IntechOpen Series
Veterinary Medicine and Science, Volume 12

Updates on Veterinary Anatomy and Physiology

*Edited by Catrin Sian Rutland
and Samir A.A. El-Gendy*

Updates on Veterinary Anatomy and Physiology

Edited by Catrin Sian Rutland and Samir A.A. El-Gendy

Contributors

Thomas Geissmann, Simone Rosenkranz-Weck, Judith J.G.M. Van Der Loo, Mathias Orgeldinger, Gabriel Alexis S.P. Tubalinal, Leonard Paulo G. Lucero, Jim Andreus V. Mangahas, Marvin A. Villanueva, Claro N. Mingala, Catrin Sian Rutland, Jennifer Hall, Emily Barker, Adam Best, Mohamed A.M. Alsafy, Samir A.A. El-Gendy, Jaco Bakker, Christophe Casteleyn, Chan I-Ping, Hsueh Tung, Wojciech Kozdruń, Jowita Samanta Niczyporuk, Natalia Styś-Fijoł, Tuba Parlak Ak, Maria Evarista Arellano-García, Maritza Roxana García-García, Sandra Castro-Gamboa, Olivia Torres-Bugarín, Yanis Toledano-Magaña, Juan Carlos García-Ramos, Cinthya Sofia Sanabria-Mora, Daniel García-Flores, Thomas Rohwedder, Cármen Nóbrega, Helena Vala, Ana Cristina Mega, Carla Santos, Catarina Coelho, Maria Aires Pereira, Rita Cruz, Fernando Esteves, João Mesquita, Isabel Brás, Paula A. Oliveira, Ana I. Faustino-Rocha, Milomir Kovac, Tatiana Vladimirovna Ippolitova, Sergey Pozyabin, Ruslan Aliev, Viktoria Lobanova, Nevena Drakul

Notice

Statements and opinions expressed in the chapters are these of the individual contributors and not necessarily those of the editors or publisher. No responsibility is accepted for the accuracy of information contained in the published chapters. The publisher assumes no responsibility for any damage or injury to persons or property arising out of the use of any materials, instructions, methods or ideas contained in the book.

We are IntechOpen,
the world's leading publisher of Open Access books
Built by scientists, for scientists

6,100+
Open access books available

149,000+
International authors and editors

185M+
Downloads

156
Countries delivered to

Our authors are among the
Top 1%
most cited scientists

12.2%
Contributors from top 500 universities

Interested in publishing with us?
Contact book.department@intechopen.com

Numbers displayed above are based on latest data collected.
For more information visit www.intechopen.com

Veterinary Medicine and Science

Aims and Scope of the Series

Paralleling similar advances in the medical field, astounding advances occurred in Veterinary Medicine and Science in recent decades. These advances have helped foster better support for animal health, more humane animal production, and a better understanding of the physiology of endangered species to improve the assisted reproductive technologies or the pathogenesis of certain diseases, where animals can be used as models for human diseases (like cancer, degenerative diseases or fertility), and even as a guarantee of public health. Bridging Human, Animal, and Environmental health, the holistic and integrative "One Health" concept intimately associates the developments within those fields, projecting its advancements into practice. This book series aims to tackle various animal-related medicine and sciences fields, providing thematic volumes consisting of high-quality significant research directed to researchers and postgraduates. It aims to give us a glimpse into the new accomplishments in the Veterinary Medicine and Science field. By addressing hot topics in veterinary sciences, we aim to gather authoritative texts within each issue of this series, providing in-depth overviews and analysis for graduates, academics, and practitioners and foreseeing a deeper understanding of the subject. Forthcoming texts, written and edited by experienced researchers from both industry and academia, will also discuss scientific challenges faced today in Veterinary Medicine and Science. In brief, we hope that books in this series will provide accessible references for those interested or working in this field and encourage learning in a range of different topics.

Meet the Series Editor

Rita Payan Carreira earned her Veterinary Degree from the Faculty of Veterinary Medicine in Lisbon, Portugal, in 1985. She obtained her Ph.D. in Veterinary Sciences from the University of Trás-os-Montes e Alto Douro, Portugal. After almost 32 years of teaching at the University of Trás-os-Montes and Alto Douro, she recently moved to the University of Évora, Department of Veterinary Medicine, where she teaches in the field of Animal Reproduction and Clinics. Her primary research areas include the molecular markers of the endometrial cycle and the embryo–maternal interaction, including oxidative stress and the reproductive physiology and disorders of sexual development, besides the molecular determinants of male and female fertility. She often supervises students preparing their master's or doctoral theses. She is also a frequent referee for various journals.

Meet the Volume Editors

Catrin Rutland is an Associate Professor of Anatomy and Developmental Genetics and Sub Dean for Postgraduate Research at the University of Nottingham, UK. She obtained her undergraduate degree from the University of Derby, UK, her master's degree from Technische Universität München, Germany, and her Ph.D. from the University of Nottingham. She undertook a post-doctoral research fellowship in the School of Medicine at the University of Nottingham before accepting tenure in Veterinary Medicine and Science, also achieving her MMedSci (Medical Education) and Postgraduate Certificate in Higher Education (PGCHE). Dr. Rutland is an author of more than 100 peer-reviewed journal articles and books/book chapters, as well as more than 100 research abstracts. She is a board member of the European Association of Veterinary Anatomists, a fellow of the Anatomical Society, and a senior fellow of the Higher Education Academy. She has written popular science books for the public.

Samir A.A. El-Gendy is a Professor of Anatomy and Embryology at the Faculty of Veterinary Medicine, Alexandria University, Egypt, where he obtained his Ph.D. in Veterinary Science in 2007. He is an author of scientific articles, books, and book chapters. His research focuses on applied anatomy, imaging techniques, and computed tomography. He has worked on various local projects on E-learning. Dr. El-Gendy is a board member of the African Association of Veterinary Anatomists and other anatomy societies.

Contents

Preface

Animal health, disease, and function are based on the fundamentals of anatomy, histology, embryology, and physiology. Therefore, these topics are essential for not only veterinary professionals but also animal owners. This book contains literature reviews and original research studies on animals ranging from primates to horses and cattle.

The first section, "Anatomy, Embryology and Function," includes four chapters. Chapter 1, "Anatomy of the Rhesus Monkey (*Macaca mulatta*): The Essentials for the Biomedical Researcher", provides easily accessible anatomical data on the rhesus monkey. It explores the muscular, digestive, respiratory, urogenital, and circulatory systems in both males and females using incredible images to aid visualization. Chapter 2, "Anatomical Guide to the Paranasal Sinuses of Domestic Animals", is useful for anatomists, radiologists, clinicians, researchers, and even veterinary students. It examines the paranasal sinuses of production animals such as cattle, buffalo, sheep, and goats, in addition to camels, canines (dogs), and equines (horses and donkeys). Chapter 3, "Biomechanics of the Canine Elbow Joint", discusses the complex elbow joint of dogs, discussing normal ranges of movement and the techniques used to investigate these. It also examines the joint under adaptive changes, such as when caused by pain and lameness. Chapter 4, "Pulmonary Vein: Embryology, Anatomy, Function and Disease", focuses on these essential cardiovascular structures from development to disease, incorporating physiology and function.

The second section, "Anatomy and Physiology of Disease and Diagnostics," also includes four chapters. Chapter 5, "Evaluation of Current and Future Diagnostic and Prognostic Techniques for Traumatic Pericarditis in Cattle", discusses bovine cardiac disease, which often has a poor prognosis. This is a situation complicated by the fact that it is often a production animal with economic viability that is affected. This chapter discusses the anatomy, physiology, and clinical presentations of traumatic pericarditis in terms of prevention, diagnosis, prognosis, and treatment. Chapter 6, "Equine Stress: Neuroendocrine Physiology and Pathophysiology", focuses on horses. The stress responses in horses maintain physiological integrity and provide protection. This chapter investigates the mechanisms behind these processes under both normal and disease states, and explores assessment, prevention, control, and management of these diseases and stress. Chapter 7, "'Marek's Disease is a Threat for Large Scale Poultry Production", discusses Marek's disease, which is a widespread infectious disease that results in huge economic losses within poultry production, from weight loss in birds to increased numbers of deaths. This chapter considers not only the causative agents but also details the anatomopathological changes that occur in the liver, spleen, and reproductive system because of the disease. It also examines diagnostic techniques. Chapter 8, "Application of Noble Metals in the Advances in Animal Disease Diagnostics", discusses how advances in molecular biology and biotechnology have greatly increased laboratory-based screening and detection of different animal diseases, whether they be caused by bacterial, viral, or fungal pathogens. Increasingly,

especially in food production, there has been a need for more field-based applications. This chapter considers the use of noble metals as diagnostic tools.

The third section, "Molecular and Cellular Structure and Function," includes two chapters relating to anatomy and physiology in the field of veterinary medicine and health. Chapter 9, "Bronchus-Associated Lymphoid Tissue (BALT) Histology and Its Role in Various Pathologies", examines the associations between the anatomy and histology of the lower respiratory tract and the relationship with infections and immunological response mechanisms. Chapter 10, "Genomic Instability and Cyto-Genotoxic Damage in Animal Species", covers genomic instability and its potential associations with carcinogenesis and/or physiological disorders. It discusses exposure of wild, captive, and domesticated vertebrates to xenobiotics as well as the links to cytogenotoxicity and the resulting disorders. The chapter also presents techniques to assess and interpret cytogenotoxicity biomarkers to assist with therapeutic management of related disorders.

The final section of the book, "Pedagogy and Psychology," includes two chapters. Chapter 11, "Virtual Physiology: A Tool for the 21st Century", is very apt during these times of increased remote learning and teaching. This chapter discusses using game-based learning, virtual experiences and laboratories, as well as other newer techniques to help reduce costs and the use of animals. These methods are especially useful when students cannot attend classes in person due to such situations as the COVID-19 pandemic. The chapter also provides a look back through history and the differing landmarks of physiology teaching. Chapter 12, "Taxon-Specific Pair Bonds in Gibbons (Hylobatidae)", investigates three generally accepted indicators of pair-bond strength (mutual grooming, behavioral synchronization, and partner distance) and presents a study of the amount of partner-directed grooming in each sex. There is no doubt that the mind and body can have incredible effects on the anatomy, physiology, and general health of an animal.

The chapter authors are experts in their field from across the world. They have investigated numerous species, using published literature, innovative research, and graphics to illustrate their work. The researchers have looked at DNA as well as entire organ systems and organisms, exploring contemporary aspects of anatomy and physiology and the impacts they have on animal health and the economy. This book discusses basic anatomy and physiology aspects as well as pathology and disease detection and diagnosis and treatment methods.

Dr. Catrin Sian Rutland
School of Veterinary Medicine and Science,
University of Nottingham,
Nottingham, UK.

Samir A.A. El-Gendy
Professor,
Faculty of Veterinary Medicine,
Alexandria University,
Alexandria, Egypt

Section 1

Anatomy, Embryology and Function

Chapter 1

Anatomy of the Rhesus Monkey (*Macaca mulatta*): The Essentials for the Biomedical Researcher

Christophe Casteleyn and Jaco Bakker

Abstract

Amongst the non-human primates, the rhesus monkey (*Macaca mulatta*) is the most commonly investigated species in biomedical research. Its similarity to humans regarding the anatomy and physiology has resulted in an increasing number of studies in which the rhesus monkey serves as a model. This book chapter aims to fulfill the researcher's need for easily accessible anatomical data on the rhesus monkey by presenting the essentials of its various anatomical systems. The cadavers of several rhesus monkeys of either gender were dissected for gross anatomical study of the muscular, digestive, respiratory and urogenital systems. The circulatory system was studied after injection of latex into the blood vessels. Not only did this technique allow for better visualization of the blood vessels, but it was also valuable during the description of the peripheral nerves. In addition, methyl methacrylate casts were prepared to gain insight into the organization of the arterial system. The arthrology of the rhesus monkey was studied during the maceration of several cadavers, which ultimately revealed the individual bones that were described. From one such cadaver the skeleton was mounted. The results of the dissections are textually described and illustrated by means of numerous figures.

Keywords: Rhesus monkey, Anatomy, Osteology, Arthrology, Myology, Digestive system, Urogenital system, Angiology, Neurology

1. Introduction

The rhesus monkey (*Macaca mulatta*) belongs to the class of the mammals (*Mammalia*), the order of the primates (*Primates*), the family of the Old World monkeys (*Cercopithecidae*) and the genus *Macaca*. This animal finds its origin in the southern parts of Asia but is widespread throughout the world as one of the most frequently used laboratory animal. This is the result of the many similarities between the rhesus monkey and humans. Both species have common ancestry with genomes that are identical for 93.5% [1]. Only great apes present a larger degree of similarity with humans, but their use in research is very strictly regulated [2].

Rhesus monkeys are commonly used in toxicity studies and play a pivotal role in unraveling the mechanisms of health and diseases and during the development of

vaccines. HIV, SARS and Covid-19 are a few examples of viral diseases that are studied in the rhesus monkey. In addition to investigations that require that the physiology of this laboratory animal parallels that of man, studies that demand a comparable anatomy are multiple as well. Examples include studies on osteoporosis, osteopenia, lordosis and kyphosis [1].

The aim of this book chapter is to provide the biomedical researcher, who studies and/or uses the rhesus monkey, with the essentials of its anatomy. Although this chapter is rather elaborate, not all the details of the rhesus monkey anatomy can be described. Where appropriate, emphasis is put on those structures that have importance during manipulations of the animal under investigation, such as the muscles that allow for intramuscular injection and the veins that can be punctured to draw blood or inject substances intravenously. Researchers can be referred to two anatomical atlases for further reading. These include the work by Hartman and Straus Jr. from 1933, entitled *The Anatomy of the Rhesus Monkey (*Macaca mulatta*)* [3] and the work by Berringer and coworkers from 1968, entitled *An Atlas and Dissection Manual of Rhesus Monkey Anatomy* [4]. However, these reference works are outdated as they present black-and-white photographs and line drawings to visualize the anatomy. In addition, they make use of human terminology that is often archaic. In the present book chapter, more than 70 full color photographs are shown. In the figure legends, the official veterinary anatomical nomenclature is used [5]. In the text, however, English terms are used to enhance the readability. All materials for this study were obtained from animals that were euthanized for ethical reasons. No animals were euthanized for the purpose of this chapter.

2. External appearance

The rhesus monkey exhibits pronounced sex differentiation (**Figure 1**). Females measure approximately 47 cm in length (crown-rump length, thus without tail) and weigh 5–8 kg, whereas males present values of 53 cm and 8–15 kg, respectively [6, 7]. They have a relatively short, nonprehensile tail. As the rhesus monkey is a despotic species, fights often occur related to their hierarchical rank order system causing

Figure 1.
External appearance of the male (A) and female (B) rhesus monkey. Notice the twins suckling their mother.

severe tail wounds all resulting in the veterinarian's decision to amputate the injured tail.

The hairs on the lateral sides of the animal are gray to brown. The inside of the arms and legs, and the belly color pale beige to white. Each finger and toe, five on each hand and foot, possesses a nail (unguis). The palms of the hands and the soles of the feet are keratinized showing epidermal ridges [7]. The face, including the ears, has very few hairs and therefore a pinkish appearance. Females possess a pair of pectoral mammary glands.

The skin covering and surrounding the genitals is also devoid of hairs. In males, the scrotum is non-pendulous and contains a pair of testes that measure 4 cm in length [8]. The penis is normally retracted within the preputium (**Figure 2**), only extracted during mating.

Menarche occurs at about 3 years of age and the length of the menstrual cycle is 28 days. The gestation length is around 165 days. Rhesus monkeys are seasonal breeders. Menstrual bleeding (menses) lasts for about 4 days. During the mating season (autumn-early winter), the skin of the face and genitals of females becomes characteristically red and/or swollen (**Figures 3** and **4**) during the period of regular cycles (sex skin coloration). These periodic changes in sex skin coloration are not valid indicators of either ovulation or menstruation. The sex skin is a secondary sex characteristic and reflects estrogenic activity. It fluctuates, as a rule, as to presence, extent, and time of year in a very unpredictable manner. In older females, the sex skin is less pronounced, and the redness may persist for longer intervals. Moreover, sex color is maintained during the entire gestational period and for several weeks after parturition: females who become pregnant during the mating season do not show the significant sex skin coloration decrease seen in nonpregnant females during the months that follow the mating season. Environmental cues, perhaps acting on a seasonal biological clock rather than social factors, are thought to be mainly responsible for the seasonal fluctuations observed. Sex skin involves the skin of the buttocks, hips, and base of tail, but the coloration and swelling can even spread in red splotches down the legs and over the calves to the heel; and there might also be a forward-tapering streak of red splotches from the symphysis to the umbilicus. Females could use color as a gauge to monitor other females' reproductive status or cyclic phase, for competitive purposes, as hindquarter color can advertise the relative timing of ovulation. The possibility

Figure 2.
External genital organs of the male rhesus monkey with the penis retracted into the preputium.

Figure 3.
Two examples of sex skin (coloration and swelling) in the face of females.
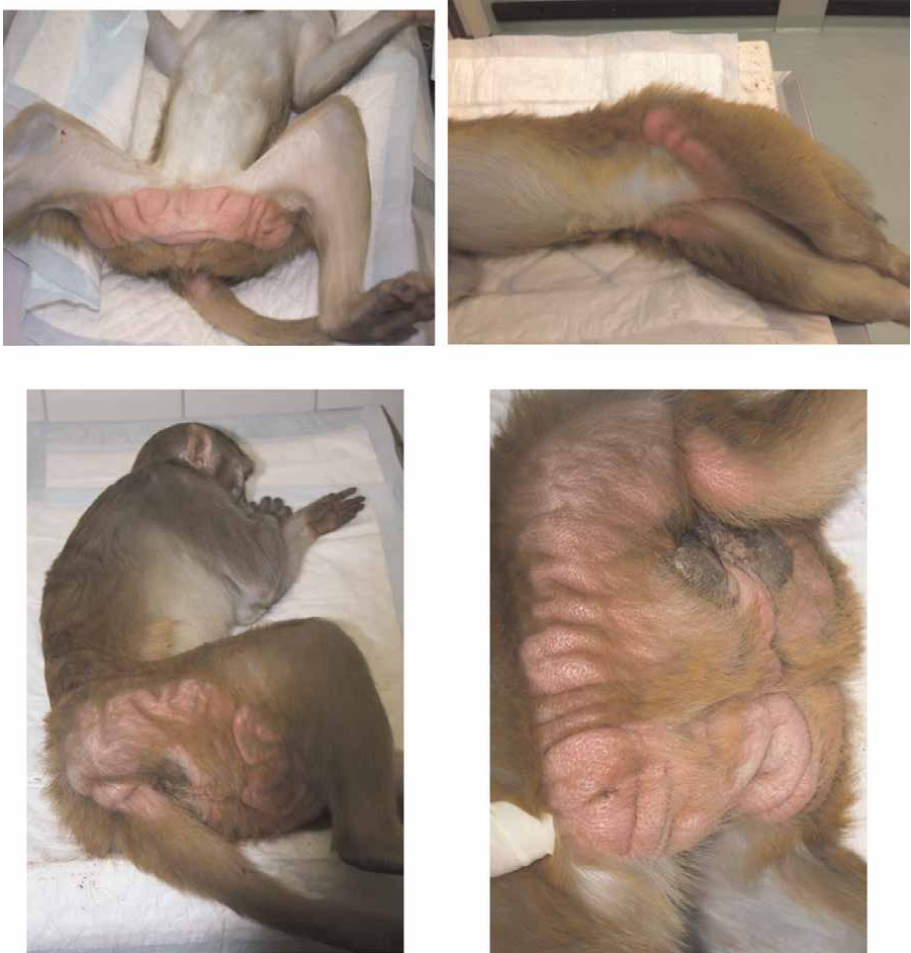
Figure 4.
Four examples of sex skin coloration and swelling on the buttocks, hips, legs and base of tail in females.
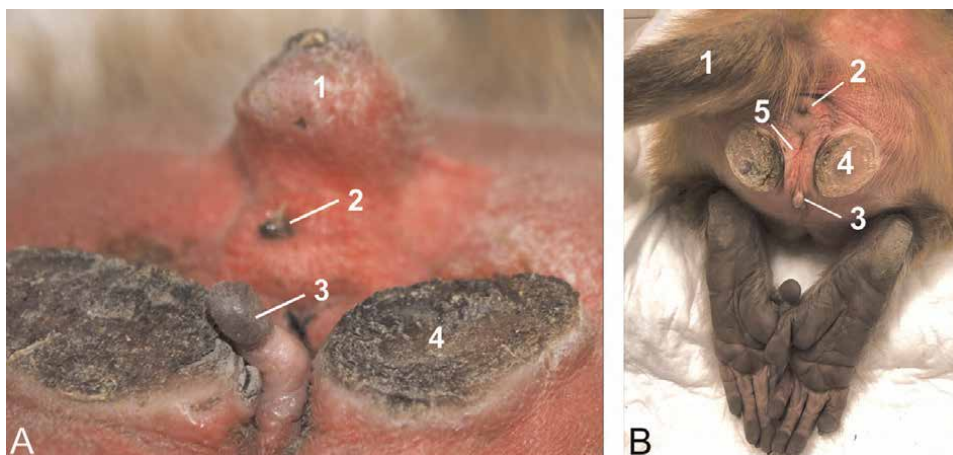
Figure 5.
(A) Perineum of a female rhesus monkey. This female is presented with a tail stump (1) that is visible just dorsal to the anal opening (2). The large clitoris (3) is present in between the sciatic protuberances (4). (B) This female has an intact tail (1) just dorsal to the anal opening (2). The clitoris (3) is less pronounced but still visible in between the sciatic protuberances (4). The prudential labia (5) can however, more readily be recognized in the female.

might not be plausible for facial color, given that the relationship between face color and cyclic phase is not predictable in rhesus monkeys.

In females, the vulva is pronounced, with a large visible clitoris between the sciatic protuberances that are covered with keratinized skin patches (callositas ischii/sciatic protuberances), which is typical for Old World monkeys, both males and females (**Figure 5**).

3. Osteology

The general build of the skeleton of the rhesus monkey is illustrated in **Figure 6**. The skull is large and heavy compared to the slender body. This contrasts with the sturdy external appearance of the rhesus monkey, as depicted in **Figure 1**, which suggests that this species has a well-developed musculature.

3.1 Skull

The skull including the mandible of an adult male rhesus monkey is depicted in **Figure 7**. Some major anatomical landmarks are indicated. The splanchnocranium is relatively large but presents a reduced length. The very large conical orbits are almost completely postorbitally closed. The neurocranium is situated caudal to the former. It contains the cranial cavity that harbors the brains. The mandible and in particular its body is relatively large. A prominent mandibular angle can be seen. The symphysis between the left and right mandibles is synostotic.

The hyoid bone of the rhesus monkey (**Figure 8**) is not directly connected to the skull. It consists of a body (corpus) and a bilaterally present pair of horns that lie caudally. The lesser horn (cornu minus) is, however, fused with the greater horn (cornu majus). The latter horns are joined with the body by means of cartilage.
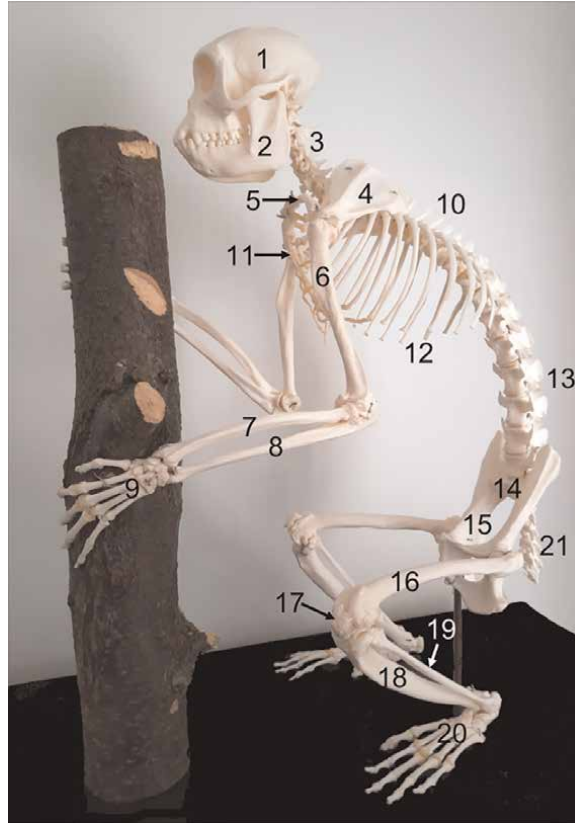
Figure 6.
Skeleton of a female rhesus monkey. 1: cranium, 2: mandibula, 3: vertebrae cervicales, 4: scapula, 5: clavicula, 6: humerus, 7: radius, 8: ulna, 9: manus, 10: vertebrae thoracales, 11: sternum, 12: arcus costalis, 13: vertebrae lumbales, 14: sacrum, 15: pelvis, 16: femur, 17: patella, 18: tibia, 19: fibula, 20: pes, 21: vertebrae caudales.
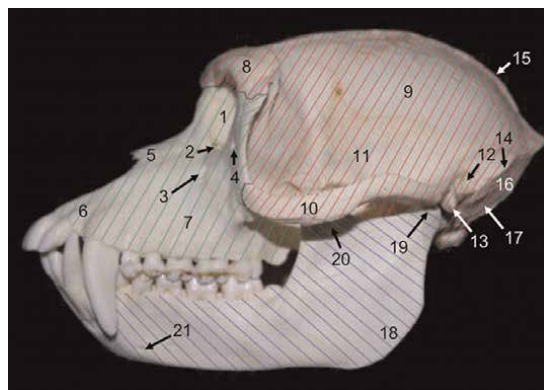
Figure 7.
Left lateral view of the skull of an adult male rhesus monkey. The splanchnocranium and neurocranium are shaded in red and green, respectively. 1: orbita, 2: canalis lacrimalis, 3: foramen infraorbitale, 4: foramen zygomaticofaciale, 5: os nasale, 6: os incisivum, 7: maxilla, 8: os frontale, 9: os parietale, 10: arcus zygomaticus, 11: fossa temporalis, 12: porus acusticus externus, 13: processus styloideus, 14: crista nuchae, 15: linea temporalis, 16: planum nuchale, 17: foramen magnum. The mandible is shaded in purple. 18: angulus mandibulae, 19: processus condylaris, 20: processus coronoideus, 21: foramen mentale.
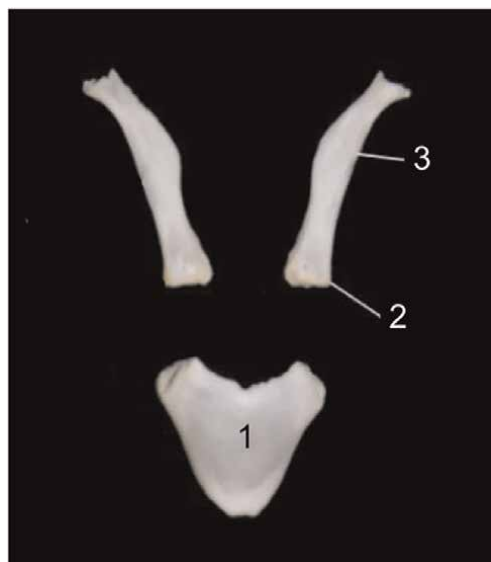
Figure 8.
Dorsal view of the hyoid bone. The large corpus (1) is caudally elongated by the bilateral cornu minus (2) and the bilateral cornu majus (3) that are fused.

3.2 Axial skeleton

The vertebral column consists of 7 cervical vertebrae, 12 thoracic vertebrae, 7 lumbar vertebrae, 3 fused sacral vertebrae and around 19 caudal vertebrae. This number is variable. The fifth, sixth and seventh caudal vertebrae possess a hemal arch that encloses the caudal artery and vein. The number of rib pairs equals the number of thoracic vertebrae, i.e. 12. Consequently, the rhesus monkey presents 24 ribs in total. These are connected to the sternum, which is composed of 7 sternebrae, by means of costal cartilages. The manubrium is the first sternebra to which not only the first pair of ribs is connected, but also the bilaterally present clavicle (**Figure 9**). This bone
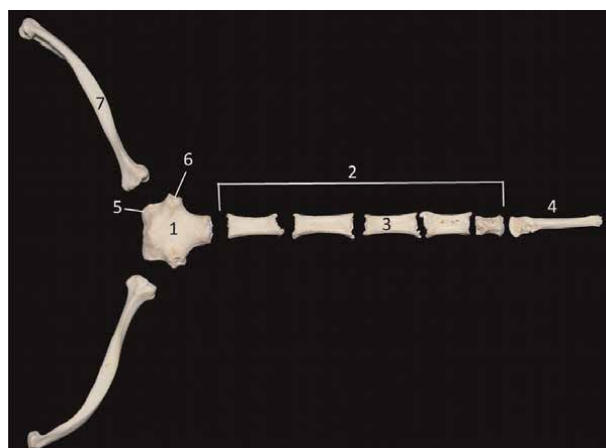
Figure 9.
Dorsal view of the sternum. 1: manubrium sterni, 2: corpus sterni, 3: sternebra, 4: processus xyphoideus, 5: incisura clavicularis, 6: incisura costalis, 7: clavicula.
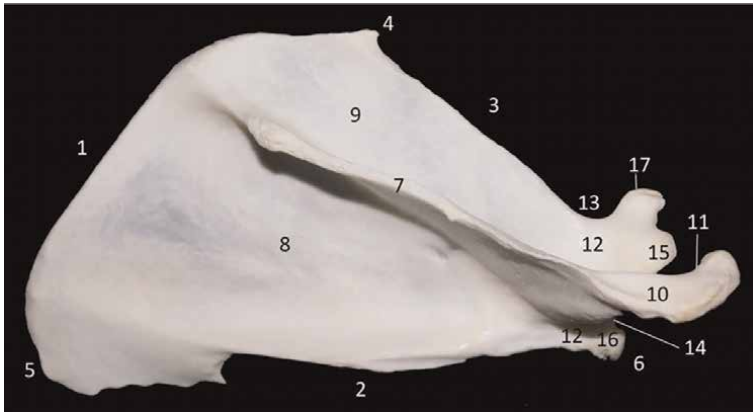
Figure 10.
Lateral view of the right scapula. 1: margo dorsalis, 2: margo caudalis, 3: margo cranialis, 4: angulus cranialis, 5: angulus caudalis, 6: angulus ventralis, 7: spina scapulae, 8: fossa infraspinata, 9: fossa supraspinata, 10: acromium, 11: facies articularis clavicularis, 12: collum scapulae, 13: incisura scapulae, 14: cavitas glenoidalis, 15: tuberculum supraglenoidale, 16: tuberculum infraglenoidale, 17: processus coracoideus.

Figure 11.
Cranial (A) and caudal (B) views of the right humerus. 1: epiphysis proximalis or extremitas proximalis, 2: diaphysis or corpus humeri, 3: epiphysis distalis or extremitas distalis, 4: caput humeri, 5: collum humeri, 6: tuberculum majus, 7: tuberculum minus, 8: crista tuberculi minoris, 9: crista tuberculi majoris, 10: sulcus intertubercularis, 11: tuberositas deltoidea, 12: epicondylus lateralis, 13: epicondylus medialis, 14: fossa radialis, 15: fossa coronoidea, 16: trochlea humeri, 17: capitulum humeri, 18: fossa olecrani, 19: sulcus nervi radialis.

connects the sternum with the thoracic limb through its junction with the acromion of the shoulder blade.

3.3 Appendicular skeleton

3.3.1 Thoracic limb

The thoracic limb, which is connected with the thorax by means of the clavicle, is composed of the shoulder blade or scapula (**Figure 10**), the humerus (**Figure 11**), the medially located radius (**Figure 12**) and the laterally located ulna (**Figure 13**) that are unfused, and the hand (**Figure 14**). The hand contains five fingers that are each composed of 3 phalanges, except the first, called the pollex, that lacks the middle phalanx.

Figure 12.
Cranial (A) and caudal (B) views of the right radius. 1: epiphysis proximalis or extremitas proximalis, 2: diaphysis or corpus radii, 3: epiphysis distalis or extremitas distalis, 4: caput radii, 5: fovea articularis, 6: collum radii, 7: tuberositas radii, 8: processus styloideus radii, 9: facies articularis carpalis, 10: tuberositas pronatoria, 11: incisura ulnaris.

Figure 13.
Cranial (A) and caudal (B) views of the right ulna. 1: epiphysis proximalis or extremitas proximalis, 2: diaphysis or corpus ulnae, 3: epiphysis distalis or extremitas distalis, 4: olecranon with tuber olecrani, 5: incisura trochlearis with processus anconeus, 6: processus coronoideus medialis, 7: processus coronoideus lateralis, 8: tuberositas ulnae, 9: crista musculi supinatorii, 10: caput ulnae, 11: facies articularis, 12: processus styloideus ulnae.

3.3.2 Pelvic limb

The pelvic limb connects to the body through the pelvis that consists of the fused left and right pelvic bones (**Figures 15** and **16**). The symphysis between these bones is synostotic. The femoral bone or femur presents a distal trochlea for the ovoid patella. Both femoral condyles, which each support a sesamoid bone on their caudoproximal aspects, articulate with the tibial plateau (**Figure 17**). The tibia (**Figure 18**) lies medial to the slender fibula (**Figure 19**). The foot (**Figure 20**) contains five toes that are each composed of 3 phalanges, except the first, called the hallux, that lacks the middle phalanx.

4. Arthrology

4.1 Head

The various bones of which the skull is composed of are connected by means of sutures that ossify during puberty. As mentioned earlier, the symphysis mandibulae is
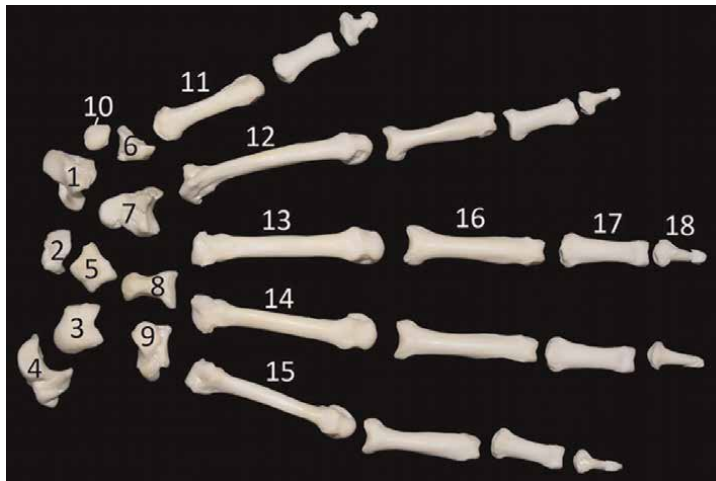
Figure 14.
Dorsal view of the skeleton of the right hand. 1: os carpi radiale (os scaphoideum), 2: os carpi intermedium (os lunatum), 3: os carpi ulnare (os triquetrum), 4: os carpi accessorium (os pisiforme), 5: os carpi Centrale, 6: os carpale primum (os trapezium), 7: os carpale secundum (os trapezoideum), 8: os carpale tertium (os capitatum), 9: os carpale quartum (os hamatum), 10: os sesamoideum m. abductoris digiti primi (pollicis), 11: os metacarpale primum, 12: os metacarpale secundum, 13: os metacarpale tertium, 14: os metacarpale quartum, 15: os metacarpale quintum, 16: Phalanx proximalis, 17: phalanx media, 18: phalanx distalis.
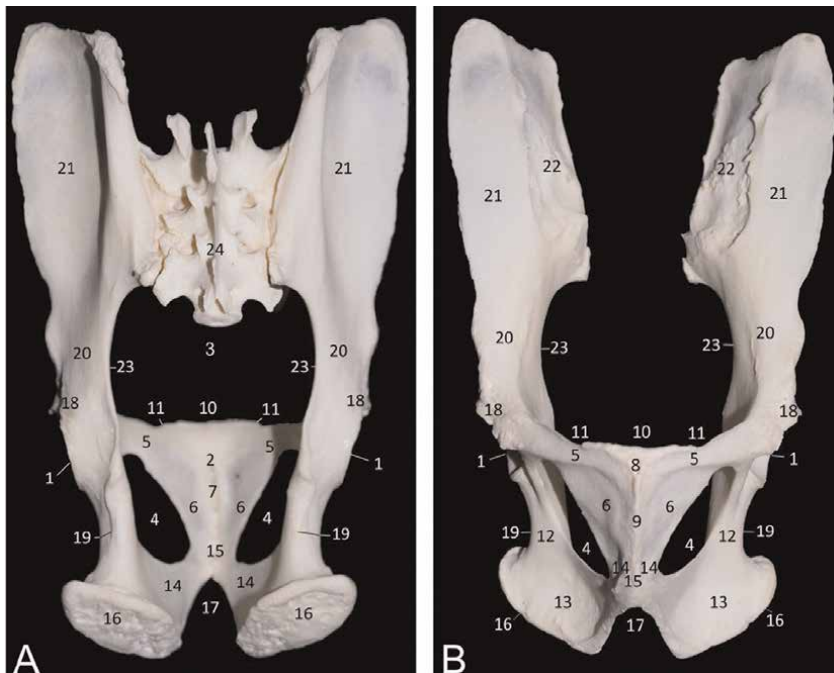
Figure 15.
Dorsal (A) and ventral (B) views of the pelvis. 1: acetabulum, 2: ossa pubicae, 3: cavum pelvis, 4: foramen obturatum, 5: ramus cranialis ossis pubis, 6: ramus caudalis ossis pubis, 7: symphysis pubica, 8: tuberculum pubicum ventrale, 9: crista pubica, 10: pecten ossis pubis, 11: eminentia iliopubica, 12: corpus ossis ischii, 13: tabula ossis ischii, 14: ramus ossis ischii, 15: symphysis ischiadica, 16: tuber ischiadicum, 17: arcus ischiadicus, 18: spina ischiadica, 19: incisura ischiadica minor, 20: corpus ossis ilii, 21: ala ossis ilii, 22: facies sacropelvina, 23: incisura ischiadica major, 24: sacrum; 7+15 = symphysis pelvina.
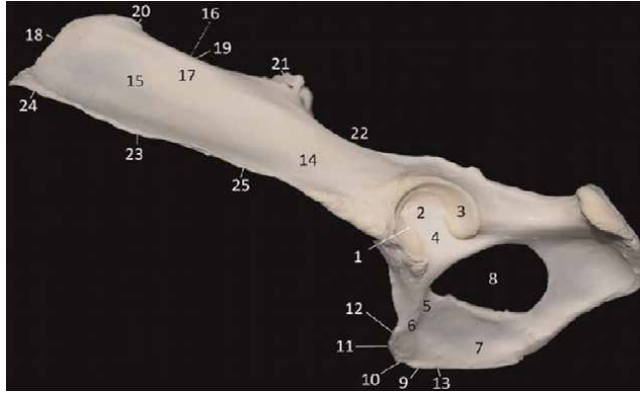
Figure 16.
Lateral view of the left os coxae. 1: acetabulum, 2: fossa acetabuli, 3: facies lunata, 4: incisura acetabuli, 5: corpus ossis pubis, 6: ramus cranialis ossis pubis, 7: ramus caudalis ossis pubis, 8: foramen obturatum, 9: symphysis pubica, 10: tuberculum pubicum ventrale, 11: pecten ossis pubis, 12: eminentia iliopubica, 13: crista pubica, 14: corpus ossis ilii, 15: ala ossis ilii, 16: facies sacropelvina, 17: facies glutea, 18: crista iliaca, 19: tuber sacrale or spina iliaca dorsalis, 20: spina iliaca dorsalis cranialis, 21: spina iliaca dorsalis caudalis, 22: incisura ischiadica major, 23: tuber coxae or spina iliaca ventralis, 24: spina iliaca ventralis cranialis, 25: spina iliaca ventralis caudalis.

Figure 17.
Cranial (A) and caudal (B) views of the right femur. 1: epiphysis proximalis or extremitas proximalis, 2: diafysis or corpus femoris, 3: epiphysis distalis or extremitas distalis, 4: caput ossis femoris, 5: fovea capitis, 6: collum ossis femoris, 7: trochanter major, 8: fossa trochanterica, 9: trochanter minor, 10: crista intertrochanterica, 11: epicondylus lateralis, 12: epicondylus medialis, 13: condylus lateralis, 14: condylus medialis, 15: trochlea ossis femoris, 16: fossa intercondylaris, 17: facies articularis sesamoidea (lateralis et medialis), 18: fossa m. poplitei.
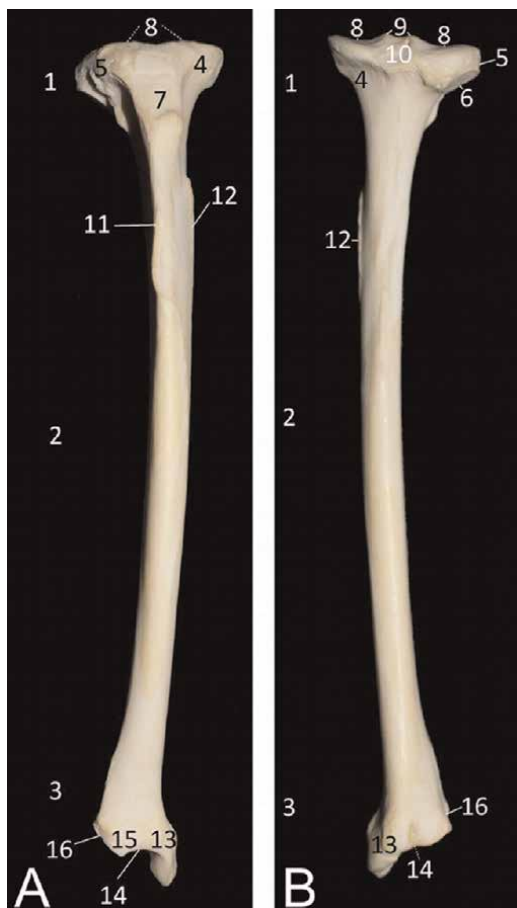
Figure 18.
Cranial (A) and caudal (B) views of the right tibia. 1: epiphysis proximalis or extremitas proximalis, 2: diaphysis or corpus tibiae, 3: epiphysis distalis or extremitas distalis, 4: condylus medialis, 5: condylus lateralis, 6: facies articularis fibularis, 7: tuberositas tibiae, 8: facies articularis proximalis, 9: eminentia intercondylaris, 10: tuberculum intercondylare laterale et mediale, 11: crista tibiae, 12: linea muscularis, 13: malleolus medialis, 14: facies articularis distalis, 15: cochlea tibiae, 16: incisura fibularis.

synostotic. The mandibular joint between the mandible and the skull presents a cartilaginous disc that eliminates the incongruence between the mandibular fossa and the condylar process (**Figure 21**).

4.2 Vertebral column

The atlanto-occipital joint between the occipital condyles of the skull and the cranial articulating foveae of the atlas (first cervical vertebra) is dorsally covered by the atlanto-occipital membrane. The bilateral articulations are laterally reinforced by the lateral ligaments.

The atlanto-axial joint has three important ligaments. The transverse ligament covers the dens axis. From this dens, the longitudinal dental ligament runs to the ventral edge of the foramen magnum. The alar ligaments connect the dens with the lateral edges of the foramen magnum.
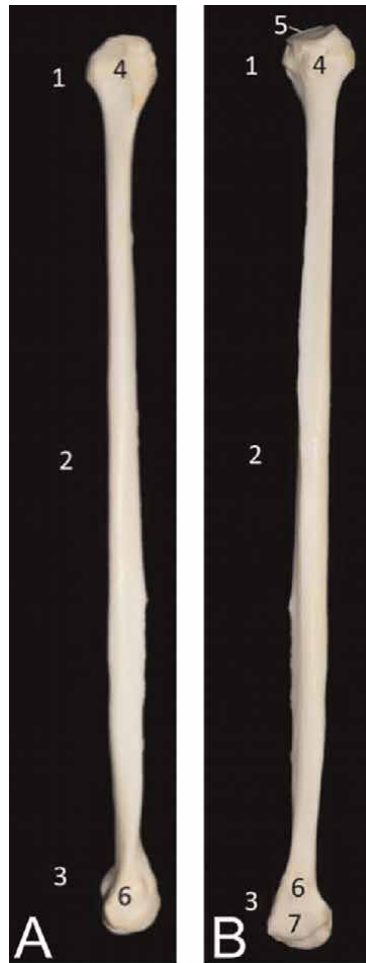
Figure 19.
Lateral (A) and medial (B) views of the right fibula. 1: epiphysis proximalis or extremitas proximalis, 2: diaphysis or corpus fibulae, 3: epiphysis distalis or extremitas distalis, 4: caput fibulae, 5: facies articularis capitis fibulae, 6: malleolus lateralis, 7: facies articularis malleoli.

The individual vertebrae, from the third cervical vertebra to the sacrum, are joined together with multiple ligaments and bands (**Figure 22**). The supraspinal ligament is the continuation of the nuchal ligament that connects the external occipital protuberance on the skull with the spinal processes of the 3rd tot 7th cervical vertebrae. The dorsal longitudinal ligament that lies immediately dorsal to the vertebral bodies, up to the sacrum, is the continuation of the tectorial membrane that covers the several ligaments of the atlanto-axial joint.

The ribs have three contact points with the thoracic vertebrae. The costal head articulates with the caudal fovea of the cranial thoracic vertebra (or the 7th cervical vertebra in the case of the first rib) and the cranial fovea of the caudal thoracic vertebra. An additional attachment is present between the costal tubercle and the transverse process of the thoracic vertebra, which number equals that of the rib (e.g., thoracic vertebra number 3 bears rib pair number 3). Ribs 11 and 12 lack the typical articulations as they have no costal tubercle.
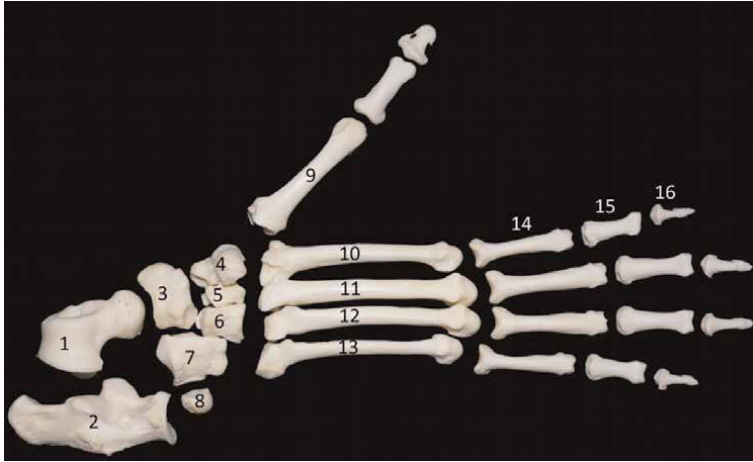
Figure 20.
Dorsal view of the skeleton of the right foot. 1: talus, 2: calcaneus, 3: os tarsi centrale (os naviculare), 4: os tarsale primum (os cuneiforme mediale), 5: os tarsale secundum (os cuneiforme intermedium), 6: os tarsale tertium (os cuneiforme laterale), 7: os tarsale quartum (os cuboideum), 8: os sesamoideum, 9: os metatarsale primum, 10: os metatarsale secundum, 11: os metatarsale tertium, 12: os metatarsale quartum, 13: os metatarsale quintum, 14: phalanx proximalis, 15: phalanx media, 16: phalanx distalis.
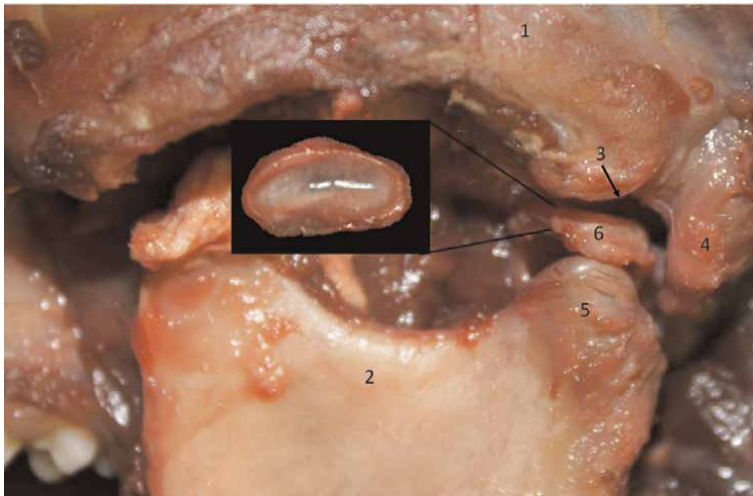
Figure 21.
Left mandibular joint formed between the cranium (1) and the mandibula (2). More specifically, the articulation is present between the fossa mandibularis (3), caudally bordered by the processus styloideus (4), and the processus coronoideus (5). The discus articularis (6), of which a higher magnification is shown in the insert, is located in between these structures.

4.3 Limbs

4.3.1 Thoracic limb

The front limb is not only connected to the thorax by means of a synsarcosis (connecting muscles) but also by means of the collar bone that attaches to the
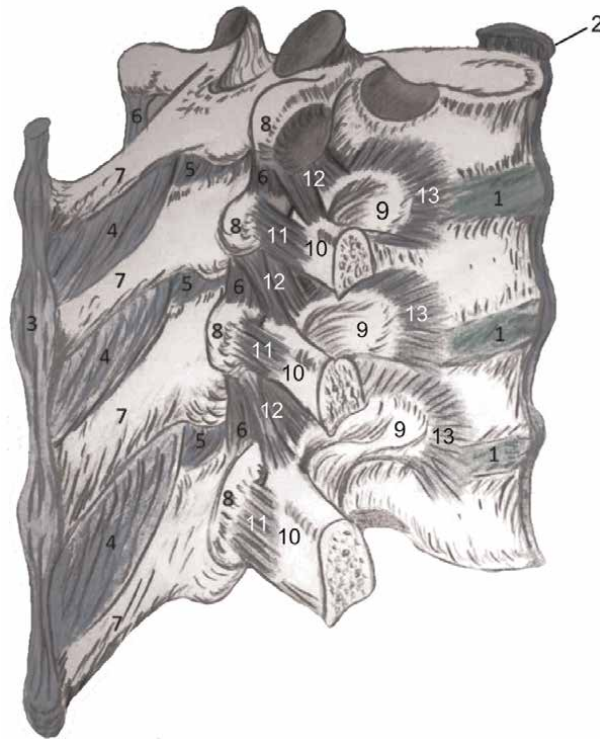
Figure 22.
Right lateral view of four thoracic vertebrae with their associated ligaments and ribs. The cranial rib has been removed entirely while the other ribs are cut proximally. 1: discus intervertebralis, 2: ligamentum longitudinale ventrale, 3: ligamentum supraspinale, 4: ligamenta interspinalia, 5: ligamentum interarcuale, 6: ligamenta intertransversaria, 7: processus spinosus, 8: processus spinosus, 9: caput costae, 10: tuberculum costae, 11: ligamentum costotransversarium laterale, 12: ligamentum costotransversarium craniale, 13: ligamenta radiata.

manubrium of the sternum, and the acromion and coracoid process of the shoulder blade. The coracoclavicular ligament is worth mentioning.

The shoulder joint between the shoulder blade and the humerus is characteristic in that the glenoid cavity of the scapula is narrower than the humeral head. Therefore, a glenoid labrum is present at the rims of the glenoid cavity. The coracohumeral ligament has its origin on the coracoid process of the scapula and inserts into the articular capsule. No collateral ligaments can be observed.

The elbow joint is formed by the humerus, radius and ulna. As such, a humeroradial and a proximal radioulnar articulation are present. The lateral collateral band originates at the lateral epicondyle of the humerus and attaches to the ulna (lateral coronoid process). It is therefore called the ulnar collateral ligament. The radial collateral ligament can be found between the medial humeral epicondyle and the radius (radial head) and ulna (medial coronoid process). The radial annular ligament attaches to both coronoid processes and encloses the radial head. In between the radius and ulna, the interosseous membrane can be seen. The distal radioulnar joint has a firm joint capsule that keeps both bones together.

The wrist or carpus/carpal joint is very complex. Numerous ligaments connect the several bones. These ligaments can be grouped into antebrachiocarpal (radiocarpal and

ulnocarpal), intercarpal and carpometacarpal ligaments. The metacarpal bones are proximally connected to each other by means of the palmar metacarpal ligaments.

Metacarpophalangeal, proximal interphalangeal and distal interphalangeal joints are the several articulations that can be found in the fingers. The pollex only shows a single interphalangeal joint. Lateral and medial collateral bands connect the phalanges to each other and to the respective metacarpal bones.

4.3.2 Pelvic limb

The hip joint is formed between the acetabulum of the pelvic bone and the femoral head. The ligament of the femoral head is stretched between these structures. Since the acetabulum is rather shallow compared to the pronounced femoral head, its rim is provided by a cartilaginous labrum (**Figure 23**). No collateral bands are present.

The knee joint is complex. It is composed of the femoropatellar, femorotibial and tibiofibular articulations. The ovoid patella bears a single straight patellar ligament that inserts on the tibial tuberosity. The incongruence between the femoral condyles and the tibial plateau is eliminated by the presence of C-shaped menisci. Both are cranially and caudally attached to the tibia by means of small meniscal ligaments. A cranial or lateral and a caudal or medial cruciate ligament can be observed between the femoral intercondylar fossa and the tibial intercondylar eminence. In addition, a meniscofemoral ligament or false cruciate ligament inserts on the caudal tip of the lateral meniscus. The lateral and medial collateral bands find their origins on the lateral and medial femoral epicondyles, respectively, and insert into the tibial epicondyle and fibular head, respectively (**Figure 24**).

The tarsal joint consists of the articulations between the tibia, the fibula, the several tarsal bones and the metatarsal bones (tarsocrural, proximal intertarsal, distal intertarsal and tarsometatarsal articulations). Numerous long and short ligaments connect the several bones. Long ligaments include the collateral ligaments and the long plantar ligament.

Metatarsophalangeal, proximal interphalangeal and distal interphalangeal joints are the several articulations that can be found in the toes. The hallux only shows a
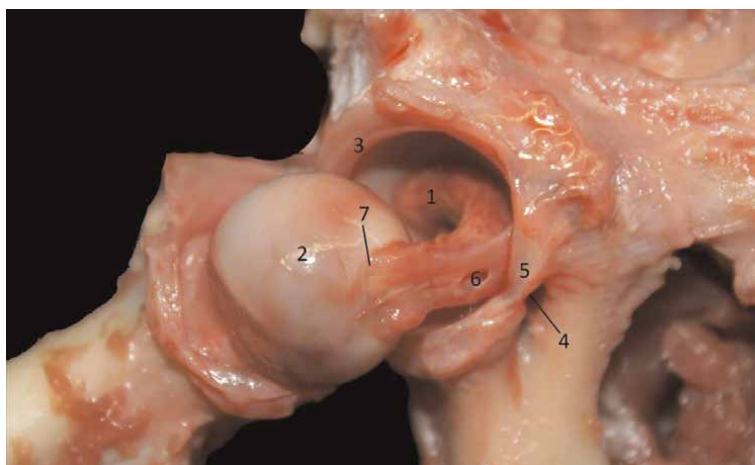
Figure 23.
Ventral view of the right hip joint. 1: acetabulum, 2: caput femoris, 3: labrum acetabulare, 4: incisura acetabuli, 5: ligamentum transversum acetabuli, 6: ligamentum capitis ossis femoris, 7: fovea capitis.
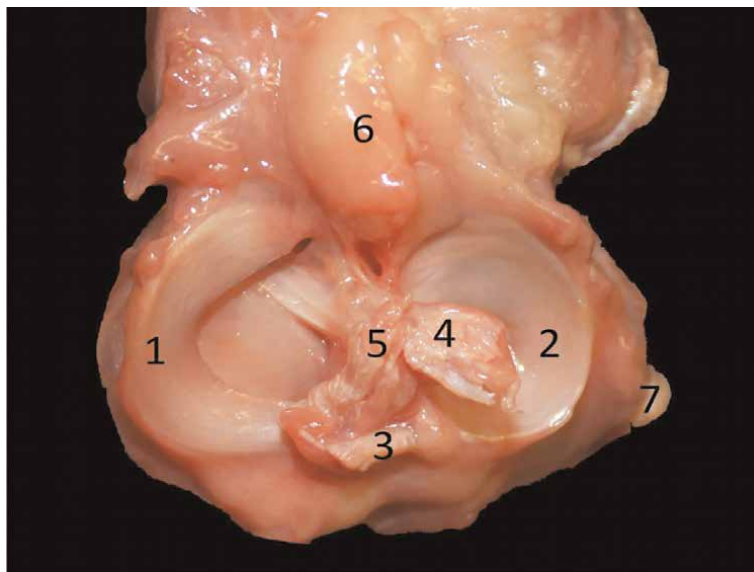
Figure 24.
View on the tibial plateau of the right limb. 1: meniscus medialis, 2: meniscus lateralis, 3: ligamentum meniscofemorale, 4: ligamentum cruciatum craniale, 5: ligamentum cruciatum caudale, 6: corpus adiposum infrapatellare, 7: ligamentum collaterale laterale.

single interphalangeal joint. Lateral and medial collateral bands connect the phalanges to each other and to the respective metatarsal bones.

5. Myology

5.1 General overview

The superficial muscles that can be observed immediately after skinning the animal are illustrated in **Figures 25** and **26**, which are ventral, dorsal and left lateral views, respectively. Below, the musculature of the rhesus monkey is briefly described per region with emphasis on the origin and insertion of each muscle. Readers are referred to anatomical atlases [3, 9] for more details.

5.2 Facial muscles

The facial muscles play a pivotal role in the facial expression and therefore the communication between animals [10, 11].

- M. platysma: This very thin superficial muscle overlies the neck region and inserts into the m. caninus, m. orbicularis oris, m. depressor anguli oris, m. depressor labii inferioris and m. mentalis (**Figure 26**).

- M. occipitalis: This cutaneous muscle lies superficial to the platysma muscle.

- M. frontalis: This broad, thin muscle covers the forehead and inserts into the m. orbicularis oculi (**Figure 26**).
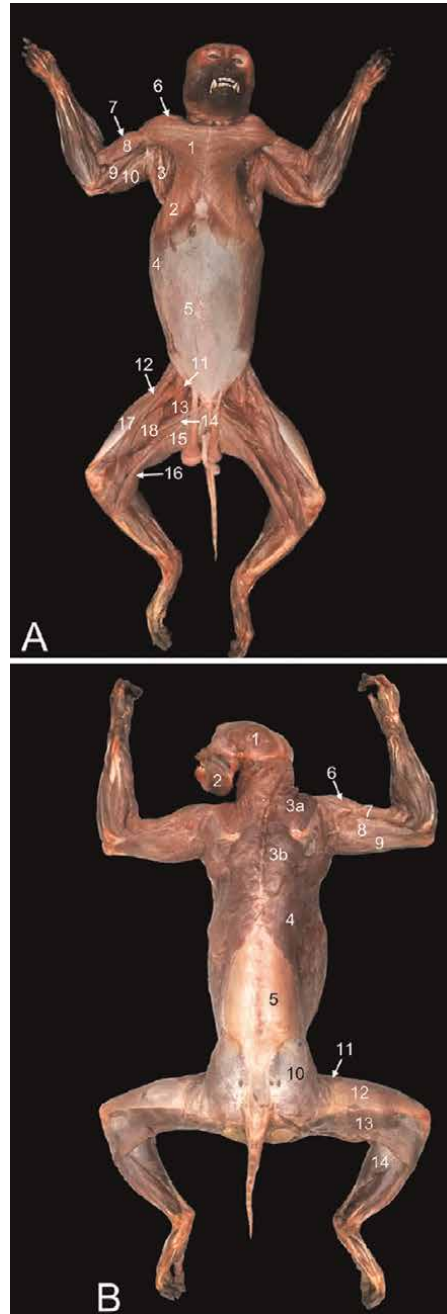
Figure 25.
Superficial musculature. A: Ventral view with 1: m. pectoralis major, 2: m. pectoralis abdominalis, 3: m. latissimus dorsi, 4: m. obliquus externus abdominis, 5: m. rectus abdominis, 6: m. deltoideus, 7: m. biceps brachii caput longum, 8: m. biceps brachii caput breve, 9: m. triceps brachii caput mediale, 10: m. triceps brachii caput longum, 11: m. iliopsoas, 12: m. sartorius, 13: m. pectineus, 14: m. adductor longus, 15: m. gracilis, 16: m. semimembranosus, 17: m. rectus femoris, 18: m. vastus medialis. B: Dorsal view with 1: m. temporal, 2: m. masseter, 3a: m. trapezius pars cervicalis, 3b: m. trapezius pars thoracica, 4: m. latissimus dorsi, 5: fascia thoracodorsalis, 6: m. deltoideus, 7: m. biceps brachii caput longum, 8: m. triceps brachii caput laterale, 9: m. triceps brachii caput longum, 10: m. gluteus superficialis covered by the fascia glutea, 11: m. tensor fasciae latae, 12: Fascia lata, 13: m. biceps femoris, 14: m. gastrocnemius caput laterale.

- M. auricularis caudalis: This muscle finds its origin in the dorsal cervical region, medial to the occipital muscle. It bifurcates to insert bilaterally at the caudal aspect of the external acoustic meatus (**Figure 26**).

- M. auricularis dorsalis: This muscle is wider and thinner than the former. It lies between the ears and inserts at the dorsal aspect of the external acoustic meatus (**Figure 26**).

- M. orbitoauricularis: This inconsistent muscle runs from the lateral orbital angle to the rostral aspect of the external acoustic meatus (**Figure 26**).

- M. orbicularis oculi: This muscle surrounds the orbit as a sphincter.

- M. zygomaticus: The origin of this band-shaped muscle is the zygomatic arch, whereas the insertion is the lateral angle of the mouth.

- M. levator labii superioris: It runs from the nasal and maxillary bones to the dorsal fibers of the orbicularis oris muscle.

- M. levator labii alaeque nasi: This muscle lies medial to the former and presents fibers that insert into the nasal wings.

- M. depressor anguli oris: This triangular muscle has insertions into the zygomatic and orbicularis oris muscles.
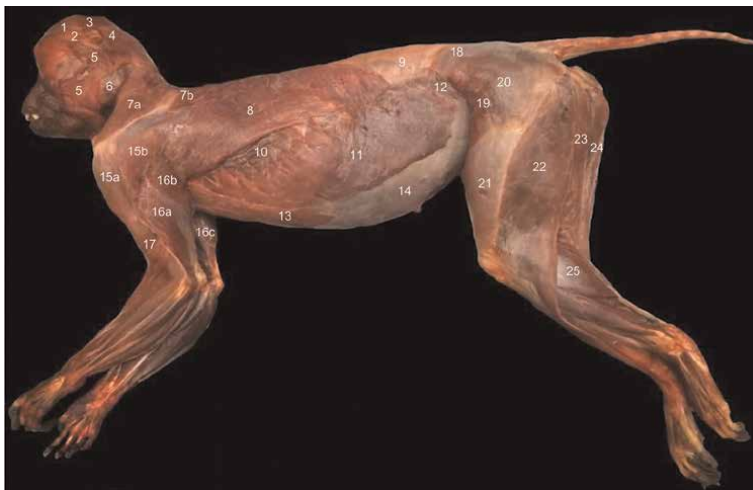
Figure 26.
Left lateral view of the superficial musculature. 1: m. frontalis, 2: m. orbitoauricularis, 3: m. auricularis dorsalis, 4: m. auricularis caudalis, 5: m. platysma, 6: m. masseter, 7a: m. trapezius pars cervicalis, 7b: m. trapezius pars thoracica, 8: m. latissimus dorsi, 9: fascia thoracodorsalis, 10: m. serratus ventralis, 11: m. obliquus externus abdominis, 12: m. obliquus internus abdominis, 13: m. pectoralis abdominalis, 14: Lamina externa vaginae m. recti abdominis, 15a: m. acromiodeltoideus, 15b: m. spinodeltoideus, 16a: m. triceps brachii caput laterale, 16b: m. triceps brachii caput longum, 16c: m. triceps brachii caput mediale, 17: m. biceps brachii, 18: fascia thoracolumbalis, 19: m. tensor fasciae latae, 20: m. gluteus superficialis, 21: fascia lata, 22: m. biceps femoris, 23: m. semitendinosus, 24: m. semimembranosus, 25: m. gastrocnemius caput laterale.

- M. caninus: This muscle lies deep to the former. It can be found at the angles of the mouth that cover the canines.

- M. orbicularis oris: This muscle surrounds the mouth opening as a sphincter.

- M. depressor labii inferioris: This muscle that lies ventromedial to the depressor anguli oris muscle runs between the ventral aspect of the orbicularis oris muscle and the skin of the chin.

- M. mentalis. This muscle covers the chin. It has insertions into the ventral aspect of the orbicularis oris muscle.

5.3 Masticatory muscles

The muscles of mastification were studied after the facial musculature was removed.

- M. masseter: The masseter originates from the zygomatic arch. It consists of a larger superficial and a smaller deep part that both insert into the mandible (**Figures 25B**, **26**, and **27**).

- M. temporalis: This muscle fills the temporal fossa. Its fibers converge on the coronoid process of the mandible (**Figures 26** and **27**).

Figure 27.
Ventrolateral view of the masticatory muscles and musculature of the ventral cervical region and tongue. 1a: m. masseter pars superficialis, 1b: m. masseter pars profunda, 2: m. temporalis, 3: m. buccinator, 4: m. pterygoideus, 5: m. digastricus venter caudalis, 6: m. sternomastoideus, 7: m. cleidomastoideus, 8: m. cleidooccipitalis, 9: m. levator scapulae cranialis, 10: m. trapezius pars cervicalis, 11: m. sternohyoideus, 12: m. sternothyroideus, 13: m. longus capitis, 14: m. longus colli, 15: m. mylohyoideus, 16: m. hyoglossus, 17: m. thyrohyoideus.

- M. buccinator: The buccinator is a deep muscle that originates from the rostral part of the zygomatic arch and the maxilla. It is inserted into the mandible (**Figure 27**)

- M. pterygoideus: The larger internal part arises from the pterygoid fossa and inserts into the mandibular angle. The smaller external part originates laterally on the pterygoid bone and inserts into the mandible at the level of the mandibular joint (**Figure 27**).

- M. digastricus: The rostral and caudal bellies are separated by an intermediate tendon. The caudal belly attaches to the mastoid process while the rostral belly inserts into the rostroventral border of the mandible (**Figure 27**).

5.4 Muscles of the ventral cervical region and tongue

- M. sternocleidomastoideus:

    The lateral portion is the m. cleidooccipitalis that arises from the clavicle and inserts into the nuchal line of the skull (**Figure 27**).

    The medial portion is the m. sternomastoideus that runs from the manubrium of the sternum to the mastoid process of the skull (**Figure 27**).

    In between both muscles, the m. cleidomastoideus can be seen. It runs from the medial side of the clavicle to the mastoid process (**Figure 27**).

- M. omohyoideus: This fusiform muscle originates from the cranial border of the scapula and inserts into the lateral aspect of the hyoid bone. It runs medial to the sternocleidomastoid muscle and lateral to the common carotid artery and vagosympathetic trunk.

- M. sternohyoideus: This muscle finds its origin on the craniodorsal aspect of the manubrium sterni and inserts into the medial aspect of the hyoid bone. As a result, it covers the trachea in the ventral midline together with its contralateral counterpart (**Figure 27**).

- M. sternothyroideus: This muscle has the same origin as the former but inserts into the thyroid cartilage. It lies medial to the common carotid artery and vagosympathetic trunk, and ventral to the trachea (**Figure 27**).

- M. longus capitis: Both the major part (m. longus capitis major) and the minor part (m. longus capitis minor) insert into the basiocciput. The former arises from the ventral sides of the bodies of the 4th to 6th cervical vertebrae, while the latter has the atlas as its origo (**Figure 27**).

- M. longus colli: This muscle lies deep against the ventral sides of all cervical and the first four thoracic vertebrae, dorsal to the trachea. The short muscle fibers interconnect the subsequent vertebrae (**Figure 27**).

- M. mylohyoideus: This muscle originates from the medial surface of the mandibular body along its entire length and inserts into the median raphe of the tongue where it meets its counterpart (**Figure 27**).

- M. hyoglossus: The hyoid bone is the origin of this muscle that inserts into the tongue (**Figure 27**).

- M. thyrohyoideus: This muscle has its origin on the thyroid cartilage and inserts into the hyoid bone.

- M. geniohyoideus: This muscle originates from the mandible at the caudal edge of the symphysis and travels caudally towards the hyoid bone.

5.5 Muscles of the dorsal and lateral cervical regions

- M. splenius: This muscle is reduced in the rhesus monkey. It originates dorsally on the first three thoracic vertebrae and runs cranially towards the occiput.

- M. complexus: This muscle arises from the transverse processes of the 3rd to 5th thoracic vertebrae and is inserted into the occipital bone below the nuchal crest near the median plane (**Figure 28**).
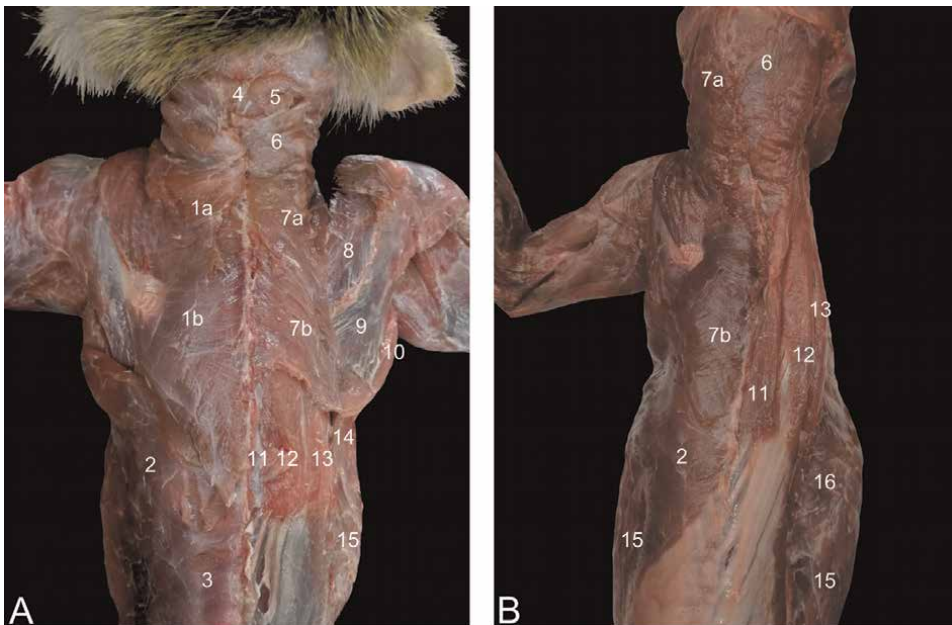
Figure 28.
Musculature of the dorsal thoracocervical region. A: Superficial layer at the left and deeper layer at the right, B: Superficial layer at the left and deeper layer at the right after removal of the right front limb. 1a: m. trapezius pars cervicalis, 1b: m. trapezius pars thoracica, 2: m. latissimus dorsi, 3: fascia thoracodorsalis, 4: m. rectus capitis, 5: m. complexus, 6: m. splenius, 7a: m. rhomboideus cervicis, 7b: m. rhomboideus thoracis, 8: m. supraspinatus, 9: m. infraspinatus, 10: m. teres major, 11: m. spinalis, 12: m. longissimus dorsi, 13: m. iliocostalis, 14: m. serratus ventralis, 15: m. obliquus externus abdominis, 16: m. serratus dorsalis.

- M. rectus capitis: The major part (m. rectus capitis major) and minor part (m. rectus capitis minor) arise from the crest of the axis and dorsal tubercle of the atlas, respectively. Both insert into the occipital bone (**Figure 28**).

- M. obliquus capitis: The cranial part (m. obliquus capitis cranialis) runs from the wing of the atlas to the occiput. The caudal part (m. obliquus capitis cranialis) arises from the crest of the axis and inserts into the wing of the atlas.

- M. trachelomastoideus: This muscle arises from the 2nd to 4th thoracic vertebrae and is inserted into the occipital bone and the mastoid process.

- M. scalenus:

     M. scalenus dorsalis (m. scalenus brevis posterior): The origin is laterocaudal to the ventral scalenus muscle. The insertion is into the transverse processes of all cervical vertebrae.

     M. scalenus medius (m. scalenus longus): The origin is on the 3rd to 5th rib. The insertion is on the transverse process of the 4th cervical vertebra (**Figure 30**).

     M. scalenus ventralis (m. scalenus brevis anterior): The origo can be found craniomedially on the first rib. The insertion is the transverse processes of the 3rd to 5th cervical vertebrae.

5.6 Muscles of the spine

- M. erector spinae:

     M. iliocostalis: This long muscle originates from the wing of the ilium and inserts into the transverse processes of the lumbar vertebrae, the ribs and transverse processes of the last two cervical vertebrae. As such, a lumbar and thoracic part can be discerned (**Figures 28** and **29**).
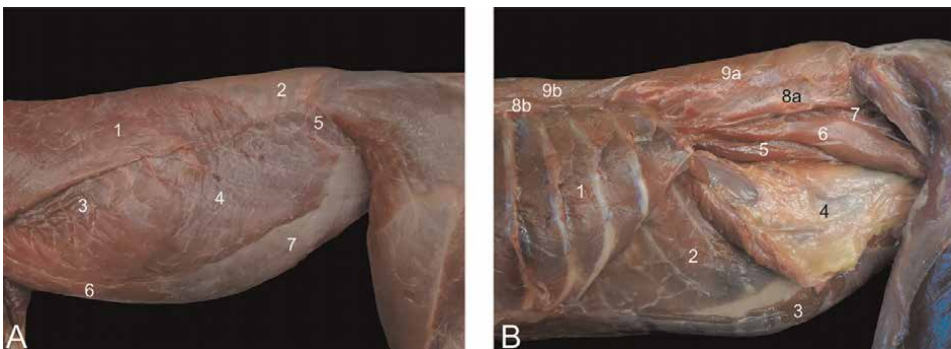
Figure 29.
Left lateral view of the abdominal muscles. A: Superficial musculature with 1: m. latissimus dorsi, 2: fascia thoracodorsalis, 3: m. serratus ventralis, 4: m. obliquus externus abdominis, 5: m. obliquus internus abdominis, 6: m. pectoralis abdominalis, 7: lamina externa vaginae m. recti abdominis. B. Deep musculature with 1: m. intercostalis externus, 2: m. transversus abdominis, 3: m. rectus abdominis, 4: fascia transversalis, 5: m. psoas minor, 6: m. psoas major, 7: m. quadratus lumborum, 8a: m. iliocostalis lumborum, 8b: m. iliocostalis thoracis 9a: m. longissimus lumborum, 9b: m. longissimus thoracis.
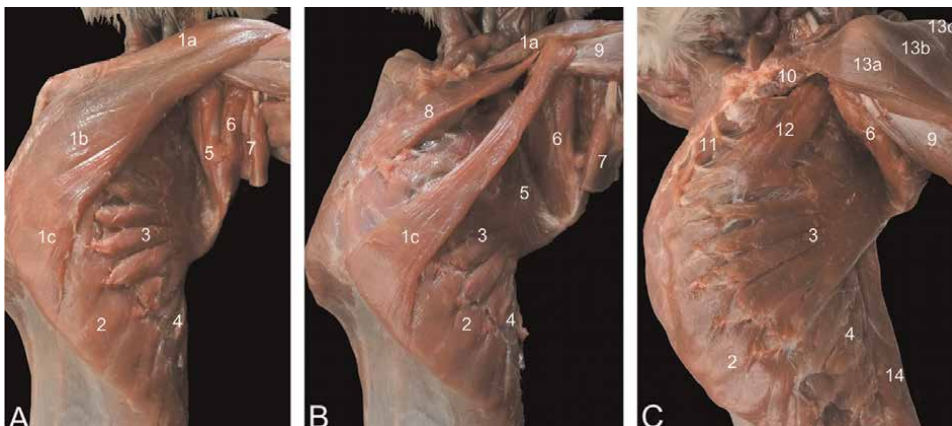
Figure 30.
Lateral views of the pectoral muscles. A: superficial layer, B: deeper layer, C: deepest layer. 1a: m. pectoralis superficialis pars sternocapsularis, 1b: m. pectoralis superficialis pars sternalis, 1c: m. pectoral superficialis pars abdominalis, 2: m. obliquus externus abdominis, 3: m. serratus ventralis, 4: m. serratus dorsalis, 5: m. subscapularis, 6: m. teres major, 7: m. latissimus dorsi, 8: m. pectoral profundus, 9: m. biceps brachii, 10: m. subclavius, 11: m. sternocostalis, 12: m. scalenus medius, 13a: m. cleidodeltoideus, 13b: m. acromiodeltoideus, 13c: m. spinodeltoideus, 14: m. latissimus dorsi.

M. longissimus dorsi: This long, cylindrical muscle that is covered by the thoracodorsal fascia lies medial to the former muscle and runs from the ilium to the mastoid process. Insertions can be found into the lumbar, thoracic and cervical vertebrae and the ribs (pars lumbalis, thoracis, cervicis and capitis) (**Figure 28**).

M. spinalis: This is the deepest muscle of this group. The origins and insertions are the spinal processes (**Figures 28** and **29**).

• M. transversospinalis:

M. semispinalis (capitis) = m. complexus: This muscle was described earlier with the muscles of the dorsal and lateral cervical region (**Figure 28**).

Mm. multifidi et rotatores: These muscles lie very deep against the vertebrae. With their origins and insertions on the transverse processes and into the spinal processes, they can rotate the vertebral column.

• M. serratus dorsalis cranialis: The cervicothoracic fascia offers the aponeurotic origin of this muscle that inserts into the 2nd to 5th ribs. The muscle fibers run in craniodorsal direction.

• M. serratus dorsalis caudalis: The lumbosacral fascia offers the aponeurotic origin of this muscle that inserts into the caudal ribs. The muscle fibers run in caudodorsal direction.

5.7 Tail musculature

The tail of the rhesus monkey is nonprehensile. The muscles found on the dorsal aspect of the caudal vertebrae are the mm. interspinales caudae, the m. extensor caudae

medialis, the m. extensor caudae lateralis, the m. abductor caudae medialis/internus and the m. abductor caudae lateralis/externus. The ventral muscles of the tail comprise the m. flexor caudae brevis, m. flexor caudae longus and the mm. intertransversarii caudae.

5.8 Abdominal muscles

- M. obliquus abdominis externus: The muscle has tendinous origins on the 4th to the 12th rib, where it interdigitates with the serratus ventralis muscle. In addition, muscle fibers originate dorsally from the lumbodorsal fascia in the lumbar region. The fibers run caudoventrally towards the linea alba onto which it attaches by means of an aponeurosis (**Figures 29**, **36**, and **37**).

- M. obliquus abdominis internus: The fibers of this muscle that lies beneath the former originate from the thoracolumbar fascia and the iliac spine. The fibers run in cranioventral direction to become tendinous (aponeurosis) at the level of the straight abdominal muscle. The aponeurosis blends with that of the external oblique abdominal muscle and forms the external sheath of the straight abdominal muscle (**Figures 29** and **36**). In the male, the cremaster muscle branches off the internal oblique abdominal muscle (**Figure 37**).

- M. transversus abdominis: This muscle arises from the costal arch, the lumbodorsal fascia and the iliac crest. The fibers run in dorsoventral direction to insert into the linea alba by means of an aponeurosis that forms the internal sheath of the straight abdominal muscle (**Figure 29**).

- M. rectus abdominis: This muscle lies between the fused aponeurosis of the external and internal oblique abdominal muscles on the one hand and the aponeurosis of the transverse abdominal muscle. The muscle runs from the sternum to the pubis and presents several tendinous intersections (**Figures 29** and **36**).

5.9 Muscles that connect the thoracic limb to the body

- Pectoral muscles:

  M. pectoralis superficialis (m. pectoralis major):

  a. Pars sternocapsularis: The sternoclavicular joint and the manubrium is the origo while the insertion is the intertubercular groove of the humerus (**Figure 30**).

  b. Pars sternalis: This part has the same insertion site as the former but finds it origin along the entire length of the sternum (**Figure 30**).

  c. Pars abdominalis: The origin is the xiphoid process and the cranial aspect of the external sheath of the straight abdominal muscle. The muscle inserts deep to the sternal part into the humerus (**Figure 30**).

  M. pectoralis minor (m. pectoralis profundus): This pectoral muscle lies deep to the superficial pectoral muscle. It has origin on the cartilages of the 2nd to 6th ribs and is inserted into the greater tuberosity of the humerus (**Figure 30**).

M. subclavius: This small fusiform muscle arises from the 1st costal cartilage and is inserted into the clavicle (**Figure 30**).

• M. trapezius: Both the cervical and thoracic parts arise from the scapular spine. The occiput and 10th thoracic vertebra are reached cranially, resp. caudally by this muscle that meets its counterpart in the dorsal midline (**Figures 25**, **26**, and **28**).

• M. rhomboideus: The cervical part (m. rhomboideus cervicis = m. levator anguli scapulae) and thoracic part (m. rhomboideus thoracis) arise from the dorsal border of the scapula and insert into the occiput and nuchal ligament, and the first 6 thoracic vertebrae, respectively (**Figure 28**).

• M. serratus ventralis: Muscle strands have attachments on the last four cervical vertebrae (m. serratus ventralis cervicis = m. levator scapulae) and first nine ribs (m. serratus ventralis thoracis) and inserts medially on the scapula (**Figures 26**, and **28–30**).

• M. latissimus dorsi: This muscle originates by means of an aponeurosis at the dorsal midline at the level of the 6th to 12th thoracic vertebrae and the lumbodorsal fascia. The insertion site is twofold, i.e. at the teres major tendon and into the bicipital groove (**Figures 25**, **26**, and **28-30**).

5.10 Muscles of the shoulder region

• M. supraspinatus: This muscle fills the supraspinous fossa and has insertion into the greater humeral tubercle (**Figure 31**).
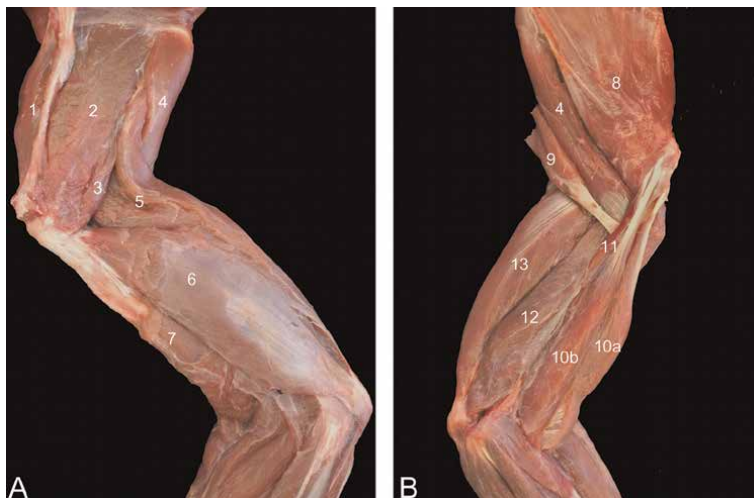
Figure 31.
Musculature of the left shoulder. A: lateral view, B: medial view. 1: m. supraspinatus, 2: m. infraspinatus, 3: m. teres minor, 4: m. teres major, 5: m. triceps brachii caput longum, 6: m. triceps brachii caput laterale, 7: m. brachialis, 8: m. subscapularis, 9: m. latissimus dorsi, 10a: m. biceps brachii caput longum, 10b: m. biceps brachii caput breve, 11: m. coracobrachialis, 12: m. triceps brachii caput mediale, 13: m. triceps brachii caput laterale.

- M. infraspinatus: The origin is the infraspinous fossa. The muscle is covered by the spinodeltoid muscle. Its tendon inserts into the greater tubercle of the humerus, in between the tendons of the supraspinous and teres minor muscles (**Figure 31**).

- M. deltoideus: The insertion is the deltoid tuberosity on the humerus. The origin is either the clavicle (M. cleidodeltoideus (M. deltoideus anterior)), the acromion (M. acromiodeltoideus (M. deltoideus medius)) or the scapular spine (M. spinodeltoideus (M. deltoideus posterior)) (**Figure 30**).

- M. teres minor: This muscle has origin at the caudodistal margin of the shoulder blade and the caudal aspect of the infraspinatus muscle. It inserts into the greater tubercle of the humerus, just caudal to the insertion of the aforementioned muscle (**Figure 31**).

- M. teres major: This muscle originates at the ventral angle and caudal border of the scapula and inserts medially into the humeral shaft in its proximal third (**Figure 31**).

- M. subscapularis: The origin and insertion of this muscle are the subscapular fossa and the lesser tubercle of the humerus, respectively (**Figure 31**).

5.11 Muscles of the upper arm

5.11.1 Extensor musculature

- M. triceps brachii: The triceps muscle inserts into the olecranon of the ulna. Its long head (caput longum), lateral head (caput laterale) and medial head (caput mediale) originate from the caudal border of the scapula, the greater tuberosity of the humerus, and the proximo-medial side of the humeral shaft, respectively (**Figures 25**, **26**, and **31**).

- M. anconeus (lateralis): This small muscle arises distally on the humeral shaft and inserts proximally on the ulna.

- M. dorsoepitrochlearis: arises from the lower margin of the latissimus dorsi muscle and attaches to the antebrachial fascia and medial epicondyle of the humerus.

5.11.2 Flexor musculature

- M. biceps brachii: The long head (caput longum) and short head (caput breve) run from the supraglenoid tubercle and coracoid process of the shoulder blade, respectively to the radial tuberosity of the radius (**Figures 25**, **26**, **30**, and **31**).

- M. coracobrachialis: Both the deep part (m. coracobrachialis profundus) and middle part (m. coracobrachialis medius) arise from the coracoid process on the shoulder blade. The former part inserts into the humeral neck, while the latter part attaches more distally at the medial side of the humeral shaft (**Figure 31**).

- M. brachialis: The lateroproximal aspect of the humerus is the site of origin of this muscle, that follows the brachial sulcus of the humerus to insert into the medial coronoid process of the ulna (**Figure 31**).

5.12 Muscles of the forearm

5.12.1 Extensor musculature

- M. extensor carpi radialis (longus et brevis): The lateral epicondylar crest of the humerus forms the origin of this muscle. The insertion is into the base of the 2nd metacarpal bone (long part) and 3rd metacarpal bone (short part) (**Figures 32–34**).

- M. extensor carpi ulnaris: This muscle arises from the lateral epicondyle of the humerus and is inserted into the base of the 5th metacarpal bone (**Figures 32** and **34**).

- M. extensor digitorum communis: This muscle arises from the lateral epicondyle of the humerus and inserts by means of four tendons into the distal phalanges of digits II to V (**Figures 32** and **34**).

- M. extensor digiti:

    primi longus (m. extensor pollicis longus): The origin is craniolaterally on the proximal half of the ulna and inserts into the distal phalanx of the pollex (**Figure 34**).
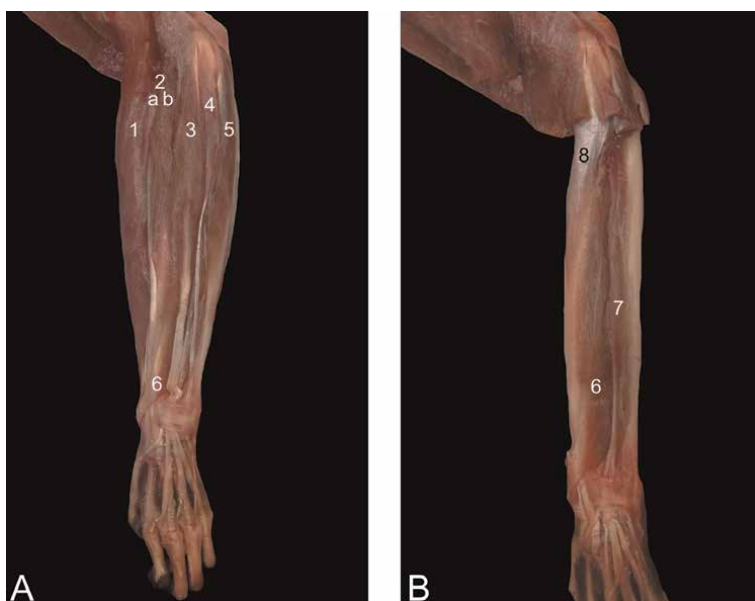
Figure 32.
Lateral view of the musculature of the left forearm. A: superficial layer with 1: brachioradialis muscle, 2a: long part of extensor carpi radialis muscle, 2b: short part of extensor carpi radialis muscle, 3: extensor digitorum communis muscle, 4: extensor digitorum quarti et quinti muscle, 5: extensor carpi ulnaris muscle, 6: abductor digiti primi longus muscle. B: deep layer with 6: abductor digiti primi longus muscle, 7: extensor digitorum secundi et tertii muscle, 8: supinator muscle.
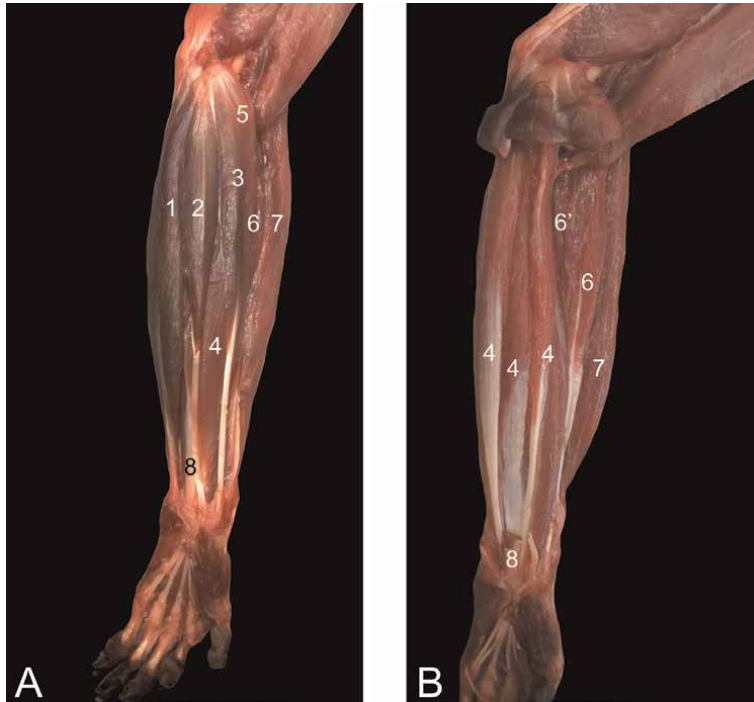
Figure 33.
Medial view of the musculature of the left forearm. A: Superficial layer with 1: m. flexor carpi ulnaris, 2: m. palmaris longus, 3: m. flexor carpi radialis, 4: m. flexor digitorum profundus, 5: m. pronator teres, 6: m. extensor carpi radialis longus, 7: m. brachioradialis. B: Deep layer with 4: m. flexor digitorum profundus, 6: m. extensor carpi radialis longus, 6': m. extensor carpi radialis brevis, 7: m. brachioradialis, 8: m. flexor digitorum superficialis.

secundi (m. extensor indicis) et tertii: This muscle arises distal to the former muscle. At the level of the carpus, the tendon splits into two tendons, one to the proximal phalanx of the 2nd digit and one for the 3rd digit (**Figures 32** and **34**).

quarti: From the lateral humeral epicondyle to proximal phalanx of the 4th digit (**Figures 32** and **34**).

quinti: From the lateral humeral epicondyle to the middle phalanx of the 5th digit (**Figures 32** and **34**).

5.12.2 Flexor musculature

- M. flexor carpi radialis: This muscle arises from the medial humeral condyle and inserts into the base of the 2nd metacarpal bone (**Figures 33** and **35**).

- M. flexor carpi ulnaris: This muscle also arises from the medial humeral epicondyle. It attaches to the pisiform carpal bone (**Figures 33** and **35**).

- M. palmaris longus: This muscle is situated in between the two aforementioned muscles. It also originates at the medial humeral epicondyle. It presents a distal
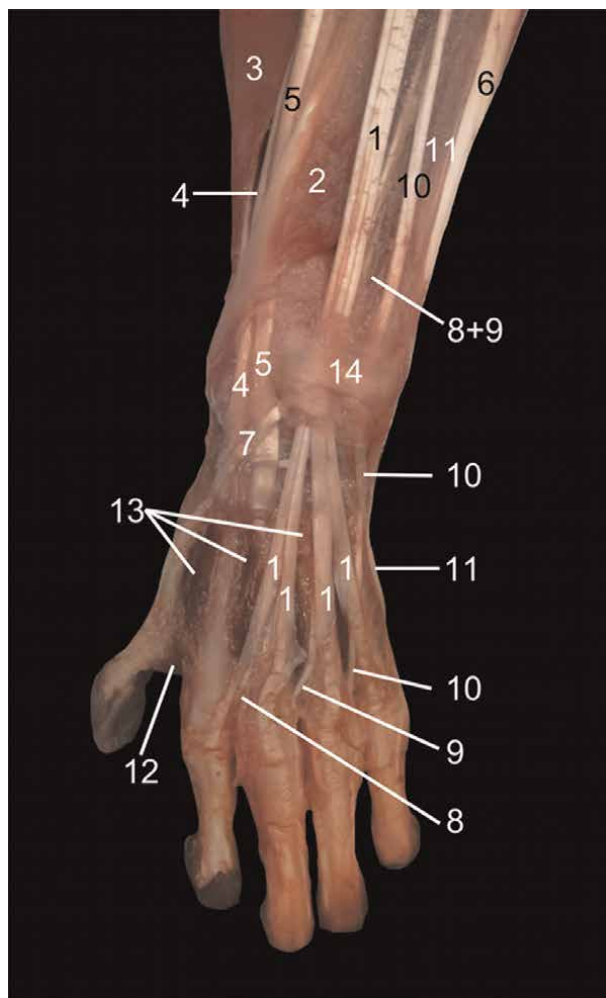
Figure 34.
Dorsal view of the musculature of the left hand. 1: m. extensor digitorum communis, 2: m. abductor digiti primi longus, 3: m. brachioradialis, 4: m. extensor carpi radialis longus, 5: m. extensor carpi radialis brevis, 6: m. extensor carpi ulnaris, 7: m. extensor digiti primi (pollicis) longus, 8: m. extensor digiti secundi, 9: m. extensor digiti tertii, 10: m. extensor digiti quarti, 11: m. extensor digiti quinti, 12: m. adductor digiti primi, 13: m. interosseous, 14: ligamentum carpi dorsale.

aponeurosis (aponeurosis palmaris) which lies superficially at the palmar side of the hand (**Figures 33** and **35**).

- M. brachioradialis: This muscle runs from the lateral humeral epicondyle to the distal aspect of the radius (**Figures 32–35**).

- M. flexor digitorum superficialis (m. flexor digitorum sublimis): This very thin muscle originates on the medial epicondyle of the humerus. Its four tendons insert on the base of the 2nd phalanx of digits I to IV (**Figures 33** and **35**).

- M. flexor digitorum profundus: This muscle arises from the proximal half of the ulna (caput ulnare) and the upper two-thirds of the radius (caput radiale). Five
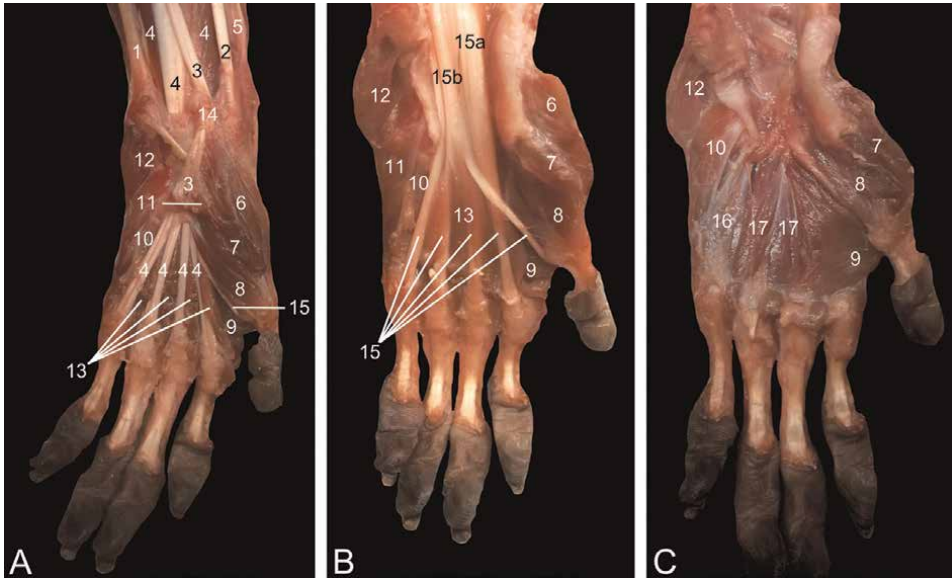
Figure 35.
Palmar view of the musculature of the left hand. A: superficial layer, B: deeper layer, C: deepest layer. 1: m. flexor carpi ulnaris, 2: m. flexor carpi radialis, 3: m. palmaris longus with cut aponeurosis, 4: m. flexor digitorum superficialis, 5: m. brachioradialis, 6: m. abductor digiti primi brevis, 7: m. flexor digiti primi brevis superficialis, 8: m. flexor digiti primi brevis profundus, 9: m. adductor digiti primi, 10: m. flexor digiti quinti brevis, 11: m. abductor digiti quinti, 12: m. palmaris brevis, 13: mm. lumbricales, 14: ligamentum carpi palmare, 15: m. flexor digitorum profundus with 15a: caput radiale and 15b: caput ulnare, 16: m. opponens digiti quinti, 17: mm. contrahentes digitorum manus.

tendons arise, which are inserted into the palmar sides of the terminal phalanges of all five digits (**Figures 33** and **35**).

- M. epitrochleoanconeus: This short muscle runs from the medial humeral epicondyle to the olecranon.

5.12.3 The pronators and supinators

- M. pronator teres: This pronator muscle of the forearm originates on the medial humeral epicondyle. It runs obliquely towards the middle third of the radius (**Figure 33**).

- M. pronator quadratus: This rectangular muscle can be found at the medial side of the forearm, running from the proximal ulna to the distal radius.

- M. supinator: The supinator of the forearm originates on the lateral humeral epicondyle. It runs obliquely towards the proximal half of the radius.

5.13 Muscles of the hand

- M. palmaris brevis: This short muscle, that lies directly subcutaneously, arises from the palmar aponeurosis and is inserted into the subcutis (**Figure 35**).

- M. abductor digiti primi (pollicis) longus: This muscle has origin at the proximolateral aspect of the ulna and the cranial side of the radius. It attaches to the proximal end of the metacarpal bone of the pollex (**Figures 32** and **34**).

- M. abductor digiti primi (pollicis) brevis: This muscle arises medially from the transverse carpal ligament. It is inserted into the base of the proximal phalanx of the pollex (**Figure 35**).

- M. flexor digiti primi (pollicis) brevis: This muscle lies just lateral to the former. It also starts on the transverse carpal ligament and is inserted into the base of the proximal phalanx of the pollex (**Figure 35**).

- M. adductor digiti primi (pollicis): This muscle runs from the 2nd and 3rd metacarpal bones towards the proximal phalanx of the pollex. The proximal and distal parts of this muscle cannot be discerned (**Figures 34** and **35**).

- M. opponens digiti primi (pollicis): This muscle lies below the short abductor of the thumb. It runs from the transverse carpal ligament to the 1st metacarpal bone.

- M. abductor digiti quinti: This muscle has origin on the transverse carpal ligament and the most lateral carpal bones. Insertion is into the proximal phalanx of the 5th digit (**Figure 35**).

- M. flexor digiti quinti brevis: This muscle runs somewhat more medial and superficial compared to the former. The insertion site is the same (**Figure 35**).

- M. opponens digiti quinti: This muscle lies deep compared to the abductor and flexor of the 5th digit. It insert along the entire length of the 5th metacarpal bone (**Figure 35**).

- Mm. lumbricales manus: These muscles, which are 4 in number, are very well developed. They arise from the medial side of the deep flexor tendons to digits II – V. They are inserted into the base of the proximal phalanx and the metacarpophalangeal joints (**Figure 35**).

- Mm. contrahentes digitorum manus: Origins are the proximal epiphyses of the 2nd and 3rd metacarpal bones. Insertion is into the proximal phalanges of the 2nd, 4th and 5th digits (**Figure 35**).

- Mm. interossei manus: These muscles form pairs of muscles that are present in each intermetacarpal cleft. They attach to the sides of the metacarpophalangeal joints (**Figure 34**).

5.14 Muscles of the hip region

5.14.1 Extensor musculature

- M. gluteus superficialis (m. gluteus maximus): The superficial gluteus muscle arises from the lumbar fascia and the first three caudal vertebrae. The tendon is inserted into fascia lata and the greater trochanter of the femur (**Figures 25**, **26** and **36**).
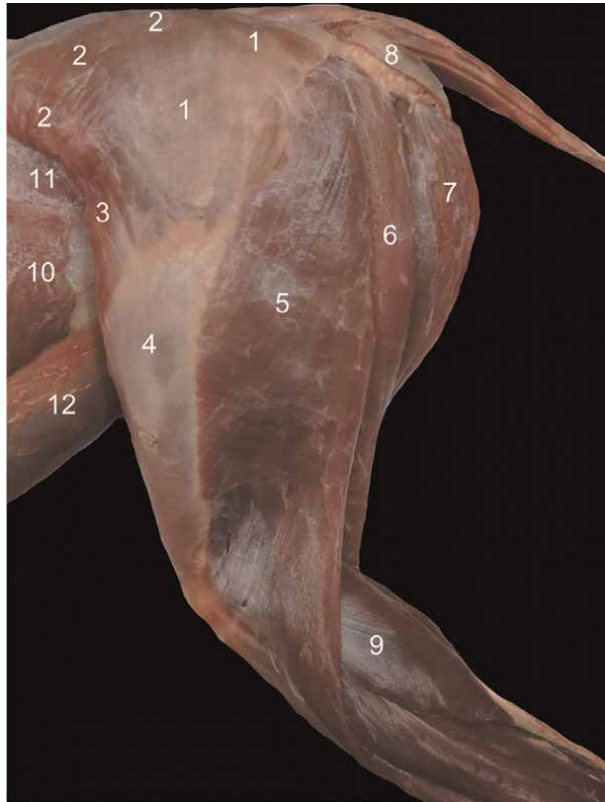
Figure 36.
Lateral view of the left thigh musculature. 1: m. gluteus superficialis, 2: m. gluteus medius, 3: m. tensor fasciae latae, 4: fascia lata, 5: m. biceps femoris, 6: m. semitendinosus, 7: m. semimembranosus, 8: callositas ischii, 9: m. gastrocnemius caput laterale, 10: m. obliquus externus abdominis, 11: m. obliquus internus abdominis, 12: m. rectus abdominis.

- M. gluteus medius: This deeper part of the gluteus musculature arises from the lateral surface of the wing of the ilium, the sacro-iliac joint and the first caudal vertebra. The large muscle is inserted into the greater trochanter of the femur (**Figures 26** and **36**).

- M. gluteus profundus (m. gluteus minimus): This deepest gluteus muscle has its origin on the dorsal aspect of the ilium and inserts into the greater trochanter of the femur.

5.14.2 Flexor musculature

- M. psoas major: The psoas major muscle arises from the ventral sides of the lumbar vertebrae. The muscle is inserted into the lesser trochanter of the femur (**Figure 29**).

- M. psoas minor: This psoas muscle lies ventromedial to the former. It originates from the ventral sides of the first four lumbar vertebrae and is inserted cranially on the pubic bone (tuberculum m. psoas minoris) (**Figure 29**).

- M. iliacus: The origin of this muscle is the medial aspect of the ilium. It first runs lateral to the psoas major and finally joins it to form the m. iliopsoas (**Figure 37**). This muscle has insertion into the lesser trochanter of the femur (**Figure 29**).

- M. quadratus lumborum: This muscle finds it origin on the crest and wing of the ilium. This thin quadrilateral muscle is inserted into the last rib and transverse processes of the lumbar vertebrae (**Figure 29**).

5.15 The adductors of the hind limb

- M. sartorius: This long, slender muscle arises from the cranioventral spine of the ilium. It inserts into the medial side of the proximal third of the tibia (**Figures 25**, **37**, and **39**).

- M. gracilis: This broad muscle starts from the pelvic symphysis and attaches to the craniomedial aspect of the proximal third of the tibia (**Figures 25**, **37**, and **39**).

- M. pectineus: This short, fusiform muscle runs from the pecten pubis to the medioproximal aspect of the femur (**Figures 25** and **37**).

- M. adductor (**Figure 37**):

  longus: The origin of the long adductor muscle is the pelvic symphysis. It lies lateral (deep) to the gracilis muscle and inserts medially, halfway the femur (**Figure 25**).

Figure 37.
Medial view of the left thigh musculature. 1: m. sartorius, 2: m. gracilis, 3: m. pectineus, 4: m. adductor, 5: m. rectus femoris, 6: m. vastus intermedius, 7: m. vastus medialis, 8: m. semimembranosus, 9: m. iliopsoas, 10: m. cremaster, 11: m. obliquus externus abdominis.

magnus: This muscle is composed of two parts that individually attach to the proximocaudal part of the femoral diaphysis. Their origins are the pelvic symphysis and tuber sciatic tuberosity, respectively.

brevis: The small adductor muscle starts just ventral to the foramen obturatum and attaches to the medioproximal aspect of the femur.

5.16 The supinators of the hind limb

- M. obturatorius externus: This muscle arises from the obturator membrane and the bone surrounding the obturator foramen, at its dorsal side. The tendon is inserted into the intertrochanteric fossa.

- M. obturatorius internus: This muscle also arises from the obturator membrane and the bone surrounding the obturator foramen, albeit at its ventral side. The insertion is at the medial side of the greater trochanter of the femur.

- Mm. gemelli: The gemelli originate from the ischium. Their tendons are inserted into the tendon of the m. obturatorius internus.

- M. quadratus femoris: This muscle runs from the sciatic tuberosity to the lesser femoral trochanter.

5.17 The extensors of the knee

- M. quadriceps: Intramuscular injections can be administered in this muscle that consists of four parts. All insert into the basis of the patella.

  M. rectus femoris: The origin is just dorsal to the acetabulum (**Figures 25** and **37**).

  M. vastus lateralis: This part of the quadriceps muscle arises from the greater trochanter of the femur.

  M. vastus medialis: This muscle arises from lesser trochanter of the femur (**Figure 37**).

  M. vastus intermedius (formerly described as the m. crureus): This deep muscle arises from the proximal three-fourths of the shaft of the femur (**Figure 37**).

- M. tensor fasciae latae: The origin of this muscle is the ilium and the fascia overlying the gluteus medius muscle. The muscle is inserted into the fascia lata (**Figures 25**, **26**, and **36**).

5.18 The hamstrings and flexors of the knee

- M. biceps femoris: The biceps femoris muscle arises from the ischial tuberosity. The muscle forms a thin aponeurosis that is inserted into the fascia cruris (**Figures 25**, **26**, and **36**). This muscle can be used to administer intramuscular injections.

- M. semitendinosus: This muscle also arises from the sciatic tuberosity, just caudal to the biceps femoris muscle. The tendon lies superficial to the semimembranosus muscle and attaches to the medial surface of the tibial shaft, deep to the tendon of the gracilis muscle (**Figures 26**, **36**, and **38**).

- M. semimembranosus: The semimembranosus muscle consists of the smaller and more lateral semimembranosus proprius muscle and larger and more medial semimembranosus accessories muscle. The origins of both is caudal on the sciatic tuberosity. The semimembranosus proprius muscle is inserted medially on the tibial tuberosity, while the accessory semimembranosus muscle is broadly inserted more proximally, at the level of the medial femoral condyle (**Figures 25**, **26**, **36**, **37**, and **39**).

- M. popliteus: This muscle is the only intrinsic flexor muscle of the knee. The fan-shaped muscle is located at the caudal side of the proximal tibial shaft. Its tendon inserts into the popliteal fossa of the femur (**Figure 39**).

5.19 Muscles of the lower leg

5.19.1 The flexors of the tarsal joint and extensors of the digits

- M. tibialis cranialis: This muscle arises from the lateral condyle of the tibia and from the upper two-thirds of its shaft. Two bellies can be observed. The medial tendon attaches to the 1st tarsal bone, whereas the lateral tendon is inserted into the head of the 1st metatarsal bone (**Figures 38–40**).

- M. extensor digitorum longus: The origins of this muscle are the lateral condyle of the tibia, and the fibular head. Three tendons arise at the level of the foot that are inserted into the middle and distal phalanges of the 2nd to 5th digits (**Figures 38** and **40**).

- M. extensor digiti primi (hallucis) longus: This very thin muscle that lies deep to the former muscle obtains its origin from the medial side of the fibular diaphysis. The tendon is inserted into the terminal phalanx of the hallux (**Figures 38** and **40**).

- M. fibularis longus: This muscle has its origin on the fibula and proximal epiphysis of the fibula. The tendon crosses the lateral malleolus and inserts into the plantar side of the 1st metatarsal bone, thus crossing the plantar side of the foot (**Figure 38**).

- M. fibularis brevis: This muscle arises from the lower two-thirds of the shaft of the fibula. Insertion is into the metatarsal bone of the 5th digit (**Figure 38**).

- M. fibularis digiti quinti: This muscle present a similar topography as the former muscle, but inserts into the distal phalanx of the 5th digit.

5.19.2 The extensors of the tarsal joint and flexors of the digits

- M. gastrocnemius: The lateral and medial heads of the gastrocnemius muscle arise from the lateral and medial epicondyle of the femur, respectively. A sesamoid

Figure 38.
Lateral view of the lower leg musculature (left hind limb). A: superficial layer, B: deeper layer, C: deepest layer. 1: m. biceps femoris, 2: m. semitendinosus, 3: m. gastrocnemius caput laterale, 4: m. tibialis cranialis, 5: m. extensor digitorum longus, 6: m. fibularis longus, 7: m. fibularis brevis, 8: m. tibialis caudalis, 9: m. plantaris, 10: m. soleus, 11: m. extensor digiti primi (hallucis) longus.
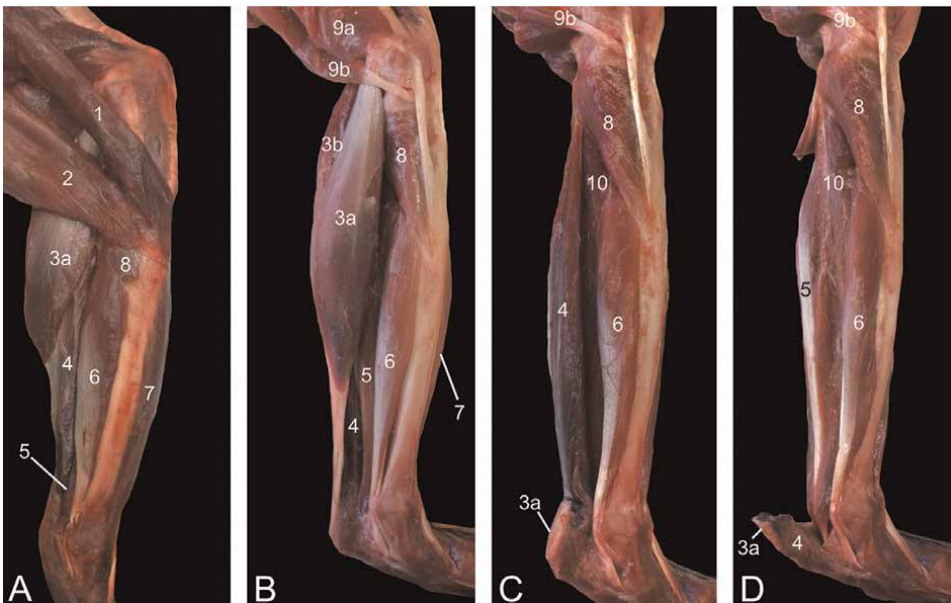
Figure 39.
Medial view of the lower leg musculature (left hind limb). A: superficial layer, B: deeper layer, C: deep layer, D: deepest layer. 1: m. sartorius, 2: m. gracilis, 3a: m. gastrocnemius caput mediale, 3b: m. gastrocnemius caput laterale, 4: m. soleus, 5: m. plantaris, 6: m. flexor digitorum tibialis, 7: m. tibialis cranialis, 8: m. popliteus, 9a: m. semimembranosus accessorius, 9b: m. semimembranosus proprius, 10: m. tibialis caudalis.
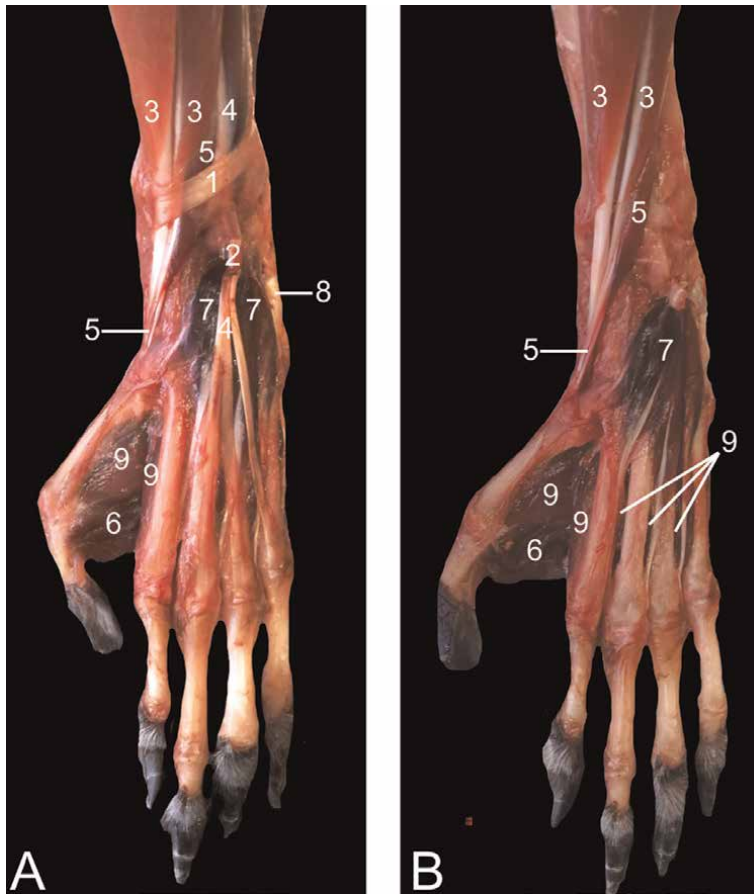
Figure 40.
Dorsal view of the musculature of the left foot. A: superficial layer, B: deep layer. 1: retinaculum proximalis, 2: retinaculum distalis, 3: m. tibialis cranialis (two bellies), 4: m. extensor digitorum longus, 5: m. extensor digiti primi (hallucis) longus, 6: m. adductor digiti primi (hallucis), 7:m. extensor digitorum et digiti primi (hallucis) brevis, 8: m. abductor digiti quinti, 9: mm. interossei.

bone is present in each tendon of origin (ossa sesamoidea m. gastrocnemii or fabellae). The tendo Achilles attaches to the tuber calcanei (**Figures 25**, **26**, **36**, **38**, and **39**).

- M. soleus: This thin muscle arises from the head of the fibula. Its tendon fuses with the gastrocnemius muscle (**Figures 38** and **39**).

- M. plantaris: The thin plantaris muscle has its origin on the lateral condyle of the femur. Its thin tendon lies on the medial side of the tendo Achilles and is inserted into the plantar fascia (**Figures 38** and **39**).

- M. flexor digitorum (longus) tibialis (can be considered as the m. flexor digitorum superficialis): This muscle arises halfway from the caudal side of the tibia. The tendon crosses the medial malleolus and splits to attach to the plantar sides of the distal phalanges of digits II to V (**Figure 41**).
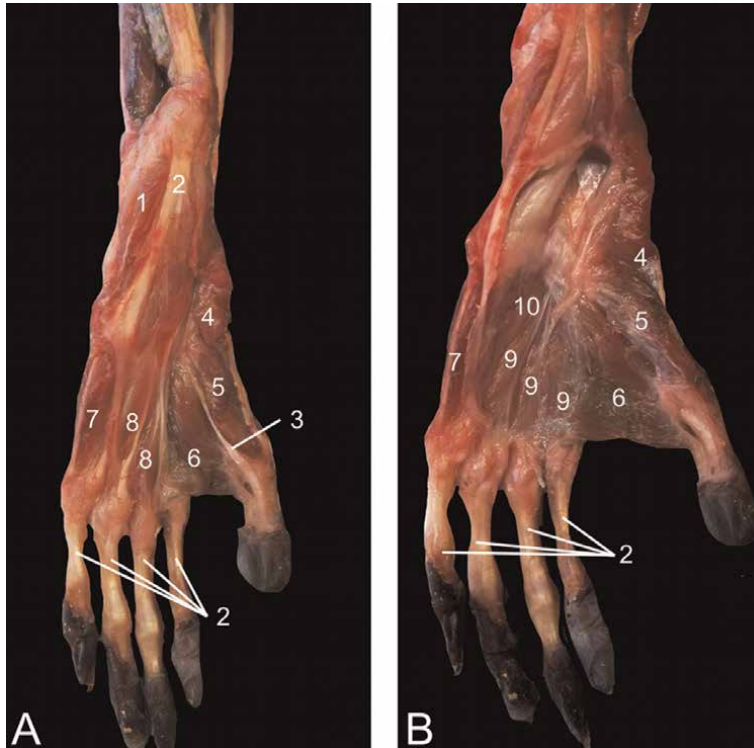
Figure 41.
Plantar view of the musculature of the left foot. A: middle layer, B: deep layer. 1: m. quadratus plantae, 2: m. flexor digitorum (longus) tibialis, 3: m. flexor digitorum (longus) fibularis (tendon to digit I), 4: m. abductor digiti primi (hallucis), 5: m. flexor digiti primi (hallucis) brevis, 6: m. adductor digiti primi (hallucis), 7: m. flexor digiti quinti brevis, 8: mm. lumbricales, 9: mm. contrahentes digitorum pedis, 10: mm. interossei.

- M. flexor digitorum (longus) fibularis (can be considered as the m. flexor digitorum profundus): This muscle lies deep to the former. It arises from the caudomedial aspect of the fibula, the interosseous membrane between the tibia and fibula, and the distal part of the tibia. The tendon travels along the plantar side of the tarsal joint, then splits in three tendons, one for digit I, III and IV (**Figure 41**).

- M. tibialis caudalis: This muscle arises from the caudal side of the tibia. Its tendon crosses the medial malleolus and inserts into the plantar sides of the metatarsal bones of digits II to IV (**Figures 38** and **39**).

5.20 Muscles of the foot

- M. flexor digitorum brevis: The superficial head has its origin on the tuber calcanei. This head forms the short flexor of digit II as it inserts into its middle phalanx. The deep head arises from the flexor digitorum tibialis tendon, at the level of the medial malleolus. The three tendons are inserted into the base of the middle phalanx of digits III to V.

- M. abductor digiti primi (hallucis): This muscle starts from the calcaneus and inserts into the plantar side of the proximal phalanx of the hallux (**Figure 41**).

- M. flexor digiti primi (hallucis) brevis: Two heads originate from the plantar side of the tarsus and insert into the proximal phalanx of the hallux (**Figure 41**).

- M. extensor digitorum et digiti primi (hallucis) brevis: This dorsally located muscle starts at the calcaneus and sends four tendons towards distal phalanx of digits I to IV (**Figure 40**).

- M. adductor digiti primi (hallucis): This broad muscle has origin at the metatarsal bones of the 2nd and 3rd digits. The proximal phalanx of the hallux is the insertion site (**Figures 40** and **41**).

- M. abductor digiti quinti: This muscle runs from the tuber calcanei towards the proximal phalanx of the 5th digit (**Figure 40**).

- M. abductor ossis metatarsi quinti: This inconsistently present muscle runs lateral from the former muscle and inserts into the metatarsal bone of the 5th digit.

- M. flexor digiti quinti brevis: This muscle has origin at the tendon of the fibularis longus muscle at the level of the metatarsal bone of the 5th digit. It inserts at the proximal phalanx of the 5th digit (**Figure 41**).

- M. quadratus plantae: The origin is on the lateral side of the calcaneus. It splits into several tendons that insert into the tendons of the flexor digitorum longus muscles (**Figure 41**).

- Mm. lumbricales pedis: Four fine muscle strands find their origins deep to the flexor digitorum brevis muscle. They run medial to the metatarsal bones of the 2nd to 5th digits to insert into their proximal phalanges (**Figure 41**).

- Mm. contrahentes digitorum pedis: These muscles have a single aponeurosis in common at the level of the fibularis longus muscle. Three muscular bands originate from here to insert into the proximal phalanges of the 2nd, 4th and 5th digit (**Figure 41**).

- Mm. interossei pedis: These muscles form pairs of muscles that are present in each intermetatarsal cleft. They attach to the sides of the metatarsophalangeal joints (**Figures 40** and **41**).

6. Splanchnology

6.1 Dentition

The rhesus monkey is omnivorous and mainly feeds on fruit, vegetables, insects and small mammals. Its dentition is very similar to that of humans as it also presents 32 teeth of which two incisors, one canine, two premolars and three molars in each quadrant. The teeth are of the brachydont type, thus with typical crowns and roots. The canines are more pronounced in the male compared to the female rhesus monkey. Furthermore, the premolars and molars are of the bunodont type, thus with typical cusps. The number of roots is one for the incisors and the canines, two for the

premolars and molars of the mandible, and three for the premolars and molars of the maxilla (**Figures 42** and **43**).

6.2 Oral cavity and tongue

It is worthwhile to mention that the rhesus monkey possesses a pair of cheek pouches [12]. The tongue plays a pivotal role in digestion and vocalization. The muscles that are responsible for the lingual movements are discussed in section 5.4. The dorsal mucosa of the tongue presents several types of papillae. Gustatory papillae
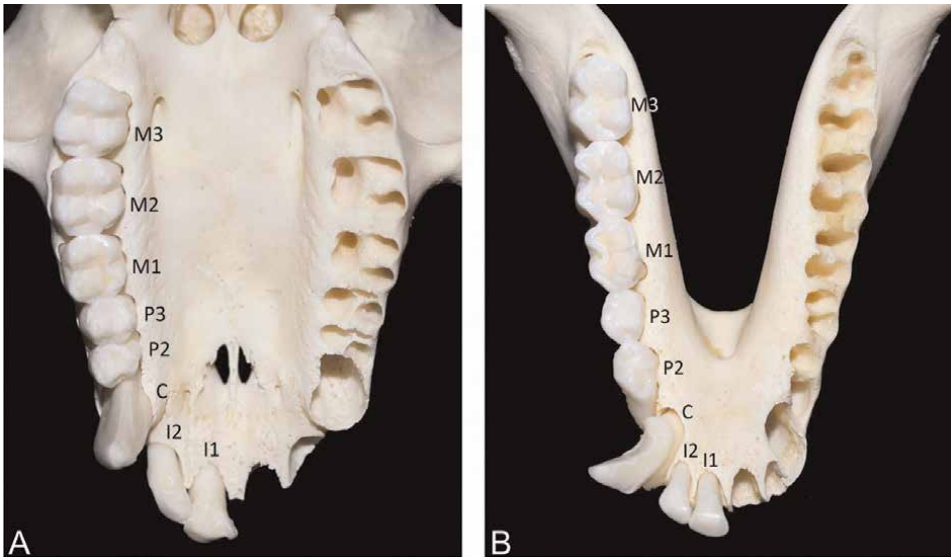
Figure 42.
Ventral view of the upper jaw (A) and dorsal view of the lower jaw (B) with the teeth unilaterally present. I1: dens incisivus primus, I2: dens incisivus secundus, C: dens caninus, P2: dens premolaris secundus, P3: dens premolaris tertius, M1: dens molaris primus, M2: dens molaris secundus, M3: dens molaris tertius.
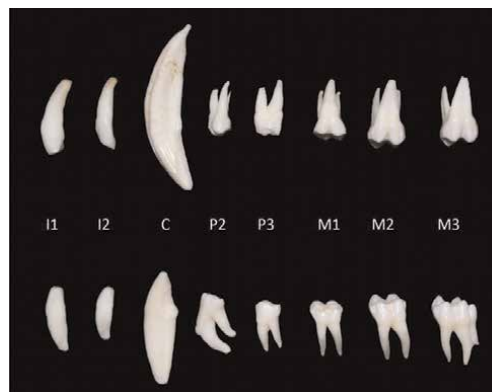
Figure 43.
Dentition of the rhesus monkey. Upper panel: teeth of the right upper jaw after extraction. Lower panel: teeth of the right lower jaw after extraction. Notice the clear distinction between the crowns and roots, and the number of roots.

include the fungiform, circumvallate and foliate papillae. The filiform papillae are of the mechanical type (**Figure 44**).

6.3 Digestive organs

After a ventral midline incision through the abdominal wall has been made, the greater omentum (omentum majus) that covers the majority of abdominal organs can be observed (**Figure 45A**). It consists of the parietal and visceral sheets that enclose the virtual omental bursa. The parietal sheet is attached to the greater curvature of the stomach, while the visceral sheet is attached to the dorsal abdominal wall. The abdominal organs can only be observed after retraction or excision of the greater omentum (**Figure 45B**).
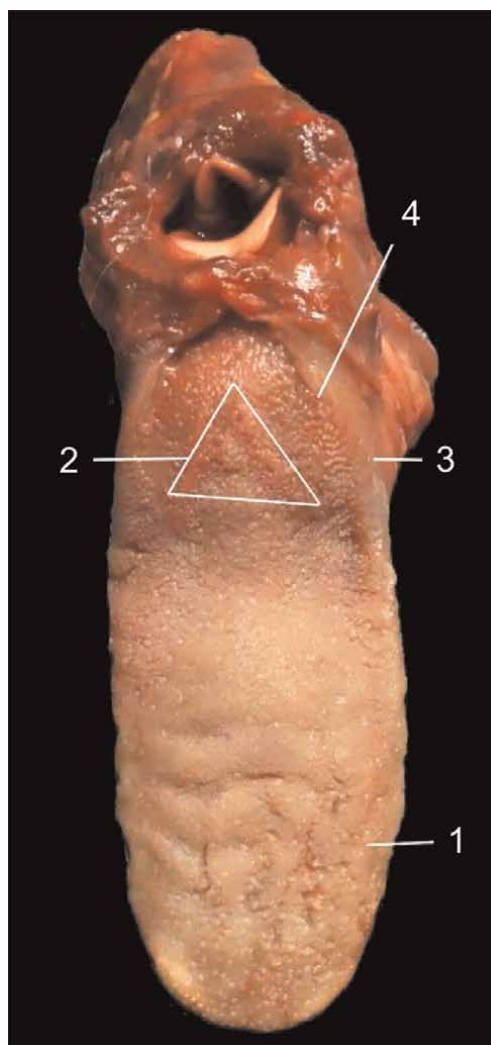
Figure 44.
Dorsal view of the tongue. 1: papillae fungiformes, 2: papillae circumvallatae, 3: papillae foliatae, 4: papillae filiformes.
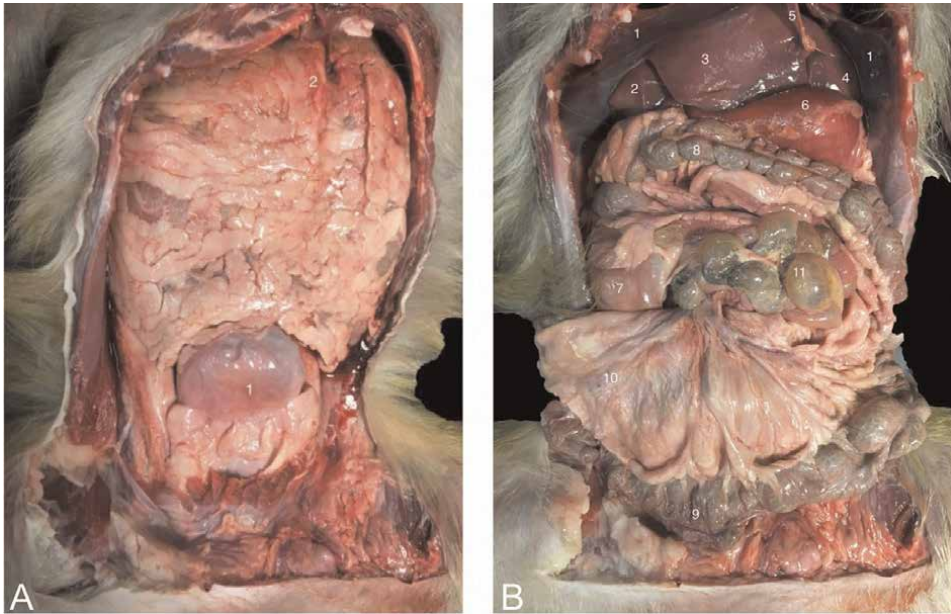
Figure 45.
Ventral view of the abdominal cavity after a ventral midline incision was performed. A: The omentum majus is still present with 1: urinary bladder, 2: parietal sheeth of the omentum majus. B: The omentum majus is excised with 1: diaphragm, 2: lobus hepatis dexter lateralis, 3: lobus hepatis dexter medialis, 4: lobus hepatis sinister medialis, 5: ligamentum falciforme, 6: curvatura major of the stomach, 7: cecum, 8: colon transversum, 9: colon descendens, 10: mesocolon, 11: jejunum.

The esophagus presents a cervical, thoracic and abdominal segment. The cervical segment lies at the left side of the trachea. It bends to the right side of the body when reaching the thorax and deviates to the left side again to perforate the diaphragm (hiatus oesophageus). Its muscular layer is composed of an outer layer of longitudinally orientated fibers and an inner layer of circular fibers that enable peristalsis. The abdominal segment contains smooth muscle cells, while the other two segments present striated muscle fibers. The esophagus finally enters the stomach a few centimeters caudal to the diaphragm. Here, the cardiac sphincter is located. Relaxation of this sphincter and antiperistalsis in the esophagus allow for vomiting.

The stomach (**Figure 46**) consists of the fundus, the body, the pyloric canal and the pyloric antrum. The fundus is large and extends cranially left to the esophagus. The corpus is continuous with the esophagus and cannot be delineated from the fundus by any anatomical landmark. The pyloric antrum is continuous with the corpus. It can be distinguished from the body by its smaller diameter. The narrow short tube that follows is the pyloric canal that ends at the pyloric sphincter.

The reddish spleen is tongue-shaped and lies at the left side of the abdomen. It is connected to the stomach by means of the gastro-splenic ligament (**Figure 46**). The spleen is, however, a lymphoid organ.

The isolated intestinal tract of the rhesus monkey is presented in **Figure 47**. The small intestine measures approximately 175 cm in length and is composed of the duodenum, the jejunum and the ileum. The duodenum presents a long descending part (duodenum pars descendens/duodenum descendens) that is located at the right side of the abdomen, a short transverse part (duodenum pars transversa/duodenum
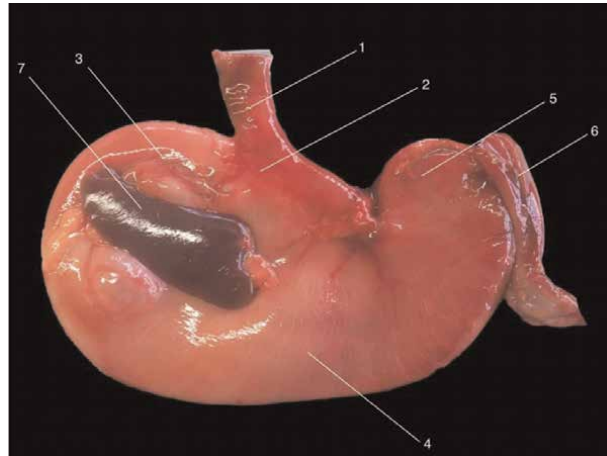
Figure 46.
Dorsal view of the stomach with the spleen attached. 1: oesophagus, 2: pars cardiaca, 3: fundus ventriculi, 4: corpus ventriculi, 5: pars pylorica, 6: pars cranialis duodeni, 7: lien.
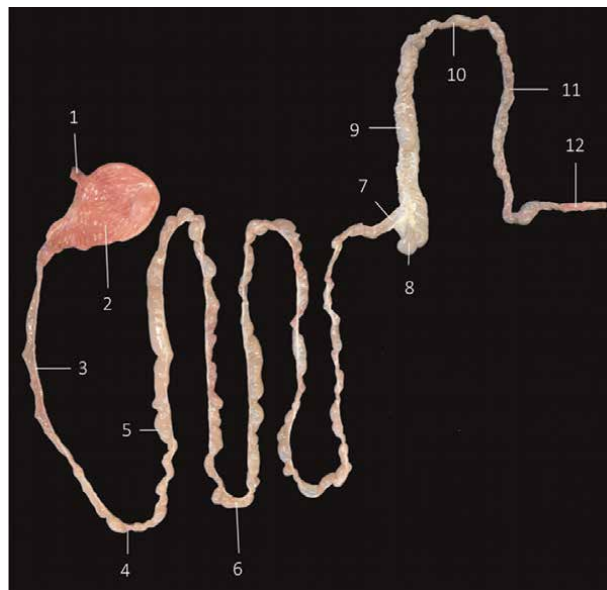
Figure 47.
Isolated intestinal tract. 1: oesophagus, 2: stomach, 3: duodenum descendens, 4: duodenum transversum, 5: duodenum ascendens, 6: jejunum, 7: ileum, 8: caecum, 9: colon ascendens, 10: colon transversum, 11: colon descendens, 12: rectum.

transversum) in which the chyme travels from right to left in the caudal half of the abdominal cavity, and a short ascending part (duodenum pars ascendens/duodenum ascendens) at the left side of the abdomen. The basis of the mesentery lies in the middle of the J-shaped duodenum. The common bile duct (ductus choledochus) and the pancreatic ducts (i.e. ductus pancreaticus and ductus pancreaticus accessorius) enter the descending part of the duodenum at 1/3 of its length. The accessory pancreatic duct enters the duodenum separately on the minor duodenal papilla, whereas the

common bile duct and the principal pancreatic duct join to terminate on the major duodenal papilla. Within the mesoduodenum descendens, the tail or lobus dexter of the pancreas is found. This organ measures approximately 12 cm by 2 cm. Its body (corpus pancreatis) and left lobe (lobus sinister pancreatis) lie within visceral sheet of the greater omentum against the stomach and in the mesocolon ascendens (**Figure 48**). The jejunum presents several loops and continues as the ileum that is anatomically defined as that segment of the small intestine that is attached to the cecum by means of the plica ileocecalis. The ileum finally enters the cecum (ostium ileocecale).

The large intestine measures approximately 63 cm in length ans consists of the cecum, colon and rectum. The cecum can be found at the junction between the ileum and colon at the right side of the abdomen (**Figure 45B**). The cecum (**Figure 49**) is relatively large, measures 7 cm in length and lacks an appendix. Ventral and dorsal teniae that consist of smooth muscle fibers are present. They give origin to the several sacculations called haustra. The U-shaped colon consists of the ascending part (colon pars ascendens/colon ascendens), the transverse part (colon pars transversa/colon transversum) and the descending part (colon pars descendens/colon descendens). Its total length is approximately 46 cm. It present two teniae that give origin to haustra. The descending colon travels along the left side of the abdomen and passes insensibly into the rectum that is approximately 10 cm long and is defined as that segment of the large intestine that is located within the pelvic cavity.

The liver lies most cranial in the abdomen (**Figure 45B**). It measures approximately 15 cm by 10 cm. Its diaphragmatic side is located against the diaphragm while its visceral side faces the viscera, in particular the stomach. The esophagus runs in a fissure between the left and the caudate lobes. The lobulation of the liver is presented in **Figure 50**. The falciform ligament runs from the umbilicus to the liver, in between the left and right liver lobes towards the diaphragmatic side. This side is attached to the diaphragm by means of the left and right triangular ligaments and the coronary ligament. At the visceral side, the gall bladder is lodged in between the quadrate lobe and the right medial lobe.

The common bile duct joins the principal pancreatic duct to enter the duodenum on the major duodenal papilla. The portal vein and hepatic artery enter the liver at the porta hepatis. Both vessels join at the level of the sinusoids. The blood within the
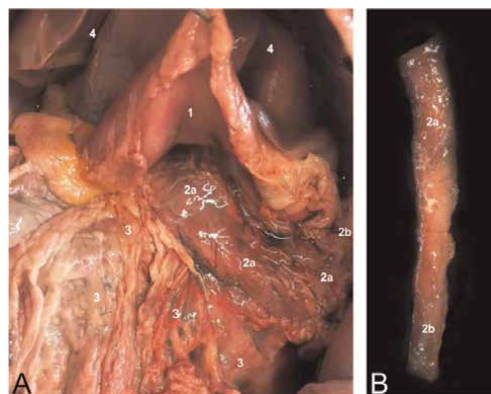
Figure 48.
Pancreas of the rhesus monkey in situ (A) and ex corpore (B) with 1: corpus ventriculi, 2a: lobus pancreatis sinister, 2b: lobus pancreatic dexter, 3: omentum majus paries profundus, 4: hepar.
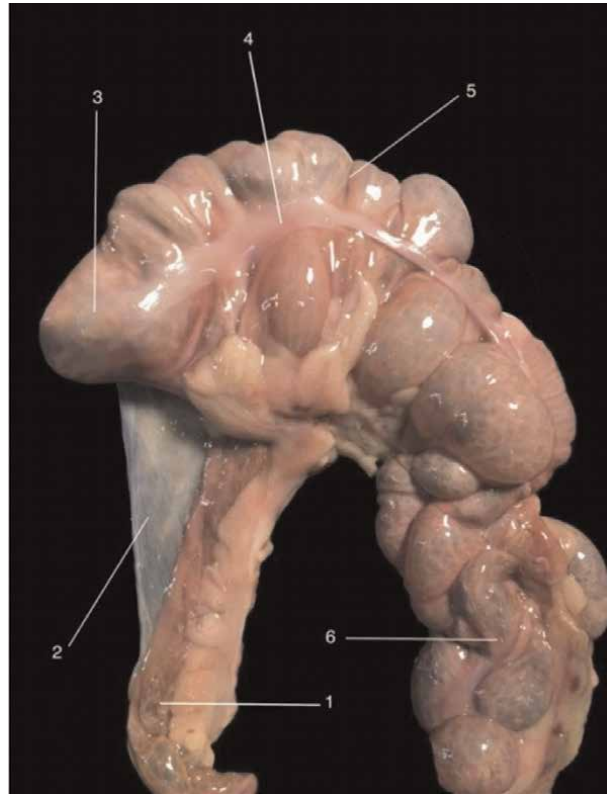
Figure 49.
Isolated cecum. 1: ileum, 2: plica ileocecalis, 3: apex ceci, 4: tenia, 5: corpus ceci, 6: colon ascendens.
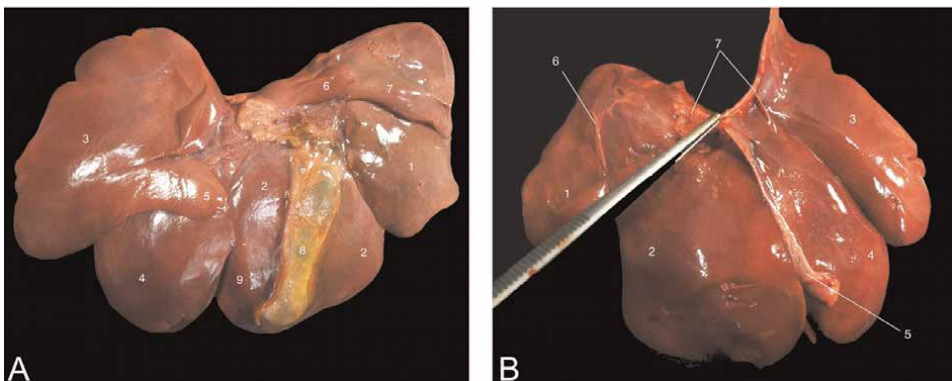
Figure 50.
Liver. A: visceral side with 1: lobus hepatis dexter lateralis, 2: lobus hepatis dexter medialis, 3: lobus hepatis sinister lateralis, 4: lobus hepatis sinister medialis, 5: processus anonimus, 6: processus papillaris of lobus caudatus, 7: processus caudatus of lobus caudatus, 8: vesica biliaris, 9: lobus quadratus. B: diaphragmatic side with 1 – 4 idem as in A, 5: ligamentum falciforme, 6: ligamentum triangulare dextrum, 7: ligamentum coronarium.

sinusoidal system flows towards the central veins in the center of the liver lobules. These finally join to form multiple hepatic veins that ultimately drain into the caudal vena cava that runs at the dorsal margin of the liver (**Figure 51**).
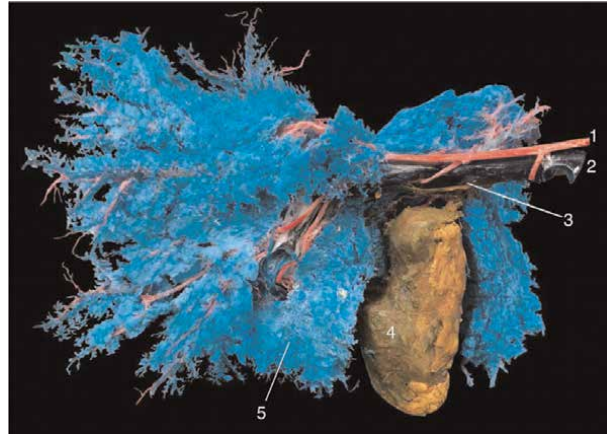
Figure 51.
Vascular corrosion cast of the liver, visceral side. 1: a. hepatica, 2: v. portae, 3: ductus choledochus, 4: vesica biliaris, 5: liver sinusoids.

6.4 Urinary tract and adrenal glands

The brownish, bean-shaped kidneys measure approximately 5 cm by 3 cm. The lateral margin is convex while the medial margin is concave (**Figure 52B**). The cranial pole of the left kidney lies against the left lobe of the pancreas and lies more caudal than the right kidney that makes contact with the caudate lobe of the liver. As a result, this liver lobe presents a renal impression. An adipose capsule surrounds the kidneys that are overlaid with a fibrous capsule (**Figure 52A**). At the hilus, the renal artery and renal vein enter the kidney, while the ureter leaves the kidney. After a longitudinal section of the kidney has been performed, the red cortex, brown medulla and the pale pelvis can be observed (**Figure 52C**).

The ureters lead the urine into the urinary bladder. Like the kidneys, they lie retroperitoneally. The abdominal part travels dorsal to the a. and v. ovarica or a. and v. testicularis. The pelvic part is located within the pelvic cavity and crosses the a. and v.
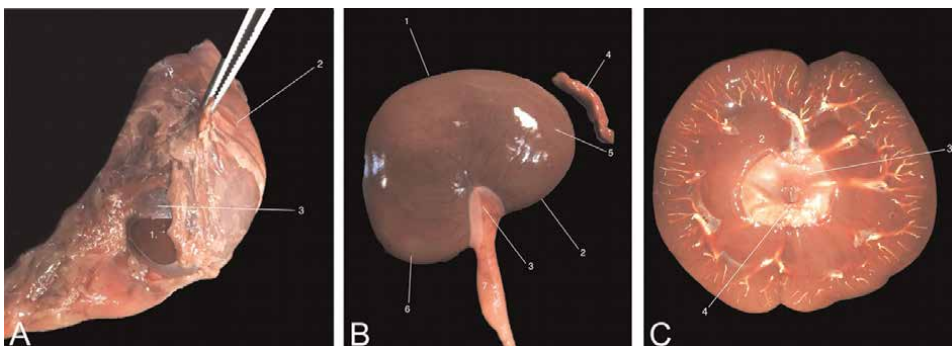
Figure 52.
A: Kidney (1) encapsulated by the capsula adiposa (2) and capsula fibrosa (3). B: Left kidney and adrenal gland ex corpore with 1: margo lateralis, 2: margo medialis, 3: hilus renalis, 4: glandula adrenalis, 5: polus cranialis, 6: polus caudalis, 7: ureter. C: Longitudinally sectioned kidney of which the blood vessels are filled with white latex rubber showing the cortex (1), medulla (2) and pelvis renalis (3).

iliaca externa ventrally. The intramural part travels obliquely within the wall of the urinary bladder.

The urinary bladder measures approximately 10 cm in length and 7 cm in width when filled with urine. It is attached to the abdominal wall by means of the median ligament (ligamentum vesicae medianum) and the left and right lateral ligaments (ligamenta vesicae lateralia). When the urinary bladder is cut longitudinally from the cervix, over the corpus to the apex, the mucosa can be studied. In the cervix, a left and right ostium ureteris is present on the respective columna ureterica. These distally elongate to form the left and right plica ureterica that distally join at the crista urethralis. As such, the trigonum vesicae is delineated. At the ostium urethrae internum, the urethra finds its origin (**Figure 53**).

The female urethra is rather short as it opens ventrally into the vagina. This opening, the ostium urethrae externum, forms the border between the actual vagina and the vestibulum vaginae.

The adrenal glands are located within the adipose capsules of the kidneys, at their cranial poles (**Figure 57B**). They have a pink color, are lobulated and measure approximately 1 cm in length and a few mm in width (**Figure 52B**). The pink cortex produces mineralocorticosteroids, glucocorticosteroids and androgens. The brown medulla produces adrenalin and noradrenalin.

6.5 Female reproductive organs

The oval-shaped ovaries measure approximately 8 mm in length and 6 mm in width. At the margo mesovaricus, they are attached to the abdominal wall by means of the mesovarium. The margo liber is devoid of any ligaments. The ligamentum suspensorium ovarii connects the ovary with the lateral pelvic wall. The a. and v. ovarica lie within this ligament. The ligamentum ovarii proprium links the ovary to the uterus.

The coiled fallopian tubes or oviducts lie lateral to the ovaries. They are attached to the abdominal wall by means of the mesosalpinx. The tapered infundibulum that lies against
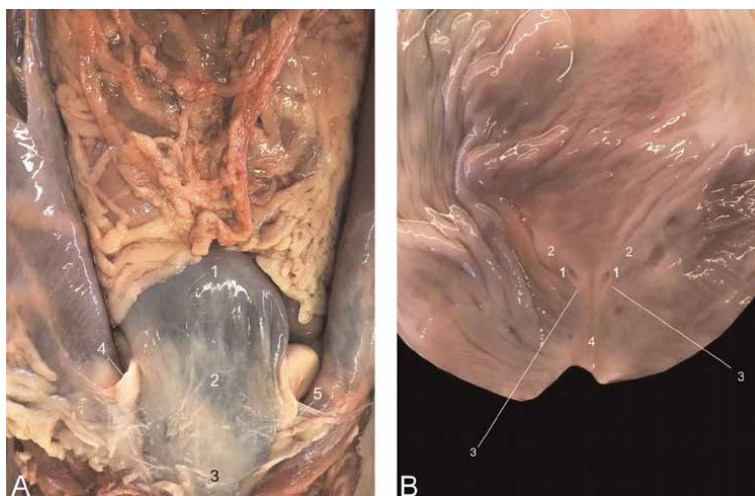
Figure 53.
A: Urinary bladder in situ showing the apex vesicae (1), corpus vesicae (2), cervix vesicae (3), ligamentum vesicae laterale dextrum (4), ligamentum vesicae laterale sinistrum (5). B: Opened urinary bladder with indication of the ostia ureteria (1), columnae uretericae (2), plicae uretericae (3), crista urethralis (4).

the ovary presents fimbriae to collect the ovulated ovum. Fertilization takes place within the wider ampulla. The isthmus is narrower and opens up into the uterus.

The uterus of the rhesus monkey is of the simplex type. The fundus uteri, corpus uteri and isthmus uteri measure approximately 5 mm, 10 mm and 5 mm in length, respectively. The isthmus is in continuation with the canalis cervicis uteri that is the central canal within the cervix. The uterus is connected with the abdominal wall by means of the mesometrium. Together with the mesosalpinx and the mesovarium, it forms the broad uterine ligament. The ligamentum teres uteri attaches to the uterine body and travels through the inguinal canal. Terminal fibers of this ligament disperse into the vulva lips (**Figure 54**).

The vagina begins distal to the cervix. The portio vaginalis cervicis is the protrusion of the cervix into the vagina. The fornix vaginae is surrounding this structure. The vaginal mucosa is slightly keratinized and presents irregular folds. The vestibulum vaginae lies more distal and can be reached through the ostium vaginae. The border between the vagina and the vestibulum is formed by the urethral opening. This perineal opening that is located ventral to the anal opening is enclosed by a pair of vulva lips.

6.6 Male reproductive organs

The primary genital glands of the male rhesus monkey are the testes. These are located in the scrotum that lies caudoventrally in the perineal region (**Figure 2**). The scrotal skin is thin and a has a limited number of hairs. This favors thermoregulation. The raphe scroti is visible in the midline and is continuous with the internal septum scroti that divides the scrotum in two separate cavities (cavum vaginale). These cavities can be reached by incision through the scrotal skin.

After transecting the wall of the vaginal cavity, i.e. the tunica vaginalis, the testis can be observed. This egg-shaped organ measures approximately 5 cm in length and 3 cm in width. It is encapsulated by the pale tunica albuginea that consist of dense connective tissue (**Figure 55**).

The a. testicularis is responsible for the testicular blood supply. It is surrounded by the venous plexus pampiniformis that cools the arterial blood. The ductus deferens is closely associated with the testicular blood vessels as they form the funiculus spermaticus that is enclosed by the tunica vaginalis. The ductus deferens is the continuation of the ductus epididymidis. This duct is extremely coiled, forming the epididymis, a solid structure adjacent to the testis. It can be divided into the caput, corpus and cauda epididymidis. The corpus lies against the medial side of the testis and is connected with this structure through the ligamentum testis proprium. The cauda epididymidis is attached to the tunica vaginalis by means of the ligamentum caudae epididymidis (**Figure 56**).

The ductus deferens leaves the vaginal cavity through the inguinal canal. After it has entered the abdominal cavity, it presents a caudal flexion dorsal to the ureter to flow into the pelvic part of the urethra. Along this urethral segment, three accessory glands are present. The ellipsoid, lobulated vesicular glands are large, 5–6 cm in length. They are positioned against the neck of the urinary bladder. Their caudal parts have contact with the prostate. This gland is spherical with a diameter of approximately 1 cm. Its body is positioned in between the caudal parts of the vesicular glands, at the dorsal side of the urethra. Some glandular tissue, however, surrounds the urethra. The bulbourethral glands are very small. They can be found caudolateral to the prostate gland (**Figure 57**).
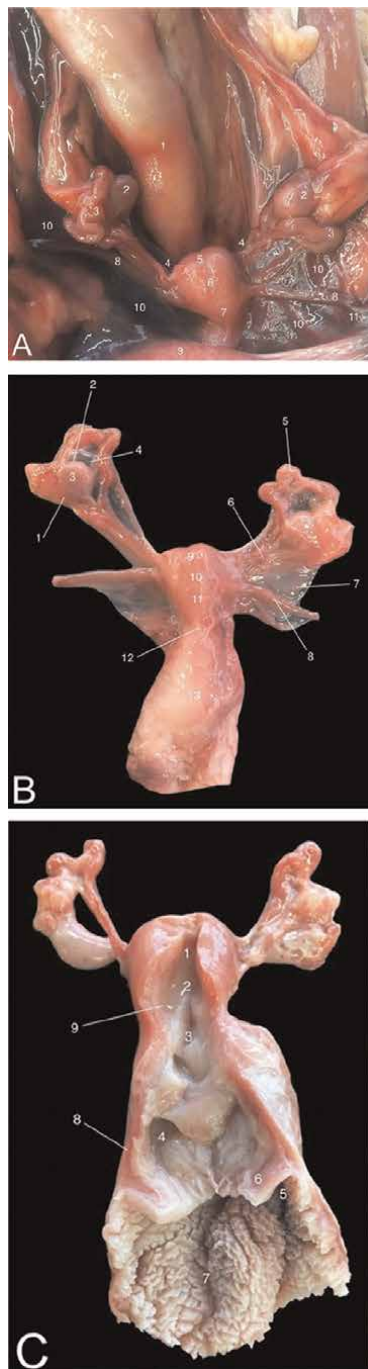
Figure 54.
A: The female reproductive tract in situ. 1: rectum, 2: ovarium, 3: tuba uterina, 4: isthmus tubae uterinae, 5: fundus uteri, 6: corpus uteri, 7: isthmus uteri, 8: ligamentum teres uteri, 9: vesical urinaria, 10: ligamentum latum uteri, 11: anulus inguinalis profundus. B: Isolated female reproductive tract. 1: margo liber ovaricae, 2: margo mesovaricus, 3: ovarium, 4: mesosalpinx, 5: tuba uterina, 6: ligamentum ovarii proprium, 7: ligamentum latum uteri, 8: ligamentum teres uteri, 9: fundus uteri, 10: corpus uteri, 11: isthmus uteri, 12: cervix, 13: vagina. C: Isolated female reproductive tract with opened uterus. 1: fundus uteri, 2: corpus uteri, 3: isthmus uteri, 4: canalis cervicis uteri, 5: fornix vaginae, 6: portio vaginalis cervicis, 7: vagina, 8: myometrium, 9: endometrium.
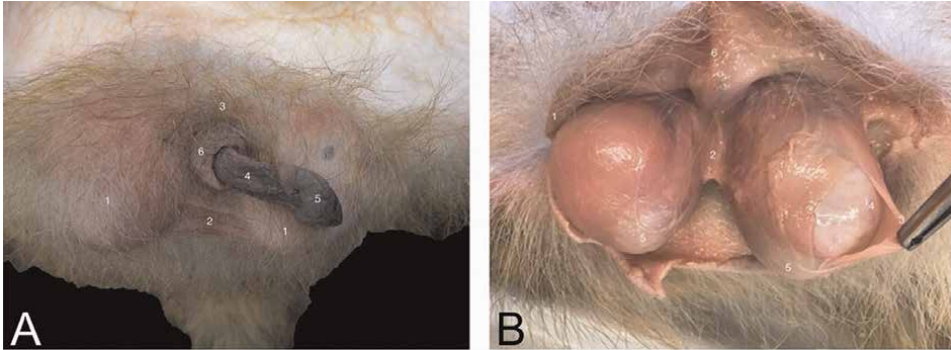
Figure 55.
A: Penis and scrotum of the male rhesus monkey. 1: scrotum, 2: raphe scroti, 3: radix penis, 4: corpus penis, 5: glans penis, 6: preputium. B: Incision through the scrotal skin showing the testes. 1: scrotal skin, 2: septum scroti, 3: tunica vaginalis (partially incised), 4: tunica albuginea, 5: cauda epididymidis, 6: raphe scroti.
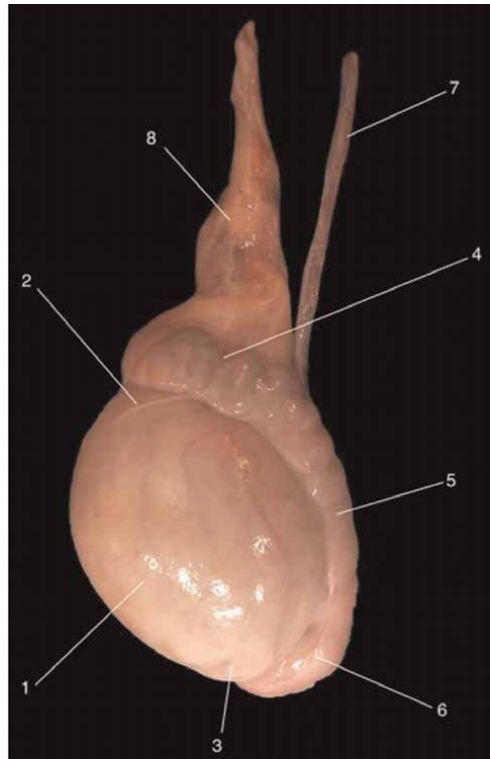
Figure 56.
Left testis and epididymis of the rhesus monkey. 1: testis, 2: extremitas dorsalis, 3: extremitas ventralis, 4: caput epididymidis, 5: corpus epididymidis, 6: cauda epididymidis, 7: ductus deferens, 8: plexus pampiniformis.

The penis of the rhesus monkey is of the cavernous type. When the penis is transected, the paired corpora cavernosa can be recognized by their pale brown color. Both are divided by the penile septum. The free part of the penis is approximately 5 cm long. It consists of the corpus penis and the glans penis. The urethral opening is
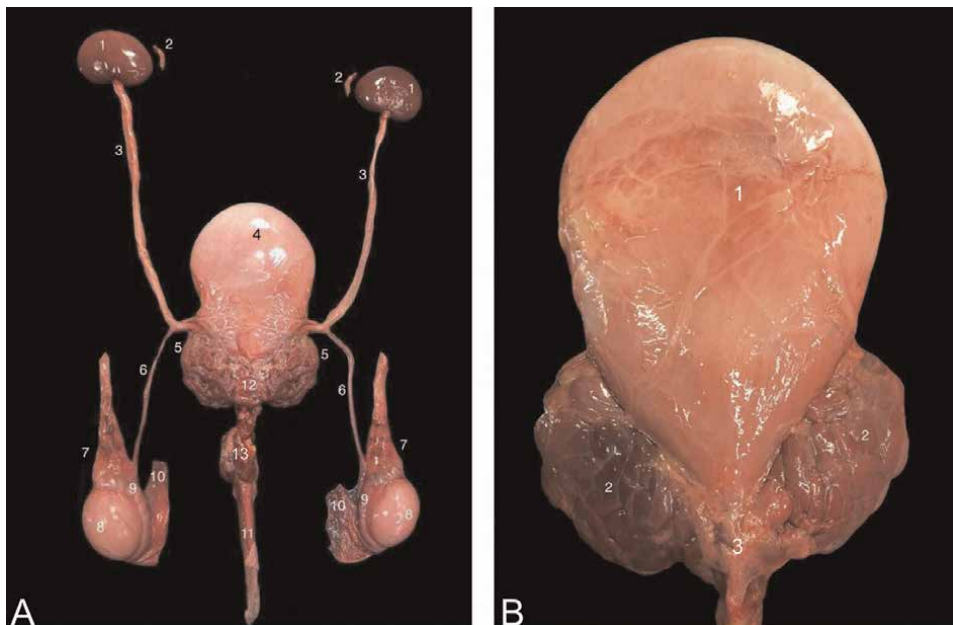
Figure 57.
A: Ventral view of the isolated male urogenital tract. 1: ren, 2: glandula adrenalis, 3: ureter, 4: vesical urinaria, 5: glandula vesicularis, 6: ductus deferens, 7: plexus pampiniformis, 8: testis, 9: epididymis, 10: tunica vaginalis, 11: penis, 12: prostata, 13: glandula bulbourethralis. B: Larger magnification of the urinary bladder (1) and the accessory genital glands comprising the glandula vesicularis (2) and the prostata (3).

located at the ventral side of the glans. The glans is covered by the preputium (**Figure 58**).

6.7 Lungs

The major intrathoracic organs are the lungs. The lungs can be examined by auscultation are medical imaging in the region from the 2nd to the 8th intercostal space. They consist of the left and right lungs that are separated by the mediastinum. Both are divided into lung lobes by fissures. The left lung consists of a cranial and caudal lung lobe that are separated by the interlobar fissure. The left cranial lung lobe is additionally divided into a cranial part and a caudal part by the cardiac scissure. The right lung has four lobes. The presence of the cranial and caudal interlobar fissures allows for the determination of the cranial, middle and caudal lung lobes. In addition, an accessory lung lobe is present in the right lung (**Figure 59**).

Each lung lobe is ventilated by a principal bronchus (bronchus principalis sinister et dexter). These are the terminal bifurcation of the trachea. This structure counts approximately 27 cartilaginous rings and measures approximately 10 cm in length and 1 cm in diameter. Intrathoracically, the trachea lies ventral to the esophagus and is crossed by the aortic arch at its left side. From the left and right principal bronchi, two and three specific bronchi (bronchi lobares) for the several lung lobes branch off, respectively. The bronchus for the left cranial lung lobe further splits into a bronchus for the cranial part and one for the caudal part. The bronchus for the accessory lobe of the right lung is a branch from the caudal lobar bronchus (**Figure 60**).
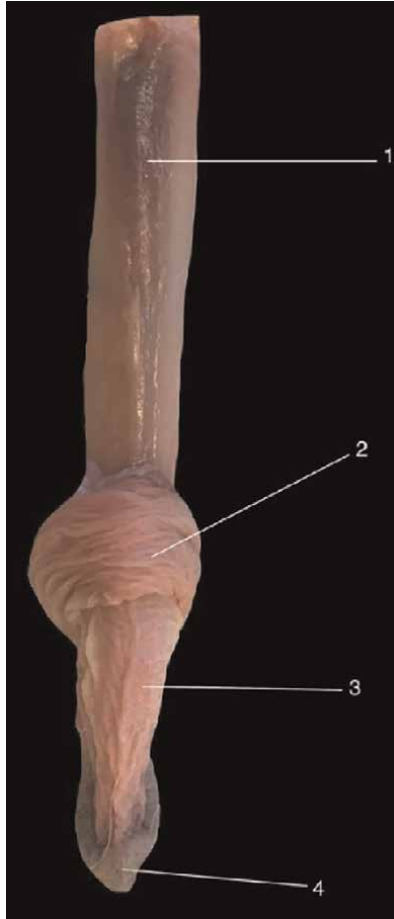
Figure 58.
Dorsal view of the penis. 1: radix penis with a. dorsalis penis, 2: preputium, 3: corpus penis, 4: glans penis.
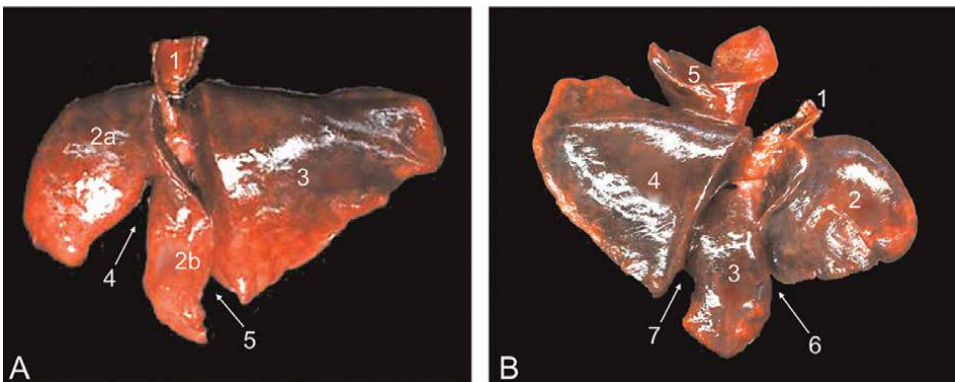
Figure 59.
Lungs. A: Left lateral view of the left lung with 1: trachea, 2a: lobus cranialis, pars cranialis, 2b: lobus cranialis, pars caudalis 3: lobus caudalis, 4: incisura cardiaca, 5: fissura interlobaris. B: Right lateral view of the right lung with 1: trachea, 2: lobus cranialis, 3: lobus medius, 4: lobus caudalis, 5: lobus accessorius, 6: fissura interlobaris cranialis, 7: fissura interlobaris caudalis.
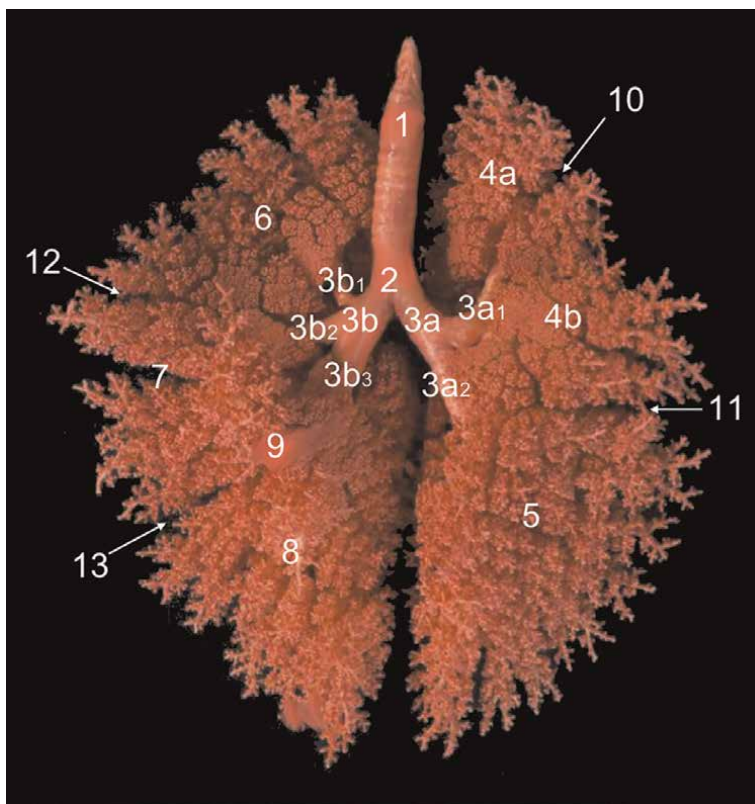
Figure 60.
Polyurethane cast of the lungs, ventral view. 1: trachea, 2: bifurcatio tracheae, 3a: bronchus principalis sinister, 3b: bronchus principalis dexter, 3a1: bronchus lobaris for the left cranial lung lobe, 3a2: bronchus lobaris for the left caudal lung lobe, 3b1: bronchus lobaris for the right cranial lung lobe, 3b2: bronchus lobaris for the right middle lung lobe, 3b3: bronchus lobaris for the right caudal lung lobe, 4a: pars cranialis lobi cranialis pulmonis sinistri, 4b: pars caudalis lobi cranialis pulmonis sinistri, 5: lobus caudalis pulmonis sinistri, 6: lobus cranialis pulmonis dextri, 7: lobus medius pulmonis dextri, 8: lobus caudalis pulmonis dextri, 9: lobus accessorius pulmonis dextri, 10: incisura cardiaca, 11: fissura interlobaris, 12: fissura interlobaris cranialis, 13: fissura interlobaris caudalis.

6.8 Heart

The heart lies in the thoracic cavity in the region from the 2nd to the 4th intercostal space. It is located between the lungs, in de middle mediastinum, and is enclosed by the pericardium. This fibrous structure dorsally attaches to the basis of the heart and ventrally to the sternum by means of the sternopericardiac ligament. After removal of the left thoracic wall, the blunt apex of the heart, which is formed by the left ventricle, can be observed in between the left cranial and caudal lung lobes as the longitudinal axis of the heart presents a deviation of approximately 45° towards the left. As a result, both the left and right auricle can be observed from the left. The left lateral aspect of the heart is therefore called the auricular side (facies auricularis). Both atria are visible from the right side. This side of the heart is the atrial side (facies atrialis). After removal of the right thoracic wall, it can be observed that the right heart including the right auricle and ventricle rests on the sternum as a result of the counterclockwise quarter rotation of the longitudinal cardiac axis (**Figure 61**).
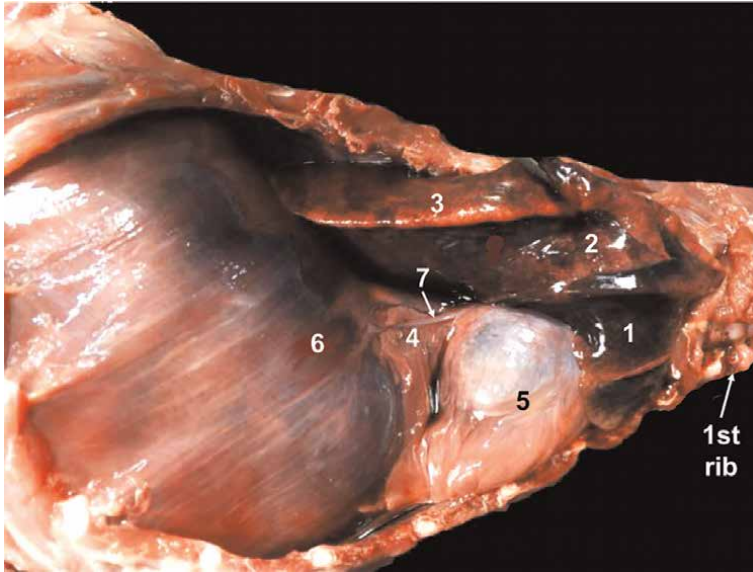
Figure 61.
Right lateral view of the thoracic cavity with 1: lobus cranialis pulmonis dextri, 2: lobus medius pulmonis dextri, 3: lobus caudalis pulmonis dextri, 4: lobus accessorius pulmonis dextri, 5: heart within the pericardium, 6: diaphragma, 7: n. phrenicus.

The left atrium, that is enlarged by the presence of the left auricle, receives oxygenated blood from the lungs via the four pulmonary veins. The left atrium is smaller in volume than the right atrium and has a smoother inner surface. From here, the blood flows to the left ventricle. The bicuspid left atrio-ventricular valve, i.e. the mitral valve, separates the left auricle from the left ventricle. It is attached to the papillary muscles in the wall of the left ventricle by means of the chordae tendineae. The latter presents a well trabeculated wall (trabeculae carneae) of approximately 6–9 mm in width. A septomarginal trabecula can be observed. Subsequently, blood flows to the ascending aorta. The aortic valve contains three valvulae.

The right atrium, with its right auricle, receives the systemic venous blood through the cranial and caudal vena cava that join at the level of the tuberculum intervenosum. Its wall is characterized by the mm. pectinati. The right auriculo-ventricular valve presents three cusps and is therefore known as the tricuspid valve. The wall of the right ventricle is also trabeculated and measures 1–2 mm in width. The right lumen contains a septomarginal trabecula. The pulmonary valve has the typical arrangement with three valvulae (**Figures 62** and **63**).

The left and right coronary arteries (a. coronaria sinistra et dextra) branch off the short ascending aorta, which runs craniodorsally, just above the aortic valve. These can initially be seen in the coronary sulcus. The a. coronaria dextra gives the a. interventricularis subsinuosus that runs in the sulcus interventricularis subsinuosus. It ultimately joins the ramus circumflexus of the a. coronaria sinistra. This coronary artery runs initially in the coronary sulcus, gives the ramus interventricularis paraconalis that runs in the sulcus interventricularis paraconalis, and continues as the ramus circumflexus that joins the right coronary artery. The left coronary artery is more pronounced than the right (**Figure 63**).
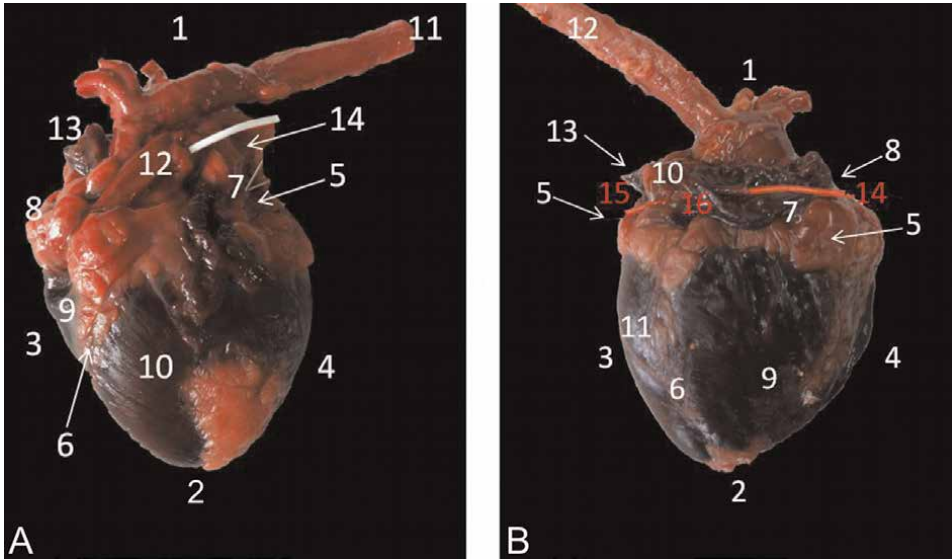
Figure 62.
External anatomical landmarks of the heart. A: Left view, facies auricularis with 1: basis cordis, 2: apex cordis, 3: margo ventricularis dexter, 4: margo ventricularis sinister, 5: sulcus coronarius, 6: sulcus interventricularis paraconalis, 7: auricula sinistra, 8: auricula dextra, 9: ventriculus dexter, 10: ventriculus sinister, 11: aorta descendens, 12: truncus pulmonalis, 13: v. cava cranialis, 14: vv. pulmonales. B: Right view, facies atrialis with 1: basis cordis, 2: apex cordis, 3: margo ventricularis sinister, 4: margo ventricularis dexter, 5: sulcus coronarius, 6: sulcus interventricularis subsinuosus, 7: atrium dextrum, 8: sulcus terminalis, 9: ventriculus dexter, 10: atrium sinistrum, 11: ventriculus sinister, 12: aorta descendens, 13: vv. pulmonales, 14: v. cava cranialis, 15: v. cava caudalis, 16: sinus venarum cavarum.
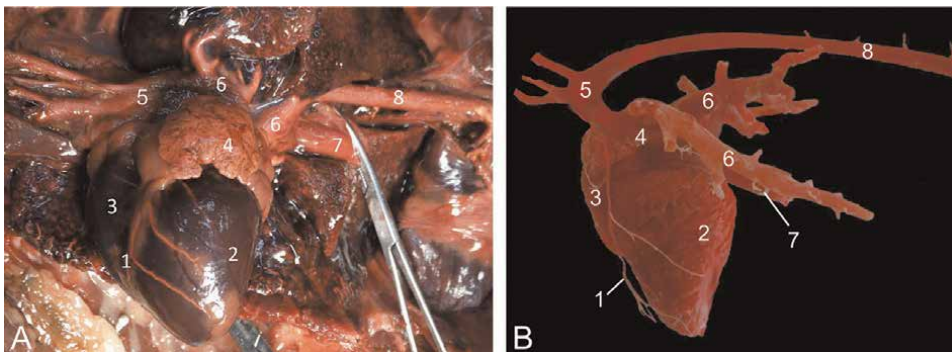
Figure 63.
Heart and larger vessels. A: Latex injected specimen, B: Vascular corrosion cast. 1: a. coronaria sinistra ramus interventricularis paraconalis, 2: ventriculus sinister, 3: ventriculus dexter, 4: atrium sinistrum, 5: arcus aortae, 6: vv. pulmonales, 7: v. cava caudalis, 8: aorta thoracica.

The aortic arch presents a branching pattern that is dissimilar to that in humans. Only two branches can be seen, the brachiocephalic trunk and the left subclavian artery. From the short initial segment of the brachiocephalic trunk, also known as the truncus communis, branches the left common carotid artery after a few mm to 1 cm. In humans, the left common carotid artery is a direct branch of the aortic arch. The right common carotid artery branches off subsequently. The continuation of the brachiocephalic trunk is the right subclavian artery (**Figure 64**).
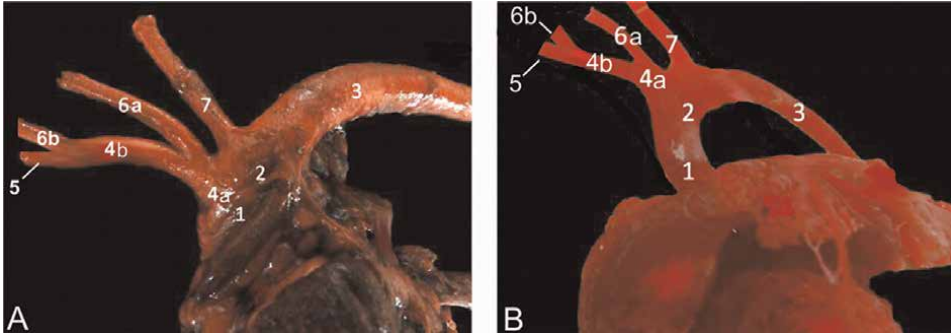
Figure 64.
Branching vessels from the aortic arch. A: Native specimen, B: Vascular corrosion cast. 1: aorta ascendens, 2: arcus aortae, 3: aorta descendens, 4a: truncus communis, 4b: truncus brachiocephalicus, 5: a. subclavia dextra, 6a: a. carotis communis sinistra, 6b: a. carotis communis dextra, 7: a. subclavia sinistra.

7. Angiology and neurology

7.1 Head

From the brachiocephalic trunk branches the left and subsequently the right common carotid artery. These arteries are laterally covered by the sternocleidomastoideus muscle. The internal jugular vein and vagal nerve are closely associated and lie just lateral to the artery. The common carotid artery divides into the internal and external carotid arteries at the mandibular angle. The former artery provides blood to the eye and the brains, while the latter gives off, amongst others, the linguofacial artery to continue as the maxillary artery.

The external jugular vein travels along the lateral aspect of the sternocleidomastoideus muscle and drains the venous blood from the head. This vein is suited for venipuncture. The accessory jugular vein lies parallel to the external jugular vein with which it fuses caudal to the collar bone. The caudal auricular veins, superficial temporal vein and maxillary vein drain into the external jugular vein. The facial vein drains partly into this vein, but mainly into the internal jugular vein. Both the external and internal jugular veins drain into the subclavian vein that in turn flow into the brachiocephalic vein. The cranial cava vein receives the left and right brachiocephalic veins.

In between the common carotid artery and the internal jugular vein lies the vagal nerve. It runs separately from the sympathetic trunk that lies deep against the cervical vertebrae. At the entrance of the thorax, the laryngeus recurrens nerve leaves the vagal nerve. The left sweeps around the aortic arch whereas the right makes a curvature around the right subclavian artery. The laryngeus recurrens nerve subsequently returns to the larynx, lateral to the trachea. Some major nerves and blood vessels of the rhesus monkey head are depicted in **Figure 65**.

7.2 Thoracic limb

After crossing the 1st rib and giving off several branches to the head, neck, shoulder and thorax, the subclavian artery continues as the axillary artery that is accompanied by the axillary vein. The latter artery continues as the brachial artery after the a. subscapularis and a. circumflexa humeri cranialis have branched off. The brachial
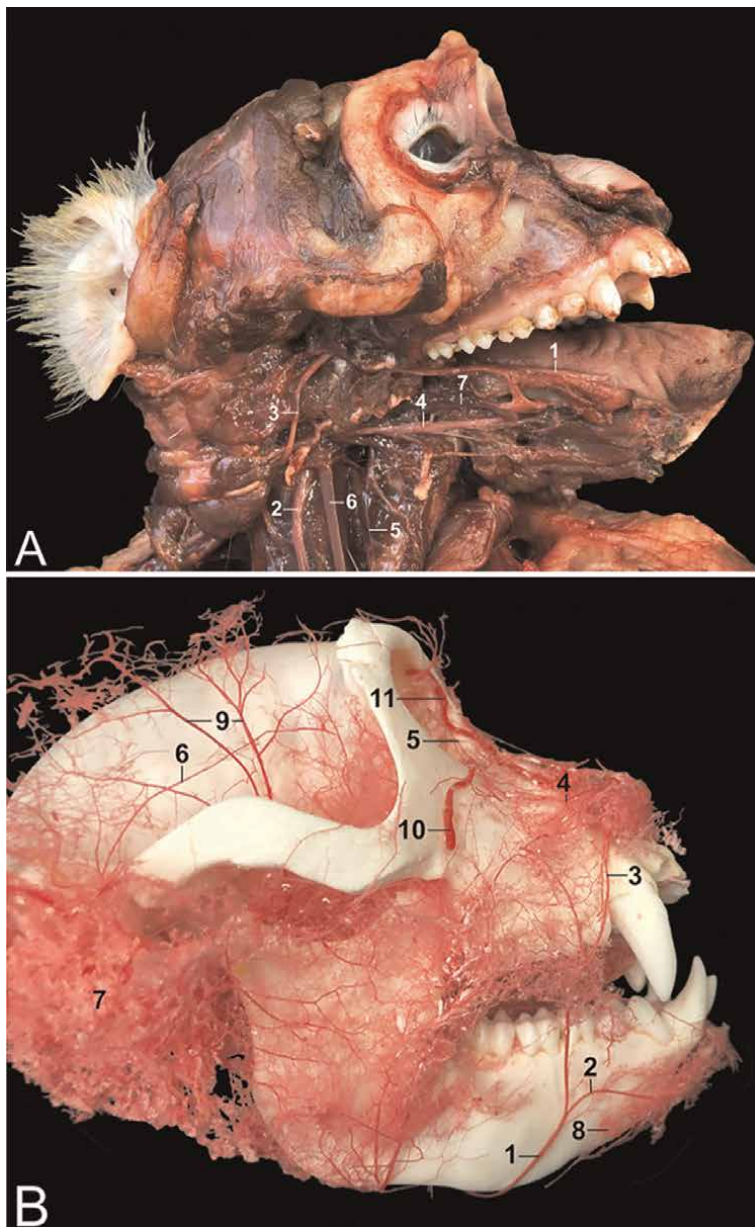
Figure 65.
A: Right lateral view of the rhesus monkey head of which the right side of the mandible has been removed with 1: n. lingualis, 2: n. vagus, 3: n. accessorius, 4: n. hypoglossus, 5: ansa cervicalis, 6: a. carotis communis, 7: a. lingualis. B: Right lateral view of a vascular corrosion cast of the rhesus monkey head with 1: a. facialis, 2: a. submentalis, 3: a. labialis superior, 4: a. nasalis lateralis, 5: a. angularis oculi, 6: a. temporalis superficialis, 7: vascular network of the parotid gland, 8: a. mentalis, 9: aa. temporales profundae, 10: v. facialis, 11: v. angularis oculi.

artery runs parallel to the n. medianus and gives off the a. profunda brachii as first branch. Subsequent branches are the collateralis ulnaris arteries that run collateral to the n. ulnaris. Just proximal to the elbow joint, the brachial artery splits into the radial and ulnar arteries. The former artery runs at the lateral side of the forearm towards the carpus where it gives origin to the dorsal and palmar arches. The ulnar artery joins

the palmar arch. These arches supply the hand and fingers. **Figures 66** and **68** present the discussed arteries.

The venous circulation of the thoracic limbs consists of a deep and a superficial system. The deep system accompanies the arteries (e.g. v. subclavia, v. axillaris, v. brachialis), while the superficial veins have no arterial counterpart. In the rhesus monkey, the superficial venous system is poorly developed since the venous drainage of the hand and forearm is mainly provided by paired vv. comitantes. The cephalic vein, which is located at the cranial side of the antebrachium, is the major superficial vein of the forelimb. It forms a common stem with the accessory jugular vein that drains into the external jugular vein. It can be used for venipuncture, but is not preferred in the rhesus monkey (**Figure 67**).

The nerves of the forelimb originate from the brachial plexus (C5 – T2) at the medial side of the upper arm. The thoracodorsal nerve innervates the latissimus dorsi muscle. The axillary nerve finds its way from medial to lateral superficially in the angle between the coracobrachialis and teres major muscles and deeper between the triceps and teres minor muscles to innervate the flexor muscles of the shoulder (deltoid, coracobrachialis and both teres muscles). The radial nerve runs from medial to lateral between the lateral and medial heads of the triceps muscle and perforates the brachioradialis muscle. Its muscular branches innervate the triceps and anconeus muscles as well as the extensor musculature of the upper arm, forearm and hand. The musculocutaneus nerve innervates the flexor muscles of the elbow joint (rami musculares to the coracobrachialis, biceps brachii and brachialis muscles). The median nerve runs parallel to the brachial artery in between the biceps brachii and
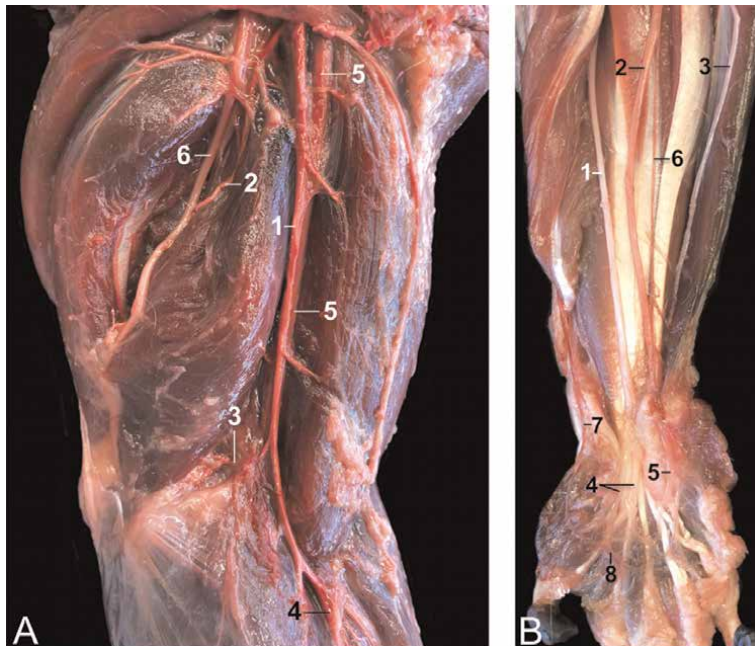
Figure 66.
Blood vessels and nerves of the thoracic limb. A: Medial view of the left upper arm with 1: a. brachialis, 2: a. collateralis ulnaris proximalis, 3: a. collateralis ulnaris distalis, 4: a. radialis, 5: n. medianus, 6: n. ulnaris. B: Medial/palmar view of the right forearm and hand with 1: n. medianus, 2: n. ulnaris, 3: ramus dorsalis (n. ulnaris), 4: nn. digitales palmares communes, 5: ramus superficialis (n. ulnaris), 6: a. ulnaris, 7: a. radialis, 8: arcus palmaris.
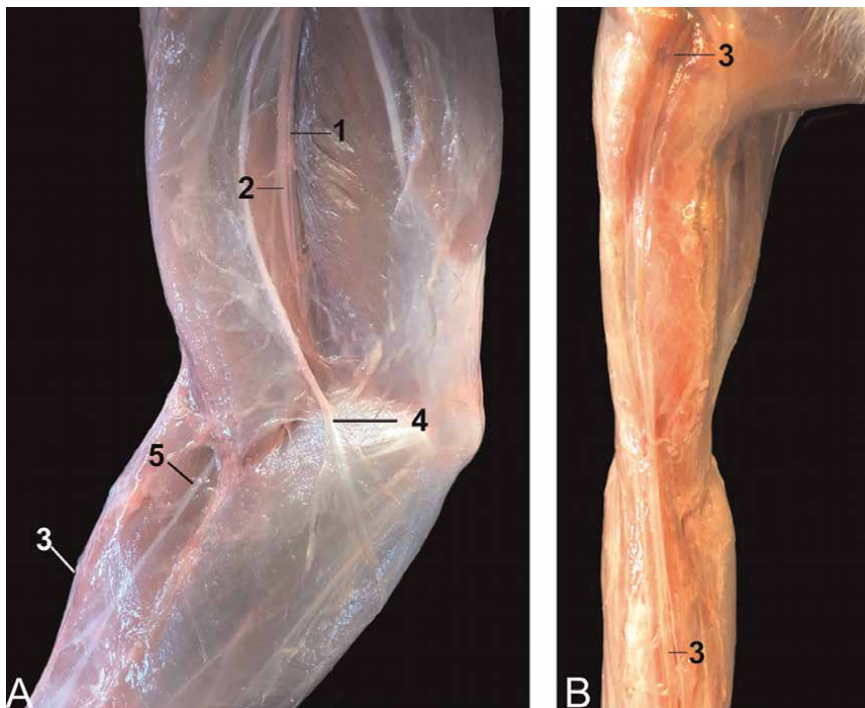
Figure 67.
Medial (A) and dorsal (B) views of the thoracic limb showing 1: v. brachialis, 2: n. medianus, 3: v. cephalica, 4: n. cutaneus brachii medialis, 5: n. cutaneus antebrachii medialis.

brachialis muscle. More distally, it lies deep to the flexor muscles of the forearm, which it innervates. Its most distal branches are the digital nerves. The ulnar nerve can be found between the medial and long head of the triceps muscle. It crosses the elbow region in between the flexor carpi ulnaris and flexor digitorum profundus muscles to reach the hand. Its dorsal, superficial and deep branches innervate the flexor musculature of the fingers in addition to the median nerve. The n. cutaneus brachii et antebrachii medialis runs initially parallel to the ulnar nerve. The brachial and antebrachial branches innervate the skin at the medial sides of the upper and lower arm, respectively. The here discussed nerves are depicted in **Figures 66–68**.

7.3 Body

In this paragraph, some essential data on the ramifications of the abdominal aorta and caudal vena cava will be shared. As regards the arterial system that is depicted in **Figure 69**, it should be noticed that the truncus celiacus is very short and soon divides into the common hepatic artery, the gastrolienalis artery and the cranial mesenteric artery. The common hepatic artery branches into the a. hepatica propria that supplies the liver and arteries for the stomach, pancreas and duodenum. The a. gastrolienalis subsequently divides into the a. lienalis and a. gastrica sinistra. The a. mesenterica cranialis ramifies into the jejunal, ileal and colic arteries. Only approximately 1 cm caudal to the celiac trunk branches the right renal artery off the abdominal aorta. The left renal artery can be found a few mm more caudal. The caudal mesenteric artery branches off a few cm caudal to the left renal artery. This artery ramifies into the a.
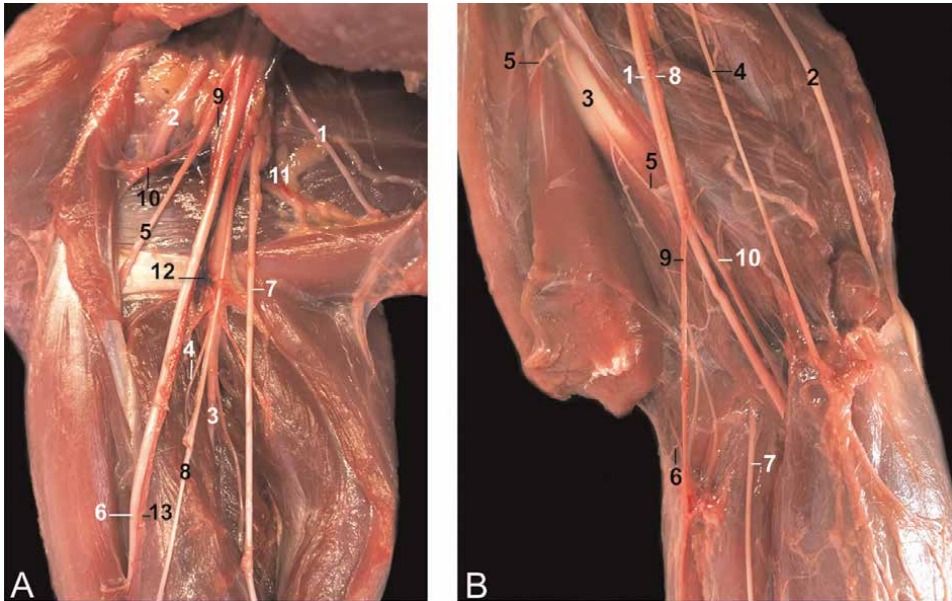
Figure 68.
Medial views of the nerves and blood vessels of the right forelimb. A: Plexus brachialis at the level of the shoulder joint with 1: n. thoracodorsalis, 2: n. axillaris, 3: n. radialis, 4: rami musculares, 5: n. musculocutaneus, 6: n. medianus, 7: n. ulnaris, 8: n. cutaneus brachii et antebrachii medialis, 9: a. axillaris, 10: a. circumflexa humeri cranialis, 11: a. subscapularis, 12: a. profunda brachii, 13: a. brachialis. B: Blood vessels and nerves at the level of the elbow joint with 1: n. medianus, 2: n. ulnaris, 3: n. musculocutaneus, 4: n. cutaneus brachii et antebrachii medialis, 5: Rami musculares, 6: n. cutaneus antebrachii lateralis, 7: n. radialis, 8: a. brachialis, 9: a. radialis, 10: a. ulnaris.

colica sinistra, a. sigmoidea and a. rectalis cranialis. Just cranial to the terminal bifurcation of the abdominal aorta into the common iliac arteries can the origin of the a. circumflexa ilium profunda be found.

Regarding the venous system, the reader should be reminded of the fact that the arterial truncus celiacus has no venous counterpart. The portal vein is described above (**Figure 51**). The veins of the caudal segment of the caudal vena cava can be studied by means of **Figure 70**.

7.4 Pelvic limb

The abdominal aorta divides into the left and right common iliac arteries within the pelvic cavity. These arteries subsequently divide into the external and internal iliac arteries (**Figure 69**). In the proximal part of the thigh, the external iliac artery continues as the femoral artery, which is suitable for palpation of the pulse, after the a. profunda femoris has branched off. This artery gives origin to the lateral circumflex artery, which branches supply the vasti muscles. The femoral artery then divides into the saphena artery and the popliteal artery. The latter artery runs deep between both heads of the gastrocnemius muscle and gives the medial and lateral a. genus distalis as branches. These branches supply the knee region together with the a. genus proximalis of the a. saphena. This artery emerges in the angle formed by the sartorius and gracilis muscles and runs superficially to the medial side of the tibia. She subsequently migrates to the cranial aspect of the tarsus to become the a. dorsalis pedis
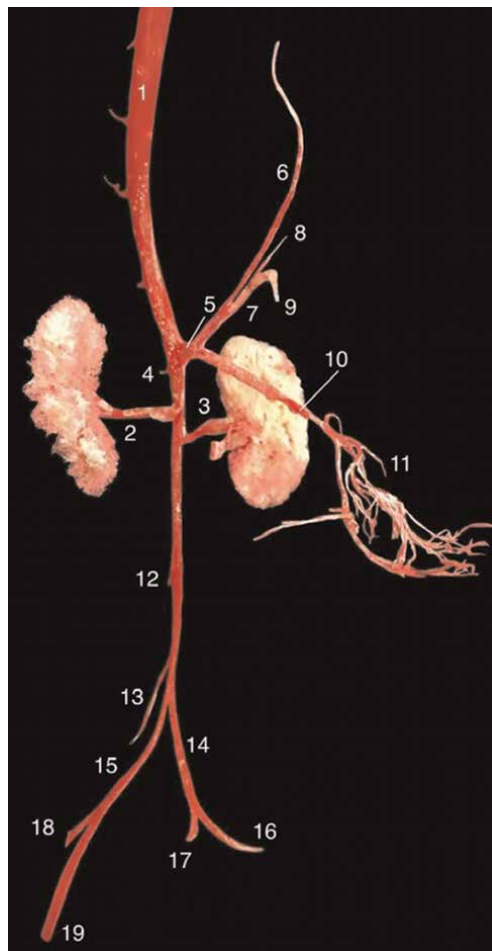
Figure 69.
Corrosion cast of the abdominal arteries, ventral view. 1: aorta abdominalis, 2: a. renalis dextra, 3: a. renalis sinistra, 4: a. adrenalis, 5: truncus celiacus, 6: a. hepatica communis, 7: a. gastrolienalis, 8: a. gastrica, 9: a. lienalis, 10: a. mesenterica cranialis, 11: aa. jejunales et ileales, 12: a. mesenterica caudalis, 13: a. circumflexa ilium profunda, 14: a. iliaca communis sinistra, 15: a. iliaca comunis dextra, 16: a. iliaca externa sinistra, 17: a. iliaca interna sinistra, 18: a. iliaca interna dextra, 19: a. iliaca externa dextra.

(superficialis et profunda). From the popliteal artery branches the a. tibialis cranialis. She becomes the a. tibialis caudalis at the level of the lower leg. At the level of the foot, the a. tibialis caudalis divides into the a. plantaris lateralis et medialis. The arterial and nerve system of the hind limb are visualized in **Figures 71** and **73**.

In analogy with the thoracic limb, the venous drainage of the pelvic limb is mainly effectuated by the vv. comitantes. The vv. marginalis medialis et lateralis pedis drain the dorsal side of the foot. The v. marginalis medialis pedis drains into the superficially located v. saphena magna that proximately flows into the femoral vein. The v. marginalis lateralis pedis drains into the v. saphena parva. It is an important vein as it drains the larger part of the hind leg and is suitable for venipuncture at the caudal aspect of the calf (**Figure 72**). In the popliteal fossa, she drains into the popliteal vein. This vein runs adjacent to the eponymous artery and flows into the femoral vein. This vein is also suitable for venipuncture. The femoral vein proximally drains into the external iliac vein that in turn flows into the common iliac vein.
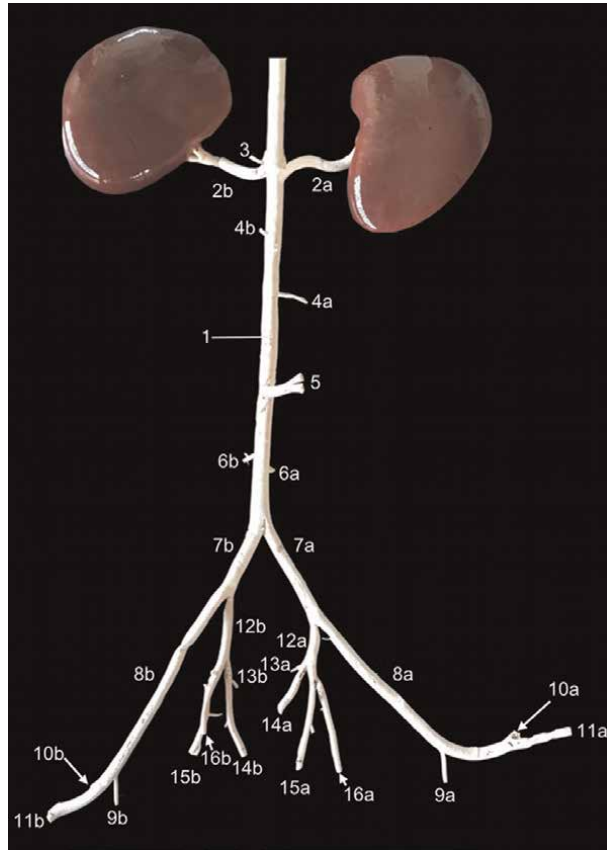
Figure 70.
Latex cast of the caudal segment of the caudal cava vein of the male rhesus monkey, ventral view. 1: v. cava caudalis, 2a: v. renalis dextra, 2b: v. renalis sinistra, 3: v. adrenalis sinistra, 4a: v. testicularis dextra, 4b: v. testicularis sinistra, 5: v. mesenterica caudalis, 6a: v. circumflexa ilium profunda dextra, 6b: v. circumflexa ilium profunda sinistra, 7a: v. iliaca communis dextra, 7b: v. iliaca communis sinistra, 8a: v. iliaca externa dextra, 8b: v. iliaca externa sinistra, 9a: v. profunda femoris dextra, 9b: v. profunda femoris sinistra, 10a: v. circumflexa femoris lateralis dextra, 10b: v. circumflexa femoris lateralis sinistra, 11a: v. femoralis dextra, 11b: v. femoralis sinistra, 12a: v. iliaca interna dextra, 12b: v. iliaca interna sinistra, 13a + 14a: v. gluteus cranialis superficialis dextra, 13b + 14b: v. gluteus cranialis superficialis sinistra, 15a + 15b: Continuation of v. iliaca interna dextra et sinistra, 16a: v. obturatoria dextra, 16b: v. obturatoria sinistra.

The nerves of the hind limb originate from the lumbosacral plexus. The femoral nerve is associated with the eponymous blood vessels. Its muscular branches innervate the extensor muscles of the knee. In addition, cranial cutaneous branches innervate the skin at the craniomedial side of the upper leg and the medial side of the knee. The distal continuation of the femoral nerve is the n. saphenus that accompanies the a. saphena and innervates the skin at the craniomedial aspect of the lower leg. The n. gluteus caudalis, that innervates the m. gluteus superficialis, emerges together with the sciatic nerve. This nerve divides into the n. fibularis communis and n. tibialis. The former nerve deviates towards the lateral head of the gastrocnemius muscle. Halfway the upper leg, the n. cutaneus surae lateralis branches off to innervate the skin at the caudolateral side of the lower leg. Here, nerve biopsy can be performed. At the level of the knee, the n. fibularis communis divides into the n. fibularis superficialis et profundus. The latter travels deep to the fibularis longus and extensor digitorum
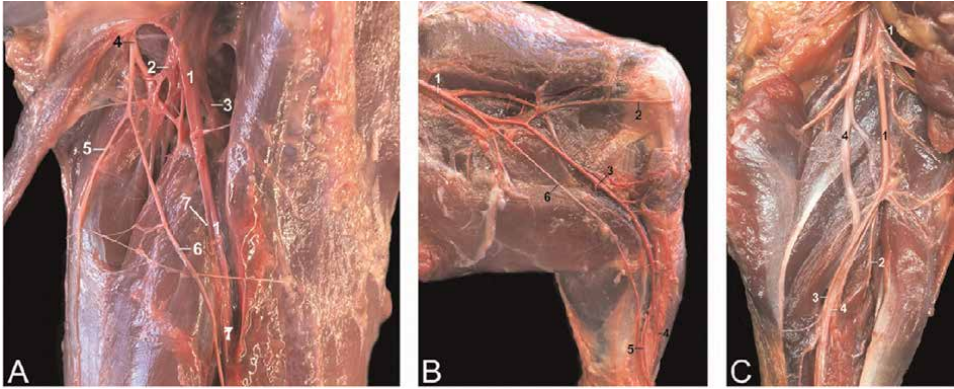
Figure 71.
Vasculature and nerves of the pelvic limb. A: Dorsomedial view of the right upper leg with 1: a. femoralis, 2: a. circumflexa femoris lateralis, 3: a. profunda femoris, 4: n. femoralis, 5: rami cutanei craniales, 6: n. saphenus. B: Medial view of the thigh and knee of the left leg with 1: a. femoralis, 2: a. genus proximalis, 3: a. saphena: 4: a. dorsalis pedis profunda: 5: a. dorsalis pedis superficialis, 6: n. saphenus. C: Caudal view of the popliteal region of the left leg with 1: a. poplitea, 2: a. tibialis cranialis, 3: a. tibialis caudalis, 4: n. tibialis.

Figure 72.
Superficial veins of the pelvic limb. A: Subcutaneous localization of the v. saphena parva. B: Catheterization of the v. saphena parva.

longus muscles to innervate the flexors of the tarsal joint and the extensors of the toes. The former gives off ramifications to the fibularis muscles and branches into the skin at the dorsolateral side of the foot. The tibial nerve presents several ramifications at the level of the knee. The majority migrate between the heads of the gastrocnemius
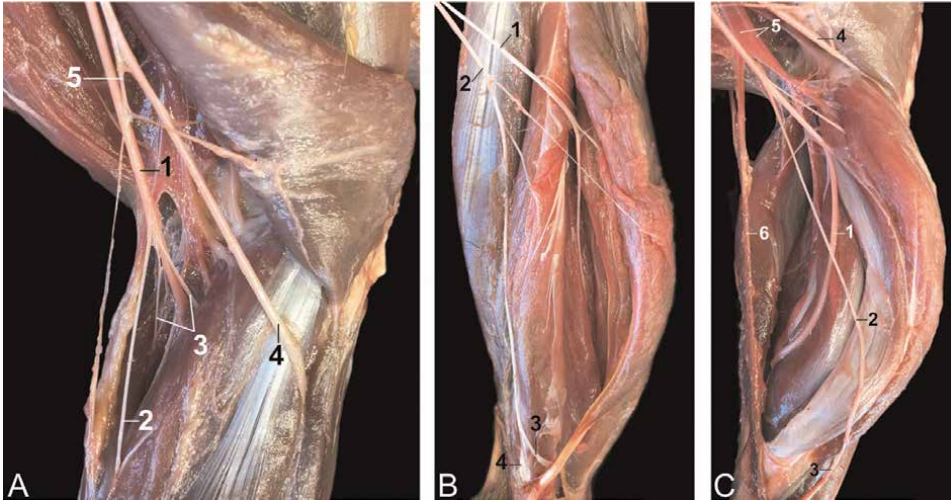
Figure 73.
Nerves and blood vessels of the right pelvic limb. Laterocaudal view of the right knee with 1: n. tibialis, 2: n. cutaneus surae medialis, 3: rami musculares, 4: n. fibularis communis, 5: n. cutaneus surae lateralis. B: Laterocaudal, superficial view of the lower leg with 1: n. fibularis profundus, 2: n. fibularis superficialis, 3: n. cutaneus pedis dorsalis medialis, 4: n. cutaneus pedis dorsalis intermedius. C: Laterocaudal, deep view of the lower leg with 1: n. tibialis, 2: n. cutaneus surae medialis, 3: n. suralis, 4: n. fibularis communis, 5: a. et v. poplitea, 6: v. saphena parva.

muscle to innervate the popliteus muscle, the extensors of the tarsal joint and the flexor musculature of the toes. A specific branch, the n. cutaneus surae caudalis, innervates the skin at the caudal side of the lower leg. More distally, it runs more laterally and is then called the n. suralis. Just proximal to the medial ankle, the tibial nerve divides into the medial and lateral plantar nerves. The n. flexoris femoris runs adjacent to the proximal part of the tibial nerve and branches into the hamstrings.

Acknowledgements

Author details

Christophe Casteleyn[1,2]* and Jaco Bakker[3]

1 Department of Morphology, Faculty of Veterinary Medicine, Ghent University, Merelbeke, Belgium

2 Laboratory for Applied Veterinary Morphology, Faculty of Pharmaceutical, Biomedical and Veterinary Sciences, University of Antwerp, Belgium

3 Animal Science Department, Biomedical Primate Research Centre, Rijswijk, The Netherlands

*Address all correspondence to: christophe.casteleyn@ugent.be

IntechOpen

References

[1] Morton WR, Kyes KB, Kyes RC, Swindler DR, Swindler KE. Use of the primate model in research. In: Wolfe-Coote S, editors. The Laboratory Primate. London: Academic Press; 2005. p. 405-415.

[2] Thew M, Bailey J, Balls M, Hudson M. The ban on the use of chimpanzees in biomedical research and testing in the UK should be made permanent and legally binding. Alternatives to Laboratory Animals. 2012;40:3-8.

[3] Hartman CG, Straus Jr WL. The Anatomy of the Rhesus Monkey (*Macaca mulatta*). London: Ballière, Tindall and Cox; 1933. 383 p.

[4] Berringer OM, Browning FM, Schroeder CR. An Atlas and Dissection Manual of Rhesus Monkey Anatomy. Tallahassee: Anatomy Laboratory Aids; 1968. 115 p.

[5] Nomina Anatomica Veterinaria, 6th edition (Internet). 2017. Available from: http://www.wava-amav.org [Accessed: 2021-05-10]

[6] Van Wagenen G, Catchpole HR. Physical growth of the rhesus monkey (*Macaca mulatta*). American Journal of Physical Anthropology. 1956;14:245-273.

[7] Lewis AD, Prongay K (2015). Basic physiology of Macaca mulatta. In: Bluemel J, Korte S, Schenck E, Weinbauer GF, editors. The Nonhuman Primate in Nonclinical Drug Development and Safety Assessment. London: Academic Press; 2015. p. 87-113.

[8] Van Wagenen G, Simpson ME. Testicular development in the rhesus monkey. The Anatomical Record. 1954; 118:231-251.

[9] Berringer OM, Browning FM, Schroeder CR. Myology. In: Berringer OM, Browning FM, Schroeder CR, editors. An Atlas and Dissection Manual of Rhesus Monkey Anatomy. 2nd ed. Tallahassee: Rose Printing Company; 1974. p. 15-54.

[10] Burrows AM, Waller BM, Parr LA. Facial musculature in the rhesus macaque (*Macaca mulatta*): Evolutionary and functional contexts with comparisons to chimpanzees and humans. Journal of Anatomy. 2009;215: 320-334.

[11] Burrows AM, Waller BM, Micheletta J. Mimetic muscles in a despotic macaque (*Macaca mulatta*) differ from those in a closely related tolerant macaque (*M. nigra*). The Anatomical Record. 2016;299:1317-1324.

[12] Murray P. The role of cheek Pouches in Cercopithecine monkey adaptive strategy. In: Tuttle RH, editor. Primate Functional Morphology and Evolution. Berlin: De Gruyter; 1975. p. 151-170.

Chapter 2

Anatomical Guide to the Paranasal Sinuses of Domestic Animals

Mohamed A.M. Alsafy, Samir A.A. El-Gendy
and Catrin Sian Rutland

Abstract

Paranasal sinuses are paired cavities within the skull, which develop by evagination into the spongy bone between the external and internal plates of the cranial and facial bones. Thus, each sinus is lined by respiratory epithelium and has direct or indirect communication to the nasal cavity. The purpose of this chapter is to present an anatomical reference guide of the paranasal sinuses in domestic animals, including large and small ruminants (cattle, buffalo, sheep, and goats), camels, canines (dog) and equines (horse and donkey), appropriate for use by anatomists, radiologists, clinicians, and veterinary students. Topographic descriptions and the relationships between the various air cavities and paranasal sinuses have been visualized using computed tomography and cadaver sections images. The anatomical features (including head bones, muscles, and soft tissues) have been compared using both dissected heads and skulls and computed tomography images. This chapter will therefore be useful as a normal reference guide for clinical applications.

Keywords: paranasal sinuses, morphology, computed tomography, domestic animals

1. Introduction

The paranasal sinuses develop via evagination into the spongy bone between the external and internal plates of the cranial and facial bones [1]. Therefore, the lining of each sinus comprises of respiratory epithelium. With the exception of the lacrimal and palatine sinuses which are diverticula of the maxillary sinus, each sinus has a direct opening into the nasal cavity. One of the largest problems with sinuses is inflammation, which can be caused by numerous problems including infection and structural abnormalities, and in itself can cause pain and increased infections. Unfortunately, when inflammation occurs, the mucous membrane swells and closes the aperture, this blocks normal sinus drainage [1]. This condition may require surgical drainage. The extensive sinus system possesses considerable clinical interest, especially as it is susceptible to infection that may spread from the nose or from an alveolar abscess [2, 3]. The paranasal sinuses of sheep include the frontal, maxillary, ethmoidal, lacrimal and palatine sinuses. Ovine sinuses differ slightly to cattle, including buffalo, which have frontal, maxillary, sphenoidal, ethmoidal, lacrimal and palatine sinuses [3–5]. Camels are somewhat similar to cattle with frontal, maxillary, sphenoidal, ethmoidal, and lacrimal sinuses [6] with an additional

palatine sinus [7–9]. However, in equids, three paranasal sinuses have been recorded: the frontal, maxillary and sphenopalatine [10–12]. Computed tomography of equine, ruminant and camel heads has enabled production of detailed cross-sectional images of structures and cavities such as the brain case, paranasal sinuses and nasal cavity whilst ensuring that other anatomical structures are not superimposed [4, 6, 11, 12].

2. The paranasal sinuses

2.1 The frontal sinus

The frontal sinus is an air-filled space which occupies the two cortical layers of the frontal bone, the dorsal part of the skull, medial and dorsal to the orbital cavity. It superimposes both the cranial and nasal cavities. The sinus divides into left and right sinuses using a complete median bony interfrontal septum.
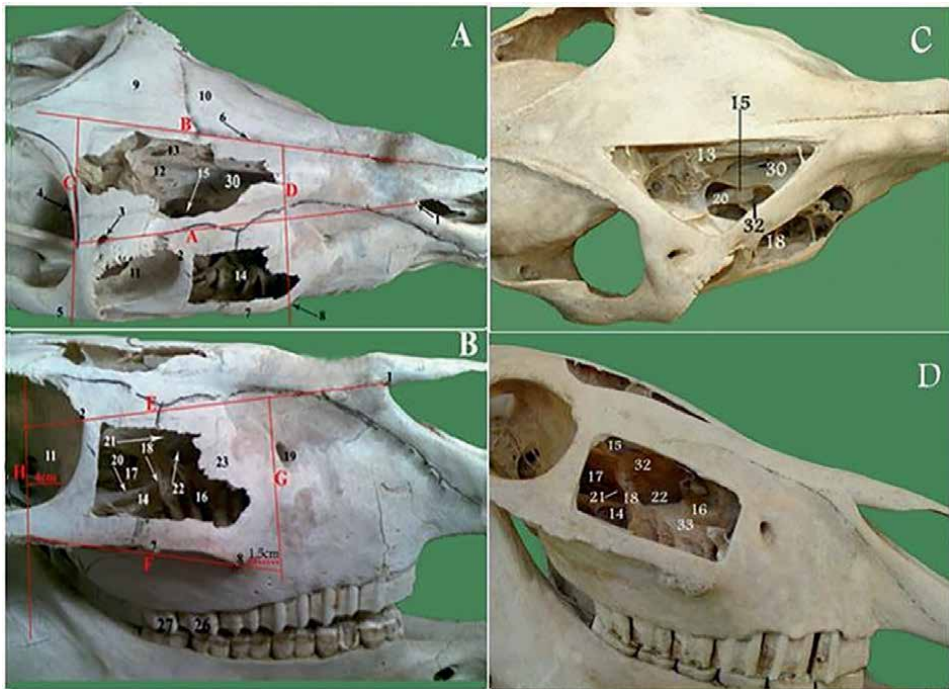
Figure 1.
Topography of frontal and maxillary sinuses in the donkey skull. 1. Nasoincisive notch. 2. Medial angle of the eye. 3. Supraorbital foramen. 4. Caudal border of supraorbital process. 5. Zygomatic arch. 6. Midline of skull. 7. Facial crest. 8. The end of facial crest. 9. Frontal bone. 10. Nasal bone. 11. Orbit. 12. Frontal sinus. 13. Frontal septum between right and left frontal sinuses. 14. Lateral compartment of caudal maxillary sinus. 15. Frontomaxillary opening. 16. Rostral maxillary sinus. 17. Medial compartment of caudal maxillary sinus. 18. Maxillary septum between rostral and caudal maxillary sinuses. 19. Infraorbital foramen. 20. Infraorbital canal. 21. Nasomaxillary opening. 22. Conchomaxillary opening. 23. Maxillary bone. 24. Dotted line indicated the caudal approach line of conchofrontal sinus. 25. Dotted line indicated the rostral approach line of conchofrontal sinus. 26. 2nd maxillary molar tooth. 27. 3rd maxillary molar tooth. 28. Site of approach of caudal maxillary sinus. 29. Site of approach of rostral maxillary sinus. 30. Dorsal Conchal sinus. 31. The lateral segment connected the lateral extent of the caudal and rostral lines. 32. Bulla of ventral nasal Conchal sinus (opened). 33. Bony plate. A, B) 5 year old donkeys, C&D) 12 year old donkeys. Reproduced with permission [13] journal of veterinary anatomy.

In the horse and donkey (**Figures 1**-**3**), the frontal sinus lies close to the dorsal nasal concha that forms the conchofrontal sinus in horse and donkey (**Figure 1**). The interior of the sinus cavity is incompletely divided by several bony spicules [11]. There is a convexity which exists on the floor of the frontal sinus due to the presence of the underlying ethmoidal labyrinth (**Figures 1** and **3**). It communicates directly with the caudal maxillary sinus by a large oval frontomaxillary opening, there is no frontomaxillary opening in any other domestic animal except in equines [1]. This opening is at the level of the caudal third of second molar tooth and extends caudally by 2–3 cm to the last molar tooth on the lateral floor of the conchofrontal sinus (**Figure 1**, see label 15) [11, 13].

In cattle and buffalo, the frontal sinus extends rostrally to the level of the middle of the third molar tooth at the level of rostral half of orbital rim, which is represented by the nasofrontal suture in the macerated skull. The caudal boundary of the sinus is the nuchal line of occipital bone. The sinus extends laterally to the medial boundary of the orbital rim and temporal line. In turn the cranial cavity bulges into the central
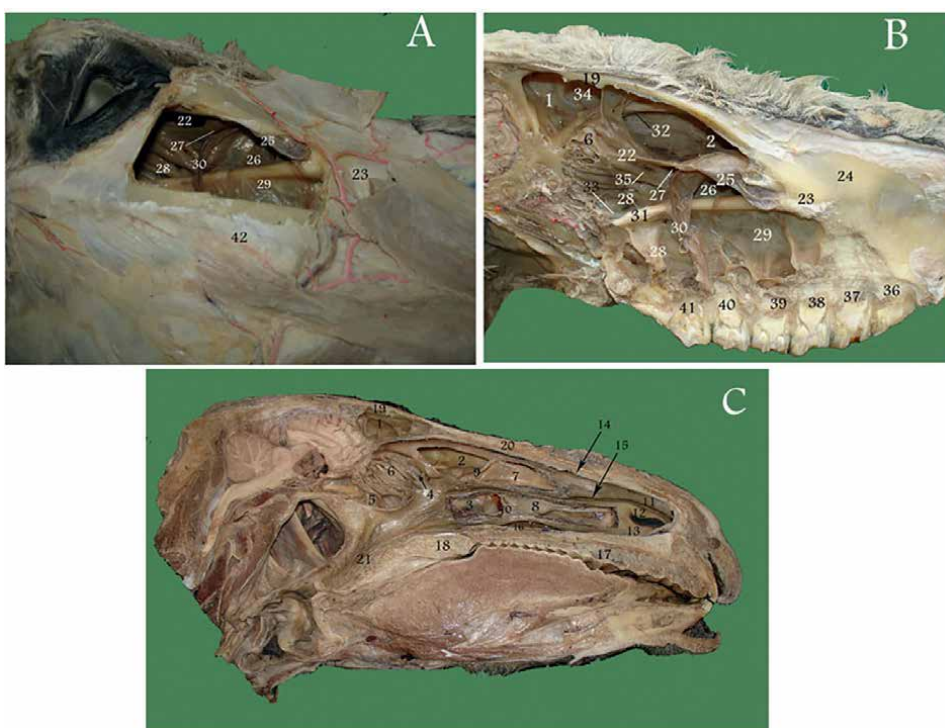
Figure 2.
Sagittal sections of the donkey head. 1. Frontal sinus. 2. Dorsal Conchal sinus. 3. Ventral Conchal sinus. 4. Middle Conchal sinus. 5. Sphenopalatine sinus. 6. Ethmoidal turbinate. 7. Bulla of the dorsal nasal concha. 8. Bulla of the ventral nasal concha. 9. Septum of ventral nasal concha. 10. Septum of dorsal nasal concha. 11. Straight fold. 12. Alar fold. 13. Basal fold. 14. Dorsal nasal meatus. 15. Middle nasal meatus. 16. Ventral nasal meatus. 17. Hard palate. 18. Soft palate. 19. Frontal bone. 20. Nasal bone. 21. Pharynx. 22. Frontomaxillary opening. 23. Infraorbital nerve. 24. Maxillary bone. 25. Bulla of ventral nasal Conchal sinus. 26. Conchomaxillary opening. 27. Nasomaxillary opening. 28. Lateral part of caudal maxillary sinus. 28′. Medial part of caudal maxillary sinus. 29. Rostral maxillary sinus. 30. Maxillary septum. 31. Infraorbital canal. 32. Nasolacrimal duct. 33. Sphenopalatine opening. 34. Frontal septum. 35. Opening of middle nasal Conchal sinus into caudal maxillary sinus. 36.1st maxillary premolar tooth; 37. Second maxillary premolar. 38. 3rd maxillary premolar. 39. 1st maxillary molar tooth. 40. 2nd maxillary molar tooth. 41. 3rd maxillary molar tooth. 42. Facial crest. Reproduced with permission [13] journal of veterinary anatomy.
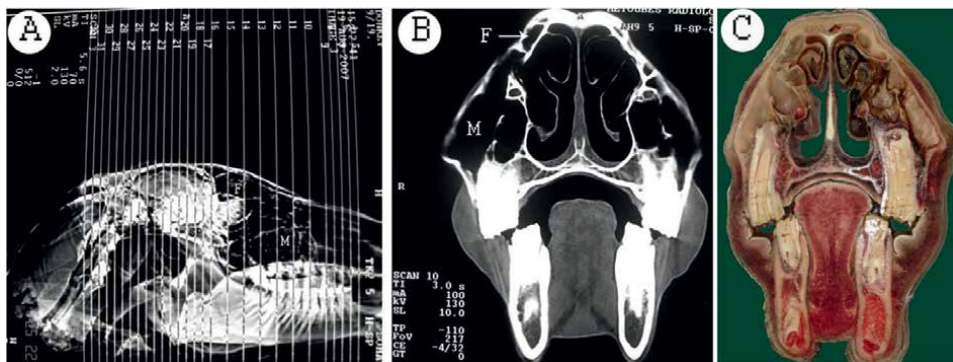
Figure 3.
Sinus anatomy in the donkey. (A) Lateral CT scan shows the levels of the section and paranasal sinus. (B) CT at the level of the second cheek tooth maxillary sinus and frontal sinus. (C) Cross section at head) showing the frontal sinus (F). Maxillary sinus (M). Sphenopalatine sinus (SP). Adapted with permission [11].

part of the frontal sinus. The sinus cavity is subdivided into several compartments; these vary in size and differ in position between differing animals and also from left and right sinus [4]. The frontal sinus cavity is divided by an oblique transverse septum creating the rostral and caudal sinuses. The rostral sinus is subdivided into several small lateral, medial and intermediate compartments by the presence of two irregular oblique longitudinal and transverse septa. The rostral sinus compartments all communicate separately with the ethmoidal meatus and rostrally with the dorsal nasal sinus via a nasofrontal opening [4]. One part of the dorsal nasal concha projects caudally between the medial and intermediate rostral sinuses, in addition the lateral rostral sinus is separated by a thin septum from the lacrimal sinus. The caudal sinus is subdivided into the large caudolateral and small rostromedial sinuses by an incomplete oblique transverse septum, the two latter are also able to communicate with each other. An oblique frontal transverse septum divides the caudolateral sinus into two sub-compartments, of which the caudolateral part is separated from nuchal diverticulum by an oblique transverse septum. The caudolateral sinus cavity has three diverticula: the nuchal, cornual and postorbital diverticula. The nuchal diverticulum is more extensive due to the well-developed parietal bone, and is itself subdivided into four sub-compartments. The cornual diverticulum extends into the cornual process of the frontal bone, and is subdivided by a septum [2]. The postorbital diverticulum is located medially, caudal to the orbital cavity, and dorsal to the cranial cavity, and occupies the space between the orbital cavity and rostral frontal small compartments. The relatively short supraorbital canal passes through the lateral border of the caudal frontal sinus through an apparently bony septum. The caudal frontal sinus opens up in the ethmoidal meatus (**Figures 4**-**6**).

In the camel, each frontal sinus is subdivided by bony plates into six large compartments; two caudal, two lateral and two rostral, surrounding eight small compartments that communicate with the nasal fundus through small openings. The supraorbital canal is traverse to the large caudolateral compartment where the supraorbital foramen is present (**Figure 7**) [6].

In sheep and goats, each frontal sinus is subdivided into interconnected lateral and medial chambers, differing in size, by many bony plates. The medial chamber has only one elongated chamber, which contains no bony plates, communicating only with the middle part of the lateral chamber. Meanwhile the lateral chamber has three portions rostral, middle and caudal, and three diverticula nuchal, cornual and orbital [14]. The
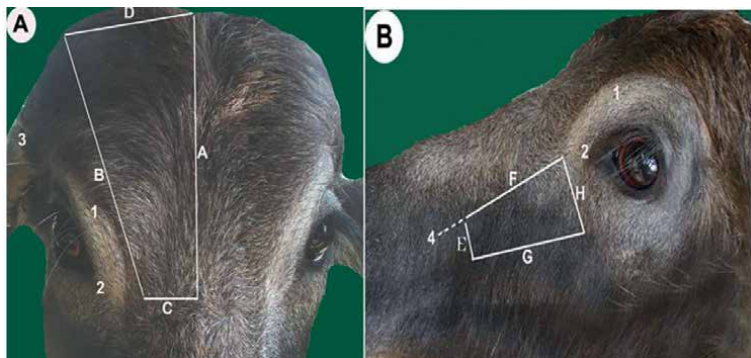
Figure 4.
Topography of the frontal and maxillary sinuses of the buffalo head (a& B). 1. Supraorbital foramen. 2. Medial angle of the eye. 3. Cornual process. 4. Infraorbital foramen. A. Medial limit of frontal sinus (Medline of the head). B. Lateral limit of frontal sinus. C. Rostral limit of frontal sinus. D. Caudal limit of frontal sinus. E. Rostral limit of maxillary sinus. F. Dorsal limit of maxillary sinus. G. Ventral limit of maxillary sinus. H. Caudal limit of maxillary sinus.
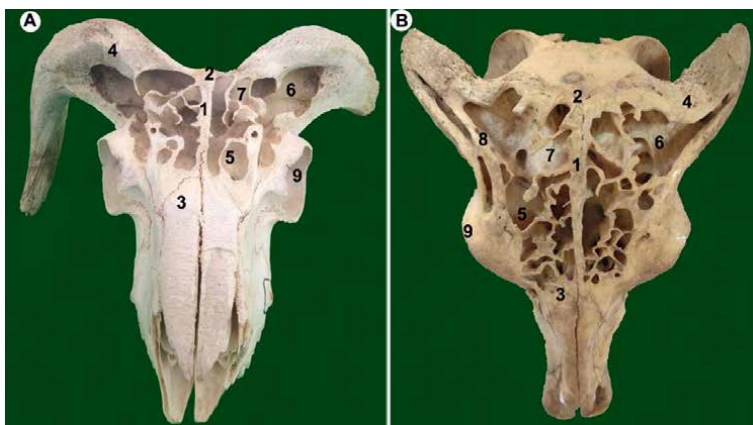
Figure 5.
Frontal surface of sheep (a) and buffalo (B) skulls showing the frontal sinuses. 1. Median interfrontal septum. 2. Parietal bone. 3. Nasal bone. 4. Cornual process of the frontal bone. 5. Postorbital diverticulum of the frontal sinus. 6. Cornual diverticulum of the frontal sinus. 7. Nuchal diverticulum of the frontal sinus. 8. Cornual septum. 9. Orbital cavity.

dorsal part of the lateral chamber communicates with the dorsal conchal sinus, the middle part communicates with the medial chamber and its caudal part communicates with the three frontal diverticula. The cornual diverticulum is the largest diverticula and is itself divided into a small dorsal part and a large ventral part by an oblique transverse septum [14]. The orbital diverticulum is surrounded by the orbital cavity dorsally and caudally, however, the nuchal diverticulum is the smallest one. The supraorbital canal meanwhile is a short canal, located at the longitudinal interfrontal septum between the lateral chamber and orbital diverticulum of each frontal sinus (**Figure 5**).

In the dog and cat, the paired frontal sinuses have open communication with the nasal cavity. The rostral frontal sinus lies between the median osseous septum of the frontal sinus and the orbit. The lateral frontal sinus is the largest of the frontal sinuses and extends into the zygomatic process of the frontal bone. The medial frontal sinus is very small and lies between the other two, occasionally it is absent.
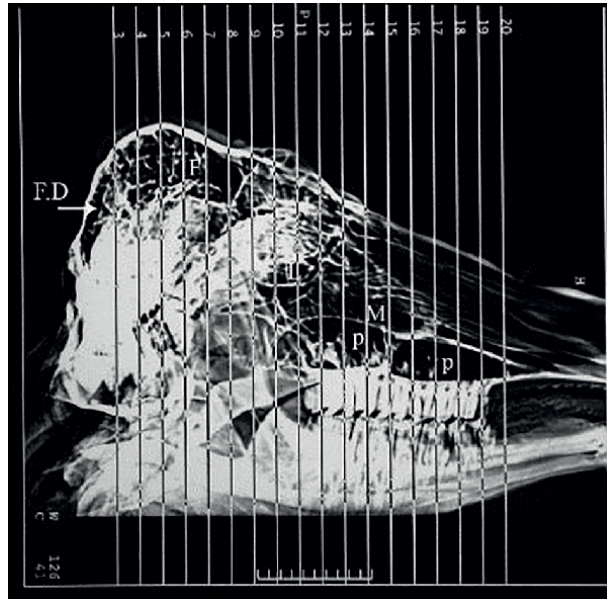
Figure 6.
Lateral CT scan shows the levels of the section and paranasal sinus in the buffalo. F. frontal sinus. C.D. Cornual diverticulum of frontal sinus. P. Palatine sinus. M. Maxillary sinus. L. Lacrimal sinus.

Figure 7.
Frontal surface of the camel skull showing the frontal sinuses.

2.2 The maxillary sinus

In the horse and donkey, the maxillary sinus divides into rostral and caudal compartments via a thin incomplete bony septum in the donkey or a complete septum in horse. The dorsal part of the septum was designed by the bulla of the ventral conchal

sinus. This septum angles obliquely caudally and its rostral aspect is varied in with regards to location; it usually crosses the roots of the second and third molar teeth, approximately 4–5 cm caudal to the rostral end of the facial crest. Most specimens have a septum measuring around 1.5 cm high, whilst the sinus can be 4–5 cm deep with bony spicules [11]. The caudal maxillary sinus is incompletely divided by the infraorbital canal into lateral and medial compartments. The canal also facilitates free communication between the two parts. Only the third maxillary molar tooth root embeds in the caudal maxillary sinus. The rostral and caudal maxillary sinuses connect with the middle nasal meatus via a slit-like nasomaxillary opening. The capacious caudal maxillary sinus appears larger than the smaller rostral maxillary sinus. The rostral maxillary sinus communicates with the ventral conchal sinus via the wide conchomaxillary opening dorsal to the infraorbital canal. The opening of which located at the level of the rostral part of the first molar tooth until the caudal part of the second molar tooth. The rostral maxillary sinus is around 4–5 cm long and 0.3–0.4 cm wide (**Figures 1**–**3**) [11, 13]. When CT imaged, the maxillary sinus is low in density but has high-density structures; the infraorbital canal, maxillary septum and bony spicules.

In cattle and buffalo, the maxillary sinus excavates into the maxillary and lacrimal bones. The sinus cavity is triangular in shape as the base is located caudally with a cranial apex behind the infraorbital foramen. The cavity extends rostrally towards the facial tuberosity at the level of the caudal border of the second premolar tooth. Around 2-3 cm ventral to the orbit and caudal to third molar tooth, the sinus continues caudally into the lacrimal bulla which has thinner walls and the zygomatic bone [4]. The dorsal limit of the cavity is determined by a line extending from the infraorbital foramen to the medial canthus of eye, while the ventral limit is around 1–2 cm above the alveolar border. Under computed tomography imaging, the more dense infraorbital canal and bony spicules of the maxillary sinus are observed. The maxillary sinus communicates with the caudal part of middle nasal meatus in common with the palatine sinuses through the nasomaxillary opening. This opening is positioned on the medial wall just ventral to the nasolacrimal canal, over the infraorbital canal and at around the midpoint between the orbit and facial tuber at a level from the first molar to third molar teeth. The maxillary and palatine sinuses communicate through an oval maxillopalatine opening, located above the infraorbital opening at a level from second premolar to the second molar teeth [4]. Caudally, it also communicates with the lacrimal sinus through maxillolacrimal opening. There is a rostral crest within the maxillary sinus (**Figure 4**).

In camels, the maxillary sinus is in an excavation of a small part of the maxillary bone and the rostral part of the zygomatic bone. The maxillary sinus extends towards the level of the rostral border of the third upper cheek tooth. The medial boundary is formed by the osseous nasolacrimal canal and it communicates dorsally with the lacrimal sinus and with the caudal part of the middle nasal meatus via the nasomaxillary opening which in turn is partly covered by the lateral part of the dorsal conchal sinus [6].

In sheep and goats, the maxillary sinus is located in a triangular excavation of the maxillary bone and rostral part of the zygomatic bone. The sinus extends to the level of the rostral border of the third upper cheek tooth and rostral to the facial tuberosity. The sinus is incompletely separated by the infraorbital canal, therefore presenting as a smaller dorsomedial part and a larger ventrolateral part, [14]. Caudally, the sinus become larger and extends by the lacrimal bulla. This lacrimal bulla presents as dorsal and ventral orbital diverticula inside the orbital cavity. The sinus communicates dorsally with the lacrimal sinus by the maxillolacrimal opening, whilst the caudal section of the sinus communicates with the palatine sinus via the maxillopalatine opening on the medial side of the infraorbital canal. In addition, the sinus communicates with

the caudal part of the middle nasal meatus via the nasomaxillary opening which is partially covered by the lateral part of the dorsal nasal conchal sinus at the level of the fourth cheek tooth (**Figure** 5) [14].

In the dog and cat, in contrast to the other domestic mammals, the canine maxilla has no paranasal sinus, but rather a laterally directed outpouching, the maxillary recess.

2.3 The sphenoidal sinus

In the horse and donkey, the sphenoidal and palatine sinuses communicate with each other. The sphenopalatine sinuses are excavated into the palatine and sphenoid bones ventromedial to the orbit and ventral to forebrain [11]. There is a septum separating the left and right sphenoidal sinuses, however, it is not frequently in the midline. The dorsal and lateral walls of the sphenopalatine sinus are thin. The sinus communicates with the caudal maxillary sinus via the sphenopalatinal opening, which is the most caudal opening of the maxillary sinus. The opening itself appears sagittal oblique and is located between the caudal origin of the infraorbital canal and the pterygopalatine fossa, caudal to the last molar tooth roots (**Figure 2** structures 5 and 33 [13]).

In cattle and buffalo, the sphenoid sinus is shallow and excavated in the body and wing of the sphenoid bone [4]. The right and left sinuses are divided by a septum forming unequal small parts, the rostral canal and caudal cavity. It opens into the ethmoidal meatus via the nasosphenoidal opening.

In camels, the sphenoidal sinus is in a cavity within the body and wing of the sphenoidal bone. The sinus contains bony plates which subdivide it into small compartments, which alongside the frontal sinus compartments encircle the cranial cavity [6]. The sphenoidal sinus opens directly into the nasal fundus through the nasosphenoidal opening [6].

In the dog and cat, in some cases a sphenoidal sinus develops but not always.

2.4 The ethmoidal sinus

In cattle and buffalo, the ethmoidal cells are small cavities in the medial wall of the orbit [4]. The ethmoid bone forms the medial wall whereas their lateral walls are formed by the frontal, palatine and the wing of presphenoid bones. The ethmoidal cells open into the ethmoidal meatus.

In camels, the ethmoidal sinus is apparent in the ethmoid labyrinths. It communicates directly with the ethmoidal meatus into the nasal fundus [6].

In sheep and goats, the ethmoidal sinus is located at the nasal fundus part of the nasal cavity [14]. The ethmoidal sinus is apparent in the five triangular projections of the ethmoidal labyrinths. It communicates directly with the ethmoidal meatus into the nasal fundus.

2.5 The lacrimal sinus

In cattle and buffalo, the lacrimal sinus is a small excavation in the lacrimal and frontal bones rostromedial to the orbit. The lacrimal bones forms the lateral wall and the lateral mass of the ethmoidal bone forms the medial wall. The sinus cavity is not divided by osseous plates and the nasolacrimal canal traverses its lateral wall. It communicates with the maxillary sinus via maxillolacrimal opening (**Figures** 5 and **6**).

In camels, the lacrimal sinus is occupies a small cavity in the lacrimal bone rostromedial to the orbit. The lacrimal bone forms the lateral wall, while the lateral mass of

	Horse and donkey	Cattle/buffalo	Sheep and goat	Camel	Dog
Maxillary	+	+	+	+	Recess
Frontal	+	+	+	+	+
Lacrimal	—	+	+	+	—
Palatine	—	+	+	+	—
Sphenoid	—	+	—	—	—
Sphenopalatine	+	—	—	—	—
+ *Present. -Absent.*					

Table 1.
The paranasal sinuses in a range of mammals.

the ethmoidal bone forms the medial wall. The lacrimal sinus is separated rostrally from the maxillary sinus by the nasolacrimal canal and it communicates with the maxillary sinus via the maxillolacrimal opening, just anterior to the orbital cavity at the level of third cheek tooth [6].

In sheep and goats, the lacrimal sinus is occupies a small cavity in the lacrimal bone rostromedial to the orbit. The lateral wall is formed by the lacrimal bone, while the medial wall is formed by the lateral border of the dorsal lamellae of the ventral nasal conchae [14]. It is separated rostrally from the maxillary sinus by the nasolacrimal canal and communicates with the maxillary sinus via the maxillolacrimal opening just anterior to the orbital cavity at the level of the third cheek tooth (**Figure 5**).

2.6 The palatine sinus

In cattle and buffalo, the palatine sinus appears larger than the maxillary sinus and is located within the horizontal part of the palatine bone and the palatine process of maxillary bone. The right and left palatine sinuses are separated by a median interpalatine septum, which is undulant caudally. The sinus extends from the caudal border of the palatine bone and rostral border of the orbit roughly 2 cm caudal to the third molar tooth to around 3–4 cm rostral to the first premolar teeth [4]. The sinus cavity contains an incomplete transverse bony crest which arises from the floor of sinus and subdivides the sinus into two unequal compartments. The caudal part of the sinus is traversed obliquely by the infraorbital canal that divides it into medial and lateral compartments. The palatine sinus communicates with the maxillary sinus via a maxillopalatine opening over the infraorbital canal (**Figure 6**).

In sheep and goats, the palatine sinuses are located within the horizontal part of the palatine bone and the palatine process of the maxillary bone, and it is the smallest sinus. The right and left palatine sinuses are separated by a median inter-palatine septum [14]. The sinus extends from the caudal border of the palatine bone and rostral border of the orbit caudal to the third molar tooth. The palatine sinus communicates with the maxillary sinus by the maxillopalatine opening over the infraorbital canal (**Table 1**) [3].

Conflict of interest

The authors declare no conflict of interest.

Author details

Mohamed A.M. Alsafy[1], Samir A.A. El-Gendy[1] and Catrin Sian Rutland[2]*

1 Faculty of Veterinary Medicine, Department of Anatomy and Embryology, Alexandria University, Egypt

2 Faculty of Medicine, School of Veterinary Medicine and Science, University of Nottingham, UK

*Address all correspondence to: catrin.rutland@nottingham.ac.uk

IntechOpen

References

[1] Budras KD et al. Bovine Anatomy: An Illustrated Text. Germany: Schlütersche Gmbh & Colorado. KG Verlag Und Druckerei; 2004

[2] Dyce KM, Sack WO, Wensing CJG. Textbook of Veterinary Anatomy. 4th ed. USA: Saunders; 2009

[3] Budras KD et al. Anatomy of the Horse. 6th ed. Germany: Schluetersche; 2012

[4] Alsafy M, El-Gendy S, El Sharaby A. Anatomic reference for computed tomography of paranasal sinuses and their communication in the Egyptian buffalo (Bubalus bubalis). Anatomia, Histologia, Embryologia. 2013;**42**(3):220-231

[5] Dyce KM, Sack WO, Wensing CJG. Textbook of Veterinary Anatomy. USA: Saunders; 2010

[6] Alsafy MA, El-gendy SA, Abumandour M. Computed tomography and gross anatomical studies on the head of one-humped camel (Camelus dromedarius). The Anatomical Record. 2014;**297**(4):630-642

[7] Ahmed AS, Shokry M, El-Keiey M. Contribution to the paranasal sinuses of the one humped camel (Camelus dromedarius). Anatomia, Histologia, Embryologia. 1985;**14**:221-225

[8] Bai ZT, et al. The Computed Tomography and Gross Anatomies of Nasal Cavity and Sinuses in the Bactrian Camel (Camelus bactrianus). 2008. Available from: http://en.paper.edu.cn/en_releasepaper/downPaper/200812-184

[9] Saber AS. Radiographic anatomy of the dromedary skull (Camelus dromedarius). Veterinary Radiology. 1990;**31**(10):161-164

[10] De Zani DS et al. Topographic comparative study of paranasal sinuses in adult horses by computed tomography, sinuscopy, and sectional anatomy. Veterinary Research Communications. 2010;**34**(Suppl. 1): S13-S16

[11] El Gendy SAA, Alsafy MAM, El Sharaby AA. Computed tomography and sectional anatomy of the head cavities in donkey (Equus asinus). Anatomical Science International. 2014;**89**(3):140-150

[12] Probst A, Henninger W, Willmann M. Communications of normal nasal and paranasal cavities in computed tomography of horses. Veterinary Radiology & Ultrasound. 2005;**46**(1):44-48

[13] El-Gendy SAA, Alsafy MAM. Nasal and paranasal sinuses of the donkey: Gross anatomy and computed tomography. Journal of Veterinary Anatomy. 2010;**3**(1):25-41

[14] Alsafy M et al. Anatomical description of the head in Ossimi sheep: Sectional anatomy and computed tomographic approach. Morphologie. 2021;**105**(348):29-44

Chapter 3

Biomechanics of the Canine Elbow Joint

Thomas Rohwedder

Abstract

The canine elbow joint is a complex joint, whose musculoskeletal anatomy is well investigated. During the last 30 years kinematic analysis has gained importance in veterinary research and kinematics of the healthy and medial coronoid disease affected canine elbow joint are progressively investigated. Video-kinematographic analysis represents the most commonly used technique and multiple studies have investigated the range of motion, angular velocity, duration of swing and stance phase, stride length and other kinematic parameters, mostly in the sagittal plane only. However, this technique is more error-prone and data gained by video-kinematography represent the kinematics of the whole limb including the soft tissue envelope. A more precise evaluation of the in vivo bone and joint movement can only been achieved using fluoroscopic kinematography. Based on recent studies significant differences in the motion pattern between healthy joints and elbows with medial coronoid disease could be detected. Thereby not only adaptive changes, caused by pain and lameness, could be described, but primary changes in the micromotion of the joint forming bones could be found, which potentially represent new factors in the pathogenesis of medial coronoid disease. This chapter gives a review of current literature on elbow joint kinematics, with particular focus onto pathologic biomechanics in dysplastic canine elbows.

Keywords: elbow, elbow dysplasia, canine, biomechanics, kinematics, joint disease, medial coronoid disease, joint contact

1. Introduction

The canine elbow joint is a complex joint, whose musculoskeletal anatomy is well investigated. However, the in vivo function of the elbow joint, the individual movement of the humerus, radius and ulna relative to each other and the load distribution within the joint is still subject of present and future research. Especially pathophysiological motion of the elbow joint, leading to a mechanical overload of certain joint compartments, is not well understood and an interesting field of present veterinary research. Canine developmental elbow disease (DED), in particular medial coronoid disease (MCD), is one of the most common reasons for forelimb lameness in the dog and therefore this topic has not only academic, but also clinical relevance.

2. Anatomical basics

The canine elbow joint is composed of the humerus proximally and the radius and ulna distally, and can be divided into three joint compartments: the humero-ulnar, humero-radial and proximal radio-ulnar joint [1, 2]. The humero-ulnar joint is formed by the humeral trochlea and intercondylar region of the condyle and the ulnar trochlear notch, which extends from the anconeal process to the radial incisure, and continues to the medial coronoid process of the ulna. The humero-radial joint is formed by the capitulum of the humeral condyle and the radial head. The radial incisure and the medial aspect of the radial head form the proximal radio-ulnar joint. Altogether the elbow joint acts as a hinge joint (ginglymus) with extension and flexion being the main motion pattern and some amount of pronation and supination, mainly taken over by the radio-ulnar joint [1].

In healthy canine elbows the radio-ulnar joint shows a congruent shape without any step formation between the ulnar and radial joint surface, at least under static conditions. However, the humero-ulnar joint is not perfectly congruent even in healthy dogs [3–6]. The radii of curvature of the humeral condyle and ulnar trochlear notch show different values along their curvilinear course, resulting in reduced contact in the central notch region [3–7]. The trochlear notch shows a slightly elliptical shape, so that the anconeal process and distal aspect of the notch as well as the coronoid process are in contact with the humeral condyle. This kind of physiological humero-ulnar incongruence was first described in humans and could be detected in the canine elbow joint, too [4–6, 8, 9].

The maximum range of motion (ROM) varies between 110 to 150 degrees, with breed-specific maximum flexion of 25 to 49 degrees and maximum extension of 155 to 175 degrees [10–14]. The main extensor muscle of the elbow joint is the triceps brachii muscle [1]. Further this muscle prevents flexion of the elbow during the stance phase. The anconeal and tensor fasciae antebrachii muscles are additional extensors of the elbow joint. Flexion is performed by the biceps brachii and brachial muscles. The extensor carpi radialis muscle contributes to flexor function to some amount. The canine antebrachium can be pronated 17 to 50 degrees and supinated 31 to 70 degrees [10, 15]. The supinator and brachioradial muscles are responsible for supination of the antebrachium. The latter contributes only minimal to supination and is missing in some individuals [16]. The pronator teres and pronator quadratus muscles are responsible for pronation and the pronator teres muscle is supposed to contribute to elbow joint flexion as well [1, 2].

Four ligaments support the elbow joint: the medial and lateral collateral ligament, the annular ligament and interosseous ligament/interosseous membrane [1, 2]. The medial and lateral collateral ligaments origin from the medial and lateral humeral epicondyle. The medial collateral divides into two crura. The cranial one is weaker and attaches at the radius, while the stronger caudal one attaches mainly at the ulna and to some amount at the radius. The lateral collateral ligament consists of two crura as well. The cranial part attaches to the radius, and the caudal part attaches to the ulna and colligates with the annular ligament, which can contain a sesamoid bone [2]. The annular ligament runs transversely around the radial head spanning from the lateral to the medial aspect of the radial incisure of the ulna. It runs underneath the medial and lateral collateral ligaments. The radius and ulna are further attached to each other by the interosseous ligament and interosseous membrane, which spans the interosseous space. Distally the radius and ulna are connected to each other by the radioulnar ligament.

3. Elbow joint kinematics

3.1 Kinematic analysis

Kinematics describe the motion of body segments without measuring the forces acting onto that segments. Kinematic analysis allows evaluation of the range of motion, angular velocities, segmental velocities of each portion of the limb, stride frequency and stride length [17]. Depending on the technique used for the kinematic analysis, motion of bones and joints can be measured with a submillimeter accuracy [18–20].

Generally two forms of kinematic analysis can be differentiated: the video-kinematography, based on a video motion capture system, and the radiostereometric kinematic analysis (RSA), based on a radiographic system, coupled with high speed video cameras. Video motion capture kinematic systems use skin markers, attached to specific body areas, which are tracked in the generated videos of the moving animal and allow for calculation of the aforementioned parameters. Radiostereometric analysis can be marker based or performed without bone markers [21–30]. Furthermore, both kinematic analysis systems can be used to evaluate motion in the two or three dimensional (2D, 3D) space, depending on the technical setup [17].

The most commonly used technique is a video motion capture system based analysis. This technique is non-invasive and allows for evaluation of overall limb, limb segment or body segment motion. However, skin mounted markers do not match exactly the movement of the underlying bones. Movement of the soft tissues results in skin motion artifacts [21, 28, 31–35], with a difference of 0.4 to 1.2 cm between the skin marker and respective underlying bony landmark in small animals [33]. Especially in the proximal joints of the forelimb skin marker based data differ significantly from fluoroscopically gained kinematic data [28]. Comparison of biplanar fluoroscopy and video-kinematography in hindlimb kinematics revealed significant differences between both techniques, too [21]. Skin marker based data tend to project different trajectories and smaller amplitudes compared to fluoroscopic kinematography with particularly contradictory results, especially in proximal joints, where increased soft tissues can be found [21].

Radiostereometric analysis, also called fluoroscopic kinematography, allows for the most accurate kinematic data acquisition [19, 21–24, 28, 30]. One or two fluoroscopic units, coupled with high speed video cameras, take x-ray movies of the moving object. Based on these x-ray movies bone movement can be calculated and transferred onto 3D bone models generated from CT scans of the individual animal. Bone motion analysis can be performed using implanted bone markers, which are tracked in one (uniplanar, 2D evaluation) or both (biplanar, 3D evaluation) x-ray movies and 3D coordinates of each marker are then transferred onto the 3D bone models. Alternatively, scientific rotoscoping or autoscoping techniques can be used to track bone movement and transfer this in vivo bone motion from the fluoroscopic images onto 3D bone models [18, 20, 36]. These techniques do not rely on bone markers, rather the shape and edges of each bone are used to project digitally reconstructed radiographs (DRR), generated from the CT scans of each bone, onto the respective bone in the fluoroscopic image. By that the 3D bone model is aligned and animated along the x-ray movies. Scientific rotoscoping is performed manually, while autoscoping is a completely computerized process. Both techniques can be described as morphology based methods of motion analysis. Marker based tacking is the gold standard of kinematic analysis with an accuracy of 0.1 mm and 0.1 degrees [20].

However, scientific rotoscoping and autoscoping show a high accuracy as well, with values ranging from 0.16 to 0.66 mm in translation and 0.43 to 2.78 degrees rotation for scientific rotoscoping and 0.07 to 1.13 mm translation and 0.01 to 3.0 degrees rotation for autoscoping [18, 37–42]. Therefore, both techniques result in a highly precise evaluation of bone and joint motion with a substantially reduced invasiveness compared to a bone marker based analysis.

Multiple studies have investigated elbow joint kinematics in healthy dogs and dogs with different joint pathologies. Results have to be interpreted cautiously due to varying breeds, different technical setups and varying gaits and gait velocities, e.g. the walk or the trot, all of which influencing the kinematic pattern. **Table 1** gives an overview of previous studies on canine forelimb and elbow joint kinematics.

Study	Technique	Breed	Number of dogs	Gait/Speed
DeCamp et al. [43]	3D marker based video-kinematography, 2D evaluation (sagittal motion)	Greyhound	8	trot, 1.8–2.3 m/s (walkway)
Allen et al. [44]	3D marker based video-kinematography, 2D evaluation (sagittal motion)	Mixed breed dogs	14	trot, 1.8–2.3 m/s (overground)
Hottinger et al. [45]	3D marker based video-kinematography, 2D evaluation (sagittal motion)	Different large breed dogs	15	walk, 0.9–1.1. m/s (overground)
Gillette and Zebas [46]	Uniplanar marker based video-kinematography, 2D evaluation (sagittal motion)	Labrador Retriever	16	trot, 2.8 m/s
Nielsen et al. [47]	3D marker based video-kinematography, 2D evaluation (sagittal motion), stance phase only	Mixed breed dogs	6	walk, 0.8–1.0 m/s (overground)
Owen et al. [48]	Uniplanar marker based video-kinematography, 2D evaluation (sagittal motion)	Greyhound	11	trot, 2.2–2.4 m/s (treadmill)
Clements et al. [49]	Uniplanar marker based video-kinematography, 2D evaluation (sagittal motion)	Labrador Retriever	10	trot, 2.0 m/s (treadmill)
Feeney et al. [50]	Uniplanar marker based video-kinematography, 2D evaluation (sagittal motion)	Labrador Retriever	10	walk, velocity not documented (overground)
Burton et al. [51]	3D marker based video-kinematography, 2D evaluation (sagittal motion)	Different mid to large breed dogs	7 (unilateral elbow disease)	trot, velocity not documented (treadmill)

Study	Technique	Breed	Number of dogs	Gait/Speed
Holler et al. [52]	3D marker based video-kinematography, 2D evaluation (sagittal motion)	Different mid to large breed dogs	8	walk, 0.89–1.1 m/s (treadmill, normal, uphill, downhill, obstacle)
Agostinho et al. [53]	3D marker based video-kinematography, 2D evaluation (sagittal motion)	Labrador Retriever Rottweiler	20 (10 each)	trot, 2.1–2.2. m/s (treadmill)
Guillou et al. [54]	3D marker based fluoroscopic kinematography	Fox hound	4	walk & trot, velocity not documented
Angle et al. [55]	Uniplanar marker based video-kinematography, 2D evaluation (sagittal motion)	Greyhound	7	Movement initiation up to 3.52 m/s (overground)
Jarvis et al. [56]	3D marker based video-kinematography, 2D evaluation (sagittal motion), stance phase only	Different breeds	40 (24 healthy, 16 front limb amputee dogs)	trot, 2.2–2.6 m/s (walkway)
Brady et al. [57]	3D marker based video-kinematography, 2D evaluation (sagittal motion)	Different breeds	16	trot, 1.8 m/s & 2.5 m/s (walkway)
Miqueleto et al. [58]	3D marker based video-kinematography, 2D evaluation (sagittal motion)	German Shepherd	20 (10 hip dysplasia, 10 healthy dogs)	trot, 2.1–2.2. m/s (treadmill)
Galindo-Zamora et al. [59]	3D marker based video-kinematography, 2D evaluation (sagittal motion)	Different mid to large breed dogs	20 (unilateral elbow disease)	walk, 0.65–1.1 m/s (treadmill)
Caron et al. [60]	3D marker based video-kinematography, 3D evaluation	Labrador Retriever	26 (13 healthy, 13 dogs with coronoid disease)	walk, 0.7 m/s (treadmill)
Fischer & Lilje, [61]	3D marker based video- & fluoroscopic kinematography, 2D evaluation (sagittal motion)	32 different breeds	327	walk & trot, 0.54–5.56 m/s (treadmill)
Catavitello et al. [62]	Uniplanar marker based video-kinematography, 2D evaluation (sagittal motion)	Labrador Retriever Golden Retriever	6 (3 each breed)	walk, 2 m/s, trot, 4 m/s & running, 9.5 m/s (overground)
Duerr et al. [63]	Uniplanar marker based video-kinematography, 2D evaluation (sagittal motion) and inertial measurements unit	Different mid to large breed dogs	16	trot, 2.4–2.5 m/s (overground)

Study	Technique	Breed	Number of dogs	Gait/Speed
Andrada et al. [28]	3D marker based video- & fluoroscopic kinematography (scientific rotoscoping), 3D evaluation	Beagle	5	walk, 0.98 m/s & trot, 2.2 m/s (treadmill)
Lorke et al. [64]	3D marker based video-kinematography, 2D evaluation (sagittal motion)	Beagle	10	trot, 1.7–1.8 m/s (treadmill)
Rohwedder et al. [22]	3D marker based fluoroscopic kinematography (first third of stance phase only)	Different mid to large breed dogs	11 (5 healthy, 6 dogs with coronoid disease)	walk, 0.6–0.9 m/s (treadmill)
Kopec et al. [65]	Uniplanar marker based video-kinematography, 2D evaluation (sagittal motion)	Different mid to large breed dogs	8	walk, 1.01–1.45 m/s (overground & stair exercise)
Rohwedder et al. [23]	3D marker based fluoroscopic kinematography (first third of stance phase only)	Different mid to large breed dogs	11 (5 healthy, 6 dogs with coronoid disease)	walk, 0.6–0.9 m/s (treadmill)
Rohwedder et al. [24]	3D marker based fluoroscopic kinematography & joint contact pattern evaluation	Labrador Retriever	1 (before and after DPUO[*])	walk, 0.6–0.9 m/s (treadmill)
Humphries et al. [66]	3D marker based video-kinematography, 2D evaluation (sagittal motion)	Labrador Retriever German Shepherd	24 (12 each breed)	trot, 2.19–2.45 m/s (walkway)
De Souza et al. [67]	3D marker based video-kinematography, 2D evaluation (sagittal motion)	American Pit Bull Terrier	11	walk, 1.17 ± 0.17 m/s trot, 2.04 ± 0.33 m/s (overground)

[*]*DPUO: dynamic proximal ulnar osteotomy.*

Table 1.
Summary of studies investigating canine forelimb and/or elbow joint kinematics.

3.2 The healthy elbow joint

Most studies on elbow joint kinematics are based on video-kinematographic analysis and have investigated the motion of the elbow only in the sagittal plane [43–45, 47–53, 55–59, 62, 63, 65, 68, 69]. Caron et al. were the first to describe the real 3D kinematics of the canine forelimb of healthy Labrador retrievers and dogs with medial coronoid disease using video-kinematographic analysis [60]. Another study evaluated the 3D motion of orthopedic healthy canine forelimbs using video-kinematography and compared that data to fluoroscopically gained motion analysis, which was additionally calculated in one of the dogs [28].

One complete gait cycle consists of the swing and the stance phase. The swing phase starts when the paw breaks contact with the ground and ends with first ground

contact of the paw. The time between initial ground contact and paw lift is defined as the stance phase. The ratio between swing and stance phase depends from the gait pattern and the dog's velocity [28, 29, 70, 71]. At the walk the swing phase of the forelimb accounts for 39 to 43% of the whole gait cycle [60] and increases to approximately 50% to two thirds of the whole gait cycle during the trot, depending from the trotting speed [28, 43, 45, 58, 62, 64, 66]. During running the swing phase is further prolonged and accounts for approximately 75% of the gait cycle [62]. Conversely, with increasing speed the stance phase decreases [45, 70, 71].

The sagittal plane range of motion of the elbow joint (flexion-extension) is between 48.1 degrees and 70 degrees during one complete gait cycle when the dog is moving on a flat surface (**Table 2**), with the majority of motion occurring during the swing phase [28, 43–45, 47–50, 52, 53, 56–61, 63–67]. Range of motion is influenced by different parameters like breed, limb and body segment length, gait, velocity, exercise, age, contralateral limb amputation and concurrent orthopedic disease. With increasing speed of the gait the range of motion of joints increases [29, 45, 57, 62, 66, 68, 69]. Obese dogs show an increased range of motion as well, especially during the stance phase [57]. However, increasing age leads to an decrease in total range of motion, even in orthopedic healthy dogs [64]. Further, different exercises like descending stairs, uphill and downhill walking influence the range of motion, with descending stairs, obstacle exercises and uphill walking increasing the range of motion, while downhill walking decreases the amount of sagittal motion in the elbow [52, 65].

Study	Breed	Range of motion (°)	Flexion/Extension (°)	Gait/Speed
DeCamp et al. [43]	Greyhound	53.7	86.8/140.5	trot, 1.8–2.3 m/s (walkway)
Allen et al. [44]	Mixed breed dogs	55.8	93.7/149.5	trot, 1.8–2.3 m/s (overground)
Hottinger et al. [45]	Different large breed dogs	48.1	—	walk, 0.9–1.1. m/s (walkway)
Gillette and Zebas [46]	Labrador Retriever	right: 69.1 left: 66.1	—	trot, 2.8 m/s
Nielsen et al. [47]	Mixed breed dogs	—	111.7 ± 12/136.3 ± 10.4 (stance phase only)	walk, 0.8–1.0 m/s (overground)
Owen et al. [48]	Greyhound	49.35–49.59	100.98–102.7/150.57–152.05	trot, 2.2–2.4 m/s (treadmill)
Clements et al. [49]	Labrador Retriever	59.3 (SD 5.5)	—	trot, 2.0 m/s (treadmill)
Feeney et al. [50]	Labrador Retriever	54.8 ± 17.9	91.4/146.3	walk, velocity not documented(overground)
Holler et a. [52]	Different mid to large breed dogs	normal: 52.9 ± 7.0 uphill: 54.2 ± 7.4 downhill: 43.1 ± 5.8 obstacle: 57.0 ± 6.9	—	walk, 0.89–1.1 m/s (treadmill, normal, uphill, downhill, obstacle)

Study	Breed	Range of motion (°)	Flexion/Extension (°)	Gait/Speed
Agostinho et al. [53]	Labrador Retriever Rottweiler	63.77 ± 4.83 54.86 ± 5.16	90.52 ± 11.66/154.28 ± 9.64 93.99 ± 10.19/148.85 ± 9.15	trot, 2.1–2.2. m/s (treadmill)
Jarvis et al. [56]	Different breeds	stance phase only: control: 33.3 ± 8.6 amputee: 39.7 ± 10.4	control: 123.0 ± 12.9/ 156.4 ± 12.2 amputee: 119.2 ± 12.8/ 158.9 ± 12.5	trot, 2.2–2.6 m/s (walkway)
Brady et al. [57]	Different breeds	lean: 52.5 (1.8 m/s) obese: 65.0 (1.8 m/s) lean: 54.0 (2.5 m/s) obese: 62.0 (2.5 m/s)	lean: 95 ± 7/147 ± 17 obese: 90 ± 11/155 ± 9 lean: 93 ± 8/147 ± 9 obese: 88 ± 14/150 ± 18	trot, 1.8 m/s & 2.5 m/s (walkway)
Miqueleto et al. [58]	German Shepherd	healthy: 68.15 ± 7.19 hip dysplasia: 63.54 ± 13.53	healthy: 61.99/131.77 ± 7.60 hip dysplasia: 69.09/133.68 ± 11.37	trot, 2.1–2.2. m/s (treadmill)
Galindo-Zamora et al. [59]	Different mid to large breed dogs	healthy: 54.18 ± 8.62 MCD: 51.45 ± 7.27	healthy: 82.36 ± 6.02/136.54 ± 9.16 MCD: 87.1 ± 10.8/138.55 ± 13.03	walk, 0.65–1.1 m/s (treadmill)
Duerr et al. [63]	Different mid to large breed dogs	63.4 ± 7.7	82.1 ± 8.6/145.5 ± 10.8	trot, 2.4–2.5 m/s (overground)
Lorke et al. [64]	Beagle	young: 68.8 ± 2.7 old: 62.9 ± 5.1	young: 83.2/152.0 ± 10.5 old: 76.8/139.6 ± 12.4	trot, 1.7–1.8 m/s (treadmill)
Kopec et al. [65]	Different mid to large breed dogs	flat: 65.81 desc. Stair: 80.43 desc. Ramp: 67.95	66.23/132.03 34.36/114.79 46.0/113.95	walk, 1.01–1.45 m/s (overground & stair exercise)
Humphries et al. [66]	Labrador Retriever German Shepherd	left: 70.63 right: 67.13 left: 67.13 right: 67.94	77.21/147.84 77.21/144.34 75.45/142.58 74.37/142.31	trot, 2.19–2.45 m/s (walkway)
De Souza et al. [67]	American Pit Bull Terrier	walk: 45.22 trot: 52.39	walk: 111.25/167.65 trot: 110.14/163.00	walk, 1.17 ± 0.17 m/s trot, 2.04 ± 0.33 m/s (overground)

Table 2.
Summary of the values for range of motion in sagittal plane and flexion and extension angles of the canine elbow joint from different kinematic studies. All values are expressed in degrees and were calculated, if necessary, based on data of each study to allow comparison between studies. 180 degrees represent maximum extension and 0 degrees maximum flexion.

The stance phase is mainly characterized by continuous extension of the elbow joint until lifting of the paw from the ground. Some studies have shown flexion of the elbow joint just after weight bearing [43, 45, 47, 53, 58, 60, 64], resulting in two peaks of extension during the gait cycle. The first peak of extension occurs during the late swing phase and the initiation of ground contact and a second peak occurs at the end of the stance phase. The amount of this flexion differs between studies by several degrees. Further, this movement has not been described using fluoroscopic kinematography, what represents the gold standard of kinematic gait analysis [28]. This might be due to breed and inter-individual differences in the gait, due to the different techniques used for kinematic analysis or due to a soft tissue artifact, which occurs with skin mounted markers, and does not represent the in vivo motion of the bony cubital joint, but the movement pattern of the complete limb including the soft tissues [28, 32, 33]. Maximum extension of the elbow joint is reached at the end of the stance phase and is followed by continuous flexion during the swing phase. The peak flexion of the elbow joint is reached at approximately the middle of the swing phase and is followed by continuous extension of the elbow joint as a preparation for paw strike [53, 60, 64].

Besides flexion and extension, which represent the main motion pattern of the elbow joint, supination and pronation of the antebrachium and abduction and adduction of the humerus and antebrachium occur during the regular locomotion. In healthy Labrador retrievers the antebrachium is positioned in mild supination at the initial stance phase and shows minimal pronation during the remainder stance phase with a mean supination of the antebrachium of 3 ± 9 degrees [60]. In healthy Beagle the forelimb is placed onto the ground in mild pronation and is kept in this position during two thirds of the stance phase and then externally rotated during the last third of stance [28]. During the initial swing phase the antebrachium is supinated and maximum supination (mean 19 ± 9 degrees) occurs at the middle of the swing phase, together with maximum flexion of the elbow joint, in healthy Labrador retrievers [60]. In orthopedic sound Beagle a similar motion pattern is present during the swing phase, with supination of the antebrachium occurring during the first third of the swing phase [28]. Prior to foot strike rapid pronation of the antebrachium occurs and the limb is placed on the ground in a slightly supinated position in Labrador retrievers and slight pronation in Beagle [28, 60].

Three dimensional micromotion of the humerus, radius and ulna relative to each other was measured in different studies using marker based fluoroscopic kinematographic analysis [22–24, 54, 72]. Results of these studies show that the bones of the antebrachium have a complex motion pattern and radius and ulna cannot be seen as one single object. At the walk and the trot an axial movement between radius and ulna occurs in healthy and MCD affected elbows [22, 54]. In healthy canine elbow joints the radius shows an mean axial movement of 0.7 (SD 0.31) mm to 0.8 mm in relation to the ulna. This axial motion was detected in different mid to large breed dogs, like Fox hounds, Australian shepherd, Labrador retriever, Eurasian, German shepherd, Bernese mountain dog and mixed breeds [22, 54]. After the initiation of ground contact the radius moves proximally and remains in a slightly elevated position relative to the ulna, resulting in a dynamic negative radio-ulnar incongruence (RUI) [22, 72]. These results correspond with data from an in vitro study, which investigated the effects of limb loading and flexion and extension onto the radio-ulnar joint conformation and intra articular contact areas and which showed, that elbow extension leads to a relative lowering of the ulna in relation to the radius [73]. Extension is the main

motion of the elbow during the weight bearing phase and therefore the induction of a dynamic negative RUI might be seen as a adaption to joint loading [72]. Further, internal and external rotation between the radius and ulna occurs during the walk. Prior to foot strike the radius is in an externally rotated position relative to the ulna und shows internal rotation during the first third of the stance phase. Mean range of motion of the in vivo internal-external radial rotation is 11.4 (SD 2.0) degrees during the initial weight bearing phase [74]. No data exist investigating the in vivo radio-ulnar movement during the later stance phase and the swing. Therefore, the in vivo motion of the antebrachial bones and the dynamic changes within the radio-ulnar joint during the complete gait cycle are still unknown.

The in vivo humero-ulnar micromotion has only been investigated in one study so far [23]. Movement between the humerus and the ulna is characterized by flexion and extension, but rotational movement of the humerus relative to the ulna takes also place during locomotion [23]. At the walk the humerus shows an relative external rotation of 2.9 (SD 1.1) degrees during the first third of the stance phase in healthy humero-ulnar joints [23, 28]. These data imply that the elbow joint is not completely restricted to sagittal motion only. One study, investigating the 3D kinematics of the whole canine forelimb showed, that at the moment of ground contact the humerus is in an internally rotated position, which is slightly less at the trot compared to the walk (mean segment angle, walk: −34 degrees; trot: −25 degrees) [28]. During the walk the humerus shows internal and external rotation and only external rotation during the trot throughout the complete stance and swing phase, with a net external rotational movement during the stance phase [28]. This external rotational motion of the humerus is contrary to the internal rotation (pronation) of the antebrachium, which occurs prior to paw strike and is maintained during the stance [28, 60].

3.3 The dysplastic elbow joint

When kinematics of the diseased canine elbow joint are evaluated two different types of changes in the kinematic pattern have to be differentiated. First, changes attributed to pain and lameness, i.e. altered kinematics as a result of the disease. Second, changes in elbow joint kinematics, which represent a causative factor of the disease process.

Due to pain, caused by different joint pathologies in the elbow with DED, multiple adaptive mechanisms occur in the affected forelimb. Decreases in stance time, angular displacement and net joint moments can all be seen in the diseased elbow joint [51].

A reduced range of motion in the sagittal plane (flexion-extension) is present in dogs with MCD [51, 59, 60]. In particular flexion of the joint is decreased and the elbow kept in a more extended position during the gait. In Labrador retrievers with MCD a faster extension of the cubital joint occurs during late swing phase and the elbow is more extended by 9 degrees (mean) during initial ground contact and the early stance phase compared to orthopedically healthy elbows [60]. This more extended gait is a compensating mechanism and aims to reduce pressure at the medial joint compartment [7, 73, 75]. At the end of the stance and beginning of swing phase the elbow joint is more rapidly flexed in affected dogs. However, no active push off occurs at the end of the stance phase indicating that the affected limb is pulled off the ground by the proximal musculature [51]. Reduction in active push off aims to reduce the pressure acting on the joint surface. The elbow is held 16 degrees more externally rotated during the end of swing and initial stance phase and the antebrachium is

in average 2 degrees more abducted throughout the gait cycle and 9 degrees more supinated during the paw strike and early stance phase [60]. These changes have to be assumed as compensating mechanisms as well. Supination leads to caudal displacement of the peak pressure at the medial ulnar joint surface and by that to a release of pressure and potentially pain at the diseased medial coronoid process. Besides the Labrador retriever a more extended elbow joint is present in other breeds with MCD, e.g. Rottweiler, Staffordshire Bullterrier, Airdale terrier, Golden retriever, Polish Lowland sheepdog, German wirehaired pointer, Belgian malinois, Irish setter and mixed breed dogs [51, 59, 60]. Therefore, these changes in the kinematic pattern represent a general secondary adaption to intra articular pathologies and the corresponding pain in canine elbow joints with MCD.

Primary changes in the kinematics of the radius, ulna and humerus are assumed to play an role in the pathogenesis of MCD. Altered kinematics in the proximal radio-ulnar joint, were suggested by different researchers to be one potential factor influencing the development of MCD [76–90]. One proposed mechanism was an increased axial translation of the radius relative to the ulna leading to an dynamic radio-ulnar incongruence. Translational movement between the radius and ulna occurs in elbows with and without MCD in vivo [22, 54], with no significant difference in the total amount of movement between both groups [22]. Therefore, increased axial movement between the radius and ulna and induction of a dynamic RUI under weight bearing conditions could be excluded as an primary factor. However, the direction of radial motion is different between normal and diseased joints, with a negative RUI being induced during the initial stance phase in healthy elbows and no significant change in the radio-ulnar joint conformation in MCD affected joints [72]. Based on the results of that study dogs with a static RUI are not able to compensate the radio-ulnar step formation by radio-ulnar translation and dogs with MCD, but without a static RUI, do not show the same amount of negative dynamic RUI as measured in healthy canine elbow joints [72]. The induction of a negative radio-ulnar step during weight bearing might be a protective mechanism in healthy canine elbow joints. Lowering of the ulna or elevation of the radius during extension of the elbow joint was previously described in vitro and leads to a decrease of intra articular pressure at the medial joint compartment [73]. The inability of the diseased canine elbow joint to adjust the radio-ulnar joint conformation during loading might be one potential biomechanical factor in the pathogenesis of MCD. Especially in dogs without a measurable static incongruence, which account for 40% of all patients with MCD [76], the insufficient adaption to intra articular joint loads can lead to mechanical overload at one distinct joint compartment. Increased radio-ulnar rotation was proposed as another potential cause of mechanical overload along the radial incisure of the medial coronoid process and subsequent cartilage and bone damage [82, 87–90]. The only study comparing in vivo radio-ulnar rotational movement in healthy joints to joints with MCD showed no significant difference in the total amount of radial rotation and in the motion pattern of the radius [74]. The radius starts in an externally rotated position during the late swing phase just before paw strike and rotates internally in relation to the ulna during the early weight bearing phase. At approximately 30 to 40% of the stance phase the radius shows an external rotation again. Values of total rotational movement and internal/external movement of the radius show no significant difference between normal and affected elbow (internal radial rotation, healthy: 5.7 [SD 2.1] degrees; MCD: 5.3 [SD 2.6] degrees; p = 0.1727; external radial rotation, healthy: - 5.8 [SD: 1.3] degrees; MCD: - 4.5 [1.7] degrees; p = 0.7705; total rotation, healthy: 11.4 [SD: 2.0] degrees; MCD: 9.8 [SD: 3.2]; p = 0.2904) [74]. Absence of
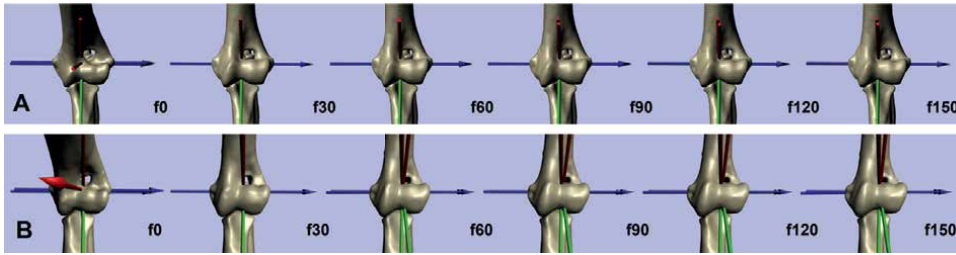
Figure 1.
Image sequence of the in vivo humero-ulnar joint motion during the late swing phase (f0), at the moment of weight bearing (f30) and the first third of the stance phase (f60 – f150). (A) Healthy joint; (B) MCD affected joint; relative external rotation of the humerus occurs just after ground contact, when the joint gets loaded. External rotation of the condyle leads to a craniolateral shift of the trochlea, impinging on the lateral aspect of the medial coronoid process [23].

increased radio-ulnar rotational motion does not exclude an biomechanical overload along the lateral aspect of the medial coronoid process of the ulna caused by interaction with the radial head. An abaxial attachment of the tendon of the biceps brachii muscle at the ulna was detected in dogs with MCD [90]. The pull of the biceps brachii muscle on the ulna could potentially lead to increased pressure between the medial coronoid and the radial head without altering the kinematics. However, no studies have investigated the forces acting between radius and ulna and compared these data between healthy and MCD affected dogs.

Another significant difference can be seen in the humero-ulnar rotational movement between healthy and MCD affected joints. Increased external rotation of the humeral condyle in relation to the ulna occurs at the first third of the stance phase in cubital joints with MCD (humeral rotation, healthy: 2.9 [SD 1.1] degrees; MCD: 5.3 [SD 2.0] degrees; p = 0.0229) [23]. This rotation of the humeral condyle leads to compression of the joint space between the medial coronoid process and the humeral trochlea, and might potentially lead to mechanical overload at the coronoid process and consequently to cartilage and subchondral bone damage (**Figure 1**). Therefore, increased humero-ulnar rotation has to be considered as one dynamic factor in the pathogenesis of MCD. If this increased humero-ulnar rotational movement is caused by soft tissue laxity, like in the dysplastic hip joint, altered muscle function or due to bony differences altering the joint function has not been investigated so far. The influence of a static positive radio-ulnar incongruence onto the contact areas and pressure distribution within the humero-ulnar joint is known [91–93]. However, the literature is lacking kinematic analysis investigating the influence of a static RUI on elbow joint motion, particular the humero-radio-ulnar micromotion. In the cited study on humero-ulnar kinematics the MCD group consisted of dogs with and without a static positive RUI [23]. Due to the small sample size no correlation could be found between the presence of static RUI and the amount of humeral rotational motion. Therefore, the influence of this significant bony deformity on the kinematics of the elbow joint remains unknown.

4. Joint contact areas and force distribution within the elbow joint

The mean body weight distribution between fore- and hindlimbs is approximately 60% : 40% in dogs [56, 94]. A large study investigating 123 different breeds found

that the grand mean proportion of mass was 60.4% on the forelimbs (range: 47.6 to 74.4%) [94]. Only sex was shown to be a significant factor altering that ratio, with females being below the mean value throughout different breeds [94]. Another study comparing kinematic and kinetic data of orthopedic healthy Labrador retrievers and German shepherds reported that Labrador retrievers carry a higher percentage of the weight on their forelimbs compared to the German shepherd (69% vs. 62%, p < 0.001) [66]. If this breed specific mechanical overload plays a role in the pathogenesis of DED and contributes to the high rate of Labrador retrievers with developmental elbow disease, in particular MCD, is not known.

Within the elbow joint load and forces are not homogenously distributed throughout the whole joint surface. It was believed that the radial joint surface is the main weight bearing surface of the radio-ulnar joint. However, more recent studies have shown, that the radius takes 51 to 52% of load [73, 75, 91]. Therefore the ulna plays a more important role in weight bearing than previously assumed. Despite an overall equal load and force distribution between the radius and the ulna, not every part of the joint surface represents an active joint contact area. Within the combined radio-ulnar joint surface three distinct contact areas can be found: the craniolateral aspect of anconeal process, the joint surface of the radial head, and the medial coronoid process [7, 24, 73]. There is no particular contact at the medial aspect of the anconeal process and the center of the trochlear notch (**Figure 2**). The latter one might be explained by the slight physiological humero-ulnar incongruence leading to a bicentrical contact

Figure 2.
Colored animation of the in vivo humero-ulnar joint contact pattern at the ulnar joint surface at the beginning of weight bearing in a healthy canine elbow joint (red: Humero-ulnar contact). Joint contact is present along the medial coronoid process and the lateral and proximal aspect of the trochlear notch. The radius is not shown in this animation.

pattern [6, 7, 9, 73, 95]. When the elbow joint is loaded the force applied by the humeral condyle is distributed along the anconeal process and the coronoid region. With increasing load the concave ulnar notch is stretched and these pressure forces are partially transformed to traction forces [8, 95–97]. Therefore this physiological incongruence leads to a more even stress distribution within the humero-ulnar joint. In human elbow joints the proximal and distal contact area confluent when high loads are acting onto the ulnar joint surface [98]. This load dependent change in contact pattern has not been described in canine elbows so far [7].

The presence of these three contact areas within the elbow joint is further supported by increased subchondral bone density measurements at these anatomic areas [95, 99]. Bone is a dynamic tissue which has the ability to remodel in response to mechanical load (Wolff's law) [100]. Therefore, increased bone density can be found in areas with increased load. Increased subchondral bone densities are present at the disto-medial and cranial aspect of the humeral trochlea and in the olecranon fossa, the anconeal and medial coronoid processes of the ulna and the cranio-medial region of the joint surface of the radius [95]. The same study showed a significant age-dependent increase in the subchondral bone density of the joint surfaces of all three bones, representing continuous adaption of the bone to mechanical stress with increasing age [95].

Though increased loading of the ulnar joint surface does not result in confluence of the bicentric contact pattern, other factors can influence the joint contact patterns of the humero-ulnar and humero-radial joint surfaces. An in vitro study investigated the influence of positive radio-ulnar incongruence (short radius) on joint contact patterns. Presence of a positive RUI leads to a shift of the contact area at the medial coronoid process towards the cranio-lateral aspect of the coronoid process and reduction of the anconeal contact area [93]. Other in vitro studies show similar results. After induction of a 1.9 mm positive RUI medial compartment contact area decreases significantly while the lateral contact area increases. Likewise the mean contact pressure and peak contact pressure increase within the medial compartment and decrease in the lateral part [91, 92]. Therefore, presence of a static positive RUI has to be assumed as an important factor in the disease process of developmental elbow disease and a correlation between the severity of cartilage damage and static RUI has been shown in affected elbows [76, 77, 101]. In vivo evaluation of the ulnar joint contact pattern during the walk in a dog with positive static RUI before and after bi-oblique dynamic proximal ulnar osteotomy (DPUO) confirmed the results of different in vitro studies [24]. Following DPUO positive static RUI decreased, leading to a significant increase of the contact area at the medial coronoid process and to a shift of the contact area from the cranio-lateral aspect (tip and radial incisure) towards the medial aspect and the base of the medial coronoid process (**Figure 3**) [24]. This positive effect of different forms of ulnar and humeral osteotomies onto humero-radio-ulnar contact and force distribution has previously been shown in vitro [75, 91, 92]. Whether a static RUI changes the kinematic pattern of humero-radial, humero-ulnar or radio-ulnar motion and by that the intra articular contact areas and pressure distribution or has a purely mechanical influence without dynamic changes has not been investigated so far.

Further, joint contact areas change during the regular locomotion. Pronation leads to reduction of the contact area in the medial and to a lesser amount in the lateral compartment of the radio-ulnar joint surface. The effect of pronation is further influenced by the elbow joint angle, with significant reduction of the medial contact area by 23% at 135 degree of flexion, what represents the average flexion angle during
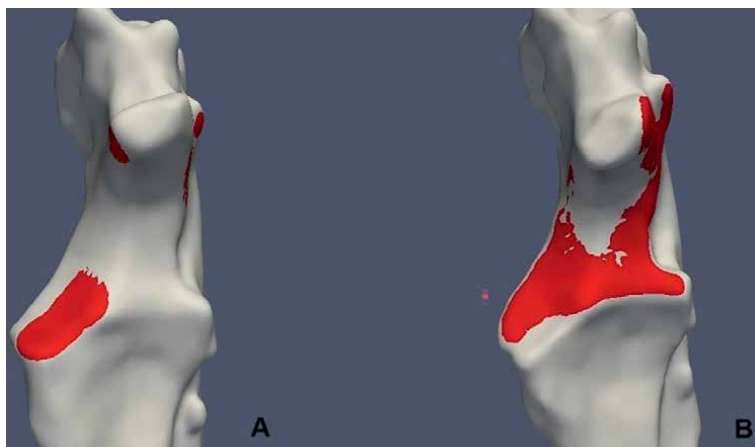
Figure 3.
Humero-ulnar joint contact pattern at the ulnar joint surface at the beginning of weight bearing in a canine elbow joint with MCD (red: Contact area). (A) Contact pattern before bi-oblique DPUO; focal concentration of joint contact at the medial coronoid process (MCP) and slight contact at the medial and lateral aspect of the anconeal process is present. (B) Contact pattern 12 weeks postoperative; joint contact is more homogenously distributed throughout the ulnar joint surface and the craniolateral aspect of the MCP is even not in contact with the corresponding humeral trochlea [24].

the stance phase [73]. A reduced contact area will result in increased pressure when the same load is applied to the joint. Further, pronation of the antebrachium leads to a shift of the peak contact pressure towards the apex of the medial coronoid process. Otherwise supination of the antebrachium leads to caudal displacement of the peak contact pressure on the medial coronoid process [73, 75]. This might explain that dogs with medial coronoid disease show a more supinated stance to release pressure from the apex of the medial coronoid [60]. Moreover, flexion and extension, the main motion pattern during the normal locomotion, influence the intra articular pressure distribution. Flexion increases peak pressure at the medial radio-ulnar joint compartment and extension decreases pressure [73]. It is assumed that this change is due to dynamic changes within the radio-ulnar joint surface in healthy canine elbows [72, 73]. In a cadaveric study extension of the elbow joint induced lowering of the radius and ulna, however more pronounced in the ulna (3.8 mm) compared to the radius (1.9 mm). This corresponds to findings of the in vivo investigation of the radio-ulnar joint cup conformation in healthy elbow joints during the walk, where a negative RUI (short ulna) was induced during weight bearing [72]. This lowering of the ulna relative to the radius might protect the medial coronoid process from mechanical overload during locomotion in healthy canine elbows. In contrast, altered radio-ulnar kinematics preventing elevation of the radius might lead to continuous excessive mechanical overload and subsequent joint pathologies.

Considering the changes of intra articular contact areas and pressure distribution as a function of limb position might explain the typical clinical signs in dogs with developmental elbow disease. Affected dogs stand with the elbow slightly abducted and the antebrachium in slight external rotation (supination) [102]. Furthermore, the elbow joint is more rapidly extended during the swing phase and kept in a more extended position during weight bearing [60]. This motion pattern aims to reduce the contact and pressure at the medial coronoid process, where most commonly lesions attributed to developmental elbow disease occur [90, 103].

5. Conclusion

Canine elbow joint kinematics are more complex than flexion and extension of the joint and influenced by multiple factors like breed, limb length, gait, exercise and joint pathologies. The precise interaction of the three joint forming bones is essential for physiologic joint contact and intra articular force and pressure distribution. Based on the current literature an significantly increased humero-ulnar rotational movement as well as an reduced adjustment of the radio-ulnar joint during the regular locomotion of the dog seem to be two essential pathological factors influencing the development of MCD. This kind of movement is only measurable using laborious techniques like 3D fluoroscopic based kinematography. Nevertheless, further studies are needed to evaluate the complex kinematics of the healthy and the diseased canine elbow joint and to understand the effect of different kinematics onto kinetics.

Conflict of interest

The author declares no conflict of interest.

Author details

Thomas Rohwedder
Small Animal Clinic, Freie University Berlin, Berlin, Germany

*Address all correspondence to: thomas.rohwedder@fu-berlin.de

IntechOpen

Biomechanics of the Canine Elbow Joint
DOI: http://dx.doi.org/10.5772/intechopen.99569

References

[1] Nickel R, Schummer A, Seiferle E. Lehrbuch der Anatomie der Haustiere. 8. ed. Stuttgart: Enke Verlag Parey; 2003.

[2] Constantinescu GM, Constantinescu IA. A clinically oriented comprehensive pictorial review of canine elbow anatomy. Vet Surg. 2009;38(2):135-143.

[3] Alves-Pimenta S, Colaco B, Fernandes AM, Goncalves L, Colaco J, Melo-Pinto P, et al. Radiographic assessment of humeroulnar congruity in a medium and a large breed of dog. Vet Radiol Ultrasound. 2017;58(6): 627-633.

[4] Alves-Pimenta S, Ginja MM, Fernandes AM, Ferreira AJ, Melo-Pinto P, Colaco B. Computed tomography and radiographic assessment of congruity between the ulnar trochlear notch and humeral trochlea in large breed dogs. Vet Comp Orthop Traumatol. 2017;30(1): 8-14.

[5] Collins KE, Cross AR, Lewis DD, Zapata JL, Goett SD, Newell SM, et al. Comparison of the radius of curvature of the ulnar trochlear notch of Rottweilers and Greyhounds. American journal of veterinary research. 2001;62(6): 968-973.

[6] Maierl J, Hecht S, Böttcher P, Matis U, Liebich HG, editors. New aspects of the functional anatomy of the canine elbow joint. 10th European Society of Veterinary Orthopaedics and Traumatology (ESVOT); 2000 2000 March 24-26; Munich, Germany.

[7] Preston CA, Schulz KS, Kass PH. In vitro determination of contact areas in the normal elbow joint of dogs. American journal of veterinary research. 2000;61(10):1315-1321.

[8] Alves-Pimenta S, Ginja MM, Colaco B. Role of Elbow Incongruity in Canine Elbow Dysplasia: Advances in Diagnostics and Biomechanics. Vet Comp Orthop Traumatol. 2019;32(2):87-96.

[9] Eckstein F, Löhe F, Schulte E, Müller-Gerbl M, Milz S, Putz R. Physiological incongruity of the humero-ulnar joint: a functional principle of optimized stress distribution acting upon articulating surfaces? Anat Embryol. 1993;188:449-455.

[10] Brunnberg L, Waibl H, Lehmann J. Lahmheit beim Hund. 1. ed. Berlin: Procane Claudo; 2014.

[11] Clarke E, Aulakh KS, Hudson C, Barnes K, Gines JA, Liu CC, et al. Effect of sedation or general anesthesia on elbow goniometry and thoracic limb circumference measurements in dogs with naturally occurring elbow osteoarthritis. Vet Surg. 2020;49(7): 1428-1436.

[12] Formenton MR, de Lima LG, Vassalo FG, Joaquim JGF, Rosseto LP, Fantoni DT. Goniometric Assessment in French Bulldogs. Front Vet Sci. 2019;6:424.

[13] Thomas TM, Marcellin-Little DJ, Roe SC, Lascelles BDX, Brosey BP. Comparison of measurements obtained by use of an electrogoniometer and a universal plastic goniometer for the assessment of joint motion in dogs. American journal of veterinary research. 2006;67(12):1974-1979.

[14] Jaegger G, Marcellin-Little DJ, Levine D. Reliability of goniometry in Labrador Retrievers. American journal of veterinary research. 2002;63(7): 979-986.

[15] Farrell M, Draffan D, Gemmill T, Mellor D, Carmichael S. In vitro validation of a technique for assessment of canine and feline elbow joint collateral ligament integrity and description of a new method for collateral ligament prosthetic replacement. Vet Surg. 2007;36(6):548-556.

[16] Wakuri H, Kano Y. Anatomical studies on the brachioradial muscle in dogs. Acta Anat Nippon. 1966;41:22-31.

[17] Sandberg GS, Torres BT, Budsberg SC. Review of kinematic analysis in dogs. Vet Surg. 2020;49(6): 1088-1098.

[18] Geiger SM, Reich E, Böttcher P, Grund S, Hagen J. Validation of biplane high-speed fluoroscopy combined with two different noninvasive tracking methodologies for measuring in vivo distal limb kinematics of the horse. Equine veterinary journal. 2018;50(2): 261-269.

[19] Brainerd EL, Baier DB, Gatesy SM, Hedrick TL, Metzger KA, Gilbert SL, et al. X-ray reconstruction of moving morphology (XROMM): precision, accuracy and applications in comparative biomechanics research. J Exp Zool A Ecol Genet Physiol. 2010;313(5):262-279.

[20] Miranda DL, Schwartz JB, Loomis AC, Brainerd EL, Fleming BC, Crisco JJ. Static and Dynamic Error of a Biplanar Videoradiography System Using Marker-Based and Markerless Tracking Techniques. J Biomech Eng. 2011;133(12): 121002-121010.

[21] Fischer MS, Lehmann SV, Andrada E. Three-dimensional kinematics of canine hind limbs: in vivo, biplanar, high-frequency fluoroscopic analysis of four breeds during walking and trotting. Sci Rep. 2018;8(1):16982.

[22] Rohwedder T, Fischer M, Böttcher P. In-vivo fluoroscopic kinematography of dynamic radio-ulnar incongruence in dogs. Open Veterinary Journal. 2017; 7(3):221-228.

[23] Rohwedder T, Fischer M, Böttcher P. In vivo axial humero-ulnar rotation in normal and dysplastic canine elbow joints. Tierarztliche Praxis Ausgabe K, Kleintiere/Heimtiere. 2018;46(2):83-89.

[24] Rohwedder T, Rebentrost P, Böttcher P. Three-Dimensional Joint Kinematics in a Canine Elbow Joint with Medial Coronoid Disease before and after Bi-Oblique Dynamic Proximal Ulnar Osteotomy. VCOT Open. 2019;02(02):e44-ee9.

[25] Tashman S, Andrest W. In-vivo measurement of dynamic joint motion using high speed biplane radiography and CT: application to canine ACL deficiency. J Biomech Eng. 2003;125(2): 238-245.

[26] Tashman S, Anderst W, Kolowich P, Havstad S, Arnoczky SP. Kinematics of the ACL-deficient canine knee during gait: serial changes over two years. J Orthop Res. 2004;22(5):931-941.

[27] Korvick DL, Pijanowski GJ, Schaeffer DJ. Three-dimensional kinematics of the intact and cranial cruciate ligament-deficient stifle of dogs. Journal of biomechanics. 1994; 27(1):77-87.

[28] Andrada E, Reinhardt L, Lucas K, Fischer MS. Three-dimensional inverse dynamics of the forelimb of Beagles at a walk and trot. American journal of veterinary research. 2017;78(7): 804-817.

[29] Kim SE, Jones SC, Lewis DD, Banks SA, Conrad BP, Tremolada G, et al.

In-vivo three-dimensional knee kinematics during daily activities in dogs. J Orthop Res. 2015;33(11):1603-1610.

[30] Rey J, Fischer MS, Böttcher P. Sagittal joint instability in the cranial cruciate ligament insufficient canine stifle. Caudal slippage of the femur and not cranial tibial subluxation. Tierarztliche Praxis Ausgabe K, Kleintiere/Heimtiere. 2014;42(3):151-156.

[31] Bauman JM, Chang YH. High-speed X-ray video demonstrates significant skin movement errors with standard optical kinematics during rat locomotion. J Neurosci Methods. 2010;186(1):18-24.

[32] Kim SY, Kim JY, Hayashi K, Kapatkin AS. Skin movement during the kinematic analysis of the canine pelvic limb. Vet Comp Orthop Traumatol. 2011;24(5):326-332.

[33] Schwencke M, Smolders LA, Bergknut N, Gustas P, Meij BP, Hazewinkel HA. Soft tissue artifact in canine kinematic gait analysis. Vet Surg. 2012;41(7):829-837.

[34] Torres BT, Whitlock D, Reynolds LR, Fu YC, Navik JA, Speas AL, et al. The effect of marker location variability on noninvasive canine stifle kinematics. Vet Surg. 2011;40(6):715-719.

[35] Torres BT, Punke JP, Fu YC, Navik JA, Speas AL, Sornborger A, et al. Comparison of canine stifle kinematic data collected with three different targeting models. Vet Surg. 2010;39(4): 504-512.

[36] Gatesy SM, Baier DB, Jenkins FA, Dial KP. Scientific rotoscoping: a morphology-based method of 3-D motion analysis and visualization. J Exp Zool A Ecol Genet Physiol. 2010; 313(5):244-261.

[37] Anderst W, Zauel R, Bishop J, Demps E, Tashman S. Validation of three-dimensional model-based tibio-femoral tracking during running. Med Eng Phys. 2009;31(1):10-16.

[38] Anderst WJ, Baillargeon E, Donaldson WF, 3rd, Lee JY, Kang JD. Validation of a noninvasive technique to precisely measure in vivo three-dimensional cervical spine movement. Spine (Phila Pa 1976). 2011;36(6): E393-E400.

[39] Giphart JE, Zirker CA, Myers CA, Pennington WW, LaPrade RF. Accuracy of a contour-based biplane fluoroscopy technique for tracking knee joint kinematics of different speeds. Journal of biomechanics. 2012;45(16):2935-2938.

[40] Li G, Van de Velde SK, Bingham JT. Validation of a non-invasive fluoroscopic imaging technique for the measurement of dynamic knee joint motion. Journal of biomechanics. 2008;41(7):1616-1622.

[41] Lin H, Wang S, Tsai TY, Li G, Kwon YM. In-vitro validation of a non-invasive dual fluoroscopic imaging technique for measurement of the hip kinematics. Med Eng Phys. 2012;35(3):411-416.

[42] Bey MJ, Zauel R, Brock SK, Tashman S. Validation of a new model-based tracking technique for measuring three-dimensional, in vivo glenohumeral joint kinematics. J Biomech Eng. 2006;128(4):604-609.

[43] DeCamp CE, Soutas-Little RW, Hauptman J, Olivier B, Braden T, A. W. Kinematic gait analysis of the trot in healthy greyhounds. American journal of veterinary research. 1993;54(4):627-634.

[44] Allen K, DeCamp CE, Braden TD, Balms M. Kinematic Gait Analysis of the

Trot in Healthy Mixed Breed Dogs. Vet Comp Orthop Traumatol. 1994;7(4): 148-153.

[45] Hottinger HA, DeCamp CE, Olivier B, Hauptman JG, Soutas-Little RW. Noninvasive kinematic analysis of the walk in healthy large-breed dogs. American journal of veterinary research. 1996;57(3):381-389.

[46] Gillette R, Zebas CJ. A Two-Dimensional Analysis of Limb Symmetry in the Trot of Labrador Retrievers. J Am Anim Hosp Assoc. 1999;35(6):515-20.

[47] Nielsen C, Stover SM, Schulz KS, Hubbard M, Hawkins DA. Two-dimensional link-segment model of the forelimb of dogs at a walk. American journal of veterinary research. 2003; 64(5):609-617.

[48] Owen MR, Richards J, Clements DN, Drew ST, Bennett D, Carmichael S. Kinematics of the elbow and stifle joints in greyhounds during treadmill trotting – An investigation of familiarisation. Vet Comp Orthop Traumatol. 2004;17(3): 141-145.

[49] Clements DN, Owen MR, Carmichael S, Reid SWJ. Kinematic analysis of the gait of 10 labrador retrievers during treadmill locomotion. Vet Rec. 2005;156(15):478-481.

[50] Feeney LC, Lin C, Marcellin-Little DJ, Tate AR, Queen RM, Yu B. Validation of two-dimensional kinematic analysis of walk and sit-to-stand motions in dogs. American journal of veterinary research. 2007;68(3):277-282.

[51] Burton NJ, Dobney JA, Owen MR, Colborne GR. Joint angle, moment and power compensations in dogs with fragmented medial coronoid process. Vet Comp Orthop Traumatol. 2008;21(2): 110-118.

[52] Holler PJ, Brazda V, Dal-Bianco B, Lewy E, Mueller MC, Peham C, et al. Kinematic motion analysis of the joints of the forelimbs and hind limbs of dogs during walking exercise regimens. American journal of veterinary research. 2010;71(7):734-740.

[53] Agostinho FS, Rahal SC, Miqueleto NS, Verdugo MR, Inamassu LR, El-Warrak AO. Kinematic analysis of Labrador Retrievers and Rottweilers trotting on a treadmill. Vet Comp Orthop Traumatol. 2011;24(3): 185-191.

[54] Guillou RP, Déjardin LM, Bey MJ, McDonald CP. Three Dimensional Kinematics of the Normal Canine Elbow at the Walk and Trot. 2011 American College of Veterinary Surgeons Veterinary Symposium November 3-5, Chicago, Illinois. Veterinary Surgery. 2011;40(7):E17-E42.

[55] Angle T, Gillette R, Weimar W. Kinematic analysis of maximal movement initiation in Greyhounds. Aust Vet J. 2012;90(3):60-68.

[56] Jarvis SL, Worley DR, Hogy SM, Hill AE, Haussler KK, Reiser RF. Kinematic and kinetic analysis of dogs during trotting after amputation of a thoracic limb. American journal of veterinary research. 2013;74(9): 1155-1163.

[57] Brady RB, Sidiropoulos AN, Bennett HJ, Rider PM, J. M-LD, P. D. Evaluation of gait-related variables in lean and obese dogs at a trot. American journal of veterinary research. 2013; 74(5):757-762.

[58] Miqueleto NS, Rahal SC, Agostinho FS, Siqueira EG, Araujo FA, El-Warrak AO. Kinematic analysis in healthy and hip-dysplastic German Shepherd dogs. Veterinary journal

(London, England : 1997). 2013;195(2):210-5.

[59] Galindo-Zamora V, Dziallas P, Wolf DC, Kramer S, Abdelhadi J, Lucas K, et al. Evaluation of thoracic limb loads, elbow movement, and morphology in dogs before and after arthroscopic management of unilateral medial coronoid process disease. Vet Surg. 2014;43(7):819-828.

[60] Caron A, Caley A, Farrell M, Fitzpatrick N. Kinematic gait analysis of the canine thoracic limb using a six degrees of freedom marker set. Study in normal Labrador Retrievers and Labrador Retrievers with medial coronoid process disease. Vet Comp Orthop Traumatol. 2014;27(6):461-469.

[61] Fischer MS, Lilje KE. Dogs in motion. 2nd ed. Dortmund: VDH Service GmbH; 2011.

[62] Catavitello G, Ivanenko YP, Lacquaniti F. Planar Covariation of Hindlimb and Forelimb Elevation Angles during Terrestrial and Aquatic Locomotion of Dogs. PLoS One. 2015;10(7):e0133936.

[63] Duerr FM, Pauls A, Kawcak C, Haussler K, Bertocci G, Moorman V, et al. Evaluation of inertial measurement units as a novel method for kinematic gait evaluation in dogs. Vet Comp Orthop Traumatol. 2016;29(6):475-483.

[64] Lorke M, Willen M, Lucas K, Beyerbach M, Wefstaedt P, Murua Escobar H, et al. Comparative kinematic gait analysis in young and old Beagle dogs. J Vet Sci. 2017;18(4):521-530.

[65] Kopec NL, Williams JM, Tabor GF. Kinematic analysis of the thoracic limb of healthy dogs during descending stair and ramp exercises. American journal of veterinary research. 2018;79(1):33-41.

[66] Humphries A, Shaheen AF, Gomez Alvarez CB. Biomechanical comparison of standing posture and during trot between German shepherd and Labrador retriever dogs. PLoS One. 2020;15(10): e0239832.

[67] de Souza MC, Calesso JR, Cenci B, Cardoso MJL, Moura FA, Fagnani R. Kinematics of healthy American Pit Bull Terrier dogs. Veterinární Medicína. 2021;66(No. 1):8-16.

[68] Gustas P, Pettersson K, Honkavaara S, Lagerstedt AS, Bystrom A. Kinematic and temporospatial assessment of habituation of Labrador retrievers to treadmill trotting. Veterinary journal (London, England : 1997). 2013;198 Suppl 1:e114-9.

[69] Gustas P, Pettersson K, Honkavaara S, Lagerstedt AS, Bystrom A. Kinematic and spatiotemporal assessment of habituation to treadmill walking in Labrador retrievers. Acta Vet Scand. 2016;58(1):87.

[70] Tian W, Cong Q, Menon C. Investigation on walking and pacing stability of german Shepherd dog for different locomotion speeds. J Bionic Eng. 2011;8(1):18-24.

[71] Colborne GR, Walker AM, Tattersall AJ, Fuller CJ. Effect of trotting velocity on work patterns of the hind limbs of Greyhounds. American journal of veterinary research. 2006;67(8): 1293-1298.

[72] Rohwedder T, Böttcher P. In vivo changes of the radio-ulnar joint conformation in canine elbow joints with and without medial coronoid process disease. 5th World Veterinary Orthopaedic Congress (WVOC); 2018 2018 September 12-15; Barcelona, Spain.

[73] Cuddy LC, Lewis DD, Kim SE, Conrad BP, Banks SA, Horodyski M,

et al. Contact mechanics and three-dimensional alignment of normal dog elbows. Vet Surg. 2012;41(7):818-828.

[74] Rohwedder T, Böttcher P. In vivo rotational movement of the radius in healthy canine elbow joints and elbows with medial coronoid process disease. Virtual ESVOT Congress, 2021 May 5-8; 2021.

[75] Mason DR, Schulz KS, Fujita Y, Kass PH, Stover SM. Measurement of humeroradial and humeroulnar transarticular joint forces in the canine elbow joint after humeral wedge and humeral slide osteotomies. Vet Surg. 2008;37(1):63-70.

[76] Eljack H, Böttcher P. Relationship between axial radioulnar incongruence with cartilage damage in dogs with medial coronoid disease. Vet Surg. 2015;44(2):174-179.

[77] Kramer A, Holsworth IG, Wisner ER, Kass PH, Schulz KS. Computed tomographic evaluation of canine radioulnar incongruence in vivo. Vet Surg. 2006;35(1):24-29.

[78] Krotscheck U, Böttcher P, Thompson MS, Todhunter RJ, Mohammed HO. Cubital subchondral joint space width and CT osteo-absorptiometry in dogs with and without fragmented medial coronoid process. Vet Surg. 2014;43(3):330-338.

[79] Smith TJ, Fitzpatrick N, Evans RB, Pead MJ. Measurement of Ulnar Subtrochlear Sclerosis Using a Percentage Scale in Labrador Retrievers with Minimal Radiographic Signs of Periarticular Osteophytosis. Veterinary Surgery. 2009;38(2):199-208.

[80] Starke A, Böttcher P, Pfeil I. [Radiologic quantification of the elbow conformation with a new method for acquiring standardized x-rays under load. Reference valus for medium sized and large dogs without dysplasia of the elbow joint]. Tierarztliche Praxis Ausgabe K, Kleintiere/Heimtiere. 2013;41(3):145-154.

[81] Starke A, Böttcher P, Pfeil I. [Comparative radiologic examination of the canine elbow with and without elbow dysplasia under standardized load]. Tierarztliche Praxis Ausgabe K, Kleintiere/Heimtiere. 2014;42(3): 141-150.

[82] Fitzpatrick N, Garcia TC, Daryani A, Bertran J, Watari S, Hayashi K. Micro-CT Structural Analysis of the Canine Medial Coronoid Disease. Vet Surg. 2016;45(3): 336-346.

[83] Fitzpatrick N, Smith TJ, Evans RB, O'Riordan J, Yeadon R. Subtotal coronoid ostectomy for treatment of medial coronoid disease in 263 dogs. Vet Surg. 2009;38(2):233-245.

[84] Fitzpatrick N, Yeadon R. Working algorithm for treatment decision making for developmental disease of the medial compartment of the elbow in dogs. Vet Surg. 2009;38(2):285-300.

[85] Gemmill TJ, Clements DN. Fragmented coronoid process in the dog: is there a role for incongruency? J Small Anim Pract. 2007;48(7):361-368.

[86] Might KR, Hanzlik KA, Case JB, Duncan CG, Egger EL, Rooney MB, et al. In Vitro Comparison of Proximal Ulnar Osteotomy and Distal Ulnar Osteotomy with Release of the Interosseous Ligament in a Canine Model. Veterinary Surgery. 2011;40(3):321-326.

[87] Baud K, Griffin S, Martinez-Taboada F, Burton NJ. CT evaluation of elbow congruity in dogs: radial incisure versus apical medial coronoid process

fragmentation. J Small Anim Pract. 2020;61(4):224-229.

[88] Burton NJ, Warren-Smith CM, Roper DP, Parsons KJ. CT assessment of the influence of dynamic loading on physiological incongruency of the canine elbow. J Small Anim Pract. 2013; 54(6):291-298.

[89] Hulse D, Young B, Beale B, Kowaleski M, Vannini R. Relationship of the biceps-brachialis complex to the medial coronoid process of the canine ulna. Vet Comp Orthop Traumatol. 2010;23(3):173-176.

[90] Veksins A, Kozinda O, Sandersen C. Computed tomographic morphometry of the biceps brachii muscle tendon of dogs affected by the medial coronoid disease. Anat Histol Embryol. 2019.

[91] Krotscheck U, Kalafut S, Meloni G, Thompson MS, Todhunter RJ, Mohammed HO, et al. Effect of Ulnar Ostectomy on Intra-Articular Pressure Mapping and Contact Mechanics of the Congruent and Incongruent Canine Elbow Ex Vivo. Vet Surg. 2014;43(3):339-346.

[92] McConkey MJ, Valenzano DM, Wei A, Li T, Thompson MS, Mohammed HO, et al. Effect of the Proximal Abducting Ulnar Osteotomy on Intra-Articular Pressure Distribution and Contact Mechanics of Congruent and Incongruent Canine Elbows Ex Vivo. Vet Surg. 2016;45(3):347-355.

[93] Preston CA, Schulz KS, Taylor KT, Kass PH, Hagan CE, Stover SM. In vitro experimental study of the effect of radial shortening and ulnar ostectomy on contact patterns in the elbow joint of dogs. American journal of veterinary research. 2001;62(10):1548-1556.

[94] Fish FE, Sheehan MJ, Adams DS, Tennett KA, Gough WT. A 60:40 split: Differential mass support in dogs. Anat Rec (Hoboken). 2021;304(1):78-89.

[95] Dickomeit MJ, Böttcher P, Hecht S, Liebich HG, Maierl J. Topographic and age-dependent distribution of subchondral bone density in the elbow joints of clinically normal dogs. American journal of veterinary research. 2011;72(4):491-499.

[96] Eckstein F, Löhe F, Müller-Gerbl M, Steinlechner M, Putz R. Stress distribution in the trochlear notch. A model of bicentric load transmission through joints. The Journal of bone and joint surgery American volume. 1994; 76(4):647-653.

[97] Merz B, Eckstein F, Hillebrand S, Putz R. Mechanical implications of humero-ulnar incongruity – finite element analysis and experiment. Journal of biomechanics. 1997;30(7):713-721.

[98] Eckstein F, Löhe F, Hillebrand S, Bergmann M, Schulte E, Milz S, et al. Morphomechanics of the humero-ulnar joint: I. Joint space width and contact areas as a function of load and flexion angle. Anat Rec. 1995;243(3):318-326.

[99] Winhard FE. Anatomische und computertomographische Untersu-chungen am gesunden und degenerativ veränderten Schulter- und Ellbogen-gelenk des Hundes (*Canis familiaris*) [Doctoral Thesis]. Munich: Ludwig-Maximilian-Universität München; 2007.

[100] Wolff J. The law of bone remodeling. 1 ed. Berlin Heidelberg: Springer-Verlag; 1986.

[101] Griffon DJ, Mostafa AA, Blond L, Schaeffer DJ. Radiographic, computed tomographic, and arthroscopic diagnosis of radioulnar incongruence in dogs with medial coronoid disease. Vet Surg. 2018; 47(3):333-342.

[102] Trostel CT, McLaughlin RM, Pool RR. Canine lameness caused by developmental orthopedic diseases. Compend Contin Educ Vet. 2003;25:112.

[103] Lavrijsen IC, Heuven HC, Voorhout G, Meij BP, Theyse LF, Leegwater PA, et al. Phenotypic and genetic evaluation of elbow dysplasia in Dutch Labrador Retrievers, Golden Retrievers, and Bernese Mountain dogs. Veterinary journal (London, England: 1997). 2012;193(2):486-92.

Chapter 4

Pulmonary Vein: Embryology, Anatomy, Function and Disease

Chan I-Ping and Hsueh Tung

Abstract

Four pulmonary veins come from respective lung lobes drain oxygen-rich blood back to the left atrium. Failure of incorporation with the left atrium can lead to a condition, called Cor triatriatum sinister, that the left atrium is separated into two chambers by an abortive fibrous tissue. The venous system of lung and whole body communicate with each other in the earlier time and they will be disconnected in the following developmental process. Total or partial anomalous pulmonary venous connection refers to that there is/are some degree of the communication exists after birth, which can occur in different sites. In the veterinary field, retrospective studies and several case reports have been published to describe these rare congenital cardiovascular diseases in several species. More cases are need for better understanding their clinical manifestation, treatment options and outcomes.

Keywords: congenital, development, Cor triatriatum sinister, anomalous pulmonary venous connection, outcome

1. Introduction

All the vessels that drain blood out of the heart are called artery, and those that drain blood into the heart are called vein. Pulmonary veins, literally, are the vessels that transport oxygenated blood from the lungs back to the left atrium. The information of those veins is hardly found in veterinary textbooks. First of all, this chapter is focus on the development of those veins in fetus. If something wrongs during the process, different type of the abnormality leads to different results. The diagnosis, treatment and prognosis in human medicines are introduced simply in this chapter. In addition, pulmonary venous abnormalities in the veterinary medicines are reported in several species. Those case reports will also be briefly reviewed in this chapter.

2. The embryology of pulmonary veins

The development of the cardiovascular system is complicated because it involves the process from before the folding of heart tube and extend to the later stage of vascular growth. In the vertebrate embryo, most discussion start from the Carnegie stage 12, which approximately equals to 28-30 days in human [1] and 2 days in chicken [2]. At this moment, the primitive pulmonary vein originates from the venous plexus of splanchnic

mesoderm. The staining characteristic of the pulmonary vein orifices in the developing heart can prove that the pulmonary vein is not part of the heart tube: it has no atrial natriuretic factor and has connexin 40 (a transmembrane protein that responsible for electrical coupling mostly found in the nodal tissue) [3]. In addition, an observation study of chicken embryo using image analysis and three-dimensional reconstruction technique also revealed that the pulmonary vein is developing from the splanchnic plexus [4]. The venous plexus of splanchnic mesoderm is a great capillary network that spread from the heart to the liver, connecting cardinal and umbilicovitelline veins. In other words, the pulmonary vein is communicating with systemic venous system in the beginning. In the subsequent developmental process, this communication will degenerate, therefore separating the systemic and pulmonary venous systems (**Figure 1**) [5].
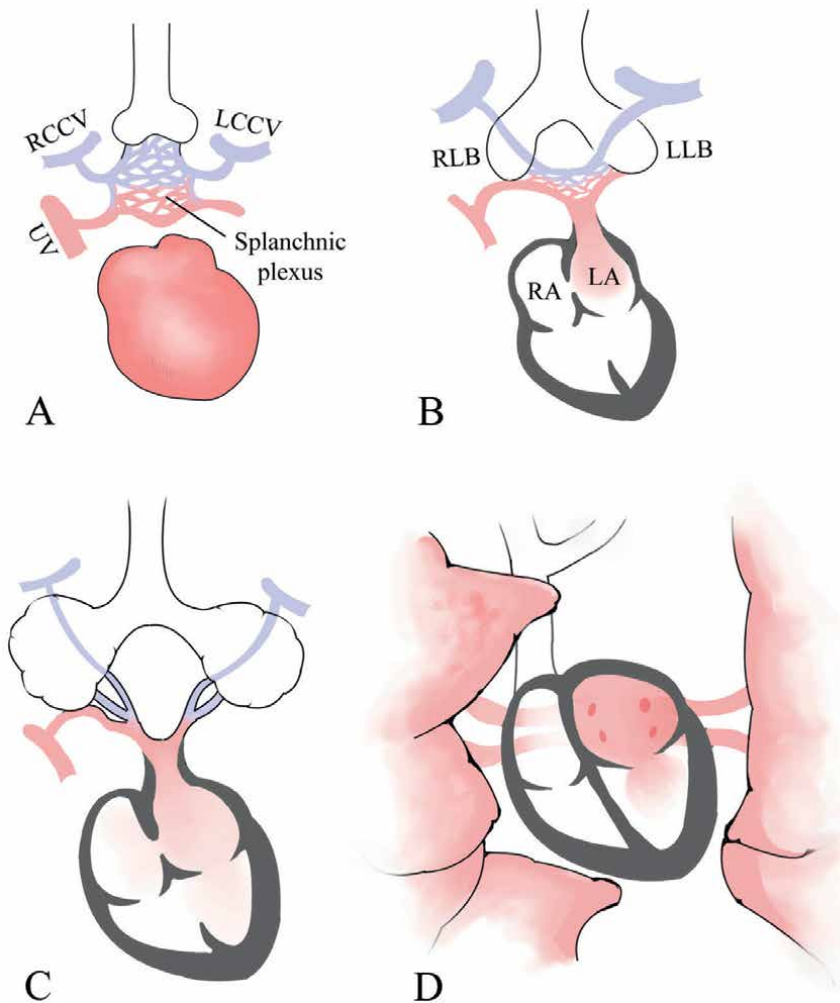
Figure 1.
The normal pulmonary venous development. A, the lung buds are surrounded the splanchnic plexus that communicates umbilical veins and cardinal veins. B, Common pulmonary vein is formed and connected with the sinoatrial part of the heart. C, the connection between pulmonary and splanchnic venous plexus is disappearing. D, the common pulmonary vein develops to four distinct pulmonary veins that incorporates separately with the left atrium. LA, left atrium; LCCV, left common cardinal vein; LLB, left lung bud; RA, right atrium; RCCV, right common cardinal vein; RLB, right lung bud; UV, umbilical vein.

This common pulmonary vein connects the lung buds to the dorsal heart tube, where would develop to left atrium after the outgrowth of intertrial septum. At the level of left atrium, the common pulmonary vein would usually divide into four branches and incorporate with left atrium, forming the smooth part of the left atrium wall [6]. In a study using 26 normal human embryos, the initial process of formation of the human pulmonary vein is very similar to that seen in animal models; marked temporal and morphological difference between the development process of right- and left-side pulmonary veins was found: a much longer tributary being formed on the left than on the right [7].

Various congenital abnormalities of pulmonary veins can occur if anything is wrong during these developmental processes. The cor triatriatum sinister (CTS), a condition that left atrium is separated into two chambers by a membranous tissue, is thought to be the consequence of the inappropriate incorporation of pulmonary veins with the left atrium [7]. In addition, if the atrophy of connection between pulmonary veins and systemic venous system is fail, total or partial anomalous pulmonary venous connection (TAPVC or PAPVC) occurs, depending on the degree of remanent communication between systemic and pulmonary venous system [8].

3. The anatomy of the pulmonary veins

The pulmonary veins, in contrast to systemic veins that collect deoxygenated blood from all organs except lungs, deliver oxygen-rich blood from the lungs to the left atrium. Generally, there are four tributaries of pulmonary vein that would form four ostia on the left atrial wall, two from the right cranial and caudal pulmonary vein and the other two from the left cranial and caudal pulmonary vein (**Figure 2**).
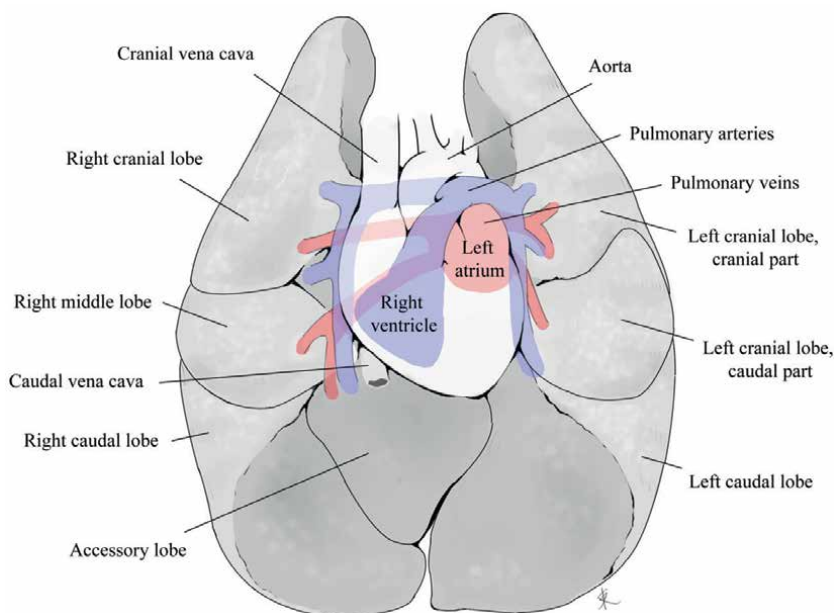
Figure 2.
Normal anatomy of pulmonary veins. The blue (deoxygenated) marks pulmonary arteries, and the red (oxygenated) marks the pulmonary veins.

The right cranial pulmonary vein collects blood from the right cranial and middle lung lobe, and the right caudal pulmonary vein receives blood from the right caudal and accessory lung lobe. The rest pulmonary veins serve for the corresponded lung lobs that they are named after [9].

In atypical but not rare situations in human, pulmonary veins that both originate from right (4%) or left (17.8%) may fuse into a common trunk before entering the left atrium [10]. Additional pulmonary veins derive from individual lung lobes can also happen. Generally, these variations of the number of pulmonary veins are not always problematic, but it may interfere with clinical decisions especially in surgical procedures.

4. The physiology and function of pulmonary veins

In the species that have two atriums, two ventricles, and execute oxygen exchange via the lungs, the oxygenated blood is pumped from the aorta and sent into tissues. The oxygen, nutrients and metabolic products diffuse and exchange in the capillaries that converge and form the vein. Vena cava collect all the venous blood and return to right atrium, right ventricle and lungs. After oxygenation in the lung, these fresh, oxygen-rich blood is returned into left atrium via pulmonary veins, therefore complete the cycle of blood circulation.

Before we go deeper into more understanding of the pulmonary veins, there is an important concept that should be explained first. The cardiovascular system has several functions that are all indispensable to keep the body works normally. Maintaining the systemic arterial pressure is the first priority of the cardiovascular system, it means that the systemic arterial pressure is the last one that the decompensation occurs. The second one is to keep the cardiac output at an adequate level that can provide enough blood flow to the peripheral tissues. Maintaining the normal capillary pressure is the last priority, and therefore it is the reason that the first sign of heart failure is commonly those that associate with congestion [11]. In the cases of pulmonary vein abnormalities, although the pathophysiological mechanisms are different among diagnosis, the loss of normal capillary and venous pressure is often the end result of the developmental disorders. Patient is commonly presented to the clinic because of signs related to congestion. Therefore, we will discuss the pulmonary venous pressure in the next paragraph.

In the fetus, the pressure of the pulmonary system is higher compared to after birth because of very high pulmonary vascular resistance and resultant low pulmonary blood flow (only account for 10 to 15% of right heart stroke volume). The pulmonary vascular resistance falls after birth, and the pressure of pulmonary system drops to a lower level than the systemic circulation in normal setting [12]. In an experiment that studying normal dogs with light sedation, the mean pulmonary venous pressure (17.1 ± 6.5 mm Hg) is consistently slightly higher than mean left atrial pressure (13.4 ± 6.3 mm Hg), which is almost the same with mean pulmonary wedge pressure (13.3 ± 6.2 mm Hg). Considering that the lungs are a large organ that occupy the thorax cavity, the pulmonary venous pressure between locations that differ from altitude (distance from left atrium) is vary [13]. Generally, the pulmonary veins share the similar intravascular pressure with left atrium because there is no valve between them.

During ventricular systole and early diastole, the blood in the pulmonary veins flow into left atrium, and part of blood in the left atrium would regurgitates back into

pulmonary veins when the atrial active pumping that corresponds to the ventricular late filling phase. The changes of pulmonary venous profile among different cardiac cycle can be record by the echocardiographic Doppler examination [14]. It is therefore reasonable that any reason that elevates pressure of the left atrium has the potential to increase the pulmonary venous pressure, because of the higher impedance of draining blood forward and larger regurgitated volume from the high-pressured left atrium.

Another important characteristic of vessel that we cannot forget when we are discussing the hemodynamic is the vascular distensibility and compliance. Distensibility is an ability of vessel whose volume can increase or decrease for every increase or decrease intravascular pressure, and the compliance is equal to distensibility times the volume of blood in the given portion of the circulation. Because of the different wall constitution between veins and arteries, the distensibility of veins is about eight times larger than that of arteries. That is, the venous system can conserve more blood and only has slightly elevation of the intravascular pressure [15]. The pulmonary veins have similar distensibility to the systemic veins, meaning that the pulmonary venous pressure would not exceed the normal range before large amount of blood is congested in the pulmonary capillary and veins.

Various congenital and acquired cardiovascular diseases that affecting pulmonary veins themselves and the left atrium could lead to the congestion of pulmonary veins. They can be simply classified into conditions that cause obstruction or pulmonary overcirculation. Occlusions of one or more pulmonary veins, and the divided left atrium (like the CTS) are examples that pulmonary venous blood flow has difficulties to get through obstacles in its normal pathway and therefore causing high pressure to the rest part of pulmonary veins. In addition, pulmonary overcirculation caused by intra- or extra-cardiac left to right shunting (atrial and ventricular septal defects, patent foramen ovale, patent ductus arteriosus, and anomalous pulmonary venous connection and so on) also has the potential to causes pulmonary congestion because of larger than normal volume that circulates the pulmonary vasculature. Among them, CTS, TAPVC and PAPVC are three of the good examples that is closely related to the development of pulmonary veins. We will discuss these diseases in the following sections.

5. Cor triatriatum sinister

The CTS is a relatively rare congenital cardiovascular disease that has been first reported in 1868 [16]. In an autopsy research, it was accounted for 0.1% to 0.4% in human patients with congenital heart disease [17]. In veterinary medicine, the true prevalence is hard to know because this abnormality is not always producing heart murmur and develops clinical signs that can be observed by the owner and the veterinarian at the general practice. By reviewing case reports, naturally-occurred CTS is identified more frequently in cats [18–23] than in dogs [24–26].

The embryonic cause of CTS is still controversial, but the theory of pulmonary venous abnormality is the most popular. In the development of pulmonary veins, they should incorporate with left atrium and form four ostia on the smooth part of the dorsal left atrial wall. If certain degree of failure in this process occurs, the left atrium could be separated by the remains of the pulmonary veins, most of the time is a fibromuscular membrane. The left atrium is therefore divided to a proximal chamber that locates between the atriopulmonary junction and the fibromuscular membrane, and a distal chamber that extends from the fibromuscular membrane to the mitral valve

annulus. The molecular cause of CTS was first reported in experimental mice without hyaluronidase 2, which is an enzyme required for the degradation of hyaluronan that is the major extracellular matrix component of the heart [27]. Later, the similar result was obtained by genetic studies in affected human families and mice [28].

Anatomic variation of the membrane exists and whether or how much of the blood flow would be impeded depends on the three-dimensional relative position between the membrane and left atrium. This intra-atrial septum can be complete, incomplete or fenestrated, and its size, shape, thickness and location can be varied among affected patients. Types of diaphragmatic, hourglass and tubular has been used to describe the variations [29]. In a retrospective study, the histopathology of the membranous tissue was investigated. Elastin fibers were found to be presence in the top and bottom side and was absent in the middle layer of the diaphragm. Cardiomyocytes with positive staining of cardiac troponin C were located in the peripheral region, more on the side that near the diaphragm and atrial septum than on the side that near the diaphragm and the atrial free wall. The remanent area was mostly made up by the fibrous collagen and other mesenchymal cells. These specimens were collected from human patients that undergo surgical repair of the Cor triatriatum sinister, without surgical death in this cohort [30].

Impendence of the blood flow in the left atrium could cause turbulence, but the pressure gradient between two chambers may be not large enough for the heart murmur to be heard. Elevated pressure in the proximal chamber of the left atrium could raise the intravascular pressure of the pulmonary veins, and signs of left-side congestive heart failure may occur. However, the natural progression of the CTS in human patients is generally stable, with more than half patients were diagnosed in adulthood. In patients that need surgical correction using cardiopulmonary bypass, the surgery is safe and effective [31].

Transthoracic echocardiography is usually helpful in making diagnosis [32]. Except for detecting Cor triatriatum sinister, the echocardiography can also identify concurrent lesions. High proportion (58%) of affected human patients had associated abnormalities, and atrial septal defect and anomalous pulmonary venous connection were the most common and should be always keep in mind [30, 31, 33]. Two feline cases had been published that one kitten had CTS combined with persistent left cranial vena cava [20], and the other was diagnosed CTS with incomplete atrioventricular septal defect [21]. Some conditions can mimic the CTS under two-dimensional imaging mode, including supramitral ring or pulmonary stenosis [34]. In cases that the echocardiographic result alone is controversial or is suspicious of having multiple cardiovascular developmental diseases, additional imaging tools should be considered. A special case that was diagnosed as CTS with TAPVC by echocardiography combined with saline contrast technique was report in 2020 [35]. In some conditions especially when our target area is located near the heart base, the transesophageal echocardiography can provide better image resolution and details than the transthoracic echocardiography. Cardiac catheterization angiography has its advantages that it can measure the true intra-lumen pressure, which is always an estimated value if only echocardiography is performed. However, its clinical utility is limited in the veterinary field because deep sedation to generalized anesthesia is usually required in veterinary patients. Other imaging tools like computed tomography angiography and magnetic resonance imaging can provide multiplaner image reconstruction and assist with the diagnosis process [29].

Early in the 1998, a kitten presented signs of respiratory distress and diagnosed with CTS was successfully surgically managed. The membrane was torn by a dilator

introduced from an opened left atrium [18]. Procedure that combining thoracotomy and cardiac catheter guided cutting balloon was performed in a cat that signs of congestive heart failure resolved completely after the hybrid technique [22]. Surgical correction under cardiopulmonary bypass was also feasible in feline patient with appropriate body size and weight [23]. In canine, the first case was published in 2012, and the patient was doing well only by internal medical treatment for the congestive heart failure [25]. A poodle case was presented with acute dyspnea and cyanosis, and was unfortunately made its definite diagnosis in postmortem examination [26]. Recently, Toaldo et al. reported a 6-year-old intact male French bulldog was accidentally diagnosed as CTS [24].

By reviewing veterinary literature, we can find that cats are more frequently presented, and their age at diagnosis is generally younger (8 weeks old to 4 years old, mostly <1 year old) than dogs (3, 5 and 6 years old). Although most of affected cats had congestive heart failure at admission (this result can be biased in veterinary patients), the surgery is usually tolerable and the patient can be free of heart failure after procedure. Medicine for controlling congestive heart failure is an alternative option if surgery is not performed. Weather the surgery is also benefit and recommended in patient without heart failure is not conclusive.

6. Anomalous pulmonary venous connection

Another important developmental abnormality of pulmonary vein is the anomalous pulmonary venous connection. In human medicine, the TAPVC was comprised of 1–5% congenital heart diseases cases [36] and 0.6 to 1.2 per 10,000 live births [37]. The PAPVC was found 0.4% to 0.7% in the routine autopsies [38, 39]. A retrospective study that reviewed 290 dogs with cardiovascular malformations from 1953 to 1965 revealed that only 1 case was diagnosed PAPVC with secundum atrial septal defect [40]. For the published case reports, there are only 3 dogs [41–43] and each 1 of chicken [44] and foal [45] that are diagnosed as TAPVC; only 4 dogs [46–48] and 2 cats [49, 50] are PAPVC. One canine case reported in 1975 did not describe its detail (TAPVC or PAPVC) [51].

As previous discussed, the primitive pulmonary veins from the lung buds develop from the splanchnic plexus, which communicates with the systemic venous system, and connects to the left atrium. As development proceeds, the connection between pulmonary veins and the systemic venous system disappears. If the communication between pulmonary veins and the systemic venous system persists, TAPVC or PAPVC would be diagnosed depending on the degree of persistent connections [8].

The TAPVC is that all pulmonary veins being abnormally connected to the systemic venous circulation, that is, the right atrium would receive both systemic and pulmonary venous return. Researchers had described four types of TAPVC depending on the connection level (**Figure 3**). Type I, or supra-cardiac type, is the most common type that consist 40–55% of cases. The pulmonary veins empty through left innominate vein, superior vena cava or azygos veins. Type II, or cardiac type, is the second common type that consist 15–30% of cases. The pulmonary veins drain into the right atrium through the coronary sinus or in the posterior wall of the right atrium. Type III, or infra-cardiac type, is accounting approximately 15–26% of cases. The pulmonary veins run to the portal venous system or inferior vena cava. And type IV, or mixed type, is representing 2–10% cases that there are at least two different drainage sites [52, 53].
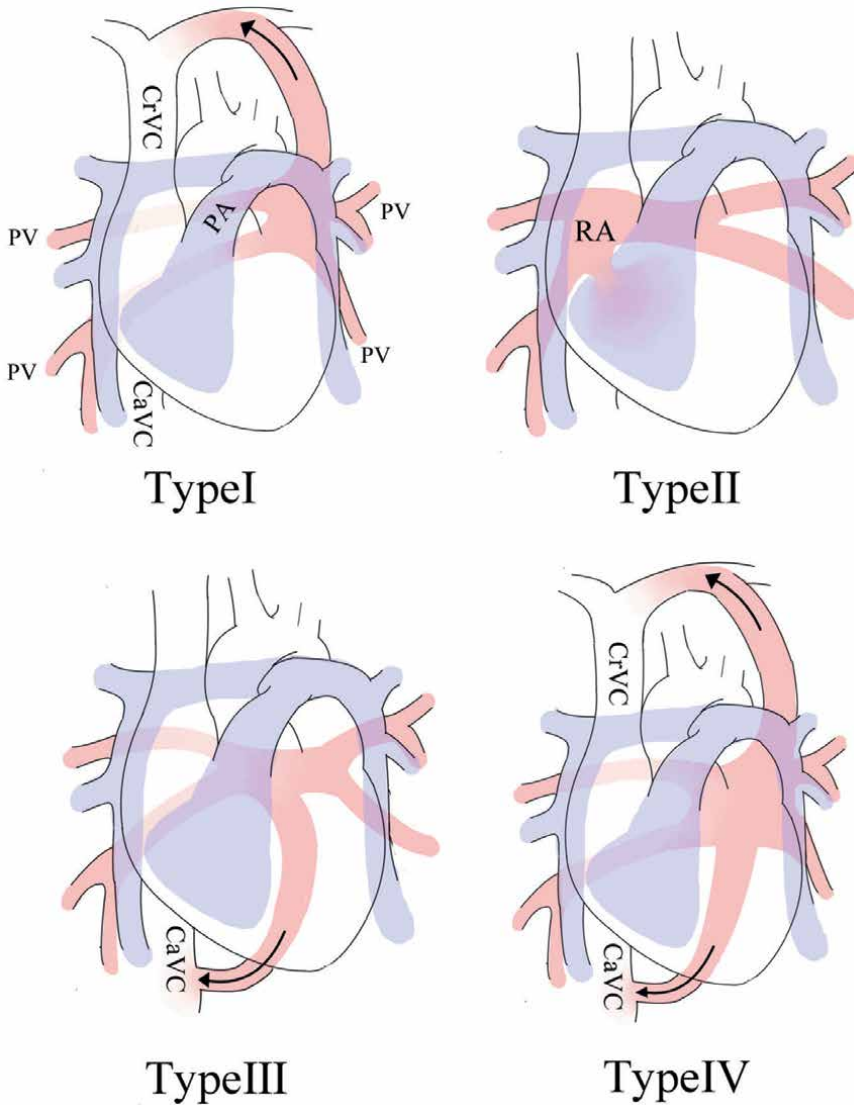
Figure 3.
The classification of TAPVR. Type I, the Supra-cardiac type; Type II, the cardiac type; Type III, the infra-cardiac type, and the Type IV, the mixed type. CaVC, caudal vena cava; CrVC, cranial vena cava; PA, pulmonary artery; PV, pulmonary vein; RA, right atrium.

In the setting of TAPVC, a right-to left shunt via an atrial septal defect (ASD), patent foramen ovale (PFO) or to a lesser extent of patent ductus arteriosus is required for completing circulation and maintaining life [54]. The presence of right (pulmonary) to left (systemic) shunting permits mixture of oxygenated and deoxygenated blood to enter the systemic circulation. Signs of dyspnea with exertion, cyanosis and exercise intolerance could be observed, and the patient is at risk of developing to pulmonary hypertension and congestive heart failure. Three veterinary cases were found to have concurrent ASD (secundum type in 1 dog [41] and 1 chicken [44]; sinus venous type in another dog [42]) and the case of foal [45] had concurrent PFO. A special child case had been recognized recently that all of his pulmonary veins

were anatomically connected to the left atrium but the blood inside actually was drained into superior vena cava via an innominate vein, therefore corresponded to the definition of supra-cardiac type of anomaly [35].

Thoracic radiography is commonly the first imaging exam, it can be normal or some classic changes may exist depending on the types of abnormal connections. A snowman sign has been described in patients with supra-cardiac TAPVC. The head is formed by superior vena cava, vertical vein (common vein that formed by the four anomalous pulmonary veins) and innominate vein, and the body is formed by enlarged right atrium. Another famous radiographic characteristic is the scimitar signs in the PAPVC. It describes the anomalous pulmonary veins like a sword with a curved blade that mostly affect the right-side lung lobes [5, 55].

In addition, the clinical utility of echocardiography in diagnosing abnormalities of pulmonary venous connection is somewhat difficult because of limited echo window, but it can provide the information of the concurrent congenital cardiac anomalies and hemodynamic consequences like the dilated right heart or possible pulmonary hypertension. Transesophageal echocardiography has the advantage that it can access from the heart base aspect, therefore providing more clear images of the structures near the heart base. Right heart catherization can opacify the right heart chambers and venous vasculature but is limited that some small accessory and anomalous vessels may be missed.

For obtaining the full picture of abnormal development of pulmonary veins, multidetector computed tomography and magnetic resonance imaging both can provide good images. The importance of advanced imaging modules in diagnosing these complex cardiovascular developmental diseases had been emphasized in these years [49, 50]. Both of multidetector computed tomography and magnetic resonance imaging are non-invasive, and they can offer multiplanar and three-dimensional reconstructive model. Small lesions and details can be further illustrated by contrast median. Lack of ionizing radiation is the advantage of magnetic resonance imaging, but this procedure needs longer time and sedation which may be risky in some patients [53].

Generally, surgical repair is recommended at the time that TAPVC is diagnosed [56]. The surgical outcome is acceptable with the 6.6% of intraoperative and late death and 15% of recurrent pulmonary venous obstruction in the survivors. Risk factors for both undesired consequences including preoperative pulmonary venous obstruction, infra-cardiac type and mixed type [57]. This result emphasizes the importance of pre- and intra-operative assessment.

Partial anomalous pulmonary venous connection refers to equal to or more than 1, but not all, pulmonary veins being connected to the systemic venous circulation rather than the left atrium. Affected animals can exhibit no clinical signs or have symptoms associates with congestive heart failure and pulmonary hypertension. In the total of 6 veterinary cases, half of them were asymptomatic (2 miniature schnauzers [46] and 1 Devon Rex cat [49]) and the other half were presented with signs of decompensation (exercise intolerance in 1 Belgian Malinois dog [47], pulmonary edema in 1 toy poodle [48] and 1 American shorthair kitten [50]). The severity of symptoms depends on the number of affected pulmonary veins, that is, the degree of left-to-right shunt. A ratio of pulmonary to systemic blood flow (Qp:Qs) can be used to estimate the magnitude of left-to-right shunt, and the ratio greater than 1.5 to 2 is generally considered hemodynamic significant because the patient is at risk of pulmonary hypertension and heart failure, and surgical treatment is usually recommended in these cases [58].

According to the affected pulmonary veins, as many as 27 different anatomic variations had been proposed [59]. The characteristic of partial APVR in pediatric and adult populations varies significantly. In a prospective survey of pediatric patients, mostly (90%) were right-sided and in association of sinus venosus atrial septal defect [60]. In other two retrospective study that focused on adult (>18 years old), abnormal development of pulmonary vein from the left upper lobe was the most (ranging from 47–79%), followed by the right upper pulmonary vein (ranging from 17–38%) [61, 62]. The human patients that were diagnosed in childhood were mostly symptomatic, and those that diagnosed until adulthood were usually an incidental finding. Related signs including dyspnea, orthopnea, fatigue, chest pain, palpitations, tachycardia, and peripheral edema [53].

Surgical repair of the PAPVC with different strategies (intracardiac baffle, pulmonary vein implantation, or superior vena cava division with reimplantation on the right atrial appendage) in children showed excellent outcomes [60]. In a case series that only contain adult patients (20 to 66 years old), conservative management with close monitoring is recommended in asymptomatic patients, and the surgical outcomes in symptomatic patients are usually excellent with low complication rate [63]. Sinus node dysfunction and postoperative venous stenosis are the possible consequences followed surgery [64]. In a recent canine case, his PAPVC and sinus venosus ASD were successfully repaired by single-patch method under cardiopulmonary bypass. The patient remained stable and free of clinical signs in the following one year, suggesting that this is a valid treatment option for other similar case [48].

We can find that the terms of "connection", "drainage" and "return" are all used in the literature to describe the abnormality. The "connection" indicates an anomalous venoatrial connection, whereas the word "drainage" or "return" describe the concept of abnormal pulmonary venous return despite normal anatomical connection [65]. Appropriate wording should be applied depending on the individual case. By reviewing veterinary literature, the clinical manifestation of TAPVC or PAPVC can vary depending on the individual. Owing to the scarcity of these diseases, we still know little about them. Future reports, including studies before and after death, treatment options and related outcome, are warrant.

7. Conclusions

In this chapter, we describe the embryology, physiological function and congenital diseases associated with pulmonary veins. The developmental process of the cardiovascular system is complicated, and every step is crucial. The CTS, TAPVC and PAPVC are rare congenital cardiovascular diseases in human and other animals, and can be asymptomatic or life-threatening. The improvement of advance imaging modules helps in diagnosing these abnormalities, particularly those have multiple concurrent developmental diseases. Knowledges regarding to the treatment intervention in the veterinary medicine is much less than the human medicine, further studies are welcome to provide more information.

Acknowledgements

Conflict of interest

The authors declare no conflict of interest.

Author details

Chan I-Ping* and Hsueh Tung
Veterinary Medical Teaching Hospital, National Chung Hsing University,
Taichung, Taiwan

*Address all correspondence to: cutejamie.tw@gmail.com

IntechOpen

References

[1] O'Rahilly R. Early human development and the chief sources of information on staged human embryos. European Journal of Obstetrics & Gynecology and Reproductive Biology. 1979;9(4):273-280. DOI: 10.1016/0028-2243(79)90068-6

[2] Hamburger V, Hamilton HL. A series of normal stages in the development of the chick embryo. Developmental dynamics. 1992;195(4):231-272. DOI: 10.1002/aja.1001950404

[3] Anderson RH, Brown NA, Moorman AF. Development and structures of the venous pole of the heart. Developmental dynamics: an official publication of the American Association of Anatomists. 2006;235(1):2-9. DOI: 10.1002/dvdy.20578

[4] van den Berg G, Moorman AF. Development of the pulmonary vein and the systemic venous sinus: an interactive 3D overview. PloS one. 2011;6(7):e22055.

[5] Hassani C, Saremi F. Comprehensive Cross-sectional Imaging of the Pulmonary Veins. Radiographics. 2017;37(7):1928-1954. 10.1148/rg.2017170050

[6] Douglas YL, Jongbloed MR, DeRuiter MC, Gittenberger-de Groot AC. Normal and abnormal development of pulmonary veins: state of the art and correlation with clinical entities. International journal of cardiology. 2011;147(1):13-24. DOI: 10.1016/j.ijcard.2010.07.004

[7] Webb S, Kanani M, Anderson RH, Richardson MK, Brown NA. Development of the human pulmonary vein and its incorporation in the morphologically left atrium. Cardiology

in the Young. 2001;11(6):632. DOI: 10.1017/s1047951101000993

[8] Neill CA. Development of the pulmonary veins: with reference to the embryology of anomalies of pulmonary venous return. Pediatrics. 1956;18(6):880-887.

[9] Holt D, Cole S, Anderson R, Miscelis R, Bridges C. The canine right caudal and accessory lobe pulmonary veins: revised anatomical description, clinical relevance, and embryological implications. Anatomia, histologia, embryologia. 2005;34(4):273-275.

[10] Polaczek M, Szaro P, Baranska I, Burakowska B, Ciszek B. Morphology and morphometry of pulmonary veins and the left atrium in multi-slice computed tomography. Surgical and Radiologic Anatomy. 2019;41(7):721-730. DOI: 10.1007/s00276-019-02210-1

[11] Kittleson MD, Kienle RD. Small animal cardiovascular medicine. 1st ed. St. Louis: Mosby; 1998. 603 p.

[12] Rudolph AM. The changes in the circulation after birth: their importance in congenital heart disease. Circulation. 1970;41(2):343-359. DOI: 10.1161/01.cir.41.2.343

[13] Chaliki HP, Hurrell DG, Nishimura RA, Reinke RA, Appleton CP. Pulmonary venous pressure: relationship to pulmonary artery, pulmonary wedge, and left atrial pressure in normal, lightly sedated dogs. Catheterization and cardiovascular interventions. 2002;56(3):432-438.

[14] Boon JA. Veterinary echocardiography. 2nd ed. Hoboken: John Wiley & Sons; 2011. 632 p.

[15] Hall JE. Guyton and Hall: Textbook of Medical Physiology. 13th ed. Philadelphia: Saunders; 2015. 1168 p. DOI: 10.4103/sni.sni_327_17

[16] Church W. Congenital malformation of heart: abnormal septum in left auricle. Trans Pathol Soc Lond. 1868;19:188-190.

[17] Jegier W, Gibbons JE, Wiglesworth F. Cor triatriatum: Clinical, hemodynamic and pathological studies: Surgical correction in early life. Pediatrics. 1963;31(2):255-267.

[18] Wander K, Monnet E, Orton E. Surgical correction of cor triatriatum sinister in a kitten. J Am Anim Hosp Assoc. 1998;34(5):383-386. DOI: 10.5326/15473317-34-5-383

[19] Koie H, Sato T, Nakagawa H, Sakai T. Cor triatriatum sinister in a cat. J Small Anim Pract. 2000;41(3):128-131. DOI: 10.1111/j.1748-5827.2000.tb03180.x

[20] Heaney AM, Bulmer BJ. Cor triatriatum sinister and persistent left cranial vena cava in a kitten. J Vet Intern Med. 2004;18(6):895-898. DOI: 10.1892/0891-6640(2004)18<895:ctsapl>2.0.co;2

[21] Nakao S, Tanaka R, Hamabe L, Suzuki S, Hsu H-C, Fukushima R, et al. Cor triatriatum sinister with incomplete atrioventricular septal defect in a cat. Journal of feline medicine and surgery. 2011;13(6):463-466. DOI: 10.1016/j.jfms.2011.01.016

[22] Stern JA, Tou SP, Barker PC, Hill KD, Lodge AJ, Mathews KG, et al. Hybrid cutting balloon dilatation for treatment of cor triatriatum sinister in a cat. J Vet Cardiol. 2013;15(3):205-210. DOI: 10.1016/j.jvc.2013.03.001

[23] Borenstein N, Gouni V, Behr L, Trehiou-Sechi E, Petit A, Misbach C, et al. Surgical treatment of cor triatriatum sinister in a cat under cardiopulmonary bypass. Vet Surg. 2015;44(8):964-969. DOI: 10.1111/vsu.12403

[24] Castagna P, Romito G, Toaldo MB. Cor triatriatum sinister in a dog. J Vet Cardiol. 2019;25:25-31. DOI: 10.1016/j.jvc.2019.07.003

[25] Almeida GL, Almeida MB, Santos ACM, Mattos ÂV, Oliveira LS, Braga RC. Cor triatriatum sinister in a french bulldog. Case Reports in Veterinary Medicine. 2012;2012. DOI: 10.1155/2012/413020

[26] Champion T, Gava F, Garrido E, Galvão A, Camacho A. Cor triatriatum sinister and secondary pulmonary arterial hypertension in a dog. Arquivo Brasileiro de Medicina Veterinária e Zootecnia. 2014;66(1):310-314. DOI: 10.1590/S0102-09352014000100042

[27] Chowdhury B, Xiang B, Muggenthaler M, Dolinsky VW, Triggs-Raine B. Hyaluronidase 2 deficiency is a molecular cause of cor triatriatum sinister in mice. International journal of cardiology. 2016;209:281-283. DOI: 10.1016/j.ijcard.2016.02.072

[28] Muggenthaler MM, Chowdhury B, Hasan SN, Cross HE, Mark B, Harlalka GV, et al. Mutations in HYAL2, encoding hyaluronidase 2, cause a syndrome of orofacial clefting and cor triatriatum sinister in humans and mice. PLoS genetics. 2017;13(1):e1006470. DOI: 10.1371/journal.pgen.1006470

[29] Jha AK, Makhija N. Cor triatriatum: a review. Seminars in cardiothoracic and vascular anesthesia. 2017;21(2):178-185. DOI: 10.1007/s00392-017-1197-8

[30] Al Kindi HN, Shehata M, Ibrahim AM, Roshdy M, Simry W,

Aguib Y, et al. Cor Triatriatum Sinister (Divided Left Atrium): Histopathologic Features and Clinical Management. The Annals of thoracic surgery. 2020;110(4):1380-1386. DOI: 10.1016/j.athoracsur.2020.01.025

[31] Fuchs MM, Connolly HM, Said SM, Egbe AC. Outcomes in patients with cor triatriatum sinister. Congenital heart disease. 2018;13(4):628-632. DOI: 10.1111/chd.12624

[32] Van Son JA, danielson GK, schaff HV, puga FJ, seward JB, hagler DJ, et al. Cor triatriatum: diagnosis, operative approach, and late results. Mayo Clinic Proceedings. 1993;68(9):854-859. DOI: 10.1016/s0025-6196(12)60693-4

[33] Yang P, Chang C, Lee C, Lin M, Shih J. Cor triatriatum sinister presenting in the fetus: beware of association with total anomalous pulmonary venous connection. Ultrasound in Obstetrics & Gynecology. 2015;45(5):622-624. DOI: 10.1002/uog.14710

[34] Fine DM, Tobias AH, Jacob KA. Supravalvular mitral stenosis in a cat. J Am Anim Hosp Assoc. 2002;38(5):403-406. DOI: 10.5326/0380403

[35] Relan J, Choubey M, Kothari SS. Supracardiac total anomalous pulmonary venous connection with cor triatriatum sinister: A rare diagnosis confirmed by saline contrast echocardiography. Echocardiography. 2020. DOI: 10.1111/echo.14914

[36] Arthur Garson, J. Timothy Bricker, McNamara DG. The science and practice of pediatric cardiology. 1st ed. Philadelphia: Lea and Febiger; 1990. 2557 p.

[37] Hoffman JI, Kaplan S. The incidence of congenital heart disease. Journal of the American college of cardiology.

2002;39(12):1890-1900. DOI: 10.1016/s0735-1097(02)01886-7

[38] Brody H. Drainage of the pulmonary veins into the right side of the heart. Arch Pathol. 1942;33:221-240. DOI: 10.1016/S0002-8703(42)91031-7

[39] Healey Jr JE. An anatomic survey of anomalous pulmonary veins: their clinical significance. Journal of Thoracic Surgery. 1952;23(5):433-444. DOI: 10.1016/S0096-5588(20)31117-X

[40] Patterson DF. Canine congenital heart disease: epidemiology and etiological hypotheses. J Small Anim Pract. 1971;12(5):263-287. DOI: 10.1111/j.1748-5827.1971.tb06231.x

[41] Hilwig R, Bishop S. Anomalous pulmonary venous return in a Great Dane. American journal of veterinary research. 1975;36(2):229-233.

[42] Hogan DF, Green HW, 3rd, Van Alstine WG. Total anomalous pulmonary venous drainage in a dog. J Vet Intern Med. 2002;16(3):303-308. DOI: 10.1892/0891-6640(2002)016<0303:tapvdi>2.3.co;2

[43] Bode EF, Longo M, Breheny C, Del-Pozo J, Culshaw GJ, Martinez-Pereira Y. Total anomalous pulmonary venous connection in a mature dog. J Vet Cardiol. 2019;21:10-17. DOI: 10.1016/j.jvc.2018.11.003

[44] Aihara N, Horiuchi N, Hikichi N, Ochiai M, Ishikawa Y, Oishi K. Total anomalous pulmonary venous connection in a chicken. Avian Dis. 2013;57(1):140-142. DOI: 10.1637/10210-041712-Case.1

[45] Seco Diaz O, Desrochers A, Hoffmann V, Reef VB. Total anomalous pulmonary venous connection in a foal. Vet Radiol Ultrasound. 2005;46(1):83-85. DOI: 10.1111/j.1740-8261.2005.00017.x

[46] Fujii Y, Ishikawa T, Sunahara H, Sugimoto K, Kanai E, Kayanuma H, et al. Partial anomalous pulmonary venous connection in 2 Miniature Schnauzers. J Vet Intern Med. 2014;28(2):678-681. DOI: 10.1111/jvim.12272

[47] Thorn CL, Ford NR, Sleeper MM. Partial anomalous pulmonary venous connection in a dog. J Vet Cardiol. 2017;19(5):448-454. DOI: 10.1016/j.jvc.2017.08.002

[48] Mizuno T, Mizuno M, Harada K, Takano H, Shinoda A, Takahashi A, et al. Surgical correction for sinus venosus atrial septal defect with partial anomalous pulmonary venous connection in a dog. J Vet Cardiol. 2020;28:23-30. DOI: 10.1016/j.jvc.2020.01.006

[49] Nicolson G, Daley M, Makara M, Beijerink N. Partial anomalous pulmonary venous connection with suspected pulmonary hypertension in a cat. J Vet Cardiol. 2015;17:S354-S359. DOI: 10.1016/j.jvc.2015.05.003

[50] Hsueh T, Yang CC, Lin SL, Chan IP. Symptomatic partial anomalous pulmonary venous connection in a kitten. J Vet Intern Med. 2020;34(6):2677-2681. DOI: 10.1111/jvim.15934

[51] Shively M. Anomalous pulmonary venous connection in a dog. J Am Vet Med Assoc. 1975;166(11):1102-1103.

[52] Craig JM, Darling RC, Rothney WB. Total pulmonary venous drainage into the right side of the heart: report of 17 autopsied cases not associated with other major cardiovascular anomalies. Lab Invest. 1957;6(1):44-64.

[53] Katre R, Burns SK, Murillo H, Lane MJ, Restrepo CS. Anomalous pulmonary venous connections. Seminars in Ultrasound, CT and MRI.

2012;33(6):485-499. DOI: 10.1053/j.sult.2012.07.001

[54] Herlong JR, Jaggers JJ, Ungerleider RM. Congenital heart surgery nomenclature and database project: pulmonary venous anomalies. The Annals of thoracic surgery. 2000;69(3):56-69. DOI:10.1016/s0003-4975(99)01237-0

[55] Ferguson EC, Krishnamurthy R, Oldham SA. Classic imaging signs of congenital cardiovascular abnormalities. Radiographics. 2007;27(5):1323-1334. DOI: 10.1148/rg.275065148

[56] Files MD, Morray B. Total Anomalous Pulmonary Venous Connection: Preoperative Anatomy, Physiology, Imaging, and Interventional Management of Postoperative Pulmonary Venous Obstruction. Semin Cardiothorac Vasc Anesth. 2017;21(2):123-131. DOI: 10.1177/1089253216672442

[57] Shi G, Zhu Z, Chen J, Ou Y, Hong H, Nie Z, et al. Total Anomalous Pulmonary Venous Connection: The Current Management Strategies in a Pediatric Cohort of 768 Patients. Circulation. 2017;135(1):48-58. DOI: 10.1161/circulationaha.116.023889

[58] Toyoshima M, Sato A, Fukumoto Y, Taniguchi M, Imokawa S, Takayama S, et al. Partial anomalous pulmonary venous return showing anomalous venous return to the azygos vein. Internal Medicine. 1992;31(9):1112-1116. DOI: 10.2169/internalmedicine.31.1112

[59] Blake HA, Hall RJ, Manion WC. Anomalous pulmonary venous return. Circulation. 1965;32(3):406-414. DOI: 10.1161/01.cir.32.3.406

[60] Alsoufi B, Cai S, Van Arsdell GS, Williams WG, Caldarone CA, Coles JG. Outcomes after surgical treatment of

children with partial anomalous
pulmonary venous connection.
The Annals of thoracic surgery.
2007;84(6):2020-2026. DOI: 10.1016/j.
athoracsur.2007.05.046

[61] Haramati LB, Moche IE, Rivera VT,
Patel PV, Heyneman L, McAdams HP,
et al. Computed tomography of partial
anomalous pulmonary venous
connection in adults. J Comput Assist
Tomogr. 2003;27(5):743-749. DOI:
10.1097/00004728-200309000-00011

[62] Ho ML, Bhalla S, Bierhals A,
Gutierrez F. MDCT of partial anomalous
pulmonary venous return (PAPVR) in
adults. J Thorac Imaging. 2009;24(2):89-
95. DOI: 10.1097/RTI.0b013e318194c942

[63] El-Kersh K, Homsy E, Daniels CJ,
Smith JS. Partial anomalous pulmonary
venous return: A case series with
management approach. Respir Med Case
Rep. 2019;27:100833. DOI: 10.1016/j.
rmcr.2019.100833

[64] Pace Napoleone C, Mariucci E,
Angeli E, Oppido G, Gargiulo GD. Sinus
node dysfunction after partial anomalous
pulmonary venous connection repair. J
Thorac Cardiovasc Surg. 2014;147(5):
1594-1598. DOI: 10.1016/j.jtcvs.
2013.07.058

[65] Mascarenhas E, Javier RP, Samet P.
Partial anomalous pulmonary venous
connection and drainage. Am J Cardiol.
1973;31(4):512-518. DOI: 10.1016/
0002-9149(73)90304-4

Section 2

Anatomy and Physiology of Disease and Diagnostics

Chapter 5

Evaluation of Current and Future Diagnostic and Prognostic Techniques for Traumatic Pericarditis in Cattle

Jennifer Hall, Emily Barker, Adam Best and Catrin Sian Rutland

Abstract

Pericarditis in cattle can be classified as traumatic pericarditis (TP), idiopathic haemorrhagic, secondary to neoplasia or septic pericarditis due to haematogenous spread of organisms, such as *Colibacilli* or *Pasturella*. In cattle, pericardial disease most commonly develops from traumatic reticuloperitonitis (TRP). Bovine cardiac disease often has a poor prognosis, and this is worsened when clinical manifestations of heart failure are present. Euthanasia is the treatment of choice in many cases, but for pregnant or high value animals, treatment of disease is often the preferred option and an early diagnosis can provide a better prognosis in these cases. This chapter looks at the anatomy, physiology and presentation of TP. In addition, a more in depth look at cardiac troponin is presented alongside present and future diagnostic and prognostic methods, in addition to treatment options surrounding this clinically important problem.

Keywords: biochemistry, cardiac abnormality, cardiac troponin, cattle, haematology

1. Introduction

Pericarditis is defined as inflammation of the pericardium resulting in accumulation of fluid or exudate between visceral and parietal pericardium and can be classified as traumatic pericarditis (TP), idiopathic haemorrhagic [1], neoplastic or septic [2, 3]. Haematogenous spread of organisms, such as *Colibacilli* or *Pasturella* species which commonly originate from pleuropneumonia, are most commonly involved. In cattle, [4] the most common classification of pericarditis is TP, resulting from traumatic reticuloperitonitis (TRP), the ingestion of sharp objects which migrate through the anterior wall of the reticulum, across the diaphragm and penetrate the pericardium, in some cases extending into the myocardium [3, 4]. This can lead to pericarditis; which is defined as inflammation of the pericardium that results in accumulation of fluid or exudate between the visceral and parietal pericardium [2].

TP is one of the most common heart diseases reported in cattle [3]. From 1989 to 1995, TP was one of the top 10 findings following necropsy examination of 321 cattle at the University of Glasgow [5]. Clinical signs of the cardiovascular condition can vary greatly as they depend on the extent of disease progression, location of the foreign object, route of migration [6, 7], and potential for other diseases to present with similar signs [8]. Cases of TP do not commonly present until the later stages of the disease process when subsequent heart failure (HF) is evident [9] (see **Figure 1**). Due to varying clinical signs and late presentation of those signs, diagnosis can be difficult and often requires more than a clinical examination. Commonly used methods include echocardiogram, pericardiocentesis and blood analysis which help to determine the presence and extent of disease [11]. Unfortunately, these diagnostic techniques are frequently not economically viable for clients in farm practice where expenses are usually focussed on herd health as opposed to the health of individual stock.

Bovine cardiac disease often has a poor prognosis, which is worsened when clinical manifestations of HF are present. Euthanasia is the treatment of choice in many cases [11]. However, for pregnant or high value animals, treatment of disease is often the preferred option and an early diagnosis can provide a better prognosis in these cases [11]. With regards to TRP, recognition of pericardial involvement (TP) needs to be recognised as early as possible in the disease process to prevent further suffering of the animal and economic losses for the farmer. Ideally, a cheap and quick method of diagnosing pericarditis in cases of cattle with TRP should be established. In this
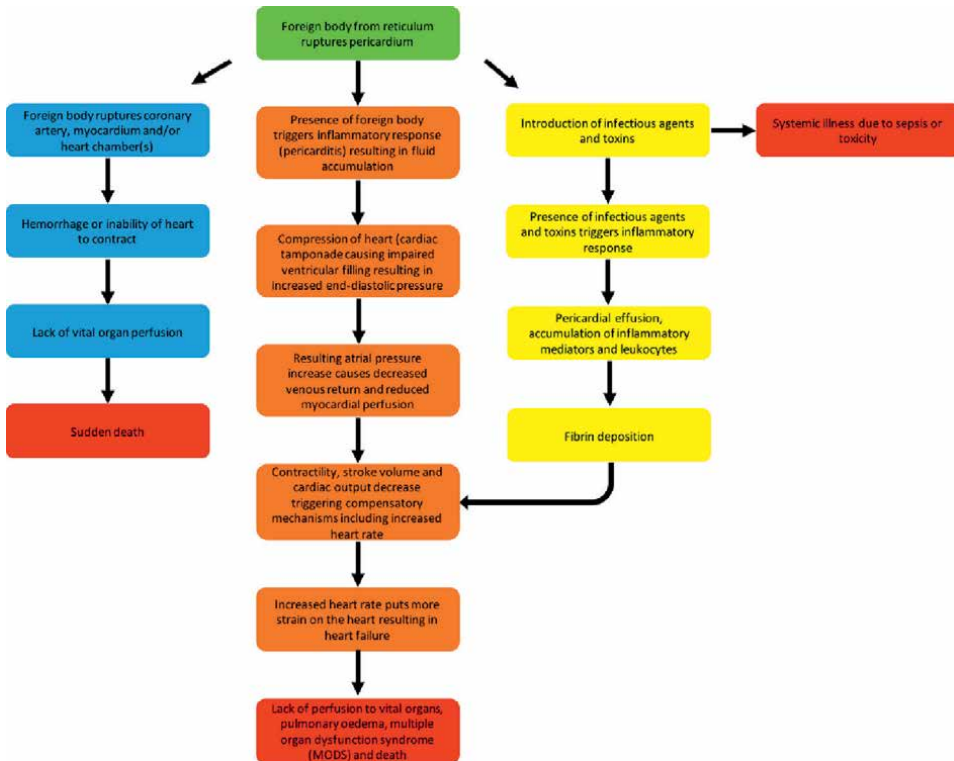
Figure 1.
Flowchart explanation of three potential outcomes of TP, with clarification of how HF can occur as a result of TP. Adapted from [10].

review, we assess the recent research focusing on concentrations of cardiac biomarkers (specifically cardiac troponin 1 (cTnI)) in the serum of TP cattle and evaluate both the current and future capabilities of such tests. The advantages and limitations of other diagnostic techniques are also explored, with reference to survival rates of TP affected cattle.

2. Clinical examination

The main presenting complaints in cases of TP are often vague and non-specific; relating to milk drop, anorexia, lethargy, and weight loss [4, 10]. A review study demonstrated that in 60 animals diagnosed with fatal traumatic reticulitis (15 of which developed TP), the most common presenting sign was a sudden reduction in milk yield, which was observed in 68% of the cases.

Early signs of pericarditis, which can be detected through a clinical exam, include muffled heart sounds with associated splashing sounds, pericardial friction rubs, tachycardia, and pyrexia [10, 12]. Fluctuations in parameters such as rumen turnover, faecal output, heart rhythm, lung sounds and demeanour may also be found [12].

Pain is also an important component of TP which may present as bruxism, grunting, unwillingness to move, abducted elbows or a positive response to the cranial bar and withers test [10, 12]. Not all signs are present in every case, and they are also not exclusive to TP [12], other pathologies and physiological changes can be associated with such signs [11].

The signs mentioned above are also commonly seen in TRP cases irrespective of known TP development [7]. Clinical examinations alone have been shown to miss instances of TP. In a group of 28 animals which had TP, confirmed by necropsy, only 15 were diagnosed with TP using clinical examinations alone [13]. The lack of consistency in clinical signs between TP cattle is attributed to individuals presenting at different stages of disease with some showing evidence of HF. In addition, differences are observed as a result of the location of the foreign object, which specific anatomical structures the object has penetrated and the volume of fluid present in the pericardium [10]. Pregnancy and parturition have been also highlighted as possible contributing factors, due to increased pressure on the reticulum [13]. The variable degree of clinical signs and contributing factors associated with TP emphasises that only a tentative diagnosis can be made on clinical examination alone [4, 12, 14].

Some publications have emphasised that auscultation of the heart is the most significant aspect of a clinical exam in identifying pericarditis [3, 9]. Evidence of muffled heart sounds or other abnormal sounds such as splashing, tinkling, and rubbing are also commonly associated with pericarditis [11]. In a previous study, it was shown that muffled heart sounds had a sensitivity of 92% and specificity of 93% to pericarditis disease in 39 confirmed cases [6]. It should be noted that the presence of muffled heart sounds does not specify the type of pericarditis and the absence of such sounds does not necessarily rule out pericarditis [12]. Muffled heart sounds have also been demonstrated in other, non-cardiac diseases. One study observed muffled heart sounds in all 7 cases of pleurisy and all 5 cases of mediastinal abscesses, compared to only 39 of 55 TP cases [15]. This study also found that splashing and tinkling heart sounds were only found in the TP cattle, and not those with pleurisy or mediastinal abscesses. The presence or absence of tinkling sounds might help to rule in but not rule out TP.

Abnormal heart sounds do not always remain constant within TP cases, their presentation can change daily and the severity and time frame of disease progression of each animal should also be taken into account [16]. This highlights the need to reassess clinical signs in dubious cases. As well as auscultation, a full cardiac clinical exam should include assessment of mucous membrane colour, capillary refill time, a description of heart sound audibility and intensity with appreciation for cardiac rhythm and rate. In addition, pulse strength, rate, quality and the rhythm of both jugular and mammary veins, auscultation of lung fields and percussion of the cardiac region to assess level of cardiac dullness should be conducted [12, 17]. This comprehensive assessment allows for clarification of the clinical status of each cow and indicates whether there is potential disruption of the cardiac system. This can help indicate the most likely disease responsible, however, further diagnostic approaches are needed to fully determine the underlying aetiology and type of pericarditis, if present.

HF is the penultimate stage of all heart disease due to failure of the compensatory mechanisms [18, 19] (see **Figure 1**). Any heart disease seen in cattle can present with or without clinical signs of HF, as demonstrated in previous cases of pericarditis [19, 20]. Most clinical signs associated with chronic late stage TP relate to congestive right sided HF which can present with signs such as jugular distension, submandibular and brisket oedema [4].

It should be noted that a lack of any of the aforementioned signs of TP found on clinical examination does not mean that TP is not present. A study using clinical examination alone identified that 2 of 28 cattle under investigation had TRP with no signs of TP. However, on post mortem examination it was discovered that all 28 cases had profound signs of TP. This demonstrated that the development of TP in cases of TRP cannot be excluded via clinical assessment alone.

TP has been reported as the most common cause of pericardial disease and congestive heart failure (CHF) in cattle [15]. Despite this, other diseases should be considered when signs of congestive HF are apparent. Differentials include other causes of

Clinical sign	% affected (N)	Reference
Tachycardia	85.7 (28)	[13]
Decreased rumen turnover	82.1 (28)	[13]
Milk drop	78.8 (85)	[4, 13]
Weight loss	63.1 (57)	[4]
Jugular vein distension	62.4 (85)	[4, 13]
Tachypnoea	60.7 (28)	[13]
Muffled heart sounds	57.6 (85)	[4, 13]
Oedema	51.8 (85)	[4, 13]
Anorexia	48.2 (85)	[4, 13]
Pain (bruxism, muscle fasciculations or Grunting)	42.9 (28)	[13]
Splashing heart sounds	25.0 (28)	[13]
Pericardial friction rubs	7.14 (28)	[13]
Tachyarrhythmia	3.57 (28)	[13]

Table 1.
Commonly observed clinical signs associated with TP in order of their frequency in scientific studies.

pericarditis, bacterial endocarditis, primary dilated cardiomyopathy, congenital heart disease, cardiac lymphoma, mediastinal abscess and non-cardiac exudative pleurisy with much research evident on these other possible diseases too [10].

In conclusion, all differential diagnoses should be taken into careful consideration by the veterinarian when considering the presenting signs in suspected cases of TP. This is especially important in cases where presenting signs are vague or inconsistent. TP cannot always be ruled out by clinical examination alone and TP should always be considered when cattle present wit TRP. A full, cardiac clinical exam (**Table 1**) is paramount when reviewing the possibility of cardiac disease, to accurately provide diagnostic and prognostic information to the client.

3. Haematology and biochemistry

The most frequent reported haematological finding with TP is reduced clotting time indicated by the glutaraldehyde test in 93% of 28 TP cases which had presented with a heart rate of more than 100 bpm, distended jugular veins and abnormal heart sounds [12]. Other recorded signs include hyperfibrinogenaemia and leucocytosis with neutrophilia and lymphocytopenia [12]. Hyperproteinaemia, hypoalbuminaemia and hyperglobinaemia have also been consistently found in buffalo TP cases [21].

Haematology and biochemistry results only support findings indicated by clinical examination and provide limited additional information on underlying disease processes. It has been previously stated that biochemistry and haematology results alone were not enough to differentiate between endocarditis, pericarditis and congenital heart defects in cattle and it could be argued that farmers' money would be better spent on the use of other diagnostic techniques [6]. However, it could also be said that haematology and biochemistry results are necessary in order to rule out disease secondary to HF such as liver congestion which is commonly found secondary to HF. Haematology and biochemistry also gives an indication to the severity of the HF and therefore can be used to determine an accurate prognosis.

4. Radiographic imaging

Radiographic imaging is considered a useful method to identify metallic objects within the reticulum and adjacent structures, as well as highlighting findings such as cardiomegaly and abnormal cardiac shape [21]. One caveat of using radiography in late-stage pericarditis is that often, fibrinous deposits, adhesions, pleural effusion and pneumopericardium can be so severe that there is a profound loss in thoracic detail making it difficult to identify offending object(s) [6, 10, 22]. A lack of a foreign object seen on thoracic radiographs does not rule out TP, and as a result, the sensitivity of radiography as a diagnostic technique is limited [11, 22]. Additionally, in cases of extensive fluid accumulation or concurrent pleural effusion with TP, radiographic changes will be indistinguishable from other cardiac pathologies such as pleuritis [10].

5. Echocardiography

Ultrasonography is currently recognized as the preferred diagnostic method for investigating cardiac abnormalities, including pericardial effusion in cattle [11].

Echocardiography is non-invasive and can be performed on the standing and compliant animal on site [5]. This does not include evaluation via Doppler due to higher expense and problems with accessibility in farm practice. When carrying out an echocardiographic assessment it has been recommended that a 3–3.5 MHz transducer is used observing caudal long, caudal short and cranial long axis views on the right side and caudal long and cranial long axis views on the left side [23, 24].

Common signs noted within the literature relating to thoracic ultrasonography and echocardiography in TP cases include displacement of the heart away from the thoracic wall, increased echogenicity of the heart, generalized thickening of the pericardium and the presence of a hypoechoic fluid exudate between the parietal and visceral pericardium, which often contains echogenic fibrin deposits [6, 25]. As a result of fluid accumulation in the pericardium, causing a subsequent cardiac tamponade, compression of ventricles and reduced ventricular motility can also be observed [11, 26–28]. The ultrasonographic findings described provide strong evidence for the diagnosis of pericarditis.

Factors to consider when using echocardiogram include the training experience of the clinician, the views obtained and the restraint and position of the cow. To ensure a full and complete assessment, ultrasound images should also be obtained from the lung fields, mediastinum pleural space and abdominal region, extending the scan from the 3rd intercostal space to the 12th [15]. It has been suggested that a productive and conclusive echocardiogram would take 20 minutes to perform in a farm setting [29]. Studies have also highlighted the importance of assessing the reticulum in retrospect to the diaphragm in order to interpret signs of abscess formation, adhesions and peritonitis, which may occur alongside TP [21]. This subsequently adds additional time to the scanning session but is performed at the farmer's request. In a study of 51 healthy cattle, it was shown that differences in cattle temperament, body condition score and rib width can result in a lack of consistency between thoracic ultrasonography assessments [26]. This further emphasises the importance of clinician experience when producing echocardiograms in cattle, alongside good anatomical comprehension to prevent over interpretation.

6. Ultrasound-guided pericardiocentesis

Ultrasonography alone is unable to explicitly determine the type of pericarditis which may be causing fluid accumulation in the pericardial sac. Pericardiocentesis is needed to characterise the fluid present and is often performed at the left fifth intercostal space, 2.5–10 cm dorsal to the olecranon [10]. Samples obtained from cases of TP are often malodourous, purulent, have elevated protein content (>3.5 g/dl) and on cytology show elevated white blood cells (>2500/μl) (mainly neutrophils) and the presence of mostly commensal bacteria [10]. In comparison to TP, idiopathic pericarditis is rare and in these cases pericardiocentesis is often haemorrhagic. Clinical signs may also improve with the pericardiocentesis, unlike with TP [1, 28].

Risks with pericardiocentesis may be reduced when it is performed with ultrasound guidance rather than blind. However, these risks are still plausible and can include pneumothorax, cardiac puncture, pericardial fluid leakage and formation of arrhythmias [13]. Pericardiocentesis has been described as a successful treatment option alongside pericardial lavage, pericardiostomy and rib resection in some cases of TP but evidence still remains variable [19]. Studies have shown that performing pericardiocentesis can prolong life when an animal has TP and is pregnant, so that it may deliver [30].

7. Necropsy

A definitive diagnosis of TP can be provided via post-mortem examination and this is carried out in most academic studies to allow correlation to other clinical findings [6, 11]. On necropsy, a malodourous, fibrinous to purulent pericarditis with extensive adhesions is found in TP cases. Other changes are also frequently found within the thorax and abdomen; these commonly include a congested liver, hepatomegaly, liver abscessation and peritoneal effusion [6, 11]. Sometimes the foreign object is located penetrating through the reticulum, diaphragm and pericardium, but not always [4, 11].

8. Serum cardiac troponin

Studies across many species have demonstrated the specificity of cardiac troponin to the heart muscle, and elevated levels of cardiac troponin subunits, especially cTnI, which shows a positive correlation with acute myocardial damage [31, 32]. Cardiac biomarkers have therefore been studied in farm practice following the need for an accessible and cheap method of detecting cardiac damage. Analysis of cardiac bio-markers in serum samples of TRP affected cattle could provide information on the prognosis and has the potential to surpass other diagnostic techniques especially in reference to TP [33–35].

There is a significant difference in cTnI levels between healthy cattle and those with cardiac disease. A study found that serum cTnI was higher in 4 out of 5 confirmed pericarditis cases, compared to 34 healthy control animals [36]. In a different study which used a cut off value of 0.08 ng/ml, elevated levels of cTnI was observed in 14/18 pericarditis cases, 12/15 endocarditis cases, 5/10 congenital heart defect cases, 3/7 mediastinal abscesses, 3/5 caudal vena cava thrombosis cases and in 4/13 cattle with chronic suppurative pneumonia [33]. All of these conditions were confirmed at necropsy. By investigating the concentrations of cTnI in 40 perceptively healthy cattle another study concluded that the normal range of cTnI in normal, healthy, lactating (Holstein) dairy cattle was 0.00–0.05 ng/ml (using iSTAT- immunoassay). Although, serum cTnI concentrations are usually increased with cardiac disease in cattle, this parameter cannot be used to differentiate pericarditis from other heart diseases (**Figure 2**), or to differentiate primary cardiac disease from other
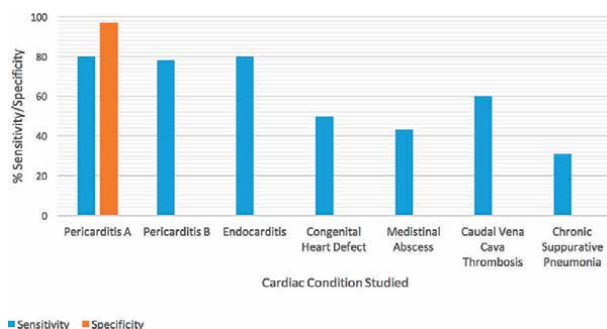
Figure 2.
Sensitivity and specificity of cTnI as a test for various cardiovascular diseases including two studies on pericarditis. Information adapted from Pericarditis A [37], and Pericarditis B, endocarditis, congenital heart defect, mediastinal abscess, caudal vena cava thrombosis, chronic suppurative pneumonia [34].

non-cardiac, intrathoracic diseases [33, 36, 37]. Despite the research conducted to date, further studies are also necessary in order to confirm the normal range of cTnI in healthy cattle which can then be used to determine specific cut off values for use in disease assessment. However, standardization of cTnI assays is difficult due to the use of different antibodies in differing assays [38]. Additionally, the assays used in cTnI investigations were designed for use in human medicine, cattle specific assays may be more appropriate.

Whilst comparison of serum cTnI levels between cardiac diseases has not been fully established, an additional complicating factor is non-cardiac disease. Elevated cTnI levels have been demonstrated in non-cardiac intrathoracic and non-intrathoracic diseases in cattle. The concentrations of serum cTnI in cattle with metritis, mastitis, left displaced abomasum, downer cow syndrome and other calving and post-calving complications determined that in 43 of the 53 diseased cattle cTnI values were above the cut off value of 0.02 ng/ml [39]. Cattle with downer cow syndrome showed the highest levels of serum cTnI out of these diseases, with a maximum value of 27 ng/ml. This illustrates the need to consider secondary myocardial involvement as a result of other disease processes [39] and again, it reflects the importance of a thorough clinical exam. The research also found that non-surviving diseased cows (which died or were euthanized) had significantly higher median cTnI than surviving cows and that the cTnI in healthy cows was in the undetectable range (<0.02 ng/ml). However, it was concluded that further standardization studies are necessary to confirm such claims.

Using cTnI to detect TP and therefore determine the prognosis for cattle with TRP has been investigated [40]. Investigations found that measurement of serum cTnI in cattle with TRP could potentially provide an earlier diagnosis of TP. Making an early diagnosis of TP could save time and money for the vet and farmer and reduce suffering for cattle, since treatment, at present, is generally unrewarding and the prognosis is poor particularly when diagnoses are made further along the disease process [10].

Concentrations of cTnI have been recorded in cattle with confirmed TRP to try and show possible myocardial degeneration [37]. In 55% of confirmed TRP cases, significantly elevated levels (>0.3 ng/ml) of cTnI were observed, with the mean cTnI recorded at 3.26 ng/ml (standard deviation of 2.1 ng/ml). This compares to 0.052 ng/ml mean serum cTnI (standard deviation 0.001 ng/ml) recorded in 10 healthy control animals that were used in the study.

It should be considered that elevated cTnI levels in the serum of TRP affected cattle may not correlate directly with the severity of myocardial damage. No post-mortem examinations, echocardiograms or thorough clinical examinations were described in the report, therefore potential correlations of cTnI concentration and the stage/severity of disease could not be established [37]. A positive correlation between the magnitude of cTnI increase and the severity of myocardial damage on histopathology has been demonstrated in cattle with monesin toxicosis [41] and in calves with Foot and Mouth disease [35]. Another study [36] concluded that increased serum cTnI might be more likely in acute presentations of TP compared to chronic cases, as is seen in human medicine. This emphasizes a need to consider the magnitude of the rise in serum cardiac biomarker levels over a significant timeframe.

A more recent study [42] assessed other cardiac biomarkers including heart-type fatty acid-binding protein (H-FABP), Pentraxin-3 (PTX-3) and thrombomodulin (TM) in cases of TP in cattle. There were significantly elevated H-FABP, TM and PTX-3 levels in the 25 Holstein TP positive cattle compared to 10 healthy control animals. The elevations in these biomarkers positively correlated with elevations

in cTnI. However, it was concluded that there is a need to correlate cTnI levels with other cardiac biomarkers not just in TP but also other cardiac diseases. Additionally the need to correlate H-FABP, PTX-3 and TM to necropsy and histological findings in TP has been highlighted. The use of multiple cardiac biomarkers in such cases could help to further confirm thoughts of pericardial involvement when no cardiac signs are observed clinically and this could assist with determining prognosis before the expense of treatment is pursued [42].

9. Conclusion

In this review, we have identified the need for a gold standard cardiac examination to be performed in all ruminant cases where cardiac disease is suspected. We have also re-emphasised the ability for echocardiogram and pericardiocentesis to provide a diagnosis of TP. These methods are also required to help review and evaluate the use of cTnI as a possible indicator of prognosis in TRP with TP. We highlight the need to correlate serum cTnI levels and other cardiac biomarkers to the severity of myocardial damage present, and the correlation of such values to the stage of TP via findings on echocardiogram, necropsy examination and histopathology. There is also a need to carry out further research into serum cTnI in larger cohorts of cattle over a significant time-frame starting from initial TRP through to severe TP cases, in order to validate its use as a commercially viable and dependable parameter. In order to do this, specific cut off values for disease level and severity, and a normal cattle cTnI reference range still needs to be defined.

However, this review suggests that with further investigation and if proven to be reliable, serum cardiac biomarkers such as cTnI have the potential to revolutionise diagnosis of traumatic pericarditis in cattle.

Acknowledgements

Conflict of interest

The authors declare no conflict of interest.

Author details

Jennifer Hall, Emily Barker, Adam Best and Catrin Sian Rutland*
School of Veterinary Medicine and Science, University of Nottingham, Nottingham,
United Kingdom

*Address all correspondence to: catrin.rutland@nottingham.ac.uk

IntechOpen

References

[1] Jesty SA, Sweeney RW, Dolente BA, Reef VB. Idiopathic pericarditis and cardiac tamponade in two cows. Journal of the American Veterinary Medical Association. 2005;**226**(9):1555-1558, 02

[2] Gründer HD. Krankheiten des Herzens und des Herzbeutels. Innere Medizin undChirurgie des Rindes. 4th ed. Berlin: Parey Buchverlag; 2002. pp. 159-181

[3] Bexiga R, Mateus A, Philbey AW, Ellis K, Barrett DC, Mellor DJ. Clinicopathological presentation of cardiac disease in cattle and its impact on decision making. The Veterinary Record. 2008;**162**(18):575-580

[4] Roth L, King JM. Traumatic reticulitis in cattle: A review of 60 fatal cases. Journal of Veterinary Diagnostic Investigation. 1991;**3**(1):52-54

[5] Knox KM, Reid SW, Irwin T, Murray M, Gettinby G. Objective interpretation of bovine clinical biochemistry data: Application of Bayes law to a database model. Preventive Veterinary Medicine. 1998;**33**(1-4):147-158

[6] Imran S, Tyagi SP, Kumar A, Kumar A, Sharma S. Ultrasonographic application in the diagnosis and prognosis of pericarditis in cows. Veterinary Medicine International. 2011;**2011**:974785

[7] Miesner MD, Reppert EJ. Diagnosis and treatment of hardware disease. The Veterinary Clinics of North America: Food Animal Practice. 2017;**33**(3):513-523

[8] McGuirk SM. Treatment of cardiovascular disease in cattle. The Veterinary Clinics of North America: Food Animal Practice. 1991;**7**(3):729-746

[9] Buczinski S, Rezakhani A, Boerboom D. Heart disease in cattle: Diagnosis, therapeutic approaches and prognosis. Veterinary Journal. 2010;**184**(3):258-263

[10] Reef VB, Mcguirk SM. Diseases of the cardiovascular system. In: Smith BP, editor. Large Animal Internal Medicine. 4th ed. USA: Mosby; 2009. pp. 474-478

[11] Braun U. Traumatic pericarditis in cattle: Clinical, radiographic and ultrasonographic findings. Veterinary Journal. 2009;**182**(2):176-186

[12] Braun U, Lejeune B, Schweizer G, Puorger M, Ehrensperger F. Clinical findings in 28 cattle with traumatic pericarditis. The Veterinary Record. 2007;**161**(16):558-563

[13] Peek SF, McGuirk SM. Chapter 3: Cardiovascular disease. In: Saunders GK, editor. Rebhun's Diseases of Dairy Cattle. 2nd ed. Amsterdam, Netherlands: Elsevier; 2008

[14] Singh CK, Kumar A, Singh N. An overview on the diagnostic and therapeutic aspects of cardiac diseases in bovine. Journal of Entomology and Zoology Studies. 2019;**7**:855-863

[15] Abd El Raouf M, Elgioushy M, Ezzeldein SA. Congestive heart failure in cattle; etiology, clinical, and ultrasonographic findings in 67 cases. Veterinary World. 2020;**13**(6): 1145-1152

[16] Nart P, Thompson H, Barrett DC, Armstrong SC, McPhaden AR. Clinical and pathological features of dilated cardiomyopathy in Holstein-Friesian cattle. The Veterinary Record. 2004;**155**(12):355-361

[17] Jackson PGG, Cockcroft PD. Clinical examination of the cardiovascular system. In: Jackson PGG, Cockcroft PD, editors. Clinical Examination of Farm Animals. New Jersey, United States: Blackwell Science Ltd; 2002. pp. 51-64

[18] De Morais HA, Schwartz DS. Pathophysiology of heart failure. In: Ettinger SJ, Feldman EC, editors. Textbook of Veterinary Internal Medicine. 6th ed. St Louis, USA: Elsevier Saunders; 2005. pp. 914-940

[19] Buczinski S, Francoz D, Fecteau G, DiFruscia R. Heart disease in cattle with clinical signs of heart failure: 59 cases. The Canadian Veterinary Journal. 2010;**51**(10):1123-1129

[20] Buczinski S, Francoz D, Fecteau G, Difruscia R. A study of heart diseases without clinical signs of heart failure in 47 cattle. The Canadian Veterinary Journal. 2010;**51**(11):1239-1246

[21] Khalphallah A, Elmeligy E, Elsayed HK, Abedellaah BEA, Salman D, Al-Lethie AA, et al. Ultrasonography as a diagnostic tool in Egyptian buffaloes (*Bubalus bubalis*) with traumatic pericarditis. International Journal of Veterinary Science and Medicine. 2017;**5**(2):159-167

[22] Misk NA, Semieka MA. The radiographic appearance of reticular diaphragmatic herniation and traumatic pericarditis in buffaloes and cattle. Veterinary Radiology & Ultrasound. 2001;**42**(5):426-430

[23] Braun U, Schweizer T, Pusterla N. Echocardiography of the normal bovine heart: Technique and ultrasonographic appearance. The Veterinary Record. 2001;**148**(2):47-51

[24] Hallowell GD, Potter TJ, Bowen IM. Methods and normal values for

echocardiography in adult dairy cattle. Journal of Veterinary Cardiology. 2007;**9**(2):91-98

[25] Yamaga Y, Too K. Echocardiographic detection of bovine cardiac diseases. The Japanese Journal of Veterinary Research. 1986;**34**(3-4):251-267

[26] Sojka JE, White MR, Widmer WR, Van Alstine WG. An unusual case of traumatic pericarditis in a cow. Journal of Veterinary Diagnostic Investigation. 1990;**2**(2):139-142

[27] Schweizer T, Sydler T, Braun U. Cardiomyopathy, endocarditis valvularis thromboticans and pericarditis traumatica in cows - clinical and echocardiographical findings in three cases. Schweizer Archiv für Tierheilkunde. 2003;**145**(9):425-430

[28] Firshman AM, Sage AM, Valberg SJ, Kaese HJ, Hunt L, Kenney D, et al. Idiopathic hemorrhagic pericardial effusion in cows. Journal of Veterinary Internal Medicine. 2006;**20**(6):1499-1502

[29] Peek SF, Buczinski S. Cardiovascular disease. In: Rebhun's Diseases of Dairy Cattle. 3rd ed. Amsterdam, Netherlands: Elsevier; 2018. pp. 46-93

[30] Bakos Z, Voros K. Intraoperative echocardiography and surgical treatment of traumatic pericarditis in a pregnant cow. Acta Veterinaria Hungarica. 2011;**59**(2):175-179

[31] O'Brien PJ, Landt Y, Ladenson JH. Differential reactivity of cardiac and skeletal muscle from various species in a cardiac troponin I immunoassay. Clinical Chemistry. 1997;**43**(12): 2333-2338

[32] England J, Loughna S, Rutland CS. Multiple species comparison of cardiac troponin T and dystrophin: Unravelling

the DNA behind dilated cardiomyopathy. Journal of Cardiovascular Development and Disease. 2017;**4**(3)

[33] Mellanby RJ, Henry JP, Cash R, Ricketts SW, Bexiga R, Truyers I, et al. Serum cardiac troponin I concentrations in cattle with cardiac and noncardiac disorders. Journal of Veterinary Internal Medicine. 2009;**23**(4):926-930

[34] Labonte J, Roy JP, Dubuc J, Buczinski S. Measurement of cardiac troponin I in healthy lactating dairy cows using a point of care analyzer (i-STAT-1). Journal of Veterinary Cardiology. 2015;**17**(2):129-133

[35] Gunes V, Erdogan HM, Citil M, Ozcan K. Assay of cardiac troponins in the diagnosis of myocardial degeneration due to foot-and-mouth disease in a calf. The Veterinary Record. 2005;**156**(22):714-715

[36] Mellanby RJ, Henry JP, Cash R, Ricketts SW, Bexiga JR, Mellor DJ. Serum cardiac troponin I concentrations in cattle with pericarditis. The Veterinary Record. 2007;**161**(13):454-455

[37] Gunes V, Atalan G, Citil M, Erdogan HM. Use of cardiac troponin kits for the qualitative determination of myocardial cell damage due to traumatic reticuloperitonitis in cattle. The Veterinary Record. 2008;**162**(16):514-517

[38] Melanson SE, Tanasijevic MJ, Jarolim P. Cardiac troponin assays: A view from the clinical chemistry laboratory. Circulation. 2007;**116**(18): e501-e504

[39] Varga A, Angelos JA, Graham TW, Chigerwe M. Preliminary investigation of cardiac troponin I concentration in cows with common production diseases. Journal of Veterinary Internal Medicine. 2013;**27**(6):1613-1621

[40] Attia NE. Cardiac biomarkers and ultrasonography as tools in prediction and diagnosis of traumatic pericarditis in Egyptian buffaloes. Veterinary World. 2016;**9**(9):976-982

[41] Varga A, Schober KE, Holloman CH, Stromberg PC, Lakritz J, Rings DM. Correlation of serum cardiac troponin I and myocardial damage in cattle with monensin toxicosis. Journal of Veterinary Internal Medicine. 2009;**23**(5):1108-1116

[42] Yildiz R, Ok M, Ider M, Aydogdu U, Erturk A. Heart-type fatty acid-binding protein (H-FABP), pentraxin-3 (PTX-3) and thrombomodulin in bovine traumatic pericarditis. Acta Veterinaria Hungarica. 2019;**67**(4):505-516

Chapter 6

Equine Stress: Neuroendocrine Physiology and Pathophysiology

Milomir Kovac, Tatiana Vladimirovna Ippolitova,
Sergey Pozyabin, Ruslan Aliev, Viktoria Lobanova,
Nevena Drakul and Catrin S. Rutland

Abstract

This review presents new aspects to understanding the neuroendocrine regulation of equine stress responses, and their influences on the physiological, pathophysiological, and behavioral processes. Horse management, in essence, is more frequently confirmed by external and internal stress factors, than in other domestic animals. Regardless of the nature of the stimulus, the equine stress response is an effective and highly conservative set of interconnected relationships designed to maintain physiological integrity even in the most challenging circumstances (e.g., orthopedic injuries, abdominal pain, transport, competitions, weaning, surgery, and inflammation). The equine stress response is commonly a complementary homeostatic mechanism that provides protection (not an adaptation) when the body is disturbed or threatened. It activates numerous neural and hormonal networks to optimize metabolic, cardiovascular, musculoskeletal, and immunological functions. This review looks into the various mechanisms involved in stress responses, stress-related diseases, and assessment, prevention or control, and management of these diseases and stress. Stress-related diseases can not only be identified and assessed better, given the latest research and techniques but also prevented or controlled.

Keywords: equine stress, physiology, pathophysiology, neuroendocrine regulation

1. Introduction

Despite approximately 100 years of intensive research (and more than 1 million citations in PubMed), stress, due to its multidimensional characteristics, remains a problematic concept not only in equine but also in human medicine; even today there is not a consensus on the question of what is stress? Stress may be defined as a relationship between an organism and external or internal factors that act to disrupt homeostasis. It has been suggested that "Living beings have evolved various specific and nespecidic reactions and pathways to mitigate the detrimental effects of stress to restore homeostasis" [1]. Thus, common acute stress responses can be evaluated as a process of constant flow moving around a homeostatic point, which is the optimal state for the existence of living beings (including horses). However, this definition also leads to a broader concept of stress, since it can include all temporary physiological adaptations to any change in

the environment. All living organisms, from the bacterium, to the horse or human, live (and lived) in potentially dangerous conditions, and in the process of evolution, they have developed specific protection mechanisms to survive before leaving offspring. There is not a consensus whether the highly variable stress environment promotes adaptation and the process of evolution itself, or only contributes to reflex defense [2]. In any case, stress responses in living organisms are constitutional—genetically programmed and are constantly modulated by environmental factors in the form of the gene–environment interactions [3, 4]. Thus, equine temperament traits (e.g., neophobic and neurotic behavior) that are known to be heritable strongly influence the intensity of the animal's stress response [4, 5]. Various specific equine genes influencing behavior have been identified [6]. For example, a frustration-related stress behavior in stabled horses is linked to an A–G substitution in the DRD4 (dopamine receptor) gene [7]. Additionally, it was found that an "A" variation of the G292A version of the DRD4 gene contributes to decreased curiosity and increased vigilance, and was more prevalent in Thoroughbreds compared with native breeds [8].

In the stress-induced disturbance of hemostasis or a possible threat to it, it is commonly noticed that a nonspecific multisystem three-stage body response occurs, which the famous Canadian endocrinologist Dr. Hans Selye (1907–1982) first termed the General Adaptation Syndrome (GAS) [9]. An alarm is the first stage or wave, where animals through a high concentration of catecholamines and activation primarily of cardiovascular, respiratory, and locomotory systems, and large energy consumption, trying to cope with adverse, threatening situations, or to escape from them ("fight-flight-or-freeze" response). In free nature, horses show usual a proactive response—flight (fearful behavior), rather than fight (or aggressive-dominant behavior), and this is considered a fundamental natural survival mechanism that increases protection in a threat environment. Logically, without this alarm phase developing through evolution, the horses would have no chance of escaping predators and ensuring their survival and continuation of the species. Occasionally, in "human controlled" environments, horses in the alarm phase show a passive response that involves behavioral inhibition, with lower locomotion, immobility, or withdrawal, but with focused attention. Which reaction horses show depends on the stress factors, and the reactivity of the neuroendocrine and sympathetic nervous systems. In this first wave of the stress response, within seconds there is an increased release of catecholamines, and it has been noticed that there is also increased secretion of corticotropin-releasing hormone (CRF), prolactin, growth hormone, and *glucagon, and a decrease in* the release of hypothalamic gonadotropin-releasing hormone (GnRH).

If the stressful situation is not resolved, the horse's body uses its additional energy resources and activates other physiological systems to protect or adapt to the stressful condition. This is the resistance stage. In this phase or the second wave, an increase in the concentration of glucocorticoids is mainly noticed. If the physiological compensatory mechanisms have succeeded in overcoming the stress, the recovery stage is entered. In contrast, if the animal body has used up its resources and is unable to maintain normal homeostasis that leads to the stage of exhaustion with various pathophysiological changes occurring.

2. Equine stress factors

There is wide consensus, that horses, by the nature of their use and management, are more likely to be exposed to different stressor factors compared to other

domesticated animals. There are numerous equine stress factors, these can roughly be divided into internal and external, acute and chronic, physical and psychological, but more often horses are exposed to numerous stress factors at the same time. From a pathophysiological and clinical point of view, strangulation intestinal obstruction causes the strongest equine stress response, as it is accompanied by several stress factors at the same time. Firstly, there is severe abdominal pain (through tissue damage and intestinal distension) [10]. Secondly, there is the occurrence of intestinal dysbacteriosis with the release of LPS, which triggers an increased concentration of proinflammatory cytokine and the *development of severe endotoxic shock* [11]. The treatment of such horses in equine clinics and the associated changes in environmental conditions (other stables, unknown people, and other horses) significantly enhance the stressful response [12]. If such horses undergo abdominal surgery and general anesthesia, this will increase stress exposure placed on the animals [13]. Numerous other equine stress factors also exist, for example for used horses in sports and competition there are associated transport conditions, the novelty of their surroundings, exposure to a noisy public, and physical overload [14, 15]. Physical exercise is a stress condition solicited in the organism creating a new dynamic equilibrium that requires adaptive responses. Exercise-induced stress is often proportional to the horse's competition level [16]. Water or food deprivation (after intestinal surgery), metabolic disorders by various equine diseases (acidosis, hypovolemia, electrolyte imbalance, and hypoglycemia), and inflammation also cause a stress response [17, 18]. Temporarily limited but very intensive psychological loads are exposed to foals at weaning [19, 20]. The lack of activity, for example constantly staying in a stall, stabling, and isolation without social contact with other horses, causes most horses to undergo chronic stress responses [21]. It should be taken into account that different horses may show stress in specific ways, and some horses respond better to stressful situations than others. The adaptive response of each horse to stress is determined by a multiplicity of genetic, environmental, and developmental factors. Equine stress response in horses is also dependent on the animal's perception of the situation. It is considered in human and equine medicine that the crucial factor that determines if a psychological stressor has a negative, neutral, or even positive outcome, is whether the central nervous system (CNS) perceives to be in control of the situation or not [22]. Certainly, it has an important role has the experience of the horse. Frequently, most horses appear to fear novel situations, and these are perceived as being threatening. In addition to all of the above, nervous riders or veterinary personnel may cause a horse to behave more reactively because they present as ambiguous stimuli [23]. Undoubtedly, nervous people also transmit their fear to horses, which enhances the equine stress response. It is well known that horses recognize angry human faces and interpret them as negative [24].

3. Neuroendocrine regulation of equine stress reaction

In contrast to rodents or humans, horses are not as well studied with regards to the neuroendocrine regulation of stress response, especially at the acellular and molecular level in brain structures, therefore rodent and human results will be partially extrapolated to horses in this review. For a long time, researchers suggested that the sympathetic-adrenal medullary (SAM) and hypothalamic–pituitary–adrenal (HPA) axis play the main role in stress responses [25–27]. This theory, up to the present, seems to limit or oversimplify the weight aspect of the animal's stress response.

There is almost no tissue or cell in animals (including microbiota) that, directly or indirectly, does not play some role in the maintenance of homeostasis during the acute or chronic stress response [28]. In a simplified version, the stress systems in horses have two essential components—controllers and effectors. The controllers or receptors of *sensory* systems monitor the value of the regulated homeostatic parameter which they are customized, compare it to the reference value and generate a neural (or hormonal) signal that is proportional to the absolute value of the difference. If the sensory signal is interpreted in the CNS as a threat, this will be acted upon through various pathways affecting different effectors, which creates physiological reactions into or out of the system in order to bring the controlled variable closer to the reference value [29]. Equine homeostasis is usually maintained through complex, coordinated mechanisms of self-regulation, among which feedback plays an important, but not determinative role.

The first step in the stress response is the perception of a stressor through the sensory system, which is composed of sensory receptor cells, neural and blood pathways, and parts of the brain involved in sensory perception. The brain interprets them as either a real or a potential threat, which triggers nonspecific and specific stress responses that are commensurate with the nature of the stimulus (**Figure 1**) [30]. Thus, the physical stressors which are well studied, for example, pain and blood loss, require an immediate "systemic" reflex reaction. On the other hand, the equine brain also responds to non-physical or "psychogenic" stressors (for example transport or weaning) based on prior experience [20, 31].

Sensory systems code for four aspects of different stress stimuli—type, intensity, location, and duration [32]. There are different receptors monitoring equine homeostasis, and among them, the nociceptors have the most important role in the induction of the acute stress reaction. As a reaction to physical trauma or another *noxious stimulus,* nociceptors send sensory *stimulation* primarily through to the preganglionic sympathetic neurons in the intermediolateral cell column of the thoracolumbar spinal cord, and from there further through the neospinothalamic, paleospinothalamic and archispinothalamic tract to different thalamic "relay" neurons [33]. Then, the thalamus sends the noxious signal to other brain structures, which initiate, spread, *memorize,* and cessation in an equine stress reaction [34]. As a reaction to homeostatic imbalance or inflammation, the brainstem is also able to generate rapid stress responses via direct projections of neurons in the paraventricular nucleus of the hypothalamus (PVN) or to preganglionic autonomic neurons [35]. It is considered that information on blood volume or oxygenation is communicated via baro- and chemoreceptors to the nucleus of the tractus solitarius (*NTS*), which then send direct noradrenergic projections to the PVN, ensuring a rapid HPA axis response [31]. The forebrain limbic regions (which mediate psychogenic stressors) have no direct connections with the HPA axis or the SAM, and thus require intervening synapses (primarily to the locus coreleus, amygdala, and bed nucleus of the stria terminalis), prior to initiating a stress response [35, 36].

Nociceptors, interneurons, and "relay" neurons of the thalamus release a variety of excitation (pain) neurotransmitters, primarily, the substance P (SP), neurokinin A, Glutamat, calcitonin-gene-related peptide (CGRP), and cholecystokinin [37]. Recently, in the equine thalamic reticular neurons (TRN neurons), unique dopaminergic projections to the thalamic relay neurons were found, whereas in primates this input arises from a variety of dopaminergic neurons within the classically defined catecholaminergic system [38]. This possibly novel, potentially dopaminergic, projection upon thalamic relay neurons within the equids may play a modulatory role in the output of
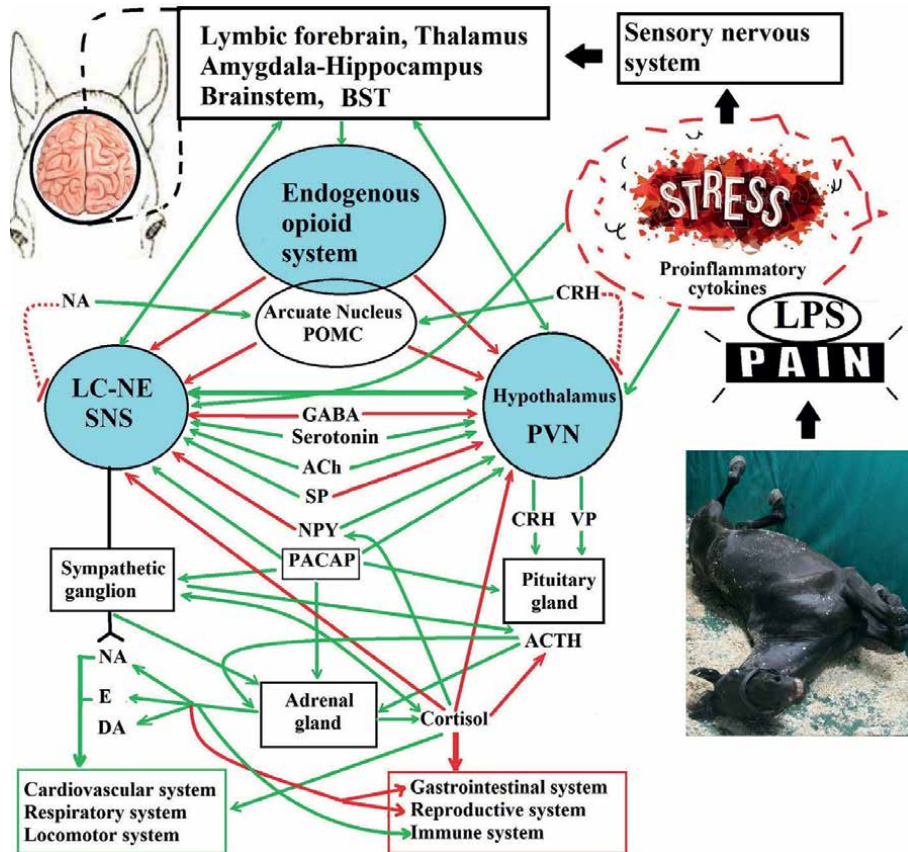
Figure 1.
Schematic representation of the central and peripheral components with regulatory pathways involved in the equine stress response caused by colic disease. LC/NE, locus coeruleus/norepinephrine system; SNS, sympathetic nervous system; PVN, paraventricular nucleus; BST, bed nucleus of the stria terminalis; POMC, proopiomelanocortin; CRH, corticotropin-releasing hormone; VP, vasopressin; GABA, γ-aminobutyric acid; ACTH, adrenocorticotropic hormone; NPY, neuropeptide Y; SP, substance P; Ach, acetylcholine; PACAP, pituitary adenylate cyclase-activating polypeptide; LPS, lipopolysaccharide; NA, norepinephrine; E, epinephrine; DA, dopamine. Activation is represented by green lines, inhibition by red lines and auto regulatory feedback loop by red dashed lines.

thalamic relay neurons to other structures of the brain [38]. It is considered, that these neurons have a strong influence on the processing of neural information, potentially providing the equid cerebral cortex with neural information that has a lower signal-to-noise ratio, making the extraction of salient neural information more precise than observed in other mammals [39]. The presence of catecholamines in the TRN neurons modifies stress behavior and may play a role in the various aspects of sleep observed in equids. It is well known that sleep in equids appears to be unusual, as they are short sleepers (around 2.9–3.3 hours per day), and have brief sleep cycles of around 15 min, with a non-rapid eye movement (REM) phase followed by a brief REM phase (less than 30 s), mostly while standing [40]. Undoubtedly, this evolutionary trait in horses on a daily basis supports a quick and effective alarm response to various acute stress factors.

After receiving a threat sensory information, most researchers argued that two areas of the brain have distinctive important roles in the stress reaction—the catecholaminergic neurons in the locus coeruleus (LC-NA system), which are mainly

responsible for activation of the SAM axis, and the hypothalamus, which is responsible for activation of HPA axis (**Figure 1**) [41–43]. Furthermore, other brain circuits modulate and fine-tune the adaptive or protective stress responses, including the amygdala-hippocampus complex, the mesocortical and mesolimbic components of the dopaminergic system, the noradrenergic cell group A2/C2 in the solitary nucleus, the A1/C1 cell groups in the ventrolateral medulla, the cuneiform nucleus and dorsal raphe nucleus, the parabrachial nucleus, and the bed nucleus of the stria terminalis [44, 45]. These structures are responsible for releasing various excitatory and inhibitory neurotransmitters, via overlapping brain circuits, in accordance with stressor modality or intensity. In addition, an alteration of the parasympathetic nervous system (PNS) with attenuation of the "vagal tone" of the heart and lungs occurs to help control the duration of activation of the SAM axis. Reconciliation of the PNS response to stress is mediated via the nucleus ambiguus and dorsal motor nucleus of the vagus nerve, possibly via input from the nucleus of the solitary tract [45].

3.1 LC/NE-sympathetic systems in the equine stress reaction

The locus coeruleus (LC) with noradrenergic neurons have been expressly implicated in the initiation and speed of acute physiological and behavioral stress changes in rodents and humans (likely in horses) [41, 42, 46, 47]. Extrapolation of results from other species to a horse should be performed with caution, to obtain a remarkable difference between equid and other animals because catecholamine metabolites are mostly glucuroconjugated and not sulfoconjugated [48]. LC receives inputs, not only from the spinal cord and thalamus, but also from the hypothalamus, medial prefrontal cortex, nucleus prepositus hypoglossi, and nucleus paragigantocellularis [49]. LPS (endotoxin) associated release proinflammatory cytokines (IL-1β, IL-6, and TNF-α) also facilitate norepinephrine (NA) release in LC [50]. Likely, this endotoxic activation of LC is especially important in horses with strangulation intestinal obstruction. After input activation, the noradrenergic neurons in the LC send then excitatory signals to different areas of the brain and to the spinal cord that are accompanied primarily by the alarm phase of the acute stress response [49]. Amplification of LC activity leads to increased signs of alertness in electroencephalographic (EEG) analysis [51]. The LC-NA system, through projections to the sympathetic preganglionic neurons in the spinal cord with activation of α_1-adrenoceptors, increases sympathetic activity and reduces parasympathetic activity, via the activation of α_2-adrenoceptors on preganglionic parasympathetic neurons [49, 52, 53]. Therefore, activation of the LC-NA system within seconds leads to the activation of the equine adrenal medulla (SAM), with a distant release of norepinephrine (NA) and other catecholamines—epinephrine (E) and dopamine (**Figure 1**). Consequently, this chain process in the alarm stress phase is more correctly denoted as activation of the LC-NA-sympathetic system, instead of activation of the SAM. In addition to NA release, the sympathetic nerve fibers also secrete adenosine triphosphate (ATP) and the neuropeptide Y (NPY), which enhance the systemic action of the catecholamines [54]. Accompanying the LC-NA-sympathetic system, the synthesis of E in the adrenal medulla partially stimulates the ACTH, cortisol, and pituitary adenylate cyclase-activating polypeptide (PACAP) [55].

3.1.1 Concentrations of equine epinephrine

The concentration of equine E in the blood depends on the tone of the sympathetic system, as it is associated with active escape, attack, and fear. In nonstress horses,

blood concentrations of E show a circadian rhythm. The mean plasma E concentrations were highest in the morning (~ 30 pg./ml at 8:00 hr), with a significant nadir in the sleeping phase at 04:00 hr. (~18 ng/ml) [56]. The concentrations of E increase up to 21 times higher during severe acute stress (fear, trauma) and intense physical activity [57]. The circadian rhythm of NA also exists, at 08:00 in the nonstressed horse, it was found to be 70–80 pg./ml, with the nadir observed at night (~50 pg./ml) [56]. In equine physical exercise stress, the NA concentration increases approximately 13-fold [58]. Thus, the response plasma levels of E and NA during exercise or other forms of acute stress in the horse is considerably greater than in people. The difference between horses and humans in SAM activity may help explain the superiority of the athletic performance of equine athletes compared to that of human athletes [59]. In horses during exercise, the increase in plasma NA is almost linearly proportional to exercise intensity, being higher after brief maximal exercise than after an endurance ride [58]. On the contrary, a marked increase in plasma E only occurs during strenuous exercise, especially if it is accompanied by psychogenic stress.

3.1.2 Roles of equine catecholamines

Basically, the equine catecholamines regulate many biochemical processes involved in energy metabolism, as well as the physical homeostasis adaptation associated with acute and rapid stress responses. Equine catecholamines have a strong impact on the bone marrow and spleen to enable the mobilization of additional blood. It has long been known that during the resting phase of horses, approximately 50–60% of blood (i.e., more than 20 L) is kept within reservoirs, in comparison to dogs (20–25%) and humans (12%) [60]. Consequently, during the alarm phase of the equine stress response, the splenic contraction under adrenergic control, ejects reservoir blood into the circulation, following significant increases in the hematocrit levels and concentrations of the erythrocytes, leucocytes, thrombocytes, hemoglobin, and plasma protein. The normal human spleen, unlike the horse spleen, does not contain many smooth muscle adrenergic receptors; therefore, it cannot strongly contract. Thus, the equine splenic contractile response to the various stress factors is more sensitive than that of any other species [60].

An increase in catecholamine release within the alarm phase leads to significant magnification of equine cardiac function. The cardiovascular system in horses is more stress sensitive than that of any other domestic species, as the increase in heart rate (HR), stroke *volume (SV),* cardiac output (CO), and blood pressure (BP) is enormous during an acute alarm stress reaction [61]. Independent of stress factors and its intensity, and through catecholamine binding to β_1 receptors in adult thoroughbreds (TB) horses, it was noticed that increasing the HR to 240 beats per minute (at rest 30–40 beats per minute), the SV to 1200 ml (at rest 900 ml), the BP to 250/120 mmHg (at rest 155/110 mmHg), the CO reached 240–340 l/min [62]. In nonstress horses, the CO is about 40 l/min, that is, by intense acute stress in horses is possible a 7–8 fold increase in cardiac function, in contrast to human athletes at approximately 2-fold [63, 64]. Commonly, these changes in cardiovascular parameters by acute stress horses are for a short time (5–60 sec), are intensively energy-consuming and straining, and the catecholamine concentrations quickly return to their resting levels [65]. It should also be remembered that these equine cardiovascular changes in acute stress are not only related to the increasing activities of the SNS and catecholamines but are also controlled by other vasoactive hormones, for example through plasma renin activity, atrial natriuretic peptide, endothelin-1 and vasopressin in the renin–angiotensin–aldosterone system.

3.1.3 Physiological changes during equine stress

Horses have a normal resting respiratory rate (RR) of 12–20 breaths per minute. During the onset of acute severe stress, in accordance with the body's need for oxygen, the RR rises as high as 180 breaths per minute [66]. In an adult TB horse at rest, the tidal volume (TV) is about 4–7 liters, rising to a maximum of about 10 liters during intense stress exercise [67]. When breathing at rest the dead space accounts for about 70% of the TV and the alveolar volume is around 30%. With exercise stress, there is a large increase in alveolar volume and a small increase in dead space. In adult nonstressed horses, the amount of air passing in and out of the lungs per minute (MV) is approximately 100 l/min. At maximal stress exercise, the MV reached 1500 l/min (due to a 7-fold increase in RR and a 2-fold increase in TV) [66]. Rate and depth of breathing are controlled in part by chemoreceptors in the blood vessels which respond to changes in pH, arterial oxygen, and carbon dioxide tension. When in gallop (stress flight) the RR is coupled with stride rate and so the mechanics of locomotion override the chemical control of breathing. This unique equine phenomenon is known as locomotor-respiratory coupling [68]. When exercise ceases, the RR decreases due to the cessation of the locomotor forces that drive respiration. These equine physiological and anatomic adaptations allow an extremely high maximal rate of use per minute of O_2 consumption (VO_2 max). By strenuous physical (stress) horse activity the VO_2 max reaches up to 200 ml/kg/min [66].

In addition, via stress activation of the LC-NA-sympathetic system, it has been noticed in horses (through contraction of the m. iris dilator) mydriasis with the appearance of tunnel vision (i.e., loss of peripheral vision) and increased body temperature, following sweating and suppression of secretion of the lacrimal and saliva glands can occur. In stressed animals, it was also noticed that decreases in gastrointestinal mobility, blood flow, and secretion could happen [69]. In the alarm phase of the stress response through catecholamines (but also through glucocorticoids), the horse's blood clotting function is accelerated to prevent excessive blood loss in the event of an injury sustained during the potential "stress fight response" [70, 71]. In the alarm phase of the equine stress response, it was noted that different immune functions were enhanced, through catecholamines binding to β-2 adrenergic receptors on immune cells (primarily on the NK cells), as well as through blood mobilization and direct sympathetic innervation of lymphoid organs (**Figure 1**) [72–74].

3.1.4 Catecholamines during stress responses

Catecholamines in an alarm phase of stress response vie β-2 adrenergic receptors induce significant lipolysis with increasing concentrations of blood fatty acids, that can be used directly as energy sources primarily by the locomotor system [75]. In different animal studies, it has been found that catecholamines, through α-adrenergic receptor binding, provoke inhibition of insulin secretion and significantly increased concentrations of glucagon (mediated through binding to the β-adrenergic receptor), and glucose, as a result of increasing either glycogenolysis or by gluconeogenesis [76, 77]. Additionally, catecholamine stimulation also releases ACTH, cortisol, and renin following the retention of sodium in the bloodstream [78].

Numerous other physiological reactions of catecholamines have also been noticed, which lead to the equine body producing additional speed and strength. For example, via the binding of alpha-1 adrenergic receptors by NA, it was noted that vasoconstriction of most blood vessels occurred in the skin, digestive tract, and kidneys [78]. These receptors are inhibited and counterbalanced by beta-2 adrenergic receptors

(stimulated by E release from the adrenal glands) in the skeletal muscles, heart, lungs, and the brain during a SAM response. At rest, in horses, only about 15% of the circulating blood is delivered to the muscles, but this increases to as much as 85% during strenuous stress exercise [66]. In other words, in the alarm phase of the stress response, through the activation of the LC-NA-sympathetic system, oxygen, and nutrient delivery is directed toward the CNS and areas of the body (primarily the cardiovascular and respiratory systems), where they are most needed to cope and escape from threat factors. In contrast, during severe acute stress responses other energy-consuming functions, such as digestion, reproduction, and growth, are temporally suppressed [59, 79, 80]. These changes are conditional and strongly depend on the type, intensity, and frequency of the stress factor. Thus, during equine stress exercise, a different picture of the hormonal background is observed in horses.

3.2 HPA axis in the equine stress reaction

In the second phase of the stress response (the stage of resistance), it is commonly observed that a strong activation of the HPA axis and the renin–angiotensin system (RAS) occurs, although a strict distinction between these stress phases is difficult to conclusively make as the reactions are dependent on the stress factor [81]. The intensity and frequency of the stressor is a major factor in determining the overall trajectory of the HPA axis response, with significantly increasing concentrations of the corticotropin-releasing factor (CRF), adrenocorticotropic hormone (ACTH), vasopressin (VP), and cortisol. Stressors of a presumptive "lesser" severity (for example the horse having 5 min exposure to a novel open field) produce lower peaks in HPA activation, in contrast to severe abdominal pain following, for example, an intestinal obstruction. The main goal of strongly activating the HPA axis during a stress reaction is the reinforcement of the homeostatic mechanisms and to provide additional energy through enhanced glycogenolysis, gluconeogenesis, and lipolysis [82, 83].

Usually, activation of the HPA axis is slightly slower than the activation of the LA-NA–sympathetic system. Commonly, after the onset of stress factor, the concentration of CRF rises immediately (as do concentrations of the NA), but the peak secretion of pituitary ACTH occurs around 5–15 s later, followed by the peak levels of cortisol 15 and 60 min later [84, 85]. There are also differences here, which are dependent on the stress factor. Commonly, various inflammatory stimuli cause prolonged HPA axis activation (2–3 hours after onset) commensurate with the need to limit immune responses [86].

3.2.1 Equine CRF

Equine CRF is a 41-amino acid peptide identical in structure to human and rat CRF. CRH is produced primarily by parvocellular neuroendocrine cells within the PVN, but this neuropeptide and specific CRH receptors have been identified in numerous extra hypothalamic regions of the brain, including the pituitary and adrenal glands [81, 87]. In addition to stimulating the secretion of the ACTH, CRH coordinates various physiological and behavioral responses, for example, induced anorectic effect, stereotyped behaviors, and enhancing the activity of the SNS [88]. Thus, one of the central actions of CRF is to appropriately facilitate "fight or flight" responses [89]. Besides this, CRF during stress responses inhibits, particularly, the secretion of GnRH, LH, testosterone, and estrogen, and through the stimulation of somatostatin secretion, it also inhibits the secretion of GH, TRH, and TSH [81].

Equine CRF concentrations in pituitary venous blood are lower compared to other species. In nonstress horses, the CRF concentration ranges from 0.25 to 0.8 pmol/l, but is very changeable day-to-day [90]. The regulation of CRF and VP secretion is complex. CRH and VP neurons in the PVN have dense connections with various structures in the brain. In the rodent and humans, the LC and other NE-synthesizing cell groups belonging to the medulla and pons have reciprocal reverberatory neural connections with the CRH neurons in the PVN and stimulate the secretion of each other through CRH receptor-1 (CRH-R1) and the α1-noradrenergic receptors, respectively (**Figure 1**) [91, 92]. It was also found that auto regulatory ultrashort negative feedback loops exist in both the PVN CRH and the catecholaminergic neurons of the LC, with collateral fibers inhibiting CRH and catecholamine secretion respectively, via inhibition of the corresponding presynaptic CRH- and α2-noradrenergic receptors [93, 94].

In addition, multiple other regulatory central pathways exist, since both CRH and the catecholaminergic neurons receive stimulatory (stress-excitatory) innervation from different brain structures through various neurotransmitters, among which is the especially important pituitary adenylate cyclase-activating polypeptide (PACAP; **Figure 1**). PACAP is a key emergency neuropeptide, mediating central and peripheral components of the stress axes [95]. This neurotransmitter is primarily expressed in the CNS and also within the sympathetic nervous system including the sympathetic preganglionic neurons that innervate the adrenal gland [96]. Thus, PACAP participates in stimulating the secretion of various hormones and neurotransmitters, including ACTH, VP, epinephrine, insulin, melatonin, prolactin, MSH, brain natriuretic peptide, follistatin, and the enkephalins [95, 97].

Serotonin, cytokines, and other inflammatory factors (e.g., nitric oxide) also participate in CRF secretion in the PVN in horses, as also seen in other mammals [98, 99]. Interestingly, NPY has multiple regulatory central pathways as it stimulates CRH neurons, whereas it inhibits the LC (**Figure 1**) [100]. On the other hand, SP, as the first responder to most noxious/extreme stimuli, has reciprocal actions to those of NPY, since it inhibits CRH neurons, whereas it activates the CA-NA system (**Figure 1**) [101, 102].

CRH and AVP neurons have reciprocal reverberatory neural connections to the pro-opiomelanocortin (POMC)-containing neurons in the arcuate nucleus (AN) of the hypothalamus. POMC-containing neurons primarily secrete β-endorphin [103]. Information on horse energy balance appears to access the PVN via projections namely, from neurons in the AC, which process circulating signals relevant to metabolic status (for example, glucose and fatty acid blood concentration) [104].

The neurons of the suprachiasmatic nucleus (SCN) of the hypothalamus also have several direct projections to the CRH neurons. The SCN is known to be the main (but not the only one) coordinator of biological circadian rhythms in mammals, described as the "CLOCK system" [105]. It is well known that the SCN neurons, through photoreception, have important roles in the basal daily and seasonal variation, not only on the equine HPA axis, but also on the hypothalamic–pituitary–*gonadal axis*, melatonin, insulin, grelin and adinopectin secretion, body temperature, and other factors [105, 106]. Thus, in resting horse conditions, through SCN input the HPA axis activity has circadian and ultradian variations. In the stress-free condition, there is a pulsatile secretion of equine CRF, VP, ACTH, and glucocorticoids (one per hour), with greater amplitudes in the morning (upon waking up) than at night [107, 108]. The circadian rhythm secretion of these hormones is disrupted under equine stressful conditions, as with other animals [109].

3.2.2 Equine vasopressin

Equine vasopressin (VP) is a nonapeptide, which is primarily produced in the magnocellular neurons of the PVN, its main effect is on the regulation of the blood pressure and ACTH secretion. VP is also expressed in other structures of the CNS, with functions in behavior, stress analgesia, and the regulation of circadian rhythms [110]. Normally, plasma vasopressin concentration in nonstress horses is less than 15 pg./mL [111]. An increase in equine VP concentrations is correlated with both the duration and intensity of the stress factor [112–114]. The basic physiological stimulus for a 5–10 fold increase in the secretion of VP is increased osmolality of the plasma, as well as the presence of hypotension due to hemorrhage or endotoxemia, for example in horses with colic [111]. Although VP has a short half-life (16–24 min), after a 3-day event endurance test, equine VP was elevated for 6 h [80].

3.2.3 Equine ACTH

Equine ACTH is a 39-amino acid peptide derived from pro-opiomelanocortin (POMC). POMC is the widespread archetypal polypeptide precursor of various hormones and neuropeptides with different functions, including several distinct melanotropins (β-MSH, α-MSH, γ-MSH), lipotropins, and endorphins (β-endorphin and met-enkephalin), corticotropin-like intermediate peptide (CLIP), that are contained within the adrenocorticotrophin and β-lipotropin peptides [115]. POMC is synthesized not only in corticotroph cells in the anterior pituitary gland, but also in the intermediate lobe of the pituitary gland, in neurons within the dorsomedial hypothalamus and brainstem, and as mentioned above it is also in the neurons within the AC of the hypothalamus. The first 18 amino acids of ACTH have the full biological activity of the whole molecule, and the first 24 amino acids are the same in all species of animals. Thus, the primary structure of equine ACTH is identical to that of the human hormone, as such, it has been suggested that they have the same biological activity [90].

CRF and VP act synergistically via specific receptors (CRF1 and V1B receptor, respectively) to trigger the release of ACTH from corticotroph cells, into the systemic circulation [116]. It has been suggested that CRF and VP mobilize different pools of pituitary ACTH. The equine pituitary gland has specific anatomical and functional features. The pars intermedia is particularly well developed in horses, and the equine pars distalis encloses the pars intermedia in a thin adherent layer as horses lack a clear hypophysial cleft [117].

ACTH production and secretion are indirectly influenced, not only by CRF, but also by the LC-NA-sympathetic system, PACAP, angiotensin II, vasoactive intestinal polypeptide, lipid mediators of inflammation, and cytokines, including TNF, IL-1β, and IL-6 [31, 81, 97]. Furthermore, endocannabinoids and endogenous opioid peptides appear to negatively regulate basal and stimulated ACTH release at multiple levels of the HPA axis (**Figure 1**) [115, 118].

The gradient in equine ACTH concentrations between pituitary effluent and jugular plasma can have an over 30-fold difference, with mean jugular plasma ACTH concentrations significantly higher in healthy horses (approximately 41 pmol/L), than in ponies [119]. Interestingly, a circadian rhythm in equine ACTH release is often undetectable. There is a disassociation between ACTH and corticosteroids during the circadian cycle suggesting a diurnal variation in the adrenal sensitivity to ACTH, with higher responsiveness during the peak phase of glucocorticoid secretion [120].

ACTH via binding specific receptors, namely type 2 melanocortin receptors (MC2-R) is the key regulator of glucocorticoid secretion (GCc) from the adrenal cortex [121, 122]. Currently, the expression of this subtype of melanocortin receptor in the equine adrenal cortex has not been characterized, but it is presumed to be similar to that described in humans. It has not been a significant relationship found between equine plasma ACTH and cortisol concentrations during exercise stress, and the maximum concentration of cortisol had no correlation with maximum ACTH concentrations [80].

3.2.4 Equine cortisol

Equine cortisol (EC) is a steroid hormone synthesized from cholesterol. EC is released into the circulation under the influence primarily of ACTH, but notably, existing evidence shows that cortisol secretion is further regulated by other hormones and/or cytokines coming from the adrenal medulla or the systemic circulation, and by neuronal signals via the autonomic innervation of the adrenal cortex (for example, as discussed above, through neuromediator PACAP) [95].

EC secretion rates are similar to humans and independent of various physiological factors, such as race, age, circadian rhythm, seasonality, exercise, and pregnancy [123]. Consequently, establishing a reference interval for the basal EC is difficult. In healthy adult horses at rest, the plasma EC levels range from 12 to 68 ng/ml or 33–187 nmol/l (total cortisol) or 10–23 nmol/l (free cortisol) [123, 124]. Under basal (nonstress) conditions, the equine adrenal gland produces cortisol at about 1 mg/kg body weight, with a pronounced pulsating rhythm in regular bursts (more as 10 per day) [124]. The highest daily value is reached shortly after waking up in the morning, before feeding and the minimum levels are observed between 6:00 and 9:00 pm [123]. The circadian rhythm of EC can be affected by various factors, such as exercise, mating, feeding, training, sleep patterns, individual activities, and especially during acute or chronic stress [125]. Plasma EC concentrations during stress responses are directly dependent on the stress factors, their duration, and frequency. Based on our unpublished studies, the total plasma EC concentration in horses with strangulated intestinal obstruction increases rapidly. We found that in colic horses independent of the degree of pain and endotoxic shock, upon admission into the clinic and before treatment commenced, there was wide individual variation in EC level (between 190 and 625 nmol/L), that is, 2–5 fold increases in comparison to the concentrations that are usually present in horses under resting conditions. We have also noticed that horses with a larger colon *volvulus, hernia* foraminis *omentalis* and *inguinal hernia* have, on average, higher EC concentrations than horses with right or left dorsal displacement of the *large colon.* The EC concentrations were significantly decreased after an abdominal surgery had been performed and steroid and non-steroidal antiphlogistics had been administered, but levels still remain more elevated than normal even when these horses had been discharged home (i.e., 10 days post-surgery). These findings are also supported by previous studies [10, 126, 127]. There is little doubt that EC levels in horses with colic are higher than those seen following transport stress [128, 129]. EC levels in transport horses correlate positively with transport duration and its conditions, but are also dependent on the individuals and their hormonal backgrounds, in this case on the stages of the estrous cycle and gestation [130, 131]. EC is frequently used to assess stress levels induced by exercise. In stress-induced exercise, a marked increase in EC levels was attributed to exercise duration and not to intensity [123]. In addition, the secretion of EC depends on the animal's prior experiences in competitions and the horse's character.

3.2.5 Interactions in the HPA axis response during equine stress

It is well known that a depletion of cortisol stores is noticed when animals are chronically stressed and thus the EC concentrations in stressed animals vary widely within the literature. Therefore, it is considered that cortisol levels are not always reliable indicators of chronic stress in horses. On the one hand, high cortisol levels can be a sign of positive stress that promotes higher performance; on the other hand, low cortisol does not necessarily mean the absence of stress. Usually, peak cortisol levels are reached 10–20 min after the onset of acute stress when transporting horses [128]. However, the ability of the adrenal glands to produce cortisol was preserved during transportation and did not decrease, and the pulsation from the transportation of horses after traveling 100–300 km persists [128]. In contrast, an elevation in ACTH concentration gradually decreases after transportation at increasing distances, and these changes were not directly associated with changes in cortisol levels. Similar to this, although an initial rise in EC levels follows a large spike in ACTH levels, if prolonged inflammatory stress occurs, ACTH levels return to near basal levels, while cortisol levels remain elevated as a result of adrenal hypersensitivity [131].

In plasma, EC binds to approximately 90% of a specific a1-glycoprotein named cortisol-binding globulin (CBG) and particularly to albumin. An inverse relationship between CBG Bmax and CBG affinity was demonstrated in mammals including the equine species [132]. The CBG maximal capacity (Bmax) was 0.22 in horses equivalent to 59% plasma cortisol concentration [123]. Equine CBG content at birth was the lowest of any species studied [132]. On the other hand, CBG concentration increased with age, whereas in other species it decreases, and the plasma of the newborn foal has a binding protein that has not been reported in other species, which binds as much cortisol as CBG does [132]. In studies on horses and other species, it has been shown that different stressors can influence CBG levels either by increasing or decreasing them in response to acute or chronic stress [133].

It is well known, those cortisol receptors are located in the cytoplasm of steroid-sensitive cells, and only the free portion of circulating cortisol is available to enter the cells by diffusion through the plasma membrane and binds to these intracellular glucocorticoid receptors (GR) [66, 81]. The steroid-sensitive cells are located in any organ and tissue of the equine body, and for this, the EC performs over a hundred different functions. This hormone has strong metabolic effects on carbohydrate balance (promoting glucose production in the liver), lipid metabolism (promoting the lipolytic effects of E and NA), protein catabolism (promoting amino acid mobilization), electrolyte and fluid balance, cardiovascular and respiratory homeostasis, sexual development and reproduction [22, 59, 73, 83, 88]. Thus, EC is critical for energy mobilization and distribution, and is needed to assure energy availability during, but also in the absence of, stress responses. EC exert their permissive effects on catecholamine release and take action in both vascular and cardiac tissue, as well as in the lungs. It has been noticed that glucocorticoids enhance cardiovascular sensitivity to catecholamines by increasing the binding capacity and affinity of β-adrenergic receptors in arterial smooth muscle cells, receptor-G protein coupling, and catecholamine-induced cAMP synthesis [134]. In addition, glucocorticoids prolong catecholamine actions in neuromuscular junctions by inhibiting catecholamine reuptake and decreasing peripheral levels of catechol-O-methyltransferase and monoamine oxidase [135]. There is not always such an unambiguous effect of cortisol with catecholamines. Sometimes, glucocorticoids can also inhibit a few features of sympathetic function and catecholamine release in response to some

stressors in rodents [136]. Along with this, glucocorticoids working through negative feedback also inhibit stress-induced NA in the PVN (**Figure 1**) [88]. Nonetheless, in acute stress the glucocorticoids facilitate sympathetic interactions, causing changes in the dopamine (DA) and noradrenaline (NA) systems, and their overall physiological effects are to permissively augment cardiovascular, respiratory, and locomotor activation. EC through inhibiting prostaglandin synthesis at basal levels blocks their vasodilatory effects. This is without doubt the central pathway by which cortisol causes increased blood pressure and the onset of laminitis in equine Cushing's syndrome (PPID) [137].

In general, glucocorticoids are powerful inhibitors of the immune system, primarily through inhibition of leukocyte traffic, secretion of cytokines by macrophages, and the production of antibodies (**Figure 1**) [138]. Due to evidence surrounding the immunosuppressive effects of cortisol, it has been proposed that a physiological function of strong stress-induced increases in this hormone is used to protect not against the source of stress itself, but against the normal defense reactions that are activated by stress. Thus, EC accomplishes this function by turning off those defense reactions, thus preventing them from overshooting themselves and threatening homeostasis [85].

Any trauma-induced hemorrhage causes a robust stress response in horses, along with the enhanced secretion of VP and renin, inducing water retention and vasoconstriction. Interestingly, EC through negative feedback inhibits the release of VP (by restoring the actions of inotropic and vasoconstrictive hormones), increases glomerular filtration rates, and increases the secretion and efficacy of atrial natriuretic polypeptide, all of which enhance water excretion [139]. From the point of view of homeostasis, the importance of suppression by EC in response to hemorrhage is that it prevents the organism from being injured or killed by its own defense mechanisms.

Cortisol also raises insulin concentrations in horses, but EC actions generally oppose but sometimes synergize with those of insulin [140]. For example, EC and insulin have opposite actions on blood glucose levels, as well as on appetite, gluconeogenesis, glucose transport, protein synthesis, muscle wastage, lipolysis, lipogenesis, and fat deposition in adipose tissue [141, 142]. Suppression of insulin and maintenance of blood glucose concentration has been related to the prevention of the onset of the central mechanism of fatigue [80]. EC also stimulates appetite over days in horses. In considering the criterion of homeostasis, it has been suggested that it aids recovery from the anorectic facet of the stress response caused by CRF. It has long been known that EC through negative feedback has indirect inhibitory effects on the CRH neuron, pituitary ACTH secretion, and POMC transcription (**Figure 1**) [43]. For energy homeostasis in stress conditions, humoral factors and neural afferents from the gastrointestinal tract communicate information to the brain to regulate energy intake and expenditure. Integrating these responses is a very important role carried out by prolactin-releasing peptide (PrRP), which is synthesized in discrete neuronal populations in the hypothalamus and brainstem [81]. Additionally, EC has a potentially disruptive effect on the reproductive function of horses through a number of mechanisms, for example, it decreases hypothalamic GnRH release and basal or GnRH-stimulated release of LH from the pituitary gland, but also through direct effects on the equine spermatogenesis and folliculogenesis in the gonads [143]. Prolonged activation of the HPA axis leads to decreased synthesis of thyroid-stimulating hormone (TSH) due to increased concentrations of CRH-induced somatostatin, which in turn suppresses both thyroid-releasing hormone (TRH) and TSH.

3.3 Endogenous opioid system in the equine stress response

It is well known that a prolonged phase of resistance is an energetically "disadvantageous" process of the metabolic load and with time the body's reserve will be depleted. Naturally, when the threatening challenge has passed, the equine body will try to shut off the stress response through various physiological mechanisms, for example, the organism trying to get into the recovery phase (or sanogenesis process). Endogenous mechanisms that oppose the stress response can determine the vulnerability or resilience of animals to the pathological consequences of stress. Turning off the equine stress reaction leads to a return to the baseline concentrations of CRF, VP, ACTH, EC, and catecholamines, and this normally happens when the danger has passed and/or the infection has been contained.

Numerous neural, endocrine, and paracrine mechanisms of physiological processes are involved in attenuating or mimicking stress responses, but one of the central roles is played by the endogenous opioids system (EOS). Thus, the EOS plays a dominant role in the third stage of GAS, just as catecholamines are the "main conductors" in the first stage, and glucocorticoids are essential in the second stage. Almost every acute stressor directly or indirectly causes the release of opioid peptides within seconds, but their action is commonly later than other stress hormones [144]. The EOS and its receptors are widely distributed throughout the CNS, and present in various organ systems and glands, such as the pituitary and adrenal glands [145]. There are three major endogenous opioid peptide families, preproopiomelanocortin (POMC), preproenkephalin, and preprodynorphin, which are cleaved active peptides, primarily endorphins, enkephalins, and dynorphin. These produce their effects through actions on μ-, δ and κ- G-protein coupled receptors, respectively [146].

The density reciprocal innervation between POMC-producing opioid peptide neurons of the hypothalamic arcuate nucleus and both the CRH/VP-producing and LC/NE-noradrenergic neurons is indicated in **Figure 1** [92]. Opiate peptides (enkephalins, dynorphins) and μ-opiate receptors are highly concentrated directly within the LC [49]. Additionally, it has been shown that μ-opiate receptors are co-localized with $α_2$-adrenoceptors in the LC, and their activation results in cellular inhibition via a shared potassium channel [49]. On the other hand, it has been shown that the LC plays an important role in the processes underlying opiate withdrawal [147]. Furthermore, endogenous opioid peptides (EOPs) strongly inhibit HPA axis activity [145].

In horses, in normal and in stressful conditions, the POMC acts as a precursor central endogenous opioid peptide β-endorphin (β-EP) and is primarily produced in the pars intermedia of the pituitary gland. Stress system activation also stimulates hypothalamus release of POMC-derived peptides, which reciprocally inhibits the activity of central stress system components [148]. The EOS performs various physiological functions, for example, it modifies the excitability of the CNS and induces control of various functional mechanisms, such as pain control, motor activity, lethargic stereotypical behaviors, feeding, immunity, thermoregulation, reproduction, antioxidation, ACTH secretion, and others [149].

3.3.1 The roles of β-EP and ACTH

Under *nonstress conditions, equine plasma* β-EP concentrations were recorded as 5.71–22.4 pmol/l [150, 151]. The daily rhythm of β-EP secretion is similar to that of ACTH and EC. The highest values of this opioid were noted in blood samples taken in

the morning. The application of an upper lip twitch resulted in a doubling of plasma β-EP concentration after 5 min [151]. It was found that the rise of equine β-EP was dependent on the type, intensity, and duration of stress physical exercise, modulates fatigue catecholamine secretion, and causes impairment of performance [152, 153]. During incremental exercise tests, plasma β-EP concentrations were positively correlated with exercise speed and intensity [154]. The critical threshold intensity of ≤60% VO_{2max} for significant increases in β-EP concentrations has been also recorded [154]. Prolonged air transportation also resulted in a sustained elevation of plasma β-EP concentrations compared to values measured at rest on the ground during the same day, but short-term road transport (i.e., for 1 hour) did not alter circulating equine plasma β-EP concentrations [151]. Other investigations noticed that concentrations of β-EP were raised when compared to the basic level only after a distance of 100 kilometers. After the ensuing 100 and 200 kilometers, a decrease was observed. Simultaneously in these horses, increases in the levels of circulating ACTH were observed after traveling distances of 100 and 200 kilometers, and levels of cortisol were higher after traversing distances of 100, 200, and 300 kilometers [150]. Horses with intestinal strangulation obstruction showed 5–10-fold elevations in plasma β-EP concentrations, which may have contributed to endotoxic shock and severe pain [151]. In contrast, horses with painful, but chronic lameness, had plasma concentrations of β-EP similar to those of normal horses, which may suggest an effect of negative feedback signaling or other factors, for example, cellular depletion of this hormone.

It may thus be assumed that upon analysis of the levels of β-EP and ACTH, the release of the opioid into the blood occurs maximally 1 hr after the appearance of the stressor [150]. The authors suggest that β-EP modulates the HPA axis activity. It may also be stated that β-EP release from the equine pituitary gland is synchronized with the initial phase of the stress reaction and may, in this way, mitigate the negative results of catecholamines and cortisol on the organism. Especially high concentrations of β-EP are found in horses with stereotypical behaviors and pituitary pars intermedia dysfunction (PPID). According to Millington *et al.*, [155], this concentration is 60 times higher in the plasma and 120 times higher in the cerebrospinal fluid of PIPD affected animals. Equine stereotypical behaviors under chronically stressful conditions help horses cope with stressors in the domesticated environment through their reputed self-rewarding effect. This behavior is highly likely to be associated with the EOS, as the use of opioid antagonists significantly reduces this equine behavioral appearance [156].

3.3.2 Stress-induced analgesia and the EOS

It has long been known that with acute stress there exists a phenomenon known as stress-induced analgesia (SIA) with a significantly increased pain threshold. From an evolutionary perspective, SIA can be viewed as a component of the predator–prey interactions, helping the survival of animals in the wild. A painful injury will not contribute toward the survival of the animal if there is a threat of further injury or death. In the process of SIA, a central role is played by the EOS [119]. SIA is primarily mediated through the binding of the μ-opioid receptor, this receptor shows greater selectivity for the β-EP, endomorphin, and enkephalins. Pharmacological studies have demonstrated that along with EOS, and a large number of other neurotransmitters and neuropeptides involved in the formation of the SIA, for example, GABA, serotonin, norepinephrine, dopamine, acetylcholine, glycine, oxytocin, vasopressin and neurotensin [92]. SIA is influenced by age, gender, and previous experiences

with stressful, painful, or other environmental stimuli. Commonly, the SIA lasts for a certain amount of time. However, when the equine body is no longer in danger, increased nociception, which manifests after the stress factor disappears, can be beneficial, since normal behavior can exacerbate the trauma.

3.3.3 Other roles of EOPs

EOP (including β-EP) also performs other functions, and one of these is transferring the body into hypobiosis, or the maximum energy-saving mode. It is characterized by heart and respiration rate decreases, changes in blood pressure, and temperature decline [144]. It turns out that hypobiosis is caused not so much by the depletion of the other two regulatory systems (SAM and HPA axis), via activation of the EOS. The shock (state of exhaustion) is an extreme degree of the stress response, in which the EOS has a very important role. Recently, it has been shown that a natural mechanism for recovering from abimal shock has "small peptides", or metabolic substances originating from the EOS, for example, the FMRFamide-related peptides (FaRPs) [157, 158]. These metabolic substances from endogenous opioids have an effect that is the opposite to them (supporting autoregulatory negative feedback). The first thing that happens during stress is the depletion of the adrenal apparatus. To return to its normal state, it must be activated in some way. FaRPs through binding of β-adrenergic receptors perform this function, thus bringing the body out of a state of exhaustion. This indicates that self-healing of stress (natural sanogenesis) is particularly associated with this peptide origin from the EOS.

3.3.4 EOS attenuation of stress

Unaccompanied, the EOS is not able to attenuate or shut off the stress response. In addition to the EOS, there are other neuromediators and hormones that have been proposed which protect against the effects of stress. Undoubtedly, to attenuate the equine stress response, it is necessary to activate the parasympathetic nervous system (PNS) with an increased tone of the vagus nerve and release of the neurotransmitter acetylcholine. Activation of PNS is mediated, among other things, via the neurons from the double reticular nucleus and the neurons from the nucleus of the solitary pathway of the medulla oblongata [81]. But this is not enough to completely "shut off" the animal's stress reaction. Numerous animal studies have shown that the hippocampus inhibits the activation of the CRH neurons in the PVN and LA through GABAergic and endocannabinoid neurotransmitters [31]. PVN neurons in the hypothalamus produce numerous neuropeptides that may contribute to activation via local paracrine actions, either by recurrent collaterals or dendritic release [159]. As mentioned above, due to mutual reverberant neural connections a gradually decreasing intensity or autoregulatory negative feedback loops exist between the CRF and the noradrenergic neurons, as in the initial stage they stimulate each other [93, 94].

Certainly, a pivotal role in attenuation of the stress response is also played via the mechanism of negative glucocorticoid feedback. Glucocorticoids have direct and indirect pathways to negative feedback to the limbic system, hypothalamus, and pituitary gland. This attenuates or decreases the primary release of CRF and ACTH. In the PVN, the binding of glucocorticoids to its receptor causes rapid synthesis and release of endocannabinoids. The released endocannabinoids bind to CB1 receptors on presynaptic terminals, inhibiting glutamate release and thereby reducing the drive to CRH neurons [160]. The effect of negative glucocorticoid feedback on equine VP

secretion is less pronounced than that for CRF because VP secreting neurons are less sensitive to glucocorticoids. Glucocorticoids may also provide positive feedback in some brain structures, particularly under chronic stress conditions [161]. In addition, neuropeptides associated with CRF, such as urocortin, also play an important role in suppressing (or activating) the function of the HPA axis during the stress response [162]. Numerous other hormones directly or indirectly attenuate deleterious effects of prolonged activation of the LA-NA-sympathetic and HPA axis in horses, foremost in that are the hormones melatonin and insulin, and therefore they are sometimes referred to anti-stress hormones [163, 164].

Through all of the physiological processes listed above, gradual decreases in the activities of the LA-NA-sympathetic axis and the HPA-axis have commonly been noticed. Depending on the stress factors (as well as their intensity and duration) a decrease in stress hormone levels in horses does not occur immediately. Commonly, it may take several hours or days for stress hormones to drop back to their baseline levels. It has also been noticed that in horses, repeated exposure to the same stressor (novelty stress) can result in habituation of the HPA axis response, characterized by decreasing glucocorticoid responses over time [165, 166]. Habituation appears to be mediated, at least in part, by the paraventricular thalamic nucleus [167]. But, it must also be noted that not all stressors cause response habituation in horses. Responses to more 'severe' stressors (e.g., pain) are maintained, therefore here it is possibly not an adaptation but only protection that comes into play.

4. Pathophysiology of equine stress

From the outset of stress research, it has been observed that not all stress reactions and the consequences are equal (despite the stereotypical neuroendocrine changes), and Selye introduced the terms "distress" (pathological) and "eustress" (physiological). Physiological stress accompanies long-term positive biological adaptation of the animal (for example, physical training, increases in horse muscle mass). The acute or chronic stress of severe intensity, which is not resolved by the adaptation of the animal, is considered distress. However, the clear contours and boundaries between eustress and distress, acute or chronic stress are difficult to define in equine practice, support for its existence is ambiguous, and there are still efforts in this area to clearly differentiate between normal homeostatic and pathophysiological responses. In other words, the chronic stress phenotype is not clearly defined [92]. Further complicating toward a clearer understanding is that equine stress responses are context-dependent and may reflect differences in the environment, timing (e.g., time of day, season), history of previous stressors, and huge among-individual variations [168]. There is widespread recognition that the effects of stress on the equine body are associated with the characteristics of the stress factor (the strength of the action, its duration, and frequency, predictability, controllability, avoidability), the breed and age, as well as some features of the stressful experience (previous contact with the same or other stress stimuli) [80, 112]. Thus, young horses and foals are much more stress reactive with more pathophysiological responses in comparison to adult animals.

The importance of acknowledging the protective, as well as the potentially damaging effects of stress reaction, has led to the introduction of different terms, for example, allostasis, allostatic load, or allostatic overload [169]. In response to a threat, allostasis maintains stability through adaptive dynamic activation of neuroendocrine, autonomic, cardiovascular, and immune systems, principally aiming to produce the new optimal

level of various physiological parameters. For example, physical exercise in horses leads to increased heart rate and blood pressure to provide optimal oxygen concentration to the vital organs. By focusing on neuroendocrine responses, allostasis involves a feed-forward mechanism rather than the negative feedback mechanisms used in homeostasis, with a continuous re-evaluation of need and continuous readjustment of all parameters toward new set points [170]. Using this theory allows us to explain the positive effects of stress on the animal body, for example, an increase in resistance to adverse factors and survival in extreme conditions. As mentioned above, the allostatic mechanism in horses must quickly disconnect once the threat has passed, as it impossible to keep a high level for a long time, due to depletion of reserve capabilities. Straining of the body supporting homeostasis under frequent or prolonged stress is called allostatic loading. It is also defined as the wear and tear associated with chronic hyperactivity or inadequate responses [171]. As allostatic load is characterized by an unstable functioning of the body, if it lasts for a long time or often, it causes the appearance of pathological changes (due to the cumulative effect), which are called allostatic overload.

Usually, under chronic stress, pathological changes are noticed simultaneously in many organs and tissues, primarily stress hormones cause the production of reactive oxygen species (ROS) or free radicals. It especially produces catecholamines, which as phenolic compounds easily undergo oxidation via a one-electron pathway involving several toxic products, such as semiquinones, quinones, and ROS, independently of the oxidation promotors. Almost any chronic stress through ROS has been shown to be responsible for the depletion of several free radical detoxifying enzymes, such as glutathione peroxidase, catalase, and superoxide dismutase [172]. It results in oxidative overloading, which has been implicated in the pathogenesis of different stress-associated pathologies, as well as in the occurrence of various mutations [173]. It is known that mutations accumulate as a result of DNA damage and imperfect DNA repair mechanisms. In animals (including horses) the accumulation of mutations is limited in two primary ways: through p53-mediated programmed cell death and cellular senescence mediated by telomeres at the end of chromosomes [174]. Telomeres shorten at every cell division and cells stop dividing once the shortest telomere reaches a critical length [175]. Cellular stress shortens the length of telomeres, and therefore it indirectly records the history of stress exposure. As a result, as biomarkers of cellular aging, telomere length and telomerase activity, have been considered for investigating the effects of chronic stress in human medicine [176]. This aspect of stress has not been adequately researched in horses to date.

There are numerous equine pathologies that are directly or indirectly associated with stress factors. According to our clinical experience, due to stress exposure, the most commonly noticed diseases in horses are—gastric ulcers, proximal enteritis, acute colitis, and pleuropneumonia [177–179]. It is important to note that for the occurrence of these diseases along with stress, other pathogenomonic factors have also had a significant impact. For example, for the occurrence of paralytic ileus or colitis, a high concentration of endotoxins in the blood also plays a very important role [177, 178]. Noxious gases (e.g., NH, NO, and CO) in the transport environment may be partially responsible for transport-related equine pleuropneumonia [179]. It is known that equine transport causes strong psychological stress reactions as it often combines the effects of neophobia, claustrophobia, social separation, and balancing. During equine transport, the physiological and endocrine stress changes prepare the horse's body for the "fight or flight" reaction, however, these actions do not actually follow, and therefore the mobilized energy is not used. Without a doubt in horses this leads to more often pathophysiological consequences, in comparison to stress physical overload, the neuroendocrine changes are accompanied by locomotion thus providing

an outlet for the mobilized energy. The reason for this phenomenon is poorly understood. It is possible, that physical activity in horses, as well as in humans, leads to the release of higher concentrations of endogenous opioids and other protective mediators against the destructive effects of stress hormones. It is also possible that the mobilized, but "unused" energy will lead to higher production of ROS.

Interestingly, of the four most common stress pathologies in the clinic in horses, three are associated with the gastrointestinal tract. The reasons for this appearance are multiple. Primarily, stress has strong adverse effects affecting the normal function of the GI tract, for example on the absorption process, mucus and stomach acid secretion, functioning of ion channels, and *peristalsis* [178, 180]. Stress induces increased intestinal permeability, allowing bacterial antigens (including LPS) to cross the epithelial barrier which activates a mucosal immune response, which in turn alters the composition of the microbiome and leads to enhanced activation of the neuroendocrine HPA axis. In other words, the equine intestinal microbiota also has been implicated in a variety of stress-pathophysiological responsiveness, but also in healthy horses, it clearly modulates the function of the immune and neuroendocrine systems, as well as various metabolic processes. The routes of communication between equine microbiota and CNS are slowly being unraveled, and include the microbial metabolites such as short-chain fatty acids, the vagus nerve, intestinal hormone signaling, and tryptophan metabolism.

Whether the horse will get sick or die from these and other stress-associated diseases depend primarily on immune systems and individual resistance. The individual characteristics of equine stress resistance are determined by the type of the nervous system, lability, or dominance of the parasympathetic or sympathetic nervous systems [168]. Based on our experience, horses with a high parasympathetic tone are much less likely to die from the stress-associated disease than animals with a high sympathetic tone (neurotic horses). Equine neuroticism is also linked to a low pain threshold, indicating such horses were more likely to be stressed by pain [181]. The effect of stress is also dependent on the initial level of hormones, which in turn depends on various factors, including the phase of the light cycle [92], but to date, there has not been a detailed investigation as to which period of the day horses are more tolerant toward stress-induced disease.

5. Indicators of equine stress

Information on equine stress levels is important when evaluating many aspects of horse management, training, and the treatment of different diseases. It is apparent that great effort is being made to improve recognition and quantitative evaluation of stress in horses. Various testing techniques are used to measure stress responses in horses, which can be roughly divided into visual, clinical and laboratory, or noninvasive and invasive methods [182]. Behavioral indicators of stress responses are very different, and very well described [183, 184]. In an attempt to quantify visual changes equine stress, the "The Horse Grimace Scale" (HGS) has recently been used, which is fine-tuned for detecting equine pain, but no validated grimace scale for detecting fear or anxiety exists yet [184].

5.1 Clinical signs of equine stress

Clinical signs of disturbance of the sympathovagal balance can be used to assess acute equine stress which primarily includes changes in cardiovascular parameters,

for example, increased heart rate (i.e., presence of sinus tachycardia) and heart rate variability (i.e., presence of nonrespiratory sinus arrhythmia) [62, 182, 185, 186]. According to our recent investigations, sinus tachycardia and sinus arrhythmia are the most frequently diagnosed arrhythmia in equine clinic praxis [187]. Other clinical signs of acute stress are altered respiratory rate and increased body/eye temperatures [66, 182]. For studying the functional state of the brain, to test its bioelectric activity it is possible to use electroencephalographic (EEG) analysis in horses with or without stress conditions. We improved the methods for recording multichannel EEG in horses with specific six unipolar leads using overhead electrodes (Ippolitova/Gauss method) (**Figure 2**) [188]. Comparative evaluation of electroencephalographic patterns in sporting horses with different types of higher nervous activity, as well as taking account for the age and training level was recently conducted for the first time. It allows the determination of an organism's potential capabilities, its resistance to stress, and thus the expected performance in competitions [188].
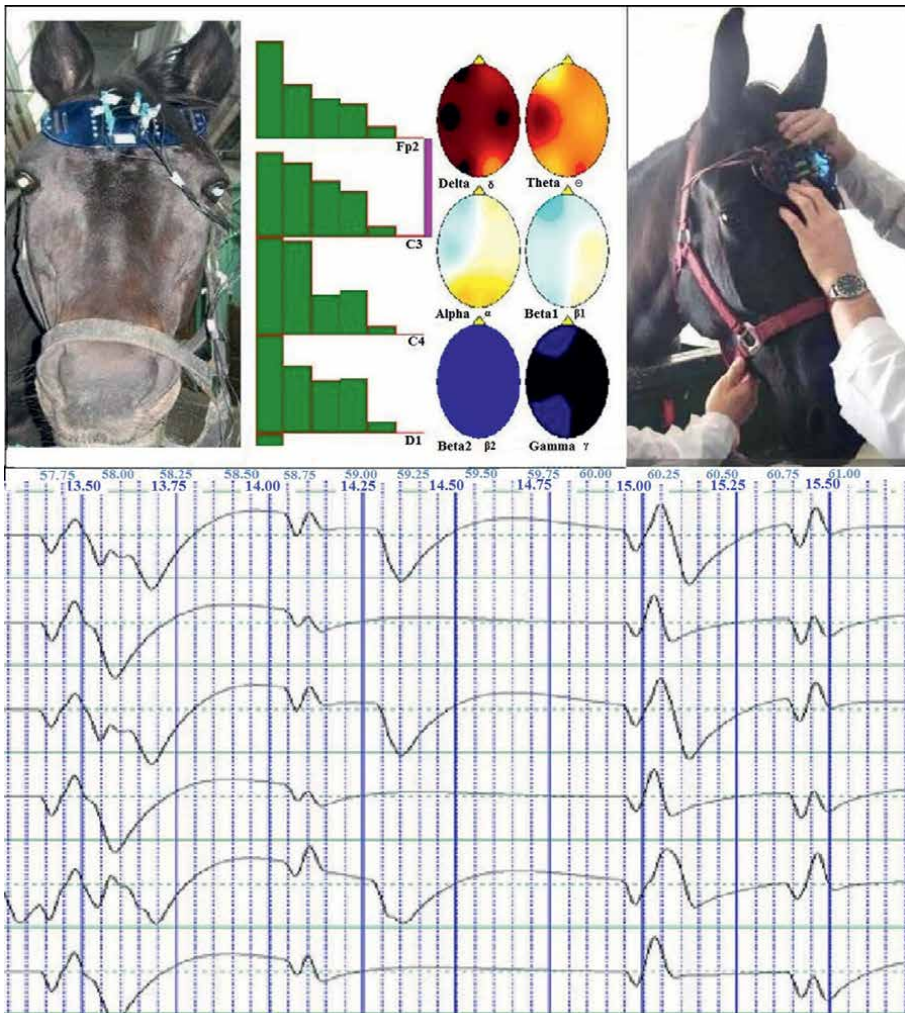
Figure 2.
Equine electroencephalographic recording of brain activity.

5.2 Blood parameters during equine stress

Various specific blood parameters can be used to assess the degree of stress activation. Commonly used were performance analyses of equine blood concentrations of E, NA, ACTH, cortisol, and β-EP [57, 111, 123, 125, 150]. However, E has a short half-life of only a few minutes, making this substance an impractical parameter for studies under field conditions [56]. Secretion of alpha-amylase from the salivary glands is controlled by autonomic nervous signals, and several studies have revealed that salivary alpha-amylase is correlated with SNS activity under stress conditions [189]. For ease of accessibility reasons equine cortisol is most often measured as a biomarker of the stress response, not only in blood but also in saliva, feces, and hair [123]. Interestingly cortisol concentration increases are noticed in saliva with a delay of approximately 20–30 min before the same observation in blood. However, it is becoming clear that relying on glucocorticoids to define stress is incomplete, and there is no current consensus that glucocorticoids should serve as the primary biomarker for defining the stress phenotype.

5.3 Pathological changes during equine stress

Stress-induced pathological changes also confirm the presence of chronic stress in the horse, for example, the occurrence of gastric ulcers. Parameters such as altered metabolism or suppressed immune function may have the potential to provide information on the long-term effects of stress, especially those which are related to blood chemistry (for example plasma or blood lactate levels, prolactin, iodothyronine, estradiol-17β, serum creatine kinase activity, IL-1, TNF). But these biochemical parameters are not specific for the measurement of stress in animals. Therefore, to date, there have been significant difficulties in measuring stress biomarkers in horses and their pathological effects, especially at the genetic, molecular, and cellular levels. In recent times in humans, different damage markers (e.g., lipid peroxidation, protein oxidation, stress-associated proteins, or oxidative stress mediators, as well length of telomeres) have been used to better reflect how people have coped with stress exposure [190].

Finally, it is necessary to take into account all these listed methods in the present day, not only in equine, but also in human medicine, and also to highlight that we have deficiencies in our abilities to analyze chronic stress before it becomes pathological. Thus far, there is a lack of understanding relating to the stress threshold, in analyses of the cumulative impact of multiple stressors over time, as well as the role of individual equine variation in reaction to stress and timing (e.g., time of day, season). Therefore, equine medicine requires improved contact sensing technology development that will allow for long-term, dynamic, noninvasive, multifactorial measurements of sets of stress mediators, as well as improvements in the diagnosis of stress damage at the cellular and genetic levels.

6. Conclusions

This review presents new aspects toward understanding neuroendocrine regulation of equine stress, and its influences on the physiological and pathophysiological processes. Horse management, in essence, is more frequently confirmed by external and internal stress factors, in comparison to other domestic animals.

In the last few decades, the initial concepts of stress have been revised. New studies have expanded the basis of stress responses to signals from various sensory receptors, through complex interactions of at least three systems that are activated in a time sequence: the locus coeruleus-norepinephrine (LC-NE)-sympathetic system, the HPA axis, and the endogenous opioid system. The interconnection of these systems provides control of norepinephrine, epinephrine, and cortisol release, but also other stress mediators, such as corticotropin-releasing hormone, adrenocortico-tropin, vasopressin, β-endorphin, dopamine, neuropeptide Y, serotonin, oxytocin, cytokines (IL-1β, IL-6), pituitary adenylate cyclase-activating polypeptide, FMRF-amide-related peptides (FaRPs), prolactin-releasing peptide (PrRP), and others. Linked into this interconnection network are other organ systems affected in one or several stages of the stress response. Commonly, these reactions in the horse are related to short-term stress responses leading to mobilization of the body's reserves in a process of constant flow around the homeostatic point. In situations of allostatic overload, a dynamic change from physiological to pathological response can be expected in horses, with the induction of primarily stomach ulcers, paralytic ileus, colitis, and pleuropneumonia. The change from equine physiological to pathological stress response depends not only on whether the stress is acute or chronic but also on the physical characteristics of the stress signals (intensity), as well as on the initial hormone levels, which in turn depend on various factors, including photoperiod sensitivity.

The development of stress-related diseases in horses dictates how long the inter-action of sanogenesis with pathogenic factors will last. These diseases can often be prevented or controlled by keeping risk factors minimal, and by assessing stress levels using a variety of testing techniques. Regardless of the nature of the stimulus, the equine stress response is an effective and highly conservative set of interconnected relationships designed to maintain physiological integrity even in the most challeng-ing circumstances. It activates numerous neural and hormonal networks to optimize metabolic, cardiovascular, respiratory, locomotory, and immunological functions.

Conflict of interest

The authors declare no conflict of interest.

Author details

Milomir Kovac[1]*, Tatiana Vladimirovna Ippolitova[1], Sergey Pozyabin[1], Ruslan Aliev[1], Viktoria Lobanova[1], Nevena Drakul[1] and Catrin S. Rutland[2]

1 Veterinary Clinic "New Century", Moscow State Academy of Veterinary Medicine and Biotechnology, Moscow, Russia

2 School of Veterinary Medicine and Science, University of Nottingham, Nottingham, UK

*Address all correspondence to: kovacmilomir@gmail.com

IntechOpen

References

[1] Daev EV. About stress, or about Hans Selye's two errors, conquered the world. Ecological Genetics. 2019;**17**(4):103-111. DOI: 10.17816/ecogen174103-111

[2] Gabriel W. How stress selects for reversible phenotypic plasticity. Journal of Evolutionary Biology. 2005;**18**(4): 873-883. DOI: 10.1111/j.1420-9101. 2005.00959.x

[3] Matsui T, Ehrenreich IM. Gene-environment interactions in stress response contribute additively to a genotype-environment interaction. PLoS Genetics. 2016;**12**(7):e1006158. DOI: 10.1371/journal.pgen.1006158

[4] Hausberger M, Bruderer C, Le Scolan N, Pierre J-S. Interplay between environmental and genetic factors in temperament/personality traits in horses (Equus caballus). Journal of Comparative Psychology. 2004;**118**(4):434-446. DOI: 10.1037/0735-7036.118.4.434

[5] McBride SD, Mills DS. Psychological factors affecting equine performance. BMC Veterinary Research. 2012;**8**(1):180. DOI: 10.1186/1746-6148-8-180

[6] Hori Y, Tozaki T, Nambo Y, Sato F, Ishimaru M, et al. Evidence for the effect of serotonin receptor 1A gene (HTR1A) polymorphism on tractability in thoroughbred horses. Animal Genetics. 2016;**47**(1):62-67. DOI: 10.1111/age.12384

[7] Ninomiya S, Anjiki A, Nishide Y, Mori M, Deguchi Y, Satoh T. Polymorphisms of the dopamine D4 receptor gene in stabled horses are related to differences in Behavioral response to frustration. Animals. 2013;**3**(3):663-669. DOI: 10.3390/ani3030663

[8] Hori Y, Ozaki T, Yamada Y, Tozaki T, Kim HS, et al. Breed Differences in

Dopamine Receptor D4 Gene (DRD4) in Horses. Journal of Equine Science. 2013;**24**(3):31-36. DOI: 10.1294/jes.24.31

[9] Selye H. Stress and the general adaptation syndrome. British Medical Journal. 1950;**1**(4667):1383-1392. DOI: 10.1136/bmj.1.4667.1383

[10] Mair TS, Sherlock CE, Boden LA. Serum cortisol concentrations in horses with colic. Veterinary Journal. 2014;**201**(3):370-377. DOI: 10.1016/j. tvjl.2014.06.005

[11] Espinosa-Oliva AM, de Pablos RM, Villaran RF, Argüelles S, Venero JL, et al. Stress is critical for LPS-induced activation of microglia and damage in the rat hippocampus. Neurobiology of Aging. 2011;**32**(1):85-102. DOI: 10.1016/j. neurobiolaging.2009.01.012

[12] Crowell-Davis SL. Social behaviour of the horse and its consequences for domestic management. Equine Veterinary Education. 1993;**5**(3):148-150. DOI: 10.1111/j.2042-3292.1993.tb01025.x

[13] Talor PM. Equine stress responses to anaesthesia. British Journal of Anaesthesia. 1989;**63**(6):702-709. DOI: 10.1093/bja/63.6.702

[14] Holbrook TC, McFarlance D, Schott HC. Neuroendocrine and non-neuroendocrine markers of inflammation associated with performance in endurance horses. Equine Veterinary Journal. 2010;**42**:123-128. DOI: 10.1111/j.2042-3306.2010.00256.x

[15] Smiet E, Van Dierendonck MC, Sleutjens J, Menheere PPCA, van Breda E, et al. Effect of different head and neck positions on behaviour, heart rate variability and cortisol levels in

lunged Royal Dutch Sport horses. The Veterinary Journal. 2014;**202**(1):26-32. DOI: 10.1016/j.tvjl.2014.07.005

[16] Peeters M, Closson C, Beckers J-F, Vandenheede M. Rider and horse salivary cortisol levels during competition and impact on performance. Journal of Equine Veterinary Science. 2013;**33**(3): 155-160. DOI: 10.1016/j.jevs.2012.05.073

[17] Hines MT. Clinical approach to commonly encountered problems. Equine Internal Medicine. 2018;**7**:232-310. DOI: 10.1016/b978-0-323-44329-6. 00007-3

[18] Houpt KA, Eggleston A, Kunkle K, Houpt TR. Effect of water restriction on equine behaviour and physiology. Equine Veterinary Journal. 2000;**32**(4):341-344. DOI: 10.2746/042516400777032200

[19] Waran NK, Clarke N, Farnworth M. The effects of weaning on the domestic horse (Equus caballus). Applied Animal Behaviour Science. 2008;**110**(1-2):42-57. DOI: 10.1016/j.applanim.2007.03.024

[20] Erber R, Wulf M, Rose-Meierhöfer S, Becker-Birck M, Möstl E, et al. Behavioral and physiological responses of young horses to different weaning protocols: A pilot study. Stress. 2011;**15**(2):184-194. DOI: 10.3109/10253890.2011.606855

[21] Hartmann E, Chritensen JW, Keeling LJ. Training young horses to social separation: Effect of a companion horse on training efficiency. Equine Veterinary Journal. 2011;**43**(5):580-584. DOI: 10.1111/j.2042-3306.2010.00326.x

[22] Folkman S. Stress: Appraisal and coping. In: Encyclopedia of Behavioral Medicine. 2nd Edition. M.D. Gellman. New York:Springer; 2013. pp. 1913-1915. DOI: 10.1007/978-1-4419-1005-9_215

[23] Gronqvist G, Rogers C, Gee E, Bolwell C, Gordon S. The challenges of using horses for practical teaching purposes in veterinary programmes. Animals. 2016;**6**(11):69. DOI: 10.3390/ ani6110069

[24] Smith AV, Proops L, Grounds K, Wathan J, McComb K. Horses give functionally relevant responses to human facial expressions of emotion: A response to Schmoll (2016). Biology Letters. 2016;**12**(9):20160549. DOI: 10.1098/ rsbl.2016.0549

[25] McCarty R, Horwatt K, Konarska M. Chronic stress and sympathetic-adrenal medullary responsiveness. Social Science & Medicine. 1988;**26**(3):333-341. DOI: 10.1016/0277-9536(88)90398-x

[26] Schommer NC, Hellhammer DH, Kirschbaum C. Dissociation between reactivity of the hypothalamus-Pituitary-adrenal Axis and the sympathetic-adrenal-medullary system to repeated psychosocial stress. Psychosomatic Medicine. 2003;**65**(3):450-460. DOI: 10.1097/01.psy.0000035721.12441.17

[27] Simic N. Changes in the activity of sympathetic-adrenal medullary system and hypothalamic-pituitary-adrenal system in humans exposed to psychogenic stressors and their effects on immunoreactivity. Acta Medica Croatica. 2010;**64**(4):273-282

[28] Bermudez-Humaran LG, Salinas E, Ortiz GG, Ramirez-Jirano LJ, Morales JA, Bitzer-Quintero OK. From probiotics to Psychobiotics: Live beneficial Bacteria which act on the brain-gut Axis. Nutrients. 2019;**11**(4):890. DOI: 10.3390/ nu11040890

[29] Kotas ME, Medzhitov R. Homeostasis, inflammation, and disease susceptibility. Cell. 2015;**160**(5):816-827. DOI: 10.1016/j.cell.2015.02.010

[30] Dedovic K, Duchesne A, Andrews J, Engert V, Pruessner JC. The brain and the

stress axis: The neural correlates of cortisol regulation in response to stress. NeuroImage. 2009;**47**:864-871. DOI: 10.1016/j.neuroimage.2009.05.074

[31] Herman JP, Figueiredo H, Mueller NK, Ulrich-Lai Y, Ostrander MM, et al. Central mechanisms of stress integration: Hierarchical circuitry controlling hypothalamo–pituitary–adrenocortical responsiveness. Frontiers in Neuroendocrinology. 2003;**24**(3):151-180. DOI: 10.1016/j.yfrne.2003.07.001

[32] Julius D, Nathans J. Signaling by sensory receptors. Cold Spring Harbor Perspectives in Biology. 2011;**4**(1): a005991-a005991. DOI: 10.1101/cshperspect.a005991

[33] Ralston HJ. Pain and the primate thalamus. Cortical Function: A View from the Thalamus. 2005;**149**:1-10. DOI: 10.1016/s0079-6123(05)49001-9

[34] Kamber N. Neuroanatomy and Pathophysiology of Pain Perception. Therapeutische Umschau. 2020;**77**(6): 239-245. DOI: 10.1024/0040-5930/a001185

[35] Ulrich-Lai YM, Herman JP. Neural regulation of endocrine and autonomic stress responses. Nature Reviews Neuroscience. 2009;**10**(6):397-409. DOI: 10.1038/nrn2647

[36] Benarroch EE. The locus ceruleus norepinephrine system: Functional organization and potential clinical significance. Neurology. 2009;**73**(20): 1699-1704. DOI: 10.1212/wnl.0b013 e3181c2937c

[37] Millan MJ. The induction of pain: An integrative review. Progress in Neurobiology. 1999;**57**(1):1-164. DOI: 10.1016/s0301-0082(98)00048-3

[38] Chaumeton AS, Gravett N, Bhagwandin A, Manger PR. Tyrosine hydroxylase containing neurons in the thalamic reticular nucleus of male equids. Journal of Chemical Neuroanatomy. 2020;**110**:101873. DOI: 10.1016/j.jchemneu.2020.101873

[39] Guillery RW, Feig SL, Lozsádi DA. Paying attention to the thalamic reticular nucleus. Trends in Neurosciences. 1998;**21**(1):28-32. DOI: 10.1016/s0166-2236(97)01157-0

[40] Williams DC, Aleman M, Holliday TA, Fletcher DJ, Tharp B, et al. Qualitative and quantitative characteristics of the electroencephalogram in Normal horses during spontaneous drowsiness and sleep. Journal of Veterinary Internal Medicine. 2008;**22**(3):630-638. DOI: 10.1111/j.1939-1676.2008.0096.x

[41] Benarroch EE. Locus coeruleus. Cell and Tissue Research. 2017;**373**(1):221-232. DOI: 10.1007/s00441-017-2649-1

[42] Ehlers MR, Todd RM. Genesis and maintenance of attentional biases: The role of the locus Coeruleus-noradrenaline system. Neural Plasticity. 2017;**2017**:1-15. DOI: 10.1155/2017/6817349

[43] Nicolaides NC, Kyratzi E, Lamprokostopoulou A, Chrousos GP, Charmandari E. Stress, the stress system and the role of glucocorticoids. Neuroimmunomodulation. 2015;**22** (1-2):6-19. DOI: 10.1159/000362736

[44] McEwen BS, Gianaros PJ. Central role of the brain in stress and adaptation: Links to socioeconomic status, health, and disease. Annals of the New York Academy of Sciences. 2010;**1186**(1):190-222. DOI: 10.1111/j.1749-6632.2009.05331.x

[45] Iversen S, Iversen L, Saper CB. Principles of Neural Science. New York: Mc-Graw Hill; 2000

[46] Sara SJ, Bouret S. Orienting and reorienting: The locus Coeruleus

mediates cognition through arousal. Neuron. 2012;**76**(1):130-141. DOI: 10.1016/j.neuron.2012.09.011

[47] William TA, Lee WD. Peripheral and central effects of circulating Catecholamines. Comprehensive Physiology. 2014;**5**:1-15. DOI: 10.1002/cphy.c140007

[48] Chiu SH, Huskey SW. Species differences in N-glucuronidation. Drug Metabolism and Disposition. 1998;**26**(9):838-847

[49] Samuels E, Szabadi E. Functional neuroanatomy of the noradrenergic locus Coeruleus: Its roles in the regulation of arousal and autonomic function part II: Physiological and pharmacological manipulations and pathological alterations of locus Coeruleus activity in humans. Current Neuropharmacology. 2008;**6**(3):254-285. DOI: 10.2174/157015908785777193

[50] Kurosawa N, Shimizu K, Seki K. The development of depression-like behavior is consolidated by IL-6-induced activation of locus coeruleus neurons and IL-1β-induced elevated leptin levels in mice. Psychopharmacology. 2015;**233**(9):1725-1737. DOI: 10.1007/s00213-015-4084-x

[51] Berridge C, Foote S. Effects of locus coeruleus activation on electroencephalographic activity in neocortex and hippocampus. Journal of Neuroscience. 1991;**11**(10):3135-3145. DOI: 10.1523/jneurosci.11-10-03135.1991

[52] Jones BE, Yang T-Z. The efferent projections from the reticular formation and the locus coeruleus studied by anterograde and retrograde axonal transport in the rat. The Journal of Comparative Neurology. 1985;**242**(1):56-92. DOI: 10.1002/cne.902420105

[53] Unnerstall JR, Kopajtic TA, Kuhar MJ. Distribution of α2 agonist binding sites in the rat and human central nervous system: Analysis of some functional, anatomic correlates of the pharmacologic effects of clonidine and related adrenergic agents. Brain Research Reviews. 1984;**7**(1):69-101. DOI: 10.1016/0165-0173(84)90030-4

[54] Macarthur H, Wilken GH, Westfall TC, Kolo LL. Neuronal and non-neuronal modulation of sympathetic neurovascular transmission. Acta Physiologica. 2011;**203**(1):37-45. DOI: 10.1111/j.1748-1716.2010.02242.x

[55] Watanabe T, Shimamoto N, Takahashi A, Fujino M. PACAP stimulates catecholamine release from adrenal medulla: A novel noncholinergic secretagogue. American Journal of Physiology. Endocrinology and Metabolism. 1995;**269**(5):E903-E909. DOI: 10.1152/ajpendo.1995.269.5.e903

[56] Kurosawa M, Takeda F, Nagata S. Circadian variations in plasma adrenaline and noradrenaline in the thoroughbred horse. Journal of Equine Science. 1997;**8**(3):81-88. DOI: 10.1294/jes.8.81

[57] Warren JB, Dalton N, Turner C, Clark TJ, Toseland PA. Adrenaline secretion during exercise. Journal of Clinical Sciences. 1984;**66**(1):87-90. DOI: 10.1042/cs0660087

[58] Nagata S, Takeda F, Kurosawa M, Mima K, Hiraga A, Kai M, et al. Plasma adrenocorticotropin, cortisol and catecholamines response to various exercises. Equine Veterinary Journal. 1999;**31**(30):570-574. DOI: 10.1111/j.2042-3306.1999.tb05286.x

[59] Jimenez M, Hinchcliff KW, Farris JW. Catecholamine and cortisol responses of horses to incremental exertion. Veterinary Research Communications. 1998;**22**(2):107-118. DOI: 10.1023/a:1006027429526

[60] Boucher JH. The equine spleen: Source of dangerous red blood cells. Journal of Equine Veterinary Science. 1987;**7**(3):140-142. DOI: 10.1016/S0737-0806(87)80022-9

[61] Thayer JF, Hahn AW, Pearson MA, Sollers JJ 3rd, Johnson PJ, Loch WE. Heart rate variability during exercise in the horse. Biomedical Sciences Instrumentation. 1997;**34**:246-251

[62] Clayton HM. Conditioning Sport Horses. Mason: Sport Horse Publication; 1991

[63] von Borell E, Langbein J, Després G, Hansen S, Leterrier C. Heart rate variability as a measure of autonomic regulation of cardiac activity for assessing stress and welfare in farm animals - a review. Journal of. Physiology & Behavior. 2007;**92**(3):293-316. DOI: 10.1016/j.physbeh.2007.01.007

[64] Fleisher AL. Heart rate variability as an assessment of cardiovascular status. Journal of Anesthesia. 1996;**10**(5):659-671. DOI: 10.1016/s1053-0770(96)80146-7

[65] Malliani A, Montano N. Heart rate variability as a clinical tool. Italian Heart Journal. 2002;**3**(8):439-445

[66] Hinchcliff KW, Geor RJ, Kaneps AJ. Equine Exercise Physiology. Churchill Livingstone: Elsevier; 2008. DOI: 10.1016/B978-0-7020-2857-1.X5001-X

[67] Butler PJ, Woakes AJ, Smale K, Roberts CA, Hillidge CJ, et al. Respiratory and cardiovascular adjustments during exercise of increasing intensity and during recovery in thoroughbred racehorses. Journal of Experimental Biology. 1993;**179**:159-180

[68] Lafortuna CL, Reinach E, Saibene F. The effects of locomotor-respiratory coupling on the pattern of breathing in horses. Journal of Physiology. 1996;**492**(Pt 2):587-596. DOI: 10.1113/jphysiol.1996.sp021331

[69] Mittal R, Debs LH, Patel AP, Nguyen D, Patel K, et al. Neurotransmitters: The Critical Modulators Regulating Gut-Brain Axis. Journal of Cellular Physiology. 2017;**232**(9):2359-2372. DOI: 10.1002/jcp.25518

[70] DeNotta SL, Brooks MB. Coagulation Assessment in the Equine Patient. Veterinary Clinics of North America: Equine Practice. 2020;**36**(1):53-71. DOI: 10.1016/j.cveq.2019.12.001

[71] Wirtz PH, Ehlert U, Emini L, Rüdisüli K. The role of stress hormones in the relationship between resting blood pressure and coagulation activity. Journal of Hypertension. 2006;**24**(12):2409-2416. DOI: 10.1097/HJH.0b013e32801098e5

[72] Cuniberti B, Badino P, Odore R, Girardi C, Re G. Effects induced by exercise on lymphocyte β-adrenergic receptors and plasma catecholamine levels in performance horses. Research in Veterinary Science. 2012;**92**(1):116-112. DOI: 10.1016/j.rvsc.2010.11.002

[73] Keadle TL. The Effects of Exercise Stress on Equine Immune Function. Baton Rouge: Diss. Louisiana State University; 1992

[74] Horohov DW, Dimock A, Guirnalda P, Folsom RW, McKeever KH, et al. Effect of exercise on the immune response of young and old horses. American Journal of Veterinary Research. 1999;**60**(5):643-647

[75] Carrington EF, Desautels M, Naylor JM. Beta-adrenergic stimulated lipolysis in pony adipocytes is exclusively via a beta2-subtype and is not affected by

lactation. Comparative Biochemistry and Physiology Part A. 2003;**136**(2):311-320. DOI: 10.1016/s1095-6433(03)00157-0

[76] Kritchevsky JE, Muir GS, Leschke DH, Hodgson JK, Hess EK, Bertin FR. Blood glucose and insulin concentrations after alpha-2-agonists administration in horses with and without insulin dysregulation. Journal of Veterinary Internal Medicine. 2020;**34**(2):902-908. DOI: 10.1111/jvim.15747

[77] Arnall DA, Marker JC, Conlee RK, Winder WW. Effect of infusing epinephrine on liver and muscle glycogenolysis during exercise in rats. American Journal of Physiology. 1986;**250**(6 Pt 1):E641-E649. DOI: 10.1152/ajpendo.1986.250.6.E641

[78] Tank AW, Lee WD. Peripheral and central effects of circulating catecholamines. Comprehensive Physiology. 2015;**5**:1-15. DOI: 10.1002/cphy.c140007

[79] de Graaf-Roelfsema E, Keizer HA, van Breda E, Wijnberg ID, van der Kolk JH. Hormonal responses to acute exercise, training and overtraining. A review with emphasis on the horse. Veterinary Quarterly. 2007;**29**(3):82-101. DOI: 10.1080/01652176.2007.9695232

[80] Ferlazzo A, Cravana C, Fazio E, Medica P. The different hormonal system during exercise stress coping in horses. Veterinary World. 2020;**13**(5): 847-859. DOI: 10.14202/vetworld. 2020.847-859

[81] Fink G. Stress: Neuroendocrinology and Neurobiology. 1st ed. Cambridge: Acad. Press; 2017;**2**:3-15. DOI: 10.1016/B978-0-12-802175-0.00001-2

[82] Van de Kar LD, Blair ML. Forebrain pathways mediating stress-induced hormone secretion. Frontiers in Neuroendocrinology. 1999;**20**(1):1-48. DOI: 10.1006/frne.1998.0172

[83] Chu B, Marwaha K, Sanvictores T, Ayers D. Physiology, stress reaction. In: StatPearls [Internet]. Treasure Island (FL): StatPearls Publishing; 2021

[84] Solomon MB, Loftspring M, de Kloet AD, Ghosal S, Jankord R. Neuroendocrine function after hypothalamic depletion of glucocorticoid receptors in male and female mice. Endocrinology. 2015;**156**(8):2843-2853. DOI: 10.1210/en.2015-1276

[85] Sapolsky RM, Romero LM, Munck AU. How do glucocorticoids influence stress responses? Integrating permissive, suppressive, stimulatory, and preparative actions. Endocrine Reviews. 2000;**21**(1):55-89. DOI: 10.1210/edrv.21.1.0389

[86] Choi DC, Furay AR, Evanson NK, Ostrander MM, Ulrich-Lai YM, Herman JP. Bed nucleus of the stria terminalis subregions differentially regulate hypothalamic-pituitary-adrenal axis activity: Implications for the integration of limbic inputs. Journal of Neuroscience. 2007;**27**:2025-2034. DOI: 10.1523/JNEUROSCI.4301-06.2007

[87] Valentino RJ, Page M, van Bockstaele E, Aston-Jones G. Corticotropin-releasing factor innervation of the locus coeruleus region: Distribution of fibers and sources of input. Journal of Neuroscience. 1992;**48**(3):689-705. DOI: 10.1016/0306-4522(92)90412-U

[88] Aguilera G. HPA axis responsiveness to stress: Implications for healthy aging. Experimental Gerontology. 2011;**46** (2-3):90-95. DOI: 10.1016/j.exger. 2010.08.023

[89] Bale TL, Vale WW. CRF and CRF receptors: Role in stress responsivity and other behaviors. Annual Review of Pharmacology and Toxicology. 2004;**44**:525-557. DOI: 10.1146/annurev. pharmtox.44.101802.121410

[90] Alexander SL, Irvine CH, Ellis MJ, Donald RA. The effect of acute exercise on the secretion of corticotropin-releasing factor, arginine vasopressin, and adrenocorticotropin as measured in pituitary venous blood from the horse. Endocrinology. 1991;**128**(1):65-72. DOI: 10.1210/endo-128-1-65

[91] Borodovitsyna O, Joshi N, Chandler D. Persistent stress-induced Neuroplastic changes in the locus Coeruleus/norepinephrine system. Neural Plasticity. 2018;**2018**:1-14. DOI: 10.1155/2018/1892570

[92] Tsigos C, Kyrou I, Kassi E, Chrousos GP. Stress: Endocrine physiology and pathophysiology. Endotext-NCBI Bookshelf (Internet), South Dartmouth, MA. 2020

[93] Silverman AJ, Hou-Yu A, Chen WP. Corticotropin-releasing factor synapses within the paraventricular nucleus of the hypothalamus. Neuroendocrinology. 1989;**49**:291-299. DOI: 10.1159/000125131

[94] Aghajanian GK, VanderMaelen CP. Alpha 2-adrenoceptor-mediated hyperpolarization of locus coeruleus neurons: Intracellular studies in vivo. Journal of Science. 1982;**215**:1394-1396. DOI: 10.1126/science.6278591

[95] Hashimoto H, Shintani N, Tanida M, Hayata A, Hashimoto R. PACAP is implicated in the stress axes. Current Pharmaceutical Design. 2011;**17**(10):985-989. DOI: 10.2174/138161211795589382

[96] Solés-Tarrés I, Cabezas-Llobet N, Vaudry D, XifróProtective X. Effects of Pituitary adenylate cyclase-activating polypeptide and vasoactive intestinal peptide against cognitive decline in neurodegenerative diseases. Frontiers in Cellular Neuroscience. 2020;**14**:221. DOI: 10.3389/fncel.2020.00221

[97] Denes V, Geck P, Mester A, Gabriel R, Pituitary. Adenylate cyclase-activating polypeptide: 30 years in research spotlight and 600 million years in service. Journal of. Clinical Medicine. 2019;**8**(9):1488. DOI: 10.3390/jcm8091488

[98] Lowry CA. Functional subsets of serotonergic neurones: Implications for control of the hypothalamic-pituitary-adrenal axis. Journal of Neuroendocrinology. 2002;**14**:911-923. DOI: 10.1046/j.1365-2826.2002.00861.x

[99] Rivest S. How circulating cytokines trigger the neural circuits that control the hypothalamic-pituitary-adrenal axis. Journal of Psychoneuroendocrinology. 2001;**26**:761-788. DOI: 10.1016/s0306-4530(01)00064-6

[100] Thorsell A., Diverse M. H. Functions of neuropeptide Y revealed using genetically modified animals. Neuropeptides. 2002; 36(2-3):182-193. DOI: 10.1054/npep.2002.0897.

[101] Ebner K, Singewald N. The role of substance P in stress and anxiety responses. Journal of Amino Acids. 2006;**31**(3):251-272. DOI: 10.1007/s00726-006-0335-9

[102] Medica P, Giunta RP, Bruschetta G, Ferlazzo AM. The influence of training and simulated race on horse plasma serotonin levels. Journal of Equine Veterinary Science. 2020;**84**:102818. DOI: 10.1016/j.jevs.2019.102818

[103] Millington GW. The role of proopiomelanocortin (POMC) neurones in feeding behavior. Journal of Nutrition

and Metabolism. 2007;**4**:18. DOI: 10.1186/1743-7075-4-18

[104] Baskin DG, Figlewicz LD, Seeley RJ, Woods SC, Porte D Jr, Schwartz MW. Insulin and leptin: Dual adiposity signals to the brain for the regulation of food intake and body weight. Brain Research. 1999;**848**:114-123. DOI: 10.1016/s0006-8993(99)01974-5

[105] Gnocchi D, Bruscalupi G, Rhythms C, Homeostasis H. Circadian Rhythms and hormonal Homeostasis: Pathophysiological implications. Biology. 2017;**6**(1):10. DOI: 10.3390/biology6010010

[106] McKeever KH. Endocrine alterations in the equine athlete: An update the veterinary clinics of North America. Equine Practice. 2011;**27**(1):197-218. DOI: 10.1016/j.cveq.2011.01.001

[107] Murphy BA. Chronobiology and the horse: Recent revelations and future directions. Veterinary Journal. 2010;**185**(2):105-114. DOI: 10.1016/j.tvjl.2009.04.013

[108] Berger A, Scheibe KM, Eichhorn K, Scheibe A, Streich J. Diurnal and ultradian rhythms of behaviour in a mare group of Przewalski horse (Equus ferus przewalskii), measured through one year under semi-reserve conditions. Applied Animal Behaviour Science. 1999;**64**(1):1-17. DOI: 10.1016/S0168-1591(99)00026-X

[109] Bertolucci C, Giannetto C, Fazio F, Piccione G. Seasonal variations in daily rhythms of activity in athletic horses. Animal. 2008;**2**:1055-1060. DOI: 10.1017/S1751731108002267

[110] Frank E, Landgraf R. The vasopressin system--from antidiuresis to psychopathology. European Journal of Pharmacology. 2008;**583**(2-3):226-242. DOI: 10.1016/j.ejphar.2007.11.063

[111] Ludders JW, Palos H-M, Erb HN, Lamb SV, Vincent SE, Gleed RD. Plasma arginine vasopressin concentration in horses undergoing surgery for colic. Journal of Veterinary Emergency and Critical Care. 2009;**19**(6):528-535. DOI: 10.1111/j.1476-4431.2009.00475.x

[112] McKeever KH. Endocrine alterations in the equine athlete: An update. Veterinary Clinics: Equine Practice. 2011;**27**(1):197-218. DOI: 10.1016/j.cveq.2011.01.001

[113] Hyyppä S. Endocrinal responses in exercising horses. Livestock Production Science. 2005;**92**(2):113-121. DOI: 10.1016/j.livprodsci.2004.11.014

[114] Aguilera G, Rabadan-Diehl C. Vasopressinergic regulation of the hypothalamic-pituitary-adrenal axis: Implications for stress adaptation. Regulatory Peptides. 2000;**96**(1-2):23-29. DOI: 10.1016/s0167-0115(00)00196-8.117

[115] Harno E, Gali RT, Coll AP, White A. POMC: The physiological power of hormone processing. Physiological Reviews. 2018;**98**(4):2381-2430. DOI: 10.1152/physrev.00024.2017

[116] Hauger RL, Dautzenberg FM. Regulation of the stress response by Corticotropin-releasing factor receptors. In: Conn PM, Freeman ME, editors. Neuroendocrinology in Physiology and Medicine. New Jersey: Humana Press; 2000. pp. 261-286

[117] van der Kolk JH, Heinrichs M, van Amerongen JD, Stooker RCJ, van den Ingh TS, et al. Evaluation of pituitary gland anatomy and histopathologic findings in clinically normal horses and horses and ponies with pituitary pars intermedia adenoma. American Journal of Veterinary Research. 2004;**65**(12):1701-1707. DOI: 10.2460/ajvr.2004.65.1701

[118] Hill MN, Tasker JG. Endocannabinoid Signaling, glucocorticoid-mediated negative feedback and regulation of the HPA Axis. Journal of Neuroscience. 2012;**204**:5-16. DOI: 10.1016/j.neuroscience.2011.12.030

[119] Dodman NH, Shuster L, Court MH, Dixon R. Investigation into the use of narcotic antagonists in the treatment of a stereotypic behavior pattern (crib-biting) in the horse. American Journal of Veterinary Research. 1987;**48**(2):311-319

[120] Couëtil L, Paradis MR, Knoll J. Plasma adrenocorticotropin concentration in healthy horses and in horses with clinical signs of hyperadrenocorticism. Journal of Veterinary Internal Medicine. 1996;**10**(1):1-6. DOI: 10.1111/j.1939-1676.1996.tb02016.x

[121] Alexander SL, Irvine CH, Donald RA. Dynamics of the regulation of the hypothalamo-pituitary-adrenal (HPA) axis determined using a nonsurgical method for collecting pituitary venous blood from horses. Frontiers in Neuroendocrinology. 1996;**17**(1):1-50. DOI: 10.1006/frne.1996.0001

[122] Katarzyna AD, Lindsey MJ, Kathryn JT, Jillian SM, et al. Multiple adrenocortical steroid response to administration of exogenous adrenocorticotropic hormone to hospitalized foals. Journal of Veterinary Internal Medicine. 2019;**33**(4):1766-1774. DOI: 10.1111/jvim.15527

[123] Touma C, Bunck M, Glasl L, Nussbaumer M, Palme R, Stein H, et al. Mice selected for high versus low stress reactivity: A new animal model for affective disorders. Journal of Psychoneuroendocrinology. 2008;**33**(6):839-862. DOI: 10.1016/j.psyneuen.2008.03.013

[124] Ambrojo KS, Corzano MM, Poggi JCG. Action mechanisms and pathophysiological characteristics of cortisol in horses. In: Corticosteroids. Rijeka: IntechOpen; 2018. DOI: 10.5772/intechopen.72721

[125] Bousquet-Melou A, Formentini E, Picard-Hagen N, Delage L, Laroute V. The Adrenocorticotropin stimulation test: Contribution of a physiologically based model developed in horse for its interpretation in different pathophysiological situations encountered in man. Endocrinology. 2006;**147**(9):4281-4291. DOI: 10.1210/en.2005-1161

[126] Pell SM, McGreevy PD. A study of cortisol and beta-endorphin levels in stereotypic and normal thoroughbreds. Applied Animal Behaviour Science. 1999;**64**:81-90. DOI: 10.1016/S0168-1591(99)00029-5

[127] Hinchcliff KW, Rush BR, Farris JW. Evaluation of plasma catecholamine and serum cortisol concentrations in horses with colic. Journal of the American Veterinary Medical Association. 2005;**227**(2):276-280. DOI: 10.2460/javma.2005.227.276

[128] Edner AH, Nyman GC, Essen-Gustavsson B. Metabolism before, during and after anaesthesia in colic and healthy horses. Acta Veterinaria Scandinavica. 2007;**49**(1):34. DOI: 10.1186/1751-0147-49-34

[129] Stull CL, Rodiek AV. Effects of cross-tying horses during 24 h of road transport. Equine Veterinary Journal. 2010;**34**(6):550-555. DOI: 10.2746/042516402776180214

[130] Friend TH. Dehydration, stress, and water consumption of horses during long-distance commercial transport. Journal of Animal Science. 2000;**78**(10):2568. DOI: 10.2527/2000.78102568x

[131] Pawluski J, Jego P, Henry S, Bruchet A, Palme R, et al. Low plasma cortisol and fecal cortisol metabolite measures as indicators of compromised welfare in domestic horses (Equus caballus). PLoS One. 2017;**12**(9): e0182257. DOI: 10.1371/journal. pone.0182257

[132] Fazio E, Medica P, Aronica V, Grasso L, Ferlazzo A. Circulating β-endorphin, adrenocorticotrophic hormone and cortisol levels of stallions before and after short road transport: Stress effect of different distances. Acta Veterinaria Scandinavica. 2008;**50**(1):6. DOI: 10.1186/1751-0147-50-6

[133] Gayarard V, Alvinerie V, Toutain PL. Interspecies variations of corticosteroid-binding globulin parameters. Domestic Animal Endocrinology. 1996;**13**(1):35-45. DOI: 10.1016/0739-7240(95)00042-9

[134] Desantis LM, Delehanty B, Weir JT. Rudy Boonstra mediating free glucocorticoid levels in the blood of vertebrates: Are corticosteroid-binding proteins always necessary? Functional Ecology. 2013;**27**(1):107-119. DOI: 10.1111/1365-2435.12038

[135] Sakaue M, Hoffman BB. Glucocorticoids induce transcription and expression of the α1B adrenergic receptor gene in DTT1 MF-2 smooth muscle cells. Journal of Clinical Investigation. 1991;**88**(2):385-389. DOI: 10.1172/JCI115315

[136] Gibson A. The influence of endocrine hormones on the autonomic nervous system. Journal of Autonomic Pharmacology. 1981;**1**(4):331-358. DOI: 10.1111/j.1474-8673.1981.tb00463.x

[137] Kvetnansky R, Fukuhara K, Pacak K, Cizza G, Goldstein DS, et al. Endogenous glucocorticoids restrain catecholamine synthesis and release at rest and during immobilization stress in rats. Endocrinology. 1993;**133**(3):1411-1419. DOI: 10.1210/endo.133.3.8396019

[138] Dianne MF. Equine Pituitary pars intermedia dysfunction. Veterinary Clinics: Equine Practice. 2011;**27**(1):93-113. DOI: 10.1016/j.cveq.2010.12.007

[139] Strehl C, Ehlers L, Gaber T, Buttgereit F. Glucocorticoids—All-Rounders tackling the versatile players of the immune system. Frontiers in Immunology. 2019;**10**:1744. DOI: 10.3389/fimmu.2019.01744

[140] Hayamizu S, Kanda K, Ohmori S, Murata Y, Seo H. Glucocorticoids potentiate the action of atrial natriuretic polypeptide in adrenalectomized rats. Endocrinology. 1994;**135**(6):2459-2464. DOI: 10.1210/endo.135.6.7988432

[141] Borer-Weir KE, Menzies-Gow NJ, Bailey SR, Harris PA, Elliott J. Seasonal and annual influence on insulin and cortisol results from overnight dexamethasone suppression tests in normal ponies and ponies predisposed to laminitis. Equine Veterinary Journal. 2013;**45**(6):688-693. DOI: 10.1111/evj.12053

[142] Harrington MKK. The endocrine system and the challenge of exercise. The Veterinary Clinics of North America. Equine Practice. 2002;**18**(2):321-353. DOI: 10.1016/S0749-0739(02)00005-6

[143] Bartolome E, Cockram MS. Potential effects of stress on the performance of sport horses. Journal of Equine Veterinary Science. 2016;**40**(5):84-93. DOI: 10.1016/j.jevs.2016.01.016

[144] AboEl-Maaty AM. Stress and its effects on horses reproduction. Veterinary Science Development. 2011;**1**(1):13. DOI: 10.4081/vsd.2011.3440

[145] McCarthy L, Wetzel M, Sliker JK, Eisenstein TK, Rogers TJ. Opioids, opioid receptors, and the immune response. Drug and Alcohol Dependence. 2001;**62**(2):111-123. DOI: 10.1016/s0376-8716(00)00181-2

[146] Sakanaka M, Magari S, Shibasaki T, Inoue N. Co-localization of corticotropin-releasing factor- and enkephalin-like immunoreactivities in nerve cells of the rat hypothalamus and adjacent areas. Brain Research. 1989;**487**:357-336. DOI: 10.1016/0006-8993(89)90840-8

[147] Nothacker HP, Reinscheid RK, Mansour A, Henningsen RA, Ardati A, et al. Primary structure and tissue distribution of the orphanin FQ precursor. Proceedings of the National Academy of Sciences of the United States of America. 1996;**93**:8677. DOI: 10.1073/pnas.93.16.8677

[148] Koob GF, Maldonado R, Stimus L. Neural substrates of opiate withdrawal. Trends in Neurosciences. 1992;**15**:186-191. DOI: 10.1016/0166-2236(92)90171-4

[149] Valentino RJ, Van Bockstaele E. Opposing regulation of the locus coeruleus by corticotropin-releasing factor and opioids. Potential for reciprocal interactions between stress and opioid sensitivity. Psychopharmacology. 2001;**158**(4):331-342. DOI: 10.1007/s002130000673

[150] Foreman JH, Ferlazzo A. Physiological responses to stress in the horse. Journal of Pferdeheilkunde. 1996;**12**(4):401-404. DOI: 10.21836/PEM19960405

[151] Golynski M, Krumrych W, Lutnicki1 K. The role of beta-endorphin in horses: A review. Veterinární Medicína. 2011;**56**(9):423-429. DOI: 10.17221/3205-VETMED

[152] Jeffcott LB, Clarke LB, Clark IJ. Preliminary studies on the use of plasma β-endorphin in horses as an indicator of stress and pain. Journal of Equine Veterinary Science. 1993;**13**(4):216-219. DOI: 10.21836/PEM20040108

[153] Ferlazzo A, Fazio E, Cravana C, Medica P. The role of circulating β-endorphin in different stress models in equines: A review. Journal of Equine Veterinary Science. 2018;**71**(12):98-104. DOI: 10.1016/j.jevs.2018.10.012

[154] Golland LC, Evans DL, Stone GM, Tyler-McGowan CM, Hodgson DR, Rose RJ. Maximal exercise transiently disrupts hormonal secretory patterns in Standardbred geldings. Equine Veterinary Journal Supplements. 1999;**30**(7):581-585. DOI: 10.1111/j.2042-3306.1999.tb05288.x

[155] Mehl ML, Schott HC 2nd, Sarkar DK, Bayly WM. Effects of exercise intensity and duration on plasma beta-endorphin concentrations in horses. American Journal of Veterinary Research. 2000;**61**(8):969-973. DOI: 10.2460/ajvr.2000.61.969

[156] Millington WR, Dybdal NO, Dawson R Jr, Manzini C, Mueller GP. Equine Cushing's disease: Differential regulation of beta-endorphin processing in tumors of the intermediate pituitary. Journal of Endocrinology. 1988;**123**(3):1598-1604. DOI: 10.1210/endo-123-3-1598

[157] Zubieta JK, Smith YR, Bueller JA, Xu Y, Kilbourn MR, Jewett DM, et al. Regional mu opioid receptor regulation of sensory and affective dimensions of pain. Journal of Science. 2001;**293**:311-315. DOI: 10.1126/science.1060952

[158] Tiniakov RL, Parin SB, Bespalova ZD, Krushinskaia IV, Sokolova NA. FMRFa and FMRFamide-like peptides (FaRPs) in the pathogenesis

of shock. Uspekhi Fiziologicheskikh Nauk. 1998;**29**(3):56-65

[159] Rőszer T, Bánfalvi G. FMRFamide-related peptides: anti-opiate transmitters acting in apoptosis. Peptides. 2012;**34**(1):177-185. DOI: 10.1016/j.peptides.2011.04.011

[160] Son SJ, Filosa JA, Potapenko ES, Biancardi VC, Zheng H, et al. Dendritic peptide release mediates interpopulation crosstalk between neurosecretory and preautonomic networks. Neuron. 2013;**78**(6):1036-1049. DOI: 10.1016/j.neuron.2013.04.025

[161] Hillard CJ. Circulating endocannabinoids: From whence do they come and where are they going? Neuropsychopharmacology. 2018;**4**(3):155-172. DOI: 10.1038/npp.2017.130

[162] Makino S, Gold PW, Schulkin J. Corticosterone effects on corticotropin-releasing hormone mRNA in the central nucleus of the amygdala and the parvocellular region of the paraventricular nucleus of the hypothalamus. Brain Research. 1994;**640**:105-112. DOI: 10.1016/0006-8993(94)91862-7

[163] Squillacioti C, Pelagalli A, Liguori G, Mirabella N. Urocortins in the mammalian endocrine system. Acta Veterinaria Scandinavica. 2019;**61**(1):46. DOI: 10.1186/s13028-019-0480-2

[164] Murphy BA, Martin AM, Furney P, Elliott JA. Absence of a serum melatonin rhythm under acutely extended darkness in the horse. Journal of Circadian Rhythms. 2011;**9**:3. DOI: 10.1186/1740-3391-9

[165] Bertin FR, Ruffin-Taylor D, Stewart AJ. Insulin dysregulation in horses with systemic inflammatory response syndrome. Journal of Veterinary Internal Medicine. 2018;**32**(4):1420-1427. DOI: 10.1111/jvim.15138

[166] Christensen JW. Object habituation in horses: The effect of voluntary versus negatively reinforced approach to frightening stimuli. Journal of Equine Veterinary Science. 2013;**45**(3):298-301. DOI: 10.1111/j.2042-3306.2012.00629.x

[167] Hada T, Onaka T, Takahashi T, Hiraga A, Yagi K. Effects of novelty stress on neuroendocrine activities and running performance in thoroughbred horses. Journal of Neuroendocrinology. 2003;**15**(7):638-648. DOI: 10.1046/j.1365-2826.2003.01042.x

[168] Bhatnagar S, Huber R, Nowak N, Trotter P. Lesions of the posterior paraventricular thalamus block habituation of hypothalamic-pituitary-adrenal responses to repeated restraint. Journal of Neuroendocrinology. 2002;**14**:403-410. DOI: 10.1046/j.0007-1331.2002.00792.x

[169] Romero ML, Platts SH, Schoech SJ, Wada H, Crespi E. Understanding stress in the healthy animal – Potential paths for progress. The International Journal on Biology of Stress. 2015;**18**(5):491-497. DOI: 10.3109/10253890.2015.1073255

[170] Sterling P, Eyer J. Biological basis of stress-related mortality. Social Science and Medicine. Part E Medical Psychology. 1981;**15**(1):3-42. DOI: 10.1016/0271-5384(81)90061-2

[171] Ramsay DS, Woods SC. Clarifying the roles of homeostasis and allostasis in physiological regulation. Psychological Review. 2014;**121**(2):225-247. DOI: 10.1037/a0035942

[172] McEwen BS, Stellar E. Stress and the individual. Mechanisms leading to disease. Archives of Internal Medicine. 1993;**153**(18):2093-2101

[173] Liu Y, Schubert DR. The specificity of neuroprotection by antioxidants. Journal of Biomedical Science. 2009;**16**:98. DOI: 10.1186/1423-0127-16-98

[174] Von Zglinicki T, Pilger R, Sitte N. Accumulation of single-strand breaks is the major cause of telomere shortening in human fibroblasts. Free Radical Biology and Medicine. 2000;**28**(1):64-74. DOI: 10.1016/s0891-5849(99)00207-5

[175] Slijepcevic P, Bryant PE. Chromosome healing, telomere capture and mechanisms of radiation-induced chromosome breakage. International Journal of Radiation Biology. 1998;**73**(1):1-13. DOI: 10.1080/095530098142653

[176] Slijepcevic P. The role of DNA damage response proteins at telomeres--an "integrative" model. DNA Repair. 2006;**5**(11):1299-1306. DOI: 10.1016/j.dnarep.2006.05.038

[177] Puterman E, Lin J, Blackburn E, O'donovan A, Adler N, Epel E. The power of exercise: Buffering the effect of chronic stress on telomere length. PLoS One. 2010;**5**:e10837. DOI: 10.1371/journal.pone.0010837

[178] Kovac M, Huskamp B, Scheidemann W, Toth J, Tambur Z. Survival and evaluation of clinical and laboratory variables as prognostic indicators in horses hospitalized with acute diarrhea: 342 cases (1995-2015). Acta Veterinaria-Beograd. 2017;**67**:356-365. DOI: 10.1515/acve-2017-0029

[179] Kovac M, Aliev R, Pozyabin S, Drakul N. Current strategies for prevention and treatment of equine postoperative ileus: A multimodal approach. In: Equine Science. Rijeka: Intechopen; 2020. DOI: 10.5772/intechopen.91290

[180] Kovac M, Pogorelov M, Aliev R, Ivanatov E. Equine pleuropneumonia - etiology, diagnosis and treatment: 18 cases (2007-2017). Veterinářství. 2017;**4**:35-41

[181] Yaribeygi H, Panahi Y, Sahraei H, Johnston T, Sahebkar A. The impact of stress on body function: A review. EXCLI Journal. 2017;**16**:1057-1072. DOI: 10.17179/excli2017-480

[182] Ijichi T, Hasegawa Y, Morishima T, Kurihara T. Effect of sprint training: Training once daily versus twice every second day. European Journal of Sport Science. 2015;**15**(2):143-150. DOI: 10.1080/17461391.2014.932849

[183] Visser K, von Borstel UK, Hall C. Indicators of stress in equitation. Applied Animal Behaviour Science. 2017;**190**:43-56. DOI: 10.1016/j.applanim.2017.02.018

[184] Rietmann T, Stuart A, Bernasconi P, Stauffacher M, Auer J, Weishaupt M. Assessment of mental stress in warmblood horses: Heart rate variability in comparison to heart rate and selected behavioural parameters. Applied Animal Behaviour Science. 2004;**88**:121-136. DOI: 10.1016/j.applanim.2004.02.016

[185] Lansade L, Bertrand M, Bouissou MF. Effects of neonatal handling on subsequent manageability, reactivity and learning ability of foals. Applied Animal Behaviour Science. 2004;**92**:143-158

[186] von Borstel UK, McGreevy P. Behind the vertical and behind the times. Veterinary Journal. 2014;**202**(3):403-404. DOI: 10.1016/j.tvjl.2014.10.005

[187] von Borell E, Langbein J, Despres G, Hansen S, Leterrier C, et al. Heart rate variability as a measure of autonomic regulation of cardiac activity for assessing stress and welfare in farm

animals -- a review. Physiology &
Behavior. 2007;**92**(3):293-316.
DOI: 10.1016/j.physbeh.2007.01.007

[188] Kovac M, Novicki S, Ippolitova TV,
Aliev R. Equine cardiac arrhythmias:
Pathogenesis, and prevalence. Veterinary
Pharmacology. 2021;**1**:24-27

[189] Viryasova NA, Ippolitova TV.
Features of EEG in sport horses
depending on age/veterinary medicine.
Journal of Animal Science and
Biotechnology. 2017;**4**:78-86

[190] Heidinger BJ, Wada H. Introduction
to the symposium: Stress phenotype:
Linking molecular, cellular, and
physiological stress responses to fitness.
Integrative and Comparative Biology.
2019;**59**(2):237-242. DOI: 10.1093/
icb/icz098

Chapter 7

Marek's Disease Is a Threat for Large Scale Poultry Production

Wojciech Kozdruń, Jowita Samanta Niczyporuk and Natalia Styś-Fijoł

Abstract

Marek's disease (MD) is one of the widespread infectious diseases that causes huge losses in large-scale poultry production. This is due to weight loss, poorer feed conversion and an increased number of deaths among infected birds. The etiological agent is a Marek's disease virus (MDV) belonging to the Herpesviridae family. It is mainly described in poultry, however, it is also found in geese. There are three MDV serotypes, and four patotypes within serotype 1. Currently, Marek's disease is very rare in its classical form. There are non-specific clinical symptoms, and anatomo-pathological changes are mainly observed in the liver, spleen and the reproductive system. This may be due to the evolution in the pathogenicity of MDV field strains over the past several decades. The presence of MDV and number of molecular diagnostic tests based on the detection of viral nucleic acids and viral proteins is already found in birds that have several weeks old. Laboratory diagnostics are based mainly on molecular biology (mainly PCR) methods. The only relatively effective method instead of biosecurity measures, of preventing MD is prophylactic vaccination of 1-day-old chickens or *in ovo* vaccination. Nevertheless, Marek's disease is still recorded in poultry flocks around the world, with estimated losses reaching several million dollars.

Keywords: Marek's disease, poultry production, poultry flocks

1. Introduction

One of the greatest threats to large-fledged poultry production besides avian influenza (AI) and infectious bronchitis (IB) is Marek's disease (MD). All these disease entities cause significant economic losses through reduced weight of birds, worse feed conversion and an increased number of dead birds. Marek's disease is a viral lymphoproliferative disease in chickens that was first described in 1907 by a Hungarian researcher - Dr. Joseph Marek [1]. Then, a year later, other researchers, ie Ellerman and Bang, described similar symptoms in hens, marked with nervous symptoms, and found lymphoid tumors in internal organs that were leukemic in nature. At that time, Marek's disease was also associated with various names such as: neuritis, paralysis, and neurophomatosis gallinarum [2, 3].

IntechOpen

It should be noted that since the initial description of this disease entity, there have been many discrepancies as to its name with regards to the visible clinical symptoms and anatomopathological changes observed in the internal organs of infected chickens.

Authors such as Biggs and Campbell have suggested keeping the name Marek's disease, instead of using avian leukemia. The disease is closely related to the presence of nervous symptoms and peripheral nerves lesions in birds [4, 5]. In the following years, Marek's disease was undoubtedly the greatest epizootic threat to birds. Within a few years, the percentage of dead birds increased significantly, usually from 10–30%, but, for example, in the case of secondary infections, even up to 60% - 80% [2]. Such a situation contributed to the undertaking of numerous scientific studies, the main aim of which was to characterize the etiological agent, to understand the mechanisms of immunity conducting after natural infection, the routes of infection, and the mechanisms of the lesions including visceral tumors and formation in internal organs and the broadly understood mechanisms of pathogenesis.

After finding that the etiological factor of Marek's disease is a virus from the Herpesviridae family, called Marek's disease virus (MDV), it was hypothesized that Marek's disease virus strains isolated from field cases may differ in their pathogenicity despite a similar clinical signs [6]. In the course of laboratory studies, it was found that the genetic material of MDV is closely related to the genetic material of the host (target-associated). The cell-free form of the virus is only found in feather follicles. This fact turned out to be useful in research on the pathogenesis of Marek's disease, mainly in terms of the mechanisms of virus spreading among birds and between buildings on the farm, but also in developing the principles of proper immunoprophylactic vaccinations. In addition, it was also helpful in determining the influence and role of antibodies raised in birds after both vaccination and natural infection [7].

The first vaccine used in the immunoprophylactic vaccinations of Mareka's disease was a vaccine based on a strain of turkey herpes virus (HVT FC126) belonging to serotype 3. It was in the form of a lyophilisate. Then came a vaccine based on the serotype 1 strain Rispens CVI 988, which required liquid nitrogen temperature for storage [8, 9]. The first studies with these vaccines were carried out to determine the efficacy of the vaccine in birds lacking maternal antibodies and in birds with maternal antibodies against Marek's disease. The vaccine used was based on the HVT (FC 126) strain in both cell-bound and cell-free form. The results of the research showed a much lower effectiveness of the vaccine based on the HVT (FC126) strain in the cell-free form. Additionally, different vaccination efficacy was found for 2 persons simultaneously vaccinating. Thus, the influence of the human factor on the process of preparation and vaccination technique on the effectiveness of the vaccination against Marek's disease was proved [10]. In subsequent studies, it was shown that there is a large variation in the incidence of Marek's disease in poultry houses located within one farm, but even in individual sectors of a given poultry houses. It has also been shown that this state of affairs can be greatly influenced by the presence of predisposing factors in the birds and on the farm in the first 8 weeks of bird life, as well as strains with different pathogenicity [11].

In 1984, Witter et al. Began research on the possibility of using a vaccine containing a strain of serotype 1, serotype 2 and serotype 3 in birds. Unfortunately, the results of these studies turned out to be unsatisfactory and the reason for this was the fact that each was the immune response of the birds. They also observed that the

incidence of the occurrence of lymphatic leukemia was significantly more frequent in vaccinated/protected birds [12, 13]. Subsequent studies have shown that Marek's disease can be divided into four successive phases: early cytolytic infection, mainly B lymphocytes, latent phase/ infection, late cytolytic infection and the phenomenon of immunosuppression, and tumor transformation of T lymphocytes [14].

Marek's disease virus strains with high pathogenicity, described as vv + (very virulent plus) strains, were found already in the early 1990s. Even then, these strains were responsible for a very high mortality among birds, even those vaccinated against Marek's disease. These studies were based mainly on classical methods in the form of a biological assay, but also molecular biology methods, mainly reaction of amplification (PCR) have already started to be used [15, 16]. In 1985, Venugopal et al. identified several genes of Marek's disease virus associated with oncogenicity/neoplastic transformation, and additionally the gen meq. They found the sequence of the latter gene only in strains classified within serotype 1. Currently, as seen, the meq gene sequence is perhaps the most frequently used sequence for the diagnosis of Marek's disease and for differentiating Marek's disease virus virulent field strains from vaccine strains [17]. A breakthrough in the research on Marek's disease was the introduction of large-scale methods of molecular biology, partial genome sequencing and then whole genome sequencing. It was mentioned that the exact sequence of individual genes and, indirectly, the mechanisms of the pathogenicity of Marek's disease virus strains and the mechanisms of the emerging immunity, both after natural infection and after vaccination, began to be studied. Efforts were also made to elucidate the full mechanism of immunosuppression caused by Marek's disease virus [18, 19]. It should also be added that the introduction of Real-Time PCR made it possible to accurately determine the viral load in 1 dose of the vaccine, which was an undoubted breakthrough in research on the effectiveness of the vaccines used [20, 21].

Our own (unpublished data) and other authors' observations confirm the fact that previously and currently used vaccines are not able to fully protect birds not only against infection, but mostly against clinical symptoms and pathological changes in internal organs of infected birds. In addition, changes in internal organs and the skin form in broiler chickens may cause confiscation on the slaughter belt up to 90% of carcasses. This is undoubtedly influenced by the progressive evolution in the pathogenicity of virus strains and the significant intensification of the scale of poultry production. That is why it seems so important to intensify research on Marek's disease [22].

It has been shown that the aforementioned meq gene can be a specific milestone by the cloning reaction of its sequence into the genome of the turkey herpes virus or the genome of the avipox virus.

A further step may be research on the sequence of the virus genome, the so-called fragmentation of non-coding RNAs in tumor cells (e.g. RNA telomerase). It is hoped that all these studies will lead to a more effective vaccine against Marek's disease [23, 24].

2. Brief characteristics of the etiological factor of Marek's disease

The etiological agent of Marek's disease is the herpesvirus (MDV) associated with the host cell (herpes virus-associated cell) of the genus Marbivirus. According to the principles of the new taxonomy announced by the International Committee on the

Taxonomy of Viruses, the division into 3 MDV serotypes is now as follows: Gallid herpesvirus 1 (serotype 1), Gallid herpesvirus 3 (serotype 2) and Meleagrid herpesvirus 1 (serotype 3) [25]. They were also divided into pathotypes of serotype 1 according to the same committee is as follows:

- classic MDV strains with moderate virulence (mMDV-mild MDV)

- virulent strains (vMDV-virulent MDV)

- very virulent strains (vvMDV-very virulent MDV)

- strains with high virulence plus (vv + MDV-very virulent plus MDV) [25].

Test the classification of individual strains into appropriate serotypes based on examining with typically specific monoclonal antibodies should be scored. The so-called patotyping of strains within serotype 1 was production based on studies (pathogenicity test) using vaccinated chickens against Marek's disease.

As previously identified with the widespread use of molecular biology, the MDV genome analysis did not define the classical markers of Marek's disease virus strains with the virulence of each of the patotypes in serotype 1 [5, 10, 26].

The MDV virion has hexagonal symmetry with a diameter of approximately 150–160 nm [4]. In turn, the nucleocapsid consists of 162 capsomers, and has a diameter of approximately 85–100 nm. The MDV genome density is approximately 1.706 g / ml (in the CsCl gradient) [4]. The differences between sequences of Marek's disease virus strains within serotypes have been presented in **Figure 1**.

The MDV genome is made of DNA and contains in its composition a unique long sequence (UL), a unique short sequence (US), which are limited by terminal repeat (TRL) sequence and internal repeat sequences (IRS) [27, 28]. Due to the high density, it is extremely difficult to divide the genetic material of the virus from the genetic material of the host. Nevertheless, the genes of the HVT FC126 strain are very often used as a vector in the production of vaccines intended for poultry, e.g. against avian influenza or infectious bursa disease.
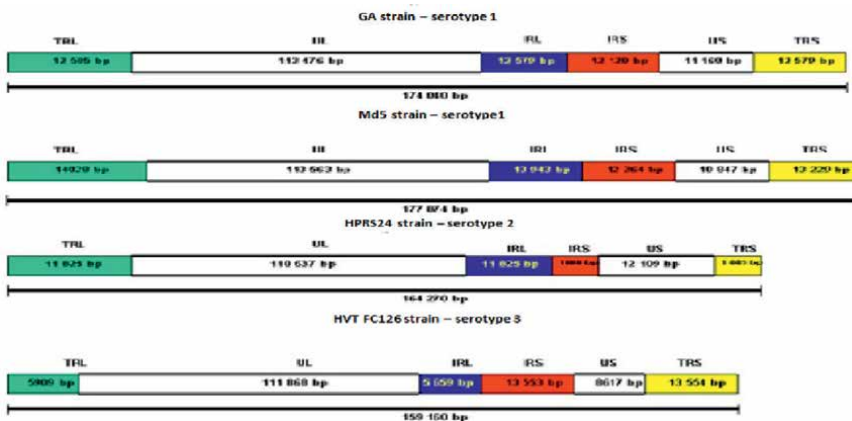
Figure 1.
Genome differences between sequences of Marek's disease virus strains within serotypes.

3. Brief characteristics of Marek's disease virus genes

MDV genes can be divided into three groups:

- genes related to oncogenicity (oncogenes),

- genes encoding glycoproteins,

- other genes.

The best described and characterized gene is the meq gene. It is a protein that is present only in serotype 1 strains. It plays an important role in oncogenesis and its sequence has been used to develop primers for an amplification reaction in which a single reaction can distinguish field strains from the Rispens CVI 988 vaccine strain [29].

Another important oncogenic gene is the pp38 gene. It occurs in both strains belonged to serotype 1 and serotype 3, where it shows a high homology [30].

4. Virus replication and the pathogenesis of Marek's disease

Marek's disease virus is an infection via the respiratory system. Subsequently, lymphocytes B and macrophages which have been found in the lungs are activated. The virus then moves to the bird's main lymphatic organs, Bursa of Fabricius, thymus, and spleen [31–33]. After replication in lymphocytes B cells, the virus spreads to T cells, mainly CD4 + cells. However, only some of the lymphocytes T are transformed and they are then a source of lymphoma formation. They are located within internal organs, mainly the kidneys, spleen, liver, ovary or testes, and even in the gizzard. They are very rarely found in peripheral nerves, skin and muscles [34]. The virus then enters a latent phase in most transformed lymphocytes T cells. Only a very small percentage of the neoplastic cells approximately (<0.001%) contain viral particles detected by electron microscopy (TEM) [35]. It should also be added that MDV occurs with a latency state only in lymphocytes, and not in neurons, as is the case with other alphaherpesviruses [36]. In the active phase of infection, the virus particles are transferred to the skin cells. Then, along with the exfoliating epithelium, it is spreader into the environment and is a direct source of infection for other birds. Of course, vertical transmission of MDV has not been confirmed, although there are reports of MDV genetic material being found in experimentally infected chicken embryos and egg surfaces [37]. On the basis of research using the immunofluorescence method, it was found that the so-called follicles play the main role in the process of MDV release into the environment of the poultry house. It has been shown that follicles can develop complete and mature virus particles which are capable of infecting other birds. It was also found that the full infectious particles of MDV in the poultry house environment is up to 7–9 months at room temperature, and much longer at lower temperatures. This time is significantly extended if the virus in the poultry house is "surrounded" by biological material such as dust or chicken droppings. That is why it is so important to thoroughly sanitize and disinfect poultry houses, especially before introducing 1-day-old chickens [38]. The results of conducted studies characterizing viral genes and proteins associated with feather follicles were also performed and published. It was confirmed that many viral proteins are expressed at a much higher level in feather follicles compared to expression in cells of internal organs [39].

Some authors believe that the replication of the virus particles in the feather follicles begins as early as 7–10 days after MDV infection. Most likely, the infected cells transmit the virus to the epithelial layer of the epidermal, where the virus replication and infects the neighboring cells of the skin, including fibroblast cells and melanocyte precursors. So far, a marker responsible for virus replication in skin epithelial cells has not been described [40]. In infected birds, 2 types of lesions may occur in the skin: neoplastic lesions in the form of tumors and lesions other than tumors. Many authors suggest that the nature of these changes does not allow them to be called the so-called "skin leukemia". It has also been shown in some studies that tumor cells do not contain viral antigens, and the research method used was immunofluorescence. Intensive research is underway on this issue [41]. As previously indicated, the genome structure of each of the MDV regions is similar, but the existing differences are nevertheless crucial. The oncogenicity of serotype 1 of MDV strains is determined primarily by the presence of the meq gene, but also the pp38 gene, vIL8 and vTR gene. They influence the oncogenic transformation processes and activated T lymphocytes. In turn, the dimmer form of the meq gene influences the expression level of cellular apoptotic factors and virus transformation [42, 43].

In molecular studies, it was found that all MDV strains represented three serotypes reduce the expression level of the Major Histocompatibility Complex (MHC). This phenomenon seems to be useful in studies to generate lines of birds resistant to MDV infection, and in particular with regard to cellular immunity, both after natural infection and prophylactic vaccination [44].

There are several unique features in the pathogenesis of Marek's disease. In the early (cytolytic) phase of the infection, lasting approximately 7 to 10 days, the virus causes a "massive destruction" of lymphoid cells and macrophages, resulting in the phenomenon of immunosuppression [45].

After this time, Marek's disease virus enters a latent phase, which lasts until the end of life in CD4 + and CD8 + T cells. Virtually all genes of Marek's disease virus are expressed at a much lower level. This condition is mainly due to neoplastic conversion of CD4 + cells and the formation / development of multiple lymphomas in several internal organs in infected birds. It causes mortality among birds starting from 3 to 4 weeks post infection and which is sometimes not "associated" with Marek's disease by producers /veterinarians. The first nervous symptoms in the form of paralysis may already appear, which results from a significant degree of lymphatic infiltration in the peripheral nerves [46].

After approximately 10 days, the virus spreads through the bloodstream to the skin epithelial cells / feather follicle cells. This is another type of interaction between Marek's disease virus and the host cell [45, 46]. On the basis of its own and many other authors' observations, it causes various symptoms of this disease or even syndromes that can be divided into two groups: oncogenic and non-oncogenic. This division depends on whether or not the birds have maternal antibodies. It should be presumed that most hatched chickens have maternal antibodies which disappear after 3–4 weeks [unpublished data].

The natural route of infection with Marek's disease virus is through the respiratory system by aspiration of the dust containing cell-free virus particles [47].

The role of lung cells in the pathogenesis, however, is not fully understood despite the presence of viral antigen in lung cells. Phagocytes present in lung tissue are believed to "capture" the virus and transmit it to the lymphoid organs (bursa of Fabricius, thymus and spleen). Infection with the virus affects of epithelial cells in internal organs and epithelial cells in blood vessels. There are already primary foci of

necrosis and symptoms of inflammation in internal organs. At this stage of the infection, the viral antigen can be detected by electron microscopy in all infected cells. This condition causes transitional immunosuppression [48].

5. Clinical symptoms and anatomopathological changes in the course of Marek's disease is most common in poultry

Laying hens, broiler chickens, turkeys and quails [47]. Recent years have also confirmed that it can also occur in geese. Several cases have already been recorded in Poland, both in the flocks of reproductive geese, but also in the flocks of geese intended for fattening [49]. In the case of breeding geese, Marek's disease is found in birds in the 2nd and 3rd laying season, while in geese intended for fattening at the age of 6–7 weeks, these changes are most often found during post-mortem examination [unpublished data].

A common feature of infections in geese is the fact that previously laying hens or broiler chickens have been reased in the same buildings as geese in which clinical Marek's disease was confirmed (unpublished data). Based on our own observations, Marek's disease conducted with rapid course of the disease in flock at the beginning of the infection, with a large number of dead birds. The infection then gradually "silences" [unpublished data]. In turn, the frequency of Marek's disease also depends on many predisposing factors, including: transport stress, vaccination stress, too high density of birds, sex or the content of undesirable substances in feed and water [47]. In the course of Marek's disease, clinical symptoms are closely related to the location of neoplastic lesions in the internal organs of the birds [47]. General apathy of the birds, stunted growth and even diarrhea are observed (it can be bloody if it becomes infected with coccidia). The paralysis and twist of the neck and head in the case of neurological disorders in the nervous system. One sided paralysis may be present. In the case of changes in the nerves of the eye and inflammation of intraocular structures, we may be dealing with blindness or pathological changes in the eye [50]. Generally, it can be assumed that the pathological changes can be classified into 3 groups: changes in internal organs, skin and in peripheral nerves [47].

Pathological changes in internal organs can be nodular, diffuse or both. If the lesions are diffuse, then the internal organs are significantly enlarged (rarely of normal size) with white or gray discoloration. When the lesions are nodular, the lymphomas appear singly or in small clusters of white or gray color [51].

As previously mentioned, skin lesions are associated with feather follicles and are best seen in featherless carcasses. The folios are greatly enlarged and in the form of diffuse lesions. Changes can also be seen on combs and bells. Red lesions and cavities on the skin of the thighs are called "Alabama Red Leg" syndrome. Such changes were described in Poland in 2005 in a flock of broiler chickens [52]. Peripheral nerve enlargement can be called the "golden sign" which we can observe during the anatomopathologiocal examinations [53]. Nerve changes can take the form of unilateral or bilateral nerves dysfunction. The altered peripheral nerves can be 2–3 times enlarged, lose their physiological shine and transverse striations, gray or yellow in color, sometimes swollen or with the presence of streaked hyperaemia [54]. In general, anatomopathological changes in Marek's disease occur most frequently in internal organs such as the liver and spleen. There are the changes described above. Of course, some changes can also occur in other organs, but much less frequently. The following can be mentioned here: the reproductive system (especially the ovary and testicle), kidneys (most often manifested significantly enlarged with a marked structure of renal

tubules), and glandular stomach (significant thickening of the wall). In addition, there may be complete atrophy of the thymus and bursa of Fabricius [47].

In the course of Mare's disease, in its non-oncogenic form, there are usually three forms: lymphodegenerative syndrome, transient paralysis and panophthalmitis (also known as "gray eye") [55]. Lymphodegenerative syndrome is observed only in unvaccinated birds against Marek's disease and in which no maternal antibodies are present. On the other hand, lymphatic organs such as the bursa of Fabricius and the thymus undergo very quick atrophy, already around 6–8 days after infection, and turn yellow-green. It has been proven that they are more atrophied after infection with Marek's disease virus of low pathogenicity in case of classical strains. If the birds are subsequently infected with highly virulent train expressing higher pathogenicity, atrophy does not progress. Additionally, necrotic foci may appear [47]. Transient paralysis is most common in birds vaccinated against Marek's disease, mostly in broiler chickens around 40 days of age. It mainly affects the neck muscles in the initial period, and then the paralysis gradually progresses in other parts of the muscles [56].

6. Diagnosis of Marek's disease

When Marek's disease is suspected and the consequences of the outbreak have been confirmed, the differential diagnosis is very important. It is based on finding clinical symptoms and pathological changes during the conduction of anatomopathological examination and comparing them with similar symptoms and macroscopic/microscopic lesions which can be suspected/visualized in other diseases (**Table 1**).

1. Lymphoproliferative syndrome in turkeys. In fallen birds, a slight enlargement of the liver is visible with the presence of small, gray-white necrotic lesions resembling tuberculosis lesions. In turn, the spleen is significantly enlarged and resembles a marbled structure [47].

Marek's disease	Other diseases
	lymphocytic leukemia
	myelogenous leukemia
	Lymphoproliferative syndrom
	Retikuloendotheliosis
	Tuberculosis
	Histomonozis
	Avian Encephalomyelitis AE
	Thiamin, Vitamin B1 deficiency
	Vitamin B2 - riboflavin deficiency
	Pseudopestis avium, Newcastle Disease, ND
	Fowl Pox FP
	Coligranulomatosis gallinarum, Hjarre's disease
	Botulismus avium, botulism

Table 1.
The most important diseases or disease syndromes included in the diagnostic differentiations of Marek's disease.

2. Lymphocytic leukemia. The pathological changes occur mainly in the liver in the form of single neoplastic tumors or, much less frequently, in the disseminated form. The changes further affect the spleen. The visible bumps vary in size and consistency of a compact (solid) or lard-like consistency. Sometimes, and especially in reproductive hens over 19–20 weeks of age, neoplastic tumors may completely fill the body cavity. These tumors may be white or cream-white in color [57].

3. Myelogenous leukemia. In this case, the neoplastic tumors are most often yellow - gray or yellow - white. They are usually diffuse, and very rarely in the form of single lesions [58].

4. Reticuloendotheliosis. During the pathological examination, significant enlargement of the liver and spleen is observed with the presence of necrotic foci of various sizes [58].

5. Tuberculosis. There is dejection, significant deterioration of the condition of birds and emaciation. Tuberculous lesions are visible in sections in the form of large, uniform tumors or scattered small nodules mainly in the gastrointestinal tract, liver and spleen. The liver and spleen are significantly enlarged also with the presence of necrotic foci [59].

6. Histomonosis. Birds are progressively emaciated. Mortality in young birds can be as high as 100%, while in older birds only 10–20%. The pathological examination reveals a significant enlargement of the liver with the presence of yellow or yellow-green necrotic foci of various sizes [60].

7. Avian encephalomyelitis AE. The disease is mainly associated with symptoms related to the nervous system. There are locomotor difficulties mainly caused by paralysis of the legs. In lying hens, tremors of the neck and head are visible. Older birds may have paralytic symptoms similar to Marek's disease [61].

8. Vitamin B1 deficiency. In this case, growth inhibition, unsteady gait and feathering have been observed. In addition, there may be paralysis of the legs, wings and neck. Birds assume a sitting position on jumps with the head tilted back [62].

9. Vitamin B2 deficiency. Birds are kachetic, even dwarfed, and differenced within the flock. Similarly, in this case, the birds sit on their legs and support themselves on the wings. In a long-term state of deficiency, birds usually lie down with their legs stretched out [69].

10. Newcastle disease. In the case of velogenic and mesogenic strains, apathy, swelling of the head and conjunctivitis occur in birds. Birds are depressed, appetite and thirst decrease, and over time the birds differentiate in body weight [63].

11. Fowl pox. In the cutaneous (chronic) form, tumors are visible in the area of the steak and lower abdomen. These changes are largely similar to those found in the skin form in broiler chickens [64].

12. Coligranulomatosis. It is a chronic disease and the incubation period can last up to several weeks. Virtually all internal organs of the bird are damaged. Numerous cocci are visible in the liver and in the lungs, reproductive system and kidneys [65].

13. Botulism (botulism). Apathy of birds, locomotor difficulties (unsteady gait) and paralysis of the neck and wings have been observed. The bird's posture with the head hanging down is a characteristic posture [66].

7. Laboratory diagnosis of Marek's disease

Generally, the diagnostic methods for Marek's disease can be divided into the following methods: serological, histopathological and virological. In the case of the latter, they include methods based on molecular biology.

Live birds (5 to 10 birds per flock) showing symptoms of the disease and an additional 20 to 25 blood or preferably serum samples should be provided for virological examination. We can also examined feathers collected from birds from the shoulder glass or the inner thigh surface. These feathers should be protected in such a way that does not dry out during the transport of the samples to the laboratory. Sick birds delivered to the diagnostic examinations should be euthanized using methods compliant with applicable legislation. Then, a thorough anatomopathological changes should be performed, describing the visible changes. During the anatomopathological examination, samples of the internal organs should be collected (in sterile way) for laboratory diagnostic tests, (classical virological and molecular). Most often samples of the liver and spleen have been collected, but also samples of other internal organs with pathological changes were examined to better understand the virus virulency. In turn, for histopathological examinations, apart from liver and spleen sections, also bursa of Fabricius, glandular stomach and peripheral nerves (sciatic and brachial plexus) have been examined. The possible presence of lesions in peripheral nerves is also diagnostic tool for differentiating between Marek's disease and avian leukemia infections, but also other neoplastic diseases. Homogenates are prepared from the collected internal organs, which are used to infect cell cultures: SPF (Specific Pathogen Free) chicken embryo fibroblast cultures (CEF) or Chicken embryo kidney cultures (CEK) or chicken embryos. The infected cell cultures are incubated at 37.5°C and the possibly cytopathic effect (CPE) in the form of clustered fine light refracting cells is observed on a daily basis. The formation of CPE in infected cell cultures indicates the presence of Marek's disease virus [67]. Sometimes, plaque formation is found, i.e. places where the connectivity of the cell layer has been interrupted by a proliferating Marek's disease virus strains.The cytopathic effect and plaques created by, for example, the vaccine strain HVT FC 126 (serotype 3) usually begins to appear as early as 72 hours after infection of the cell culture. In turn, field strains form CPE only in the 2nd or even 3rd passage. Under the microscope, starting from the 5th day after infection of the culture, a cytopathic effect is visible in the form of clustered small cells, strongly refracting light, and it most often appears between 7 and 9 days after infection. The final results of incubation are read under the microscope after about 12–14 days culture incubation. Clusters of small cells may also be visible, often overlapping each other and forming so-called focuses [68].

Marek's disease virus can also be isolated directly in a sterile culture prepared from kidney cells collected from diseased birds in a similar manner as described above. Isolation of Marek's disease virus strains in chicken embryos is used very

rarely, mainly due to the time cost consuming nature of this method. Commercial Marek's disease virus antigen and commercial anti-MDV serum are used in serological method. Blood is taken from the examined birds in a sterile manner, from which the serum is obtained after centrifugation. Feathers, are collected from places where there is an intensive replication of complete virus particles (wings, thighs and shoulder pathway). The presence of the specific anti-MDV antibodies in the serum samples collected from infected birds is determined by the agar gel immunodiffusion method (AGID), while the agar gel radial immunodiffusion test (RID) is used to detect the presence of the specific antigen of Marek's disease virus in the feather follicles of sick birds.

Among the molecular methods, the most frequently used technique is the polymerase Chain Reaction (PCR) is the amplification method with other variations. The amplification reaction allows the detection of the genetic material of Marek's disease virus strains and the differentiation of field and vaccine strains.Organ samples, blood, feather follicles, as well as dust collected from poultry houses serve as a matrix for DNA isolation. Traditional PCR consists in amplifying a fragment of a gene specific for MDV. Primers whose nucleotide sequence is complementary to the amplified fragment of the MDV genome are most often used for this purpose. The primers used are usually complementary to the sequence of genes such as: meq gene, 132 bp repeat sequence, pp38 gene or fragment of the SORF1 gene specific for turkey herpesvirus FC 126 strain (serotype 3) [69]. The advantage of the PCR method is its high sensitivity and specificity. The high specificity of the PCR allows the differentiation between field strains belonging to serotype 1 and the vaccine strain HVT FC 126 belonging to serotype 3 and the vaccine strain Rispens CVI 988 belonging to serotype 1.The results of PCR methods have been used to answer the question whether the birds have been vaccinated correctly or not, and whether the birds were infected with a virulent, field strains of Marek's disease virus.

Frequently in birds vaccinated with the bivalent vaccine (Rispens CVI 988 and HVT FC 126), in the case of infection with the field strain, DNA of the Rispens CVI 988 strain is absent. This is most often the case in birds over 6 weeks of age. On the other hand, these birds have DNA of the vaccine strain HVT FC 126 in practically every case. Such a PCR result clearly proves that the examined birds were vaccinated against Marek's disease. It should be remembered that vaccination does not protect birds against infection with a field strain, but only against the manifestation of the clinical symptoms and the occurrence of pathological changes.

8. Immunoprophylaxis of Marek's disease

The one effective way of preventing Marek's disease is prophylactic vaccinations, mainly performed in 1-day-old chickens. *In ovo* vaccination is also used, however, due to its high costs, it is used to a very limited extent. At this point, it should be recalled once again that vaccination against Marek's disease does not protect birds against infection, but against clinical symptoms and pathological changes in the internal organs of the birds. Marek's disease continues to cause heavy economic losses on account of these latter aspects. In 2020 and 2021, a slight upward trend was observed in the number of cases of the clinical form of the disease in field conditions. Practically from the beginning, when the immunoprophylaxis against Marek's disease was introduced, vaccines based on Marek's disease virus serotype 1 and serotype 3 have been used. Marek's disease virus vaccines based on serotype 3, contain the

turkey herpesvirus strain HVT (FC126), which occurs naturally in turkeys and is a non-pathogenic strain for these birds. This strain comes in two forms: as a target-associated virus and as a cell-free virus. Cell-bound virus must be stored at liquid nitrogen temperature (−1960°C) and cell-free virus in lyophilisate form at 2–8°C. Vaccines based on the serotype 1 (strain Rispens CVI988) are in the form of a liquid suspension and absolutely must be stored at liquid nitrogen temperature (−196°C). There are also vaccines on the market consisting of two strains: HVT (Fc126) and the Rispens CVI988 strain, and here, also, liquid nitrogen temperature is required.

In the United States, a vaccine based on serotype 2 (strain SB1) is additionally used. However, this vaccine is not used in Poland, although the results obtained in several laboratories indicate that this strain may already be present in poultry flocks in Poland [70].

Administration of the vaccine against Marek's disease in the correct manner causes the reduction of the multiplication process in the body of the virulent field strain and the spreading of the infection in the flock horizontally (lower level of replication in feather follicles). As a result, the formation of pathological changes in internal organs, mainly in lymphatic tissues, is limited. The viral load of infected birds is also reduced [24, 71]. A very important aspect of vaccination against Marek's disease is the fact that vaccine immunity significantly reduces the risk of immunosuppression. It is important due to the possibility of contact of birds on the farm with immunosuppressive factors, mainly from the infectious background [72].

There are a few important information's to keep in mind when prophylactic vaccinations against Marek's disease have been conducted:

- birds of one age (usually 1 day old) must be vaccinated

- strictly follow the safety rules

- only birds without any disease symptoms should be vaccinated

- vaccination should be carried out by qualified staff and under the supervision of a veterinarian.

Most often, the birds are vaccinated on the first day of their life in the hatchery or immediately after being placed on the farm.

An important aspect at the time of vaccination is the fact that Marek's disease vaccine should not be combined with other vaccines. The exceptions are, of course, the recommendations of the vaccine recommendations.

The information that in the field conditions very different volumes of the vaccine are used (not to be confused with the dose of virus in 1 dose of the vaccine) arouse much controversy of scientific and field nature (in terms of vaccine effectiveness). The recommended volume for a 1 day old chickens is 0.2 ml, which contains approximately 2000–3000 PFU (focus-forming units in cell cultures).

Research studies indicated that the use of a 0.1 ml volume of vaccine will not provide adequate protection for the birds from clinical Marek's disease. On the other hand, a vaccine volume of 0.5 ml is used in areas where Marek's disease virus may be endemic. Neither one solution nor the other can find any justification [unpublished data]. According to our own observations, there is a very frequent breakdown of post-vaccination (cellular) immunity, and then we are dealing with the classic course of Marek's disease in a given flock. A very important step in the correct vaccination

against Marek's disease is the storage and transport of the vaccine. Recently, vaccines based solely on vaccination with HVT (FC 126) strain in the form of lyophilisate have been used. Therefore, vaccines based on the Rispens CVI 988 strain or in combination with HVT (FC 126) must be strictly stored under the conditions recommended by the vaccine protocol [73]. In some cases, after removing the vaccine, the entire contents of the vaccine remain in the upper part of the ampoule. This clearly proves that the contents of such an ampoule were previously thawed and then frozen again. This vaccine is no longer usable and should be disposed of. The fall in the titter of the vaccine virus is then 100% [73]. Storing the vaccine at a temperature of 40°C or over 25°C for more than 1 hour causes a significant decrease in the viral load. After 24 hours, the decrease in titter is close to 80–90% [73]. The vaccine after removing from the container with liquid nitrogen should be dissolved up to 2 minutes, because a longer time causes a significant decrease in the titter of the vaccine virus in 1 dose of the vaccine. We should not use water over 37°C to defrost the vaccine.

After dissolving the contents of the vaccine in a suitable solvent, use the entire contents within 1 hour or a maximum of 2 hours. Research carried out at PIWet-PIB in Puławy showed a decrease in the viral load with the duration of vaccination.

Another important aspect of correct vaccination is the number of chickens vaccinated subcutaneously or intramuscularly. On this point, veterinarians are much divided. It is recommended to vaccinate about 2000–2500 birds within 1 hour. The more vaccinated birds per hour, the lower the number of correctly vaccinated birds should be presumed. You should also take into account the method of vaccination, whether we vaccinate with an automatic syringe or a special vaccination machine. Many companies offer suitable dyes that are added to the solvent. In this way, the vaccination veterinarian can very easily assess the quality of the vaccination performed. It should also be remembered that birds should not be given any antimicrobials or substances with immunosuppressive activity (e.g. immunostimulators) with the vaccine. In the case of vaccination in breeding flocks and commercial hens it is recommended to use vaccines based on the Rispens CVI 988 strain or vaccines containing the Rispens CVI 988 and the HVT (FC 126) strains. In broiler chicken flocks, vaccines based on the HVT (FC 126) strain are used, however, due to the presence of Marek's disease virus strains with high pathogenicity, it is recommended to use vaccines based on the Rispens CVI 988 strain. For turkey herds, the use of vaccines based on Rispens (CVI 988) is recommended. If vaccination is already performed on the farm, it should be remembered that all proper sanitary and hygienic conditions are maintained. We should apply the very simple but extremely effective "full farm - full empty farm" principle. This means that only one-age birds should be existed on the farm. This is a barrier protecting young birds against the possibility of transmission of pathogens from older birds. Among these pathogens there may be immunosuppressive pathogens, which adversely affect the effectiveness of the vaccination against Marek's disease.

After vaccination, it is very important to deal with chickens for the first 2 weeks of life, i.e. until immunity is developed. In this period, there should be close cooperation between the hatchery, the poultry producer and the veterinarian providing services to the poultry producer [74]. The in ovo method is used to inoculate the embryos on the 17.5-19th day of incubation, most often when the embryos are transferred from the incubation chamber to the brood chamber. The site of *in ovo* vaccination is the amniotic, allantoic or yolk sac (extra embryonic - EE), but also the body of the embryo (intra embryonic - IE) [75]. The place where the vaccine is administered depends on the age of the embryo, the egg placement, the size of the egg and the breed of the

parent flock. Within one hour, up to 50,000–60,000 embryos can be vaccinated. Properly conducted *in ovo* vaccination reduces the incidence of vaccine breakdown and clinical form/expression of Marek's disease in the field. In addition, it protects or significantly reduces hatched chickens from the possibility of early infection of chickens with virulent, field strain of Marek's disease virus. Like any vaccination method, it has advantages and disadvantages [76]. The advantage of the *in ovo* vaccination is that there is no stress that may occur in vaccinated chickens. There are significantly fewer infections associated with the *in ovo* technique alone compared to the subcutaneous or intramuscular vaccination of 1-day-old chickens. It is important to compare the effectiveness of *in ovo* vaccination compared to that of 1-day-old chickens vaccination. Our own observations at NVRI show that the effectiveness of both methods is probably at a similar level. When *in ovo* vaccination was used, a lower percentage of so-called seizures at the slaughterhouse associated with coetaneous Marek's disease were observed in broiler chickens.

Another controversial issue is the vaccination of chickens already vaccinated on 1 day of life. Immunization is used even in the first day of life after a few hours' break from the first vaccination. However, it seems that there is no scientific justification for this, and moreover, it was not observed in the field that vaccination, e.g. on the 3rd, 7th or even 10/21 days, had an impact on the possible course of Marek's disease in infected birds.

Recently, there has also been a limited amount of data collected on the field (unpublished data) on additional vaccination of birds, especially in breeding flocks 35–37 weeks of age. Also, such a scheme is a bad scheme and should not be used, especially since the vaccination process itself is a great stress for the birds.

9. Conclusion

Despite several decades of immunoprophylactic vaccinations and research on bird breeds resistant to infection, it was not possible to fully combat Marek's disease. The slow evolution in the pathogenicity of MDV strains should accelerate the pace of research into such bird breeds, but above all into other, more effective vaccines. Progress must alsw be made in laboratory diagnostics.
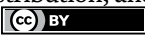
Author details

Wojciech Kozdruń*, Jowita Samanta Niczyporuk and Natalia Styś-Fijoł
National Veterinary Research Institute, Pulawy, Poland

*Address all correspondence to: wkozdrun@piwet.pulawy.pl

IntechOpen

References

[1] Marek J. Multiple Nervenentzuendung (polyneuritis) bei huehnern. Deutsch. Tierarztl Wochenschr. 1907;**15**: 417-421

[2] Biggs PM, Nair V. 40 years of Marek's disease research and Avian Pathology. Avian Pathol.2012;**41**:3-9.doi:10.1080/030 79457.2011.646238

[3] Adldinger HK, Calnek BW. Pathogenesis of Marek's disease: early distribution of virus and viral antigens in infected chickens. J Natl Cancer Inst.1973;**50**:1287-1298

[4] Biggs PM. Marek's disease. Current state of knowledge. Curr Top Microbial Immunol. 1968;**43**:93-125

[5] Biggs PM. The history and biology of Marek's disease virus. Curr Top Microbiol Immunol. 2001;**255**:1-24

[6] Cho BR, Kenzy SG. Isolation and characterization of an isolate (HN) of Mareks' diseasevirus with low pathogenicity. Appl Microbiol. 1972;**24**:299-306

[7] Davidson L, Maray T, Malkinson M, Becker Y. Detection of Marek's Marek's disease virus antigens and DNA in feathers from infected chickens. J Virol Meth. 1986;**13**:231-244

[8] Gimeno IM, Mareks's disease vaccines: a solution for today but worry for tomorrow? Vaccine. 2008;**26**:31-41

[9] Islam T, Waldken Brown SW, Renz KG, Fakhrul Islam AF, Ralapanawe S. Vaccination-challange interval markedly influences protection provided by Rispens CVI 988 vaccine against very virulent Marek's disease virus challenge. Avian Pathol. 2013;**42**:516-526.doi:10.1080/03079457.2 013.841312

[10] Miles AM, Anderson AS, Bernberg EL, Kent J, Rosenberger JK, Pope CR, Morgan RW. Comparison of two serotype 1 MDV isolates. Acta Virol. 1999;**43**:102-105

[11] Wozniakowski G, Samorek-Salamonowicz E. Molecular evolution of Marek's disease virus (MDV) field strains in a 40-year time period. Avian Dis. 2014;**58**:550-557.doi: 10.1637/10812-030614-Reg1

[12] Witter RL, Lee LF. Polyvalent Marek's disease vaccines: Safety, efficacy and protective synergism in chicken with maternal antibodies. Avian Pathol. 1984;**13**:75-92

[13] Witter RL, Sharma JM. Lee LF, Opitz HM, Henry CW. Field trials to test the efficacy of polyvalent Marek's disease vaccines in broilers. Avian Dis.1984;**28**: 44-60

[14] Baaten BJ, Staines KA, Smith LP, Skinner H, Davison TF, Butter C. Early replication in pulmonary B cells after infection with Marek's disease herpesvirus by the respiratory route. Viral Immunol.2009;**22**:431-444. doi:10.1089/vim.2009.0047

[15] Baigent SJ, Davison TF. Development and composition of lymphoid lesions in the spleens of Marek's disease virus-infected chickens: association with virus spread and the pathogenesis of Marek's disease. Avian Pathol.1999;**28**:287-300

[16] Biggs PM. Marek's disease-long and difficult beginnings. In: Marek's Disease. An Evolving Problem. Davison F and Venugopal V. 2004. Eds.Elsevier Academic Press.London, 8-16

[17] Venugopal N, Bland AP, Ross LJN, Payne LN. Pathogenicity of an unusual

highly virulent Marek's disease virus isolated in the United Kingdom. In: Current Research on Marek's Disease. Silva RF, Cheng HH, Coussens PM, Lee LF, Velicer LF. 1996. Eds. American Association of Avian Pathologists, Kennet Square, PA.119-124

[18] Becker Y, Asher Y, Tabor E, Davidson I, Malkinson M, Weisman Y. Polymerase chain reaction for differentiation between pathogenic and non-pathogenic serotype 1 Marek's disease viruses (MDV) and vaccine viruses of MDV-seerotypes 2 and 3. J Virol Methods.1992;**40**:307-322

[19] Davidson I, Borenstein R. Multiple infection of chickens and turkeys with avian oncogenic viruses: prevalence and molecular analysis. Acta Virol.1999;**43**: 136-142

[20] Islam A, Harrison B, Cheetham BF, Mahony TJ, Young PI, Waldken Brown. Differential amplification and quantitation of Marek's disease viruses using real-time polymerase chain reaction. J Virol Methods.2004;**119**:103-113.doi:10.1016/j. jviromet.2004.03.06

[21] Baigent SJ, Petherbridge LJ, Howes K, Smith LP, Currie RJ, Nair VK. Absolute quantitation of Marek's disease virus genome copy number in chicken feather and lymphocyte samples using real-time PCR. J Virol Methods.2005;**123**:53-64. doi: 10.1016/j.viromet.2004.08.19

[22] Barrow A, Venugopal K. Molecular characteristics of very virulent European isolates. Acta Virol.1999;**43**:90-93

[23] Brown AC, Baigent SJ, Smith LP, Chattoo JP, Petherbridge LJ, Hawes P, Allday MJ, Nair V. Interaction of MEQ protein and C-terminal-binding protein is critical for induction of lymphomas by Marek's disease virus. Proc Natl Acad Sci USA.2006;**103**:1687-1692

[24] Schat KA. History of the first generation Marek's disease vaccines: the science and little-known facts. Avian Dis.2016;**60**:715-724.doi: 10.1637/11429-050216.doi:10.1637/11429-050216-Hist

[25] https://talk.icvonline.org/taxonomy/

[26] Lee LF, Liu X, Witter RL. Monoclonal antibodies with specificity for three different serotypes of Marek's disease viruses in chickens. J Immunol.1983;**130**:1003-1006

[27] Lee LF, Wu D, Sui D, Ren D, Kamil J, Kung HJ, Witter RL. The complete unique long sequence and the overall genomic organization of the GA strain of Marek's disease virus. Proc Natl Acad Sci.2000;**97**;6091-6096

[28] Nair V. Latency and tumorigenesis in Marek's disease. Avian Dis.2013;**57**:360-365.doi:10.1637/10470-121712-Reg1

[29] Nair V, Zavolan M. Virus-encoded microRNAs:novel regulators of gene expresion. Trends Microbiol.2006;**14**: 169-175.doi:10.1016/j.tim.2006.02.007

[30] Naito M, Nakajima K, Iwa N, Ono K, Yoshida I, Konobe T, Ikuta K, Ueda S, Kato S, Hirai K. Demonstration of a Marek's disease virus-specific antygen in tumour lesions of chickens with Marek's disease using monoclonal anibody against a virus phosphorylated protein. Avian Pathol.1986;**15**:503-510

[31] 2013.Proceedings of the Ninth International Symposium on Marek's disease and avian herpesviruses. Avian Dis.2012;**57**:329-571

[32] Barrow AD, Burgess S.C., Howes K, Venugopal K. Invasion of avian macrophages by highly virulent Marek's disease virus strain C12/130 represents a tropic shift in the pathogenesis. In: Current Progress on Marek's Disease

Research. Schat KA, Morgan RM, Parcells MS, Spenceer JL.Eds. American Association of Avian Pathologists, Kennet Square, PA, 63-67

[33] Boodhoo N, Gurung A, Sharif S, Behboudi S. Marek's disease in chickens: review with Focus on immunology. Vet Res.2016;**47**:119.doi:10.1186/s13567-016-0404-3

[34] Burgess S.C. Marek's disease lymphomas. In: Marek's disease: An Evolving Problem. Davidson F, Nair V.Eds. Elsevier Academic Press. London;98-111

[35] Dunn JR, Auten K, Heidari M, Buscaglia C. Correlation between Marek's disease virus pathotype and replication. Avian Dis.2014;**58**;287-292. doi:10.1637/10678-092513-Reg1

[36] Gimeno IM, WItter RL, Cortes AI, Reed WM. Replication ability of three highly protective Marek's disease vaccines: implications in lymphoid organ atrophy and prptection. Avian Pathol.2011;**40**:573-579.doi:10.1080/03079457.2011.617725

[37] Davison F, Nair V. Marek's disease: an evolving problem. Eds.2004. Elsevier Academic Press. London

[38] Hirai K. Marek's disease.ed.2001. Springer-Verlag, Berlin

[39] Liu HC, Soderblomm EJ, Goshe MB. A mass spectrometry-based proteomic aprooach to study Marek's disease virus genome gene expression.J Virol Methods.2006;**135**:66-75.doi:10.1016/jviromet.2006.02.01

[40] Nair V, Kung HJ. Marek's disease virus oncogenicity: molecular mechanisms. In Marek's disease. An evolving problem. Davison F, Nair V. Eds. Elsevier Academic Press. London.32-48

[41] Nakamura K, Ito M, Fujino K, Yamamoto Y, Mase M, Yamada M, Kobayashi H, Harada T. Pathology and microbiology of dermal squamos cell carcinoma in young brown chickens reared on reused liter. Avian Dis.2010;**54**:1120-1124.doi:10.1637/9366-041210-Case1

[42] Parvizi P, Andrzejewski K, Read LR, Behboudi S, Sharif S. Expression profiling of genes associated with regulatory functions of T-cell subsets in Marek's disease virus-infected chickens. Avian Pathol.2010;**39**:367-373.doi:10.1080/03079457.2010.508776

[43] Reddy SM, Lupiani B, Gimeno IM, Silva RF, Lee LF, Witter RL. Rescue of a pathogenic Marek's disease virus with overlapping cosmid DNAs:use of a pp38 mutant to validate the technology for the study of gene function. Proc Natl Acad Sci.**99**:7054-7059

[44] Hearn C, Preeyanon L, Hunt HD, York LA. An MHC class 1 immune evasion gene of Marek's disease virus. Virology.2015;**475**:88-95.doi:10.1016/j.virol.2014.11.008

[45] Gimeno IM, Schat KA. Virus-induced immunosupression in chickens. Avian Dis. 2018;**62**:272-275.doi:10.1637/11841-041318-Review.1

[46] Parvizi P, Read L, Abdul-Careem MF, Lusty C, Sharif S. Cytokine gene expresion in splenic CD4(+) and CD8(+) T-cell subsets of chickens infected with Marek's disease virus. Viral Immunol.2009;**22**:31-38.doi:10.1089/vim.2008.0062

[47] Morrow C, Fehler F. Marek's disease: a worldwide problem. In Marek's disease. An evolving problem. Davison F, Nair V. Eds. Elsevier Academic Press. London. 49-61

[48] Bertzbach LD, Conradie AM, You Y, Kaufer BB. Latest insights into Marek's

disease virus pathogenesis and tumorgenesis. Cancers.2020;**12**:647. doi:103390/cancers12030647

[49] Murata S, Chang KS, Yamamoto Y, Okada T, Lee SI, Konnai S, Onuma M, Osa Y, Asakawa M, Ohashi K. Detection of the virulent Marek's disease virus genome from feather tips of wild geese in Japan and the Far East region of Russia. Arch Virol.2007;**152**:1523-1526. doi:10.1007/s00705-007-0982-5

[50] Kennedy DA, Cairns C, Jones MJ, Bell AS, Salathe RM, Baigent SJ, Nair VK, Dunn PA, Read AF. Industry-wide surveillance of Marek's disease on commercial poultry farms. Avian Dis.2017;**61**:153-164.doi: 10.1637/11525-110216-Reg1

[51] Jarosiński KW, Tischer BK, Trapp S, Osterrieder N. Marek's disease virus: lytic replication, oncogenesis and control. Expert Rev Vaccines.2006;**5**:761-772. doi:10.1586/14760584.5.6.761

[52] Szeleszczuk P, Samorek-Sala-inducedmonowicz E, Kozdruń W., Szatraj KJ, Malicka E, Karpińska E. First case of Alabama Red Leg Syndrome i broiler chickens in Poland. Medycyna Weterynaryjna.2006; **62**:1391-1394

[53] Gimeno IM, Witter RL, Fadly AM, Silva RF. Novel criteria for the diagnosis of Marek's disease virus-induced lymphomas. Avian Pathol.2005;**34**: 332-340.doi:10.1080/0307945000179715

[54] Gall S, Korosi L, Cortes AL., Delvecchio A, Prandini F, Mitsch P, Gimeno IM. Use of Real-Time PCR to rule out Marek's disease in the diagnosis of peripheral neuropathy. Avian Pathol.2018;**47**:427-433.doi:10.1080/0307 9457.2018.1473555

[55] Ficken MD, Nasisse MP, Boggan GD, Guy JS, Wages DP, Witter RL,

Rosenberger JK, NOrdgren RM. Marek's disease virus isolates with unusual tropism and virulence for ocular tissues: clinical findings, challenge studies and pathological features. Avian Pathol.1991.;**20**:461-474

[56] Kornegay JN, Gorgacz EJ, Parker MA, Brown J, Schierman LW. Marek's disease virus induced transient paralysis: clinical and electrophysiologic findings in susceptible and resistant lines in chickens. Am J Vet Res.1983;**44**:1541-1544

[57] Fadly AM. Isolation and identification of avian leucosis virus. Avian Pathol.2000;**29**:529-535. doi:10.1080/03079450020016760

[58] Payne LN, Venugopal K. Neoplastic disease, Marek's disease, avian leucosis and reticuloendoteliosis. Rev Sci Tech Off Inst Epiz.2000;**19**:544-564

[59] Tell LA, Woods L, Cromie RL. Tuberculosis in birds. Rev Sci Tech Off Inst Epiz.2001;**20**:180-203

[60] Liebhart D, Ganas P, Sulejmanovic T, Hess M. Histomonosis in poultry: previous and current strategies for prevention and therapy. Avian Pathol.2017;**46**:1-18.doi:10. 1080/03079457.2016.1229458

[61] Tannock GA, Sharfen DR. Avian encephaloyelitis: a review. Avian Pathol.1994;**23**:603-620. doi:10.1080/03079408419031

[62] Moszczyński P, Pyć R. Vitamin B and coenzimes. PWN Warszawa.1998;124-129

[63] Ganar K, Das M, Sinha S, Kumar S. Newcastle disease virus: current status and our understanding. Virus Res.2014;**184**:71-81.doi:10.1016/j. virusres.2014.02.016

[64] Gholami-Ahangaran M, Zia-Jahromi N, Namjoo A. Molecular

detection of avian pox virus from nodular skin and mucosal fibrinonecrotic lesions of Iranian backyard poultry. Trop Anim Health Prod.2014;**46**:349-353. doi:10.1007/s11250-013-0495-z

[65] Rahimi M, Siavash Haghighi ZM. An outbreak of visceral coligranuloma in a backyard chicken flock. Comp Clin Pathol.2012;**23**:382-384

[66] Holmes P. Avian botulism-a recurring paralytic disease of wild UK waterbirds. Vet Rec.2019;**185**:261-261. doi:10.1136/vr.I5417

[67] Wen L, Zhang A, Li Y, Lai H, Li H, Luo Q, Jin S, Chen R. Suspension culture of Marek's disease virus and evaluation of its immunological effects. Avian Pathol.2019;**48**:183-190.doi:10.1080/03079457.2018.1556385

[68] Li X, Schat KA. Quail cell lines supporting replication of Marek's disease virus serotype 1 and 2 and herpesvirus of turkeys. Avian Dis.2004;**48**:803-812. doi:10.1637/7182-032604R

[69] Kozdruń W, Styś-Fijoł N, Czekaj H, Piekarska K, Niczyporuk JS, Stolarek A. Occurence of Marek's disease in Poland on the basis of diagnostic examination in 2015-2018. J Vet Res.2020;**64**:503-507.doi:102478/jvetres-2020-0079

[70] Reddy SM, Izumiya Y, Lupiani B. Marek's disease vaccines: Current status, and strategies for improvment and development of vector vaccines. Vet Microbiol.2017;**206**:113-120.doi:10.1016/j.vetmic.2016.11.024

[71] Kim T, Spatz SJ, Dunn JR. VAccinal efficacy of moleculary cloned Gallid aplpahherpesvirus 3 strains 301B/1 agaisnt very virulent Marek's disease virus challenge. J Gen Virol.2020;**101**:542-552. doi:10.1099/jgv.0.001403

[72] Heidari M, Wang D. Sun S. Early immune responses to Marek's disease vaccines. Viral Immunol.2017;**30**:167-177. doi:10.1089/vim.2016.0126

[73] Ralapanawe S, Walden-Brown SW, Renz KG, Islam AF. Protection provided by Rispens CVII988 vaccine against Marek's disease virus isolates of different pathotypes and early prediction of vaccine take and MD outcome. Avian Pathol.2016;**45**:26-37.doi:10.1080/03079457.2015.11108

[74] Baigent SJ, Smith LP, Nair VK, Currie RJ. Vaccinal control of Marek disease: current challenges,and future strategies to maximize protection. Vet Immunol Immunopathol.2006;**112**:78-86. doi:10.1016/j.vetimm.2006.03.01

[75] Peebles ED. In ovo vaccination in poultry: A review. Poult Sci. 2018;97:2322-2338.doi:10.3382/ps/pey081

[76] Dobner M, Auerbach M, Mundt E, Presinger R, Icken R, Rautenschlein S. Immune respones upon in ovo HVT-IBD vaccination vary between diffrent chickens lines. Dev Comp immunol. 2019;100:103422.doi:10.1016/j.dci.2019.103422

Chapter 8

Application of Noble Metals in the Advances in Animal Disease Diagnostics

Gabriel Alexis S.P. Tubalinal, Leonard Paulo G. Lucero,
Jim Andreus V. Mangahas, Marvin A. Villanueva
and Claro N. Mingala

Abstract

The advent of molecular biology and biotechnology has given ease and comfort for the screening and detection of different animal diseases caused by bacterial, viral, and fungal pathogens. Furthermore, detection of antibiotics and its residues has advanced in recent years. However, most of the process of animal disease diagnostics is still confined in the laboratory. The next step to conduct surveillance and prevent the spread of animal infectious diseases is to detect these diseases in the field. Through the discovery and continuous development in the field of nanobiotechnology, it was found that incorporation of noble metal nanoparticles to biotechnology tools such as the loop-mediated isothermal amplification (LAMP), lateral flow assays (LFAs) and dipsticks provided a promising start to conduct point-of-care diagnostics. Moreover, the modification and application of nanoparticle noble metals has increased the stability, effectiveness, sensitivity and overall efficacy of these diagnostic tools. Thus, recent advances in disease diagnostics used these noble metals such as gold, silver and platinum.

Keywords: Animal Diseases, Biotechnology, Nanotechnology, Noble Metals

1. Introduction

The fastest growing and expanding agricultural sectors worldwide are the livestock, poultry and aquaculture industries. These industries need to grow and expand fast to sustain the needs of the growing population. However, this massive growth is in constant threat of outbreak of different infectious and/or zoonotic diseases [1]. Furthermore, the globalization of animal trade can further contribute to the spread of diseases such as spread of *Trypanosoma evansi* from the tse tse belt of Africa toward the rest of the world [2]. Thus, unforeseen entry of disease in a country or area may lead to rapid undetected spread of disease with late diagnosis. To prevent or slow down spread of animal diseases, the World Organization for Animal Health (OIE)

prescribed the use of rapid, accurate and highly sensitive identification and detection of these different infectious agents [1].

The application of molecular tool such as Polymerase Chain Reaction (PCR) has become one of the most important routine diagnostic procedure in the laboratory [3]. Furthermore, the development of Loop-mediated isothermal amplification (LAMP) by Japanese researchers further advanced disease diagnostics with its simplicity and cost-effectiveness [4]. However, even with the new PCR or LAMP techniques developed to detect different animal diseases, still, most of animal diseases are not properly diagnosed. Thus, development of methods and techniques that are more sensitive, specific, cost-effective, and can be used under field conditions are of paramount importance.

Noble metals are metals that have outstanding resistance to corrosion and oxidation at elevated temperature. These metals have a long and rich history and was reported to be used as early as the First Egyptian Dynasty. Noble metals include the metals of groups VIIb, VIII and 1b of the second and third transition series of the periodic table such as rhodium (Rh), ruthenium (Ru), palladium (Pd), silver (Ag), osmium (Os), iridium (Ir), platinum (Pt) and gold (Au) [5]. These metals belong to a group of elements with wide variety of use and applications in fields of aerospace, electronics and most significantly, health [6].

Nanotechnology is an emerging science and is the study of matter with one or more dimensions in between 1 to 100 nm. The combination of nanoscience and biotechnology has created a new growing field of research in the form of nanobiotechnology with massive opportunities [5] to further improve healthcare, medical treatments, therapeutics and biomedical [7] uses such as radiotherapy enhancers [8–10], drug and gene delivery vehicles, and highly specific and sensitive diagnostic assays [11, 12].

Among all noble metals, gold (Au) and silver (Ag) are the most extensively studied due to the well-established synthesis routes, their relatively higher content in the earth's crust and better safety profile. Furthermore, gold and silver nanoparticles demonstrated the most fascinating properties for biosensing. Gold nanoparticles (AuNPs), commonly known as colloidal gold or gold colloids, are the most stable metal nanoparticle. AuNPs present distinctive characteristics like size-related optical, electronic and magnetic properties, individual particle behavior and specially, compatibility with biomolecules [10, 11]. These characteristics of AuNPs attracted researchers from the field of human and animal medicine to apply these properties in a point-of-care or field diagnosis of various infectious diseases. In 1996, it was originally reported the capability of nucleotide functionalized AuNP can detect DNA colorimetrically [11, 13]. Moreover, AuNPs had been used for the detection of pathogenic DNA, single nucleotide polymorphisms and sequence discrimination [11, 14]. Researchers used AuNP in the development of numerous disease detection or screening platforms or techniques. This made gold as the most used noble metal in the field of point-of-care or field diagnostics [15].

AuNPs remain the most studied noble metal for disease diagnostics due to its biocompatibility and chemical stability [10, 16–18]. However, silver nanoparticles (AgNPs) are reported to habitually result in better sensitivity compared to AuNPs [18, 19]. Furthermore, Ag has higher thermal and electrical conduciveness, and more efficient to transfer electron than gold with shaper extinction band and AgNPs are more stable in water and air. Thus, the use of Ag has also attracted researchers to be used in drug delivery, environmental, electronics, antimicrobial agents and in diagnostics. Furthermore, AgNPs have been prominent in the field of biosensor and imaging [15].

Aside from Au and Ag, platinum (Pt) is another noble metal that has been note-worthy scientific tool explored by researchers in the field of biotechnology, nano-medicine and pharmacology [20].

In this book chapter, the different routes of synthesis and application of noble metal nanoparticles were discussed in order to give an overview on the recent advances and/or point-of-care animal disease diagnostics using these noble metals.

2. Advances in animal disease diagnostics

2.1 Synthesis of Noble metal nanoparticles

Throughout the emergence of nanotechnology, there have been many techniques developed on how to synthesize nanoparticles which include physical, chemical, and biological approaches. Among the three, synthesis of nanoparticles from physical and chemical methods are considered the best methods for they can provide more uniform-sized nanoparticles with long-term stability. Biological approach on the other hand is also used to lessen the production of toxic by-products from physical and mostly from chemical approaches [21].

2.1.1 The Turkevich method

The most common method of synthesis of nanoparticles is probably through the Turkevich method used to make spherical gold and silver nanoparticles [22]. This method is a chemical approach which makes use of a single phase water-based reduc-tion where gold or silver salt undergo reduction by citrate (sodium tri-citrate) at boiling temperature (100°C). The citrate ions, which serves as both reducing and non-aggrega-tion agent, stabilize the nanoparticles by providing negatively charged ions which gets absorbed onto the surface of each particle (see **Figure 1**). Individual particles which are now stabilized and surrounded by negative charges will tend to repel each other causing a more stable nanoparticle dispersion and preventing them from aggregation [23].

Furthermore, the concentration of the citrate ions used in the solution determines the average size of the nanoparticles. Higher concentration of citrate ions (citrate to gold ratio) produces smaller nanoparticle size (average of 10 nm) due to higher stabilization and particle repulsion. On the other hand, reducing the concentration of sodium tri-citrate limits the number of citrate ions that will stabilize the particles. This causes aggregation and forms bigger particles (>15 nm) [24].
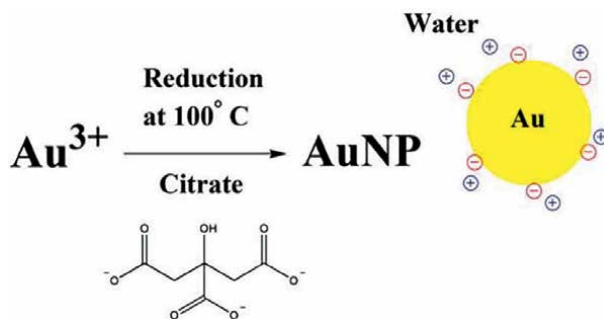
Figure 1.
Synthesis of AuNP using Turkevich method [23].

2.1.2 Physical methods of synthesizing nanoparticles

Several ways of producing nanoparticles using physical methods are already reported [25, 26]. Generally, some of these methods are using Plasma, Chemical Vapor Deposition, Microwave Irradiation, Pulsed Laser, Sonochemical Reduction and Gamma Radiation.

2.1.3 Green synthesis of nanoparticles

Green synthesis or biological synthesis are alternative pathways to produce nanoparticles in an eco-friendly way. This approach (in comparison with the physical and chemical methods) has lower energy consumption, lower cost, and less harmful to the environment. This pathway utilizes the use of microorganisms or plants (phytosynthesis) as source of reducing agents [26]. The main limitation of this approach is how to control the size and shape of the product. Different phyto-chemical compositions from organic sources have different influences on the particles' size and shape which can be attributed to purity of the extract used as reducing agents [27].

2.2 Characterization of synthesized gold nanoparticles

Synthesis of nanoparticles are verified mainly through their size and shape using Scanning Electron or Transmission Electron Microscopes (SEM/TEM). Additional characterization methods include spectroscopic analysis (UV–Vis Spectroscopy), dynamic light scattering (DLS), Zeta Potential, Inductively-coupled Plasma Mass Spectroscopy (ICP-MS), dark field microscopy, and more [28, 29]. Aside from their size and shapes, nanoparticles can have other unique properties based on their method of synthesis and precursor metals. These characteristics affect how they react with light due to surface plasmon resonance [30]. A good example on how to demonstrate the effect of size of nanoparticle on how they interact with light can be seen in **Figure 2** [31].

2.3 Advances in animal disease diagnostics using Noble metals

Serological (e.g. Enzyme-linked immunosorbent assay – ELISA) and molecular detection (e.g. PCR) of different animal pathogens has been one of the routine diagnostic techniques is most animal disease diagnostics. However, this requires well-trained laboratory technicians and expensive, sophisticated equipment [3]. Thus, the LAMP method developed by Japanese researchers that is claimed to be cost-effective without sacrificing sensitivity and specificity became a promising point-of-care molecular method [4]. However, this technique still has drawbacks such as less versatility compared to PCR, cannot be used in cloning purposes, limitation in multiplexing and difficulty in primer designing.

Colorimetric-based nanoparticle DNA detection is an eye-catching method due to its rapidity and cost-effectiveness compared to current generation of DNA detection or amplification. This method enables a direct or visual detection of amplified DNA even without expensive, sophisticated equipment. The incorporation of nanoparticles in platforms such as LAMP addresses the issue with regards to false positive results due to the addition of intercalating dyes as amplification indicators. Furthermore, hybridizations of nanoparticles with complementary DNA make this method more specific and overcoming the weaknesses of test format such as LAMP. Thus, LAMP and other

Figure 2.
Variations in color of gold nanoparticle suspension as particle size increases. Synthesized gold nanoparticles tend to have wine-red color (average size of 10–15 nm) and turns blue to purple as particles aggregate and get bigger.

point-of-care diagnostic tools coupled with nanoparticle has become a promising, sensitive, specific, cost-effective and rapid animal disease diagnosis techniques.

2.3.1 Point-of-care animal disease diagnosis using gold nanoparticles (AuNPs)

AuNPs are the most studied nanoparticle and has a fascinating property for biosensing. Furthermore, AuNPs can be synthesized to gold nanoprobes (AuPr) for detection of colorimetric detection of different animal diseases.

2.3.1.1 Bacterial diseases

Paratuberculosis or Johne's Disease, caused by *Mycobacterium avium subsp. para-tuberculosis* (MAP), is a chronic gastro-enteric disease of ruminants marked with diarrhea and irreversible wasting leading to death [32, 33]. The problem with paratuberculosis is that it can exist in the herd for years and remain undetectable. However, recent reports reveal that an estimated 200–250 million USD is lost in US Cattle industry due to paratuberculosis [11]. Furthermore, sub-clinically infected cattle produce 15–16% less milk that amounts to 1300–1500 pound's loss in every lactation. In addition, there is no approved treatment for paratuberculosis and no effective vaccine available. Thus, screening and removal of the infected animal from the herd is the most effective way of controlling and preventing spread of paratuberculosis [33]. Ganareal *et al.* [11] developed a gold-nanoparticle based probe for the colorimetric detection of MAP DNA. The developed nano-probe was specific to detect MAP with a detection limit of 103 ng of MAP PCR product per reaction. Furthermore, UV–Vis and SEM showed dispersion and aggregation of the AuNPs for the positive and negative results with no observed particle growth.

2.3.1.2 Viral diseases

Foot-and-Mouth Disease (FMD) is one of the most devastating and highly contagious disease of cloven-hoofed animals (e.g. ruminants and swine) that may threaten food security [34]. The causative agent, Foot-and-Mouth Disease virus (FMDV) has multiple modes of transmission, fast replication rate and viral excretion that makes FMD one of the acute and highly contagious diseases of cloven-hoofed animals [34, 35]. Southeast and East Asian countries such as Cambodia, Laos, Thailand, Vietnam and China show varying FMD prevalence [34]. Eradication and control strategy for FMD is mainly controlled by vaccination. However, discrimination between naturally infected versus immunized animals against FMD is a must especially in the event of mass importation of cloven-hoofed animals. Furthermore, the rapidity of development of antibody against FMD and the differentiation of naturally infected vs. immunized animals are important in the disease control and prevention strategies. Conventionally, serological methods such as FMD structural proteins (SPs)-based virus neutralization test (VNT), liquid phase blocking enzyme-linked immunosorbent assay (LPB-ELISA) and solid-phase competition ELISA (SPCE) can evaluate the antibody level and non-structural proteins (NSPs)-based ELISA can discriminate naturally infected from immunized animals. However, with the advent and success of immunochromatographic strip (ICS) in the field due to its high specificity, sensitivity, rapidity, low cost and portability for field detection and high sample throughput, Yang *et al.* [34] developed an immunochromatographic gold nanoparticle strip that can differentiate FMD type O-naturally infected from immunized animals using serum. Both epitopes of FMDVs SPs (T1) and NSPs (T2) were dispensed in the nitrocellulose membranes to be the two test lines and as for control line a goat anti-pig antibody IgG was used. The result of their experiment shows 95.17% and 100% specificities for T1 and T2, respectively with the sensitivity comparable to the commercial ELISA kits. Furthermore, the coincidence rate of the develop AuNP strip is 95.5% and 93.13% for 3ABC monoclonal antibody (Mab)-ELISA and LPB-ELISA, respectively. Thus, the developed AuNP strip can provide a point-of-care differentiation test between naturally-infected and immunized FMD animals that is easy-to-use, economical, faster without sacrificing sensitivity and specificity of the test.

Nam *et al.* [36] developed a bio-barcode amplification (BCA) and used to measure respective protein and nucleic acid targets of different living organisms. In 2011, Ding *et al.* [35] developed an AuNP improved immuno-PCR for the detection of FMDV. The target particles were captured using a polyclonal antibody on a microplate followed by the addition of primers with AuNP and FMDV Mab 1D11 to form the sandwich complex. Then, immuno-complex will be formed and the signal DNA will be released by heating and then characterized by PCR and real time PCR. The developed FMDV BCA has a detection limit of 10 fg/ml purified FMDV particles and can detect clinical samples of FMDV with high sensitivity as compared to the traditional ELISA techniques with 100 ng/ml. Thus, FMDV AuNP BCA provided a detection test for FMDV with high sensitivity.

Bluetongue disease (BTD) is an arthropod-borne viral disease that affects ruminants worldwide. Bluetongue can cause massive socio-economic effects and is one of OIE listed diseases [36, 37]. Diagnosis of BTD includes viral isolation, serology and molecular diagnostics. In 2011, Yin *et al.* [37] developed a BCA BTD VP7 test. However, traditional BCA is time-consuming and complex. Thus, Yin *et al.* [38] improved their previous BCA BTD VP7 [36] test by incorporating gold nanoparticle probe to make the test easy and more sensitive to detect BTD VP7. Their platform

captures the protein VP7 using AuPr coated with the anti-VP7 polyclonal antibodies and single-stranded signal DNA. Then, magnetic microplate (MMP) probes coated with the anti-VP7 monoclonal antibodies were added to form the sandwich immuno-complex. Using PCR and real-time fluorescence PCR using Taqman probe, the single-stranded signal DNA in the immuno-complex can be detected. This technique has a detection limit of 10^{-2} fg/ml which is 8 orders of magnitude (100,000,000x) greater than conventional antigen capture ELISAs and 1 order (10x) than conventional BCA. The developed AuNP BCA test is a highly sensitive and an easier detection test for VP7 protein of bluetongue. Furthermore, this technique can be modified to measure the presence of other proteins.

Caprine arthritis encephalitis virus (CAEv) is one of the economically important diseases of goats that causes mostly polyarthritis in adults and progressive paresis (leukoencephalomyelitis) in kids. However, other clinical manifestations include inter-stitial pneumonia, mastitis and chronic wasting diseases that lead to eventual death of the animal. Detection of CAEv infection is mostly done through serological testing such as Agar Gel Immunodiffusion (AGID) and Enzyme-linked immunosorbent assay (ELISA) [39, 40]. However, application of polymerase chain reaction to detect CAEv became a routine assay due to its rapidity and ability to detect CAEv in early stage of the disease [41]. Furthermore, Huang *et al.* [42] and Balbin *et al.* [41] optimized loop-mediated isothermal amplification (LAMP) to detect CAEv. Moreover, Balbin *et al.* [43] developed a LAMP test coupled with AuPr that can provide a specific colorometric detection CAEv. The specificity of this test was evaluated by subjecting other economi-cally important small ruminant pathogens such as *Leptospira* spp., Bovine Leukemia Virus (BLV), *Trypanosoma evansi*, *Babesia* spp., *Anaplasma marginale,* and *Theileria* spp. The AuPr was not able to hybridize with the DNA amplification products of these pathogens, thus the designed oligonucleotide in the AuPr is only CAEv-specific. Furthermore, the result of AuPr colorimetric detection corroborated with the result of SYBR green and gel electrophoresis result of CAEv LAMP amplification.

Acute hepatopancreatic necrosis disease (AHPND) is one viral disease that causes devastating economic effects due to 100% mortality that occurs at 35 days after stocking of shrimp post-larvae in ponds [44–46]. De Guia *et al.* [12] developed a AuPr-based detection *pir*A^{vp} toxin gene that causes AHPND without PCR amplifica-tion. The sensitivity of the developed test was as low as 20 fg/µl of extracted genomic DNA and positive samples had decreased absorbance value of 0.048 from 0.210 as compared to the negative controls with 0.137 absorbance value. Thus, most of the AuNPs aggregated due to the presence of *pir*A^{vp} toxin in the samples. Furthermore, the sensitivity of this technique was tested with AHPND uninfected shrimp samples and non-vibrio DNA extracts of *Staphylococcus haemolyticus* isolate 1, *Staphylococcus haemolyticus* isolate 2, *Plesiomonas shigelloides, Staphylococcus arlettae, Edwardshiella tarda, Bacillus cereus* and *Citrobacter freundii*. The specificity and sensitivity of the test was conducted in 5 replications to assure the reliability of the test results. The posi-tive result of the test will reveal a colorimetric change from pink red to purple, while negative will retain the pink red color.

2.3.1.3 Fungal diseases

Epizootic ulcerative syndrome (EUS) also known as mycotic granulomatosis, red spot disease or ulcerative mycosis is an economically important disease of wild and cultured fresh-water and estuarine finfish species [45]. This disease is caused by a fungus, *Aphanomyces invadans*. The conventional detection method for the

disease includes culturing of causative agent, gross observation of clinical signs and symptoms and histopathology [45]. Molecular techniques such as PCR and fluorescent *in-situ* hybridization (FISH) have also been used for diagnosis of EUS [47, 48]. Furthermore, electrochemical DNA biosensors have been used to detect diseases for their relatively lower cost, higher sensitivity and specificity, portability, greater analyte discrimination, fast result and easy-to-use [49]. Thus, application of noble metal nanoparticle on these electrochemical DNA biosensors have been used to further improve disease diagnosis [47, 48]. Kuan *et al.* [49] developed an EUS electrochemical genosensors for the detection of *18S rRNA* and the internal transcribed spacer (IRS) of *A. invadans.* Kuan *et al.* research group described their platform as novel application for the detection of PCR product from real sample of *A. invadans* using a premix of sandwich hybridization assay. This assay was easier to use and more specific and sensitive compared to conventional techniques. The limit of detection of the EUS-genosensor was 0.5 fM (4.99 zmol) of linear DNA target and 1 fM (10 zmol) of PCR product. The developed EUS-genosensor will be highly suitable for surveillance and diagnostics of EUS in the aquaculture industry worldwide.

2.3.1.4 Parasitic diseases

Visceral Leishmaniasis, caused by *Leishmania infantum* that is transmitted by sandflies, is a fatal zoonotic diseases of domesticated dogs, wild canids and humans [50, 51]. Canine Leishmaniasis (CanL) can be diagnosed through the use of parasitological [52, 53], serological [50] and molecular testing approaches [54–58]. However, the limitations of using this test to diagnose CanL are reported to be the need to skilled workers/laboratory staff, expensive and the need to send samples to reference laboratories [50]. Furthermore, a lateral flow assay (LFA) test for the detection of CanL, however, the detection limit is the drawback as it cannot detect low level of CanL antibody in the blood [59–61]. Molecular tool, PCR, have proven effective as it is considered as the confirmatory and gold standard test. However, molecular diagnostic tool has its drawbacks like the need of expensive and sophisticated equipment for the precise and repeated heating required for amplification [50]. Thus, de la Escosura-Muñiz *et al.* [50] developed a point-of-care test kit for the detection of CanL using primers labeled by AuNPs and magnetic beads (MBs) using isothermally amplified DNA products. This test kit successfully discriminated CanL infected blood from healthy dog's blood. Further qualitative studies revealed that less than 1 *Leishamania* parasite can be detected per microliter of blood (8×10^{-3} parasites per isothermal amplification reaction). The result of study of de la Escosura-Muñiz *et al.* [50] provided a pioneering approach to advance diagnostic testing in animals using noble metals as it makes diagnostics faster, economical and easy-to-use.

2.3.1.5 Antibiotics and antibiotic residues

Antimicrobial resistance has emerged as one of the most essential problems in public health for the 21st century. This phenomenon is a threat to the effective disease prevention and treatment as increasing number of pathogens gain resistance to common medicines that used to treat them. In recent years, steady increase and intensification of animal production due to the increasing demand for animal protein has also lead to the increase in the use of antimicrobials as growth promoters in addition the specific use of antibiotics to treat specific diseases and to prevent the spread of particular diseases. This practice has been an essential contributor to the development

and spread of resistance. On the other side of the coin, the livestock industry cannot support the growing demand for animal protein to the growing population without this modern miracle – antibiotics.

Research groups around the world has developed aptamer nanoparticle-based detection of antibiotics and its derivatives. Point-of-care detection of antibiotics is important in One Health approach as tainted products with antibiotics and its derivatives can be intercepted before penetrating the market and table of consumers.

Oxytetracycline (OTC) is one of the most commonly used tetracyclines (TCs) in veterinary medicine. TCs are extensively used as growth promoters that can lead to bioaccumulation in livestock products and by-products. This bioaccumulation of antibiotics may lead to serious human health issues ranging from allergies to incurable disease such as aplastic anemia, however, still the greatest threat is antimicrobial resistance. Thus, point-of-care detection for antimicrobials and its derivative is important to prevent the development and spread of antimicrobial resistance. Kim *et al.* [62] developed a colorimetric aptasensor using gold nanoparticle for the detection of OTC. Using a highly specific ssDNA aptamer to bind to OTC that can discriminate to doxycycline (DOX) and tetracycline (TET), aggregation of AuNPs was specifically induced via desorption of OTC binding aptamers (OBAs) from the surface of AuNPs as a result of aptamer-target interaction, thus a colorimetric change from red to purple. Kim *et al.* [62] aptasensor can detect up to 25 nM of OTC which is 20-fold lower than the limit of USA-EPA regulations. Thus, this colorimetric aptasensor is advantageous over traditional methods with simple signal generation and detection with naked eye specially during on-site detection of antimicrobial agents.

Kanamycin is one the frequently used aminoglycoside antibiotics produced by *Streptomyces kanamyceticus* [63, 64]. The increasing use of kanamycin is a threat to human health due to is ototoxicity, nephrotoxicity and neurotoxicity due to its residue in animal-derived products [65, 66]. The European Commission has set the maximum residue limits (MRLs) or kanamycin in milk at 150 μg/kg [64, 67, 68]. Thus, a convenient, fast, economical, accurate and sensitive point-of-care detection test is vital to promote healthy and safe animal derived products [69, 70]. Ou *et al.* [64] developed an aptamer-based strip biosensor for visual detection of kanamycin. The strip design uses the easy separation of magnetic microspheres (MMS) with target-mediated chain displacement of ssDNA and capture of the visible DNA-functionalized AuNP probe. The presence of kanamycin will competitively bind to the aptamer and release the cDNA to the supernatant. The free cDNA concentration is directly proportional to the concentration of kanamycin. The capture of DNA functionalized AuNPs on the test zone is through cDNA-induced hybridization that provide visual detection signal or the presence of line in the test zone. The limit of detection of the aptamer test strip is 50 nM and 4.96 nM for visual detection limit by naked eye and quantitative determination, respectively. This lateral flow strip biosensor can detect presence of kanamycin in different food samples and has a potential in medicine and for everyday use. Furthermore, this is vital as kanamycin side effects from animal derived foods has become a serious public health issue on a global scale [68].

2.3.2 Point-of-care animal disease diagnosis using silver nanoparticles (AgNPs)

2.3.2.1 Antibiotics and antibiotic residues

Aminoglycosides (AMG) antibiotics are known for their broad-spectrum activities to gram-negative aerobic bacteria [71]. However, the discrepancy of administered

AMG and the presence in blood is an important concern [72]. Thus, emergence of AMG-resistant bacteria is a pressing concern due to its abuse in animal husbandry and agricultural practices [73–75]. One of the important AMG is Streptomycin, an effective antibiotic for gram-negative bacterial treatment and is used not only for human diseases but also for diseases of veterinary concern [76, 77]. The presence of streptomycin residues in animal-derived products is a threat to human health due to its nephrotoxicity, ototoxicity and allergic reactions [77, 78]. The European Commission has set a MRL for streptomycin of 500 and 200 µg kg $^{-1}$ for meat and milk, respectively [77, 79]. Thus, development of sensitive and selective detection of streptomycin residues in animal derived products is vital to ensure food quality and safety and one health. Ghodake *et al.* [77] developed a silver nanoparticle (AgNP) probe for the colorimetric detection of picomolar-level sensitivity toward streptomycin in water, serum and milk samples. A color change of yellow to orange/red was observed in samples with streptomycin. A detection limit of 36 pmol L $^{-1}$ was observed in the developed AgNP probe. The AgNP probe can successfully detect streptomycin residues in serum and milk and is a rapid and cost-effective detection of low molecular weight analytes. Thus, this method can provide practical application is the ultrasensitive detection of AMGs.

2.3.3 Point-of-care animal disease diagnosis using platinum nanoparticles (PtNPs)

2.3.3.1 Bacteria

Salmonella is one primary risk factor for bacterial food poisoning and can be transmitted via contaminated animal-derived foods like meats, eggs milk, etc. Millions of people are infected with *Salmonella* sometimes with severe and fatal results. Most highly developed countries have zero tolerance to *Salmonella* in foods, especially to ready to eat food. Thus, ultrasensitive detection is important. However, food testing is complex and usually low concentration of *Salmonella* is found in ready to eat foods [80]. The need for rapid, sensitive and cost-effective point of care *Salmonella* screening test is of great importance. Wang *et al.* [80] developed a *Salmonella* biosensor using a platinum nanoparticle loaded manganese dioxide nanoflowers (Pt@ MnO$_2$ NFs) and thin-film pressure detector. The biosensor test starts by separating *Salmonella* from the sample using capture antibodies (CAbs) modified magnetic nanobeads (MNB) forming MNB-CAbs-*Salmonella* complex (magnetic bacteria). Then, detection antibodies (DAb) were used for labelling magnetic bacteria to form MNB-CAb-*Salmonella*-DAb-Pt@MnO$_2$ NFs complex (nanoflower bacteria). The nanoflower bacteria will be resuspended into H$_2$O$_2$ in a sealed centrifuge tube. H$_2$O$_2$ was catalyzed by PtMnO$_2$ to produce O$_2$ that results in increased pressure. This increased in pressure is monitored in real-time by piezoresistor-based pressured detector and transfer data to smartphone by Bluetooth for analysis and detection of *Salmonella* in the samples. The developed biosensor by Wang *et al* [80] can quantitatively detect *Salmonella* from 1.5 x 10^1 to 1.5 x 10^5 CFU/mL in 1.5 h with low detection limit of 13 CFU/mL.

2.3.3.2 Drug residues

β$_2$-adrenergic receptor agonists (β2-agonists) is a drug group which is usually used for the treatment of pulmonary diseases in animals [81, 82]. However, they can promote animal growth and increase feed efficiency by enhancing protein accretion and

reducing fat deposition producing "lean meats" [82–84]. The use of this drug group in veterinary medicine is illegal since prolonged consumption of residues in animal-derived products can cause headache, chest tightness, nausea, and more. One of this β2-agonists is ractopamine (RAC), however RAC is a derivative of clenbuterol which causes high blood pressure and heart disease in human. Thus, the use of RAC is illegal in Europe and China but RAC is still used around the world due to its effectiveness and low cost [82]. Thus, detection of RAC and its residue using simple and accurate method is important. Sun *et al* [82] developed a colorimetric immunosensor based PtNPs immobilized on Power Vision (PV) as signal probes and Fe_3O_4@β-cyclodextrin as capture probes for ractopamine detection in pork. PtNPs-PV double catalyzed the chromogenic substrate 3,3′-diaminobenzidine (DAB), which induced changes in DAB's color and chromogenic absorbance. Incubation temperature, pH, and incubation time were systematically optimized, and under optimum conditions, the measured absorbance values exhibited a linear relationship with the RAC concentrations in the range of 0.03 to 8.1 ng mL^{-1}. The detection limit was 0.01 ng mL^{-1}. The sensor exhibited high sensitivity and specificity, which was demonstrated by testing structurally similar organic compounds such as salbutamol (SAL), clenbuterol (CLE), and dopamine (DOA). The practicality of the developed colorimetric immunosensor was supported by the successful detection of RAC in pork samples with recovery ranging from 94.00% to 106.00%.

3. Conclusions

In conclusion, this review has provided the application of noble metals (gold, silver and platinum) in the advances in animal disease diagnostics. The versatility of these noble metals to be able to detect virtually all types of animal pathogens such as bacteria, virus, fungi, parasites to detecting drug and its residues is a promising foundation for point-of-care diagnostics/field diagnostics of animal diseases in the near future.

Acknowledgements

Conflict of interest

The authors declare no conflict of interests.

Author details

Gabriel Alexis S.P. Tubalinal[1], Leonard Paulo G. Lucero[2], Jim Andreus V. Mangahas[2], Marvin A. Villanueva[1,2] and Claro N. Mingala[1,2]*

1 Biosafety and Environment Section, Philippine Carabao Center National Headquarters and Gene pool, Science City of Muñoz, Nueva Ecija, Philippines

2 Livestock Biotechnology Center, Philippine Carabao Center National Headquarters and Gene pool, Science City of Muñoz, Nueva Ecija, Philippines

*Address all correspondence to: cnmingala@hotmail.com

IntechOpen

References

[1] Malik D, Yashpal S, Verma A, Naveen K, Deol P, Kumar D, Ghosh S, Dhama K. Biotechnological innovations in farm and pet animal disease diagnosis. Genomics and Biotechnological Advances in Veterinary, Poultry and Fisheries. 2020: 287-309. DOI: 10.1016/B978-0-12-816352-8.00013-8.

[2] Villanueva MA, Mingala CN, Tubalinal GAS, Gaban PBV, Nakajima C, Susuki Y. Emerging Infectious Diseases in Water Buffalo - An Economic and Public Health Concern. InTech. Janeza Trdine 9, 51000 Rjeka, Croatia, 2018.

[3] Valones MAA, Guimarães RL, Brandão RCL, De Souza PRE, De Albuquerque Tavares Carvalho P, Crovela S.Principles and applications of polymerase chain reaction in medical diagnostic fields: A review. Brazilian Journal of Microbiology. 2009: 40(1):1-11. DOI: 10.1590/S1517-83822009000100001.

[4] Notomi T, Okayama H, Masubuchi H, Yonekawa T, Watanabe K, Amino N. Loop-mediated isothermal amplification of DNA. Nucleic Acid Research. 2000: 28(12):e63

[5] Azharuddin M, Zhu GH, Das D, Ozgur O, Uzun L, Turner APF, Patra HK. A repertoire of biomedical applications of noble metal nanoparticles. Chemical Communications. 2019: 55(49):6964-6996. DOI: 10.1039/c9cc01741k.

[6] Begerow J, Neuendorf J, Turfeld M, Raab W, Dunemann L. Long-term urinary platinum, palladium, and gold excretion of patients after insertion of noble-metal dental alloys. Biomarkers. 1999: 4(1): 27-36. DOI: 10.1080/135475099230976.

[7] Sanvicens N, Marco MP. Multifunctional nanoparticles – properties and prospects for their use in human medicine. Trends in Microbiology. 2008: 26(8):425-433. DOI: 10.1016/j.tibtech.2008.04.005.

[8] Huang X, El-sayed IH, El-sayed MA. Gold nanoparticles : interesting optical properties and recent applications in cancer diagnostics and therapy. Nanomedicine. 2007: 2(5): 681-693.

[9] Hainfeld JF, Dilmanian FA, Slatkin DN, Smilowitz HM. Radiotherapy enhancement with gold nanoparticles. Journal of Pharmacy and Pharmacology. 2008:60: 977-985. DOI: 10.1211/jpp.60.8.0005.

[10] Hainfeld JF, Slatkin DN, Smilowitz HM. The use of gold nanoparticles to enhance radiotherapy. Physics in Medicine and Biology. 2004: 49:N309-N315. DOI: 10.1088/0031-9155/49/18/N03.

[11] Ganareal TACS, Balbin MM, Monserate JJ, Salazar JR, Mingala CN. Gold nanoparticle-based probes for the colorimetric detection of Mycobacterium avium subspecies paratuberculosis DNA. Biochemical and Biophysical Research Communications. 2018:496(3): 988-997. DOI: 10.1016/j.bbrc.2018.01.033.

[12] de Guia ACM, Fernando SID, Medina NP, Eugenio PJG, Pilare R, Velasco RR, Domingo CYJ, Monsarate JJ, Quiazon KMA. Gold nanoparticle-based detection of pirAvp toxin gene causing acute hepatopancreatic necrosis disease (AHPND). SN Applied Sciences. 2020:2(8):3-10. DOI: 10.1007/s42452-020-3073-9.

[13] Loiseau A, Asila V, Boitel-Aullen G, Lam M, Salmain M, Boujday S. Silver-based plasmonic nanoparticles for and their use in biosensing. Biosensors. 2019: 9(78). DOI: 10.3390/bios9020078.

[14] Anker JN, Hall WP, Lyandres O, Shah NC, Zhao J, Van Duyne RP. Biosensing with plasmonic nanosensors. Nature Materials, 2008: 7:308-319

[15] Mayer K, Hafner JH. Localized Surface Plasmon Resonance Sensors. Chemical Reviews 2011: 111: 3828-3857. DOI: 10.1021/cr100313v.

[16] Doria G, Baumgartner BG, Franco R, Baptista PV. Optimizing Au-nanoprobes for specific sequence discrimination. Colloids Surfaces B: Biointerfaces. 2010:77(1)1:22-124. DOI: 10.1016/j.colsurfb.2010.01.007.

[17] Mirkin CA, Letsinger RL, Mucic RC, Storhoff JJ. A DNA-based method for rationally assembling nanoparticles into macroscopic materials. Nature. 1996:382(6592):607-609. DOI: 10.1038/382607a0.

[18] Tan P, Li HS, Wang J, Gopinath SBC. Silver nanoparticle in biosensor and bioimaging: Clinical perspectives. Biotechnology and Applied Biochemistry. 2020:1-7. DOI: 10.1002/bab.2045.

[19] Boisselier E, Astruc D. Gold nanoparticles in nanomedicine: preparations, imaging, diagnostics, therapies and toxicity. Chemical Society Reviews. 2009: 38(6):1759-1782. DOI: 10.1039/b806051g.

[20] Dreaden EC, Alkilany AM, Huang X, Murphy CJ,El-Sayed MA. The golden age: Gold nanoparticles for biomedicine. Chemical Society Review. 2012:41(7): 2740-2779. DOI: 10.1039/c1cs15237h.

[21] Rycenga M, Cobley CM, Zeng J, Li W, Moran CH, Zhang Q, Quin D, Xia Y. Controlling the synthesis and assembly of silver nanostructures for plasmonic applications. Chemical Review. 2011:111(6):3669-3712. DOI: 10.1021/cr100275d.

[22] Jeyaraj M, Gurunathan S, Qasim M, Kang MH, Kim JH. A comprehensive review on the synthesis, characterization, and biomedical application of platinum nanoparticles. Nanomaterials. 2019:9(12):2019. DOI: 10.3390/nano9121719.

[23] Augustine R, Hasan A. Chapter 11 - Multimodal applications of phytonanoparticles. In: Thajuddin N, Mathew SBPT, editors. Micro and Nano Technologies. Elsevier; 2020. p. 195-219.

[24] Kimling J, Maier M, Okenve B, Kotaidis V, Ballot H, Plech A. Turkevich Method for Gold Nanoparticle Synthesis Revisited. The Journal of Physical Chemistry B. 2006:110(32):15700-15707. DOI: 10.1021/JP061667W.

[25] Nayfeh M. Fundamentals and Applications of Nano Silicon of Nano Silicon in Plasmonics and Fullerines. Micro and Nano Technologies, Elsevier;2018:p. 169-203.

[26] Cele T. Preparation of Nanoparticles. Janeza Trdine 9, 51000 Rjeka, Croatia: InTech; 2020. DOI:10.5772/intechopen.90771

[27] Pal G, Rai P, Pandey A. Chapter 1 - Green synthesis of nanoparticles: A greener approach for a cleaner future. Shukla AK, Iravani S, editors. Green Synthesis, Characterization and Applications of Nanoparticles. Elsevier; 2019, p. 1-26.

[28] Khan A, Rashid R, Murtaza G, Zahra A. Gold Nanoparticles: Synthesis and Applications in Drug Delivery. Tropical Journal of Pharmaceutical Research.2014: 13(7):1169-1177. DOI: 10.4314/tjpr.v13i7.23.

[29] Mourdikoudis S, Pallares RM, Thanh NTK. Characterization techniques for nanoparticles: Comparison and

complementarity upon studying nanoparticle properties. Nanoscale. 2018:10(27):12871-12934. DOI: 10.1039/c8nr02278j.

[30] Pereira RMS, Borges J, Smirnov DV, Vaz F, Vasilevskiy MI. Surface Plasmon Resonance in a Metallic Nanoparticle Embedded in a Semiconductor Matrix: Exciton–Plasmon Coupling. ACS Photonics. 2019:6(1):204-210. DOI: 10.1021/acsphotonics.8b01430.

[31] Imbraguglio D, Giovannozzi AM, Rossi AM. Nanometrology. Proceeding of the International School of Physics "Enrico Fermi,". 2013:185(2018):193-220. DOI: 10.3254/978-1-61499-326-1-193.

[32] Facciuolo A, Kelton DF, Mutharia LM. Novel secreted antigens of Mycobacterium paratuberculosis as serodiagnostic biomarkers for Johne's disease in cattle. Clinical and Vaccine Immunology. 2013:20(12):1783-1791. DOI: 10.1128/CVI.00380-13.

[33] Hermon-Taylor J. Mycobacterium avium subspecies paratuberculosis, Crohn's disease and the Doomsday scenario. Gut Pathology. 2009:1(1):15. DOI: 10.1186/1757-4749-1-15.

[34] Yang S, Sun Y, Yang J, Liu Y, Feng H Zhang G. A gold nanoparticle strip for simultaneously evaluating FMDV immunized antibody level and discriminating FMDV vaccinated animals from infected animals. RSC Advances. 2019:9(52):30164-30170. DOI: 10.1039/c9ra04810c.

[35] Ding YZ, Liu YS, Zhou JH, Chen HT, Wei G, Ma LN, Zhang J. A highly sensitive detection for foot-and-mouth disease virus by gold nanopariticle improved immuno-PCR Virology Journal. 2011:8(148):1-5. DOI: 10.1186/1743-422X-8-148.

[36] Nam JM, Thaxton CS,Mirkin CA. Nanoparticle-Based Bio-Bar Codes for the Ultrasensitive Detection of Proteins. Science. 2003:203(5641): 1884-1884.

[37] Yin HQ, Jia MX, Shi LJ, Yang S, Zhang LY, Zhang QM. Wang SQ, Li G, Zhang JG. Nanoparticle-based bio-barcode assay for the detection of bluetongue virus. Journal of Virological Methods. 2011:178(1-2):225-228. DOI: 10.1016/j.jviromet.2011.05.014.

[38] Yin HQ, Jia MX, Yang S, Jing PP, Wang R, Zhang JG. Development of a highly sensitive gold nanoparticle probe-based assay for bluetongue virus detection. Journal of Virological Methods. 2012:183(1): 45-48. DOI: 10.1016/j.jviromet.2012.03.027.

[39] Herrmann-Hoesing LM. Diagnostic assays used to control small ruminant lentiviruses. Journa; of Veterinary Diagnostic Investigation. 2010:22(6):843-855. DOI: 10.1177/104063871002200602.

[40] Brinkhof JMA, van Maanen C, Wigger R, Peterson K, Houwers DJ. Specific detection of small ruminant lentiviral nucleic acid sequences located in the proviral long terminal repeat and leader-gag regions using real-time polymerase chain reaction. Journal of Virological Methods. 2008:147(2):338-344. DOI: 10.1016/j.jviromet.2007.10.013.

[41] Balbin MM, Lertanantawong B, Suraruengchai W, Mingala CN. Colorimetric detection of caprine arthritis encephalitis virus (CAEV) through loop-mediated isothermal amplification (LAMP) with gold nanoprobes. Small Ruminant Research. 2017:147:48-55. DOI: 10.1016/j.smallrumres.2016.11.021.

[42] Huang J, Sun Y, Liu Y, Xiao H, Zhuang S. Development of a

loop-mediated isothermal amplification method for rapid detection of caprine arthritis-encephalitis virus proviral DNA. Archives of Virology. 2012:157(8):1463-1469. DOI: 10.1007/s00705-012-1322-y.

[43] Balbin MM, Belotindos LP, Abes NS, Mingala CN. Caprine arthritis encephalitis virus detection in blood by loop-mediated isothermal amplification (LAMP) assay targeting the proviral gag region. Diagnostic Microbiology and Infectious Disease. 2014:79(1):37-42. DOI: 10.1016/j.diagmicrobio.2013.12.012.

[44] SirikharinR, Taengchaiyaphum S, Sanguanrut P, Chi TD, Mavichak R, Proespraiwong P, Nuangseng B, Thitamadee S, Flegel TW, Sritunyalucksana K. Characterization and PCR detection of binary, pir-like toxins from vibrio parahaemolyticus isolates that cause acute hepatopancreatic necrosis disease (AHPND) in shrimp. PLoS One. 2015:10(5):1-16. DOI: 10.1371/journal.pone.0126987.

[45] Te Lee C, Chen IT, Yang YT, Ko TP, Huang YT, Huang JY, Huaag MF, Lin SJ, Chen CY, Lin SS, Lightner DV, Wang HC, Wang AHJ, Wang HC, Hor LI, Lo CF. The opportunistic marine pathogen Vibrio parahaemolyticus becomes virulent by acquiring a plasmid that expresses a deadly toxin. Proceedings of the National Academy of Sciences of the United States of America. 2015:112(39):E5445. DOI: 10.1073/pnas.1517100112.

[46] Boys CA, Rowland SJ, Gabor M, Gabor L, Marsh IB, Hum S, Callinan RB. Emergence of epizootic ulcerative syndrome in native fish of the murray-darling river system, Australia: Hosts, Distribution and Possible Vectors. PLoS One. 2012:7(4). DOI: 10.1371/journal.pone.0035568.

[47] Vandersea MW, Litaker RW, Yonnish B, Sosa E, Landsberg JH, Pullinger C, Moon-Butzin P, Green J, Morris JA, Kator H, Noga EJ, Tester PA. Molecular Assays for Detecting *Aphanomyces invadans* in Ulcerative Mycotic FIsh Lesions. Applied and Environmental Microbiology. 2006:72(2):1551-1557. DOI: 10.1128/AEM.72.2.1551.

[48] Phadee P, Kurata O, Hatai K, Hirono I, Aoki T. Detection and identification of fish-pathogenic Aphanomyces piscicida using Polymerase Chain Reaction (PCR) with species-specific primers. Journal of Aquatic Anial Health. 2004:16(4):220-230. DOI: 10.1577/H03-047.1.

[49] Kuan GC, Sheng LP, Rijiravanich P, Marimuthu K, Ravichandran M, Yin LS, Lertanantawong B, Surareungchai W. Gold-nanoparticle based electrochemical DNA sensor for the detection of fish pathogen Aphanomyces invadans. Talanta. 2013:117:312-317. DOI: 10.1016/j.talanta.2013.09.016.

[50] De La Escosura-Muñiz A, Baptisa-Pires L, Serrano L, Altet L, Francio O, Sanchez A, Merkoci A. Magnetic Bead/Gold Nanoparticle Double-Labeled Primers for Electrochemical Detection of Isothermal Amplified Leishmania DNA. Small. 2016:12(2):205-213. DOI: 10.1002/smll.201502350.

[51] Chappuis F, Sundar S, Hallu S, Ghalib H, Rijal S, Peeling RW, Alvar J, Boelaert M. Visceral leishmaniasis: What are the needs for diagnosis, treatment and control?. Naturet Reviews Microbiology. 2007:5(11):873-882. DOI: 10.1038/nrmicro1748.

[52] Solano-Gallego L, Fernandez-Bellon H, Morell P, Fondevila D, Alberola J, Ramis A, Ferrer L. Histological and immuno-histochemical study of clinically normal

skin of Leishmania infantum-infected dogs. Journal of Comparative Pathology. 2004:130(1):7-12. DOI: 10.1016/S0021-9975(03)00063-X.

[53] Xavier SC, De Andrade HM, Monte SJH, Chiarelli IM, Lima WG, Michalic MSM, Tafuri WL, Tafuri WL. Comparison of paraffin-embedded skin biopsies from different anatomical regions as sampling methods for detection of Leishmania infection in dogs using histological, immunohistochemical and PCR methods. BMC Veterinary Research. 2006:2:1-7. DOI: 10.1186/1746-6148-2-17.

[54] Reithinger R, Dujardin JC. Molecular diagnosis of leishmaniasis: Current status and future applications. Journal of Clinical Microbiology. 2007:45(1):21-25. DOI: 10.1128/JCM.02029-06.

[55] Srividya G, Kulshrestha A, Singh R, Salotra P. Diagnosis of visceral leishmaniasis: Developments over the last decade. Parasitology Research. 2012:110(3):1065-1078. DOI: 10.1007/s00436-011-2680-1.

[56] Lombardo G, Pennisi MG, Lupo T, Migliazzo A, Caprì A, Solano-Gallego L. Detection of Leishmania infantum DNA by real-time PCR in canine oral and conjunctival swabs and comparison with other diagnostic techniques. Veterinary Parasitology. 2012:184(1):10-17. DOI: 10.1016/j.vetpar.2011.08.010.

[57] Naranjo C, Fondevilla D, Altet L, Francino O, Rios J, Roura X, Peña T. Evaluation of the presence of Leishmania spp. by real-time PCR in the lacrimal glands of dogs with leishmaniosis. The Veterinary Journal. 2012:193(1):168-173. DOI: 10.1016/j.tvjl.2011.10.001.

[58] Van Der Meide W, Guerra J, Schoone G, Farenhorst M, Coelho L, Faber W, Peekel I, Schallig H. Comparison between quantitative nucleic acid sequence-based amplification, real-time reverse transcriptase PCR, and real-time PCR for quantification of Leishmania parasites. Journal Clinical Microbiology. 2008:46(1):73-78. DOI: 10.1128/JCM.01416-07.

[59] Chappuis F, Mueller Y, Nguimfack A, Rwakimari JB, Couffignal S, Boelaert M, Cavailler P, Loutan L, Piola P. Diagnostic accuracy of two rK39 antigen-based dipsticks and the formol gel test for rapid diagnosis of visceral leishmaniasis in northeastern Uganda. Journal Clinincal Microbiology. 2005:43(12):5973-5977. DOI: 10.1128/JCM.43.12.5973-5977.2005.

[60] Salotra P, Sreenivas G, Ramesh V, Sundar S. A simple and sensitive test for field diagnosis of post kala-azar dermal leishmaniasis. British Journal of Dermatology. 2001:145(4):630-632. DOI: 10.1046/j.1365-2133.2001.04434.x.

[61] Sundar S, Maurya R, Singh RK, Bharti K, Chakravarty J, Parekh A, Rai M, Kumar K, Murray HW. Rapid, noninvasive diagnosis of visceral leishmaniasis in India: Comparison of two immunochromatographic strip tests for detection of anti-K39 antibody. Journal Clinincal Microbiology. 2006:44(1):251-253. DOI: 10.1128/JCM.44.1.251-253.2006.

[62] Kim YS, Kim JH, Kim IA, Lee SJ, Jurng J, Gu MB. A novel colorimetric aptasensor using gold nanoparticle for a highly sensitive and specific detection of oxytetracycline. Biosensor and Bioelectronics. 2010:26(4):1644-1649. DOI: 10.1016/j.bios.2010.08.046.

[63] Chen J, Li Z, Ge J, Yang R, Zhang L, Qu LB, Wang HQ, Zhang L. An aptamer-based signal-on bio-assay for sensitive and selective detection of Kanamycin A by using gold nanoparticles. Talanta. 2015:139:226-232. DOI: 10.1016/j.talanta.2015.02.036.

[64] Ou Y, Jin X, Liu L, Tian Y, Zhou N. Visual detection of kanamycin with DNA-functionalized gold nanoparticles probe in aptamer-based strip biosensor. Analytical Biochemistry. 2019: 587:113432. DOI: 10.1016/j.ab.2019. 113432.

[65] Robati TY, Arab A, Ramezani M, Langroodi FA, Abnous K, Taghdisi SM. Aptasensors for quantitative detection of kanamycin. Biosensors and Bioelectronics. 2016:82:162-172. DOI: 10.1016/j.bios.2016.04.011.

[66] Song HY, Kang TF, Li NN, Lu LP, Cheng SY. Highly sensitive voltammetric determination of kanamycin based on aptamer sensor for signal amplification. Analytical Methods. 2016:8(16):3366-3372. DOI: 10.1039/c6ay00152a.

[67] European Commission. COMMISSION REGULATION (EU) No 37/2010. Official Journal European Union. 2010: L 15/1:1-72.

[68] Xing YP, Liu C, Zhou XH, Shi HC. Label-free detection of kanamycin based on a G-quadruplex DNA aptamer-based fluorescent intercalator displacement assay. Sciemtific Reports. 2015:5:14-16. DOI: 10.1038/srep08125.

[69] Zhu Y, Chandra P, Song KM, Ban C, Shim YB. Label-free detection of kanamycin based on the aptamer-functionalized conducting polymer/gold nanocomposite. Biosensors and Bioelectronics. 2012:36(1):29-34 DOI: 10.1016/j.bios.2012.03.034.

[70] Wang H, Wang Y, Liu S, Yu J, Guo Y, Xu Y, Huang J. Signal-on electrochemical detection of antibiotics at zeptomole level based on target-aptamer binding triggered multiple recycling amplification. Biosensensors and Bioelectronics. 2016:80:471-476. DOI: 10.1016/j.bios.2016.02.014.

[71] He X, Han H, Liu L, SHi W, Lu X, Dong J, Yang W, Lu X. Self-Assembled Microgels for Sensitive and Low-Fouling Detection of Streptomycin in Complex Media. ACS Applied Materials and Interfaces. 2019:11(14):13676-13684. DOI:10.1021/acsami.9b00277.

[72] Mahmoudi L, Nikman R, Mousavir S, Ahmadi A, Honarmand H, Ziaie S, Mojtahedzadeb M.Optimal aminoglycoside therapy following the sepsis: How much is too much?. Iranian Journal of Pharmaceutical Research. 2013:12(2):261-269. DOI: 10.22037/ ijpr.2013.1298.

[73] Schwake-Anduschus C, Langenkämper G. Chlortetracycline and related tetracyclines: detection in wheat and rye grain. Journal of the Science of Food and Agriculture. 2018:98(12): 4542-4549. DOI: 10.1002/jsfa.8982.

[74] Chander Y, Gupta SC, Kumar K, Goyal SM, Murray H. Antibiotic use and the prevalence of antibiotic resistant bacteria on turkey farms. Journal of the Science of Food and Agriculture. 2008:88:714-719.

[75] Ben Said L, Klibi N, Dziri R, Borgo F, Boudabous A, Slama KB, Torres C. Prevalence, antimicrobial resistance and genetic lineages of Enterococcus spp. from vegetable food, soil and irrigation water in farm environments in Tunisia. Journal of the Science of Food and Agriculture. 2016:96(5):1627-1633. DOI: 10.1002/jsfa.7264.

[76] Krause KM, Serio AW, Kane TR, Connolly LE.Aminoglycosides : An Overview. Cold Spring Harbor Perspective in Medicine. 2016 pp. 1-18, 2016: 6(a2729):1-18.

[77] Ghodake G, Shinde S, Saratale RG, Kadam A, Saratale GD, Syed A, Marraiki N, Elgorban AM, Kim DY. Silver

nanoparticle probe for colorimetric detection of aminoglycoside antibiotics: picomolar-level sensitivity toward streptomycin in water, serum, and milk samples. Journal of the Science of Food and Agriculture.2020:100(2):874-884. DOI: 10.1002/jsfa.10129.

[78] Ramatla T, Ngoma L, Adetunji M, Mwanza M. Evaluation of antibiotic residues in raw meat using different analytical methods. Antibiotics. 2017:6(4):1-17. DOI: 10.3390/antibiotics 6040034.

[79] Zhao J, Wu Y, Tao H, Chen H,Yang W, Qiu S. Colorimetric detection of streptomycin in milk based on peroxidase-mimicking catalytic activity of gold nanoparticles. RSC Advances. 2017:7(61):38471-38478. DOI: 10.1039/ c7ra06434a.

[80] Wang L, Hao L, Qi W, Huo X, Xue L, Liu Y, Zhang Q, Lin J.A sensitive Salmonella biosensor using platinum nanoparticle loaded manganese dioxide nanoflowers and thin-film pressure detector. Sensors and Actuators B: Chemical. 2020:321:128616. DOI: 10.1016/j.snb.2020.128616.

[81] Chen C, Meng L, Li M, Zhu Z. Simultaneous separation and sensitive detection of four β2-agonists in biological specimens by CE-UV using a field-enhanced sample injection method. Analytical Methods. 2015:7(1):175-180. DOI: 10.1039/c4ay02385d.

[82] Sun Y, Du T, Chen S, Wu Z, Guo Y, Pan D, Gan N. A novel colorimetric immunosensor based on platinum colloid nanoparticles immobilized on Power Vision as signal probes and Fe_3O_4@β-cyclodextrin as capture probes for ractopamine detection in pork,. Journal of the Science of Food and Agriculture. 2019:99(6):2818-2825. DOI:10.1002/ jsfa.9492.

[83] Schiavone A, Tarantola M, Perona G, Pagliasso S, Badino P, Odore R, Cuniberto B, Lussiana C. Effect of dietary clenbuterol and cimaterol on muscle composition, β-adrenergic and androgen receptor concentrations in broiler chickens. Journa of Animal Physiology and Animal Nutrition. 2004:88(3-4):94-100. DOI:10.1111/ j.1439-0396.2003.00464.x.

[84] Li Z, Wang Y, Kong W, Li C, Wang Z, Fu Z. Highly sensitive near-simultaneous assay of multiple 'lean meat agent' residues in swine urine using a disposable electrochemiluminescent immunosensors array. Biosensors and Bioelectronics. 2013:39(1):311-314. DOI: 10.1016/j.bios.2012.07.007.

Section 3

Molecular and Cellular Structure and Function

Bronchus-Associated Lymphoid Tissue (BALT) Histology and Its Role in Various Pathologies

Tuba Parlak Ak

Abstract

The lower respiratory tract is in direct communication with the external environment for gas exchange to occur. Therefore, it is constantly exposed to allergens, antigens, bacteria, viruses, and a wide variety of airborne foreign bodies. Bronchus-associated lymphoid tissue (BALT), which develops in response to these exposures and is one of the most prominent representatives of mucosa-associated lymphoid tissue (MALT), is important for generating rapid and specific bronchopulmonary adaptive immune responses. Therefore, this chapter focuses on the lymphoid architecture of BALT, which was first discovered in the bronchial wall of rabbits, its inducible form called inducible BALT (iBALT), its immunological response mechanisms, and its roles in certain pathologies including infectious and autoimmune diseases as well as in allergic and malignant conditions. In conclusion, it is hypothesized that BALT plays an important role in maintaining health and in the development of lower respiratory tract diseases; thanks to the pulmonary immune system in which it functions as a functional lymphoid tissue.

Keywords: Bronchus-associated lymphoid tissue, local immune response, histology, inducible bronchus-associated lymphoid tissue, lung diseases

1. Introduction

The respiratory system is anatomically divided into the following two parts: upper respiratory tract (organs outside the chest: nose, pharynx, and larynx) and lower respiratory tract (organs inside the chest: trachea, bronchi, bronchioles, alveolar ducts, and alveoli). This system that performs three basic functions, i.e., air transmission, air filtration, and gas exchange (respiration), is functionally divided into two zones. These are the conductive zones (from the nose to the bronchioles) that act as a pathway for the delivery of inhaled gases, and the respiratory zone (from the alveolar canal to the alveoli) where gas exchange occurs. The branching pattern of the conducting passages is known as the tracheobronchial tree as it resembles the branching of a tree [1].

The lungs, the main organ of the respiratory system, are divided into two sections depending on the functions of their structural parts. These are the tubes that conduct air (bronchi and bronchioles) and respiratory tissue (alveolar ducts, alveolar sacs, and alveoli). Ventilated by a secondary (lobar) bronchus, each lobe of the lung is divided into smaller pyramidal-shaped segments known as the bronchopulmonary segments and is ventilated by a tertiary (segmental) bronchus [2].

The bronchi of the lower respiratory tract are vital in terms of respiratory aspects because they are responsible for the transmission and filtration of air as well as for key immunological functions.

1.1 Bronchial structure

The bronchial wall is microscopically composed of the following five sections: mucosa, muscle, submucosa, cartilage, and peribronchial connective tissue (adventitia) (**Figure 1**) [3].

The epithelial and lamina propria layers constitute the bronchial mucosa layer, which has the characteristics of the respiratory mucosa. The initial part of the bronchi exhibits a similar structure to that of the trachea, which is a pathway responsible for the transmission of air taken from the external environment into the lungs. The structure of the bronchial wall changes histologically at the point where it enters the lungs and transforms into intrapulmonary bronchi. In the beginning, the bronchial mucosa comprises a layer of respiratory epithelium with the same cellular composition as the trachea. The height of the cells of this ciliated layer, also known as the pseudostratified columnar epithelium, decreases in proportion to the diameter of the bronchus.
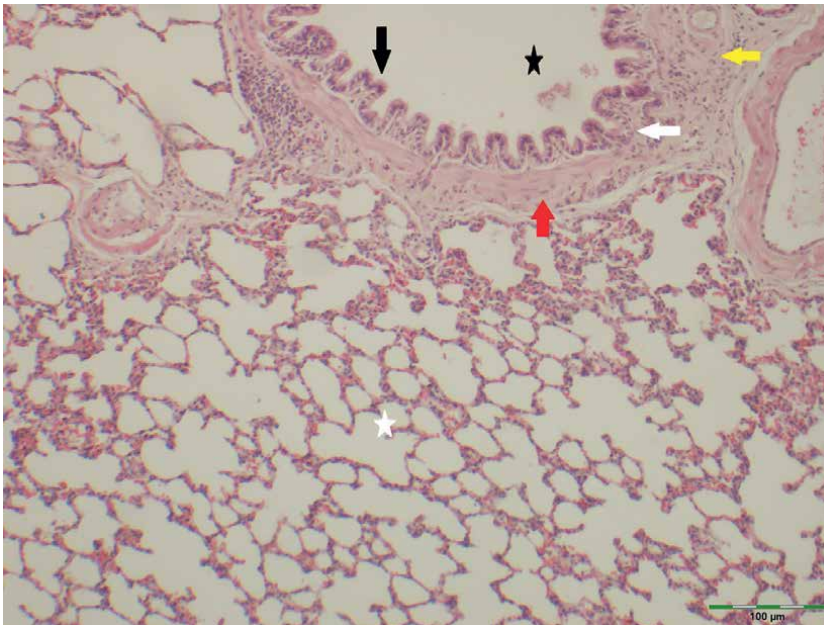
Figure 1.
Light microscopic view of the bronchial wall, rat lung (H-E). Black star: bronchial lumen, black arrow: respiratory epithelium layer, white arrow: lamina propria layer, red arrow: smooth muscle layer, yellow arrow: submucosa layer, white star: distinctive lung tissue (LT) showing the many empty spaces of pulmonary alveoli.

The prominent cell types in the epithelium are ciliated cells, goblet cells, basal cells, brush cells, and neuroendocrine cells. The epithelial layer is separated from other mucosal layers by a basement membrane [4].

The basement membrane is prominent in the primary bronchi; however, it rapidly decreases in thickness and disappears as a separate structure in the secondary bronchi. The lamina propria layer is similar to the trachea, but it decreases in proportion to the diameter of the bronchi. The lamina propria layer, which appears as a typical loose connective tissue with abundant elastic and collagen threads, is rich in cellular structures. In addition to the cell types such as plasma cells, mast cells, eosinophils, and fibroblasts, it comprises a large number of lymphocyte cells. The lymphocytes in this layer gather in the form of infiltrates at some places and lymph follicles at some [3].

The muscularis layer, which comprises multiple rows of circular smooth muscle cells, is a continuous layer of smooth muscles in the large bronchi. However, in the small bronchi, it is weakly and loosely organized because it may appear discontinuous due to its spiral route. This layer is responsible for determining the appropriate airway diameter for airflow regulation. In the large bronchi, the loose connective tissue submucosa layer is evident, whereas in the small bronchi, it is only observed as a narrow patch. In addition to the venous plexus and lymph follicles, bronchial glands known as GI. bronchioles are quite common in this layer. These glands, similar to salivary gland tissue, comprise a mixture of serous and mucinous cells and decrease in quantity as the diameter of the bronchi decreases (**Figure 2**) [3, 5].

The cartilage layer is observed as a whole in the trachea, whereas it is irregularly present at the beginning of the bronchi in the form of hyaline cartilage. As the diameter of the bronchus decreases, the fragmented cartilage layer becomes smaller and appears as elastic cartilage. On the other hand, the peribronchial connective tissue (adventitia) layer is dense that limits the bronchi from the alveoli and is rich in nerve and elastic fibers in addition to large blood and lymph vessels [3].
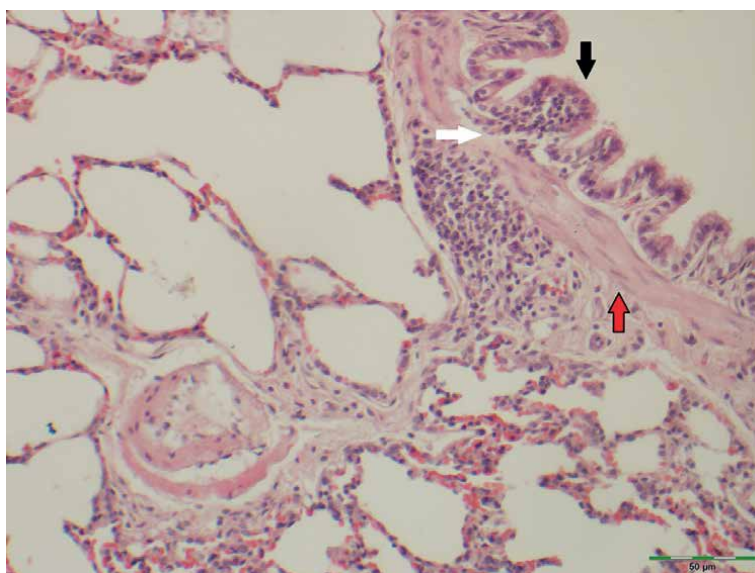
Figure 2.
A higher power light microscopic view of the bronchial wall, rat lung (H-E). Black arrow: respiratory epithelium layer, white arrow: lamina propria layer, red arrow: smooth muscle layer.

2. Bronchi immunology

The lower respiratory tract is constantly exposed to a wide variety of airborne for-eign bodies because it is in direct communication with the external environment for gas exchange [6]. Both the trachea and bronchi function as filters against this expo-sure due to some of their structural features. The bronchial epithelium has a similar histological structure to the trachea and can capture foreign bodies through the smear of the mucus film secreted by the goblet cells to the kinocilium at the apical ends of the prismatic cells present in its structure. These bodies are captured and removed from the lungs by the movement of the kinocilium toward the larynx [7]. Mechanical filtering of inhaled air is thus ensured due to this primary defense mechanism.

The lower respiratory tract is constantly exposed to allergens, antigens, bacte-ria, and viruses during gas exchange. This is a very sensitive area for various types of pathogen invasions, such as influenza virus, measles virus, and *Mycobacterium tuberculosis* [8]. Producing rapid and specific adaptive immune responses against these factors are important for survival [6]. At the initial stage of an adaptive immune response, naive T cells migrate through the endothelial venules of blood vessels to secondary lymphoid tissues, where they are stimulated by antigen-bearing cells. This is critical for the development of appropriate adaptive immunity. This migra-tion therefore leads to the generation of antigen-specific effector and memory T and B cells released from the secondary lymphoid tissue into the bloodstream. In the effector stage of the adaptive immune response, some memory T and B cells migrate from blood vessels to non-lymphoid tissues containing cognate antigens or pathogens [9, 10]. Bronchial lymphoid tissue and lymphatic nodes, two types of secondary lymphoid tissue found in the bronchial mucosa of the lower respiratory tract, are important in this regard [11, 12]. These secondary lymphoid tissues play a key role in the development of bronchopulmonary immune responses. Therefore, the broncho-pulmonary adaptive immune system plays an important role in maintaining health as well as in the development of lower respiratory tract diseases [6].

The tracheobronchial tree, which is considered as an immunological organ, [13] is important for the defense mechanism of microorganisms reaching the lungs through inhaled air as well as for hypersensitive reactions that occur through respiration. The lymphoid tissue of the tracheobronchial system contains specialized diffuse, clus-tered, and solitary lymphatic nodules known as bronchus-associated lymphoid tissue [14, 15]. This secondary lymphoid tissue is a representative of the mucosal immune system in the bronchial wall, which is common in different parts of the body. It forms the immunoglobulins as a result of the immune defense reaction, thus forming a special protective mechanism of the lower respiratory system.

3. Mucosa-associated lymphoid tissue (MALT)

The immune system can recognize a wide range of unknown antigens and elicit an appropriate respond due to the lymphocytes that have a wide variety of antigen recep-tors [16]. This system has evolved into a system of secondary lymphoid organs such as the spleen, lymph nodes, Peyer's patches, and other MALT, in line with the defense targets [17]. Highly organized secondary lymphoid organs contain architectural domains that facilitate sequential cellular interactions between antigen-presenting cells and lymphocytes and efficiently promote the activation, selection, and differentiation of B and T cells [16]. Therefore, the immunological response becomes more effective.

MALT can function independently of the systemic immune system and therefore encompasses the mucosal immune system, which is a crucial part of immunopathology [18]. It plays an important role in immunological defense by eliciting immune responses against specific antigens encountered along the surfaces of all mucosal tissues [19]. Although MALT is anatomically divided into regions, these regions are functionally interconnected under the name of the common mucosal immune system. In this way, events such as antigen presentation and B-cell activation in a mucosal region can trigger the secretion of immunoglobulin A (IgA) in the mucosal regions of different organs [18, 20]. Due to MALT, which mainly functions to produce and secrete IgA along the mucosal surfaces in antigen-specific, T helper 2-dependent reactions, T helper 1 and cytotoxic T-cell-mediated reactions can occur. This may then result in immunotolerance [20, 21].

The best-known representatives of MALT, which contains approximately half of the lymphocytes of the immune system, [22] are gut-associated lymphoid tissue (GALT), nasal-associated lymphoid tissue (NALT), and BALT. However, structures such as conjunctival-associated lymphoid tissue (CALT), larynx-associated lymphoid tissue, and duct-associated lymphoid tissue (DALT) are other MALT representatives [20, 21].

MALT is divided into the two following functional parts: inducer sites and effector sites. Inducer sites include secondary lymphoid tissues, where the clonal expansion of B cells and IgA class transition occur in response to antigen-specific T-cell activation [19]. GALT, BALT, NALT, and CALT in mice, dogs [23], and baboons [24] and DALT in cynomolgus macaques [25] constitute these inducing sites. These sites are known as secondary immune tissues where antigen sampling occurs, and immune responses are initiated. Although there are many differences between inducing sites in various organs, they all contain the same functional segments as follows: lymphoid follicles, interfollicular zones, subepithelial dome zones, and follicle-associated epithelium or lymphoepithelium containing microfold (M) cells [19].

Effector sites distributed as diffuse lymphoid tissue throughout the lamina propria layer on all mucosal surfaces [26] are known as the transport sites of IgA along the mucosal epithelium. After activation and IgA class transition, T- and B cells migrate from inducing sites to these sites [19]. CD^{4+} and CD^{8+} T cells, IgA-, IgG- and IgM-plasma cells, B cells, antigen-presenting dendritic cells, and macrophages [19] constitute the cellular content of these effector regions where secreted IgA (S-IgA) is secreted along the mucosal epithelium [27]. Mast cells and eosinophils can occasionally be seen in the interfollicular area. Thus, all the cell types required to initiate an immune response are present here.

4. Bronchus-associated lymphoid tissue (BALT)

BALT, an important part of MALT, is classically used to refer to intrapulmonary lymphoid tissue in connection with the pulmonary vessels and adventitia of the bronchi [11, 28]. Macklin [29] named this lymphoid tissue in 1955 as 'sumps' or 'pulmonary tonsils' in which dust and organisms are retained. Subsequently, Bienenstock et al. [28, 30] identified these formations as subepithelial follicular lymphoid aggregates, primarily composed of lymphocytes, organized in the bronchial mucosa in contact with the surface epithelium, and coined the term BALT to describe them.

Although BALT, a secondary lymphoid tissue that plays an important role in the maintenance and regulation of lung mucosal immune homeostasis [8], was initially claimed to resemble Peyer's patches in the small intestine [11]; it was later revealed

that it was quite different from these formations [31]. Compared to GALT where in the founder Peyer's patches are located, it is accepted that BALT is not regularly present during fetal life due to embryonic preprogramming; however, it occurs with antigenic stimulation during the postnatal period [32, 33]. In other words, it is claimed that there is a relatively special lymphoid tissue in the development of BALT. However, studies have shown that BALT exhibits great differences between species [34, 35].

BALT, which was first identified in the bronchial wall of rabbits by Bienenstock et al. [28], is frequently detected in these animals and has the highest number of regions [28, 34]. In terms of the presence and distribution of BALT, rats and guinea pigs [34] follow rabbits, whereas germ-free pigs [28, 34], cats, dogs, and Syrian hamsters [34, 36] do not have this lymphoid tissue. BALT is frequently present in poultry, particularly hens [37]. In mice and humans, the situation with BALT is a little more contradictory [19]. Some scientists suggest that BALT is present in germ-free mice when antigenic stimulation is absent [12], whereas others report that it is not [38, 39]. Besides the differing viewpoints on the presence of BALT in mice, it is assumed that it is only observed infrequently after the neonatal period.

Further, it is claimed that BALT is not present in structurally healthy humans [31] because the features similar to BALT in mice are also found in humans [8]. BALT, in particular, is detectable if it is induced in adults; however, it is only observed in 40% healthy children and adolescents. Factors inducing the presence and distribution of BALT in these adults include infection, pathogen exposure, chronic pulmonary inflammation or autoimmune disease, etc. [32, 33, 40]. Moreover, it is suggested that the formation, size, and amount of BALT depend on the type and duration of exposure [41]. Therefore, it is concluded that BALT varies in different species as well as indifferent physiological states of the same species [8].

4.1 Inducible BALT (İBALT)

Most of the secondary lymphoid organs found in mice and humans develop embryonically in the absence of microbial stimulation or environmental antigens [42]. Furthermore, the structure and function of several secondary lymphoid organs, particularly those on the mucosal surfaces, are dramatically altered upon exposure to foreign antigens and commensal organisms [43]. Peyer's patches of MALT demonstrate a striking increase in size and complexity following the colonization of commensals [44, 45]. Similarly, in rodents, NALT is not completely developed until the postnatal period; however, microbial exposure accelerates this process [46]. On the other hand, the appendix tissue of rabbits has the characteristics of the primary and secondary lymphoid tissues in terms of being functionally dependent on microbial colonization [47]. However, some lymphoid tissues, known as tertiary lymphoid tissues, develop only after environmental exposure to microbes, pathogens, or inflammatory stimulations. Interestingly, although the lungs of mice and humans normally lack organized lymphoid tissue, tertiary lymphoid structures are frequently observed in lung tissue [38, 48].

BALT is recognized as an inducible tertiary or ectopic lymphoid tissue, unlike the related secondary lymphoid organs. BALT develops during the postnatal period and at anatomically non-lymphoid sites. In terms of disease states characterized by chronic inflammation, infection, or autoimmunity, BALT formation can be induced, and these areas are then known as iBALT [32, 38]. iBALT is a classic example of tertiary lymphoid tissue because it does not develop on a preprogrammed basis; its creation, size, and number in the lungs depend on the type and duration of antigenic

exposure [31, 49]. iBALT regions are best characterized in the lungs of rodents and humans. They are observed in the lungs of mammals and birds as well as in possibly all air-breathing vertebrates [41]. The emerging arguments confirm the role of infectious agents, such as isolated lymphoid follicles in the gut, indicating that iBALT may develop in response to microbial exposure [32]. In contrast, BALT is said to have been discovered in germ-free rats [28] and mice [50] as well.

Unlike the classical BALT structure, iBALT does not always have an overlying lymphoepithelium, is not associated with a continuous airway, and can be located adjacent to small pulmonary arteries in the lung parenchyma [32]. However, as both BALT and iBALT have the same function, both tissue types are called BALT [48].

4.2 Microscopic structure of BALT

Microscopically, BALT is defined as a densely packed cluster of lymphocytes with follicular structures enveloped in a network of reticular stromal cells beneath a specialized airway epithelium devoid of cilium. These structures are claimed to be located along the main bronchial airways embedded in the airway wall with extensive lymphocytic infiltration of the epithelial layer forming a classical dome epithelium (**Figures 3** and **4**) [11].

Further, it is stated that BALT is present in bronchial tree bifurcations to capture respiratory antigens. In species, BALT develops in response to various stimulations rather than being constitutively present in the lung, whereas iBALT does not always have such a defined structure or precise localization in the lung [51].

As a part of the integrated mucosal system including GALT, NALT, and other secondary lymphoid tissue representatives, BALT is known to contain cell types that are responsible for eliciting an appropriate immune response. BALT is mainly defined as an organized structure comprising T- and B-cell domains, dendritic cells (DCs), stromal cells, and high endothelial venules (HEVs) in the T-cell region [38, 52–55].
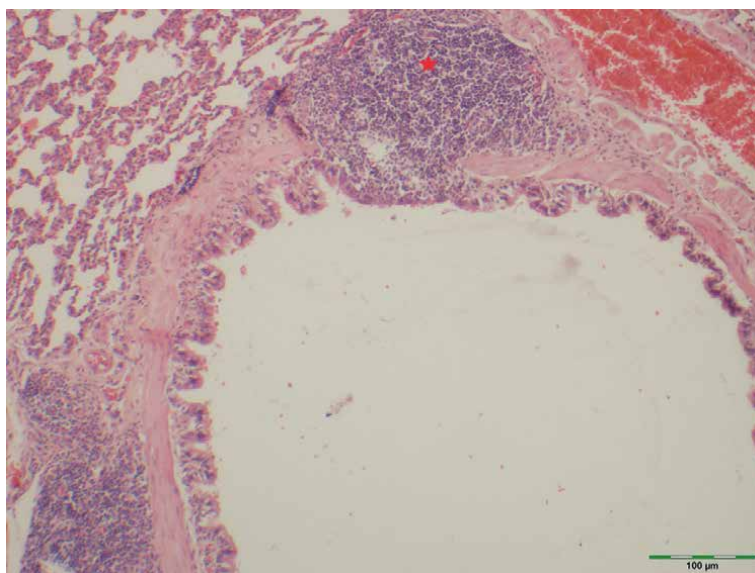
Figure 3.
Light microscopic view of the BALT structure, rat lung (H-E). Red star: BALT formation.
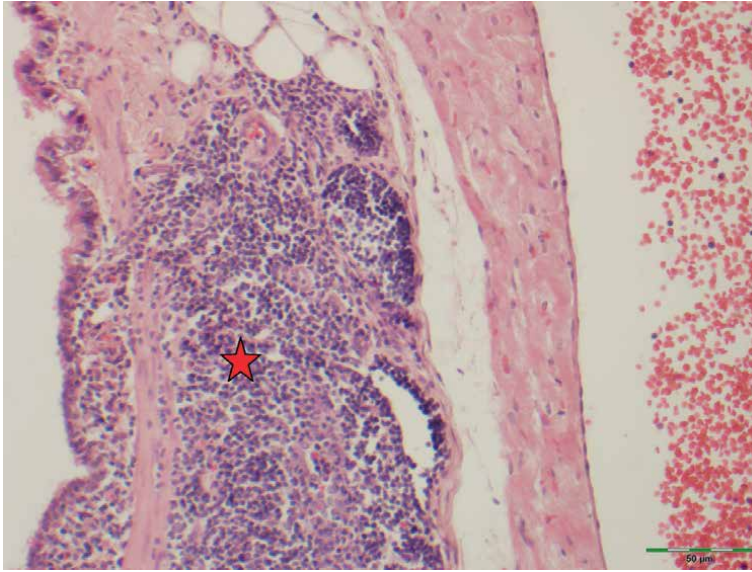
Figure 4.
A higher power light microscopic view of the BALT structure, rat lung (H-E). Red star: BALT formation.

Furthermore, it is stated that most of its cellular component consists of B cells expressing IgM^{lo} IgD^{hi}; however, depending on the nature of the microbe and/or antigen to which the cells respond, IgG-, IgA-, and even IgE-positive plasma cells may also be present [50, 56–58].

Moreover, in BALT, the most prominent structure is follicular-like lymphocyte accumulation, which is the common microscopic appearance of secondary lymphoid tissues, forming a classical germinal center (active site) [59, 60]. In this structure, surrounded by more mature, small lymphocytes, most of the germinal center comprises antigen-presenting macrophages [58, 61]. Lymphocytes leave the blood and migrate to BALT in the walls of HEVs, which are present at the periphery of the tissue. As there are no afferent lymphatics, these HEVs are thought to be the only entry site where lymphocytes migrate to BALT [59, 60]. In addition, the expression of chemokines in HEVs ensures accurate targeting of lymphocytes to lymphoid tissues [62].

However, in the direction of the bronchial epithelium, a dome-like protrusion similar to Peyer's patches toward the bronchial lumen is sometimes clearly observed [31]. The B-cell follicle, which is the most noticeable characteristic in classic BALT tissues with dome epithelium, is positioned below the epithelium [11]. CD^{4+} T cells are abundant in B-cell follicles, especially in reactive follicles with germinal centers [63], and CD^{8+} T cells are uncommon. Moreover, BALT is covered by a lymphoepithelium, which contains M cells that are similar to the M cells present in the dome epithelium of Peyer's patches in some species [31]. M cells are thought to transport antigens from the mucosal lumen to DCs that are in close contact with the dome epithelium [48]. Rabbits, the first and important representative of BALT, have fewer ciliated cells, few goblet cells, and many lymphocytes between epithelial and M cells. Although this basic structure appears to be valid for all species, there are some differences in details [31].

Another cell type that makes up the cellular component of BALT is follicular DCs (FDCs). These cells depend on the lymphotoxin signaling pathway to differentiate

into conventional lymphoid tissues and BALT [38]. Located at the center of B-cell follicles, these cells present antigen to B cells [64] and provide costimulatory signals that increase B-cell activation and proliferation in germinal centers [65, 66]. FDCs in mice are characterized by their ability to bind to antibodies against CD_{21}/CD_{35} [38], $FDCM_1$, or $FDCM_2$ [57] and to sequester their immune complexes [67]. In addition, FDCs are responsible for the organization of the follicle and expression of $CXCL_{13}$, which is responsible for the recruitment of B cells and some T cells in the B-cell area [68]. DCs located at the highest concentration in the T-cell areas of BALT are reportedly capable of preserving the BALT architecture as well as their antigen-presenting ability [48].

BALT is induced to produce IgA^+ cells that secrete polymeric IgA, mainly due to its role in immunity. When polymeric IgA is transported into the lumen, it induces the formation of S-IgA, which has considerable immunological importance [8]. Thus, when BALT is identified as part of the integrated mucosal immune system, the term should be restricted to structures tightly associated with an epithelium infiltrated by lymphocytes. In the integrated mucosal immune system, specific antigen uptake and antigen presentation by M cells occur and immune reactions are initiated, including IgA responses [31].

Immunohistological studies in humans show a preferential central localization of B cells mixed with some CD^{4+} lymphocytes and macrophages. CD^{4+} lymphocytes are also present in the area around the HEV, at the edge resembling a crown, and in the epithelium. In addition to the few proliferative cells positive for Ki67 observed in the follicles, many cells positive for the human leukocyte antigen-DR isotype, which is associated with various autoimmune conditions, disease susceptibility, and disease resistance, are evenly distributed in the follicle [69]. This basic structural distribution of lymphoid and non-lymphoid cells has also been noted in BALT in pathological conditions such as rheumatoid arthritis [70], hypersensitivity pneumonia [71], or diffuse panbronchiolitis [72]. Therefore, it is reasonable to conclude that BALT plays an important role in many respiratory system-related pathologies.

4.3 Role of BALT in various pathologies

BALT plays an important role in pulmonary immunity such as regulating microbial homeostasis [73], inducing immune tolerance [74], inhibiting inflammation [75], and supporting immune clearance [76]. Therefore, BALT frequently encounters many pathologies associated with infectious disease agents, allergens, environmental antigens, air-borne particles, autoimmune disease agents, and factors causing malignancy. As these pathological conditions have a broad spectrum, it is not possible to discuss all the roles of BALT; therefore, only a few have been addressed.

4.3.1 Role of BALT in resistance to infectious diseases

The respiratory tract is a typical entry site for viruses. This makes it difficult for the immune system to effectively eliminate viruses and virus-infected cells without causing much damage and inflammation, which jeopardizes the lung's structural and functional integrity. The balance between eliciting an immune response to effectively eliminate viruses and virus-infected cells and to cause less damage and inflammation is maintained by a complex network of innate and adaptive immune mechanisms as well as immunomodulatory and anti-inflammatory mechanisms. Accordingly, BALT could be one of the mechanisms that facilitates viral clearance by eliciting immune

responses and decreasing inflammatory responses [48]. BALT reportedly initiates pulmonary immune responses that are faster and more protective than those initiated at systemic sites. It has been proposed that once generated, BALT could play a key role in combating successive rounds of the same infection as well as assisting in establishing local immunity against unrelated viruses or pathogens [51]. For example, it has been suggested that $Lta^{-/-}$ mice without lymph nodes and Peyer's patches are more susceptible to the influenza virus and although they elicit immune responses, both B- and T-cell responses are delayed. Based on flow cytometric identification of germinal center B cells in the lung to question where immune responses might be initiated, it was concluded that both B- and T-cell responses are probably produced in the lungs [77]. BALT is suggested to be formed in the lungs of $Lta^{-/-}$ mice and locally initiates immune responses against influenza because the germinal center is present only in secondary lymphoid tissues. Another study reported that, in addition to germinal centers, plasma cells specific to influenza nucleoprotein were detected in BALT after influenza infection [58]. However, B-cell responses to influenza are accelerated in mice with pre-existing BALT, and morbidity and mortality rates are markedly reduced in response to a variety of viruses, including influenza, severe acute respiratory syndrome coronavirus, and mouse pneumovirus [78].

Mycobacterium tuberculosis (Mtb) infection is one of the serious health threats worldwide and is typically confined to the lungs. Although local immune mechanisms are primarily responsible for keeping Mtb infection under control, once the infection has settled in the lungs, immune mechanisms alone do not appear to be capable of eliminating these bacteria [79]. In humans, Mtb is localized to the granulomas comprising a central nucleus surrounded by macrophages, multinucleated giant cells, and lymphocytes [80]. The lymphocyte clusters surrounding these granulomas are B cells that form structures similar to BALT. These BALT areas associated with granuloma have B-cell follicles, and T-cell areas are present at the outer edge of the follicles [81]. Similar BALT domains, for example, have been discovered in murine models of Mtb infection, where B-cell clusters surrounding the granuloma were observed. Well-defined B-cell domains with FDCs are formed as early as day 42 after pulmonary infection and are protected from infection until at least day 90 [82]. Considering the link between B follicular structures surrounding the granuloma and Mtb uptake, another study showed that B-cell follicles formed around Mtb lesions in mice developed large germinal centers, and the B cells responded to the antigen [83]. Therefore, it is indicated that BALT initiates local pulmonary immune responses against Mtb infection via B cells.

4.3.2 Role of BALT in pulmonary responses to allergens and environmental antigens

Endotoxin, known as lipopolysaccharide (LPS), is a component of the gram-negative bacteria [84, 85] that is commonly present in the environment [86, 87]. The development or exacerbation of asthma [86, 87], bronchitis, and chronic obstructive pulmonary disease [88, 89] is linked to considerable LPS exposure. LPS, a classical T-cell-independent B-cell antigen, and mitogen are thought to bind to TLR_4 signaling pathway [84, 85], triggering B-cell activation, proliferation, and differentiation into antibody-secreting cells [90]. TLR_4 signaling activates macrophages and DCs, epithelial cells, and even fibroblasts, causing them to produce inflammatory cytokines and chemokines [91, 92]. Experimentally, pulmonary exposure of rats to endotoxin has been found to cause increases in pre-existing BALT and pulmonary plasma cells,

ultimately leading to the formation of germinal centers [93]. Sustained dosing of LPS prior to pulmonary inflammation in BALT-deficient mice appeared to result in BALT development in the major airways with an accumulation of B cells, T cells, and macrophages in the lungs, and even in BALT-deficient areas [94]. Thus, environmental exposures to LPS, often with additional antigenic or inflammatory components, cause BALT reactivity and pulmonary physiology alterations [95].

Considering the importance of pulmonary inflammation in asthma, a correlation between BALT development and asthma is likely. However, some believe that the presence of BALT is not always associated with asthma [96], but that the reactivity of BALT in patients with asthma is elevated [97]. Further, there is evidence that specific allergens, such as *Aspergillus fumigatus*, might cause pulmonary allergies that are similar to asthma. In allergic bronchopulmonary aspergillosis, large BALT regions characterized by diffuse and IgE-stained germinal centers have been found [98]. Thus, it is suggested that BALT can potentially contribute to allergic reactions by producing IgE locally in response to *A. fumigatus*.

Hypersensitivity pneumonia is defined as an inflammatory disease of the alveoli induced by hypersensitivity to inhaled organic antigens [99]. In contrast to asthma, which affects the airways, this condition affects the alveoli [48]. An occupational exposure often is the cause of hypersensitivity pneumonia; it can occur particularly when farmers are exposed to mold and fungi in barns [100]. Considering that hypersensitivity pneumonia results from chronic pulmonary exposure to the antigen, the emergence of well-developed BALT areas with vast germinal centers and FDC networks is not surprising for researchers [61].

4.3.3 Role of BALT in response to particles

The lungs are exposed to a wide range of particles, many of which are naturally inflammatory because they cannot be metabolized and persist in phagocytes or because their components bind to specific receptors that trigger an inflammatory response. Silicosis, for example, is a chronic diffuse parenchymal lung disease caused by prolonged exposure to inhaled crystalline silica particles. Pulmonary silica exposure reportedly results in nodules of mononuclear cell infiltration at the location of silica deposition, leading to pulmonary fibrosis [101]. It has been proposed that pulmonary exposure of rats to silica causes silica-loaded alveolar macrophages to migrate across the epithelium and accumulate in BALT [102]. This is analogous to the kinetic observation of virus-activated DCs in the airways migrating from the epithelium to BALT [40].

4.3.4 Role of BALT in autoimmune diseases

Rheumatoid arthritis (RA) and Sjögren's syndrome (SS) are autoimmune disorders characterized by the formation of ectopic lymphoid follicles in target tissues. Ectopic lymphoid follicles in the joints are common in patients with RA [103]; whereas ectopic follicles in the salivary and lacrimal glands are common in those with SS [104]. These follicles are hypothesized to contain separate B- and T-cell domains, germinal centers, FDCs, and HEVs, and they contribute toautoimmunity by generating high-affinity autoreactive B cells and sparing autoreactive effector T cells. BALT areas are observed in lung biopsies from a subset of patients with RA and SS who develop lung disease. It has been suggested to range from very small isolated lymphoid follicles to large, highly organized clusters of B-cell follicles [61].

4.3.5 Role of BALT in pulmonary malignancy

BALT formation is frequently linked to lung inflammation and exposure to a variety of inflammatory stimuli. Therefore, it is not surprising that experimental exposure to an inflammatory agent via the pulmonary route results in BALT hyperplasia in rats. However, it is possible that an inflammatory agent, which has been linked to tumorigenesis, could also cause pulmonary adenocarcinoma [105]. Therefore, inflammatory responses in the lung can promote BALT and neoplasia at the same time. Indeed, considering the links between chronic inflammation and cancer development [106], it seems probable that BALT formation precedes tumorigenesis in such cases [48].

Local immune responses to pulmonary pathogens and antigens are clearly associated with BALT formation; thus, it is predicted that BALT development adjacent to pulmonary malignancies would also be beneficial for antitumor immune responses. A study demonstrated tertiary lymphoid tissue neogenesis induced by lymphotoxin: antitumor antibody fusion protein with the accumulations of CD^{4+} and CD^{8+} T cells, B cells, and PNAd-expressing HEVs [107]. Thus, it was hypothesized that the immune response necessary for tumor eradication was produced locally in tertiary lymphoid tissues [108]. Therefore, it is concluded that local BALT induction surrounding pulmonary metastases may be beneficial in inducing antitumor immunity and tumor regression [48].

In addition, it is suggested that the development of a lymphoid environment surrounding tumors may trigger antitumor immunity or immunological tolerance due to some unknown factors. Further, some studies indicate that lymphoid-like stromal elements surrounding tumors can impair antitumor immunity and lead to tolerance [109]. Despite the discrepancies and gaps in the literature, the ability of BALT to be spontaneously developed as a clear response to the development of pulmonary tumors or metastasis of other tumors to the lung as well as to boost immunity against lung tumors is an intriguing and research-worthy topic.

5. Conclusions

BALT covers a large area in the lungs, from small irregular lymphocytes and DC clusters to B-cell follicles, germinal centers, FDCs, HEV lymphatics, well-developed dome epithelium, and highly organized lymphoid tissues. It has the potential to help researchers better understand the mechanisms underlying chronic lung diseases, particularly in mammals. The potential contributions of BALT at this point are the collection of antigens from the pulmonary airways, priming B- and T-cell responses, and aiding in the clearance of pulmonary diseases. BALT becomes a functional tissue due to the induction of T cells and the production of deep lymphoid tissue, which functions in priming immune responses in the lung, including IgA-secreting plasma cells. The development of effective vaccines, particularly in the prevention of viral infections, will be aided by lymphoid tissue production.

Acknowledgements

Author details

Tuba Parlak Ak
Munzur University, Tunceli, Turkey

*Address all correspondence to: tubaparlakak@munzur.edu.tr

IntechOpen

References

[1] Patwa A, Shah A. Anatomy and physiology of respiratory system relevant to anaesthesia. Indian J. Anaesth. 2015;59(9):533-41. DOI: 10.4103/0019-5049.165 849

[2] Chaudhry SR, Bordoni B. Anatomy, Thorax, Lungs. StatPearls [Internet]. 2021. Available from: https://www.ncbi.nlm.nih.gov/books/NBK 482513/ [2021-05-05]

[3] Ross MH, Pawlina W.Histology: a Text and Atlas with correlated cell and molecular biology. 6nd ed. Philadelphia: Wolters Kluwer-Lippincott Williams & Wilkins; 2011. 974 p.

[4] Murray JF. The structure and function of the lung. Int. J. Tuberc. Lung. Dis. 2010;14(4):391-396.

[5] Khan YS, Lynch DT. Histology, Lung. In: StatPearls [Internet]. 2021. Available from: https://pubmed.ncbi.nlm.nih.gov/30521210/ [2021-05-10]

[6] Kawamata N, Xu B, Nishijima H, Aoyama K, Kusumoto M, et al. Expression of endothelia and lymphocyte adhesion molecules in bronchusassociated lymphoid tissue (BALT) in adult human lung. Respir. Res. 2009;10(97):1-11. DOI: 10.1186/1465-9921-10-97

[7] Ganesan S, Comstock AT, Sajjan US. Barrier function of airway tract epithelium. Tissue Barriers. 2013;1(4): e24997. DOI: 10.4161/tisb.24997

[8] He W, Zhang W, Cheng C, Li J, Wu X, Li M, Chen Z, Wang W. The distributive and structural characteristics of bronchusassociated lymphoid tissue (BALT) in Bactrian camels (*Camelus bactrianus*). Peer J. 2019;7(e6571):1-17. DOI: 10.7717/peerj.6571.

[9] Jenkins MK, Khoruts A, Ingulli E, Mueller DL, McSorley SJ, Reinhardt RL, Itano A, Pape KA: In vivo activation of antigen-specific CD4 T cells. Annu. Rev. Immunol. 2001;19:23-45. DOI: 10.1146/annurev.immunol.19.1.23

[10] Sprent J, Surh CD. T cell memory. Annu. Rev. Immunol. 2002;20:551-579. DOI: 10.1146/annurev.immunol.20.100101.151926

[11] Sminia T, van der Brugge-Gamelkoorn GJ, Jeurissen SH. Structure and function of bronchus-associated lymphoid tissue (BALT). Crit. Rev. Immunol. 1989;9:119-150.

[12] Bienenstock, J, McDermott MR. Bronchus- and nasal-associated lymphoid tissues. Immunol Rev. 2005;206:22-31. DOI: 10.1111/j.0105-2896.2005.00299.x

[13] Alonso JM. Immunity and pathophysiology of respiratory tract infections. Med Mal Infect. 2008;38:433-437. DOI: 10.1016/j.medmal.2008.06.013

[14] Marin ND, Dunlap MD, Kaushal D, Khader SA. Friend or Foe: The Protective and Pathological Roles of Inducible Bronchus-Associated Lymphoid Tissue in Pulmonary Diseases. J. Immunol. 2019;202(9):2519-2526. DOI: 10.4049/jimmunol.1801135

[15] Sanchez-Guzman D, Le Guen P, Villeret B, Sola N, Le Borgne R, Guyard A, Kemmel A, Crestani B, Sallenave JM, Garcia-Verdugo I. Silver nanoparticle-adjuvanted vaccine protects against lethal influenza infection through inducing BALT and IgA-mediated mucosal immunity. Biomaterials. 2019;217:119308. DOI: 10.1016/j.biomaterials.2019.119308

[16] Goodnow CC. Chance encounters and organized rendezvous. Immunol Rev. 1997;156:5-10. DOI: 10.1111/j.1600-065X.1997.tb00954.x

[17] Danilova N. The evolution of adaptive immunity. Adv Exp Med Biol. 2012;738:218-235. DOI: 10.1007/978-1-4614-1680-7_13

[18] Kuper C.F, De Heer E, van Loveren H, Vos JG. Immune System. In Handbook of Toxicologic Pathology (WM. Hascheck-Hock, C.G. Rousseaux M.A. Wallig, eds.), Vol. 2. New York; Academic Press: 2002. 585-644 p.

[19] Cesta MF. Normal Structure, Function, and Histology of Mucosa-Associated Lymphoid Tissue. Toxicologic Pathology, 2006;34:599-608. DOI: 10.1080/01926230600865531

[20] Kiyono H, Fukuyama S. NALT-versus Peyer's-patch-mediated mucosal immunity. Nat. Rev. Immunol. 2004;4:699-710. DOI: 10.1038/nri1439

[21] Gormley PD, Powell-Richards AO, Azuara-Blanco A, Donoso LA, Dua HS. Lymphocyte subsets in conjunctival mucosa-associated lymphoid-tissue after exposure to retinal-S-antigen. Int. Ophthalmol. 1998;22:77-80. DOI: 10.1023/A:1006191022900

[22] Croitoru K, Bienenstock J. Characteristics and Functions of mucosa-associated lymphoid tissue. In Handbook of Mucosal Immunology. Ogra P.L, MesteckyJ, Lamm ME, Strober W, McGhee J.R, Bienenstock J. editors.Academic Press: San Diego; 1994. pp. 141-151.

[23] Giuliano EA, Moore CP, Phillips TE. Morphological evidence ofMcells in healthy canine conjunctiva-associated lymphoid tissue. Graefe's Arch Clin Exp

Ophthalmol. 2002;240:220-226. DOI: 10.1007/s00417-002-0429-3.

[24] Astley RA, Kennedy RC, Chodosh J. Structural and cellular architecture of conjunctival lymphoid follicles in the baboon (Papio anubis). Exp. Eye Res. 2003;76:685-94.DOI: 10.1016/s0014-4835(03)00062-9

[25] Sakimoto T, Shoji J, Inada N, Saito K, Iwasaki Y, Sawa M. Histological study of conjunctiva-associated lymphoid tissue in mouse. Jpn. J. Ophthalmol. 2002;46:364-369. DOI: 10.1016/s0021-5155(02)00503-8

[26] Yan Z, Wang JB, Gong SS, Huang X. Cell proliferation in the endolymphatic sac in situ after the rat Waldeyer ring equivalent immunestimulation. Laryngoscope. 2003;113:1609-1614. DOI: 10.1097/00005537-200309000-00038

[27] Pabst R. The anatomical basis for the immune function of the gut. Anat Embryol (Berl). 1987;176:135-144. DOI: 10.1007/BF00310046.

[28] Bienenstock J, Johnston N, Perey DY. Bronchial lymphoid tissue II.Morphologic characteristics. Lab Invest. 1973a;28:686-692.

[29] Macklin CC. Pulmonary sumps, dust accumulations, alveolar fluid and lymph vessels. Acta Anat. 1955;23:1-33. DOI: 10.1159/000140979

[30] Bienenstock J, Johnston N, Perey DY. Bronchial lymphoid tissue II. Functional characteristics. Lab Invest. 1973b;28: 693-698.

[31] Tschernig T, Pabst R. Bronchus-associated lymphoid tissue (BALT) is not present in the normal adult lung but in different diseases. Pathobiology. 2000;68:1-8. DOI: 10.1159/000028109

[32] Foo SY, Phipps S. Regulation of inducible BALT formation and contribution to immunity and pathology. Mucosal Immunology. 2010;3(6):537-544. DOI: 10.1038/mi.2010.52

[33] Pabst R, Tschernig T. Bronchus-associated lymphoid tissue: an entry site forantigens for successful mucosal vaccinations? American Journal of Respiratory Cell and Molecular Biology. 2010;43(2):137-141 DOI: 10.1165/rcmb.2010-0152RT

[34] Pabst R, Gehrke I. Is the bronchus-associated lymphoid tissue (BALT) an integral structure of the lung in normal mammals including man? Am J Respir Cell Mol Biol. 1990;3:131-135. DOI: 10.1165/ajrcmb/3.2.131

[35] Brandtzaeg P, Farstad IN, Haraldsen G. Regional specialization in the mucosal immune system: Primed cells do not always home along the same track. Immunol. Today. 1999;20:267-277. DOI: 10.1016/S0167-5699(99)01468-1

[36] Brownstein DG, Rebar AH, Bice DE, Muggenburg BA, Hill JO. Immunology of the lower respiratory tract. Serial morphologic changes in the lungs and tracheobronchial lymph nodes of dogs after intrapulmonary immunization with sheep erythrocytes. Am. J. Pathol. 1980;98:499-514.

[37] Reese S, Dalamani G, Kaspers B. The avian lung-associated immune system: A review. Vet Res. 2006;37:311-324. DOI: 10.1051/vetres:2006003

[38] Moyron-Quiroz JE, Rangel-Moreno J, Kusser K, Hartson L, Sprague F, Goodrich S, Woodland DL, Lund FE, Randall TD. Role of inducible bronchus associated lymphoid tissue (iBALT) in respiratory immunity. Nature Medicine. 2004;10(9):927-934.DOI: 10.1038/nm1091

[39] Seymour R, Sundberg JP, HogenEsch H. Abnormal lymphoid organ development in immune deficient mutant mice. Vet Pathol. 2006;43:401-423. DOI: 10.1354/vp.43-4-401

[40] Halle S, Dujardin HC, Bakocevic N, Fleige H, Danzer H, Willenzon S, Suezer Y, Hammerling G, Garbi N, Sutter G, Worbs T, Forster R. Induced bronchus-associated lymphoid tissue serves as a general priming site for T cells and is maintained by dendritic cells. J. Exp. Med. 2009;206:2593-2601. DOI: 10.1084/jem.20091472

[41] Hwang JY, Randall TD, Silva-Sanchez A. Inducible bronchus-associated lymphoid tissue: taming inflammation in the lung. Front Immunol. 2016;7:258. DOI: 10.3389/fimmu.2016.00258

[42] Rennert PD, Browning JL, Mebius R, Mackay F, Hochman PS. Surface lymphotoxin alpha/beta complex is required for the development of peripheral lymphoid organs. J. Exp. Med. 1996;184:1999-2006. DOI:10.1084/jem.184.5.1999.

[43] Randall TD, Mebius RE. The development and function of mucosal lymphoid tissues: a balancing act with micro-organisms. Mucosal Immunol. 2014;7:455-66. DOI: 10.1038/mi.2014.11

[44] Hashi H, Yoshida H, Honda K, Fraser S, Kubo H, Awane M, et al. Compartmentalization of Peyer's patch anlagen before lymphocyte entry. J. Immunol. 2001;166:3702-3709. DOI: 10.4049/jimmunol.166.6.3702

[45] Nishikawa S, Nishikawa S, Honda K, Hashi H, Yoshida H. Peyer's patch organ-ogenesis as a programmed inflammation: a hypothetical model. Cytokine Growth Factor Rev.

1998;9:213-220. DOI: 10.1016/
S1359-6101(98)00014-8

[46] Krege J, Seth S, Hardtke S, Davalos-Misslitz AC, Forster R. Antigen dependent rescue of nose-associated lymphoid tissue (NALT) development independent of LTbetaR and CXCR5 signaling. Eur. J. Immunol. 2009;39:2765-2778. DOI: 10.1002/eji.200939422

[47] Pospisil R, Mage RG. Rabbit appendix: a site of development and selection of the B cell repertoire. Curr Top Microbiol Immunol. 1998;229:59-70. DOI: 10.1007/978-3-642-71984-4-6

[48] Randall TD. Bronchus-associated lymphoid tissue (BALT) structure and function. Adv. Immunol. 2010;107:187-241. DOI: 10.1016/B978-0-12-381300-8.00007-1

[49] Delventhal S, Hensel A, Petzoldt K, Pabst R. Effects of microbial stimulation on the number, size and activity of bronchus-associated lymphoid tissue (BALT) structures in the pig. Int. J. Exp. Pathol. 1992;73:351-357.

[50] Kocks JR, Davalos-Misslitz ACM, Hintzen G, Ohl L, Forster R. Regulatory T cells interfere with the development of bronchus-associated lymphoid tissue. J. Exp. Med. 2007;204:723-734. DOI: 10.1084/jem.20061424

[51] Moyron-Quiroz JE, Rangel-Moreno J, Hartson L, Kusser K, Tighe MP, Klonowski KD, Lefrancois L, Cauley LS, Harmsen AG, Lund FE, Randall TD. Persistence and responsiveness of immunologic memory in the absence of secondary lymphoid organs. Immunity. 2006;25:643-654. DOI: 10.1016/j.immuni.2006.08.022

[52] Pankow W, von Wichert P. M cell in the immune system of the lung.

Respiration. 1998;54:209-219. DOI:10.1159/000195527

[53] Matsuura Y, Matsuoka T, Fuse Y. Ultrastructural and immune histochemical studies on the ontogenic development of bronchus-associated lymphoid tissue(BALT) in the rat: special reference to follicular dendritic cells. European Respiratory Journal. 1992;5(7):824-828.

[54] Xu BH, Wagner N, Pham LN, Magno V, Shan ZY, Butcher EC, Michie SA. Lymphocyte homing to bronchus-associated lymphoid tissue (BALT) is mediatedby L-selectin/PNAd, _1_4 integrin/VCAM-1, and LFA-1 adhesion pathways. The Journal of Experimental Medicine. 2003;197(10):1255-1267. DOI:10.1084/jem.20010685

[55] Corr SC, Gahan CC, Hill C. M-cells: origin, morphology and role inmucosal immunity and microbial pathogenesis. FEMS Immunol. Med. Microbiol. 2008;52:2-12. DOI: 10.1111/j.1574-695X.2007.00359.x

[56] Milne RW, Bienenstodk J, Perey DY. The influence of antigenic stimulation on the ontegeny of lymphoid aggregates and immunoglobulin containing cells in mouse bronchial and intestinal mucosa. J. Reticuloendothel. Soc. 1975;17:361-369.

[57] Chvatchko Y, Kosco-Vilbois MH, Herren S, Lefort J, Bonnefoy JY. Germinal center formation and local immunoglobulin E (IgE) production in the lung after an airway antigenic challenge. J. Exp. Med. 1996;184:2353-2360. DOI: 10.1084/jem.184.6.2353

[58] Geurtsvan Kessel CH, Willart MA, Bergen IM, van Rijt LS, Muskens F, Elewaut D, Osterhaus AD, Hendriks R, Rimmelzwaan GF, Lambrecht BN.

Dendritic cells are crucial for maintenance of tertiary lymphoid structures in the lung of influenza virus-infected mice. J. Exp. Med. 2009;206:2339-2349. DOI: 10.1084/jem.20090410

[59] Chamberlain DW, Nopajaroonsri C, Simon GT. Ultrastructure of the pulmonary lymphoid tissue. Am. Rev. Respir. Dis. 1973;108:621-631. DOI: 10.1164/arrd.1973.108.3.621

[60] Otsuki Y, Ito Y, Magari S. Lymphocyte subpopulations in high endothelial venules and lymphatic capillaries of bronchus-associated lymphoid tissue (BALT) in the rat. Am J Anat. 1989;184:139-146. DOI: 10.1002/aja.1001840205

[61] Rangel-Moreno J, Hartson L, Navarro C, Gaxiola M, Selman M, Randall TD. Inducible bronchus-associated lymphoid tissue (iBALT) in patients with pulmonary complications of rheumatoid arthritis. J. Clin. Invest. 2006;116:3183-3194. DOI: 10.1172/JCI28756.

[62] Campbell JJ, Hedrick J, Zlotnick A, Siani MA, Thompson DA, Butcher EC. Chemokines and the arrest of lymphocytes rolling under flow conditions. Science. 1998;279:381-384. DOI: 10.1126/science.279.5349.381

[63] Woodland DL, Randall TD. Anatomical features of anti-viral immunity in the respiratory tract. Semin. Immunol. 2004;16:163-170. DOI: 10.1016/j.smim.2004.02.003

[64] Suzuki K, Grigorova I, Phan TG, Kelly LM, Cyster JG. Visualizing B cell capture of cognate antigen from follicular dendritic cells. J. Exp. Med. 2009;206:1485-1493. DOI: 10.1084/jem.20090209

[65] van der Brugge-Gamelkoorn GJ, van de Ende MB, Sminia T. Non-lymphoid cells of bronchus-associated lymphoid tissue of the rat in situ and in suspension. With special reference to inter digitating and follicular dendritic cells. Cell Tissue Res. 1985a;239:177-182. DOI: 10.1007/BF00214917

[66] Kosco-Vilbois MH, Gray D, Scheidegger D, Julius M. Follicular dendritic cells help resting B cells to become effective antigen presenting cells: induction of B7/BB1 and upregulation of majör histocompatibility complex class II molecules. J. Exp. Med. 1993;178:2055-2066. DOI: 10.1084/jem.178.6.2055

[67] Haberman AM, Shlomchik MJ. Reassessing the function of immune-complex retention by follicular dendritic cells. Nat. Rev. Immunol. 2003;3:757-764. DOI: 10.1038/nri1178

[68] Ansel KM, Ngo VN, Hayman PL, Luther SA, Forster R, Sedgwick JD, Browning JL, Lipp M, Cyster JG. A chemokine-driven positive feedback loop organizes lymphoid follicles. Nature. 2000;406:309-314. DOI: 10.1038/35018581

[69] Hiller AS, Kracke A, Tschernig T, Kasper M, Kleemann WJ, Tröger HD, Pabst R. Comparison of the immunohistology of mucosa-associated lymphoid tissue in the larynx and lungs in cases of sudden infant death and controls. Int. J. Legal. Med. 1997;110:316-322. DOI: 10.1007/s004140050095

[70] Sato A, Hayakawa H, Uchiyama H, Chida K. Cellular distribution of bronchus-associated lymphoid tissue in rheumatoid arthritis. Am. J. Respir. Crit. Care Med. 1996;154:1903-1907. DOI: 10.1164/ajrccm.154.6.8970384

[71] Suda T, Chida K, Hayakawa H, Imokawa S, Iwata M, Nakamura Y, Sato A. Development of bronchus-associated lymphoid tissue in chronic

hypersensitivity pneumonitis. Chest. 1999;115:357-363. DOI: 10.1378/ chest.115.2.357

[72] Sato A, Chida K, Iwata M, Hayakawa H. Study of bronchus-associated lymphoid tissue in patients with diffuse panbronchiolitis. Am. Rev. Respir. Dis. 1992;146:473-478. DOI: 10.1164/ajrccm/146.2.473

[73] Peterson DA, Mcnulty NP, Guruge JL, Gordon JI. IgA response to symbiotic bacteria as a mediator of gut homeostasis. Cell Host and Microbe. 2007;2(5):328-339. DOI: 10.1016/j. chom.2007.09.013

[74] Hapfelmeier S, Lawson MAE, Slack E, Kirundi JK, Stoel M, Heikenwalder M, Cahenzli J, Velykoredko Y, Balmer ML, Endt K. Reversible microbial colonization of germ-free mice reveals the dynamics of IgA immune responses. Science. 2010;328(5986):1705-1709. DOI: 10.1126/ science.1188454

[75] Macpherson AJ, Uhr T. Induction of protective IgA by intestinal dendritic cells carrying commensal bacteria. Science. 2004;303(5664):1662-1665. DOI: 10.1126/science.1091334

[76] Corthesy B. Multi-faceted functions of secretory IgA at mucosal surfaces. Frontiers in Immunology. 2013;4:(185)1-11. DOI:10.3389/fimmu.2013.00185

[77] Lund FE, Partida-Sanchez S, Lee BO, Kusser KL, Hartson L, Hogan RJ, Woodland DL, Randall TD. Lymphotoxin-alpha-deficient mice make delayed, but effective, T and B cell responses to influenza. J. Immunol. 2002;169(9):5236-5243. DOI: 10.4049/ jimmunol.169. 9.5236

[78] Wiley JA, Richert LE, Swain SD, Harmsen A, Barnard DL, Randall TD,

Jutila M, Douglas T, Broomell C, Young M. Inducible bronchus-associated lymphoid tissue elicited by a protein cage nanoparticle enhances protection in mice against diverse respiratory viruses. PLoS ONE. 2009;4:e7142. DOI: 10.1371/ journal.pone.0007142

[79] North RJ, Jung YJ. Immunity to tuberculosis. Annu. Rev. Immunol. 2004;22:599-623. DOI: 10.1146/annurev. immunol.22.012703.104635

[80] Actor, JK, Olsen M, Jagannath C, Hunter RL. Relationship of survival, organism containment, and granuloma formation in acute murine tuberculosis. J. Interferon Cytokine Res. 1999;19:1183-1193. DOI: 10.1089/107999099313136

[81] Ulrichs T, Kosmiadi GA, Trusov V, Jorg S, Pradl L, Titukhina M, Mishenko V, Gushina N, Kaufmann SH. Human tuberculous granulomas induce peripheral lymphoid follicle-like structures to orchestrate local host defence in the lung. J. Pathol. 2004;204:217-228. DOI: 10.1002/ path.1628

[82] Kahnert A, Hopken UE, Stein M, Bandermann S, Lipp M, Kaufmann SH. Mycobacterium tuberculosis triggers formation of lymphoid structure in murine lungs. J. Infect. Dis. 2007;195:46-54. DOI: 10.1086/508894

[83] Maglione PJ, Chan J. How B cells shape the immune response against *Mycobacterium tuberculosis*. Eur. J. Immunol. 2009;39:676-686. DOI: 10.1002/eji.200839148

[84] Hoshino K, Takeuchi O, Kawai T, Sanjo H, Ogawa T, Takeda Y, Takeda K, Akira S. Cutting edge: Toll-like receptor 4 (TLR4)-deficient mice are hyporesponsive to lipopolysaccharide: Evidence for TLR4 as the Lps gene product. J. Immunol. 1999;162(7): 3749-3752.

[85] Takeuchi O, Hoshino K, Kawai T, Sanjo H, Takada H, Ogawa T, Takeda K,Akira S. Differential roles of TLR2 and TLR4 in recognition of gram-negative and gram-positive bacterial cell wall components. Immunity. 1999;11:443-451. DOI: 10.1016/ S1074-7613(00)80119-3

[86] Becker S, Fenton, MJ, Soukup, JM. Involvement of microbial components and toll-like receptors 2 and 4 in cytokine responses to air pollution particles. Am. J. Respir. Cell Mol. Biol. 2002;27:611-618. DOI: 10.1165/rcmb.4868

[87] Murakami D, Yamada H, Yajima T, Masuda A, Komune S, Yoshikai Y. Lipopolysaccharide inhalation exacerbates allergic airway inflammation by activating mast cells and promoting Th2 responses. Clin. Exp. Allergy. 2007;37:339-347. DOI: 10.1111/ j.1365-2222.2006.02633.x

[88] Droemann D, Goldmann T, Tiedje T, Zabel P, Dalhoff K, Schaaf B. Toll-like receptor 2 expression is decreased on alveolar macrophages in cigarette smokers and COPD patients. Respir. Res. 2005;6(68):1-8. DOI: 10.1186/ 1465-9921-6-68

[89] Mizutani N, Fuchikami J, Takahashi M, Nabe T, Yoshino S, Kohno S. Pulmonary emphysema induced by cigarette smoke solution and lipopolysaccharide in guinea pigs. Biol. Pharm. Bull. 2009;32:1559-1564. DOI: 10.1248/bpb.32.1559

[90] Pike BL, Alderson MR, Nossal GJ. T-independent activation of single B cells: An orderly analysis of overlapping stages in the activation pathway. Immunol. Rev. 1987;99:119-152. DOI: 10.1111/j.1600-065x.1987.tb01175.x

[91] Kawai T, Takeuchi O, Fujita T, Inoue J, Muhlradt PF, Sato S, Hoshino K, Akira S. Lipopolysaccharide stimulates the MyD88-independent pathway and results in activation of IFN-regulatory factor 3 and the expression of a subset of lipopolysaccharide-inducible genes. J. Immunol. 2001;167:5887-5894. DOI: 10.4049/jimmunol.167.10.5887

[92] Takeda K, Akira S. Regulation of innate immune responses by Toll-like receptors. Jpn J. Infect. Dis. 2001;54:209-219.

[93] van der Brugge-Gamelkoorn G, van de Ende M, Sminia T. Uptake of antigens and inert particles by bronchus associated lymphoid tissue (BALT) epithelium in the rat. Cell Biol. Int. Rep. 1985b;9(6):524. DOI: 10.1016/ 0309-1651(85)90011-6

[94] Vernooy JH, Dentener MA, van Suylen RJ, Buurman WA, Wouters EF. Long-term intratracheal lipopolysaccharide exposure in mice results in chronic lung inflammation and persistent pathology. Am. J. Respir. Cell Mol. Biol. 2002;26:152-159. DOI: 10.1165/ ajrcmb.26.1.4652

[95] Charavaryamath C, Janardhan KS, Townsend HG, Willson P, Singh B. Multiple exposures to swine barn air induce lung inflammation and airway hyperresponsiveness. Respir. Res. 2005;6:1-13. DOI: 10.1186/1465-9921-6-50

[96] Heier I, Malmstrom K, Pelkonen AS, Malmberg LP, Kajosaari M, Turpeinen M, Lindahl H, Brandtzaeg P, Jahnsen FL, Makela MJ. Bronchial response pattern of antigen presenting cells and regulatory T cells in children less than 2 years of age. Thorax. 2008;63:703-709. DOI: 10.1136/ thx.2007.082974

[97] Elliot JG, Jensen CM, Mutavdzic S, Lamb JP, Carroll NG, James AL. Aggregations of lymphoid cells in the

airways of nonsmokers, smokers, and subjects with asthma. Am. J. Respir. Crit. Care Med. 2004;169:712-718. DOI: 10.1164/rccm.200308-1167OC

[98] Slavin RG, Gleich GJ, Hutcheson PS, Kephart GM, Knutson AP, Tsai CC. Localization of IgE to lung germinal lymphoid follicles in a patient with allergic bronchopulmonary aspergillosis. J. Allergy Clin. Immunol. 1992;90:1006-1008. DOI: 10.1016/0091-6749(92) 90479-l

[99] Mohr LC. Hypersensitivity pneumonitis. Curr. Opin. Pulm. Med. 2004;10:401-411. DOI: 10.1097/01. mcp.0000135675.95674.29

[100] Seal RM, Hapke EJ, Thomas GO, Meek JC, Hayes M. The pathology of the acute and chronic stages of farmer's lung. Thorax. 1968;23:469-489. DOI: 10.1136/ thx.23.5.469-489.

[101] Davis GS, Pfeiffer LM, Hemenway DR. Expansion of interferon gamma producing lung lymphocytes in mouse silicosis. Am. J. Respir. Cell Mol. Biol. 1999;20:813-824. DOI: 10.1165/ ajrcmb.20.4.3407

[102] Lee KP, Kelly DP. Translocation of particle-laden alveolar macrophages and intra-alveolar granuloma formation in rats exposed to Ludox colloidal amorphous silica by inhalation. Toxicology. 1993;77:205-222. DOI: 10.1016/0300-483X(93)90161-K

[103] Takemura S, Braun A, Crowson C, Kurtin PJ, Cofield RH, O'Fallon WM, Goronzy JJ, Weyand CM. Lymphoid neogenesis in rheumatoid synovitis. J. Immunol. 2001;167:1072-1080. DOI: 10.4049/jimmunol.167.2.1072

[104] Gatumu MK, Skarstein K, Papandile A, Browning JL, Fava RA, Bolstad AI. Blockade of lymphotoxin-beta receptor signaling reduces aspects of Sjogren's syndrome in salivary glands of non-obese diabetic mice. Arthritis Res. Ther. 2009;11(R24):1-12. DOI: 10.1186/ar2617

[105] Silva BAK, Silva IS, Pereira DM, Aydos RD, Carvalho Pde T, Facco GG. Experimental model of pulmonary carcinogenesis in Wistar rats. Acta Cir. Bras. 2007;22:16-20. DOI: 10.1590/ S0102-86502007000700005

[106] Marx J. Inflammation and cancer: The link grows stronger. Science. 2004:306:966-968. DOI: 10.1126/ science.306.5698.966

[107] Schrama D, thor Straten P, Fischer WH, McLellan AD, Brocker EB, Reisfeld RA, Becker JC. Targeting of lymphotoxin-alpha to the tumor elicits an efficient immune response associated with induction of peripheral lymphoid-like tissue. Immunity. 2001;14:111-121. DOI: 10.1016/S1074-7613(01)00094-2

[108] Schrama D, Voigt H, Eggert AO, Xiang R, Zhou H, Schumacher TN, Andersen MH, thor Straten P, Reisfeld RA, Becker JC. Immunological tumostruction in a murine melanoma model by targeted LTalpha independent of secondary lymphoid tissue. Cancer Immunol. Immunother. 2008;57:85-95. DOI: 10.1007/s00262-007-0352-x

[109] Shields JD, Kourtis IC, Tomei AA, Roberts JM, Swartz MA. Induction of lymphoid -like stroma and immune escape by tumors that express the chemokine CCL21. Science. 2010;328:749752. DOI: 10.1126/ science.1185837

Genomic Instability and Cyto-Genotoxic Damage in Animal Species

María Evarista Arellano-García, Olivia Torres-Bugarín,
Maritza Roxana García-García, Daniel García-Flores,
Yanis Toledano-Magaña, Cinthya Sofia Sanabria-Mora,
Sandra Castro-Gamboa and Juan Carlos García-Ramos

Abstract

Genomic instability is a condition that may be associated with carcinogenesis and/or physiological disorders when genetic lesions are not repaired. Besides, wild, captive, and domesticated vertebrates are exposed to xenobiotics, leading to health disorders due to cytogenotoxicity. This chapter provides an overview of tests to assess cytogenotoxicity based on micronuclei (MNi) formation. Bone marrow micronuclei test (BmMNt), peripheral blood erythrocyte micronuclei test (PBMNt), and lymphocyte cytokinesis blocking micronuclei assay (CBMN) are discussed. The most illustrative studies of these techniques applied in different vertebrates of veterinary interest are described. The values of spontaneous basal micronuclei in captive, experimental, and farm animals (rodents, hamsters, pigs, goats, cattle, horses, fish) are summarized. In addition, a flow cytometry technique is presented to reduce the time taken to record MNi and other cellular abnormalities. Flow cytometry is helpful to analyze some indicators of genomic instability, such as cell death processes and stages (necrosis, apoptosis) and to efficiently evaluate some biomarkers of genotoxicity like MNi in BmMNt, PBMNt, and CBMN. The intention is to provide veterinary professionals with techniques to assess and interpret cytogenotoxicity biomarkers to anticipate therapeutic management in animals at risk of carcinogenesis or other degenerative diseases.

Keywords: Genomic instability, Micronuclei, MNi in erythrocytes, CBMN, Flow cytometry

1. Introduction

Genetic instability results from alterations induced by agents that severely damage DNA. The nature of the damage may be silent when it occurs in non-coding regions and therefore does not affect the cellular processes of organisms. Still, when damage

occurs in key DNA segments, the biological functionality of cells, tissues, organs, and eventually organisms in a population is compromised [1]. In this sense, genotoxic and cytotoxic damage are indicators of genomic instability. Genotoxicity involves changes in DNA structure such as aneugenic (loss of whole chromosomes) and clastogenic effects (loss of chromosome fragments); whereas cytotoxicity involves alterations in proliferation and cell cycle rate, as well as the magnitude and type of cell death (necrosis and apoptosis) [2, 3].

Various toxicological techniques can assess genotoxicity and cytotoxicity induced by physical, chemical, or biological agents. There are numerous models that can evaluate genotoxicity and cytotoxicity, ranging from biochemical and spectrophotometric tests. These assays depend on sophisticated equipment and the use of expensive reagents and consumables, compared to the set of techniques presented here, which do not require expensive equipment and are accessible to any laboratory with an optical microscope and cell staining systems. Above all, these techniques provide a deep understanding of the biological and cellular mechanisms involved in each model [4].

Assays that record the number of micronuclei (MNi) and other nuclear abnormalities are very versatile, inexpensive, and can be used in a wide variety of *in vitro* and *in vivo* models. Various techniques are based on MNi formation with applicability in the veterinary field, starting from the theoretical principle described in mouse bone marrow [5, 6]. Different techniques were also developed, such as MNi formation in mouse peripheral blood erythrocytes [7, 8] and other mammals (primates, ungulates, felines, and a wide variety of vertebrates, fish, birds, and amphibians) [9–11]. Also, MNi in lymphocytes by cytokinesis blockade (CBMN) is widely applicable in veterinary medicine because it can be developed both in cell lines and in almost any organism (humans, rodents, rabbits, fish, dogs, primates, etc.), whose entire blood volume allows extraction of at least 0.5 mL of whole venous blood [4, 12].

Despite these advantages, techniques based on MNi formation require manual counting with light or fluorescence microscopy. Therefore, reviewer training is crucial due to the time expenditure (2 to 4 hours per slide) and accuracy in distinguishing MNi and other cellular abnormalities [13, 14]. Besides, flow cytometry offers an alternative to reduce the time spent on the microscope by standardizing observations. Initially, this technique required lysing the cytoplasm to release MNi, and thus facilitate their identification [15, 16]. However, this prevents the observation of nuclear buds (NBUDs) nucleoplasmic bridges (NPBs), which are observed in binucleated cells [17]. Subsequently, flow cytometry was improved with image flow cytometry (IFC) techniques that efficiently and automatically record mono-, bi-, and polynucleated cells with and without MNi, NBUDs, and NPBs, which is possible by combining the image flow cytometry technique with the machine learning approach [18].

2. Basis of the bone marrow micronucleus test (BmMNt)

In 1973, the bone marrow micronucleus test (BmMNt) was reported as being a more effective in determining chromosomal damage than the metaphase scoring method used at that time. Nevertheless, limitations of this method included the use of high concentrations of metaphase cells to quantify significant differences, in addition to the animal sacrifice requirement [19]. Then, in 1975 W. Schmid reported the principles of BmMNt, describing that MNi result from a malfunction in the cell division process, mainly in two different ways [5]:

Case 1: Acentric or fragment chromosomes do not migrate to the spindle poles in anaphase stage of cell division. Then MNi can be seen in the daughter cells.

Case 2: After one or more mitoses of exposed cells to mutagen agents, if the mitotic spindle is damaged, the nucleus of daughter cells could contain many MNi of a larger size than those produced in case 1.

Schmid manuscript also describes erythrocytes derived from the bone marrow as the best cell type to perform the assay since distinguishing between immature erythrocytes (polychromatic) and mature (normochromic) erythrocytes is possible, considering immature erythrocytes remain in circulation for 24 to 48 hours, while mature erythrocytes remain for about 30 days [5].

2.1 Mammalian bone marrow erythrocyte micronucleus test (MEMT)

Chromosomal damage, genome instability, and cancer risk assessment are the main objectives of bone marrow erythrocyte micronucleus assay (BmMNt) [20]. Its robustness lies in the fact that it determines in a simple and relatively fast way the clastogenicity or aneugenicity of chemicals [21]. The mammalian erythrocyte micronucleus test (MEMT) has been widely reported and reviewed by different research groups and government agencies. However, since its publication, more than 30 years of evidence was compiled to standardize the procedure to ensure its applicability. In addition, MEMT has been compared with other mutagenicity assays, which include the mutation in mouse lymphoma cells L5178Y, *Salmonella typhimurium*, sister chromatid exchanges, and chromosomal aberrations in Chinese hamster ovary cells [22].

The number of cells required for an appropriate genotoxicity analysis was defined by the statistical analyses of all the techniques used to evaluate MNi formation, including the MEMT technique [23, 24]. On the other hand, the preferred species for this technique are mice, rats, and Chinese hamsters. Therefore, in vivo testing is usually performed on rodent's bone marrow erythrocytes. However, other mammals, in which the spleen does not filter efficiently micronucleated erythrocytes, are accepted if stain accuracy is evaluated [24–26].

3. Potential uses of peripheral blood micronucleus test (PBMNE)

The peripheral blood erythrocyte micronucleus test (PBMNE) is used for eco-toxicological studies, monitoring of health effects from anthropogenic contamination, and genotoxic evaluation of pharmacological therapy administered in patients with chronic diseases [1]. Regarding the experimental procedure, mice are the most commonly used animals [2]. However, there are more animal models such as the rat and hamster [3] and others not as common like primates [4], birds [5], reptiles [6, 7], amphibians [8, 9], embryos [10], and fish [11]. Peripheral blood is the most versatile tissue for genotoxic and cytotoxic analysis. It is possible to use polychromatic and normochromatic erythrocyte conditions to explain the effects of myelosuppression and DNA damage [12]. Like all diagnostic tests, it has its limitations, which must be considered to avoid false negatives. One of them is that it does not detect substances that do not produce fractures or anaphase lags (aberrations that do not imply the occurrence of acentric fragments, for example, translocations and inversions); it is also not valuable for cells exhibiting a low rate of cell division or when organ-specific or species-specific carcinogens are tested [13].

Therefore, if all industrialization processes have the potential to generate large amounts of genotoxic substances, it is necessary to implement new models, such as plants or animals, to evaluate whether a particular substance or agent is harmful in the short/long term due to its mutagenic, clastogenic or aneuploidogenic, and teratogenic properties. Furthermore, to define toxic doses with greater precision, studies in several bioindicator models and not only in one must be carried out [14]. For the selection of any organism (plant or animal) as a toxic biomonitor, its cost, convenience, sensitivity, and possible extrapolation to other organisms or situations must be justified [15].

3.1 Peripheral red blood micronuclei assay

Peripheral blood was selected as a non-invasive sample to perform the MNi assay considering the invasive procedure implicated in a bone marrow sample. MNi are characterized by having a round or almond shape, with a diameter that varies from 1/20 to 1/5 (0.4 to 1.6 μ) of the average erythrocyte size (6 to 8 μ in diameter). William Henry Howell and Justin Marie Jolly identified MNi in erythrocyte precursors at the end of the 19th century and described them as remnants of the nucleus of circulating erythrocytes. Therefore, they are called Howell-Jolly bodies [16]. Subsequently, Dawson described MNi in the bone marrow of patients with several pathologies, including deficiency of cobalamin and folates; thereafter, MNi were described in lymphocytes [17].

Young or polychromatic erythrocytes (EPC) lose ribosomes within 24 hours after enucleation but retain MNi; later, they reach maturity and are transformed into normochromatic erythrocytes (ENC). These are stained blue-gray with the Giemsa stain or red with acridine orange, facilitating their identification when they are counted in tests of short exposure periods [1, 18]. Under certain circumstances, micronucleated erythrocyte (MND) values are often altered. Regardless of the tissue that is used in the MNi test, the data obtained are highly informative since it is a diagnostic tool to detect the loss of genetic material when these structures are identified in the cytoplasm of cellular compartment of the analyzed sample [19, 20].

3.2 Peripheral blood and mononuclear phagocytic system MNi test

The mononuclear phagocytic system (MPS), formerly called the reticuloendothelial system, is responsible for eliminating old or altered red blood cells, including micronucleated cells. In addition, the MPS system plays a key role in regulating innate immunity and it is constituted by dendritic cells, macrophages, and monocytes. The spleen, which is rich in macrophages, is the most sensitive detector for any red blood cell abnormality. By filtering the blood, the spleen eliminates foreign particles through phagocytic cells and destroys old erythrocytes or their fragments caused by structural changes that reduce their flexibility, making it difficult to pass through the microcirculation, undergoing cell lysis and splenic clearance [14, 21].

In mammals, two types of spleen are described, "defensive" and "storage." The former is smaller in size, has less muscle, but is abundant in lymphatic tissue and sinusoids; the latter, is larger, scarce in sinusoids, rich in the red pulp, and stores a more significant amount of blood [21]. Nevertheless, some species have a "defensive" spleen, which eliminates the abnormal erythrocytes in their entirety, making it impossible to observe MNi in peripheral blood. On the other hand, species with "storage" spleen are deficient in their phagocytic function and allow MNi to be observed at any time during the life of the species, as in the case of mice [14].

Group	Species	E / Ex	Treatment (Doses) /Analyzed zone	Frequency	Total Erythrocytes	Ref
Primates	Capuchin monkeys *Cebus capucinus*	E	Captivity	20.5 ± 2.0	10, 000	[4, 14]
	Common marmoset *Callithrix jacchus*	Ex	- Water 0.2 ml - Methotrexate 2.5 mg/kg - Cytosine arabinoside 3 mg/kg	8.0 ± 3.3 22.0 ± 5.7 31.2 ± 10.3	10, 000	
Carnivores	Cougar *Puma concolor*	E	Captivity	18.5 ± 0.7	10, 000	[14]
	Tiger *Panthera tigris*	E	Captivity	20.5 ± 2.9	10, 000	
	Lion *Panthera leo*	E	Captivity	0.6 ± 0.1	10, 000	[28]
Rodents	Guinea pig *Cavia porcellus*	E	Captivity	0.3 ± 3.0	10, 000	[28]
	Yellow-necked mouse *Apodemus flavicollis*	E	Captivity	0.2 ± 0.01	2, 000	[3]
	Common vole *Microtus arvalis*	E	Captivity	0.03 ± 0.01	2, 000	
	Mouse *Mus macedonicus*	E	Captivity	0.02 ± 0.01	2, 000	
	C57BL / 6	E	Captivity	0.3 ± 0.1	2, 000	[29]
Chiropters	Bat *Pteronotus mexicanus*	E	Captivity	0.06 ± 0.04	1, 000	[30]
Marines	Common Bottlenose dolphin *Tursiops truncatus*	E	Captivity	24.3 ± 6.1	10, 000	[31]

Group	Species	E / Ex	Treatment (Doses) / Analyzed zone	Frequency	Total Erythrocytes	Ref
Ungulates	Beef cattle *Bos taurus*	E	Captivity	0.08 ± 0.2	3,000	[32]
	Sheep *Ovis aries*	E	Captivity	1.0 ± 0.7	3,000	[32]
	Horse *Equus ferus caballus*	E	Captivity	0.2 ± 0.3	3,000	[32]
Birds	Helmeted manakin *Antilophia galeata*	E	Captivity	1.1 ± 1.2	10,000	[5]
	Golden-crowned warbler *Basileuterus culicivorus*	E	Captivity	2.0 ± 1.2	10,000	
	Gray-headed tanager *Eucometis penicillata*	E	Captivity	2.4 ± 1.6	10,000	
	Flavescent warbler *Myiothlypis flaveola*	E	Captivity	2.0 ± 1.8	10,000	
	Orange-fronted Parakeet *aratinga canicularis*	Ex	Mitomycin C 2 mg/kg	6.0 ± 3.3	10,000	[33]
Reptiles	Lizard *Tupinambis merianae*	E	Captivity	1.0 ± 0.2	1,000	[6]
	Caiman *Caiman latirostris*	E	Captivity	1.1 ± 0.7	1,000	[7]
Amphibians	American bullfrog *Lithobates catesbeianus*	E	Captivity	3.6 ± 2.8	1,000	[34]
		Ex	Radiation 3.3 Gy	7.3 ± 3.1	1,000	
	Frog *Physalaemus cuvieri*	E	Emas National Park	0.2 ± 0.6	1,000	[9]
	Lesser Treefrog *Dendropsophus minutus*	E		0.2 ± 0.4	1,000	
	Mole salamanders *Ambystoma sp.*	Ex	Cyclophosphamide 75.0 mg	6.4 ± 2	2,000	[8]

Group	Species	E / Ex	Treatment (Doses) /Analyzed zone	Frequency	Total Erythrocytes	Ref
Fishes	Brown trout *Salmo trutta*	E	Gafo River	2.4 ± 1.9	1, 000 (renal erythrocytes)	[11]
		E	Trubia River	4.1 ± 1.3		
	Common carp *Cyprinus carpio*	E	Trasimeno River	0.5 ± 0.2	25, 000	[35]
		Ex	CH_3COO_2H NaClO ClO_2	0.8 ± 0.3 2.5 ± 0.5 1.7 ± 0.4	25, 000	
	Fish *Tilapia, sp.*	E	Xochimilco River	7.4 ± 5.7	10, 000	[36]
	Astyanax bimaculatus	Ex	Cyclophosphamide 16 mg/ kg	2.0 ± 0.7	1, 000	[37]
		Ex	Vinblastine Sulfate 8 mg/kg	1.2 ± 0.6	24, 000	

E: environmental, Ex: experimental

Table 1.
Examples of experimental species used in the MNi erythrocyte test as environmental biomonitors.

The number of MNi in peripheral blood is practically null in humans [22]. However, they can be observed in impaired splenic function secondary to pathologies that directly affect it, for example, when patients have been splenectomized or were born prematurely. Since it is ethically not allowed to carry out biomonitoring programs in humans, these type of bioassays provide the opportunity to test genotoxic agents [14, 17, 22].

The organism's age influences the variability in the number of MND [23] demonstrated when analyzing their frequency in splenectomized patients since adults showed a higher frequency than children [24, 25]. Similar results are described in rodent spermatids, where old mice and hamsters have more MNi than young ones, probably because genetic damage continually accumulates throughout the organism's life [25, 26]. Some organisms present a higher frequency of MNi in juvenile stages due to the immaturity of their nuclear phagocytic system; upon reaching adulthood, their system becomes efficient and prevents the visualization of MNi [14, 25].

3.3 Selection of a suitable peripheral red blood micronucleogenicity bioindicator

To properly select a biomonitor for the MNi test in peripheral blood, at least six MNi in a total count of 10,000 erythrocytes should be identified [25]. The analyzed tissue must meet the following requirements: be in constant division, have abundant quantified cells, sufficient cytoplasm-nucleus relationship to identify MNi clearly, and a regular shape of the nucleus without lobes must be present to facilitate their observation [27]. This assay has been applied in a broad diversity of organisms to take advantage of the available resources in the environment (**Table 1**). The investigations carried out by Dr. Zúñiga's group concluded that the organisms with the best potential are felines, the capuchin monkey, and the atolero parakeet, among others [4, 14, 19, 38, 39].

4. The cytokinesis blocking micronucleus assay (CBMN)

The cytokinesis blocking micronucleus assay in lymphocytes (CBMN) was developed by a Ph.D. student more than 30 years ago [40], who anecdotally relates that while reviewing a biochemistry textbook [41]. He noticed that cytochalasin-B had the ability to block the action of actin *in vitro* cultures of human lymphocytes and thus obtain binucleated cells capable of recording clastogenic or aneugenic events resulting from exposure to xenobiotics. This biochemical principle is a fundamental aspect, enabling binucleated cells to remain in telophase (**Figure 1**). CBMN ensures that binucleated cell have undergone a single cell duplication in culture 72 hours after its initiation (**Figure 1**), making it possible to record cytotoxic or genotoxic events before blocking cytokinesis based on the following biomarkers: micronuclei (MNi), nuclear buds (NBUDs), nucleoplasmic bridges (NPBs), as well as mononucleated, binucleated, trinucleated and tetranucleated cells, which are used to calculate the cell duplication index (NDI); also the number of cells in necrosis and apoptosis can be recorded to perform a complete analysis of genomic instability [42–44].

4.1 General procedure for the cytokinesis-block micronucleus (CBMN) assay in lymphocytes

The experimental procedure begins by extracting whole venous blood in heparinized tubes. According to the designed experiment, cultures are prepared with 6.3 mL
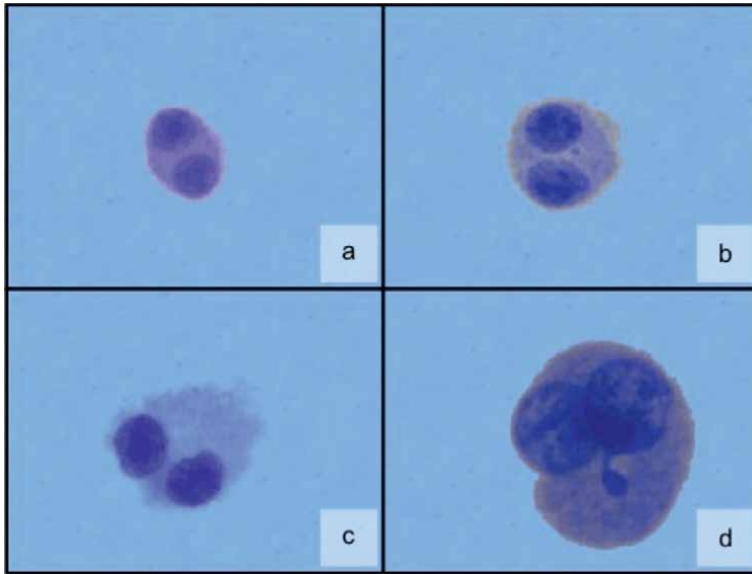
Figure 1.
Human lymphocyte binucleated cells: a) Binucleated normal cell (BNC), b) Binucleated cell with micronucleus (MNi), c) Binucleated cell with nucleoplasmic bridge (NPBs), d) Binucleated cell with nuclear bud (NBUDs).

of RPM1–1640 medium supplemented with non-essential amino acids, 0.2 mL of phytohemagglutinin, and 0.5 mL of whole venous blood incubated for 44 hours at 37°C. After this time, between 3 and 6 μg/mL of cytochalasin-B is added to avoid the division of the cytoplasm (blocking cytokinesis), and incubation is resumed until 72 hours are completed (**Figure 2**).

Once the 72-hour incubation period is finished, cells must be fixed with Clarke's solution and washed 3 to 5 times until a clear cell button is obtained. If necessary,
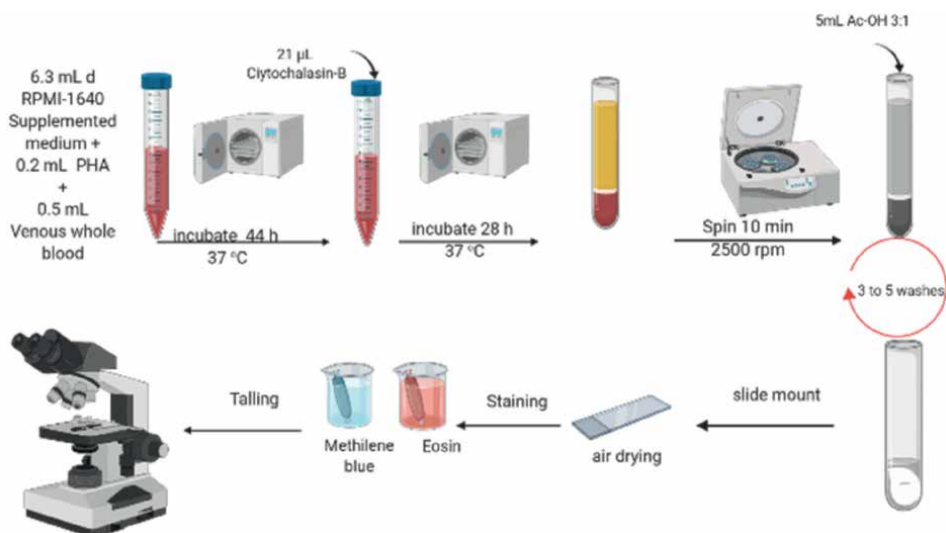
Figure 2.
The general procedure of the cytokinesis-block micronucleus assay in lymphocytes.

impurities are removed with a trypsin solution. The cell button is transferred on slides and stained with eosin and methylene blue to record nuclear abnormalities (**Figure 1**) in a total of 1000 binucleated cells and count in 500 cells those mononucleated, binucleated, trinucleated, and tetranucleated cells to calculate the cell proliferation index (NDI) and also record the number of cells in necrosis and apoptosis as indicated in the protocol [45, 46].

4.2 Application of the cytokinesis-block micronucleus (CBMN) assay in animal species

CBMN has been used to determine genomic instability in several models. Initially developed for human lymphocytes [47], it has been tested in other animal models of veterinary interest, such as cow [48–51], goat [52, 53], pig [54–56], rabbit [57, 58], horse [54], rodents [59], hamster cell lines [60], and rodent cell lines [61].

Taxonomic Group Order, Family	Species, common name	n	CBPI	MNi frequency	BN cells counted	Ref
Artiodactyla Bovidae	*Bos primigenius* Taurus, cow	20	1.45	12.3 ± 4 .1	500	[48]
		3	1.57 ± 0.06	39 ± 2.5	1000	[49]
		1	1.3 ± 0.03	11.0 ± 3.2	1000	[50]
		2	1.28 ± 0.001	13.5 ± 0.71	1000	[51]
	Capra, goat	3	ND	5 ± 2	500	[53]
Artiodactyla, Suidae	*Sus scrofa*, pig	5	ND	5.8	1000	[54]
		3		8.33 ± 1.528	1000	[58]
Carnívora, Canidae	Canis canis, dog	?	ND	35 ± 4	1000	[62]
		20	1.67 ± 0.21	11.0 ± 3.29	1000	[55]
		30	ND	4.61 ± 0.88	1000	[56]
Lagomorpha, Leporidae	*Oryctolagus cuniculus*, rabbit	5	1.55 ± 0.01	6.33 ± 0.94	2000	[57]
		3	ND	5.0 ± 2.0	500	[53]
		1	ND	6.8	1000	[54]
Perissodactyla, Equidae	*Equus caballus*/ horse	N/A [*]	1.914 ± 0.002	16.33 ± 0.298	1000	[60]
Rodentia, Cricedae	*Cricetulus barabensis*)/ Hamster	N/A [**]	1.67 ± 0.016	3 ± 1	2000	[61]
Rodentia, Muridae	*Mus musculus*/ mice	6	ND	51 ± 2.16	1000	[59]
	Mus musculus/ mice L-929	N/A [**]	1.67 ± 0.016	3 ± 1	2000	[61]

Sample size (n), Cytokinesis proliferation block index (CBPI), Frequency of binucleated cells with micronucleus (MNi frequency), Number of binucleated cells counted (BN cells Counted).
[*]*Chinese hamster ovary cells (CHO-K1).*
[**]*L-929 murine fibroblast cell line.*

Table 2.
CBMN studies in different vertebrates.

In most of the published articles presented in **Table 2**, only the MNi number was reported, eight included NDI, and only three took into account other nuclear abnormalities, such as NBUDs [50] and NPBs [49, 60]; no articles that considered the count of cells in necrosis and apoptosis were found.

CBMN is a valuable model for testing genomic instability effects in veterinary pharmacology experiments, such as the one performed in cows to test the mixture of an antiparasitic (cypermethrin) and a pesticide (chlorpyrifos), which reported 16.1 ± 2.3 NBUDs and found no evidence of cytogenotoxicity compared to the gamma radiation exposure [50]. The cytotoxic potential of epoxiconazole and fenpropimorph was also evaluated in bovine lymphocytes, and findings showed no genotoxic effects, however, the cell proliferation index decreased [51]. Moreover, in a trial using the antibiotic enrofloxacin [49], authors found that by increasing the dose, the number of MNi also increased. Another study with dogs analyzed the effect of oral administration of cadmium oxide (10 mg/K), where no significant differences after administration for 3 and 28 days [56] were observed. Finally, it has been reported that loperamide reduces cell proliferation and produces a significant increase in the number of MNi [57].

In general, it has been established that the number of spontaneous MNi in bovines is 3 times higher compared to human lymphocytes [48]. On the other hand, CBMN in goat estimates a better dosimetry fit for gamma radiation than in humans and rabbits. However, pigs and horses also show an excellent dosimetry correlation against X-rays and gamma rays [52, 54, 63].

CBMN has shown that dogs as human pets are excellent sentinels of exposure to environmental factors [55], partly because canine lymphocytes are three times more sensitive than humans to radiation [62].
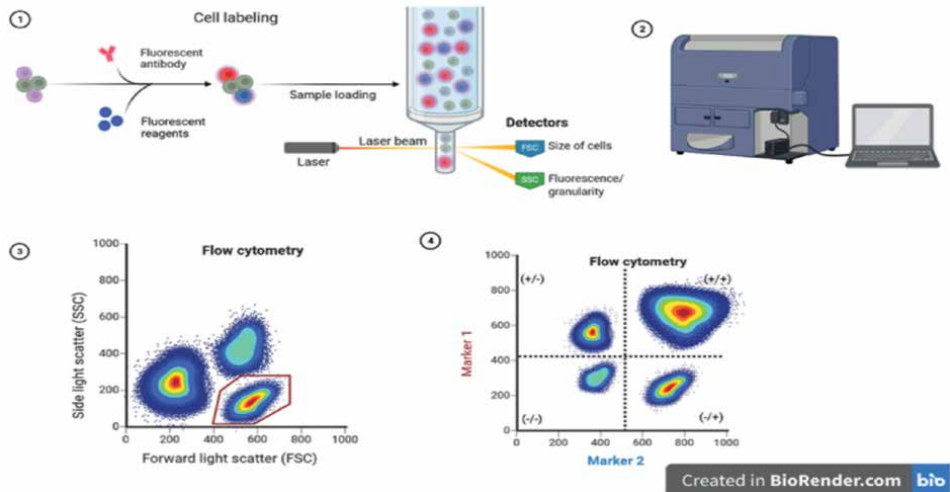
5. Flow cytometry

Flow cytometry is a technique that started as an immunological technique at the beginning; however, currently, it represents a tool to perform fast and multiparametric analyses in molecular biology, microbiology, virology, toxicology, cancer biology, and infectious diseases that can affect any organism [1].

The equipment needed to perform flow cytometry is a cytometer. This is a machine capable of analyzing cells or particles mixed in a liquid solution that makes them pass one by one into tubes with a unique system of fluids. The positioning of cells in a line allows the exposure of every single cell to a laser light, which interrogates each cell individually. Then, the interpretation is performed by a computer that analyzes the light as numeric and graphical data in a standardized format (*.fcs), which can later be read and analyzed by any flow cytometry software [1, 2].

For the flow cytometry data analysis, the first step involves standardizing the studied cell population. Then, the cohort points for the negative and positive phenotypic screening molecules should be identified in the selected cell population. To reach a better identification of the phenotypic molecules, it is necessary to use a fluorescent positive control that can be a sample of cells from the same population with the maximal expression of the molecule; also, a negative control without a fluorescent signal should be considered (**Figure 3**) [2, 4].

To assess cell damage, the measurement of several indicators is available. In this context, cell viability is used as an indicator of cytotoxicity and involves the use of kits with contrast fluorescent colors (red and green). The viable cells will be the ones that have no damage at all, and they will be detected with a green color (495–515 nm);

Figure 3.
Flow cytometry methodology. 1) Labelling of cells or particles with fluorescent molecules. 2) Cell mixture leaves the nozzle in droplets, laser beam strikes each cell or particle by the FSC detector, which identifies cell size, and the SCC detector, which identifies fluorescence/granularity/complexity. 3) Conversion of luminescent signals into numerical and graphical data to select the cell population according to its size and complexity. 4) Detection of fluorescent markers in cells by a pseudocolor quadrant density plot: Negative cells without fluorescence (-/-). Positive cells to fluorescent marker 1(+/-). Positive cells to fluorescent marker 2 (-/+). Positive cells to both fluorescent markers (+/+).

whereas cells with severe damage are discriminated by red brilliant (495–615 nm); the positive cells to both of the parameters, are in a process of early death, but still viable [64]. To be more specific in the cell death state, it is possible to define the apoptosis level using an annexin V/propidium iodide (PI) kit, which discriminates live cells by the absence to both fluorescent dyes; whereas the positive cells for only annexin V are in early apoptosis, while the positive cells for only PI are in necrosis; and the positive cells for both annexin V and PI dyes, are in frank or late apoptosis [65, 66].

5.1 Detection of MNi and other abnormalities by flow cytometry

Cytotoxicity and genotoxicity can be evaluated by flow cytometry. The initial approach to estimate genotoxicity by MNi detection is possible by ethidium monoazide bromide (EMA) staining to label the chromatin of necrotic and mid/late-stage apoptotic cells. In addition, stripping of cytoplasmic membranes and incubation with the pan-nucleic acid dye SYTOX Green plus RNase to provide a suspension of free nuclei also allows detection of MNi [67, 68].

Some authors have used cytometric techniques to quantify MNi in normochromatic and polychromatic erythrocytes, leading to a significant reduction of the counting time by 100 orders of magnitude and also reducing the number of experimental animals needed to perform the studies with the *in vivo* peripheral blood erythrocyte technique [67–69]. Flow cytometry is also used for counting MNi in bone marrow-derived erythrocytes and peripheral blood erythrocytes through *in vivo* experiments. Still, the most relevant advantage has been the adaptation of three approaches: flow cytometry, image recognition, and machine learning to detect both MNi and other nuclear abnormalities (NBUDs, NPBs) as well as necrotic and apoptotic cells, which opens a new perspective in the CBMN assay with lymphocytes [70–73].

6. Conclusions

The evolution of techniques that analyze genetic instability as micronuclei (MNi) and other cellular abnormalities has opened a new strategy to prevent cytogenotoxic effects on captive, farm, pet, and wild animals. On the other hand, these techniques contribute to better understand the pharmacology of drugs and the permissible environmental exposure levels to xenobiotics in laboratory studies.

BmMNt, PBMNE, and CBMN genomic instability tests have their sphere of applicability, advantages, and limitations. While BmMNt is mainly applied for *in vivo* experiments, its biomarkers are the end point, and it is not possible to follow up the effect for a long time. On the other hand, PBMNE allows daily monitoring, especially in pharmacological, toxicological, and dosimetry experiments. CBMN is one of the most comprehensive MNi-based assays. Although it can only be performed in animal models, of which, collecting at least half a milliliter of intravenous blood is possible to record six biomarkers of genomic instability: MNi, NBUDs, NPBs, NDI, and cellular death (necrosis and apoptosis).

Lastly, the flow cytometry improvements based on the synergy between flow cytometry, image recognition, and machine learning opens a new clinical scenery in micronucleus-based tests to detect genomic instability in all types of species, especially in those of veterinary interest.

Acknowledgements

Conflict of interest

"The authors declare no conflict of interest."

Author details

María Evarista Arellano-García[1*], Olivia Torres-Bugarín[2],
Maritza Roxana García-García[3], Daniel García-Flores[3],
Yanis Toledano-Magaña[4], Cinthya Sofia Sanabria-Mora[3], Sandra Castro-Gamboa[5]
and Juan Carlos García-Ramos[4]

1 Autonomous University of Baja California, Ensenada, Mexico

2 Department of Internal Medicine II, Dean of Health Sciences, Autonomous
University of Guadalajara, Guadalajara, Mexico

3 School of Medicine, Autonomous University of Guadalajara, Guadalajara, Mexico

4 School of Health Sciences, Autonomous University of Baja California, Ensenada,
Mexico

5 School of Medicine, Autonomous University of Guadalajara, and University Center
for Health Sciences (CUCS), University of Guadalajara, Guadalajara, Mexico

*Address all correspondence to: evarista.arellano@uabc.edu.mx

IntechOpen

References

[1] Heddle JA, Cimino MC, Hayashi M, Romagna F, Shelby MD, Tucker JD, et al. Micronuclei as an index of cytogenetic damage: Past, present, and future. Environ Mol Mutagen [Internet]. 1991;18(4):277-291. Available from: http://doi.wiley.com/10.1002/em.2850180414

[2] Hayashi M. The micronucleus test—most widely used in vivo genotoxicity test—. Genes Environ [Internet]. 2016 Dec 1;38(1):18. Available from: http://genesenvironment.biomedcentral.com/articles/10.1186/s41021-016-0044-x

[3] Mitkovska V, Chassovnikarova T, Atanassov N, Dimitrov H. Environmental genotoxicity evaluation using a micronucleus test and frequency of chromosome aberrations in free-living small rodents. J Biosci Biotechnol [Internet]. 2012;1(1):67-71. Available from: http://www.jbb.uni-plovdiv.bg

[4] Zúñiga-González GM, Gómez-Meda BC, Zamora-Perez AL, Ramos-Ibarra ML, Batista-González CM, Lemus-Varela ML, et al. Micronucleated erythrocyte frequencies in old and new world primates: Measurement of micronucleated erythrocyte frequencies in peripheral blood of Callithrix jacchus as a model for evaluating genotoxicity in primates. Environ Mol Mutagen. 2005 Dec;46(4):253-259.

[5] Baesse CQ, Tolentino VC de M, Morelli S, Melo C. Effect of urbanization on the micronucleus frequency in birds from forest fragments. Ecotoxicol Environ Saf [Internet]. 2019 Apr;171:631-637. Available from: https://linkinghub.elsevier.com/retrieve/pii/S0147651319300259

[6] Schaumburg LG, Poletta GL, Siroski PA, Mudry MD. Baseline values of Micronuclei and Comet Assay in the lizard Tupinambis merianae (Teiidae, Squamata). Ecotoxicol Environ Saf. 2012 Oct 1;84(10):99-103.

[7] Poletta GL, Larriera A, Kleinsorge E, Mudry MD. Caiman latirostris (broad-snouted caiman) as a sentinel organism for genotoxic monitoring: Basal values determination of micronucleus and comet assay. Mutat Res Toxicol Environ Mutagen [Internet]. 2008 Feb 29 [cited 2021 Jun 25];650(2):202-9. Available from: https://linkinghub.elsevier.com/retrieve/pii/S1383571807003580

[8] Zamora-Perez A, Zúñiga-González GM, Gómez-Meda BC, Ramos-Ibarra ML, Batista-González CM, Torres-Bugarín O. Induction of micronucleated cells in the shed skin of salamanders (Ambystoma sp.) treated with colchicine or cyclophosphamide. Environ Mol Mutagen. 2004;44(5):436-440.

[9] Borges RE, Santos LR de S, Benvindo-Souza M, Modesto RS, Assis RA, de Oliveira C. Genotoxic Evaluation in Tadpoles Associated with Agriculture in the Central Cerrado, Brazil. Arch Environ Contam Toxicol. 2019;77(1):22-28.

[10] Ceyca JP, Torres-Bugarín O, Castillo-Guerrero JA, Betancourt-Lozano M. Seabird Embryos as Biomonitors of Micronucleogenic Genotoxic Agents: Potential Application for the Coasts of Mexico. Avian Biol Res [Internet]. 2014 Dec 1;7(4):223-234. Available from: http://journals.sagepub.com/doi/10.3184/175815514X14162211300859

[11] Ayllón F, Suciu R, Gephard S, Juanes F, Garcia-Vazquez E. Conventional armament wastes induce micronuclei in wild brown trout Salmo trutta.

Mutat Res - Genet Toxicol Environ Mutagen. 2000 Oct 31;470(2):169-176.

[12] Norppa H, Falck GC-MCM. What do human micronuclei contain? Mutagenesis [Internet]. 2003;18(3):221-33. Available from: http://www.ncbi.nlm.nih.gov/pubmed/12714687

[13] Mavournin KH, Blakey DH, Cimino MC, Salamone MF, Heddle JA. The in vivo micronucleus assay in mammalian bone marrow and peripheral blood. A report of the U.S. Environmental Protection Agency Gene-Tox Program. Vol. 239, Mutation Research/Reviews in Genetic Toxicology. Elsevier; 1990. p. 29-80.

[14] Zúñiga-González G, Torres-Bugarín O, Zamora-Perez A, Gómez-Meda BC, Ramos Ibarra ML, Martínez-González S, et al. Differences in the number of micronucleated erythrocytes among young and adult animals including humans - Spontaneous micronuclei in 43 species. Mutat Res - Genet Toxicol Environ Mutagen. 2001;494(1-2):161-164.

[15] Alimba CG, Bakare AA. In vivo micronucleus test in the assessment of cytogenotoxicity of landfill leachates in three animal models from various ecological habitats. Ecotoxicology. 2016;25(2):310-319.

[16] Adhikari A. Micronuclei (MN), an Important Cancer Biomarker. Edelweiss Cancer Open Access. 2019;(November): 37-42.

[17] Schmid W. The micronucleus test. Mutat Res Mutagen Relat Subj. 1975 Feb 1;31(1):9-15.

[18] Hayashi M, MacGregor JT, Gatehouse DG, Blakey DH, Dertinger SD, Abramsson-Zetterberg L, et al. In vivo erythrocyte micronucleus assay. III.

Validation and regulatory acceptance of automated scoring and the use of rat peripheral blood reticulocytes, with discussion of non-hematopoietic target cells and a single dose-level limit test. Mutat Res - Genet Toxicol Environ Mutagen. 2007 Feb 3;627(1):10-30.

[19] Zúñiga-González G, Torres-Bugarín O, Zamora-Perez AL, Gómez-Meda BC, Ramos-Ibarra ML, Gallegos-Arreola P, et al. Induction of micronucleated erythrocytes in mouse peripheral blood after cutaneous application of 5-fluorouracil. Arch Med Res. 2003;34(2):141-144.

[20] Valenzuela-Salas LM, Girón-Vázquez NG, García-Ramos JC, Torres-Bugarín O, Gómez C, Pestryakov A, et al. Antiproliferative and antitumour effect of nongenotoxic silver nanoparticles on melanoma models. Oxid Med Cell Longev. 2020;2019:4528241.

[21] Udroiu I. Storage of Blood in the Mammalian Spleen: an Evolutionary Perspective [Internet]. Vol. 24, Journal of Mammalian Evolution. 2017. p. 243-60. Available from: http://link.springer.com/10.1007/s10914-016-9342-0

[22] Schlegel R, MacGregor JT. The persistence of micronucleated erythrocytes in the peripheral circulation of normal and splenectomized Fischer 344 rats: Implications for cytogenetic screening. Mutat Res - Fundam Mol Mech Mutagen. 1984;127(2):169-174.

[23] Wojda A, Ziętkiewicz E, Witt M. Effects of age and gender on micronucleus and chromosome nondisjunction frequencies in centenarians and younger subjects. Mutagenesis. 2007;22(3):195-200.

[24] Ramírez-Muñoz MP, Zúñiga G, Torres-Bugarín O, Portilla E, García-Martínez D, Ramos A, et al.

Evaluation of the micronucleus test in peripheral blood erythrocytes by use of the splenectomized model. Lab Anim Sci. 1999;49(4):418-420.

[25] Zúñiga G, Torres-Bugaŕín O, Ramírez-Muñoz MP, Ramos A, Fanti-Rodríguez E, Portilla E, et al. Spontaneous micronuclei in peripheral blood erythrocytes from 35 mammalian species. Mutat Res - Genet Toxicol. 1996;

[26] Allen JW, Collins BW, Setzer RW. Spermatid micronucleus analysis of aging effects in hamsters. Mutat Res - DNAging Genet Instab Aging. 1996;316(5-6):261-266.

[27] Zamora-Perez A, Gomez-Meda B, Ramos-Ibarra M, Batista-Gonzalez C, Luna-Aguirre J, Gonzalez-Rodriguez A, et al. Felines: An alternative in genetic toxicology studies? Rev Biol Trop. 2008;56(2):969-974.

[28] Zúñiga G, Torres-Bugaŕín O, Ramírez-Muñoz MP, Ramos A, Fanti-Rodríguez E, Portilla E, et al. Spontaneous micronuclei in peripheral blood erythrocytes from 35 mammalian species. Mutat Res - Genet Toxicol. 1996 Jul 10;369(1):123-127.

[29] Dass SB, Ali SF, Heflich RH, Casciano DA. Frequency of spontaneous and induced micronuclei in the peripheral blood of aging mice. Mutat Res - Fundam Mol Mech Mutagen. 1997;381(1).

[30] Sandoval-Herrera N, Paz Castillo J, Herrera Montalvo LG, Welch KC. Micronucleus Test Reveals Genotoxic Effects in Bats Associated with Agricultural Activity. Environ Toxicol Chem. 2021;40(1).

[31] Zamora-Perez A, Camacho-Magaña C, Gómez-Meda B, Ramos-Ibarra M, Batista-González C, Zúñiga-González G.

Importance of spontaneous micronucleated erythrocytes in bottlenose dolphin (Tursiops truncatus) to marine toxicology studies. Acta Biol Hung. 2006;57(4):441-448.

[32] Cristaldi M, Ieradi LA, Udroiu I, Zilli R. Comparative evaluation of background micronucleus frequencies in domestic mammals. Mutat Res Toxicol Environ Mutagen. 2004;559(1-2):1-9.

[33] Gómez-Meda BC, Zamora-Perez AL, Luna-Aguirre J, González-Rodríguez A, Ramos-Ibarra ML, Torres-Bugarín O, et al. Nuclear abnormalities in erythrocytes of parrots (Aratinga canicularis) related to genotoxic damage. Avian Pathol. 2006;

[34] Krauter PW, Anderson SL, Harrison FL. Radiation-induced micronuclei in peripheral erythrocytes of *Rana catesbeiana*: An aquatic animal model for in vivo genotoxicity studies. Environ Mol Mutagen. 1987;10(3).

[35] Buschini A, Martino A, Gustavino B, Monfrinotti M, Poli P, Rossi C, et al. Comet assay and micronucleus test in circulating erythrocytes of Cyprinus carpio specimens exposed in situ to lake waters treated with disinfectants for potabilization. Mutat Res - Genet Toxicol Environ Mutagen. 2004;557(2).

[36] Flores-Galván MA, Daesslé LW, Arellano-García E, Torres-Bugarín O, Macías-Zamora J V., Ruiz-Campos G, et al. Genotoxicity in fishes environmentally exposed to As, Se, Hg, Pb, Cr and toxaphene in the lower Colorado River basin, at Mexicali valley, Baja California, México. Ecotoxicology [Internet]. 2020;29(4):493-502. Available from: http://dx.doi.org/10.1007/ s10646-020-02200-9

[37] Matsumoto FE, Cólus IMS. Micronucleus frequencies in Astyanax

bimaculatus (Characidae) treated with cyclophosphamide or vinblastine sulfate. Genet Mol Biol. 2000;23(2).

[38] Zúñiga-González G, Torres-Bugarín O, Luna-Aguirre J, González-Rodríguez A, Zamora-Perez A, Gómez-Meda BCC, et al. Spontaneous micronuclei in peripheral blood erythrocytes from 54 animal species (mammals, reptiles and birds): Part two. Mutat Res - Genet Toxicol Environ Mutagen [Internet]. 2000 Apr;467(1):99-103. Available from: https://linkinghub.elsevier.com/retrieve/pii/S1383571800000218

[39] Zúñiga-González G, Ramírez-Muñoz MP, Torres-Bugarín O, Pérez-Jiménez J, Ramos-Mora A, Zamora-Pérez A, et al. Induction of micronuclei in the domestic cat (Felis domesticus) peripheral blood by colchicine and cytosine-arabinoside. Mutat Res - Genet Toxicol Environ Mutagen. 1998;413(2):187-189.

[40] Heddle JA, Fenech M, Hayashi M, MacGregor JT. Reflections on the development of micronucleus assays. Vol. 26, Mutagenesis. 2011. p. 3-10.

[41] Lehninger LA. Bioquímica. 2da ed. Barcelona: Ediciones Omega; 1985. 1-1117 p.

[42] Ruiz-Ruiz B, Arellano-García ME, Radilla-Chávez P, Salas-Vargas DS, Toledano-Magaña Y, Casillas-Figueroa F, et al. Cytokinesis-Block Micronucleus Assay Using Human Lymphocytes as a Sensitive Tool for Cytotoxicity/Genotoxicity Evaluation of AgNPs. ACS Omega. 2020;

[43] Ye CJ, Sharpe Z, Alemara S, Mackenzie S, Liu G, Abdallah B, et al. Micronuclei and Genome Chaos: Changing the System Inheritance. Genes (Basel) [Internet]. 2019 May 13;10(5):366.

Available from: https://www.mdpi.com/2073-4425/10/5/366

[44] Terradas M, Martín M, Tusell L, Genescà A. Genetic activities in micronuclei: Is the DNA entrapped in micronuclei lost for the cell? Mutat Res - Rev Mutat Res [Internet]. 2010 Jul;705(1):60-67. Available from: http://linkinghub.elsevier.com/retrieve/pii/S138357421000027X

[45] Fenech M. Cytokinesis-block micronucleus cytome assay. Nat Protoc [Internet]. 2007 May 3;2(5):1084-1104. Available from: http://www.nature.com/doifinder/10.1038/nprot.2007.77

[46] Fenech M, Bonassi S, Turner J, Lando C, Ceppi M, Chang WP, et al. Intra- and inter-laboratory variation in the scoring of micronuclei and nucleoplasmic bridges in binucleated human lymphocytes: Results of an international slide-scoring exercise by the HUMN project. Mutat Res - Genet Toxicol Environ Mutagen. 2003;534(1-2):45-64.

[47] Fenech M, Morley AA. Cytokinesis-block micronucleus method in human lymphocytes: effect of in vivo ageing and low dose X-irradiation. Mutat Res - Fundam Mol Mech Mutagen. 1986;

[48] Scarfi MR, Lioi MB, Diberardino D, Zeni O, Coviello AMR, Matassino D. Measurement of micronuclei by cytokinesis-block method in bovine lymphocytes. Mutat Res. 1993 Oct;289(2):291-295.

[49] Anchordoquy JP, Anchordoquy JM, Nikoloff N, Gambaro R, Padula G, Furnus C, et al. Cytotoxic and genotoxic effects induced by enrofloxacin-based antibiotic formulation Floxagen ® in two experimental models of bovine cells in vitro: peripheral lymphocytes and cumulus cells. Environ Sci Pollut Res

[Internet]. 2019 Jan 30;26(3):2998-3005. Available from: http://link.springer.com/10.1007/s11356-018-3776-2

[50] Ferré DM, Jotallan PJ, Lentini V, Ludueña HR, Romano RR, Gorla NBM. Biomonitoring of the hematological, biochemical and genotoxic effects of the mixture cypermethrin plus chlorpyrifos applications in bovines. Sci Total Environ [Internet]. 2020 Jul;726:138058. Available from: https//doi.org/101016/j.scitotenv.2020.138058

[51] Drážovská M, Šiviková K, Holečková B, Dianovský J, Galdíková M, Schwarzbacherová V. Evaluation of potential genotoxic/cytotoxic effects induced by epoxiconazole and fenpropimorph-based fungicide in bovine lymphocytes in vitro. J Environ Sci Heal - Part B Pestic Food Contam Agric Wastes. 2016;51(11):769-776.

[52] Kim SR, Kim TH, Ryu SY, Lee HJ, Oh H, Sung KJ, et al. Surement of micronuclei by cytokinesis-block method in human, cattle, goat, pig, rabbit, chicken and fish peripheral blood lymphocytes irradiated in vitro with gamma radiation. In Vivo (Brooklyn). 2003;17(5):433-438.

[53] Kim SH, Han DU, Lim JT, Jo SK, Kim TH. Induction of micronuclei in human, goat, rabbit peripheral blood lymphocytes and mouse splenic lymphocytes irradiated in vitro with gamma radiation. Mutat Res Toxicol Environ Mutagen. 1997 Oct;393(3):207-214.

[54] Danica H, Dunja R. Micronuclei in lymphocytes of horses and pigs after in vitro irradiation. Acta Vet Brno. 2007;57(4):341-350.

[55] Backer LC, Grindem CB, Corbett WT, Cullins L, Hunter JL. Pet dogs as sentinels for environmental contamination. Sci Total Environ. 2001;274(1-3):161-169.

[56] Dönmez-Altuntas H, Hamurcu Z, Liman N, Demirtas H, Imamoglu N. Increased micronucleus frequency after oral administration of cadmium in dogs. Biol Trace Elem Res. 2006;112(3):241-246.

[57] Mamoulakis C, Fragkiadoulaki I, Karkala P, Georgiadis G, Zisis IE, Stivaktakis P, et al. Contrast-induced nephropathy in an animal model: Evaluation of novel biomarkers in blood and tissue samples. Toxicol Reports [Internet]. 2019;6(January):395-400. Available from: https://doi.org/10.1016/j.toxrep.2019.04.007

[58] HaeJune L, ChangMo K, SeRa K, JinHee L, JoongSun K, JongChoon K, et al. Incidence of micronuclei in lymphocytes of pig in the high background radiation area (Cheongwon-gun and Boeun-gun). Korean J Vet Res. 2005;45(4):469-475. 31 ref.

[59] Turner HC, Shuryak I, Taveras M, Bertucci A, Perrier JR, Chen C, et al. Effect of dose rate on residual γ-H2AX levels and frequency of micronuclei in X-irradiated mouse lymphocytes. Radiat Res. 2015;183(3):315-324.

[60] Melchior K, Saska S, Coelho F, Scarel-Caminaga RM, Capote TS de O. Bonefill® block as alternative for bone substitute: A toxicological evaluation. Brazilian J Pharm Sci. 2018;54(2):1-9.

[61] Pittol M, Tomacheski D, Simões DN, Ribeiro VF, Santana RMC. Evaluation of the Toxicity of Silver/Silica and Titanium Dioxide Particles in Mammalian Cells. Brazilian Arch Biol Technol. 2018;61(0).

[62] Catena C, Conti D, Villani P, Nastasi R, Archilei R, Righi E.

Micronuclei and 3AB index in human and canine lymphocytes after in vitro X-irradiation. Mutat Res Mutagen Relat Subj. 1994;312(1):1-8.

[63] Kang CM, Lee HJ, Ji YH, Kim TH, Ryu SY, Kim SR, et al. A cytogenetic study of Korean native goat bred in the nuclear power plant using the micronucleus assay. J Radiat Res. 2005 Jun;46(2):283-287.

[64] Sanlioglu AD, Dirice E, Aydin C, Erin N, Koksoy S, Sanlioglu S. Surface TRAIL decoy receptor-4 expression is correlated with TRAIL resistance in MCF7 breast cancer cells. BMC Cancer. 2005;5.

[65] Crowley LC, Marfell BJ, Scott AP, Waterhouse NJ. Quantitation of apoptosis and necrosis by annexin V binding, propidium iodide uptake, and flow cytometry. Cold Spring Harb Protoc. 2016;2016(11).

[66] Pietkiewicz S, Schmidt JH, Lavrik IN. Quantification of apoptosis and necroptosis at the single cell level by a combination of Imaging Flow Cytometry with classical Annexin V/ propidium iodide staining. J Immunol Methods. 2015;423.

[67] Bryce SM, Bemis JC, Avlasevich SL, Dertinger SD. In vitro micronucleus assay scored by flow cytometry provides a comprehensive evaluation of cytogenetic damage and cytotoxicity. Mutat Res - Genet Toxicol Environ Mutagen. 2007;630(1-2).

[68] Avlasevich SL, Bryce SM, Cairns SE, Dertinger SD. In vitro micronucleus scoring by flow cytometry: Differential staining of micronuclei versus apoptotic and necrotic chromatin enhances assay reliability. Environ Mol Mutagen [Internet]. 2006 Jan;47(1):56-66. Available from: http://doi.wiley.com/10.1002/em.20170

[69] Grawé J, Nüsse M, Adler ID. Quantitative and qualitative studies of micronucleus induction in mouse erythrocytes using flow cytometry. I. Measurement of micronucleus induction in peripheral blood polychromatic erythrocytes by chemicals with known and suspected genotoxicity. Mutagenesis. 1997;12(1):1-8.

[70] Rodrigues MA, Beaton-Green LA, Wilkins RC, Fenech MF. The potential for complete automated scoring of the cytokinesis block micronucleus cytome assay using imaging flow cytometry. Vol. 836, Mutation Research - Genetic Toxicology and Environmental Mutagenesis. 2018. p. 53-64.

[71] Chen Y, Huo J, Liu Y, Zeng Z, Zhu X, Chen X, et al. Development of a novel flow cytometry-based approach for reticulocytes micronucleus test in rat peripheral blood. J Appl Toxicol. 2021;41(4).

[72] Rodrigues MA, Probst CE, Zayats A, Davidson B, Riedel M, Li Y, et al. The in vitro micronucleus assay using imaging flow cytometry and deep learning. npj Syst Biol Appl. 2021;7(1).

[73] Fenech M. Cytokinesis-block micronucleus cytome assay evolution into a more comprehensive method to measure chromosomal instability. Genes (Basel). 2020;11(10):1-13.

Section 4

Pedagogy and Psychology

Virtual Physiology: A Tool for the 21st Century

Carmen Nóbrega, Maria Aires Pereira, Catarina Coelho,
Isabel Brás, Ana Cristina Mega, Carla Santos, Fernando Esteves,
Rita Cruz, Ana I. Faustino-Rocha, Paula A. Oliveira,
*João Mesquita and Helena Vala*

Abstract

Veterinary physiology is a basic curricular unit for every course within the veterinary field. It is mandatory to understand how the animal body works, and what to expect of a healthy body, in order to recognize any misfunction, and to be able to treat it. Classic physiology teaching involves wet labs, much equipment, many reagents, some animals, and a lot of time. But times are changing. In the 21st century, it is expected that the teaching and learning process can be more active and attractive, motivating students to learn better. It is necessary to understand what students like, and to introduce novelties into the school routine. The use of a game-based learning, using "new" technologies, creating virtual experiences and labs, reducing the costs of reagents, equipment, and especially reducing the use of animals, will be the future for physiology teaching.

Keywords: learning, physiology, teaching, game based learning, Z generation

1. Introduction

It was in the 15th century that anatomy (still undistinguished from physiology) started to strongly develop. It was part of the core of the European society developments, upon the development of the Late Middle Ages, the Early Renaissance, and the early Modern period, the melting pot for important medical developments, announcing the "European miracle" of the following centuries [1]. But for all practical purposes, physiology was considered to be born in the 17th century, most likely upon the publication of William Harvey's book on the circulation of the blood, in 1628 (**Figure 1A**) [2].

It was on Harvey's work that for the first time traditional (and unquestionable) beliefs about the heart and the circulation (dating back to Galen, 1500 years earlier) have been dethroned. Harvey declined to consider uncritically what he had been taught and insisted on relying on his own scientific observations. This approach is considered to be one of the most revolutionary ideas in science in the 17th century, and Harvey's greatest contribution to science [3].
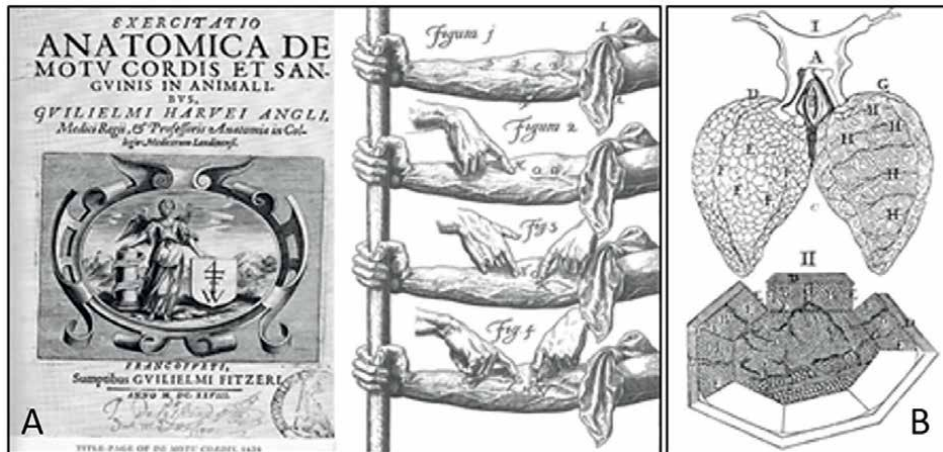
Figure 1.
A: Title page of William Harvey's De Motu Cordis (1698) to the left and demonstration of blood flow in the veins of the forearm to the right. B: Above; Malpighi's drawing of the pulmonary capillaries and alveoli: 2 lungs with the alveoli on the left and the capillaries on the right. Below; pulmonary capillaries in a diagram of an alveolus that has been opened up.

However, this was not without controversy. Many have initially opposed to the concept of physiology however great names such as Marcello Malpighi (**Figure 1B**) and Antoni van Leeuwenhoek have supported the thoughts on human function, joining efforts in developing modern physiology.

Following the initial scientific developments, a halt followed between 1750 and 1850 throughout Europe with critical thinking of medicine as a science coming to a stop and being replaced by an artistic view of medical science, resourcing to texts in Latin. This came to such an extent that the microscope was not made available to students in Leiden as was auscultation not included in the teaching curricula, albeit having been discovered in 1819 [4].

In the middle of the 1800's German doctors proposed the 'medicine equals science' concept and pointed towards the reintroduction of science in the curricula, motivated by Rudolf Virchow (cellular pathology) and by significant scientific advances at that time such as the periodic table (Dmitri Mendelejev) and upon the publication of the "Origin of Species" (Charles Darwin). Noteworthy, important technological advancements were also made at that time such as the development of steam locomotives and railroads, and the first steel steamship crossing the Atlantic. For the above, ideal conditions for the advancing of physiology has also occurred giving rise to physiologists like Carl F.W. Ludwig in Germany and Claude Bernard in France [5].

Specializations within general physiology also started, namely on gastrointestinal physiology (William Beaumont); pathology (Rudolf Virchow) and bacteriology (Louis Pasteur, Robert Koch), with scientific journals being written as the basis for solidification of these new physiology branches such as the "Archiv für Pathologische Anatomie und Physiologie und für klinische Medicin" (Virchow and Reinhardt; today called Virchows Archiv) and Pflügers Archiv (today called Pflügers Archiv - European Journal of Physiology), laying the basis for modern physiology in the 19th–20th century with names such as Pavlov (psychophysiology), Sherrington (neurophysiology), Mosso (ergograph, sphygmomanometer), Golgi (nervous system, malaria), and Ringer (Ringer's solution). This great evolution was supported (and recognized) with the creation of the Nobel Prize of Physiology or Medicine, first awarded in 1901 [5].

The rapid changes observed in modern societies have caused higher level education providers (i.e. Higher Education) to face a variety of challenges in order to cope with today's demands [6]. This has, in all, lead to the training of more enthusiastic students in an array of interdisciplinary fields [7], generating effective pedagogical methods and strategies to the point that these are now recognized as one of the most important necessities of educational systems [8].

Physiology is today recognized as the bedrock of medical curriculum [9] and, as such, the preference for a particular content delivery method has been vastly investigated by to pass knowledge logically and strategically to students [10]. A greater focus has been given now on critical thinking skills in contrast to emphasis on the systems-based didactic lectures [11]. This has been done also due to the longstanding recognition of the Physiology Science as a challenging discipline for students to grasp, assimilate and employ in clinical sciences. Furthermore, as a core science in the disease process, its understanding is of the utmost importance for an integrated knowledge [12, 13].

As such, physiology educationists are making great efforts towards focusing on ways to obtain vertical and horizontal integration in the discipline of Physiology, exceeding the typical periodical assessment of the medical curriculum by further stimulating and introducing a myriad of new teaching and learning approaches to captivate and augment students' knowledge acquisition [14].

2. The teaching and learning experience in the 21st century

The 21st century is demanding profound changes in veterinary education. Scientific knowledge grew at a dizzying speed, so even for researchers, it is difficult to keep up with the literature. The world is completely different and never the expression "times are changing" heard in the transition from our parents' generation to ours, was applied with as true sense as now. As in all sectors of society, Education systems are also changing. Big transformations occurred following the Bologna treaty that changed the educational paradigm, advocating greater student autonomy and self-learning. These changes must now be optimized considering technological evolution, that have begun to change how students acquire information [15]. It is imperative to occupy the fast fingers of students on smartphones in favor of teaching and science. This is a challenge for today's teachers, according to the idea that "The more complex the world becomes, the more creative we need to be to meet its challenges" [15, 16]. Another issue is the curricula reforms, that resulted in a reduction of teaching hours. In some core disciplines such as physiology, this reduction has resulted in serious reviews of the way it is taught [15].

2.1 Who are the 21st century students?

Current higher education students are generally in their late teens and early adulthood (although naturally some are older and a small number may be younger), and belong to the so-called Generation Z, born between 1995 and 2009. Generation Z follows members of Generation Y, more commonly known as Millennials, who were born between 1975 and 1995. Most of them do not remember life without the internet, and have had technology like smartphones, iPads, smartboards and other devices available throughout most of their schooling years [17, 18]. They grew up around gaming and have great affinity with not just technology platforms, but also with game-like settings

that provide, among other components such as continuous challenges, captivating storylines, immediate rewards and feedback, and sometimes fun [19].

Students from the so-called Generation Alpha, born between 2010 and 2025, future students in the higher education system, are younger than smartphones, the iPad, 3D television, Instagram, and music streaming apps like Spotify. This will be the first generation to be born entirely within the 21st century and likely to live in the 22nd century in large numbers. They are also the first generation to experience a pandemic situation in their early childhood: the SARS-CoV-19 pandemic (**Figure 2**) [17, 18].

Interestingly, Generation Alpha started at the same year that Apple launched its iPad, Instagram made its debut and the American Dialect Society crowned "app" as its word of the year. Surrounded by technology, this generation does not live without it, as an extension of itself. Digital tools are omnipresent in their lives, being the "most materially endowed and technologically literate generation to ever grace the planet!" [18].

This generation has grown up like no other, surrounded by technology from childhood, making it, certainly, the fittest generation in terms of digital skills. They are immersed in technology, almost as an extension of their way of being. It is widely accepted that technology can bring countless benefits. Let's think about the SARS-CoV-19 pandemic. Although too early to know exactly the pandemic impact, in early 2020, the coronavirus pandemic forced schools and most employers to operate remotely, and technology was the one who came to the rescue. This crisis has driven unpredictable direct and indirect effects on the entire educational system. Although technology can be extremely useful, when it is overkill, it can create some drawbacks, such as shorter attention spans and delayed social development [17, 18]. The impact of all this crisis is yet to be determined for years and years to come.

At this point we all understand that the entire educational system (including higher education), must undergo a phenomenal adaptation to keep up with this distinct new generation of students [18]. Past/traditional methods of teaching and learning may already make little sense to today's students who learn and think differently, and to their future workplace, where change is a constant, and where making use of information is now far more valuable than simply knowing things. Schools are probably failing to teach students to respond to rapid changes and how to handle new information because they are clinging to obsolete methods, namely memorize facts for a test when all the information will be fully available at a click [17]. To avoid demotivation, the learning process has been advocating new strategies, including activities
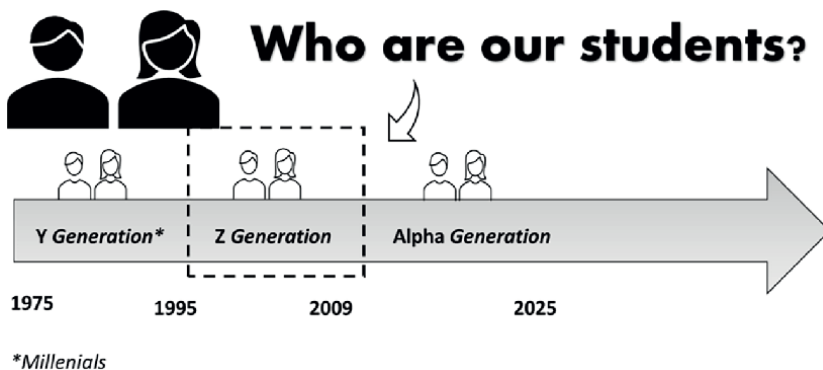
Figure 2.
The 21st century students in higher education system in 2021.

student-centred, to achieve the expected learning outcomes and at the same time, to maintain student's engagement [20, 21]. In order to increase students' knowledge, understanding, and at same time enhancing their motivation and engagement, teachers must create a joy, an excitement, and a love for learning, while inspiring students. It is imperative for teachers to demonstrate how to learn, rather than dictating what they know [22]. New strategies will lead to success, reducing the frustration of a lonely, passive study, reducing despair, depression and poor quality of life.

2.2 How do they learn?

Designing learning interventions requires careful consideration of how information is perceived and cognitively processed by students. Perceptual preferences refer to the preferred way to receive information and include visual, auditory, and kinesthetic learners [23, 24]. It was observed that 73% of students learn effectively if the teacher combines visual, auditory, and kinesthetic activities, but the remaining students fail to understand the subject matter unless it is presented in their preferred way [25].

Visual students learn by watching, have a keen visual memory and are very imaginative. They are targeted by the presence of models and demonstrations, and extract detail from the background information, remembering faces rather than names. These students usually sit in front of the room and take notes or doodle. They understand better if they can see the facial expression and the body language of the teacher. Visual students normally prefer a quiet environment to study. Computer assisted learning (CAL) is an interesting option for these students, because it allows the schematic representations of information, through charts, graphs, diagrams, and flow charts [23, 24, 26].

Auditory learners prefer verbal instructional methods, such as lecture, discussion, work in groups, debates, games, and answering questions. They find it hard to study from notes and have difficulty with reading and writing tasks. Distinctions that are important to them include pitch, time, volume, rhythm, and resonance. These students often remember names but not faces, do not take notes in class, humor talk to themselves when bored or concentrating, and read aloud. They prefer to study in a noisy environment, as sounds can evoke memory of information [23, 24, 26].

Kinesthetic students also called as tactile learners require whole body movement and real-life experience to absorb and retain information, appreciating to manipulate models and role playing. They learn from external stimuli and movement and are often risk takers and disorganized. These students use highlighters and pictures to study. They learn best when there is music in the background and snacks are available. Kinesthetic learning methods include build, design, visit, interview, and play [23, 24, 26].

Thus, learning interventions need to incorporate the perceptual preferences of the students and help them to develop alternative modes of learning [23] through the incorporation of multisensory and diverse instructional methods (**Figure 3**).

2.3 Learning outcomes for 21st century

The competitive workspace of the 21st century requires students to develop expertise across the four domains of knowledge, that includes the ability to think (cognitive skills), the capacity to valuing (affective skills), a skilled behavior (psychomotor skills), and strive to perform at highest levels (conative skills). However, the acquisition of expertise across all four domains of learning requires appropriate training [23, 27] and assessment [27].
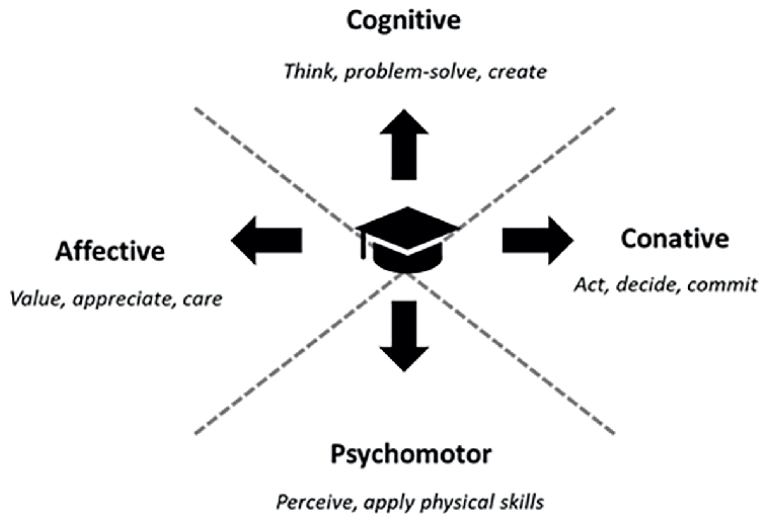
Figure 3.
Learning preferences (visual, auditory, kinesthetic).

Cognitive skills include six levels of complexity [28], ranging from lower-order skills (remember, understand, and apply) that require less cognitive processing to higher-order skills (analyze, evaluate, and create) that require greater degree of cognitive processing [29]. These cognitive skills can be contextualized into four types of knowledge (factual, conceptual, procedural and metacognitive) that need to be achieved in the learning activities [28]. Factual knowledge refers to the acquisition of basic elements (terminology and discrete facts) that will allow students to solve problems. Conceptual knowledge is related to the generalizable principles (categories, theories, principles, and models) that transcend the specific contexts of a task or procedure and is commonly described as "knowing why". Procedural knowledge refers to the technique, process, or methodology that allow executing a task or procedure proficiently and is described as "knowing how". Finally, metacognition includes self-assessment ability and knowledge of various learning skills and techniques [23, 29, 30].

Most instruction in higher education is focused on the cognitive learning skills [29, 31], however, the development of the affective and psychomotor domains are crucial to the success of health professionals [29]. The affective domain refers to emotions and feelings, especially in relationship to a set of values, and is related to the way in which we deal with things emotionally. This domain includes five categories listed from the simplest behaviors (receiving, responding and valuing a particular phenomenon) to the most complex ones, related to organizing and characterizing values [23, 27]. The development of affective skills is fundamental in the veterinary field. Veterinary health professionals face difficult situations on a daily basis. It is necessary to be empathic with clients, to deliver bad news, to deal with animal cruelty, and to see clients struggling to balance financial needs with the needs of their pets. It is imperative for these students, future professionals, to develop affective skills, to create a culture of wellbeing that will allow to deal with all difficult and stressful situations.

The psychomotor domain is related to the mastery of physical skills, including reflective movements, fundamental movement, perceptual skills, physical abilities, skilled movement, and non-discursive communication [23]. Psychomotor skills are important in the veterinary field, since professionals perform delicate/sensitive

Figure 4.
Comprehensive learning outcomes for the 21st century college graduates.

physical tasks, handle sensitive medical equipment and frightened animals. The exhibition of an appropriate body language is also highly desired to efficiently communicate with colleagues/peers and clients.

The conative domain refers to the will, desire, drive, level of effort, mental energy, intention, striving, and self-determination to perform at the highest standards possible [27, 32]. It is important that students understand the importance of physiology for their professional career and have the internal desire to understand it, rather than memorizing concepts for assessment, which are soon forgotten and do not lead to effective learning (**Figure 4**) [23].

Learning outcomes that cut across the four domains of the knowledge include the capacity to access and use information, communicate using multiple media, demonstrate understanding, apply rules and procedures, be creative and curious, think critically, make sound judgments, solve problems, be committed to life-long learning, proactively seek to extend knowledge and exhibit an ethical behavior [27]. However, these meta-outcomes must be assessed to guarantee that they are learned, since students choose to focus their study efforts on subjects, they know that will be tested [27, 33].

3. Teaching-learning approaches

It is not new and has been assumed since the Bologna treaty that the teaching and learning processes should be student centered, and a shift from an "instruction paradigm" towards a "learning paradigm" should be followed. Therefore, students must build their own understanding of concepts, relationships and procedures, and teachers can encourage this process by carefully considering the type and organization of information, as well as instructional strategies. Specifically, teachers should reduce the total amount of factual information students are expected to memorize, reduce passive lecture format, and devote much more effort to helping students to become active, independent learners and problem solvers. Collaborative learning

activities, interactive models, educational games, and establishing a culture of inquiry/scholarship are critical for achieving these goals [22]. In this context, the teacher assumes the role of facilitator of learning experiences, designing structured classroom environments to maximize student learning, and promote at the same time "classrooms equity" [34, 35].

3.1 Active learning methodologies

Active learning strategies meet perceptual preferences of all types of learners [22, 36, 37]. The implementation of evidence-based active learning interventions, physiology-specific, particularly in large-enrolment class environments can be a challenge [35, 38]. However, active learning strategies range in scale from simple, "low risk" to more complex, "higher risk" activities.

3.1.1 From "simple" to more "complex" active learning activities

Simple activities require little planning from the instructor and little involvement from the students (did not require verbal feedback to the teacher) and are easy to implement. They include pause procedure, minute papers, think pair-share activities, and classroom assessment techniques. More complex activities require more interaction and commitment of the students and more planning by the teacher. Students can work in informal, cooperative learning groups to solve problems, answer inquiry-type questions, analyze case studies and discuss articles among themselves and with the class. These active learning activities can be interspersed between lecture periods (basic active-learning lecture) [39] or replace completely lecturing. In this case, content can be transmitted before class, asking students to watch videos, or read certain material and then lecturing time can be exclusively used for active learning [35].

3.1.2 Game-based learning

The use of games for teaching and learning purposes is not new. Games although fun and entertainment provides engaging experiences, interactive learning environments and collaborative learning activities [40].

Game-based learning (GBL) is an active learning approach that uses different types of game with defined learning outcomes [41–43]. It includes the so-called serious games, when its main goal is teaching and learning, besides entertainment [36, 44]. GBL is useful whether we are addressing basic disciplines or more specific ones. Physiology is considered difficult by many students from different courses in the area of veterinary health, namely veterinary medicine and nursing. They attribute the difficulty to the need to memorize content, an excessive quantity of information, difficulty in understanding the relations between the morphology and function of organs and systems, and the perception of some topics as being too abstract [45]. GBL creates a beneficial learning environment, requiring the interaction of the students in questions and answers that assist in retaining information and improving performance. In addition to the positive impacts on student learning, the use of educational games can increase involvement with activities related to the content of the course, as well as promote greater perception of improved learning by the students [45, 46]. On the other hand, games bring an element of pleasure and can reduce anxiety; students are promoted as participants and share their knowledge and engage in teaching each other; and students can combine theory and practice [47, 48].

3.1.2.1 Digital games/ board games

Games used can be digital games, but it also can be other types of games, like board games.

Digital games, also called computer games, are games that use the advance of digital technology and offers new and engaging teaching method that allow students a most effective learning, once it is active, experiential, situated, problem-based oriented and provides immediate feedback [36]. Based in the use of computers and internet, this learning and teaching strategy has been increased, conducting to the production of several games with educational purposes in the veterinary field [49, 50].

Board games are games with rules, a playing surface, and tokens that enable interaction between or among players and facilitate face-to-face interactions with peers and teachers [51, 52].

When comparing board games with computer games, the first are more effective in terms of acquiring knowledge, but computer games yield better results when it comes to motivation, self-efficacy, or skill enhancement [42, 52]. When we combine motivation and engagement in the learning and teaching process, learning outcomes will be successfully achieved.

3.1.3 Gamification

The meaning of gamification varies widely and is often confused with GBL. Gamification is an umbrella term, that involves the application of game elements such as points, levels, time constraints and awards, and use them as non-game settings to other areas of interest [42, 53, 54]. Gamification has been characterized as well adapted to the learning style of Z generation [21, 42, 53–55]. Applied to an educational context, a gamified learning experience can positively influence student engagement by using gamification principles to affect the cognitive, emotional, and social aspects of the learning experience [54]. The cognitive aspect is stimulated through goal-oriented and learning objectives-based activities that challenge students within the gamified environment. The emotional aspect plays an important part in a gamified learning platform: curiosity, frustration, joy, pride and optimism are present during the experience [42]. Most importantly, the gamified learning experiences give feedback and allow repetition, encouraging resilience and reframing of failure, reinforcing the idea that repeated failures will eventually lead students to level completion and achieving learning goals [56]. The social aspect involves the participation of students within an environment where they interact with their peers and are part of a group. In this learning environment, students can have new identities and roles (using avatars and role play), and through branching mechanisms, they are asked to make choices and decisions. Also, gamification allows students to publicly identify themselves as "masters," once they reach a higher level of mastery, and gain social credibility - for example, via a leaderboard [57] - as well as academic recognition by accumulating points [58].

3.1.4 Simulations/virtual laboratories

A virtual laboratory is any online environment that is based on interactive learning either individually or in groups, allowing students to explore topics in an asynchronous manner that has no immediate physical reality [59].

In the last decade, there has been a gradual shift of conventional physical, in-person laboratories towards virtual alternatives, motivated by several reasons. Physical laboratories are expensive. They need advanced instruments and equipment, space, professional personnel, and maintenance. Moreover, the student population is increasing, conducting to higher experimental costs. Virtual laboratories and tools provide significant long-term cost savings. Whilst the initial development or purchase costs may be large, once developed, the majority do not require the ongoing purchase of consumables, the provision of physical space, laboratory equipment or support staff time [60].

Animal-based laboratories, very useful in the past for physiology teaching and learning, can be associated with ethical concerns, while virtual animal model simulations reduce the ethical dilemmas and broadens the types of experiments that can be conducted. Moreover, virtual laboratories exhibit higher levels of efficiency and safety, enabling students to learn in their own time and pace [61–63]. This is also another great advantage when we think of all the students undertaking part-time employment to support their studies. For them, the possibility to study at their own time and pace, at home or elsewhere, and to access virtual laboratories and experiments that always work, and with consistent data, is unvaluable. With these simulations, experiments are far shorter; students can undertake more experiments in the time available increasing their learning. Several studies have already proven that virtual laboratory tools were equally effective as traditional laboratories in increasing student knowledge and understanding, when evaluated by student performance in examinations [62, 64–66].

Nevertheless, virtual laboratories have intrinsic constraints and limitations. They do not provide students with the opportunity to develop key practical or technical skills (hands-on experience), or how to use specific items of equipment or to promote awareness of ethical, health and safety issues. They will always give the characteristic and correct data, like a perfect scenario, and we all know that in real life it's not always like that [60, 63].

Although virtual laboratories have become increasingly common as a form of teaching aid in different learning situations, creating a virtual laboratory for teaching and learning is, however, overly complex, incorporating skills in diverse areas such as interaction design, visualization, and pedagogy. It involves design and production of texts, images, 3D environments and interactivity, and the production requires programming and animation [63, 67]. There are some virtual labs already deposited in open educational resource (OER) repositories (https://libguides.mines. edu/oer/simulationslabs) that can be easily used and are invaluable strategies for this demanding learning/teaching process [63]. When asked whether virtual or traditional laboratories should be discontinued, students saw a place for both within the curriculum, recommending that they should be used in parallel [68].

3.2 How we teach?

In this enthusiastic process of teaching and learning physiology, our option is for a blended/mixed approach, meaning a process that brings together what we consider the best from different approaches: experiments hands-on, virtual experiments, digital games/simulations, board games, crosswords and word search games.

This way we intend to avoid boredom, to promote curiosity, motivation, and engagement, and to create learning opportunities for all students (visual, auditory and kinesthetic students) to go beyond rote memorization of terms and processes, and towards developing mental models of physiological phenomena.

Reflecting the importance of technology in the Z Generation, all students own at least one Internet-ready device (e.g., iPad, laptop, tablet, smartphone), enabling the use of online resources in this approach.

3.2.1 Crosswords

Crosswords are an easy and fun way to engage students. Crossword puzzles have the purpose of encourage students to form words or phrases which lead to the answers. It can be used as a means of enhancing general and scientific information, assuming a facilitative role for problem-solving skills.

This is an in-house crossword (**Figure 5**). Starting from physiologic concepts or definitions, and using online free tools (https://worksheets.theteacherscorner.net/make-your-own/crossword/), the puzzle shown in the image is created.

3.2.2 In-house created learning board games

In a combined work of teachers and students, through a Pedagogical project financed by Polytechnique Institute of Viseu (IPV), The MacVet Project (Create, Simulate and Learn), three in-house learning games were created from classic games: Vetpoly, Physiohedbanz and Pictionaryvet (**Figure 6**).

The traditional Monopoly board game has been converted to VetPoly. The original game has been adapted by creating a new board, community box cards and lucky cards, so that the game would reflect the veterinary field environment. The community box cards have been turned into Quizz timecards. Whenever the player lands on a Quizz time house they will have to answer a physiology question. If the player gets it right, he will receive a monetary reward; if he makes a mistake, he will be penalized and will have to return the amount indicated on the card to the bank. This game adapts to various curriculum units, just by replacing the Quizz time cards.
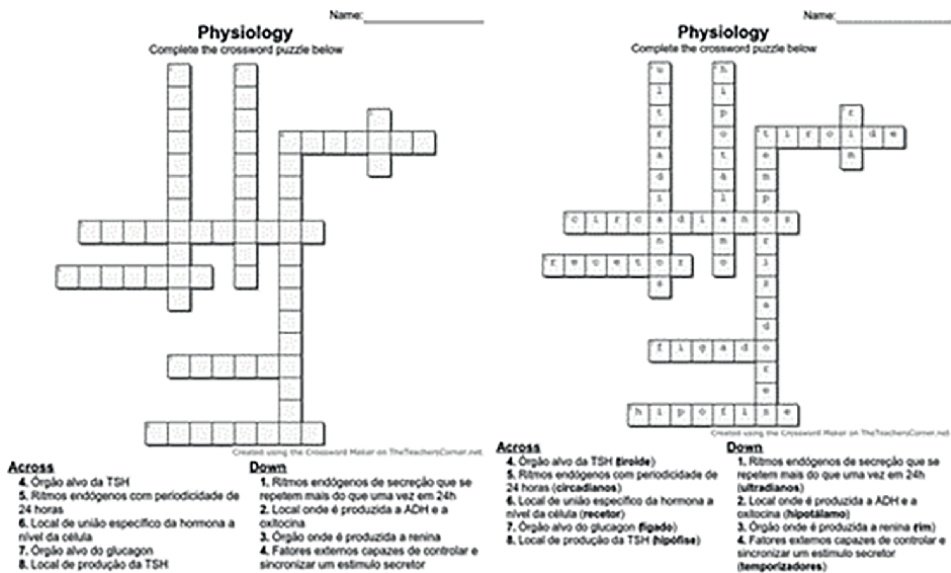

Figure 5.
Physio crosswords. (in English, for example n° 1: Across1: TSH target organ. Answer: Thyroid).

Figure 6.
Vetpoly board and game; Physiohedbanz game and rules' card; Pictionaryvet rules' card.

The Hedbanz was converted to Physiohedbanz. Using cards with figures/concepts related to physiology, that students must identify without seeing it. The game is based in old game of "What am I?" Player has to ask "yes" or "no" questions before time runs out (e.g., ADH. The student with the ADH card, must ask if it is a hormone, if it acts in the renal tubules, if it inhibits diuresis). In the end wins the player with more scoring badges.

The Pictionaryvet, similar to the classic Pictionary game, requires some drawing skills. Students are invited to draw the concepts/terms/processes, all related to physiology. Like Physioheadbanz, there are time restrictions for each team.

3.2.3 Virtual rats

Animals' experiments, classically used in the learning process of physiology, have been gradually replaced by "virtual animals", with enormous advantages: reduction of the live animals used and replacing them by alternatives. The use of "virtual rats" is one of the best known alternatives. We use, for several years and with remarkable academic success, a "Laboratory exercise using "virtual rats" to teach endocrine physiology" [69] and "Virtual rat: a tool for understanding hormonal regulation of gastrointestinal function" [70]. Although may be considered "old" papers, they remain actual. Through the description of the experiment and by the analysis of the results given, students are invited to actively enhance their understanding of physiology and foster logical thinking and problem-solving skills.

3.2.4 Kahoot and online quizzes

Z generation and technology are always holding hands. Most students (in many cases all students) not only own smartphones and other gadgets but are also attached

to them (both physically and emotionally), and in some cases are inseparable. Smartphones provide convenience, portability, comprehensive learning experiences, multi sources and multitasks, and are environmentally friendly. Students use their smartphones for a great variety of tasks: to be connected to their friends, to be on top of every event, and to access teaching materials or supporting information, normally accessible through the Internet. They also use smartphones to interact with teachers and group colleagues outside classes.

Students using interactive quizzing in an online setting reported increased engagement whilst learning due to the fun, joyful and attractive environment, and because of the interaction that occurs. It has also other advantage: the fact that it promotes a healthy competition, conducting to better learning outcomes. A great advantage of Kahoot! is that it is equally effective across both face-to-face and online teaching sessions (**Figure 7**).

Other online quizzes available on the internet, like Socrative, are also utilized in the process of teaching and learning physiology.

3.2.5 Virtual laboratories

As mentioned, simulations can be a practical and effective alternative to traditional laboratory experiences, sparing the need to use subjects (e.g., animals) and/or expensive equipment. There are some online resources available, but our main experience is with Labster [71] (https://www.labster.com/), a platform of laboratory virtual simulations, aiming to increase the learning outcomes. Upon launch a simulation, students are invited to go through a tutorial to know how to navigate in the simulation (arrows that will indicate where to look, or where to go, holograms that show were to
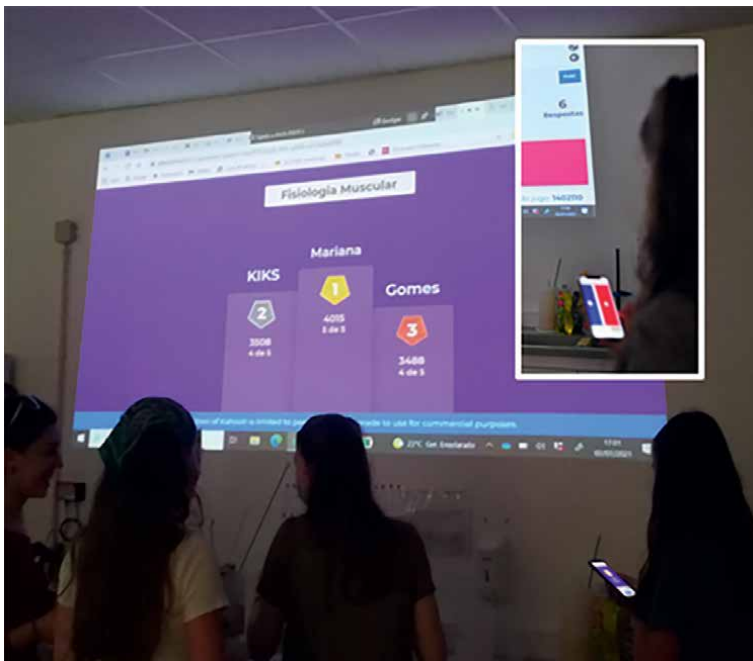
Figure 7.
Muscular physiology Kahoot! Performed in a face-to-face teaching lesson.
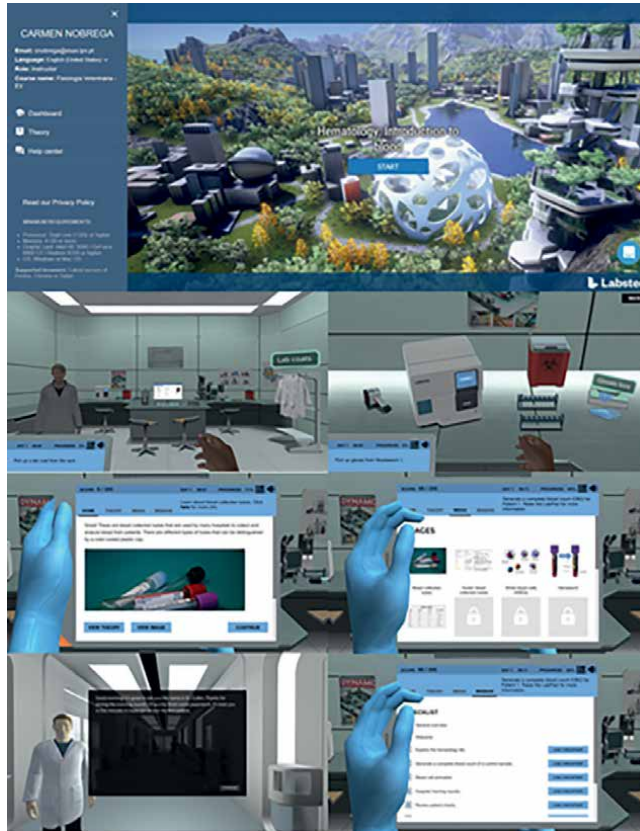
Figure 8.
Labster simulation: Hematology. Introduction to blood.

go or where to place objects, like pipettes, glass slides, beakers…). There is a lab pad, available during all the simulations that help the student with four sections: the Home page provides instructions and quiz questions, the Theory page gives access to all the information needed in order to answer the quiz questions, the Media page stores all the images seen during the simulation, and finally the Mission page provides an overview of all the simulation steps (**Figure 8**).

4. Conclusions

The benefits of using active learning strategies, and in understanding the student that is in front of us, are tremendous, since the potential of every student can be elevated, resulting in better learning outcomes and student satisfaction and enjoyment.

Remaining in a traditional and lecture-based method of curriculum delivery has been attributed to be one of the causes for school dropout and failure. Z generation is technology oriented and its inclination to turn to the digital world must be faced as a teaching ally. We also showed that besides technology, there are also other strategies, more economic ones, that can be applied. What matters is to stimulate learners. We all know that physiology is a complex science. Our job, as teachers, is to provide

the correct tools for the students to learn by developing their cognitive skills, their reasoning ability and their critical thinking, and to develop affective, psychomotor and conative skills. From here, the need for constant learning and the fascination for science will be a natural consequence. We cannot forget that in the 21st century, information is just a click away. What each one does with this information is what it counts.

Acknowledgements

Conflict of interest

The authors declare no conflict of interest.

Author details

Carmen Nóbrega[1,2*], Maria Aires Pereira[1,3], Catarina Coelho[1,2,4], Isabel Brás[5,6],
Ana Cristina Mega[1,2], Carla Santos[1,7], Fernando Esteves[1,7], Rita Cruz[1,7],
Ana I. Faustino-Rocha[2,8,9], Paula A. Oliveira[2,10], João Mesquita[11,12] and Helena Vala[1,2]

1 Agrarian School of the Polytechnic Institute of Viseu, Viseu, Portugal

2 Centre for the Research and Technology of Agro-Environmental and Biological
Sciences (CITAB), University of Trás-os-Montes and Alto Douro, Vila Real, Portugal

3 Global Health and Tropical Medicine (GHTM), Institute of Hygiene and Tropical
Medicine (IHMT), New University of Lisbon, Lisbon, Portugal

4 Animal and Veterinary Research Center (CECAV), University of Trás-os-Montes
and Alto Douro, Vila Real, Portugal

5 Superior School of Technology and Management of Viseu, Campus Polytechnic of
Repeses, Viseu, Portugal

6 Centre for Research in Digital Services (CISeD), Polytechnique Institute of Viseu,
Viseu, Portugal

7 Center of Studies in Education, Technologies and Health (CIDETS), Institute
Polythecnic of Viseu, Portugal

8 Comprehensive Health Research Center, University of Évora, Évora, Portugal

9 Department of Zootechnics, School of Sciences and Technology, University of
Évora, Évora, Portugal

10 Department of Veterinary Sciences, University of Trás-os-Montes and Alto Douro,
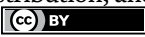Vila Real, Portugal

11 Institute of Biomedical Sciences Abel Salazar (ICBAS), University of Porto, Porto,
Portugal

12 Public Health Institute (ISPUP), University of Porto, Porto, Portugal

*Address all correspondence to: cnobrega@esav.ipv.pt

IntechOpen

References

[1] Jones E. The European miracle: environments, economies, and geopolitics in the history of Europe and Asia. 6th ed. Cambridge University Press; 1981

[2] Harvey W. Exercitatio Anatomica De Motu Cordis et Sanguinis ia Animalibus - Being a facsimile of the 1628 Francofurti edition together with the Keynes. English Translation. Birmingham: The Classics of Cardiology Library; 1985

[3] Bolli R. William Harvey and the Discovery of the Circulation of the Blood. Circulation Research. 2019;124(9):1300-1302. DOI:10.1161/CIRCRESAHA.119.314977. PMID: 31021729

[4] Lindeboom GA. De geschiedenis van de medische wetenschap in Nederland, 2nd edn. Fibula-Van Dishoeck, Haarlem; 1981

[5] Westerhof N. A short history of physiology. Acta Physiologica (Oxf). 2011; 202(4):601-603. DOI: 10.1111/j.1748-1716.2011.02286.x

[6] Bidabadi NS, Isfahani AN, Rouhollahi A., Khalili R. Effective Teaching Methods in Higher Education: Requirements and Barriers. Journal of Advances in Medical Education and Professionalism. 2016;4(4):170-178

[7] Anderson A. The European project semester: A useful teaching method in engineering education project approaches to learning in engineering education. Journal of Engineering Education. 2012;8:15-18

[8] Khodaparast HA. New perspectives in engineering education: the promotion of traditional models to innovative

solutions. Journal of Engineering Education. 2005;7(28):11-22

[9] Rehan R, Ahmed K, Khan H, Rehman R. A way forward for teaching and learning of Physiology: Students' perception of the effectiveness of teaching methodologies. Pakistan Journal of Medical Sciences. 2016;32(6):1468-1473. DOI:10.12669/pjms.326.10120

[10] Rehman R, Afzal K, Kamran A. Interactive lectures: A perspective of students and lecturers. J Postgrad Med Inst. (Peshawar-Pakistan). 2013; 27(2):152-156

[11] Huang GC, Lindell D, Jaffe LE, Sullivan AM. A multi-site study of strategies to teach critical thinking: 'why do you think that?' Medical Education. 2016;50(2):236-249. DOI:10.1111/medu.12937 3

[12] Michael J. What makes physiology hard for students to learn? Results of a faculty survey. Advances in Physiology Education. 2007;31(1):34-40. DOI: 10.1152/advan.00057.2006 4

[13] Michael J. Where's the evidence that active learning works? Advances in Physiology Education. 2006;30(4):157-167. DOI: 10.1152/ advan.00053.2006

[14] Iqbal T. Physiology is a complete subject in its own right. Pakistan Journal of Physiology. 2015;11(2):1-2

[15] González HL, Palencia AP, Umaña LA, Galindo L, Villafrade MLA. Mediated learning experience and concept maps: A pedagogical tool for achieving meaningful learning in medical physiology students. Advances in physiology education. 2009;32. 312-316. DOI:10.1152/advan.00021.2007

[16] Robinson. Out of Our Minds: The Power of Being Creative Hardcover. Wiley. 2011. ISBN:9781907312472. Online ISBN:9780857086549. DOI:10.1002/9780857086549

[17] Ding D, Guan C, Yu Y. Game-Based Learning in Tertiary Education: A New Learning Experience for the Generation Z. International Journal of Information and Education Technology. 2017;7(2):148-152

[18] Hernandez-de-Menendez M, Escobar Díaz C, Morales-Menendez R. Educational experiences with Generation Z. International Journal on Interactive Design and Manufacturing. 2020;14:847-859. DOI:10.1007/s12008-020-00674-9

[19] Bruder P. GAME ON: Gamification in the Classroom. The Education Digest; Ann Arbor. 2015; 80(7): 56-60

[20] Pintrich PR. A Motivational Science Perspective on the Role of Student Motivation in Learning and Teaching Contexts. Journal of Educational Psychology. 2003;95(4):667-686. https://doi.org/10.1037/0022-0663.95.4.667

[21] Mora Carreño A, Melià-Seguí J, Arnedo-Moreno J. Lessons learned on adult student engagement in an online gameful course. In: 1st Workshop on Gamification and Games for Learning (GamiLearn'17). 2017. Universidad de La Laguna. http://riull.ull.es/xmlui/handle/915/4774

[22] Lujan HL, DiCarlo SE. Too much teaching, not enough learning: what is the solution? Advances in Physiology Education. 2006;30(1):17-22. DOI:10.1152/advan.00061.2005

[23] Eagleton S. Designing blended learning interventions for the 21st century student. Advances in Physiology Education. 2017;41(2):203-211. DOI: 10.1152/advan.00149.2016. PMID: 28377434

[24] Eagleton S, Muller A. Development of a model for whole brain learning of physiology. Advances in Physiology Education. 2011;35(4):421-426. DOI: 10.1152/advan.00007.2011. PMID: 22139781

[25] Nageswari KS, Malhotra AS, Kapoor N, Kaur G. Pedagogical effectiveness of innovative teaching methods initiated at the Department of Physiology, Government Medical College, Chandigarh. Advances in Physiology Education. 2004;28(1-4):51-58. DOI: 10.1152/advan.00013.2003. PMID: 15149960

[26] Sadhasivam J, BabuKalivaradhan R. MOOC: A framework for learners using learning style. International Education and Research Journal. 2017;3(2).:21-24. ISSN 2454-9916

[27] Reeves T. How do you know they are learning? The importance of alignment in higher education. International Journal of Learning Technology. 2006;2, 294-309. DOI:10.1504/IJLT.2006.011336

[28] Anderson LW, Krathwohl DR, Airasian PW, Cruikshank KA, Mayer RE, Pintrich PR, Raths J, Wittrock MC. A Taxonomy for Learning, Teaching, and Assessing: A Revision of Bloom's Taxonomy of Educational Objectives. New York. 2001. ISBN: 080131903X

[29] Adams NE. Bloom's taxonomy of cognitive learning objectives. Journal of the Medical Library Association. 2015;103(3):152-153. DOI: 10.3163/1536-5050.103.3.010. PMID: 26213509; PMCID: PMC4511057

[30] Cheung JJH, Kulasegaram KM, Woods NN, Brydges R. Why Content and

Cognition Matter: Integrating Conceptual Knowledge to Support Simulation-Based Procedural Skills Transfer. Journal of General Internal Medicine. 2019;34(6):969-977. DOI: 10.1007/s11606-019-04959-y. PMID: 30937667; PMCID: PMC6544739

[31] Sperber M. How undergraduate education became college lite – and a personal apology. In: Hersh RH, Merrow J, editors. Declining by Degrees: Higher Education at Risk. New York. Palgrave Macmillan, 2005. p.131-143. ISBN 1403969213

[32] Snow R. Aptitude, instruction and individual development. International Journal of Educational Research. 1989;13:869-881. DOI:10.1016/0883-0355(89)90070-0

[33] Napoli AR, Raymond LA. How reliable are our assessment data?: a comparison of the reliability of data produced in graded and un-graded conditions. Research in Higher Education. 2004;45(8): 921-929

[34] Tanner KD. Structure matters: twenty-one teaching strategies to promote student engagement and cultivate classroom equity. CBE—Life Sciences Education. 2013;12(3):322-31. DOI: 10.1187/cbe.13-06-0115. PMID: 24006379; PMCID: PMC3762997

[35] Goodman BE, Barker MK, Cooke JE. Best practices in active and student-centered learning in physiology classes. Advances in Physiology Education. 2018;42(3):417-423. DOI: 10.1152/advan.00064.2018. PMID: 29972063

[36] Boyle E, Connolly TM, Hainey T. The role of psychology in understanding the impact of computer games. Entertainment Computing. 2011;2(2):69-74. DOI:10.1016/j.entcom.2010.12.002.

[37] Collins S, Hewer I. The impact of the Bologna process on nursing higher education in Europe: A review. International Journal of Nursing Studies. 2014;51:150-156. DOI: doi.org/10.1016/j.ijnurstu.2013.07.005

[38] Allen D, Tanner K. Infusing active learning into the large-enrollment biology class: seven strategies, from the simple to complex. Cell Biology Education 2005;4(4):262-268. DOI:10.1187/cbe.05-08-0113

[39] Wilke RR. The effect of active learning on student characteristics in a human physiology course for nonmajors. Advances in Physiology Education. 2003;27:207-223. DOI:10.1152/advan.00003.2002

[40] Li MC, Tsai CC. Game-based learning in science education: A review of relevant research. Journal of Science Education and Technology. 2013;22(6): 877-898

[41] Shaffer DW. Epistemic games. Innovate: Journal of Online Education. 2005; 1(6) Article 2. Available at: https://nsuworks.nova.edu/innovate/vol1/iss6/2

[42] Plass JL, Homer BD, Kinzer CK. Foundations of Game-Based Learning, Educational Psychologist. 2015;50(4): 258-283, DOI: 10.1080/00461520.2015.1122533

[43] Karagiorgas DN, Niemann S. Gamification and Game-Based Learning. Journal of Educational Technology Systems. 2017;45(4):499-519. DOI:10.1177/0047239516665105

[44] Ritterfeld U, Cody M, Vorderer P. Serious Games-Mechanisms and Effects. New Yourk. Routledge-Taylor&Francis Group; 2009. 552 DOI:10.1177/1359105306061185

[45] Abdulmajed H, Park YS, Tekian A. (2015) Assessment of educational games for health professions: A systematic review of trends and outcomes, Medical Teacher. 2015;37(sup1):S27-S32, DOI: 10.3109/0142159X.2015.1006609

[46] Luchi KCG, Cardozo LT, Marcondes FK. Increased learning by using board game on muscular system physiology compared with guided study. Advances in Physiology Education. 2019;43(2):149-154. DOI:10.1152/advan.00165.2018. PMID: 30933536.

[47] Gibson V, Douglas M. Criticality: The experience of developing an interactive educational tool based on board games. Nurse Education Today. 2013;33(12):1612-1616. DOI:10.1016/j.nedt.2013.01.022

[48] Lickiewicz J, Hughes P, Makara-Studzińska M. The use of board games in healthcare teaching. Nursing Problems. 2020;28(2):71-74. DOI:10.5114/ppiel.2020.98766

[49] Sharma, R. Computer assisted learning-A study. Journal of Advanced Research in Education and Technology (IJARET). 2017; 4(2), 102-105.

[50] Gunawardhana P. Introduction to Computer-Aided Learning. Global Journal of Computer Science and Technology. 2020;20:34-38. DOI:10.34257/GJCSTGVOL20IS5PG35.

[51] Barbara J. Measuring user experience in multiplayer board games. Games and Culture. 2017;12(7-8), 623-649. DOI:10.1177/1555412015593419

[52] Gauthier A, Kato PM, Bul KCM, Dunwell I, Walker-Clarke A, Lameras P. Board Games for Health: A Systematic Literature Review and Meta-Analysis.

Games for Health Journal. 2019;8(2): 85-100. DOI: 10.1089/g4h.2018.0017

[53] Deterding S, Dixon D, Khaled R, Nacke L. From game design elements to gamefulness: defining gamification. In: Proceedings of the 15th international academic MindTrek conference: Envisioning future media environments. ACM: 2011. p. 9-15

[54] Amir B, Ralph P. Proposing a theory of gamification effectiveness. Systems Research. 2014;3(1): 60- 95.

[55] Lee JJ, Hammer J. Gamification in Education: What, How, Why Bother? Definitions and uses. Exchange Organizational Behavior Teaching Journal. 2011;15(2):1-5

[56] Deterding, S. Gamification: Designing for motivation. Interactions. 2012;19(4):14-17. DOI: 10.1145/2212877.2212883

[57] Mekler EDE, Brühlmann F, Opwis K, Tuch AN. 2013. Disassembling Gamification: The Effects of Points and Meaning on User Motivation and Performance. In: CHI 2013 Extended Abstracts on Human Factors in Computing Systems. New York. ACM Press. 2013; p. 1137-1142

[58] Kapp KM. Gamification Designs for Instruction. In: Reigeluth CM, Beatty BJ, Myers RD, editors. Instructional Design Theories and Models: The Learner-Centered Paradigm of Education. Vol. IV. New York: Routledge;2016

[59] Chan CKY. Laboratory learning. In: Encyclopedia of the Sciences of Learning, edited by Seel N. M. Boston, MA: Springer; 2012

[60] Flint, S., & Stewart, T. Food microbiology – design and testing of a

virtual laboratory exercise. Journal of Food Science Education, 2010. 9(4): 84-89.

[61] Bell JT, Fogler HS. Virtual laboratory accidents designed to increase safety awareness. ASEE Annual Conference Proceedings. North Carolina; 1999

[62] Zhang X, Al-Mekhled D, Choate J. Are virtual physiology laboratories effective for student learning? A systematic review. Advances in Physiology Education. 2021;45(3):467-480. DOI: 10.1152/advan.00016.2021. PMID: 34142876

[63] Lewis DI. The pedagogical benefits and pitfalls of virtual tools for teaching and learning laboratory practices in the Biological Sciences. University of Leeds. 2014;1-27

[64] Dobson JL. Learning style preferences and course performance in an undergraduate physiology class. Advances in Physiology Education. 2009;33(4):308-314. DOI: 10.1152/advan.00048.2009. PMID: 19948680.

[65] Gibbons NJ, Evans C, Payne A, Shah K, Griffin DK. Computer Simulations Improve University Instructional Laboratories. Cell Biology Education. 2004;3(4): 263-269.

[66] Sancho JC, Barker KJ, Kerbyson DJ, Davis K. Quantifying the Potential Benefit of Overlapping Communication and Computation in Large-Scale Scientific Applications.In: Proceedings of the 2006 ACM/IEEE Conference on Supercomputing; 2006. p. 17-17, DOI: 10.1109/SC.2006.51

[67] Achuthan, K., Francis, S.P. & Diwakar, S. Augmented reflective learning and knowledge retention perceived among students in classrooms involving virtual laboratories. Education and Information Technologies. 2017;22:2825-2855. DOI:10.1007/s10639-017-9626-x

[68] Macaulay, JO, Van Damme MP, Walker KZ. The use of contextual learning to teach biochemistry to dietetic students. Biochemistry and Molecular Biology Education. 2009;37(3):137-142.

[69] Odenweller CM, Hsu CT, Sipe E, Layshock JP, Varyani S, Rosian RL, DiCarlo, S. Laboratory exercise using "virtual rats" to teach endocrine physiology. Advances in Physiology Education. 1997;18(1):S24-S40. DOI: 10.1152/advances.1997.273.6.S24

[70] Hsu CT, Bailey CM, DiCarlo SE. "Virtual rat": a tool for understanding hormonal regulation of gastrointestinal function. Advances in Physiology Education. 1999;21(1):S23-S38. DOI: 10.1152/advances.1999.276.6.S23.

[71] Brás I, Silva ME, Nóbrega C, Albuquerque C. Virtual laboratories in Polythecnic of Viseu – VLAB: Sciencies & Enginneering Teaching Innovation. In: Proceedings of the CISPEE 4th International Conference of the Portuguese Society for Engineering Education (CISPEE 2021) 21-23 Junho 2021, Instituto Superior Técnico, Lisbon, Portugal, p40

Chapter 12

Taxon-Specific Pair Bonding in Gibbons (Hylobatidae)

Thomas Geissmann, Simone Rosenkranz-Weck,

Judith J.G.M. Van Der Loo and Mathias Orgeldinger

Abstract

This study provides the first statistically significant evidence that the mechanisms of how pair bonds are created or maintained differ between gibbon taxa. We examine the pair bond in captive pairs of three genera of gibbons (Hylobatidae): siamangs (*Symphalangus*, N = 17 pairs), crested gibbons (*Nomascus*, N = 7 pairs), and pileated gibbons (*Hylobates pileatus*, N = 9 pairs). In the first part of this study, we determine three generally-accepted indicators of pair-bond strength (mutual grooming, behavioral synchronization and partner distance). A pairwise comparison of our samples reveals a difference in relative partner distances between siamangs and pileated gibbons, suggesting that siamangs may have a stronger pair bond than pileated gibbons. No difference among the three taxa was found in other variables believed to indicate pair bond strength. In the second part we examine the amount of partner-directed grooming in each sex. In siamangs, males invest significantly more into pair bonds than females, whereas the opposite is true in crested and pileated gibbons. Our results for siamangs correspond to predictions derived from the 'mate-defense hypothesis' for the evolution of pair bonds, whereas our results for crested gibbons and pileated gibbons correspond to predictions derived from the 'male-services hypothesis'.

Keywords: social structure, pair bond, *Symphalangus*, *Nomascus*, *Hylobates*, sex-specific investment, Hylobatidae

1. Introduction

Whereas the genera of great apes are known to differ strongly among each other in their social structure, the small apes or gibbons clearly are a more uniform group [1–3]. Distributed in Asian rain forests, its members typically live in socially monogamous, unimale unifemale, territorial groups [4, 5], although some flexibility in group composition and sexual behavior occurs [6–8]. Non-monogamous (extra-pair) matings and groups with multiple adult males and multiple adult females occasionally occur in gibbons [7, 9–15].

It has repeatedly been suggested, however, that gibbon taxa may differ in subtle details of their social organization [16]:

Wild family groups of Malayan siamangs (*Symphalangus syndactylus*) appear to be more tightly knit than those of white-handed gibbons (*Hylobates lar*), with siamang intra-group distances being shorter and intra-group communicatory signals being fewer or less conspicuous to observers, and paternal infant-carrying only occurring in siamangs [17–21]. A greater heterosexual cohesion in pair bonds of siamangs, as compared to white-handed gibbons, was also found in a field study in Sumatra [22], but differences in paternal investment appear to be less clear-cut. Paternal infant-carrying appears to be absent in some wild and many captive siamang groups and varies dramatically among males of the same population [10, 23–25], while it may occasionally occur in other gibbon taxa, at least in captive groups [23, 26].

Several reports suggest that the black-cheeked species of the crested gibbons (genus *Nomascus*) differ from other hylobatids in their social organization by more often forming bi-female groups [27–33]. This may not appear to apply to light-cheeked crested gibbon species [34, 35], but see [36].

Recent studies on gibbon calls documented that the various taxa strongly differ in how they present their long and loud morning song bouts [37–40]. In some taxa, mated pairs produce duet song bouts but usually no solo songs (genera *Hoolock*, *Nomascus* and *Symphalangus*), others produce sex-specific solo songs in addition to duets (*Hylobates agilis*, *H. lar*, *H. muelleri*, *H. pileatus*), and others yet produce sex-specific solo song bouts only (*H. klossii*, *H. moloch*). In all members of the genus *Nomascus* and most species of the genus *Hylobates*, for instance, most of the singing is produced by males, whereas in *H. moloch*, males sing rarely and most songs are produced by females. This pronounced diversity of sex-specific investment in resource defense provides indirect evidence for taxon-specific differences in social organization, and, possibly, in previously unrecognized factors of ecological adaptation or inter-specific competition.

Moreover, duets strongly differ in their complexity among taxa, with the most complex ones being uttered by siamangs (*S. syndactylus*) [41, 42]. These differences in song organization also strongly suggest differences in social organization. Because duet song bouts are believed to serve, among other things, to strengthen or advertise pair bonds, duetting and non-duetting gibbon species should differ either in their pair bond strength or in how the pair bond strength is achieved [43, 44].

Although the reports cited above suggest that some gibbon taxa may differ in social organization, very little quantitative evidence for such species-specific differences in the social structure are currently available. Previous comparisons have been limited to sample sizes of 2–3 pairs per genus [17, 19, 22, 23], thus precluding statistical testing. Palombit [3] correctly identified a great need for detailed data on more hylobatid pair bonds, so that we may identify consistent social patterns in light of intra-specific variation.

Early reviews on monogamy found shared behavioral traits in monogamous primates and suggested that the males generally initiate grooming and groom females more often than the reverse situation occurs [45]. In socially monogamous pairs, pair partners usually maintain close spatial association and often perform spectacular, well-coordinated, pair-specific display behavior. This does not necessarily imply, however, that the sexes share mutual socioreproductive interests [46]. Shared interests may be not be required for the evolution of social monogamy, and pair formation does not require an absence of sexual conflict, or symmetric costs and benefits for males and females.

Several of the hypotheses explaining the evolution and maintenance of social monogamy in mammals make predictions regarding female and male contributions to the pair bond [47].

1. According to the 'resource-defense hypothesis', both a male and a female benefit from pair bonding to defend resources together [48]. In this case, a male and a female should be equally interested in maintaining proximity and affiliation with a pair mate and defending their territory.

2. According to the 'mate-defense hypothesis', a male should bond with a female when either the spatial distribution of females or the temporal distribution of fertile periods makes it difficult for males to defend access to more than one female at a time [49]. In this case, a male should be more interested in maintaining proximity and affiliation with the partner.

3. According to the 'male-services hypothesis', a female benefits from bonding with a male when the male provides important services such as territorial or anti-predator defense, infant care, or protection from infanticide by competing males [48, 50–52]. In this case, a female should to be more interested in maintaining proximity and affiliation with the partner while the male should provide some significant services.

The goal of our study was to answer the following two questions: (1) Do gibbon taxa differ in the strength of their pair bonds? (2) Do gibbon taxa differ in the way pair bonds are created and maintained?

We present the first comparative and quantitative study on differences of the pair bond among multiple gibbon taxa. We have collected observational data on several captive groups of siamangs (genus *Symphalangus*), three species of the crested gibbons (genus *Nomascus*), and the pileated gibbon (*Hylobates pileatus*) as a representative of the dwarf gibbons (genus *Hylobates*). Our study will focus, therefore, on a comparison of these three genera. Photographs of three of the species we studied are shown in **Figure 1**. In addition, a compilation of previously-published data also permits us to make a limited comparison with other gibbons of the genus *Hylobates*.

In order to estimate pair bond strength, we quantified the following three generally-accepted indicators of pair bond strength (behavioral synchronization, relative distance between mates, and amount of partner directed grooming) following [44, 53].

In order to gain insight in the pair bonding mechanism, we examined which sex invests more in the pair bond by measuring the amount of grooming directed at the respective partner.

Although allogrooming *per se* may serve hygienic, social, communicatory, stress relief or thermal functions [54–59], these functions may be influenced by a species's social organization. For social systems with stable pair structures, allogrooming has been proposed to serve a pair-bonding function [45, 60, 61] and to reflect the investment into a pair bond [62, 63] and, therefore, the ultimate costs and benefits which partners can expect from a relationship [64]. Thus, sex-specific differences in partner-directed allogrooming indicate – on a proximate level – ultimate sex-specific strategies.
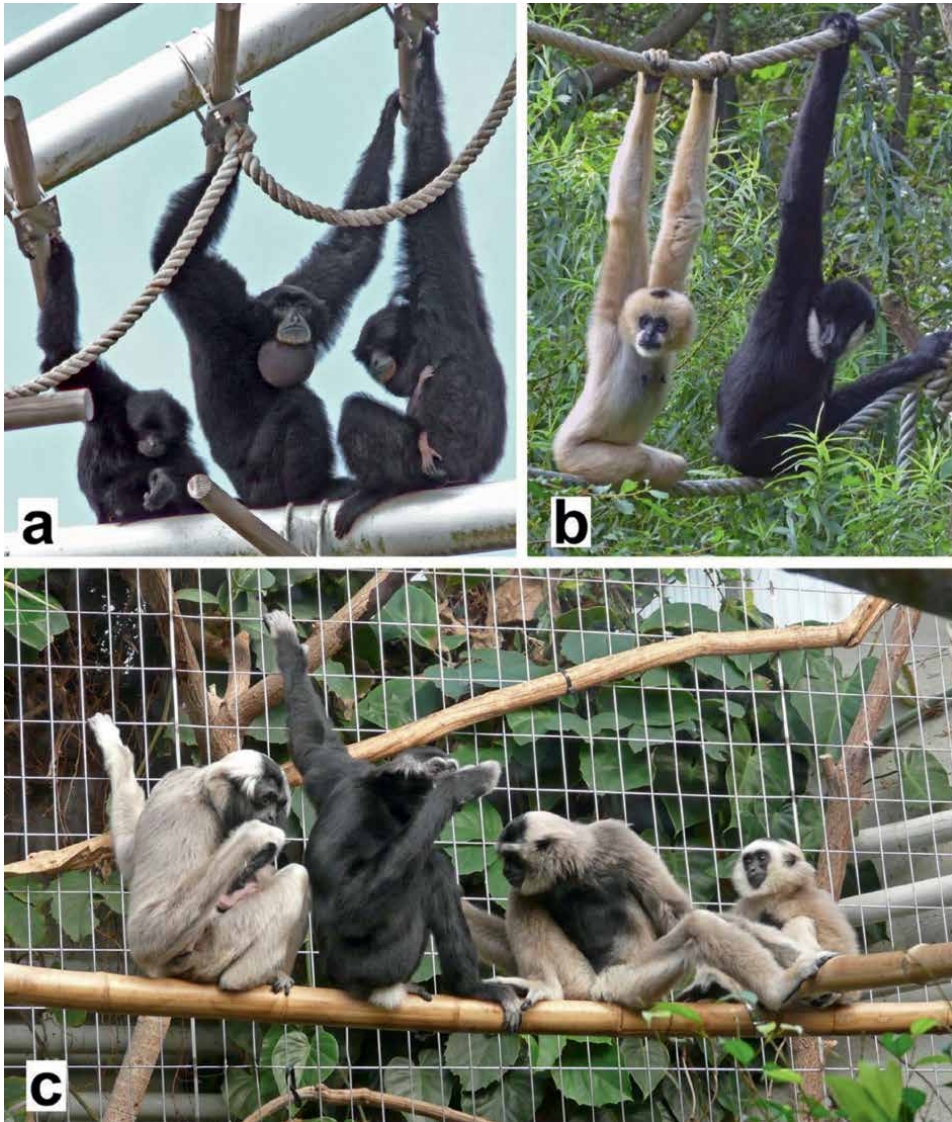
Figure 1.
Three of the gibbon species that were observed during this study. (a) Siamang (Symphalangus syndactylus), family group, showing from left to right: juvenile, adult male, and adult female carrying an infant. Siamangs are of mostly blackish fur coloration. Notice the half-inflated throat sacs, which play a role in siamang territorial vocalizations and can be inflated to about the size of the animals' head. (b) Northern White-cheeked Crested Gibbon (Nomascus leucogenys) pair, showing from left to right: adult female, and adult male. Adult male and female differ markedly in their fur coloration. Females are mostly yellowish, and males are blackish. (c) Pileated Gibbon (Hylobates pileatus) family group, showing from left to right: adult female carrying a neonate infant, adult male, subadult male, and juvenile male. Adult male and female of this species also differ markedly in their fur coloration. Females are pale grey or fawn-buff with black on crown, cheeks and chest, while males are blackish with white facial border, corona, digits, and genital tuft. Photographs by Thomas Geissmann.

2. Methods

Our data collection methods have previously been described [44, 53]. Siamang (*Symphalangus syndactylus*) data were collected in a consistent form by one of us

(M.O.) between April 1985 and March 1993. A total of 17 siamang groups were observed at the following zoos: Antwerp (An), Belgium, Branféré (Br1, Br2, Br3), France, Budapest (Bu), Hungary, Berlin Zoo (Be), Dortmund (Do), Dresden (Dr1, Dr2), Duisburg (Du), Frankfurt (Fr), Krefeld (Kr1, Kr2), Munich (Mn), Germany, Studen (St), Zurich (Zh), Switzerland and Washington (Wa), U.S.A., with group size ranging from two to six animals.

Crested gibbon data were collected in the same way by S.R.-W. between August and October 2001. A total of seven crested gibbon groups (*Nomascus*) were observed at the following zoos: Duisburg (Du), Eberswalde (Eb), Osnabrück (Os1, Os2), Germany, and Mulhouse (Mu1, Mu2, Mu3), France, with group sizes ranging from two to five animals. Three crested gibbon species are represented in our sample, including the Northern White-cheeked Crested Gibbon (*N. leucogenys*): Du, Mu1 and Os2; the Southern White-cheeked Crested Gibbon (*N. siki*): Mu2; and the Southern Yellow-cheeked Crested Gibbon (*N. gabriellae*): Eb, Mu3 and Os1. The gibbon classification used here follows [65].

Data for Pileated Gibbons (*Hylobates pileatus*) were collected in the same way by J.v.d.L. and K.N between February and May 2007. A total of nine groups were observed at the following zoos: Phnom Tamao, Cambodia (PT1–7), and Zurich, Switzerland (Zu1, Zu2), with group size ranging from two to five animals.

In order to assure comparability of data collected by the observers M.O., S.R., J.v.d.L. and K.N., dual observations were carried out on 31 July 2001 and on 13 February 2007, respectively, until consistent values of inter-observer concordance were obtained [66].

At each zoo, observation time for each sampling method was distributed evenly across the animals' activity period between 0700 and 1800 h (until 1700 h during the winter months, and between 0800 and 1800 h for crested gibbon groups Du, Eb, Mu, Os2).

We used focal animal sampling with the continuous recording rule [66–69] to collect information on the frequency and duration of grooming behavior between mates. Focal animals were changed every 20 min. Each of 11 siamang pairs was observed for 80 h, except for pairs Mu (50 h) and Du (90 h), and each crested and pileated gibbon pair for 35 h. Grooming occurred in discrete sessions that could be counted. We allowed an interval of up to 10 seconds between bouts of grooming before we counted them as two sessions, rather than one.

We used scan sampling to record behavioral synchronization of activities between mates. We defined 11 behavioral categories: socio-positive behavior (including allogrooming, embracing) and infant care, play, agonistic, territorial, sexual, comfort-related, feeding and food-related behavior, observe, rest and sleep, excretion, and locomotion. Scans were made every 1 min (or every 2 min in siamang groups Dr1, Kr1, Kr2, St). Siamang pairs were scanned for synchronization of behavioral categories during blocks of 5 or 10 min, separated by intervals of 20 min. Crested and pileated gibbon pairs were scanned for synchronization in parallel to the focal animal observations of grooming behavior. Each of 13 siamangs pairs was observed for 20 h, except pairs Zu (15 h), Be and Fr (30 h), and Du (40 h). Each crested and pileated gibbon pair was observed for 35 h. The occurrence of synchronized behavior between pair-mates is expressed in % of the total number of scans for a given pair.

We also used scan sampling to record the distance between mates. Distances were recorded to an accuracy of 0.5 m. If the individuals were closer to each other than 0.5 m, we recorded distance according to the following definitions: 0.3 m: shortest distance without body contact, 0.2 m: body contact through extremities, 0 m: body contact through trunk. Siamang pairs were scanned during blocks of 10 min,

separated by intervals of at least 10 min. During each scan sampling block, distance was recorded every 10 s. Crested and pileated gibbon pairs were scanned for the distance between mates every 1 min, and scans were carried out in parallel to the focal animal observations of grooming behavior. Each of 17 siamangs pairs was observed for 10 h, except pairs BrA, Bu, DrA (20 h), Be, Du, KrA (30 h), and Fr (210 h). Each crested and pileated gibbon pair was observed for 35 h.

The size of the enclosure varied between zoos (some gibbon groups were held in cages, others on islands). In small cages, the cage walls set outer limits to the inter-individual distances. Because small cages may have forced our pairs into closer proximity than bigger enclosures, we did not directly use absolute inter-individual distances in our comparisons. Instead, we calculated the relative distance (%) between mates, i.e. the inter-individual distance relative to the maximal possible distance in the pair's given environment (cage or island). This method was described by [44]. In order to test whether cage size had an influence on pair bonding behavior, we used the maximal possible distance in the pair's given environment as an indicator of cage size. In siamangs, our largest sample, this value ranged from 5.7 m in the smallest cage to 43.5 m on the largest island. We arbitrarily defined cages with values of less than 10 m as "small enclosures", the others as "large enclosures".

In addition to determining relative distance, we used scan sampling to estimate the time pair partners spent in each of the following distance classes: 1: body contact or distance of less than 0.3 m, 2: 0.3–1 m, 3: >1 m–3 m, 4: >3 m.

For comparison of our data on partner-directed behavior with literature data, we used male and female proportions of these behavioral variables, where male and female proportions complement each other to 100%. Proportions should be independent of the observation method and permit comparison of data from different observers.

One-sample sign test tests were used to compare classes of sex-specific grooming proportions within genera. For comparison of data among three genera, we used Kruskal-Wallis tests with Dunn's *post hoc* tests [70]. In order to compare data between *H. pileatus* and *H. lar* (i.e. after inclusion of data compiled from the literature), we used the Mann–Whitney *U* tests [71]. All tests were two-tailed, and the null hypothesis was rejected at P = 0.05. Statistical were calculated using the software StatView 5.0.1 and SPSS 17.0 on a Macintosh G4 computer.

3. Results

3.1 Strength of pair bonds

3.1.1 Synchronization of behavioral variables

The average degree of behavioral synchronization across 11 behavioral variables is shown in **Figure 2**. Values range from 15.5% to 63.9% in siamangs, from 8.0% to 38.7% in crested gibbons, and from 19.2% and 42.7%. As shown in **Table 1**, however, the overall degree of behavioral synchronization does not differ significantly between the genera (Kruskal-Wallis test, P = 0.186).

3.1.2 Relative partner-distance

Average relative partner distances and time proportions spent in four distance classes for each study group are listed in **Table 2**. Considerable differences were found
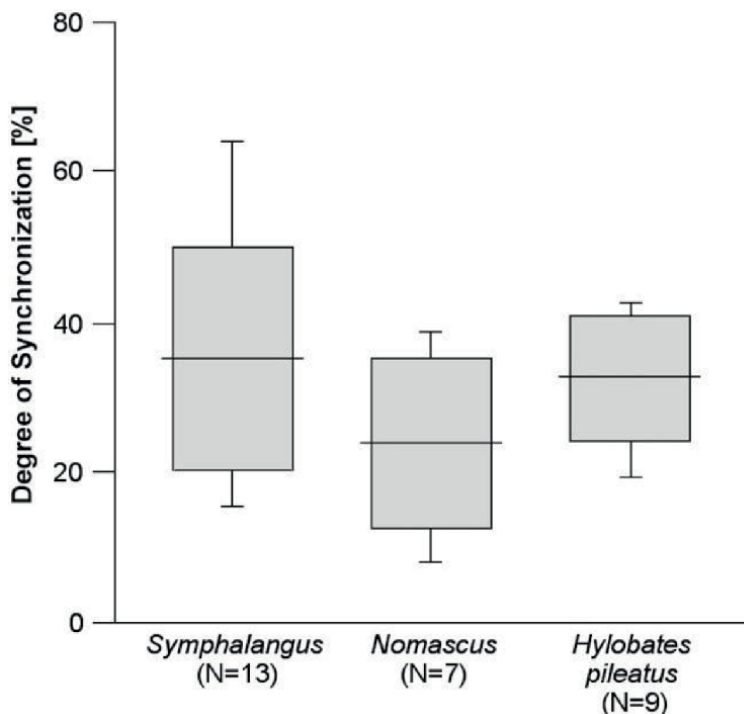
Figure 2.
Comparison of the average degree of behavioral synchronization between siamangs (Symphalangus, N = 13 pairs), crested gibbons (Nomascus, N = 7 pairs), and pileated gibbons (Hylobates pileatus, N = 9 pairs). Box plots show mean values, standard deviations and minimum and maximum values. The difference between the genera is not statistically significant (Kruskal-Wallis test, P > 0.05, see text).

	Taxon			Kruskal-Wallis test (p)
	Symphalangus	*Nomascus*	*Hylobates pileatus*	
Taxon mean	35.02 ± 15.39 (N = 14)	23.73 ± 11.30 (N = 7)	32.69 ± 7.95 (N = 9)	0.186

Table 1.
Average degree of synchronization [% ± standerd deviation] across 11 behavioral variables for siamangs (Symphalangus syndactylus), crested gibbons (Nomascus spp.), and pileated gibbons (Hylobates pileatus). Abbreviation: p = error probability.

among pairs. Time spent in distance class 1, for instance, varies from 0.3% to 49.7% in siamangs, from 5.6% to 32.3% in crested gibbons, and from 0.0% to 20.5% in pileated gibbons. Similarly, time spent in distance class 4 varies from 1.3% to 61.2% in siamangs, from 14.1% to 47.4% in crested gibbons, and from 31.6–84% in pileated gibbons. The time gibbon pairs spent in each of the four partner distance classes are shown in **Figure 3**. The three taxa do not differ significantly among each other in the time groups spent in any of the four partner distance classes (Kruskal-Wallis tests, P > 0.05), except for time spent in distance class 4 (P = 0.014). Dunn *post-hoc* tests revealed that pileated gibbon pairs spent more time in distance class 4 than siamangs (P < 0.02). Moreover, the difference in distance class 2 is close to significance (P = 0.051).

Group	Relative distance	Distance classes [%]			
	[%]	1	2	3	4
(a) Siamangs					
Antwerp	32.80	11.90	14.00	50.00	24.10
Berlin Zoo	29.80	13.70	10.00	40.80	35.50
Branféré 1	14.50	5.40	19.50	31.20	43.90
Branféré 2	12.10	10.30	29.70	23.90	36.10
Branféré 3	18.30	1.80	17.00	20.00	61.20
Budapest	29.30	10.70	21.10	34.10	34.10
Dortmund	10.10	29.50	34.80	16.60	19.10
Dresden 1	29.00	12.50	18.10	67.50	1.90
Dresden 2	24.00	12.90	31.10	54.70	1.30
Duisburg	29.10	12.30	12.20	48.70	26.80
Frankfurt	40.40	3.30	12.60	62.30	21.80
Krefeld 1	30.90	3.50	15.10	37.60	43.80
Krefeld 2	35.90	0.30	7.40	38.60	53.70
Munich	31.20	24.90	13.80	16.20	45.10
Studen	11.50	49.70	22.40	19.30	8.60
Washington	26.50	20.50	14.90	21.40	43.20
Zurich	36.10	1.30	17.80	62.30	18.60
Mean	25.97	13.21	18.32	37.95	30.52
(b) Crested gibbons					
Duisburg	33.68	5.70	39.19	41.04	14.07
Eberswalde	12.12	32.30	17.01	15.68	35.01
Mulhouse 1	30.40	7.65	19.52	25.40	47.42
Mulhouse 2	23.31	23.68	14.33	15.85	46.14
Mulhouse 3	21.12	30.73	14.79	17.03	37.45
Osnabrück 1	21.99	17.80	16.22	24.09	41.89
Osnabrück 2	21.63	5.64	30.05	27.01	37.30
Mean	23.47	17.64	21.59	23.73	37.04
(c) Pileated gibbons					
Phnom Tamao 1	28.77	7.30	14.20	28.20	50.30
Phnom Tamao 2	7.28	10.70	17.70	17.70	54.40
Phnom Tamao 3	41.99	0.00	3.90	11.30	84.80
Phnom Tamao 4	23.18	20.50	6.00	28.90	44.60
Phnom Tamao 5	24.58	11.30	16.70	23.60	48.40
Phnom Tamao 6	12.82	13.80	11.20	26.40	48.50
Phnom Tamao 7	23.13	5.50	9.70	53.20	31.60
Zurich 1	18.29	14.90	20.10	24.70	40.40
Zurich 2	34.83	0.90	7.40	17.20	47.50
Mean	23.47	9.43	11.88	25.69	50.06

Table 2.
Average relative partner distances and time proportions spent in four distance classes: (a) siamangs (Symphalangus syndactylus, N = 17 groups), (b) crested gibbons (Nomascus spp., N = 7 groups), (c) pileated gibbons (Hylobates pileatus, N = 9 groups).
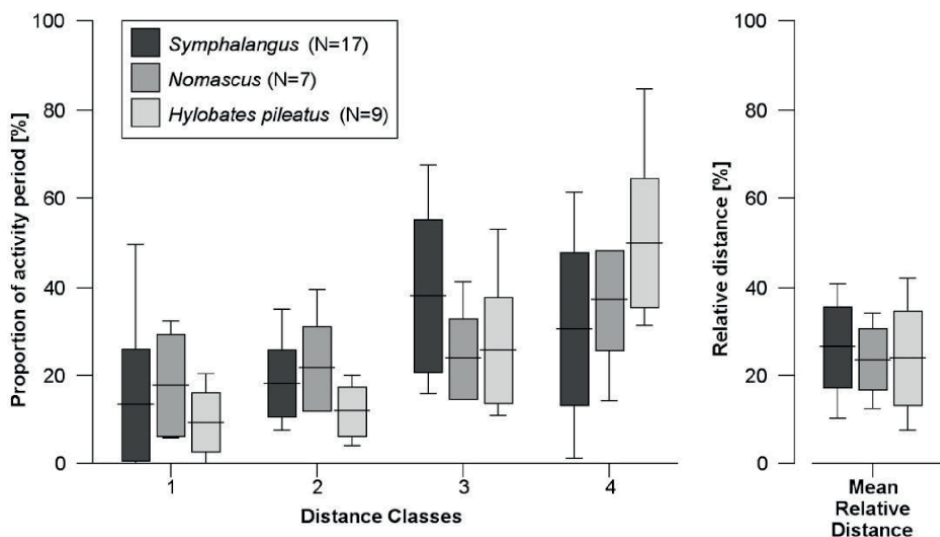
Figure 3.
Time proportion spent in 4 distance classes (left) and of the mean relative partner distances (right) in siamangs (Symphalangus, N = 17 pairs), crested gibbons (Nomascus, N = 7 pairs), and pileated gibbons (Hylobates pileatus, N = 9 pairs). Box plots show mean values, standard deviations and minimum and maximum values. In a comparison between the genera (Kruskal-Wallis tests), only one of the five variables (distance class 4) are statistically significant (P < 0.05, see text).

The relative distance between pair partners is also shown in **Figure 3**. The three taxa do not differ in this variable (Kruskal-Wallis test, $P > 0.05$).

3.1.3 Allogrooming

The number of grooming sessions/hour (average of male and female) varies from 0.0 to 3.9 in siamangs (*Symphalangus*, N = 12 pairs), from 0.5 to 2.0 in crested gibbons (*Nomascus*, N = 7 pairs), and from 0.0 to 2.1 in pileated gibbons. The difference is not statistically significant (Kruskal-Wallis test, $P > 0.05$). The average duration of grooming sessions varies from 0 s to 76.0 s in siamangs, from 50.5 s to 132.1 s in crested gibbons, and from 0 s to 101.0 s in pileated gibbons. This difference is not statistically significant (Kruskal-Wallis test, $P > 0.05$). The proportion of time spent grooming varies from 0% to 66.9% in siamang pairs, from 9.3% to 28.7% in crested gibbon pairs, and from 0% to 57.7% in pileated gibbons. The difference is not statistically significant (Kruskal-Wallis test, $P > 0.05$). As a result, siamang pairs, crested gibbon pairs, and pileated gibbon pairs spend similar amounts of time grooming (**Figure 4**).

3.2 Mechanism of pair bonds

In order to study which sex invested more in maintaining the pair bond, we determined the %-proportion of partner-directed grooming for each adult. Because male and female proportions in a pair complement each other to 100%, the grooming proportion of one sex will suffice to provide the full information. The results are summarized in **Figure 5**.

In these analyses, one pair of siamangs (Kr2) and one pair of pileated gibbons (PT3) had to be excluded because pair partners were not observed to groom each
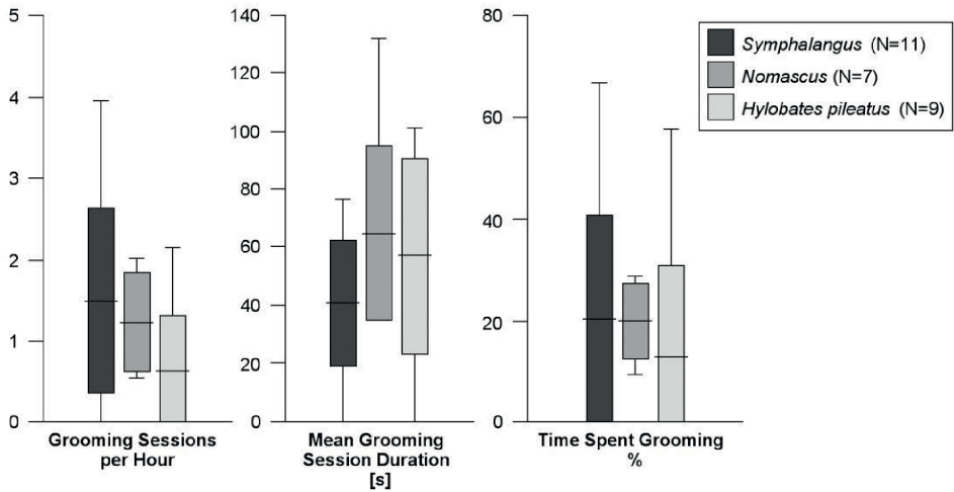
Figure 4.
Average intra-pair grooming frequency per hour, mean duration of grooming sessions, and proportion of time spent grooming in siamangs (Symphalangus, N = 11 pairs), crested gibbons (Nomascus, N = 7 pairs), and pileated gibbons (Hylobates pileatus, N = 9 pairs). Box plots show mean values, standard deviations and minimum and maximum values. In a comparison between the genera (Kruskal-Wallis tests), none of the three variables are statistically significant (P > 0.05, see text).
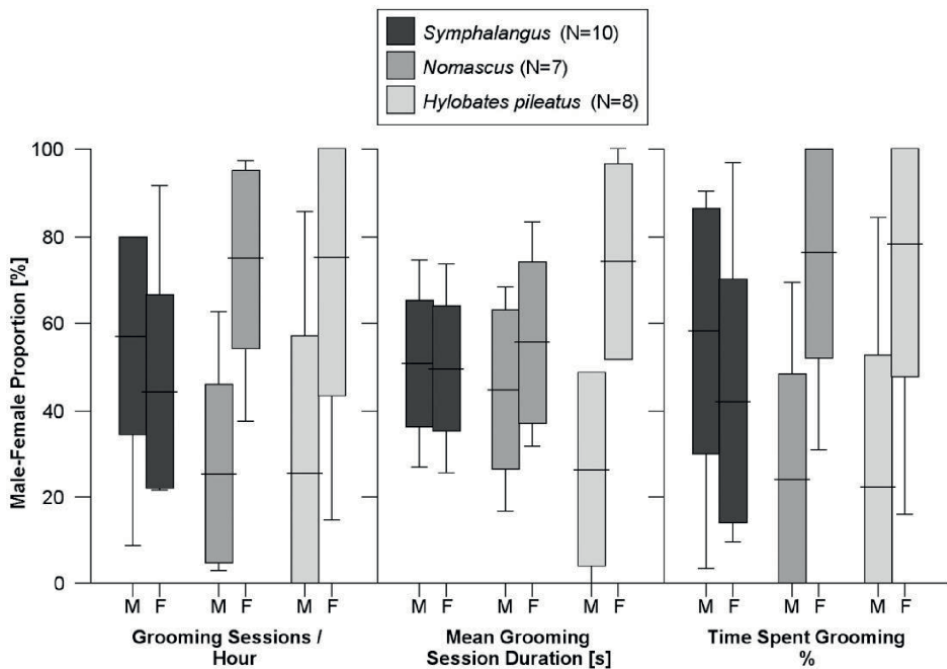
Figure 5.
Average male-female proportions of intra-pair grooming frequency per hour, mean duration of grooming sessions, and time spent grooming in siamangs (Symphalangus, N = 10 pairs), crested gibbons (Nomascus, N = 7 pairs), and pileated gibbons (Hylobates pileatus, N = 8 pairs). Box plots show mean values, standard deviations and minimum and maximum values. In a comparison between the genera (Kruskal-Wallis tests), all three variables are statistically significant (P < 0.05, see text). Abbreviations: M = males, F = females.

other at all and male–female proportions of grooming variables could, therefore, not be calculated. Neither Kr2 nor PT3 were newly formed pairs, and the reason why no grooming occurred among pair partners is unknown.

Male proportions in the number of grooming sessions per hour varied from 8.5% to 78.3% in siamangs, from 2.9% to 62.5% in crested gibbons, and from 0.0% to 85.4% in pileated gibbons. The difference between the genera is statistically significant (Kruskal-Wallis test, P = 0.032). The Dunn *post-hoc* test revealed no significant pair-wise differences, but as a trend, male proportions were higher in siamangs than in pileated gibbons (P < 0.1). Male proportions in grooming session duration varied from 26.7% to 74.6% in siamangs, from 16.6% to 68.2% in crested gibbons, and, and from 0.0% to 48.0% in pileated gibbons. The difference between the genera is statistically significant (Kruskal-Wallis test, P = 0.043), and the Dunn *post-hoc* test revealed that male proportions were higher in siamangs than in pileated gibbons (P < 0.05). Male proportions in the time spent grooming varied from 3.3% to 90.4% in siamangs, from 0.9% to 69.1% in crested gibbons, and from 0.0% to 84.3% in pileated gibbons. The difference between the genera is statistically significant (Kruskal-Wallis test, P = 0.035), and the Dunn *post-hoc* test revealed that male proportions were higher in siamangs than in pileated gibbons (P < 0.05). As a result, siamang males groom partners in longer sessions and spend more time grooming them than pileated gibbon males. Only as a trend, siamang males also tend to groom their partners during more grooming sessions than pileated gibbons.

In addition to the grooming data collected by focal animal sampling, we also collected data on male–female grooming proportions for three additional siamang groups (An, Be, Zu) during the scan sampling observations. Male grooming proportions in these groups amounted to 95.4%, 85.7% and 100%, respectively.

Finally, we compiled data from the pertinent literature on other gibbon groups. If several reports were available on the same group, we used the study with the larger data base. These data are summarized in **Table 3** and also includes members of the dwarf gibbons (*Hylobates*) and hoolock gibbons (*Hoolock*) other that the species observed by us. The sample size for the hoolocks (**Table 3d**), however, comprises only three groups and is too small for statistical analysis. Pairs that did not exhibit partner-directed grooming are also excluded from the analysis. Our resulting sample comprises 76 pairs. For summary statistics, we split male grooming contribution evenly into three classes: (1) 0–33%, (2) >33–66%, (3) >66%. Pairs should be evenly distributed across these classes if male and female contributions were balanced. As shown in **Table 3**, this is not the case in siamangs (N = 28). Most pairs fall into class 3, suggesting that siamang males, as a rule, provide most of the intra-pair grooming. In crested gibbons (N = 22) and dwarf gibbons (N = 26), the situation is exactly reversed. Most pairs fall into class 1, indicating that females provide most of the intra-pair grooming in *Nomascus* and *Hylobates*. The difference from the expected value of 50% is statistically significant for the genera *Nomascus* and *Symphalangus* (One-sample sign test, P = 0.002, and P = 0.013), but not for *Hylobates* (One-sample sign test, P > 0.05). As indicated by the species labels in **Figure 6c**, the distribution appears to differ among species of the genus *Hylobates*. Whereas partner-directed grooming is mainly provided by females in *H. pileatus* (N = 11), the distribution appears to be more randomly distributed in *H. lar* (N = 11). Although the difference between the two species is statistically significant (Mann–Whitney *U* test, P = 0.032), the samples are relatively small and the result should be regarded with caution. If only *H. pileatus* is considered, the difference from the expected value of 50% is still not significant (One-sample sign test, P > 0.05), but the sample is very small in this case (N = 11).

Group	Cap-tive/ wild	Data type	Classes of male grooming proportion [%]			Source
			1	2	3	
(a) Siamangs (*Symphalangus*)						
An	c	f			95.4	ts
Be	c	f			85.7	ts
Br1	c	f	8.5			ts
Br2	c	f			78.3	ts
Br3	c	f			74.1	ts
Bu	c	f	29.5			ts
Do	c	f		60.1		ts
Dr1	c	f			69.7	ts
Dr2	c	f		51.5		ts
Du	c	f		49.2		ts
Fr	c	f	—	—	—	ts
Kr1	c	f			76.7	ts
Kr2	c	f			72.0	ts
Mu	c	f	8.5			ts
St	c	f			78.3	ts
Wa	c	f			74.1	ts
Zh	c	f			100.0	ts
TS1	w	t		60.5		[19]
RS2	w	t			73.7	[19]
Milwaukee	c	f	26.0			[72]
Tulsa	c	f?			88.8	[73]
Berlin	c	f	—	—	—	[74]
Cheyenne, MH 21	c	t			86.3	[75]
Cheyenne, MH 23	c	t	7.0			[75]
Melbourne	c	?		60.8		[76]
Ketambe, CH-CJ	w	f		ca 48.0		[10]
Ketambe, PP-PN	w	f			ca 84.0	[10]
Ketambe, Pm-Pn	w	f		ca 60.0		[10]
Lourosa, pair 1	c	t			88.9	[77]
ICGS	c	t		56.9		[26]
Siamangs, total number of pairs			5	8	15	
(b) Crested gibbons (*Nomascus*)						
Du (*Nle*)	c	f	4.4			ts

(b) Crested gibbons (*Nomascus*)						
Eb (*Nga*)	c	f	24.7			ts
Mu1 (*Nle*)	c	f		62.5		ts
Mu2 (*Nsi*)	c	f	20.6			ts
Mu3 (*Nga*)	c	f	22.1			ts
Os1 (*Nga*)	c	f		38.3		ts
Os2 (*Nle*)	c	f	2.9			ts
Twycross (*Nco + Nle mixed pair*)	c	t	17.7			[78]
Twycross (*Nle*)	c	t	18.0			[78]
Perth, old pair (*Nle*)	c	t		36.4		[79]
Perth, new pair (*Nle*)	c	t		50.0		[79]
Perth, family gr. (*Nle*)	c	t		37.9		[79]
Melbourne (*Nle*)	c	f	19.5			[76]
Besançon (*Nga*)	c	t	6.0			[80]
Mulhouse, group 1 (*Nga*)	c	t	0			[81]
Mulhouse, group 2 (*Nle*)	c	t	—	—	—	[81]
Mulhouse, group 3 (*Nsi*)	c	t	0			[81]
Amsterdam (*Nle*)	c	t	16.0			[82]
Beekse Bergen (*Nle*)	c	t	22.2			[82]
Hannover (*Nle*)	c	t		57.5		[82]
ICGS (*Nle*)	c	t			100	[26]
Lincoln Park (*Nle*)	c	f	0			[83]
San Antonio (*Nle*)	c	?	1.6			[84, 85]
Nomascus gabriellae, total number of pairs			4	1	0	
Nomascus leucogenys, total number of pairs			8	5	1	
Crested gibbons, total number of pairs			15	6	1	
(c) Dwarf gibbons (*Hylobates*)						
Phnom Tamao 1 (*Hpi*)	`c	f		55.7		ts
Phnom Tamao 2 (*Hpi*)	c	f	0			ts
Phnom Tamao 3 (*Hpi*)	c	f	—	—	—	ts
Phnom Tamao 4 (*Hpi*)	c	f	8.1			ts
Phnom Tamao 5 (*Hpi*)	c	f	0			ts
Phnom Tamao 6 (*Hpi*)	c	f			85.4	ts
Phnom Tamao 7 (*Hpi*)	c	f	12.5			ts
Zurich 1 (*Hpi*)	c	f		38.2		ts
Zurich 2 (*Hpi*)	c	f	0			ts

			(1)	(2)	(3)	
(c) Dwarf gibbons (*Hylobates*)						
ICGS (*Hpi*)	c	t			69.6	[26]
Perth, group 6 (*Hpi*)	c	f?	0			[86]
Blackpool (*Hpi*)	c	f	0			[87]
Hylobates pileatus, total number of pairs			7	2	2	
Bronx, New York (*Hla*)	c	t			71.3	[88]
Portland, Oregon (*Hla*)	c	f		45.0		[89]
Berlin (*Hla*)	c	f	25.0			[74]
Besançon (*Hla*)	c	t		53.6		[80]
Melbourne (*Hla*)	c	f	10.8			[76]
Ketambe, AS-AY (*Hla*)	w	f			ca 81.0	[10]
Ketambe, GD-GM (*Hla*)	w	f			93.0	[10]
Khao Yai, Pair A (*Hla*)	w	t		64.3		[13]
Khao Yai, Pair B (*Hla*)	w	t		37.5		[13]
Khao Yai, Pair C (*Hla*)	w	t			71.4	[13]
Khao Yai, Pair T (*Hla*)	w	t	20.0			[90]
Hylobates lar, total number of pairs			3	4	4	
Berlin (*Hmo*)	c	f	—	—	—	[74]
ICGS (*Hmo*)	c	t	0			[26]
Munich (*Hmo*)	c	f		50.7		Average of [91–93]
Perth (*Hmo*)	c	t		50.0		[79]
Hylobates moloch, total number of pairs			1	2	0	
ICGS (*Hag*)	c	t	0			[26]
Dwarf gibbons, total number of pairs			12	8	6	
(d) Hoolock gibbons (*Hoolock*)						
Gibbon Wildlife Sanctuary, Assam, 1 (*Hho*)	w	f	25.0			[94]
Gibbon Wildlife Sanctuary, Assam, 2 (*Hho*)	w	f		50.0		[94]
Gibbon Wildlife Sanctuary, Assam, 3 (*Hho*)	w	f		41.5		[94]
Hoolock gibbons, total number of pairs			1	2	0	

Table 3.
Male contributions (%) to intra-pair grooming in gibbons. Classes of male grooming proportion are defined as (1) 0–33%, (2) >33–66% and (3) >66%. Abbreviations: Hoolock: Hho = H. hoolock; Hylobates: Hag = H. agilis, Hla = H. lar, Hmo = H. moloch, Hpi = H. pileatus. Nomascus: Nco = N. concolor, Nga = N. gabriellae, Nle = N. leucogenys, Nsi = N. siki. Captive/wild: c = captive, w = wild. Data type: f = frequency, t = time. Grooming: — = no partner-directed grooming observed. Source: ts = this study.

Especially in siamangs and crested gibbons, the unilateral distribution of male grooming proportion is surprisingly consistent. We wondered whether there was something about the pairs which do not exhibit consistent results. Of the gibbons we observed, only the siamang sample was large enough to test several potential influences statistically. In the 16 siamang pairs that showed grooming, "Having infants" had no influence on the proportion of male grooming (Mann–Whitney U test, 16 pairs, U = 15.5, P > 0.05). However, "Having a family group" did: Pairs without a family showed a smaller proportion of male grooming than pairs with offspring in the family (Mann–Whitney U test, 16 pairs, U = 11.0, P = 0.03). We also wondered whether there were any differences between pairs kept in smaller cages and pairs kept in bigger enclosures. In order to study the effect of cage size on the male proportion of pair-grooming in siamang pairs, we used the maximal possible distance in the pair's given environment as an indicator of cage size. We compared male grooming proportion between siamangs kept in small enclosures (N = 9 groups) to siamangs kept in large enclosures (N = 7 groups). The difference was not statistically significant (Mann–Whitney U test, P > 0.05). The correlation between cage size and male grooming proportion was also not significant (Spearman rank correlation, Rho = −0.165, P > 0.05).

Results for the dwarf gibbons are less consistent than those for siamangs or crested gibbons (**Table 3**). Could the differences within the first two genera be influenced by wild *vs.* captive gibbons? In siamangs, captive pairs did not differ from wild ones (Mann–Whitney U-test, 23 captive pairs vs. 5 wild pairs, U = 51.0, P > 0.05). In dwarf gibbons, on the other hand, captive pairs differ significantly from wild ones
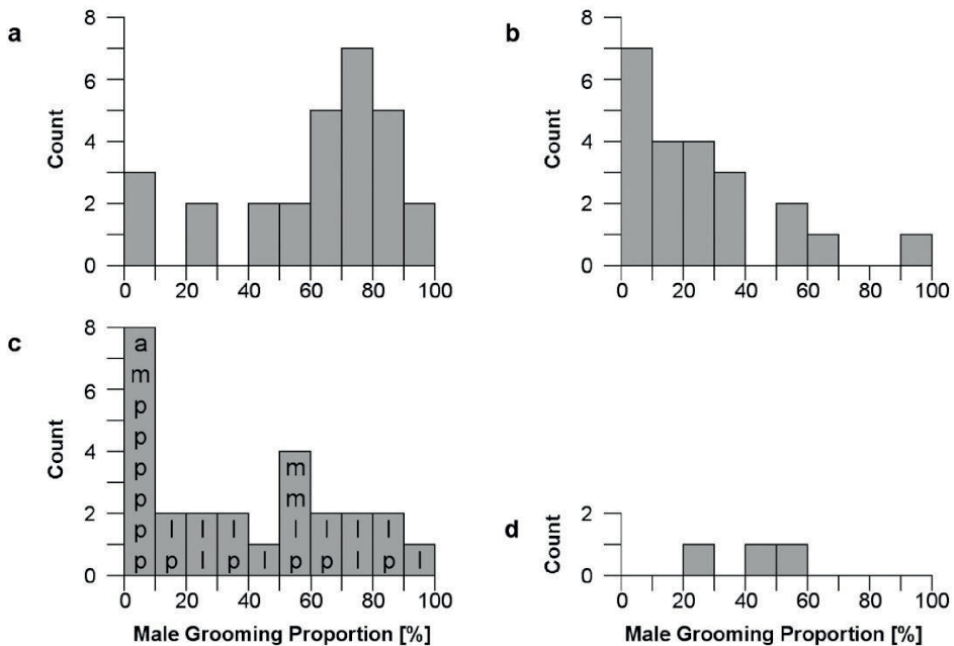
Figure 6.
Male contributions to intra-pair grooming in gibbons. (a) Siamangs (Symphalangus, N = 28 pairs); (b) crested gibbons (Nomascus, N = 18 pairs); (c) dwarf gibbons (Hylobates, N = 23 pairs); (d) hoolock gibbons (Hoolock, N = 3 pairs). Abbreviations in (c) identify the following species: a – H. agilis, l – H. lar, m – H. moloch, and p – H. pileatus.

(Mann–Whitney *U* test, 20 captive pairs vs. 6 wild pairs, U = 24.0, P = 0.027). It should be noted, however, that all available data for wild dwarf gibbons stem from only one species (*H. lar*), whereas several other species are represented in the captive sample of the same genus. If the comparison is restricted to *Hylobates lar*, the difference is not statistically significant (Mann–Whitney *U* test, 5 captive pairs vs. 6 wild pairs, U = 8.0, P > 0.05). Therefore, the variability of male grooming proportion among dwarf gibbons may be influenced by, and differ among, the species.

The frequency distribution of male grooming proportion is shown in **Figure 6**. These data differ significantly among the genera (Kruskal-Wallis test, df = 2, P < 0.0001). As revealed by the Dunn *post-hoc* tests, the male proportion in partner grooming is significantly higher in *Symphalangus* than in both *Nomascus* (P < 0.001) and *Hylobates* (P < 0.005), whereas no differences were found between *Hylobates* and *Nomascus* (P > 0.05).

4. Discussion

Monogamy is common among birds [95], but established in only about 3–9% of all mammals and about 15–29% of all primate species [45, 48, 96]. Among hominoid apes, only gibbons typically live in social monogamy (in the sense of [46]).

Various hypotheses explaining the proximate and ultimate mechanisms, which led to the evolution of social monogamy among gibbons are under debate [48, 97–99]. In these discussions, monogamy among gibbons is usually treated as, and implicitly assumed to be, a comparable, uniform entity. Cowlishaw [100], for instance, assumes that the pair bond is created by the different resource interests of the partners. The female is interested in the territory and the food resources in it, whereas the male is interested in the female partner.

Although several reports suggested that gibbon taxa might exhibit subtle distinctions in their group coherence or group composition (see Introduction), quantitative data for representative numbers of pairs have been lacking. It is generally assumed that pair bonds in all gibbon taxa are built up and maintained in the same way, and that males are mainly responsible for maintaining the pair bonds [3, 52].

As will be discussed below, this study provides evidence to the contrary. We compared indicators of pair bond strength and sex-specific pair bond investment between 7 pairs of crested gibbons, 9 pairs of pileated gibbons, and 11–17 pairs of siamangs (depending on the variable in question).

4.1 Pair bond strength

We determined three variables to compare pair bond strength between siamangs and crested gibbons (synchronization of behavioral variables, relative partner-distance, and allogrooming).

1. Synchronization of behavioral variables: The overall degree of behavioral synchronization does not differ significantly among the genera, suggesting that they do not differ in the strength of the pair bond as expressed by behavioral synchronization.

2. Relative partner-distance: The three gibbon taxa did not differ in the time spent in any of the four partner distance classes, except that siamang pairs spent less

time in the largest distance class 4 (>3 m) than pileated gibbon (*H. pileatus*) pairs, suggesting that pair bond strength in siamangs may be more pronounced than in pileated gibbons. Similarly, Palombit [22] found that siamang pairs spent significantly more time in close proximity to one another than white-handed gibbons (*H. lar*). However, we found no significant differences in the other distance classes or in the mean relative distance between pair partners.

3. Allogrooming: The three gibbon taxa did not differ in the number of grooming sessions/hour (average male and female), the proportion of time spent grooming, and the average duration of grooming sessions. As a result, siamang pairs, crested gibbon pairs and pileated gibbon pairs are involved in similar numbers of grooming sessions and spend similar amounts of time grooming.

In summary, pileated gibbons appear to spend more time apart by the largest distance class than siamangs. Based on this variable alone, their pair bond may be weaker than that of siamangs. No consistent differences in pair bond strength were found between siamangs and crested gibbons or between crested gibbons and pileated gibbons.

4.2 Pair bond maintenance

We examined which sex invests more in the pair bond by measuring the amount of grooming directed at the respective partner. For simplicity, we indicate the male proportion only; the female partner's proportion is its complement to 100%.

Our results show that in pileated and crested gibbon pairs partner-directed grooming is mostly provided by females, whereas males are the main groomers in siamang pairs. This result is further supported by additional data we collected from the literature. In most siamang pairs, males are the main groomers. Furthermore, male proportion in grooming session duration and time spent grooming are higher in siamangs than in pileated gibbons, whereas the male proportions in the numbers of grooming sessions per hour do not differ between siamangs and pileated gibbons. Siamang males groom their partners more often than crested gibbon males do, but time spent grooming and male proportion in duration of grooming do not differ between siamangs and crested gibbons. Our pairwise comparison revealed statistically significant differences for *Symphalangus*/*Nomascus*, but not for *Symphalangus*/*Hylobates* or *Hylobates*/*Nomascus*.

These results suggest that each genus differs in the mechanism of how pair bonds are created or maintained. Especially siamangs differ compared to pileated and crested gibbons: male-driven in the former, female-driven in the latter two. Obviously, the pair bond in gibbons does not appear to be a uniform entity. Date compiled in **Table 3** also suggest that field and zoo observations are consistent (except that only one wild pair exhibits a "Class 1" male grooming proportion of 0–33%).

Our results support vocal and molecular studies suggesting that gibbons are a much less homogenous group than generally assumed [39, 101, 102]. It is becoming more and more obvious that including one gibbon taxon into comparative studies in order to represent "the gibbon" is not useful practice anymore.

In our overall sample of dwarf gibbon pairs (*Hylobates*, N = 26) as well as in the subset of *H. pileatus*-pairs (N = 11), females provided more partner-grooming than males in most pairs. In *H. lar*-pairs (N = 11), on the other hand, the amount of grooming provided by males and females was very variable (**Table 3**) and the reason for this variability in this sample is not clear.

Kleiman [45] proposed that males should be the more active groomers in monogamous primates because their dominance situation is reversed as compared to primates with polygynous social organizations. Simple dominance relationships, however, do not seem the only variables influencing partner-directed allogrooming in gibbons.

If partner-directed allogrooming reflects the investment into a pair bond [62, 63], then our results document that the readiness to invest differs among pairs. In most (but not necessarily all) pairs, both partners appeared to be interested in maintaining the pair pond, and both partners provided at least some allogrooming. In addition to individual differences, the interest in a pair partner may vary with time. Probably, the benefit of a pair bond is related to the reproductive potential of a partner. Observations on wild *H. lar* and *H. moloch* suggest that the reproductive status of females may play an important role [13, 103, 104]. Males may have a higher interest to invest into the pair bond with females when they are receptive, in order to guard them more efficiently, copulate more frequently and improve the probability of their paternity. If partner-directed grooming is part of a mate-guarding strategy with fluctuating relevance to the groomer, it becomes clear why data of relatively large numbers of pairs need to be compared in order to discover species-specific differences.

How do our findings compare to the predictions of the three hypotheses for the evolution of pair bonds presented in the Introduction?

1. The 'male-services hypothesis' predicts that a female will invest substantially in a social relationship with a male willing to assume the costs of territorial or antipredator defense, infant care or protection from infanticidal males. This should result in females investing more than males in maintaining the pair bond. This prediction is met by our samples of crested gibbons (N = 22 pairs, **Table 3**), pileated gibbons (N = 11 pairs) and the combined sample of all dwarf gibbons (N = 26 pairs). In all three samples, females were the main groomers in most pairs.

2. The 'mate-defense hypothesis' predicts that bonding with a female is beneficial for a male when either the spatial distribution of females or the temporal distribution of fertile periods makes it difficult for the males to defend access to more than one female at a time. This should result in males investing more than females in maintaining the pair bond. This prediction is met by our sample of siamangs (N = 28 pairs), where males were the main groomers in most pairs.

3. The 'resource-defense hypothesis' predicts that both a male and a female benefit from pair bonding to defend resources together. This should result in a male and a female being equally interested in maintaining proximity and affiliation with a pair mate and defending their territory. None of the gibbon samples of this study appears to meet this prediction.

Only very limited information on the direction of partner-grooming is available for the fourth of the gibbon genera, the hoolocks (genus *Hoolock*). Ahsan [105], who studied three groups of the western hoolock gibbon (*H. hoolock*) at two sites in Bangladesh, reported that grooming was most frequent between adult pairs and that it was "mostly performed by the adult male". Unfortunately, the author did not publish the quantitative data in support of his statement. Sankaran [94] observed three

groups of the same species in the Gibbon Wildlife Sanctuary in Assam. However, none of his males provided more than 50% of the partner-grooming (**Table 3**). Apparently, the results of the two studies differ, but the overall sample size is too small to assess the directionality of partner grooming in hoolock gibbons with any reliability.

It has also been reported that allogrooming between pair mates is virtually non-existent in wild *Hylobates agilis* [21] and *H. klossii* [106], in contrast to the situation in wild *H. lar* and siamangs [10, 13, 19, 103]. This suggests that the range of variation in gibbon pair bonds may be larger than what we covered in our study. Several species of dwarf gibbons (*Hylobates*) are hardly represented or not represented at all in our data, including *H. agilis* and *H. klossii*.

Within crested gibbons (*Nomascus*), most of our data are from one species, *N. leucogenys* (N = 14 pairs), whereas few pairs of other light-cheeked species and only one male of a black-cheeked species (*N. concolor* in a mixed pair) are available.

5. Conclusions

1. A comparison of pair bond strength in three gibbon taxa – siamangs (*Symphalangus*), crested gibbons (*Nomascus*) and pileated gibbons (*Hylobates pileatus*) revealed a difference in relative partner distances between siamangs and pileated gibbons, suggesting that siamangs may have a stronger pair bond than pileated gibbons. No difference between the three taxa was found in other variables believed to indicate pair bond strength: degree of behavioral synchronization and amounts of grooming (both numbers of events and actual grooming time).

2. This study provides the first statistically significant evidence that the mechanisms of how pair bonds are created or maintained, differ between gibbon taxa. As indicated by the amount of partner-directed grooming, siamang males invest significantly more into the pair bond than females, whereas the opposite is true in crested gibbons, pileated gibbons, and an enlarged sample of dwarf gibbons (genus *Hylobates*). Additional species-specific differences may, however, occur within the latter group, with partner-grooming investment being highly variable in *H. lar*.

3. Our results for crested gibbons, pileated gibbons, and a combined sample of dwarf gibbons correspond to predictions derived from the 'male-services hypothesis' for the evolution of pair bonds. According to this hypothesis, a female will invest substantially in a social relationship with a male willing to assume the costs of territorial or antipredator defense, infant care or protection from infanticidal males.

4. In contrast, our results for siamangs correspond to predictions derived from the 'mate-defense hypothesis'. According to this hypothesis, bonding with a female is beneficial for a male when either the spatial distribution of females or the temporal distribution of fertile periods makes it difficult for the males to defend access to more than one female at a time.

5. Species-specific analyses are recommended for additional species of the genera *Hylobates*, *Nomascus* (especially the black-cheeked taxa) and *Hoolock*.

Acknowledgements

Conflict of interest

There is no financial/personal interest, or contractual employment involving matters in this article or belief that could affect the authors' objectivity.

Author details

Thomas Geissmann[1]*, Simone Rosenkranz-Weck[2], Judith J.G.M. Van Der Loo[3] and Mathias Orgeldinger[4]

1 Department of Anthropology, Zurich University, Zurich, Switzerland

2 Department of Biology, Hamburg University, Hamburg, Germany

3 Institute of Food, Agricultural and Horticultural Sectors, University of Applied Sciences HAS Den Bosch, The Netherlands

4 Nuremberg Zoo, Nuremberg, Germany

*Address all correspondence to: thomas.geissmann@aim.uzh.ch

IntechOpen

References

[1] Tuttle, RH. Apes of the World. Their Social Behavior, Communication, Mentality and Ecology. Park Ridge, NJ: Noyes Publications; 1986. xix+421 p.

[2] Fleagle JG. Primate Adaptation and Evolution. 3rd ed. San Diego and London: Academic Press; 2013. 441 p.

[3] Palombit RA. Infanticide and the evolution of pair bonds in nonhuman primates. Evolutionary Anthropology. 1999;7:117-129. DOI: 10.1002/(SICI)1520-6505(1999)7:4<117::AID-EVAN2>3.0.CO;2-O

[4] Chivers DJ. The Lesser Apes. In: Prince Rainier III of Monaco, Bourne GH, editors. Primate Conservation. New York: Academic Press; 1977. p. 539-598.

[5] Leighton DR. Gibbons: Territoriality and monogamy. In: Smuts BB, Cheney DL, Seyfarth RM, Wrangham RW, Struhsaker TT, editors. Primate Societies. Chicago and London: University of Chicago Press; 1987. p. 135-145.

[6] Chivers DJ, Anandam MV, Groves CP, Molur S, Rawson BM, Richardson MC, Roos C, Whittaker DJ. Family Hylobatidae (Gibbons). In: Mittermeier RA, Rylands AB, Wilson DE, editors. Handbook of the Mammals of the World, Vol 3: Primates. Barcelona: Lynx Edicions; 2013. p. 754-791.

[7] Lappan S. Social relationships among males in multimale siamang groups. International Journal of Primatology. 2007;28:369-387. DOI: 10.1007/s10764-007-9122-z

[8] Whittaker DJ, Lappan S. The diversity of small apes and the importance of population-level studies. In: Lappan S, Whittacker DJ, editors. The Gibbons: New Perspectives on Small Ape Socioecology and Population Biology. New York: Springer; 2009. p. 3-10.

[9] Lappan S. Biparental care and male reproductive strategies in siamangs (*Symphalangus syndactylus*) in southern Sumatra [Ph.D. thesis]. New York: Department of Anthropology, New York University; 2005.

[10] Palombit RA. Pair bonds and monogamy in wild siamang (*Hylobates syndactylus*) and white-handed gibbon (*Hylobates lar*) in northern Sumatra [Ph.D. thesis]. Davis: University of California; 1992.

[11] Palombit RA. Dynamic pair bonds in hylobatids: Implications regarding monogamous social systems. Behaviour. 1994;128:65-101. DOI: 10.1163/156853994X00055

[12] Palombit RA. Extra-pair copulations in a monogamous ape. Animal Behaviour. 1994;47:721-723. DOI: 10.1006/anbe.1994.1097

[13] Reichard U. Sozial- und Fortpflanzungsverhalten von Weisshandgibbons (*Hylobates lar*): Eine Freilandstudie im thailändischen Khao Yai Regenwald. [Ph.D. thesis]. Göttingen: Mathematisch-Naturwissenschaftliche Fachbereiche, Georg-August-Universität; 1995.

[14] Reichard UH. The social organization and mating system of Khao Yai white-handed gibbons: 1992-2006. In: Lappan S, Whittacker DJ, editors. The Gibbons: New Perspectives on Small Ape Socioecology and Population Biology. New York: Springer; 2009. p. 347-384.

[15] Savini T, Boesch C, Reichard R. Varying ecological quality influences the probability of polyandry in white-handed gibbons (*Hylobates lar*) in Thailand. Biotropica. 2009;41:503-513. DOI: 10.1111/j.1744-7429.2009.00507.x

[16] Bartlett TQ. Intragroup and intergroup social interactions in white-handed gibbons. International Journal of Primatology. 2003;24:239-259. DOI: 10.1023/A:1023088814263

[17] Chivers DJ. Communication within and between family groups of siamang (*Symphalangus syndactylus*). Behaviour. 1976;57:116-135. DOI: 10.1163/156853976X00136

[18] Chivers DJ. The siamang and the gibbon in the Malay peninsula. In: Rumbaugh DM, editor. Gibbon and Siamang, Vol. 1. Basel and New York: Karger; 1972. p. 103-135.

[19] Chivers DJ. The Siamang in Malaya: A Field Study of a Primate in Tropical Rain Forest (Contributions to Primatology vol. 4). Basel and New York, Karger; 1974. xiii+335 p.

[20] Chivers DJ. Gibbons. In: MacDonald, D., editor. The Encyclopedia of Mammals, Vol. 1. London: Allen & Unwin; 1984. p. 415-419.

[21] Gittins SP, Raemaekers JJ. Siamang, lar and agile gibbons. In: Chivers DJ, editor. Malayan Forest Primates: Ten Years' Study in Tropical Rain Forest. New York: Plenum Press; 1980. p. 63-105.

[22] Palombit RA. Pair bonds in monogamous apes: A comparison of the siamang *Hylobates syndactylus* and the white-handed gibbons *Hylobates lar*. Behaviour. 1996;133:321-356. DOI: 10.1163/156853996X00486

[23] Fischer JO, Geissmann T. Group harmony in gibbons: Comparison between white-handed gibbon (*Hylobates lar*) and siamang (*H. syndactylus*). Primates. 1990;31:481-494. DOI: 10.1007/BF02382532

[24] Jones AR. Infant transfer in a captive family of siamangs (*Hylobates syndactylus*) [Master's thesis]. Monroe: Faculty of the Graduate School, Northeast Louisiana University; 1995.

[25] Lappan S. Patterns of infant care in wild siamangs (*Symphalangus syndactylus*) in southern Sumatra. In: Lappan S, Whittacker DJ, editors. The Gibbons: New Perspectives on Small Ape Socioecology and Population Biology. New York: Springer; 2009. p. 327-345.

[26] Eardley J. Attachment and social relationships between members of gibbon and siamang families with a discussion on human-infant attachment figures and implications of these relationships [Master's thesis]. Fullerton: California State University; 2000.

[27] Fan P-F, Jiang X-L, Liu C-M, Luo W-S. Polygynous mating system and behavioural reason of black crested gibbon (*Nomascus concolor jingdongensis*) at Dazhaizi, Mt. Wuliang, Yunnan, China. Zoological Research. 2006;27: 216-220 (Mandarin text, English abstract).

[28] Fan P-F, Bartlett TQ, Fei H-L, Ma C-Y, Zhang W. Understanding stable bi-female grouping in gibbons: Feeding competition and reproductive success. Frontiers in Zoology. 2015;12:5. DOI 10.1186/s12983-015-0098-9

[29] Haimoff EH, Yang X-J, He S-J, Chen N. Census and survey of wild black-crested gibbons (*Hylobates concolor concolor*) in Yunnan Province, People's Republic of China. Folia Primatologica. 1986;46:205-214. DOI: 10.1159/000156254

[30] Haimoff EH, Yang X-J, He S-J, Chen N. Preliminary observations of wild black-crested gibbons (*Hylobates concolor concolor*) in Yunnan Province, People's Republic of China. *Primates*. 1987;*28*:319-335. DOI: 10.1007/BF02381015

[31] Jiang XL, Wang YX. Population and conservation of black-crested gibbon (*Hylobates concolor jingdongensis*) in Wuliang Nature Reserve, Yunnan. Zoological Research. 1999;20:421-425.

[32] Liu Z, Jiang H, Zhang Y, Liu Y, Chou T, Manry D, Southwick C. Field report on the Hainan gibbon. Primate Conservation. 1987; 8: 49-50.

[33] Liu Z, Zhang Y, Jiang H, Southwick C. Population structure of *Hylobates concolor* in Bawanglin Nature Reserve, Hainan, China. American Journal of Primatology. 1989;19:247-254. DOI: 10.1002/ajp.1350190406

[34] Geissmann T, Nguyen Xuan Dang, Lormée, N, Momberg, F. Vietnam Primate Conservation Status Review 2000. Part 1: Gibbons (English Edition). Hanoi: Fauna & Flora International, Indochina Programme; 2000. 135 p.

[35] Kenyon MA. The ecology of the golden-cheeked gibbon (*Nomascus gabriellae*) in Cat Tien National Park, Vietnam [Ph.D. thesis]. Cambridge: Department of Anatomy, University of Cambridge; 2007.

[36] Barca B, Vincent C, Khang Soeung, Nuttall M, Hobson K. Multi-female group in the southernmost species of *Nomascus*: Field observations in eastern Cambodia reveal multiple breeding females in a single group of southern yellow-cheeked crested gibbon *Nomascus gabriellae*. Asian Primates Journal. 2016;6:15-19.

[37] Dallmann R, Geissmann T. Different levels of variability in the female song of

wild silvery gibbons (*Hylobates moloch*). Behaviour. 2001;138,629-648. DOI: 10.1163/156853901316924511

[38] Dallmann R, Geissmann T. Individuality in the female songs of wild silvery gibbons (*Hylobates moloch*) on Java, Indonesia. Contributions to Zoology. 2001; 70: 41-50. DOI: 10.1163/18759866-07001003

[39] Geissmann T. Duet-splitting and the evolution of gibbon songs. Biological Reviews. 2002;77:57-76. DOI: 10.1017/s1464793101005826

[40] Geissmann T, Bohlen-Eyring S, and Heuck A. The male song of the Javan silvery gibbon (*Hylobates moloch*). Contributions to Zoology. 2005;74:1-25. DOI: 10.1163/18759866-0740102001

[41] Geissmann T. Duet songs of the siamang, *Hylobates syndactylus*: I. Structure and organisation. Primate Report. 2000;56:33-60.

[42] Geissmann T. Gibbon songs and human music from an evolutionary perspective. In: Wallin NL, Merker B, Brown S, editors. The Origins of Music. Cambridge, Massachusetts: MIT Press; 2000. p. 103-123. DOI: 10.7551/mitpress/5190.003.0011

[43] Geissmann T. Duet songs of the siamang, *Hylobates syndactylus*: II. Testing the pair-bonding hypothesis during a partner exchange. Behaviour. 1999;136:1005-1039. DOI: 10.1163/156853999501694

[44] Geissmann T, Orgeldinger M. The relationship between duet songs and pair bonds in siamangs, *Hylobates syndactylus*. Animal Behaviour. 2000;60:805-809. DOI: 10.1006/anbe.2000.1540

[45] Kleiman DG. Monogamy in mammals. Quarterly Review of Biology. 1977;52:39-69. DOI: 10.1086/409721

[46] Reichard UH. Monogamy: Past and present. In: Reichard UH., Boesch C., editors. *Monogamy: Mating Strategies and Partnerships in Birds, Humans and other Mammals*. Cambridge: Cambridge University Press; 2003. p. 3-25. DOI: 10.1017/CBO9781139087247.001

[47] Dolotovskaya S, Walker S, Heymann EW. What makes a pair bond in a Neotropical primate: Female and male contributions. Royal Society Open Science. 2020;7:191489. DOI: 10.1098/rsos.191489

[48] van Schaik CP, Dunbar RIM. The evolution of monogamy in large primates: A new hypothesis and some crucial tests. Behaviour. 1990;115:30-62. Doi:10.1163/156853990X00284

[49] Emlen ST, Oring LW. Ecology, sexual selection, and the evolution of mating systems. Science. 1977;197:215-223. Doi:10.1126/science.327542

[50] Birkhead TR, Møller AP. Sperm Competition in Birds: Evolutionary Causes and Consequences. London: Academic Press; 1992. 288 p.

[51] Opie C, Atkinson QD, Dunbar RIM, Shultz S. Male infanticide leads to social monogamy in primates. Proceedings of the National Academy of Sciences, USA. 2013;110:13328-13332. Doi:10.1073/pnas.1307903110

[52] Palombit RA. Infanticide and the evolution of male-female bonds in animals. In: van Schaik CP, Janson CH, editors. Infanticide by Males and its Implications. Cambridge: Cambridge University Press; 2000. p. 239-268. DOI: 10.1017/CBO9780511542312.013

[53] Orgeldinger M. Paarbeziehung beim Siamang-Gibbon (*Hylobates syndactylus*) im Zoo: Untersuchung über den Einfluss von Jungtieren auf die Paarbindung. Münster: Schüling Verlag; 1999.

[54] Akinyi MY, Tung J, Jeneby, M, Patel NB, Altmann J, Alberts, SC. Role of grooming in reducing tick load in wild baboons (*Papio cynocephalus*). Animal Behaviour. 2013;85:559-568. DOI: 0.1016/j.anbehav.2012.12.012

[55] Aureli F, Preston SD., de Waal FBM. Heart rate responses to social interactions in free-moving rhesus macaques (*Macaca mulatta*): A pilot study. Journal of Comparative Psychology. 1999;113:59-65. DOI: 10.1037/0735-7036.113.1.59

[56] Barton R. Grooming site preferences in primates and their functional implications. International Journal Primatology. 1985;6:519-532. DOI: 10.1007/BF02735574

[57] Goosen C. Social grooming in primates. In: Mitchell G, Erwin J, editors. Comparative Primatology, Vol. 2B: Behavior, Cognition, and Motivation. New York: Alan R. Liss; 1987. p. 107-131.

[58] Hutchins M, Barash DP. Grooming in primates: Implications for its utilitarian function. Primates. 1976;17:145-150. DOI: 10.1007/BF02382848

[59] McFarland R., Henzi SP, Barrett L, Wanigaratne A, Coetzee E, Fuller A, Hetem RS, Mitchell D, and Maloney SK. Thermal consequences of increased pelt loft infer an additional utilitarian function for grooming. American Journal of Primatology. 2016;78:456-461. DOI: 10.1002/ajp.22519

[60] Harrison CJO. Allopreening as agonistic behaviour. Behaviour. 1965;24:161-209. DOI: 10.1163/156853965X00011

[61] Kunkel P. Mating systems of tropical birds: The effects of weakness or absence of external reproduction-timing factors with special reference to prolonged pair

bonds. Zeitschrift für Tierpsychologie. 1974;34:265-307. DOI: 10.1111/j.1439-0310.1974.tb01802.x

[62] O'Brien TG. Allogrooming behaviour among adult female wedge-capped capuchin monkeys. Animal Behaviour. 1993;46:499-510. DOI: 10.1006/anbe.1993.1218

[63] Seyfarth RM. A model of social grooming among adult female monkeys. Journal of Theoretical Biology. 1977;65:671-698. DOI: 10.1016/0022-5193(77)90015-7

[64] Colvin J. Familiarity, rank and structure of rhesus male peer networks. In: Hinde RA, editor. Primate Social Relationships: An Integrated Approach. Sunderland: Sinauer Associates; 1983. p. 190-200.

[65] Burgin CJ, Wilson DE, Mittermeier RA, Rylands AB, Lacher TE, Sechrest W. Illustrated Checklist of the Mammals of the World, Vol. 1: Monotremata to Rodentia. Barcelona: Lynx Editions; 2020. 631 p.

[66] Martin P, Bateson P. Measuring Behaviour. An Introductory Guide, 3rd edition. Cambridge: Cambridge University Press; 2007. xi+176 p.

[67] Altmann J. Observational study of behavior: Sampling methods. Behaviour. 1974;49:227-267. DOI: 10.1163/156853974X00534

[68] Geissmann T. Verhaltensbiologische Forschungsmethoden: Eine Einführung. Münster: Schüling Verlag; 2002. 54 p.

[69] Lehner PN. Handbook of Ethological Methods. Cambridge: Cambridge University Press; 1998. 694 p.

[70] Zar JH. Biostatistical Analysis. 4th ed. Upper Saddle River, NJ: Prentice Hall; 1999. 663 p.

[71] Siegel S, Castellan NJ Jr. Nonparametric Statistics for the Behavioral Sciences, 2nd Edition. New York: McGraw Hill; 1988. 330 p.

[72] Fox GJ. Social dynamics in siamang [Ph.D. thesis]. Milwaukee: University of Wisconsin; 1977.

[73] Kawata K. Notes on comparative behavior in three primate species in captivity. Der Zoologische Garten (N.F.). 1980;50:209-224.

[74] Dielentheis TF, Zaiss E. Lokomotions- und Sozialverhalten dreier Hylobatiden-Arten [Praktikumsarbeit]. Berlin: AG Humanbiologie, Institut für Tierphysiologie, Freie Universität Berlin; 1987.

[75] Philippart M. Captive siamang monogamous pairs at the Cheyenne Mountain Zoo [Undergraduate research report, primatology]. Colorado Springs: Anthropology Department, The Colorado College; 1991.

[76] Bricknell S. A comparative study of the behaviour in captivity of three species of gibbon: *Hylobates syndactylus*, *Hylobates leucogenys* and *Hylobates lar*. BA [Honour's thesis]. Canberra: Department of Archaeology and Anthropology, Australian National University; 1992.

[77] Caeiro Pereira de Sousa A. Estudo e comparação dos laços de união ("pair bonds") em dois casais de siamangs (*Hylobates syndactylus*) em cativeiro [M.Sc. thesis]. Lisbon, Portugal: Instituto Superior de Psicologia Aplicada; 1998.

[78] Pollard GM. The behaviour of captive hylobatids and a comparison with the behaviour of those species in the wild [B.Sc. (Honours Biol. Sci.) thesis]. Wolverhampton, UK: Polytechnic Wolverhampton; 1983.

[79] Dooley H. Social behaviour in gibbon groups of gibbons (*Hylobates leucogenys* and *Hylobates moloch*) at Perth Zoo [Honour's thesis]. Perth: School of Anatomy and Human Biology, The University of Western Australia; 2006.

[80] Hénon C. Étude des interactions comportementales dans le cadre d'un déplacement induisant la proximité spatiale de deux espèces proches de gibbon [Maîtrise de biologie des populations et des écosystèmes]. Besançon: Université de Franche-comté; 2002.

[81] Schlegel K. Ethologische und endokrinologische Untersuchungen an Schopfgibbons *Hylobates concolor* in Gefangenschaft [Lizentiatsarbeit thesis]. Zurich: Psychologisches Institut, Biologisch-mathematische Abteilung, Philosophische Fakultät I, Zurich University; 1995.

[82] Hold A. Das Verhaltensrepertoire des Weisswangen-Schopfgibbons (*Hylobates leucogenys*) [Diploma thesis]. Hannover: Institut für Zoologie, Tierärztliche Hochschule Hannover; 1998.

[83] Lukas KE, Barkauskas RT, Maher SA, Jacobs BA, Bauman JE, Henderson AJ, Calcagno JM. Longitudinal study of delayed reproductive success in a pair of white-cheeked gibbon (*Hylobates leucogenys*). Zoo Biology. 2002;21:413-434.

[84] Poyas AL. Pair bonding and parental care in socially monogamous primates: A comparative study of the white-cheeked gibbon (*Nomascus leucogenys*) and the white-faced saki (*Pithecia pithecia*) [Master's thesis]. San Antonio: Department of Anthropology, University of Texas; 2008.

[85] Poyas AL, Bartlett TQ. Pair bonding in socially monogamous primates: A comparative study of the white-cheeked gibbon (*Nomascus leucogenys*) and the white-faced saki (*Pithecia pithecia*). American Journal of Physical Anthropology Supplement. 2009;48:214 (Abstract only).

[86] Embury AS. A study of the behaviour of captive gibbons [B.Sc. (Honour's) thesis]. Parkville: Department of Zoology, University of Melbourne; 1983.

[87] Skyner L. The effect of visitors on the self-mutilation behaviour of a male pileated gibbon (*Hylobates pileatus*) at Blackpool Zoological Gardens [BSc (Honour's) Animal Behaviour and Welfare thesis]. Myerscough: Myerscough College, in association with The University of Central Lancashire, UK; 2002.

[88] Riess BF. The behavior and social relations of the gibbon (*Hylobates lar*) observed under restricted free-range conditions. Zoologica. 1956;41:89-99.

[89] Steen, JC. Behavior of captive gibbons (*Hylobates* sp.): Study of a group of six animals in the Portland (Oreg.) Zoo [MSc (Master of Arts) thesis]. Portland: Department of Anthropology, University of Oregon; 1969.

[90] Ebert J. Paarungsverhalten weiblicher Weisshandgibbons (*Hylobates lar*) [Diploma thesis]. Berlin: Fachbereich Biologie, Chemie, Pharmazie, Freie Universität Berlin; 1999.

[91] Eichmüller P. Verhaltensbiologische Beobachtung der Silbergibbons (*Hylobates moloch*) des Tierparks Hellabrunn, München [Praktikumsarbeit zur Vorlesung Tierökologie und Verhalten, Sommersemester 2006, betreut durch Prof. Dr. Gerstmeier]. Munich: Lehrstuhl für Zoologie, Technische Universität München; 2006.

[92] Heufelder S. Eltern-Kind Beziehung und juveniles Spielverhalten von *Hylobates moloch* im Tierpark Hellabrunn, München [Praktikumsarbeit zur Vorlesung Verhaltensbiologie, betreut durch Prof. Dr. R. Gerstmeier]. Munich: Lehrstuhl für Zoologie, Technische Universität München; 2007.

[93] Schneider H. Verhaltensbiologische Beobachtung der Silbergibbons (*Hylobates moloch*) des Tierparks Hellabrunn, München [Praktikumsarbeit zur Vorlesung Verhaltensbiologie, betreut durch Prof. Dr. R. Gerstmeier]. Munich: Lehrstuhl für Zoologie, Technische Universität München; 2009.

[94] Sankaran S. Social behaviour and duetting in hoolock gibbons in Gibbon Wildlife Sanctuary, Assam [Master's thesis]. Rajkot: Wildlife Science, Saurashtra University; 2009.

[95] Dunn PO, Whittingham LA, Pitcher TE. Mating systems, sperm competition, and the evolution of sexual dimorphism in birds. Evolution. 2001;55:161-175. DOI: 0.1111/j.0014-3820.2001.tb01281.x

[96] Lukas D, Clutton-Brock TH. The evolution of social monogamy in mammals. Science. 2013;341:526-530. Doi: 10.1126/science.1238677

[97] Brockelman WY, Srikosamatara S. Maintenance and evolution of social structure in gibbons. In: Preuschoft H, Chivers DJ, Brockelman WY, Creel N, editors. The Lesser Apes: Evolutionary and Behavioural Biology. Edinburgh: Edinburgh University Press; 1984. p. 298-323.

[98] Brockelman WY, Reichard U, Treesucon U, Raemaekers JJ. Dispersal, pair formation and social structure in gibbons (*Hylobates lar*). Behavioural Ecology and Sociobiology. 1998;42:329-339. DOI: 10.1007/s002650050445

[99] van Schaik CP. Social evolution in primates: The role of ecological factors and male behaviour. Proceedings of the British Academy. 1996;88:9-31.

[100] Cowlishaw G. Song function in gibbons. Behaviour. 1992;121:131-153. DOI: 10.1163/156853992X00471

[101] Geissmann T, Bohlen-Eyring S, Heuck A. The male song of the Javan silvery gibbon (*Hylobates moloch*). Contributions to Zoology. 2005;74:1-25. DOI: 10.1163/18759866-0740102001

[102] Roos C, Geissmann T. Molecular phylogeny of the major hylobatid divisions. Molecular Phylogenetics and Evolution. 2001;19:486-494. DOI: 10.1006/mpev.2001.0939

[103] Ellefson JO. A natural history of white-handed gibbons in the Malayan Peninsula. In: Rumbaugh DM, editor. Gibbon and Siamang, Vol. 3. Basel and New York: Karger; 1974. p. 1-136.

[104] Yi Y. Intra-group and inter-group social interactions in a pair-living primate, the Javan gibbon (*Hylobates moloch*) [Ph.D. thesis]. Seoul: Ewha Womans University; 2020.

[105] Ahsan MF. Socio-ecology of the hoolock gibbon (*Hylobates hoolock*) in two forests of Bangladesh. In: Chicago Zoological Society, editor. The Apes: Challenges for the 21st Century. Conference Proceedings; 10-13 May 2000; Brookfield Zoo. Brookfield, Illinois: Chicago Zoological Society; 2001. p. 286-299.

[106] Whitten AJ. The Kloss gibbon in Siberut rain forest [Ph.D. thesis]. Cambridge: Sub-Department of Veterinary Anatomy, University of Cambridge; 1980.

*Edited by Catrin Sian Rutland
and Samir A.A. El-Gendy*

Knowledge of veterinary anatomy and physiology is essential for veterinary students, professionals, and researchers, as well as animal owners who wish to gain greater levels of understanding. This book reflects the diverse and dynamic research being undertaken on a variety of different species worldwide. It includes four sections and twelve chapters that address a myriad of topics, ranging from animal cardiovascular and musculoskeletal systems to pathology and infections, and immunity. Chapters present recent research on animals ranging from primates to horses and cattle.

*Rita Payan Carreira,
Veterinary Medicine and Science Series Editor*